MASSACHUSETTS INSTITUTE OF TECHNOLOGY

RADIATION LABORATORY SERIES

LOUIS N. RIDENOUR, *Editor-in-Chief*

RADAR SCANNERS AND RADOMES

MASSACHUSETTS INSTITUTE OF TECHNOLOGY

RADIATION LABORATORY SERIES

---

1. RADAR SYSTEM ENGINEERING—*Ridenour*
2. RADAR AIDS TO NAVIGATION—*Hall*
3. RADAR BEACONS—*Roberts*
4. LORAN—*Pierce, McKenzie, and Woodward*
5. PULSE GENERATORS—*Glasoe and Lebacqz*
6. MICROWAVE MAGNETRONS—*Collins*
7. KLYSTRONS AND MICROWAVE TRIODES—*Hamilton, Knipp, and Kuper*
8. PRINCIPLES OF MICROWAVE CIRCUITS—*Montgomery, Dicke, and Purcell*
9. MICROWAVE TRANSMISSION CIRCUITS—*Ragan*
10. WAVEGUIDE HANDBOOK—*Marcuvitz*
11. TECHNIQUE OF MICROWAVE MEASUREMENTS—*Montgomery*
12. MICROWAVE ANTENNA THEORY AND DESIGN—*Silver*
13. PROPAGATION OF SHORT RADIO WAVES—*Kerr*
14. MICROWAVE DUPLEXERS—*Smullin and Montgomery*
15. CRYSTAL RECTIFIERS—*Torrey and Whitmer*
16. MICROWAVE MIXERS—*Pound*
17. COMPONENTS HANDBOOK—*Blackburn*
18. VACUUM TUBE AMPLIFIERS—*Valley and Wallman*
19. WAVEFORMS—*Chance, Hughes, MacNichol, Sayre, and Williams*
20. ELECTRONIC TIME MEASUREMENTS—*Chance, Hulsizer, MacNichol, and Williams*
21. ELECTRONIC INSTRUMENTS—*Greenwood, Holdam, and MacRae*
22. CATHODE RAY TUBE DISPLAYS—*Soller, Starr, and Valley*
23. MICROWAVE RECEIVERS—*Van Voorhis*
24. THRESHOLD SIGNALS—*Lawson and Uhlenbeck*
25. THEORY OF SERVOMECHANISMS—*James, Nichols, and Phillips*
26. RADAR SCANNERS AND RADOMES—*Cady, Karelitz, and Turner*
27. COMPUTING MECHANISMS AND LINKAGES—*Svoboda*
28. INDEX—*Linford*

RADAR SCANNERS AND RADOMES

Edited by

W. M. CADY
HEAD, PHYSICS DIVISION, U.S. NAVAL ORDNANCE TEST STATION, PASADENA ANNEX

M. B. KARELITZ
ASSISTANT DIRECTOR OF RESEARCH GENERAL PRECISION LABORATORY, INC.

LOUIS A. TURNER
HEAD, DEPARTMENT OF PHYSICS STATE UNIVERSITY OF IOWA

OFFICE OF SCIENTIFIC RESEARCH AND DEVELOPMENT
NATIONAL DEFENSE RESEARCH COMMITTEE

FIRST EDITION

NEW YORK · TORONTO · LONDON
McGRAW-HILL BOOK COMPANY, INC.
1948

RADAR SCANNERS AND RADOMES

THE MAPLE PRESS COMPANY, YORK, PA.

RADAR SCANNERS AND RADOMES

EDITORIAL STAFF

Louis A. Turner
R. G. Herb
W. M. Cady
M. B. Karelitz

CONTRIBUTING AUTHORS

V. G. Bruce
W. M. Cady
L. L. Davenport
W. Ellis
W. B. Ewing
R. J. Grenzback
D. D. Jacobus
M. B. Karelitz
H. Leaderman
F. B. Lincoln
J. K. McKendry
E. B. McMillan
F. J. Mehringer
R. M. Robertson
R. Sher
H. A. Straus
F. E. Swain
Louis A. Turner
J. S. White

Foreword

THE tremendous research and development effort that went into the development of radar and related techniques during World War II resulted not only in hundreds of radar sets for military (and some for possible peacetime) use but also in a great body of information and new techniques in the electronics and high-frequency fields. Because this basic material may be of great value to science and engineering, it seemed most important to publish it as soon as security permitted.

The Radiation Laboratory of MIT, which operated under the supervision of the National Defense Research Committee, undertook the great task of preparing these volumes. The work described herein, however, is the collective result of work done at many laboratories, Army, Navy, university, and industrial, both in this country and in England, Canada, and other Dominions.

The Radiation Laboratory, once its proposals were approved and finances provided by the Office of Scientific Research and Development, chose Louis N. Ridenour as Editor-in-Chief to lead and direct the entire project. An editorial staff was then selected of those best qualified for this type of task. Finally the authors for the various volumes or chapters or sections were chosen from among those experts who were intimately familiar with the various fields, and who were able and willing to write the summaries of them. This entire staff agreed to remain at work at MIT for six months or more after the work of the Radiation Laboratory was complete. These volumes stand as a monument to this group.

These volumes serve as a memorial to the unnamed hundreds and thousands of other scientists, engineers, and others who actually carried on the research, development, and engineering work the results of which are herein described. There were so many involved in this work and they worked so closely together even though often in widely separated laboratories that it is impossible to name or even to know those who contributed to a particular idea or development. Only certain ones who wrote reports or articles have even been mentioned. But to all those who contributed in any way to this great cooperative development enterprise, both in this country and in England, these volumes are dedicated.

L. A. DUBRIDGE.

Preface

A RADAR scanner, or antenna mount, is the assembly consisting of the antenna and the mechanism that causes the radiated beam to scan. In this volume we are concerned mainly with the engineering of the scanner and its housing. The electrical design of the antenna and the transmission line are discussed in Vol. 12 of the Radiation Laboratory Series. Since the reader is presumed to have an engineering background, the discussion of radar antenna mounts in Part I deals only with those features of the design which are peculiar to radar antenna mounts. The treatment is incomplete in two respects. There is almost no reference to equipment operating at wavelengths longer than 10 cm, and there is little discussion of scanners that were not developed at the Radiation Laboratory. These omissions, particularly the latter, should not be regarded as indication of editorial complacency; they result from lack of information by the authors. Many valuable radar systems and radar antenna mounts have been devised for use at 20 cm and longer wavelengths; many have been developed by industry and the armed services. These systems get only passing mention or none at all because of our reluctance to write about unfamiliar topics.

It has been necessary to omit much pertinent material for reasons of military security. The editors have sought to include as much technical information as permissible and the advisory group on security has been cooperative. Deletions and revisions had to be made in the proof, however, in accord with recommendations of the final review board and it was not possible at the late date to smooth out the resulting gaps by thorough revision. The editors regret the deletions but believe that the material which remains will prove to be of value.

Part I is written largely for the mechanical engineer; in Part II electrical considerations predominate. This second part is the first comprehensive discussion of radomes, the plastic enclosures for antennas. Radome development has opened a new field of electromechanical engineering. Because the electrical aspects are less familiar, they are more fully treated here.

All the authors wrote as staff members of the Radiation Laboratory. Their contributions are indicated in each chapter. The book was

planned and guided through several stages of revision by W. M. Cady and M. B. Karelitz; after their departure in February 1946, L. A. Turner took over. M. B. Karelitz assumed the principal responsibility for editing the chapters on ground-based and shipborne antenna mounts; W. M. Cady for the airborne scanners; and L. A. Turner for Part II on radomes.

The techniques of preparing the volume were in the hands of Louise P. Butler, Betty S. Karasik, Martha T. Romanak and Joyce H. Randall. The multiple authorship and the changes of editorial staff that occurred while the volume was being prepared are doubtless reflected in some lack of homogeneity. We hope that this will not interfere with the usefulness of the book.

The nature of the development work at Radiation Laboratory has been so highly cooperative that very often the originators of an idea are unknown and credit cannot be given. It is the labor of these anonymous workers that we most wish to acknowledge, for they are the ultimate authors. Throughout the writing and editing of the volume we have benefited from the friendly criticisms of many of our colleagues in this Laboratory.

The publishers have agreed that ten years after the date on which each volume in this series is issued, the copyright thereon shall be relinquished, and the work shall become part of the public domain.

THE AUTHORS.

April, 1948.

Contents

PART II. RADOMES

PART I

RADAR SCANNERS

CHAPTER 1

USES OF RADAR SCANNERS

By M. B. Karelitz

INTRODUCTION

A scanner or antenna mount is an essential part of every radar set. Its function is to support the antenna and to direct the radiation in space in a manner dictated by the operational use of the set. The scanner also receives the reflected energy from targets or terrain under surveillance and provides means for presenting information regarding the bearing angle, range, and sometimes height of the target.

There is a wide variety of radars for land, ship, and airborne installations. No other part of the set varies so much in its design as the mount, and it is the mount that may to a great extent impose limitations on the performance and various uses of the set. Although the size and weight of the antenna mount are important factors in any set, it is evident that they are not so critical for ground and ship installations as they are for those in an airplane.

THE SCANNER IN USE

1·1. Surface-based Antenna Mounts.—The primary function of surface-based search radar is to provide early warning of approaching aircraft. Maximum coverage of scanned space, good resolution, and long range of detection are essential to its proper performance. As will be seen later, high power and large antennas are required to accomplish these results. Early-warning mounts are therefore large and are usually permanently installed on high ground or towers in order to clear surrounding obstructions. When the mounts are used in warfare for early warning and voice control of friendly airplanes in forward areas, provisions for rapid dismantling and reassembly are essential. This feature of the mount becomes of still greater importance in portable early-warning and height-finding ground radars of limited range suitable for use near combat areas. Some mounts are installed on heavy trailers for greater mobility.

Height-finding is essential for control of air traffic. In some antenna mounts the search and height-finding features are combined; this necessarily makes them more complicated to construct. Other height-finding radars have been built to supply the existing early-warning stations with

height information. The essential feature of mounts for height-finding radars of this type is their capability of being trained rapidly on a target located by the search radar to establish the elevation angle of the target.

A ship-based radar performs all the functions required of a ground radar and, in addition, is called upon as an important aid to navigation. The so-called "surface-search" radar is the most common type found on a ship. The necessity of placing the ship antenna mounts at mast height imposes a very definite limitation on their size and weight, since the stability of a ship is affected by topside weight and by increased wind forces that impose increased overturning moments. Except for a few portable emergency sets, most antenna mounts of ship radars are fixed installations continuously exposed to the elements and required to perform their function without interruption 24 hr a day.

1·2. Airborne Scanners.—Airborne scanners are also fixed installations, commonly mounted in the nose or tail of an aircraft, in faired-in enclosures below the fuselage, or on the wing. These enclosures, or radomes, are built from materials transparent to microwave radiation. The operation of airborne scanners is not nearly so continuous as that of surface radars, but airborne scanners are subject to more severe vibration and shock and to rapid and extreme variations of pressure and temperature.

There are many types of airborne scanner for microwave radars suitable for navigation, bombing, night-fighting, gunlaying, and early warning. Of these, the scanners for navigation and bombing are the most widely used. In these scanners a beam in the shape of a vertical fan sweeps continuously around and illuminates in turn the ground objects that lie at various azimuth angles. The advantage of this beam over a "pencil" beam is that it allows search of the foreground as well as of the more remote parts of the terrain. In the most recent navigation radars the antenna is stabilized so that its scanning is not affected by maneuvers of the aircraft.

1·3. Nonradar Scanners.—Scanners are also employed for various nonradar applications on ground, ship, and airborne installations. They are an essential part of countermeasure equipment such as locators of enemy radar and communication stations and of jamming equipment that neutralizes the effectiveness of enemy radars. Although IFF (identification of friend or foe) equipment can have an independent mount, it is at times combined with the radar antenna mount.

From the preceding superficial enumeration, it is evident that it will not be possible in this book to cover the design of every conceivable scanner or mount that might be required for a specific application. The scope of the book is therefore limited to microwave radars only, the main characteristic of which is a sharp beam permitting good resolution and

good bearing accuracy. To attain the desired results and obtain the desired accuracy of the data presentation, precision is required in the design and manufacture of both antennas and mounts.

ELEMENTS COMMON TO ALL SCANNERS

Regardless of their particular form and function, most radar scanners or mounts have certain components in common. These components, varied in their design, are the antenna, r-f transmission lines and their power-driven supports, and the means for transmission of data.

1·4. Antenna.—The microwave energy from the r-f oscillator travels along a transmission line to the antenna. Typically, the antenna consists of two parts: the antenna feed or termination of the transmission line and the parabolic reflector. The effect of a parabolic antenna is similar to that of a searchlight in that it sends out energy in a beam. The feed takes the place of the lamp, and the antenna reflector that of the parabolic searchlight mirror.

In certain antennas the feed may consist of an array of radiating elements. The reflector may be of a shape other than parabolic, or it may be entirely absent.

Two forms of parabolic reflectors are used: cylindrical parabolas associated with a linear feed and paraboloids of revolution which may or may not be trimmed to a special contour. A reflector of the latter type requires a feed that is a point source placed at its focal point. The width and shape of the resultant beam of energy depends on the wavelength of the radiation and the size and shape of the paraboloid. A complete paraboloid transmits a concentrated symmetrical pencil beam, whereas a cut or distorted paraboloid transmits a fan beam wider in one direction than in the other. The source of energy may be in the form of one or several dipoles, a pillbox, a slotted diaphragm (Cutler feed), or a horn terminating the transmission line.[1]

1·5. Transmission Line.—The r-f transmission line used in 10-cm-band radar scanners or mounts may be a rigid coaxial line or a waveguide. Waveguide, a thin-walled rectangular or round tubing, has the inherent advantages of simplicity, rigidity, and ability to conduct a larger amount of energy without internal arcing. For 3-cm or higher frequency radiation, rectangular waveguide is used almost exclusively, since the outside dimensions of the guides are small. It is desirable to avoid the use of long lines because (1) the attenuation per meter is appreciable, (2) the "long-line effect"[2] may cause instability of the magnetron transmitter,

[1] Antennas are fully discussed in Vol. 12 of this series, *Microwave Antenna Theory and Design.*

[2] See Glossary.

(3) the installation and cleaning of a long line is troublesome, and (4) in airborne scanners weight is at a premium.

Table 1·1 presents some data on transmission lines. The values of attenuation in this table are calculated for copper transmission line; with brass and aluminum the loss is about doubled. The calculations agree fairly well with experimental results. The maximum length tabulated is that which may potentially cause the long-line effect in a typical application. In a coaxial line, the inner conductor is usually supported by metal side arms soldered to projections on the outer conductor (stub supports).

TABLE 1·1.—SOME PROPERTIES OF TRANSMISSION LINES

Wavelength band, cm	Size of line, in.	Mode	Attenuation, db/m	Recommended maximum length, m
1	Guide 0.5 × 0.25 0.040 wall	TE_{10}	0.35	2
3	Guide 1.0 × 0.5 0.050 wall	TE_{10}	0.12	5
3	Guide 1.25 × 0.625 0.064 wall	TE_{10}	0.072	5
3	Guide $1\frac{3}{16}$ ID, round	TM_{01}		
8–10	Guide 3 × 1.5 0.080 wall	TE_{10}	0.020	5
10	Guide 3 ID, round	TE_{11}	0.014	5
10	Coaxial 0.875 OD 0.032 wall 0.375 diam inner conductor	TEM	0.075	8
10	Coaxial $1\frac{5}{8}$ OD 0.049 wall 0.625 diam inner conductor	TEM	0.04	7
8	Coaxial $1\frac{1}{4}$ OD 0.049 wall 0.500 diam inner conductor	TEM	0.05	6

Special rotary joints in the line are required to enable it to pass through the moving axes of the scanner or to rotate the feed. Transition sections are necessary to join the cylindrical sections of the rotary joints to the rectangular waveguide.

It should be noted that the dimensions of rotary joints and the length of round waveguide or coaxial line at the rotary joints are critical and must be properly chosen so that standing waves are not set up in the line by complete or partial reflection of energy. When standing waves are present, there is a variation of the amplitudes of the voltage and current along the line with alternating maxima and minima. In a properly designed transmission line, the ratio of the maximum to minimum voltage

(standing-wave ratio) should not greatly exceed 1.2. Each rotary joint in the r-f line causes a small energy loss varying from 0.1 to 0.3 db.

Where separable sections of waveguide are bolted together, special choke couplings are required to prevent arcing and leakage of energy into space at the joints. The efficiency of the transmission line decreases with its length and with the number of rotary joints employed. It is therefore advantageous to place the transmitter so that it will move with the antenna, thus shorten the line, and eliminate one to three rotary joints. This may be feasible on some ground and shipborne radar sets but is difficult to accomplish on airborne scanners.

The presence of moisture inside the transmission line increases its attenuation and tendency to arc over. To prevent condensation that may be caused in the line by rapid temperature variations and, especially in airborne equipment, to prevent arc-over because of the reduction of the atmospheric pressure at high altitudes, the transmission line[1] can be pressurized by keeping it filled with dried air at a pressure slightly above atmospheric.

1·6. Scans.—Depending on their operational use or function, different radar sets may require different space coverage. The cyclic geometric pattern described by the beam emerging from the antenna as it covers the surrounding space is known as the "scan"; from this comes the word "scanner."

Most surface-based sets for surface or air search radiate a beam narrow in the horizontal plane and fanned out in the vertical plane. The same is true for airborne surface-search radar. The 360° circular or horizon scan obtained by continuous rotation of the antenna about its vertical axis will thus cover solidly a portion of space surrounding the antenna. When, instead of rotating continuously, the antenna oscillates about its vertical axis through a small angle of an arc, sector scan is obtained. The usual rate of circular or sector scan for ground- or ship-search sets is 4 to 6 rpm. The rate of rotation of airborne scanners may be as high as 30 rpm.

Another simple scan widely employed in gunlaying or fire-control radars is the conical scan which may be obtained by rapid rotation of a feed whose axis is slightly offset from the axis of rotation. The path described by the conically scanning beam is a circle of about a beamwidth in diameter.

The *simple* scans are those in which the beam sweeps repeatedly with but one degree of freedom. Radars employing simple scan are used in establishing the range of the target and only one of its angular coordinates, usually bearing. When an additional coordinate, such as elevation angle

[1] For further information on transmission lines the reader is referred to *Waveguide Handbook*, Vol. 10 of this series.

or height of the target, is required for obtaining the exact location of the target in space, the motion of the transmitted beam must have two degrees of freedom; a *complex* scan results. Complex scan is also required when greater and more rapid space coverage is necessary than can be obtained by means of a simple scan. Thus, conical scan is often combined with horizon or sector scan. The resulting motion of the beam, known as "Palmer scan," is used in radar to facilitate its locking in on a target encountered during search.

By slowly elevating and lowering the antenna between limits while it rotates more rapidly about its vertical axis, a helical scan is obtained. Any desired zone of the surrounding sphere may thus be covered by a pencil beam.

Spiral scan is another complex motion of the beam used. This motion is a rapid conical scan in which the diameter of the circle described by the beam is continuously varied from 0° to a maximum of possibly 60° and back to 0°.

Although these briefly described scans are most commonly employed, other complex scans may be devised to satisfy the requirements of scanning coverage and data presentation called for in the functional design of the set.

1·7. Kinematics of the Scanner.—Electromechanical means must be provided to support and impart scanning motion to the antenna and to transmit the position of encountered targets to the indicating instruments. This is the function of the pedestal, or mount. The complete assembly of the pedestal and antenna is known as the antenna mount for ground-based and shipborne radars or as the scanner for airborne radars. A simple search radar requires a pedestal consisting of a single vertical spindle (azimuth axis) capable of rotating in its bearings. Pedestals for surface-based radars with a complex scan must have an additional elevation axis, supported by and rotating with the azimuth axis, to permit angular displacement of the antenna in elevation.

Additional servo-driven axes of rotation may be provided in stabilized mounts to maintain the azimuth axis of the antenna in a horizontal plane even when the ship or airplane is rolling and pitching.

Provision must be made in the mount for carrying electric power to all motors, data take-offs, electronic equipment, limit switches, interlocks, heaters, etc., that may be located on the rotating parts. Slip rings and contacting brushes are most commonly used for this purpose. More than one hundred slip rings are required on some antenna mounts. Flexible cables, attached at one end to the stationary part and at the other to the moving part of the pedestal, may be employed when rotation of the azimuth axis involves only a part of a revolution or, at most, one or two revolutions in one direction of rotation.

1·8. Data Transmission.—The angular position of the antenna in space must be accurately known at all times if the coordinates of the target or of prominent features of the surveyed terrain are to be indicated. This is accomplished by introducing into the antenna mount a data-transmission system coordinating the movement of the antenna beam with the motion of the sweep on the cathode-ray tube screen of the indicators or by indicating the antenna position on remote dials. The data indicating the direction and elevation of the antenna on its mount or the angular position of the rotating feed are most often transmitted as variable voltages. Potentiometers or sine-wave generators are occasionally used, but self-synchronous units, generally known as "synchros" (or by their trade names of Selsyns, Autosyns, etc.), are more commonly used for data transmission. The simplest form of the synchro system consists of a generator, or transmitter, geared to the rotating axis of the mount and electrically connected with a motor, or receiver, driving a remotely located dial or coil of the indicator. Whatever the rotation of a synchro generator may be, it is duplicated by that of the synchro motor, which assumes an angular position very nearly the same as that of the generator. If accuracy better than 0.5° is desired, the generator should be driven from the input shaft by step-up gearing, and the motor should drive the output shaft through step-down gearing of the same ratio. The synchro error is thus reduced in proportion to the gear ratio used. Cam switches must be added on the mount, however, and also on the indicator to prevent locking in of the motor when it is out of step with the generator during the starting of the pedestal. This limits the possible speed-up of the synchro drive with respect to the rotating axis to about 12 to 1. Ten-speed indicators have been commonly used.

If it is desired to have the angular position of an output shaft equal to the sum or difference of the angular positions of two input shafts, *differential* synchros are used.

When high accuracy is desired, two pairs of synchros are used in the data-transmission system of a servo-driven antenna mount. One pair, geared to a higher speed, often 36-speed, is used for fine indication of error; another pair, geared 1 to 1, or at 1-speed, is used for coarse indication of error. This pair of synchros prevents the output and input shafts from locking in out of step during interruption and restoration of power.

These simple synchro systems transmit angular motion without torque amplification and are subject to error if the output shaft is overloaded. To avoid this, servomechanisms (motor control systems with amplification) are used. In such a system the load is driven by a reversible variable-speed electric or hydraulic motor. The speed and direction of rotation of the motor are controlled by the magnitude and sign of the

error or by the difference of angular position of a synchro generator and a synchro control transformer, geared respectively to the output and input shafts. The synchro control transformer indicates this error as a voltage that, when amplified, drives the power motor in the direction that will reduce the angular displacement between the input and output shafts to zero. Servomechanisms are often employed to drive radar antenna mounts and thereby enable the operator to exercise remote control over the direction of the antenna. They are also employed for stabilizing ship- and airborne antennas in space and may be controlled by gyroscopic instruments.

ANTENNA-MOUNT FUNCTION AND DESIGN

1·9. Fundamental Equations.[1]—In the design of a radar system the most important aim is to obtain both the desired maximum range on the target and resolution high enough for separating closely spaced targets. These properties depend on the detection of a weak signal returned from a distant reflecting object. Transmission and reception are influenced by the amount of energy radiated to and reflected from a target, the effective size of the target, the minimum power to which the receiver will respond, and the antenna gain.

If the total amount of power that a transmitting antenna could radiate isotropically or uniformly in all directions is denoted by P_t, the power flow through unit area at a distance R from the antenna would be $P_t/4\pi R^2$. In microwave radars, however, the antennas are directional and radiate energy in a concentrated sharp beam. The ratio of the power flow observed at a distance R in any direction from such a directive antenna to the power that would be produced by an isotropic antenna radiating the same amount of power is known as the "antenna gain," G. The maximum gain of a parabolic antenna reflector is given by

$$G_0 = \frac{4\pi AF}{\lambda^2}, \tag{1}$$

where A = area of the parabolic antenna reflector aperture,
λ = wavelength,
F = dimensionless factor.

If the excitation is uniform in phase and intensity over the entire reflector aperture, F is equal to 1. In actual antennas, the value of F is between 0.5 and 0.7.

A complementary property of an antenna is its effective receiving cross section A_r, related to gain as follows:

$$A_r = \frac{G\lambda^2}{4\pi}. \tag{2}$$

[1] E. M. Purcell, *Radar System Engineering*, Vol. 1, Chap. 2.

When A_r is multiplied by the power density of an incident plane wave, the total signal power available at the receiving antenna is obtained. If σ denotes the effective scattering cross section of the target at a distance R from the radar antenna, then the strength of the signal power received from it is given by

$$S = \left(\frac{P_t G}{4\pi R^2}\right)\left(\frac{\sigma}{4\pi R^2}\right)\left(\frac{G\lambda^2}{4\pi}\right) = \frac{P_t G^2 \lambda^2 \sigma}{(4\pi)^3 R^4}. \tag{3}$$

The quantity in the first parentheses is the power density of energy reaching the target from the transmitter. The product of this value and the quantity in the second parentheses is the power density in the returning radiation at the radar antenna. The quantity in the last parentheses is the receiving cross section of the antenna reflector.

By substituting in Eq. (3) the value of the maximum gain G_0, from Eq. (1), and solving for R, the maximum range of a radar set, the equation known as the "radar equation" is obtained:

$$R_{max} = \sqrt[4]{\frac{P_t A^2 \sigma F^2}{4\pi S_{min} \lambda^2}}, \tag{4}$$

where R_{max} = the maximum range,
P_t = power transmitted.
A = area of the parabolic antenna reflector aperture,
σ = effective scattering cross section of the target,
F = dimensionless factor ($0.5 < F < 1$),
S_{min} = minimum power to which the receiver will respond,
λ = wavelength of radiation energy.

From this formula it is seen that the range depends directly on the amount of power radiated, the size of the reflector, and the effective size of the target and inversely on the sensitivity of the receiver and the wavelength used.

The resolution of the radar set depends upon the beamwidth emitted by the antenna. The beamwidth produced by a parabolic reflector may be expressed by an approximation derived from the laws of wave optics:

$$\Theta \text{ (radians)} \approx \frac{1.2\lambda}{D}; \qquad \Theta \text{ (degrees)} \approx 70\,\frac{\lambda}{D}; \tag{5}$$

where Θ = width of beam between directions for half power in a plane passing through the projected diameter,
λ = wavelength,
D = projected diameter of the paraboloid antenna reflector.

In other words, the beamwidth produced by an antenna varies directly with the wavelength and inversely with the linear dimensions of the reflector.

1·10. Examples of Design.—When a certain wavelength is chosen for the operation of the radar set and the electronic components such as the transmitter and receiver are decided upon, the size and shape of the paraboloid antenna reflector must be chosen to meet the range and beamwidth specifications as closely as possible. The size and weight of the antenna mount are largely influenced by the size of the reflectors, the size of the r-f transmission line used, the kinematical complexity of the required scan, and the operational use of the set.

Comparison of an experimental lightweight 1-cm shipborne set that has high resolution and is intended for navigation, and a surface-search set with a small 3-cm portable height-finder set, AN/TPS-10 ("Little Abner"), will serve as illustration.

The pulse-power output of the transmitter of the 1-cm set is 40 kw. For good resolution on surface targets and shore line, a beam that is sharp in the horizontal section is required. Since the mount is not stabilized, it must have a fan beam that is wide in the vertical section in order to avoid a loss of targets because of the rolling and pitching of the ship. A beamwidth 0.7° in azimuth and 10° in elevation is obtained with an antenna consisting of a horn feed and a paraboloidal reflector $7\frac{1}{4}$ in. high by 58 in. wide. The small-size reflector permits the use of a solid surface without incurring high wind resistance. It is mounted on a simple single-axis pedestal that permits horizon scan at 6 or 0.6 rpm. Although the antenna mount is long-lived, compact, and able to withstand the action of the elements, it weighs only 75 lb.

On the other hand, AN/TPS-10, being primarily a height-finder with an antenna oscillating through an angle of 25° at a rate of 60 cpm, requires a beam narrow in the vertical plane for accurate determination of the angular position of the target in elevation. A beam fairly wide in the horizontal plane is needed to facilitate training the antenna on a target previously discovered by an associated search set. In order to detect aircraft at a range sufficiently great for ground control of interception, GCI, and to track the aircraft with comparatively little interference from rain clouds, 3-cm radiation is used. A horn-fed reflector 10 ft high by 3 ft wide is required to obtain a beam 0.7° wide in elevation and 2° wide in azimuth.

Because the r-f pulse power of the AN/TPS-10 transmitter is only 60 kw, transmission-line losses must be kept to a minimum. The r-f transmitter and modulator are therefore placed on the rotating part of the mount so that the waveguide line is short, with only a single rotary joint at the elevation axis of the mount. Since the transmitter and modulator rotate together, there is no need for a rotary joint in the pulse cable between the modulator and the transmitter.

An open antenna reflector with a tubular grid surface is used to cut

down the effect of wind forces; it is rigid enough to withstand, without distortions, the dynamic forces imposed on it by the oscillatory motion. Although still in the lightweight class (portable when dismantled), the AN/TPS-10 antenna mount with its electrical components weighs 1200 lb. Other details of this mount are given in Sec. 3.6, and a description of the 1-cm mount is found in Sec. 5·9.

1·11. Mounts with Two Antennas.—By placing two antennas on the same mount it is possible, in certain cases, to obtain from a single radar set information that could otherwise be obtained only with less efficiency from two separate radar sets.

Separate transmitters and receivers for each antenna may or may not be required, depending on the operational function of the set. Thus, surface search and zenith coverage may be obtained through a single mount with its transmitter and receiver components by the addition of an r-f switch in the transmission line on the mount, alternately feeding the two separate antennas. Two separate radar sets, the SG for surface search and SO-11 for zenith search, were previously required to obtain the complete coverage needed on aircraft carriers or other ships.

When a single antenna is used for both search and height-finding, the all-important search function is lost whenever the set is used to track a target in order to establish its height. By installing two antennas with two independent r-f systems on a single mount, there is obtained a combination early-warning, search, and height-finding radar set with greater traffic-handling capacity than would otherwise be possible. Naturally, the advantage of a mount with two antennas is obtained at a cost of greater complexity. Greater efficiency of operation is gained, however, with an over-all reduction in the amount of total equipment required. This should be especially important for ships that have only a limited amount of space available for radar equipment.

1·12. Stabilization.—Stabilization of ship- or airborne antennas is required for automatically maintaining the position of the radar beam in space despite the roll and pitch of the craft, caused by execution of maneuvers, heavy sea, or rough air. Stabilization is essential to obtain sufficient accuracy of target indication and to increase the efficiency of the system. It is a "must" for shipborne height-finding radar, since an error of 1° in indication of the target elevation angle causes an error in height indication of over 3000 ft at a range of 30 miles. Stabilization, however, greatly contributes to the complexity of antenna mounts and scanners.

The weight and cost of the shipborne radar antenna mounts for surface search are considerably increased by the addition of servo-driven axes required to achieve stabilization of the radar beam. This results in a paradox: Small ships require stabilization most, since they are sub-

ject to large angles of roll and pitch in a heavy sea, but small craft can least afford the increase in weight of the radar installation. The majority of stabilized radar installations are on large ships on which the effect of heavy sea is far less violent than on a small craft.

1·13. Structural Design.—Rigidity of radar antennas and mounts is of paramount importance. This is strongly apparent in the design of antenna mounts, since the deflection of component parts under dynamic loading must be kept within required limits. The parts used may have to be heavier than necessary for strength alone. Recourse is often taken to the utilization of structural sections, such as tubing, box sections, etc., with an inherently high ratio of moment of inertia to weight. Light metals such as aluminum and magnesium are often used to advantage where their low modulus of elasticity is no detriment in order to effect a reduction in weight of the antenna mount. The welding of light metal castings and structural shapes is, however, more difficult. Also, care must be taken to minimize the effect of difference of temperature expansion in the assembly of parts made of dissimilar metals.

Most radar antenna mounts have to perform under adverse climatic and weather conditions. Special precautions must therefore be taken during the design of antenna mounts to select corrosion-resistant materials and finishes. Proper lubricants able to withstand large temperature variations without separation or excessive change in viscosity must be used in order to attain satisfactory trouble-free performance of the mechanisms.

Past experience has shown that the success of a radar system depends largely on the proper performance of the scanner or antenna mount. It cannot be too strongly emphasized that careful analysis is required of all the features that the scanner or mount must possess for the proper performance of a particular set. Competent engineers and mechanical designers must then coordinate to the best advantage requirements that may be conflicting, having always in view the best performance obtainable from the radar set as a whole.

CHAPTER 2

GROUND AND SHIP ANTENNAS

By D. D. Jacobus, R. J. Grenzeback, H. A. Straus, M. B. Karelitz and V. G. Bruce[1]

PROPERTIES OF REFLECTORS

Electromagnetic energy is usually radiated into space by terminating or tapping into a transmission line with a suitable dipole feed or by terminating a conducting waveguide with a horn feed. The emergent energy is then focused in the form of a concentrated beam by the use of a reflector or a special lens. In the terminology used in this series the word *feed* includes not only the radiating dipole or horn but also the immediately adjacent portion of the transmission line. The antenna is properly described as the combination of a feed with a focusing device. The only focusing devices that will be described in this chapter are reflectors. The reflectors used on ground and ship installations are distinguishable from those used on airborne equipment because they are usually larger in size and generally are not shielded from wind forces by a radome as are airborne antennas. A discussion of considerations applicable to all microwave reflecting surfaces will be attempted before describing the particular reflectors that have found wide usefulness.

2·1. Reflection of Microwave Radiation.—All metals or continuous metalized surfaces are suitable as microwave reflectors. Aluminum and steel are the metals most usually employed because of their structural properties. A smooth continuous metallic surface is an ideal reflector, but grids and screens are widely employed to reduce the weight and wind resistance of the antenna.

A solid reflector should be smooth but is still effective when there are local inequalities in the surface as large as 3 per cent of the wavelength of the radiation. If there are variations, they should not occur in the form of a regular pattern so as to act as a ruled grating and produce side lobes.

Gratings or screens will allow a small portion of the incident radiation to pass through the reflecting surface. They are therefore unsuitable for use on parabolic cylinders employing linear arrays as feeds, because the small fraction of radiation that leaks through the reflector will produce a

[1] The greater part of this chapter is by D. D. Jacobus. Sections written by other authors are as follows: Sec. 2·5, R. J. Grenzeback; Sec. 2·16, H. A. Straus; Secs. 2·17 and 2·18, M. B. Karelitz; Sec. 2·19, V. G. Bruce.

sharp back lobe of the same pattern as the one that would exist in the absence of the reflector. They can be used on any of a wide variety of paraboloidal reflectors, however, because the radiation escaping through the grill is not focused in a sharp beam. Even here, leakage of radiation in excess of 5 per cent is considered undesirable.

2·2. Structural Rigidity.—The primary mechanical requirement affecting antenna design, particularly with large reflectors, is structural rigidity. Certain types of airfoil construction may possess remarkable combinations of lightness and strength, but their elasticity renders them unsuitable for microwave antennas. At a given wavelength, the width of a beam of radiated energy is inversely proportional to the projected diameter of the reflecting surface. With the use of a large reflector it is possible to secure a narrow and concentrated beam of energy, i.e., an antenna pattern of high gain. For example, with a true paraboloidal reflector (*dish*) trimmed to a rectangular contour 25 ft wide and 10 ft high and illuminated with 10-cm radiation, the beam of radiation will be elliptical in a section about 0.8° wide and 2° high. If the reflector is deflected from its true form by so much as 1 in., the width of the beam will be increased to about 1.6°, thereby halving the antenna gain. It is obvious, therefore, that distortions which are due to the weight and the manner of mounting a reflector and to wind forces must be eliminated. Since the absolute accuracy of a reflecting surface is a primary factor affecting antenna design, a brief study of this problem will be attempted in the following analysis.

2·3. Allowable Manufacturing Tolerances.—A paraboloidal reflector having a surface of theoretically perfect accuracy will produce an emergent beam whose width is a function of the wavelength of the reflected energy and of the projected aperture of the dish according to the previously stated approximation

$$\Theta \approx 70 \frac{\lambda}{D},$$

where Θ is the beamwidth parallel to the projected aperture in degrees at the half-power level.

It is undesirable to specify that an antenna surface have greater accuracy than is necessary, because close tolerances will increase the weight of the antenna as well as the difficulty of manufacture. The calculation of the shape of the beam produced by a surface that deviates from a true paraboloid is complicated. In general, however, it can be said that if a beam is to be broadened no more than a certain percentage of its width, the permissible departure from the true shape can be no more than a corresponding absolute amount, regardless of the size of the reflector (assuming that reflectors for the same wavelength are being compared). Another way of stating this is as follows: If a large reflector

and a small one are both warped out of their true paraboloidal shapes by the same number of inches, the beam of the smaller one will be broadened by a greater number of degrees. The original beam of the smaller reflector was broader, however, and the percentage increase of beamwidth will be found to be the same for both reflectors.

The following considerations do not purport to be a proof of this proposition, but it is hoped that they will make it seem more plausible. Consider a paraboloidal reflector that has a horizontal axis and a horizontal projected diameter D to be rotated through an angle of $\delta\theta$ radians about a vertical line passing through the center of the dish. The principal effect will be a shift of the beam through an angle $2\ \delta\theta$ as with a plane mirror. There will be a broadening of the beam, but as a secondary effect that we shall ignore here. The edge of the reflector will have been moved a distance $X = (D/2)\ \delta\theta$. The width of the beam to the approximation given in the first paragraph of this section is $70\lambda/D$ degrees or $(70/57.3)\ (\lambda/D)$ radians. The ratio of the shift of the beam to its width is thus

$$\frac{\Delta\theta}{\theta} = 2\ \delta\theta \times \frac{57.3D}{70\lambda} = \frac{1.64D\ \delta\theta}{\lambda} = 3.28\ \frac{X}{\lambda}.$$

The ratio of angles is thus seen to be proportional to the linear shift of the edge of the reflector. Its size dropped out when the ratio was taken. A similar argument applies to the parts of the beam that must be added vectorially to get the resultant beam of a warped dish.

2·4. Weight.—The range of a particular system [*cf.* Eq. (1·4)] is obviously improved by the use of larger reflecting surfaces. On the other hand, rigid weight limitations are generally imposed on the same system. This is particularly true of ship antennas, the location of the antenna at the masthead requiring a light mount. It is also true of land-based portable equipment and especially of antennas that must be oscillated rapidly. For these reasons, antenna construction strives for the very minimum of weight that is consonant with the required structural strength, rigidity, and mechanical durability.

The thin-walled box girder and trusses built up of light-wall tubular members have been widely used in the fabrication of reflector supports. Aluminum is a common building material, although very large antennas can advantageously be constructed of light-wall steel tubing because of the high modulus of elasticity of steel as compared with aluminum. Thin-walled stainless steel tubing is an effective material because there is no danger of corrosion.

TYPES OF REFLECTING SURFACES

2·5. Solid Surfaces.—From purely electrical considerations, a solid, continuous, metallic surface makes the ideal reflector. There is also,

within limits, an economic advantage accruing from the structural simplification as compared with certain open-type surfaces. Solid surfaces may profitably be employed when wind loading is not a primary factor, as with a unit that is to operate within a radome or other shelter or when restrictions on weight and power consumption are not severe.

Most surfaces are fabricated from sheet metal, either steel or aluminum alloy. Paraboloids are formed by spinning or by pressing.

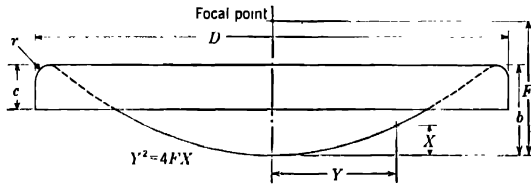

FIG. 2·1.—Dimensions for spun paraboloids.

Spinning is the preferred method when the quantity is small, because of the relatively inexpensive wooden forms used. Spun paraboloids, or dishes, have been made ranging from 4 in. to 10 ft in diameter. Figure 2·1 and Table 2·1 give data for spun aluminum reflectors often used for experimental purposes. The rim of the paraboloid is spun back to form a stiffening flange.

TABLE 2·1.—DIMENSIONS FOR SPUN ALUMINUM PARABOLOIDS

D, in.	b, in.	c, in.	r, in.	F, in.	Gauge No.	Blank diam, in.	Weight, lb
4	0.80	$\frac{3}{8}$	$\frac{1}{8}$	1.3	18	8	0.10
8	1.20	$\frac{7}{16}$	$\frac{1}{8}$	2.0	18	12	0.30
10	1.74	$\frac{7}{16}$	$\frac{1}{8}$	3.6	18	14	0.45
12	2.50	$\frac{9}{16}$	$\frac{1}{8}$	3.6	18	16	0.60
16	2.96	$\frac{5}{8}$	$\frac{1}{8}$	5.4	18	20	1.00
18	3.40	$\frac{3}{4}$	$\frac{1}{8}$	6.0	18	22	1.25
18	3.75	$\frac{3}{4}$	$\frac{1}{8}$	5.4	18	22	1.25
20	4.63	$\frac{3}{4}$	$\frac{1}{8}$	5.4	18	24	1.50
24	4.50	$\frac{3}{4}$	$\frac{1}{8}$	8.0	16	28	2.60
24	5.00	$\frac{3}{4}$	$\frac{1}{8}$	7.2	16	28	2.60
30	5.30	$\frac{3}{4}$	$\frac{1}{8}$	10.6	16	34	4.00
30	5.60	$\frac{3}{4}$	$\frac{1}{8}$	10.0	16	34	4.00
40	8.30	$\frac{7}{8}$	$\frac{1}{8}$	12.0	16	46	7.00
48	9.94	1.0	$\frac{1}{4}$	14.5	14	55	13.00
72	15.40	1.5	$\frac{3}{8}$	21 1	$\frac{3}{32}$	82	42.80
120	25.10	2.5	$\frac{1}{2}$	35.8	$\frac{1}{8}$	136	158.00

When the quantity is sufficient to justify more costly tooling, press-forming may be done. A notable example of press-forming is the SCR-584 reflector. This reflector (6 ft in diam, 15 in. deep, with a focal length

of 21.1 in.) was formed in a single drawing operation using a 16-gauge SAE 1015 mill-run cold-finish steel blank. After forming, a quadrant punch was used for perforating, and the reflector was then sized in the original forming dies to within $\pm\frac{1}{64}$ in. of the true paraboloidal surface. Generally speaking, closer tolerances can be maintained by press-forming than by spinning, although the latter method produces results adequate for most applications.

Cylindrical reflectors are readily built by fastening sheet metal to a series of ribs cut to the desired profile. This type of reflector is illustrated in Fig. 3·6 (see Sec. 3·3).

Special surfaces have been constructed by cementing metal foil to a plywood backing. Copper foil is most often used because it combines good workability with excellent electrical properties.

When it is desired to construct a special surface to be used for experimental pattern measurements only, accuracy can be achieved with metalized wood at small cost in time and money, and tolerances as close as $\pm\frac{1}{64}$ in. may be specified without hesitation. Two-inch soft pine planks are used to build up a laminated block which is hollowed on one side to give the desired surface, as shown in Fig. 2·2. Each plank is rough-cut to the approximate contour of its surface element before assembly of the block. The surface is finished to fit to templates. All paint, varnish, glue, etc., are thoroughly removed from the surface, and it is then sprayed with two coats of molten metal with a Mogul metalizer gun utilizing $\frac{1}{8}$-in. diameter wire. The conducting metal coating is applied in two layers. The first layer is pure zinc and very thin (estimated 0.003 in. thick). Because of its low melting point, the zinc does not char the wood and forms a good bonding surface for the second layer, which is pure aluminum. The aluminum layer is built up until it is approximately 0.006 to 0.010 in. thick. This completes the reflecting surface. No attempt is made to alter the granular nature of the natural sprayed finish by buffing or polishing.

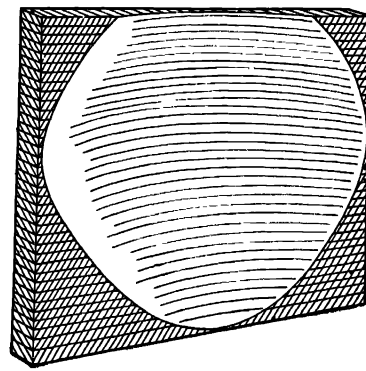

FIG. 2·2.—Experimental metalized wood reflector.

Solid reflectors up to a projected area of 24 by 48 in. have been sand-cast from aluminum alloy and give good service in the 10-cm band. These are generally used in the "as cast" condition except for a cursory going over with a disk sander to knock off minor imperfections. Even with good foundry techniques, however, there is a high percentage of

rejections, mainly because of warpage. Solid cast reflectors are rugged and do not require a radome, but their limitations have resulted in the more widespread use of the grid reflector that is described in Sec. 2·7.

2·6. Mesh Surfaces.—The large variety of open surfaces that are suitable for microwave reflectors can be subdivided into two general classifications: surfaces not critical to polarization and surfaces with parallel grating elements that are critical to polarization.[1] Mesh can broadly be defined as any screen, grillwork, or perforated sheet having continuous paths of electrical conductivity. These surfaces are not critical to polarization. The following examples are representative of the various meshes that have been employed.

A. Hardware Cloth.—Common galvanized-iron hardware cloth, 0.047-in. diameter wire on $\frac{1}{4}$-in. centers, has been widely used in the 10-cm band for large reflectors. Hardware cloth has considerable flexibility and can be manually pressed into place to take the form of the supporting framework. If the supporting framework is steel, the cloth can be attached by soft-soldering. If the supporting framework is wood, the cut edges of the cloth can be served with a thin strip of metal and then firmly nailed to the wooden supports.

B. Stainless Steel Wire Screen.—Stainless steel wire has been woven into a special screen[2] in which the wires are firmly spaced by crimping them into a rectangular pattern. This screen is difficult to form but makes excellent flat surfaces. The cut edges are generally attached to retaining strips, but the free areas have considerable structural rigidity. The screen can be woven in any desired pattern. In a marine application, 0.063-in. diameter wires on 1-in. centers were employed for 50-cm radiation.

C. Expanded Metal.—Expanded metal can be die-stamped to form paraboloidal surfaces. After the stamping operation has been completed, it is difficult to produce any further major alterations in the curvature of the surface. The supporting framework need not be contoured accurately other than at the points of support. Expanded metal can be held in place either by tack-welding or with suitable bolted connections. A flat diamond mesh, $\frac{1}{2}$ by 1 in. on the diagonals, formed from $\frac{1}{16}$ in. steel stock into connecting strips that are $\frac{7}{64}$ in. wide has been widely used on both naval and land-based antennas for 10-cm-band radiation.

D. Perforated Sheet Metal.—Metal reflectors fabricated by die-stamping may be perforated to reduce their weight and also to decrease the wind resistance of the antenna, as mentioned in Sec. 2·5. Such surfaces are suitable for mass production. The example recorded in Table 2·2 is

[1] W. D. Hayes, "Gratings and Screens as Microwave Reflectors," RL Report No. 268, April 1943.

[2] W. S. Tyler Co., Cleveland, Ohio.

made of steel 0.0363 in. thick, with $\frac{3}{8}$-in. diameter holes located in a staggered rectangular pattern on $\frac{1}{2}$-in. centers.

E. Knit Wire Mesh.—The intersection of three mutually perpendicular plane surfaces at a point to form the interior corner of a cube comprises an element of a device that is known as a "corner reflector." A cluster of these elements forms the complete corner reflector, which is capable of reflecting energy in the direction of a radar transmitting set irrespective of the angle of incidence of the incoming beam of energy. Corner reflectors as used in life-raft kits, are made by tightly stretching a knit wire mesh over a very light metal framework. A knit mesh is used because the interaction of the loops enables the material to be stretched taut more easily than a woven mesh. Particular effort must be made to ensure the proper method of binding the edges of the mesh with cloth tape to permit advantageous mounting.

A corner reflector is not a component of a radar antenna. The mesh that forms the surfaces, however, is very much lighter than any other materials that have been used as radar reflecting mediums, and it is interesting because of its unique properties. The most effective material employed to date consists of 0.0035-in. diameter round monel wire, knit into a mesh containing seven loops per inch.[1] Reflectivity is excellent with both 10- and 3-cm radiation when the mesh is new; but because the conductivity between loops is reduced by corrosion or oil films, the reflectivity may be lowered by as much as 50 per cent. This material is of interest as a reflecting medium, but it obviously does not constitute a rigid antenna surface.

TABLE 2·2.—MESH REFLECTING SURFACES

Mesh No.	Radiation wavelength, cm	Transmission of radiation, %	Open area, %	Service,* mph	Weight per ft², † lb
A	10	< 1	60	90	0.65
B	50	< 1	80	110	0.3
C	10	< 2	47	110	1.0
D	10	1.6	51	90	0.73
E	3	< 15	95	...	0.007

* Specified wind velocities that the reflectors can withstand without structural damage.
† Weight includes surface elements only.

2·7. Grating Surfaces.—A reflecting grating may be defined as any system of parallel electrical conductors spaced in such a manner that an effective microwave reflecting surface will be produced. A grating provides adequate reflection only to correctly polarized radiation, and its

[1] Manufactured by Metal Textile Corp., Orange, N.J.

elements must be parallel to the electrical vector of the incident radiation wave. For example, a vertically polarized wave demands that the grating elements be vertical if excessive transmission through the grating is to be avoided. A series of parallel wires can be a grating reflector. If the wires are replaced by similarly spaced slats of appreciable depth, the amount of radiation that leaks through will greatly decrease.[1] For this reason, a grating can be designed that has excellent reflecting properties and at the same time has very low resistance to winds normal to the surface.

Several experimental gratings have been molded in plastic and then metalized to secure the requisite conductivity. These plastic reflectors were readily damaged by rough handling. Some plastics were dimensionally unstable, and the metal plating tended to crack off others. They were therefore never employed in durable equipment and will not be included in the following tabulation.

Slats.—True paraboloidal surfaces are quite commonly formed by suitably spacing a series of identical flat parabolic strips. The intersection of a plane with a paraboloidal surface is a true parabola, provided the plane is parallel to the principal axis of the parabola. Furthermore, the shape of the parabolic intercept remains unaltered as the plane is displaced laterally away from the axis of revolution. This geometric property of the paraboloid of revolution makes it possible to build up an entire surface of revolution from a large number of identical pieces of flat stock. It is necessary that only one edge of each flat element have the identical parabolic form. This can be accomplished either by cutting a stacked pile of flat elements to a jig form or by a die-stamping operation.

Stainless steel reflectors are commonly made by die-stamping the similarly shaped grid elements. These thin elements are held in place with suitably notched strips, one strip being inserted from each side of the grating to surround the grid element. The notched strips are spot-welded together to complete the support. Notching is done in a special manner, a small, slightly outstanding tab being left at each slit. When forced against the grating elements, these tabs serve to stiffen each intersection. For added stiffness, small angle clips are used at the intersection of the midsection supports and at every sixth grid element. A reflector of this type is shown in Fig. 2·3.

When aluminum is used, it is common practice to fix the ends of the flat parabolic elements by welding or brazing them to the structural member that forms the periphery of the reflector. Midsection supports are commonly made by suitably notching a deep web. These midsection supporting points may be brazed or welded, but a more rapid and an entirely adequate technique is to crimp the metal of the deep web directly

[1] Hayes, *op. cit.*, Sec. 2·6.

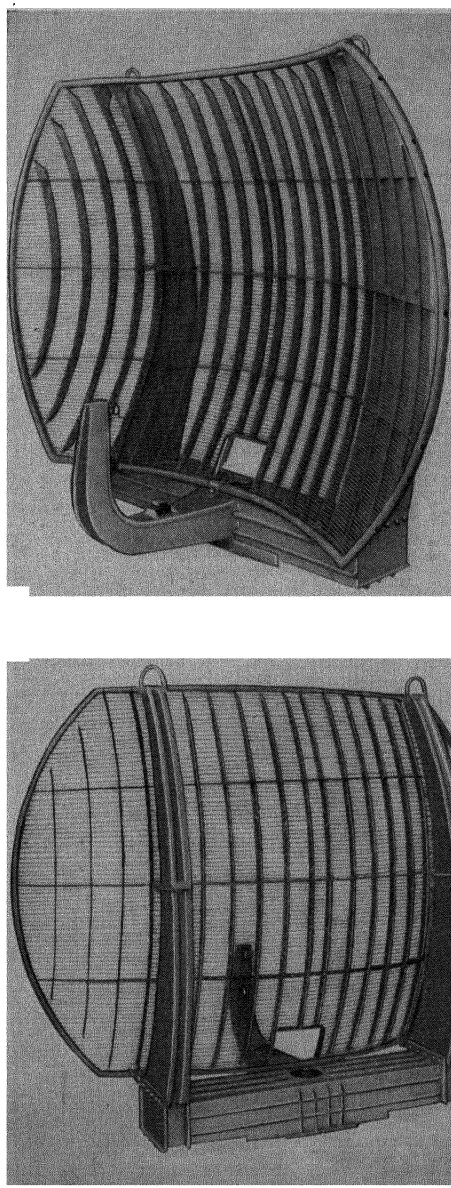

FIG. 2·3. SG-2S stainless steel reflector and support for feed. (*Courtesy of Raytheon Manufacturing Company.*)

adjacent to the insert. An effective crimping tool is a pair of pliers having a special nose designed to make indentations approximately $\frac{1}{8}$ in. long and $\frac{1}{64}$ in. deep.

The structural characteristics of some aluminum and stainless steel surfaces are given in the following examples; other properties of these surfaces are recorded in Table 2·3.

A. Aluminum slats $\frac{1}{16}$ in. thick and $\frac{7}{16}$ in. deep, spaced on $\frac{7}{16}$-in. centers; spot-welded at the periphery to $\frac{5}{8}$-in. OD aluminum tubing; midsection supports spaced approximately 10 in. apart.

B. Stainless steel slats 0.020 in. thick and 0.4 in. deep, spaced on 0.4-in. centers; ends bent and spot-welded to periphery frame; midsection supports spaced approximately 4 in. apart.

C. Aluminum slats $\frac{1}{16}$ in. thick and 1.5 in. deep, spaced on 1.5-in. centers; ends brazed to periphery frame; midsection supports spaced approximately 13 in. apart.

D. Stainless steel slats 0.030 in. thick and 1.5 in. deep, spaced on 1.5-in. centers; ends bent and spot-welded to periphery frame; midsection supports spaced approximately 6 in. apart.

Tubes.—Effective reflecting gratings can be fabricated of parallel bars of aluminum tubing. The tubing grill will have a slightly higher wind resistance than an electrically equivalent grill composed of slats. On the other hand, tubing generally weighs about 10 per cent less than slats of equal strength. The tubing can be bent into approximate form by the use of rollers. It is not essential that the tube have the exact shape finally required of the surface. Final shaping is secured by accurately fixing the points of support so that the tubing will assume the true form of the reflector after it is rigidly fastened in place. The ability to form a tubular member to a particular contour is of great value in fabricating asymmetric reflecting surfaces, in which each surface element may require a curvature slightly different from that of the adjacent surface elements.

Aluminum tubing has been fixed in place with clips that are bolted or riveted to the supporting structure. Such a method is tedious. A more effective method is achieved by punching the upstanding leg of a small aluminum angle with a series of properly spaced holes large enough to permit the tubing to be readily threaded into place. Final anchoring is secured by crimping the aluminum angle adjacent to the tube. A further virtue of this manner of anchoring tubing is that the holding angle can be easily shimmed. The shims are placed between the supporting structure and the contacting face of the holding angle. Shimming in this manner permits the correction of any irregularities that may exist in the surface of the supporting structure. The structural characteristics

of some surfaces with tubular elements are given in the following examples; other properties of these surfaces are recorded in Table 2·3.

E. 52S aluminum tubing, $\frac{1}{2}$-in. OD, 18 gauge (0.049 in. wall) on $1\frac{3}{8}$-in. centers.

F. 24ST aluminum tubing, $\frac{1}{4}$-in. OD, 20 gauge (0.035-in. wall) on $\frac{1}{2}$-in. centers.

TABLE 2·3.—GRILL REFLECTING SURFACES

Grill No.	Radiation wavelength, cm	Transmission of radiation,* %	Open area, %	Service,† mph	Weight per ft²,‡ lb
Slats:					
A	3	1.0	86	110	0.86
B	3	1.0	95	100	0.84
C	10	1.0	98	100	0.90
D	10	1.0	96	100	1.20
Tubes:					
E	11	3.0	64	110	0.71
F	3	1.5	50	90	0.76

* Hayes, *op. cit.*, Sec. 2·6.

† Specified wind velocities that the reflectors can withstand without structural damage.

‡ Weight includes surface elements only.

REFLECTOR FORMS AND TEMPLATES

Most reflectors take the form of a true paraboloid of revolution. However, reflectors with special curvatures have been devised to secure dispersal of radiation in the form of a "fan" beam. Astigmatic paraboloids are employed with certain electrically scanning feeds, of which the Robinson scanning feed and its reflector are an example. The parabolic cylinder is employed when the feed is not a point source but is a linear array. These geometric forms and the templates used in their fabrication are discussed in the following sections.

2·8. True Paraboloids.—A parabola having a focal length F is defined by the equation $X = Y^2/4F$. A true paraboloidal surface is generated by rotating the parabola about its principal axis. The focal point of this paraboloid of revolution lies on the principal axis, here the x-axis, at a distance F in front of the vertex.

The range required of a radar system is usually one of the first factors to be considered. It therefore follows that the first step in the design of an antenna is the selection of the size of reflector that the system will require. The size of the reflector is generally recorded in terms of its

projected diameter. With this dimension fixed, it then becomes necessary to select a commensurate focal length.

The r-f energy leaving a horn feed or other emitting source will be dispersed, especially if the horn is narrow, when the energy passes through the free space between the end of the feed and the surface of the reflector. The primary pattern of radiation from the feed can be controlled by proper design. Uniform illumination of the reflector is undesirable, since it causes serious side lobes in the secondary pattern radiated into space. If the illumination is too greatly tapered toward the edges of the reflector, the side lobes are reduced but the beam becomes wider. If the edges of the reflector receive an insignificant amount of energy, the size of the reflector can be reduced without lowering the gain of the system. With a reflector of fixed diameter and unspecified focal length it is apparent that the edges of the reflector will receive increasing amounts of illumination as the feed is moved farther away from the surface. The choice of the optimum focal length for a given combination of reflector and feed is a basic feature of antenna design and has been the subject of extended experimentation. Table 2·4 records the focal lengths and projected reflector diameters of certain widely used antennas.[1]

TABLE 2·4.—RATIO OF PROJECTED DIAMETER TO FOCAL LENGTH

Radiation wavelength band, cm	Size of reflector		Focal length F, in.	$\frac{D}{F}$
	Minor diam d, in.	Major diam D, in.		
10	96	96	27.5	3.6
10	60	168	60.0	2.8
3	36	120	35.5	3.4
10	120	384	99.0	3.9
10	120	300	78.0	3.8

In laying out a template for a particular reflector it is convenient first to compute the rectilinear coordinates of the parabola. These coordinates are readily transferred to suitable flat stock, which can then be accurately shaped to form the template. If the axis of the parabolic template is centered on the axis of the paraboloidal surface, the template should fit the surface at all points. In making these observations, it is highly desirable that the template be mounted on a fixed journal. A template that is merely laid against a surface in a variety of different positions may fail to disclose the over-all magnitude of the distortion. The position of the vertex is needed to determine the position of the feed relative to the reflector. It is therefore considered good practice to

[1] Vol. 12, *Microwave Antenna Theory and Design*.

indicate the vertex of the paraboloidal surface while the template is in place, because of the difficulty of accurately determining this point from measurements.

FIG. 2·4.—Reflector and template. (*Courtesy of Walsh* ***Construction Company.***) 1. Template rotary truck. 2. Top chord of template truss. 3. Track. 3a. Track support. 4. Walkway. 5. Template. 6. Center support. 7. Reflector.

Small and moderate sizes of templates are generally cut directly out of a piece of sheet metal; the template is then rigidly fastened to a shaft whose center of rotation lies on the axis of the paraboloidal surface. The

templates for certain very large reflectors were fabricated structures. The template was suspended downward inside a circular track and carried at its extremities by two trucks. To secure an accurate calibration of the surface, the circular track was carefully leveled and centered on the axis of the paraboloid reflector as shown in Fig. 2·4.

2·9. Special Surfaces. *Astigmatic Paraboloids.*—The astigmatic paraboloidal surface that is used in conjunction with trapezoidal feeds (*cf.* Sec. 2·15) is shown in Fig. 2·5. The trapezoidal feed *BCDE* consists of two parallel sheets of metal with the source of radiation at the point *S*. In Fig. 2·5, the trapezoid lies in the *XY*-plane. The vertex of the

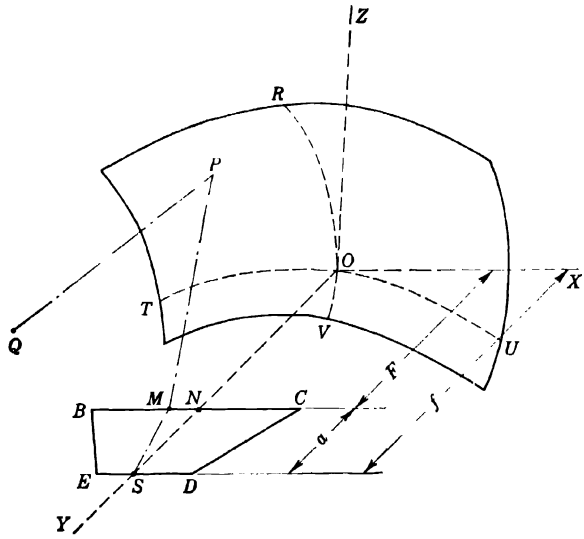

FIG. 2·5.—Astigmatic reflector with trapezoidal feed.

reflecting surface is at the point *O*. Radiation from the trapezoidal feed will be confined to the *XY*-plane until it passes from the feed into space at the line *BC*. The intercept of the *YZ*-plane with the reflecting surface is the curve *ROV*, a true parabola with focal point at *N*, having the equation $Y = Z^2/4F$. The intercept of the *XY*-plane with the reflecting surface is the curve *TOU*, a true parabola with its focal point at *S*, having the equation $Y = X^2/4f$. The point *Q* represents the intercept of a reflected ray with the plane that contains the point *S* and is parallel to the *XZ*-plane. Point *P* is a reflecting point on the surface. The reflected energy emanating from the point source at *S* will be in phase at all points on this plane if the summation of the distances *SM*, *MP*, and *PQ* remains constant, irrespective of the location of the point *M*. This condition is met if the total distance traversed by any ray $SMPQ = 2f$. Either one

of the following equations defines a surface that satisfies the condition $SMPQ = 2f$, in terms of the focal lengths f and F, where $a = f - F$.[1]

$$Z^2 = -2a(f - Y)^2 - X^2 + 2(f + F)Y - X^2 + 2af; \quad (1)$$
$$X^2 = -2a(F - Y)^2 + Z^2 + 2(f + F)Y - Z^2 + 2af. \quad (2)$$

For the fabrication of templates, it would be preferable to have an equation that expresses Y in terms of X and Z. Such an equation can be derived but is exceedingly cumbersome. The points T, R, V, and U can be determined by use of the simple equations $Y = Z^2/4F$ and $Y = X^2/4f$. The value of Y at intermediate points on the reflecting surface can then be assumed. The substitution of the assumed values of Y and X or Y and Z, in either Eq. (1) or (2), will yield accurate solutions for the third coordinate.

The template for the astigmatic paraboloid is necessarily a three-dimensional structure whose surface elements form a pattern that is the converse of the reflecting surface. The following example illustrates the manner in which such a template can be constructed. The parabolic curve TOU is inscribed on a piece of flat sheet metal, and the edge of the sheet cut and finished to the true form. In a series of planes that are parallel to the XY-plane but with each plane displaced an equal distance farther away from the origin O, when Z is small, the intercept will be a curve that closely approaches the form of the true parabola TOU. When Z is large, the intercept will differ considerably from the parabola TOU. However, the successive intercepts will differ from one another by gradual and uniform increments. Equation (2) can be used to calculate the X and Y coordinates of each of these series of curves, where Z is assigned a fixed value for each curve. Each of these curves can be inscribed on sheet metal, which is then cut and finished to form a flat element of the template.

A similar series of flat transverse elements can be fabricated, starting with the true parabola ROV. A grid can now be formed by interlocking the transverse elements with the longitudinal elements, which is accomplished by suitably slotting both sets of elements. The surface of the completed grid constitutes a lattice that defines the astigmatic paraboloid surface.

Parabolic Cylinder.—A linear array of suitably spaced and energized dipoles will radiate energy in the form of a fan beam. The linear array is commonly used with a parabolic cylinder as a reflector. The length of the array determines the sharpness of the beam, and the reflector serves to limit the broad dimension of the radiation pattern. The direction of the fan beam relative to the array is determined by the r-f wavelength inside the waveguide by which the dipoles are energized. It will be

[1] H. Krutter, *Microwave Antenna Theory and Design*, Vol. 12, Chap. 15.

perpendicular to the linear array if the probe of each dipole taps energy at the same point on each succeeding wavefront. The radiation pattern secured from a linear array with a cylindrical parabolic reflector is shown in Fig. 2·6. The fact that the surface has only one degree of curvature facilitates the fabrication of this type of reflector.

Other Surfaces.—Some special surfaces have been developed to produce a selective dispersal of the reflected energy. For example, the lower edge of a reflector may be curved more sharply than the true parabolic form in order to deflect energy upward into the form of an extended fan beam.

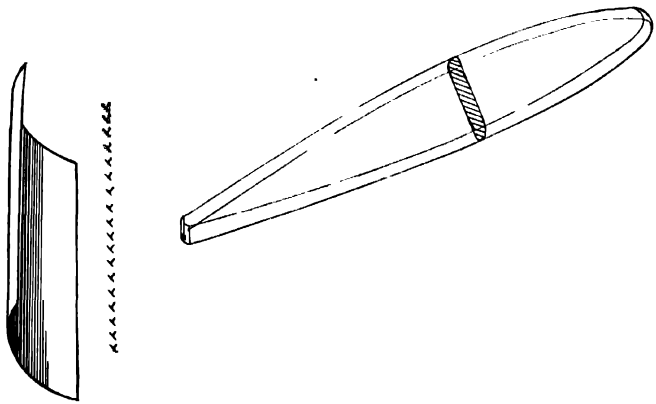

FIG. 2·6.—Linear array with cylindrical parabolic reflector.

Template construction for these surfaces presents problems similar to those discussed for the astigmatic paraboloid surface.

2·10. Shape of the Periphery.—The fan beam, narrow in its azimuth dimension and wide in vertical height, has come into almost universal use for purposes of radar search. Side lobes in the vertical plane are not so objectionable as ones in the horizontal plane. A true paraboloidal reflector with a horizontal aperture larger than the vertical aperture will produce a fan beam similar to that illustrated in Fig. 2·7. Auxiliary feeds, either horns or dipoles, may be located below the main feed to produce a wider dispersal of energy in the vertical plane. The oblong reflector will usually have a horizontal aperture that is 2.5 to 3.5 times as large as the vertical aperture. If a reflector of rectangular shape were employed, the extreme corners would receive a negligible fraction of the total radiation. It is therefore advantageous to cut the periphery to coincide with a contour of constant illumination of the edge of the reflector, which results in a form that closely approximates a projected ellipse.[1]

[1] *Cf.* S. J. Mason, "General Design Procedure for Pencil-Beam Paraboloid Antennas Having Horn Feeds," RL Report No. 690, Jan. 22, 1946.

Figures 2·7 and 2·8 illustrate two distinctly different forms of contouring. The areas of both reflectors are approximately equal, and they have identical focal lengths. In Fig. 2·8 the paraboloid is split on the major axis. The contour of the projected periphery is the half-section of an

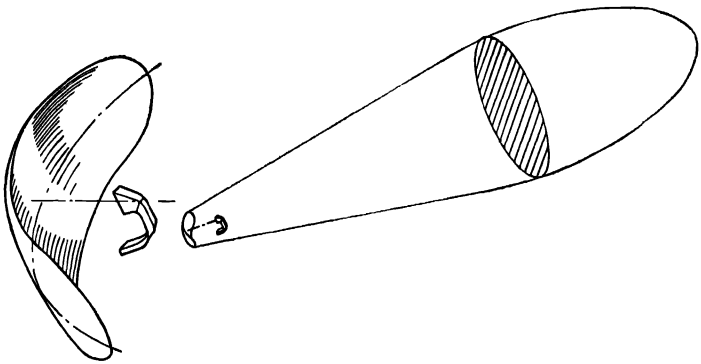

FIG. 2·7.—Radiation pattern from a paraboloidal reflector with an elliptical periphery.

ellipse. A ground plane G is required to prevent dispersal of energy past the bottom of the reflector. A narrow metallic strip S, having a parabolic contour similar to that of the reflector, is sometimes inserted to effect an upward dispersal of the radiation. With this type of reflector, a single horn feed can be used to produce a broad fan beam. A corollary advantage is that the feed and its supports do not obstruct the primary radiation pattern.

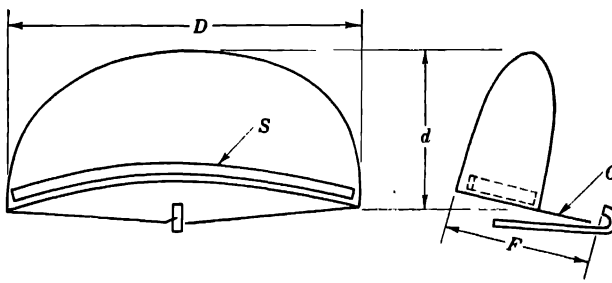

FIG. 2·8.—Paraboloidal reflector with a periphery that is a half-elliptical section. D, projected horizontal diameter; d, projected vertical diameter; F, focal length; G, ground plane; S, deflection strip.

Figure 2·9 also illustrates a paraboloidal reflector with full elliptical contour. This particular antenna design utilizes a multiple feed to secure a broad fan beam. With the triple horn feed indicated, the horn A delivers the major fraction of the total energy to produce a strong search lobe. The horns B and C deliver an amount of auxiliary energy sufficient to secure the necessary coverage in height.

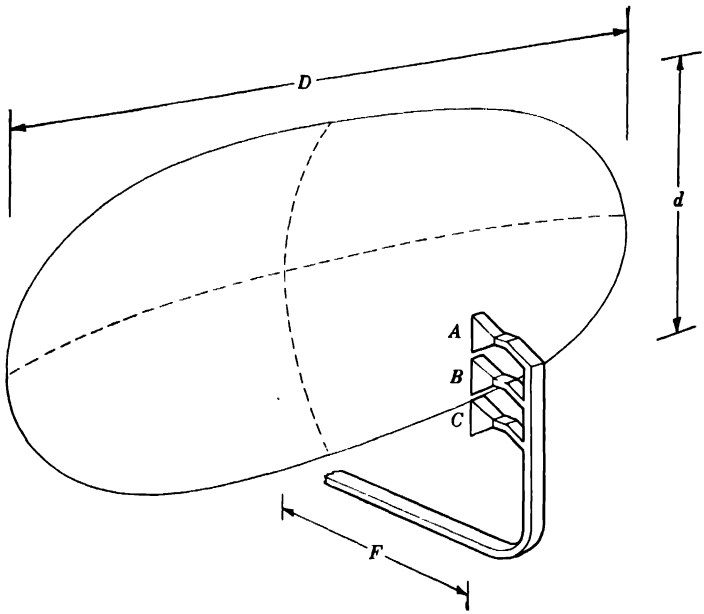

FIG. 2·9.—Paraboloid with an elliptical periphery and a multiple feed. *A*, horn feed for lower beam; *B*, horn feed for intermediate beam; *C*, horn feed for upper beam; *D*, projected horizontal diameter; *d*, projected vertical diameter; *F*, focal length.

2·11. Feed Supports.—To prevent defocusing and secondary pattern variation under conditions of vibration or shock loading, the antenna feed must be so supported that the radiating elements maintain a fixed relationship to the reflector. The type of support will vary with the nature of the feed and with the focal length of the reflector. Cantilever construction of the feed is desirable in any case and is essential if the feed is to rotate or nutate.

Feeds having long focal lengths require some type of bracing by struts or wires. The flexibility of a feed is determined by the transverse stiffness and the length of the unsupported conducting r-f line. In ordinary applications (standard brass waveguide with point-source dipole termination) any feed with a focal length over thirty to forty times the smaller outside dimension of the waveguide cross section requires external support. For single or multiple horn feeds, the possibility of torsional oscillations of the extension of the waveguide should not be overlooked.

Ideally, no structural supports should clutter the area in front of the reflector. This condition cannot always be realized, but the percentage of projected area of the reflector that is obstructed by bracing should be kept to the minimum consistent with requirements of

weight and rigidity. Obstruction of the primary pattern is especially to be avoided. Struts or wires supporting the feed should not be parallel to the plane of polarization.

The configuration of the bracing will be determined by the type of feed and its position with respect to the geometrical center of the reflector. Braces have been fabricated from impregnated Fiberglas tubing or other dielectric material in an attempt to minimize undesirable reflections. This expedient is normally unnecessary and should be applied with caution, since dielectric bracing may actually distort the pattern more seriously than metal bracing.

The design of supports for the feed should permit removal and replacement of the feed without impairing its alignment with respect to the reflector. It is desirable to have an arrangement that will permit removal of the feed without removal of its supports. Permissible variations in alignment between feed and reflector should be determined by actual measurement of the pattern. The design should be such that reflectors and feeds are interchangeable within the allowed tolerances.

WIND LOADS ON REFLECTORS

The land-based and particularly the shipborne antennas are designed for operation in winds of high velocity. The resultant wind forces exert a drag on the reflector at all times. With solid surfaces, this drag is a maximum when the wind impinges perpendicularly against the front of the parabolic reflector. Reflectors having open surfaces of mesh or grating give a total wind drag that is lower than for a similarly shaped solid surface. The maximum drag on such an open surface may not occur when the wind is directed squarely into the face of the reflector but rather when the reflector is turned about 50° away from the wind direction.

As the antenna rotates on the azimuth axis of the mount, torques of considerable and varying magnitude will be caused by wind loads. The magnitude of these torques not only is affected by the character of the reflector and its associated supports but is also critically influenced by the location of pivot around which the antenna is rotated. Wind drag and the torques exerted by wind forces on specific parabolic reflectors are discussed quantitatively in the following sections.

2·12. Wind Drag.—A series of reflectors ranging in size from 1.34 to 35 ft^2 have been tested in a wind tunnel. Winds were directed against the reflectors at varying angles. The component down-wind and cross-wind forces and the resultant developed torques were measured.

Before making tests on various reflectors, observations were made at a range of wind velocities up to 100 mph on a 4-ft-wide by 1½-ft-high paraboloidal reflector with a solid surface. A reflector having an

identical shape, but with a surface composed of flat parallel slats, was also tested at a similar range of wind velocities. The down-wind and the cross-wind forces, measured both on the solid surface and on the slatted surface, were all strictly proportional to the square of the wind velocity. No discontinuity was observed at any single wind velocity up to the maximum measurement at 100 mph. The results secured from the tests of the various reflectors are recorded in the form of the equation

$$F = K_f V^2, \tag{3}$$

where V = wind velocity, mph,
F = resultant wind force, lb,
K_f = coefficient of wind force for the reflector as a whole.

The wind drag on reflectors of different shapes and sizes is not strictly proportional to their areas. Although each reflector is somewhat unique because of its supporting structure, the composite data can be evaluated most effectively by transposing all observations into forces acting on a unit square foot of the projected area of the reflector under test. Equation (3) will then take the form

$$F = k_f A V^2,$$

where A = projected area of the reflector, ft^2,
k_f = coefficient of wind force.

The values of k_f, multiplied by a factor of 100 for convenience of tabulation, are recorded in Table 2·5. The tabulated values times 100 give the force in pounds exerted by a 100-mph wind on 1 ft^2 of the projected area of the reflector. It will be noted that this value does not exceed 40 lb/ft^2 for any of the solid surfaces in any test position. This figure is comparable with 33 lb/ft^2, the value calculated from the conventional aerodynamic formula for the force exerted by air flowing at 100 mph against a flat plate normal to the air stream. With the exception of the grilled Reflector 6, the highest value recorded for a grilled surface is 18.9 lb/ft^2. The higher values recorded for Reflector 6, which is the smallest reflector tested, are undoubtedly due largely to the wind resistance of the supporting framework. The grilled surfaces were all composed of slats 0.025 in. thick by 0.4 in. deep on 0.4-in. centers.

From these observations, it appears that the maximum force exerted by a 100-mph wind can be taken as 40 lb/ft^2 on solid surfaces and 20 lb/ft^2 on the grilled surfaces. These figures are generally acceptable as satisfactory for use in the design of naval antenna mounts.

The average values of the coefficient of wind drag on each of the seven separate slatted reflectors are plotted as a broken line on Fig. 2·10. The plotted values of k_f are then composite figures indicating the magnitude of the unit force that may be exerted on a slatted reflector when

TABLE 2·5.—WIND FORCES ON PARABOLOID REFLECTORS*

Reflector					Coefficient of wind force: $100k_f$ $F = k_f A V^2$ Wind direction									
No.	Type	Width, ft	Height, ft	Area, ft²	0°	20°	40°	60°	80°	100°	120°	140°	160°	180°
1	Slatted	4.	1.25	5.0	0.100	0.120	0.128	0.126	0.104	0.098	0.120	0.136	0.140	0.126
2	Slatted	4.	2.	8.0	0.100	0.117	0.110	0.094	0.078	0.069	0.088	0.092	0.081	0.081
3	Slatted	5.	3.	15.0	0.115	0.133	0.136	0.115	0.080	0.089	0.119	0.113	0.085	0.080
4	Slatted	7.	5.	35.0	0.069	0.112	0.165	0.189	0.152	0.114	0.157	0.177	0.143	0.074
5	Slatted	5.	3.	15.0	0.096	0.159	0.187	0.160	0.120	0.135	0.150	0.150	0.117	0.085
6	Slatted	2.	0.67	1.34	0.097	0.104	0.246	0.261	0.216	0.202	0.224	0.216	0.164	0.082
7	Slatted	3.	0.75	2.25	0.084	0.098	0.115	0.098	0.071	0.089	0.112	0.129	0.115	0.102
8	Solid	4.	1.25	5.0	0.386	0.390	0.382	0.400	0.180	0.120	0.140	0.190	0.250	0.274
9	Solid	5.	1.50	7.5	0.353	0.366	0.333	0.200	0.107	0.100	0.133	0.206	0.267	0.267
10	Solid	2.5	1.	2.5	0.368	0.372	0.372	0.280	0.224	0.196	0.160	0.200	0.244	0.280

* Based on data supplied through courtesy of Raytheon Manufacturing Company.

the wind approaches the paraboloidal surface from various directions. This curve indicates that the wind drag is at a maximum at about 50° and that another region of high drag occurs at about 130° to 140°. The shape of this curve is characteristic of the behavior of the slatted paraboloidal reflector.

Observations on three solid surfaces were similarly averaged and plotted as a solid line on Fig. 2·10. This curve shows, as would be anticipated, that k_f is a maximum when the wind is blowing directly against the front of the solid paraboloidal surface. As the reflector is turned edgewise to the wind direction, the wind drag is decreased and reaches a minimum at about 100° to 110°. Aerodynamic considerations lead to a theoretical value, $k_f = 0.0033$, for a flat plate facing the wind, in fair agreement with Fig. 2·10.

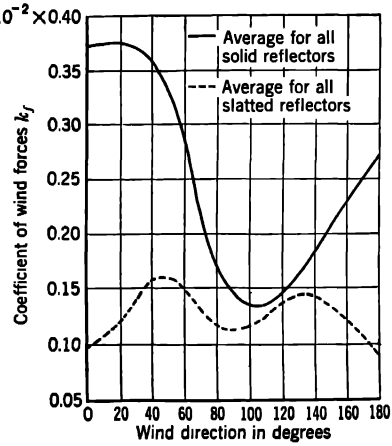

FIG. 2·10.—Wind forces on paraboloidal reflectors.

2·13. Wind Torques.—The direction of the resultant wind drag on a particular reflector can be computed from the magnitudes of the measured down-wind and cross-wind component forces. The center of wind pressure and the point of application of the resultant force will vary as the antenna rotates. If the wind force acts on the azimuth axis through a long lever arm, a high torque will be developed. The pivot point for a reflector would be in an ideal location if at all times it lay on the line of the resultant wind force. This cannot be achieved, and hence an attempt is made to secure a compromise that will keep the peak torque at a minimum value.

The torques resulting from wind loads are recorded in Table 2·6 in terms of the value of the coefficient k_t, which is employed in the equation

$$T = k_t A V^2,$$

where T = resultant wind torque, lb-ft,
A = projected area of the reflector, ft^2,
V = wind velocity, mph,
k_t = coefficient of wind torque.

These data show that the torques are reduced by placing the pivot in front of the vertex of the paraboloid surface. With grilled surfaces the

TABLE 2·6.—TORQUES RESULTING FROM WIND LOADS ON PARABOLOID REFLECTORS*

Reflector						Coefficient of wind torque: $1000k_t$ $T = k_t A V^2$ Wind direction									
No.	Type	Width, ft	Height, ft	Area, ft²	Pivot point	0°	20°	40°	60°	80°	100°	120°	140°	160°	180°
1	Slatted	4.	1.25	5.0	15 in. front	0	0.37	0.62	0.51	0.48	0.50	0.67	0.69	0.76	0
2	Slatted	4.	2.	8.0	7 in. back	0	0.85	1.08	1.19	0.90	0.88	1.07	1.15	0.40	0
3	Slatted	5.	3.	15.0	10 in. back	0	1.27	1.76	1.91	1.24	1.27	1.88	1.43	0.60	0
4	Slatted	7.	5.	35.0	$5\frac{11}{16}$ in. front	0	0 11	0.53	0.53	0.40	0.52	0.35	0	−0.13	0
5	Slatted	5.	3.	15.0	$2\frac{1}{4}$ in. front	0	0.89	1.13	1.05	0.69	0.96	0.90	0.93	0.55	0
6	Slatted	2.	0.67	1.34	3 in. front	0	0.25	0.11	−0.25	0.33	−0.22	−0.05	−0.03	−0.03	0
7	Slatted	3.	0.75	2.25	$3\frac{1}{8}$ in. front	0	−0.13	0	0.11	0.11	0.13	0.21	0	−0 16	0
8	Solid	4.	1.25	5.0	15 in. front	0	−0.33	−0 32	0	0.58	0.53	0.59	0.62	0.36	0
9	Solid	5.	1.5	7.5	0 in. front	0	−0 67	0	1 75	2.24	1 87	1 72	1.47	0.69	0
10	Solid	2.5	1.	2.5	3 in. front	0	−0.08	−0.16	0 56	1.07	1 26	0.72	0.60	0.28	0

* Based on data supplied through courtesy of Raytheon Manufacturing Company.

pivot needs to be displaced forward only a small distance, but with solid surfaces it is advantageous to place the pivot a substantial distance in front of the vertex.

The torques induced by wind loading of a particular reflector can be altered by as much as 100 per cent if the pivot point is moved a short distance. Hence, torque data of the kind recorded in Table 2·6 are unique to each reflector. A rough correlation has been attempted by averaging the data on only those reflectors which are pivoted in front of the vertex. These average values are plotted in Fig. 2·11. The curves show that the solid surface may exert less torque than the slatted surface

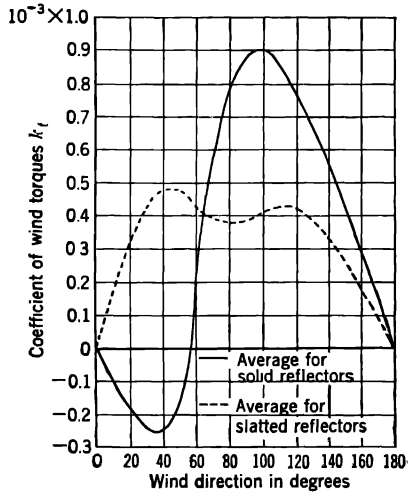

FIG. 2·11.—Wind torques on paraboloidal reflectors. The solid reflectors are Nos. 8 and 10. The slatted reflectors are Nos. 1, 4, 5, 6, and 7 in Table 2·6.

when the wind direction is not too far from the axis of the reflector but that the solid surface tends to develop a high peak torque as it is revolved.

STRUCTURAL CHARACTERISTICS OF SPECIFIC REFLECTORS

2·14. Photographs and Tables.—Some widely used reflectors are illustrated in the figures indexed in Table 2·7. This table gives the weight and, where available, the manufacturing cost of each reflector. Additional structural data are given in the supplement to Table 2·7.

In comparing the weights of reflectors that are similar but vary in size, it is reasonable to assume that the total weight varies roughly with the three-halves power of the projected area. This assumption is based on the postulate that when all dimensions of a specific reflector are retained in exact proportion as size is changed, the weight will vary with the cube of any linear dimension.

TABLE 2·7.—MICROWAVE REFLECTORS

Reflector No.	Illustration Fig. No.	Radiation, cm	Focal length, in.	Horizontal projected aperture, ft	Vertical projected aperture, ft	Projected area, ft²	To operate under wind velocities, mph	To withstand structurally wind velocities, mph	Weight, lb	Wt/ft², lb	Cost	Cost/ft²
1	3·5, 3·6	10	43.2	25.	8.	200.	60	120	2200	11.00	$2035	$10.20
2	3·5, 3·6	10	30.0	25.	5.	125.	60	120	1870	15.00	1331	10.70
3	3·16	10	60.0	5.	20	78.5	40	60	355	4.53	1100	14.00
4	3·9, 3·10	10	78.0	25.	10.	238.	45	90	1631	6.85	6000	25.20
5	3·9, 3·10	10	99.0	32.	10.	311.	45	90	2282	7.35	7700	24.80
6	2·12	10	60.0	14.	5.	55.	70	120	210	3.82	.....	.....
7	2·13	8	{108.0 / 60.0}	5.	15.	62.	70	120	240	3.87	.....	.....
8	2·14	3	35.5	3.	10.	24.	45	90	94	3.91	890	37.00
9	5·4	3	14.5	4.5	2.	7.7	70	100	18	2.34	300	39.00
10	2·15*a*, *b*	3	21.6	6.5	2.5	13.3	70	100	30	2.26	. .	....

TABLE 2·7.—MICROWAVE REFLECTORS (SUPPLEMENTARY DATA)

Reflector 1 (Figs. 3·5 and 3·6, Sec. 3·3):	
Form	Parabolic cylinder
Projected contour	Rectangle
Reflecting surface	Solid steel sheet, 12 gauge
Supporting framework	Welded structural steel. Eleven individual reflector sections, each 27 $\frac{3}{16}$ in. wide, fabricated of welded sheet steel and structural angles are bolted onto a centrally supported tubular cantilever beam
Reflector 2 (Figs. 3·5 and 3·6, Sec. 3·3):	Same as Reflector 1
Reflector 3 (Fig. 3·16, Sec. 3·6):	
Form	True paraboloid
Projected contour	Ellipse
Reflecting surface	Expanded metal, 18-gauge steel, $\frac{1}{2}$-in. mesh with the long dimension of the diamond vertical, arc-welded to the framework
Supporting framework	Carbon steel seamless tubing, $\frac{3}{4}$-in. and $1\frac{1}{4}$-in. OD, arc-welded at joints
Reflector 4 (Figs. 3·9 and 3·10, Sec. 3·5):	
Form	True paraboloid
Projected contour	Rectangle with corners cut away on a 45° angle
Reflecting surface	Galvanized iron hardware cloth, 18-gauge wire on $\frac{1}{4}$-in. centers, soldered to grillwork of $\frac{1}{2}$-in. OD by 18-gauge steel tubing
Main Truss	Welded steel tubular structure with reinforcement of the K-frame type, chord members $2\frac{1}{4}$-in. OD by 14-gauge tubing, reinforcing members $1\frac{1}{8}$-in. OD by 16-gauge tubing. For transportation purposes, the main truss is made in five separate sections. The joints are bolted together with male and female flanged connectors. The male connector is centered on a machined stud that accurately fits the mating female receptacle. Ten individual reflector sections, each 30 in. wide, are made by reinforcing the screen and grillwork surface with ribs of 14-gauge sheet steel. Each of the individual reflector units is held in exact alignment on the truss by a series of bolting pads that are welded to the main truss. The main truss weighs 808 lb, and the 10 individual reflectors weigh a total of 823 lb
Reflector 5 (Figs. 3·9 and 3·10, Sec. 3·5):	
Form	True paraboloid
Projected contour	Rectangle with corners cut away on a 45° angle
Reflecting surface and supporting framework.	Galvanized iron hardware cloth, 18-gauge wire on $\frac{1}{4}$-in. centers, soldered to grillwork of $\frac{1}{2}$-in. OD by 18-gauge steel tubing
Main Truss	Welded steel tubular structure with reinforcement of the K-frame type, chord members $2\frac{1}{4}$-in. OD by 14-gauge tubing, reinforcing members $1\frac{1}{8}$-in. OD

TABLE 2·7.—MICROWAVE REFLECTORS (SUPPLEMENTARY DATA)—(*Continued*)

by 16-gauge tubing. The construction is similar to that of Reflector 4, except that the main truss is in six separate sections and the complete reflecting surface is a composite of 14 individual reflectors. The main truss weighs 1154 lb, and the 14 individual reflectors weigh a total of 1128 lb

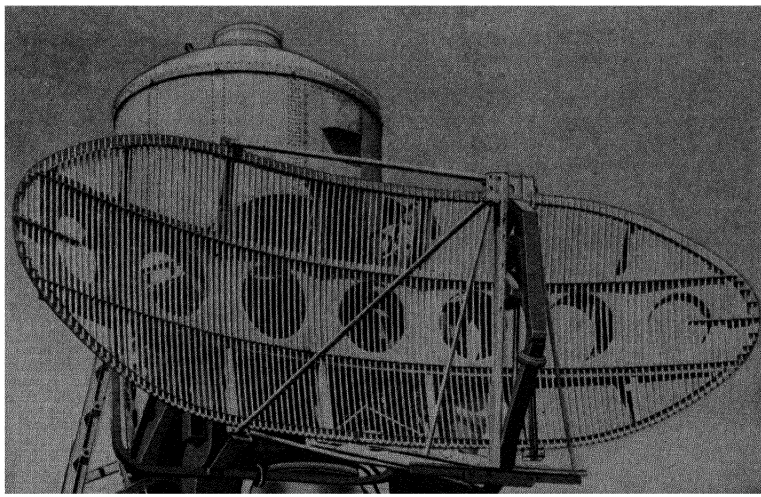

FIG. 2·12.—Experimental search antenna reflector.

Reflector 6 (Fig. 2·12):	
Form	True paraboloid
Projected contour	Ellipse
Reflecting surface	24ST aluminum tubing $\frac{1}{2}$-in. OD by 0.035-in. wall on $1\frac{1}{2}$-in. centers. The tubing is threaded through punched holes in $\frac{3}{4}$- by $\frac{3}{4}$- by $\frac{3}{32}$-in. 24ST aluminum angles and is anchored in place by crimping the angles adjacent to the tubes
Supporting framework	Box girder of 61SW aluminum sheets 0.081 in. thick, relieved with 14-in.-diameter cutouts, and riveted with $\frac{5}{16}$-in. aluminum rivets
Reflector 7 (Fig. 2·13):	
Form	Astigmatic paraboloidal surface
Projected contour	Rectangle with three corners cut on 19° angles
Reflecting surface	24ST aluminum tubing $\frac{1}{2}$-in. OD by 0.035-in. wall on $1\frac{3}{8}$-in. centers. The tubing is threaded through punched holes in $\frac{3}{4}$- by $\frac{3}{4}$- by $\frac{3}{32}$-in. 24ST aluminum angles and is anchored in place by crimping the angles adjacent to the tubes
Supporting framework	Box girder of 61SW aluminum sheets 0.081 in. thick, relieved with 14-in.-diameter cutouts, and riveted with $\frac{5}{16}$-in. aluminum rivets

TABLE 2 7.—MICROWAVE REFLECTORS (SUPPLEMENTARY DATA)—(*Continued*)

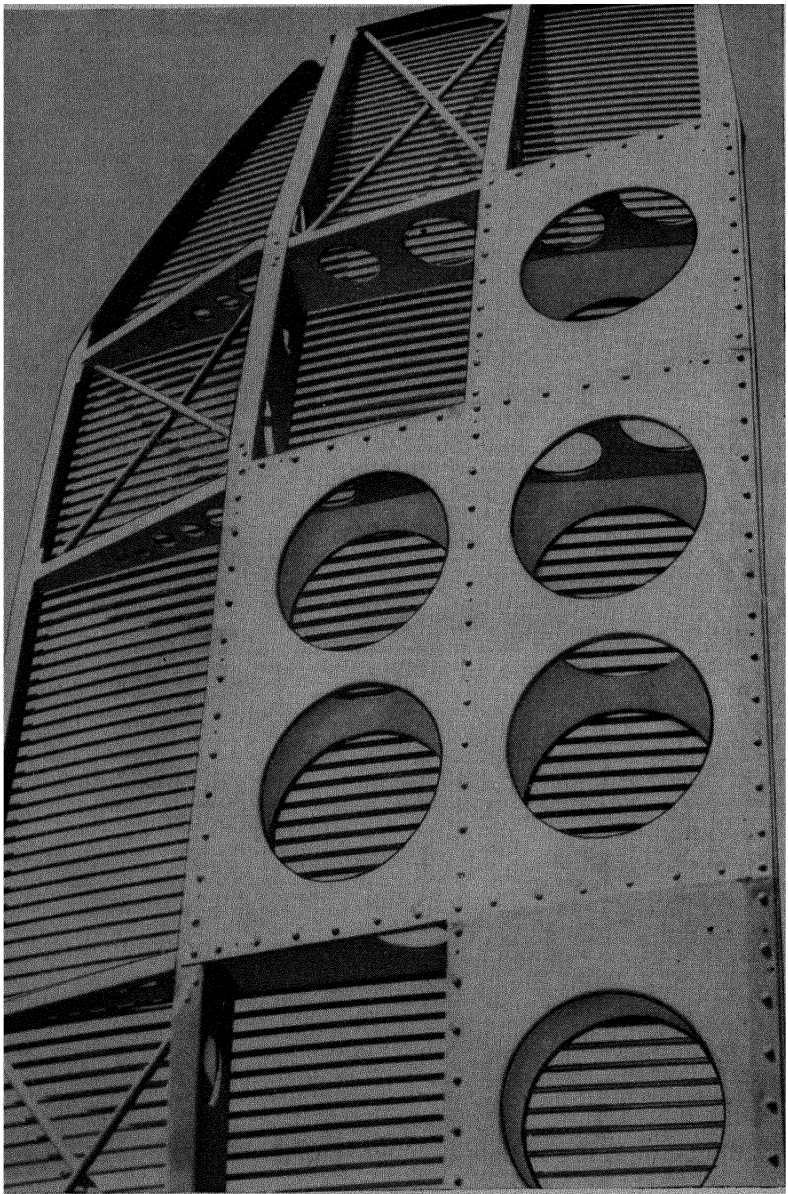

FIG. 2·13.—Reflector of antenna for height finder.

TABLE 2·7.—MICROWAVE REFLECTORS (SUPPLEMENTARY DATA)—(*Continued*)

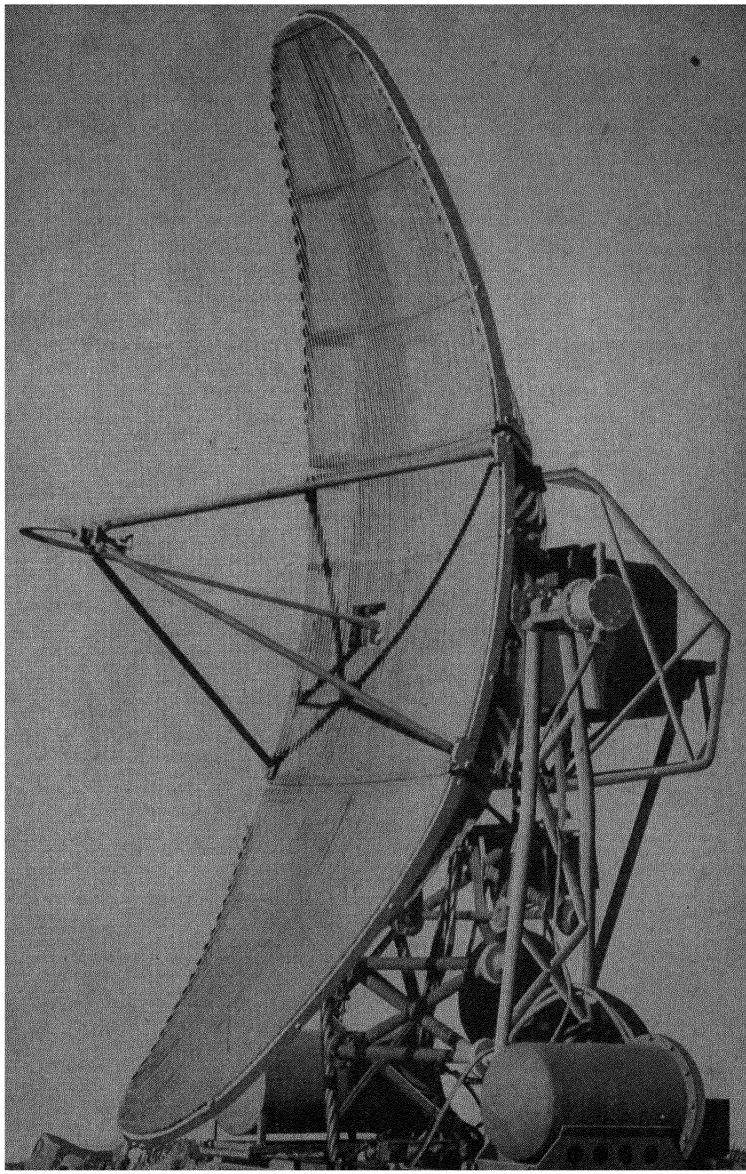

FIG. 2·14.—AN/TPS-10 antenna reflector.

TABLE 2·7.—MICROWAVE REFLECTORS (SUPPLEMENTARY DATA)—(*Continued*)

Reflector 8 (Fig. 2·14):	
Form	True paraboloid surface
Projected contour	Ellipse
Reflecting surface	24ST aluminum tubing ¼-in. OD by 20-gauge (0.035-in.) wall on ½-in. centers. The tubing is parallel to the long dimension of the dish to give vertical polarization. The tubing is threaded through punched holes in ½- by ½-in. 24ST aluminum angles and is anchored in place by crimping the angles adjacent to the tubes
Supporting framework	Deep webbed channel sections of 61SW aluminum sheet, with lightening holes cut into the webs. Structural sections are formed to approximate the shape of the dish. For transportation purposes, the reflector is made in three sections, a center section and two end sections that are bolted fast to the center section upon assembly

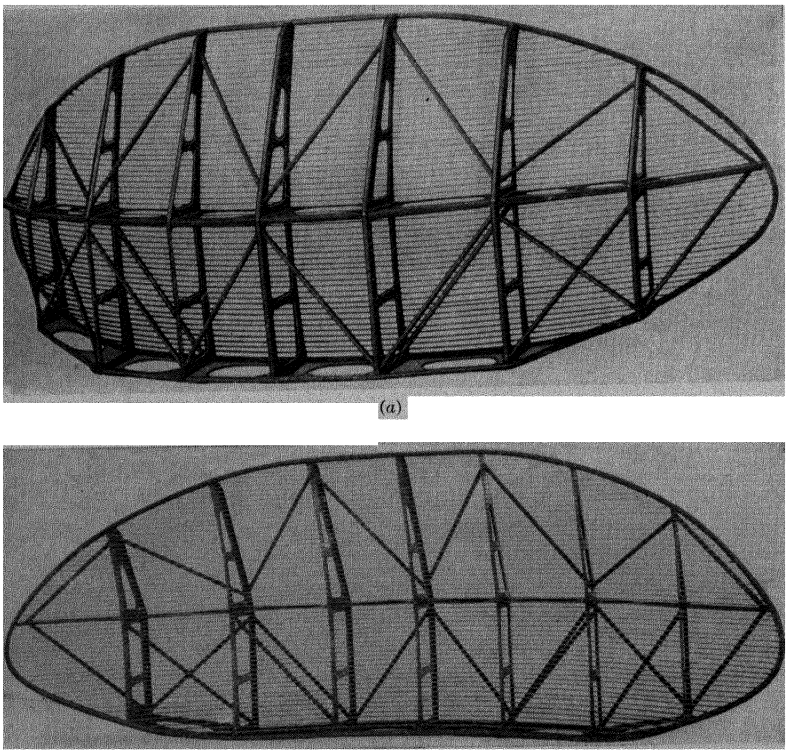

FIG. 2·15 Antenna reflector. (*a*) rear view; (*b*) front view.

TABLE 2·7.—MICROWAVE REFLECTORS (SUPPLEMENTARY DATA)—(*Continued*)

Reflector 9 (Fig. 5·4, Sec. 5·9):	
Form	Paraboloid of revolution
Projected contour	Cut to conform to the −14-db contours of the projected primary illumination
Reflecting surface	Flat aluminum strips, $\frac{1}{16}$ in. thick by $\frac{5}{8}$ in. deep, spaced $\frac{1}{2}$ in. apart. Ends brazed to $\frac{5}{8}$-in. OD by $\frac{1}{16}$-in. wall periphery tube
Supporting framework	$\frac{1}{16}$-in. aluminum uprights and longitudinal members with $\frac{1}{2}$-in. OD by 0.062-in. wall tubing for cross-bracing. All joints between sheet metal parts riveted with $\frac{1}{8}$-in.-diameter rivets. Tubing to sheet metal joints brazed. Reflecting slats crimped in place
Reflector 10 (Fig. 2·15*a* and *b*).	Identical with Reflector 9 except that the lower longitudinal frame member is $\frac{1}{8}$-in. aluminum

ELECTRICALLY SCANNING FEEDS

Any device that produces a scanning beam of radiant energy without the motion of either the reflector or the external portion of the feed is termed an electrically scanning antenna. Two distinctly different electrical scanners are described in the following sections. A third electrical scanner, the Delta a or Eagle scanner, is described in Sec. 6·14.

2·15. The Robinson Scanning Feed.[1]—The use of a trapezoidal feed with an astigmatic paraboloid reflector is discussed in Sec. 2·9. It is advisable to become familiar with that section prior to making a detailed study of the construction of the Robinson scanning feed,[2] which is a trapezoidal feed.

Properties of a Trapezoidal Feed.—Figure 2·5 illustrates a flat trapezoid in front of an astigmatic paraboloid reflector. In this figure, the line *ED* represents a locus of points on which the antenna feed may be located. The line *BC* is the boundary at which r-f energy leaves the feed and is radiated to the reflecting surface. Equations (1) and (2) in Sec. 2·9 define the astigmatic reflecting surface on the basis of radiation of energy from the point *S*. The trapezoid *BCDE* is illustrated in Fig. 2·5 as a single flat surface. In actual construction this trapezoid consists of two parallel surfaces $\frac{3}{4}$ in. apart. The energy from the feed at the point *S* is confined by these surfaces and is not free to diverge in the direction of the *OZ*-axis until it passes the boundary line *BC*.

If a reflector that is a paraboloid of revolution is illuminated by a point source, the beam may be tilted off the axis of the paraboloid by moving the feed in a direction perpendicular to the axis. The pattern of the beam deteriorates and the gain falls off when this is done. Experi-

[1] Photographs in this section are through the courtesy of the American Machine and Foundry Co.

[2] C. V. Robinson, *Microwave Antenna Theory and Design*, Vol. 12, Chap. 16.

ments have shown that the deterioration at a given tilt angle is approximately inversely proportional to the beamwidth and decreases as the value of the ratio f/D is increased.[1] In the design here considered, a reflector having a 9-ft focal length and 15-ft projected diameter gives $f/D = 0.6$. With this reflector, the deterioration is not rapid until a tilt angle of $5\frac{1}{2}°$ is reached. At this angle the deterioration becomes rapid, and this Robinson scanning feed is limited to an over-all scan of 11°.

The Folded Trapezoidal Feed.—Referring again to Fig. 2·5, scanning is accomplished by moving the feed back and forth along the line *ED*. The system is in true focus when the feed is at the point *S* but is still sufficiently in focus at either of the extreme points *E* or *D* to cause no more than a loss of 1 db in the over-all antenna system. It is entirely possible to construct a trapezoidal feed of two flat sheets as illustrated in Fig. 2·5, with a mechanical device for moving the feed backward and forward along the line *ED*. Such a device would be extremely cumbersome, and the speed at which the feed could be moved would be limited by the mechanical properties of the system. The trapezoid *BCDE* is therefore folded in such a manner that it forms a true circle of the line *ED*. The uniform $\frac{3}{4}$-in. spacing is maintained throughout. The folded feed has the electrical properties of the flat trapezoid but is now in a structural form that allows the feed to be rotated rapidly around the annular aperture *EDS*.

Schematic Diagram of the Folded Feed.—Figure 2·16 shows a schematic arrangement of the Robinson scanning feed, which is essentially the folded trapezoid discussed in the preceding paragraph. The designations *B*, *C*, *D*, *E*, *N*, and *S* that are used in Fig. 2·5 are duplicated in Fig. 2·16 in order to correlate the two diagrams. The line *ED* now appears as an annular aperture of two concentric cylinders whose inner faces are $\frac{3}{4}$ in. apart, the points *E* and *D* being superposed at the point where the folded ends of the trapezoid join. The line *BC* remains a straight line and on Fig. 2·16 is a rectangle $\frac{3}{4}$ in. wide and approximately 8 ft long. The scanning feed could be terminated at the boundary line *BC*, but a short flared section is added to reduce the dispersal of energy as it leaves the feed. The point *S* appears 180° from the points *D* and *E*, and the point *N* immediately below it. The folded surfaces run directly backward from the point *S* to the point *O* and are there reversed to return to the point *N*. Energy is supplied through the rotating waveguide *H*, which is counterbalanced and can be rotated rapidly. The cylindrical housing within which the feed rotates is grooved and shaped to form conventional choke sections and waveguide conducting surfaces, so that the energy from the waveguide will flow into the Robinson scanning feed at various points along the annular aperture *EDS*.

[1] J. R. Risser, *Microwave Antenna Theory and Design*, Vol. 12, Chap. 11.

Power Absorber.—If the folded surface is joined at *ED* to form a metal barrier, r-f mismatching will be produced as the feed *H* rotates past this barrier. The metal barrier at *ED* is therefore replaced with a material

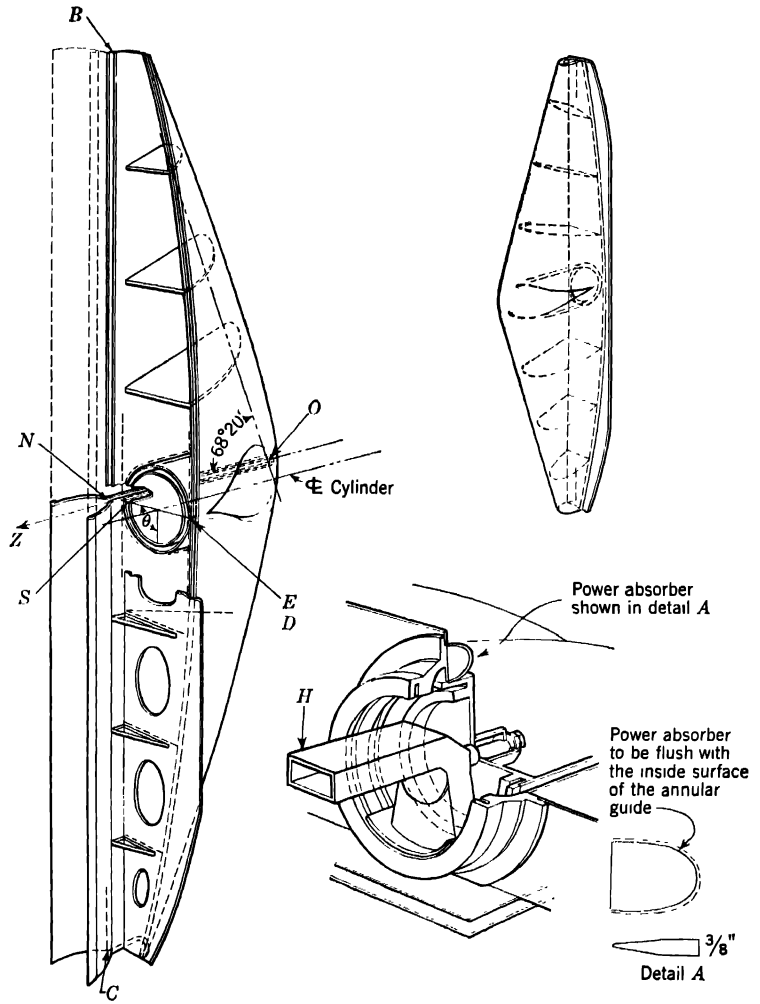

FIG. 2·16.—Schematic arrangement of Robinson scanning feed.

that will absorb such energy as impinges upon it and convert that energy into heat. A typically shaped power absorber is shown in Fig. 2·16. The choice of a suitable power-absorbing material is critical in the design of the scanning feed. Finely divided iron in a matrix of organic binder,

known as Polyiron D-1, was originally employed. Although the power-absorbing properties of the Polyiron are excellent, it was found that the Polyiron absorber was disintegrated by thermal shock. Furthermore, the heat generated in the absorber was sufficient to destroy the plastic binding material and leave a residue with very poor absorbing properties. An absorbing material of 40 parts silicon carbide and 100 parts porcelain[1] was substituted for Polyiron and proved to be entirely satisfactory. The matrix of silicon carbide and porcelain is a ceramic that can be heated to a dull red without injury to its r-f absorbing properties, and it has an adequate resistance to thermal shock.

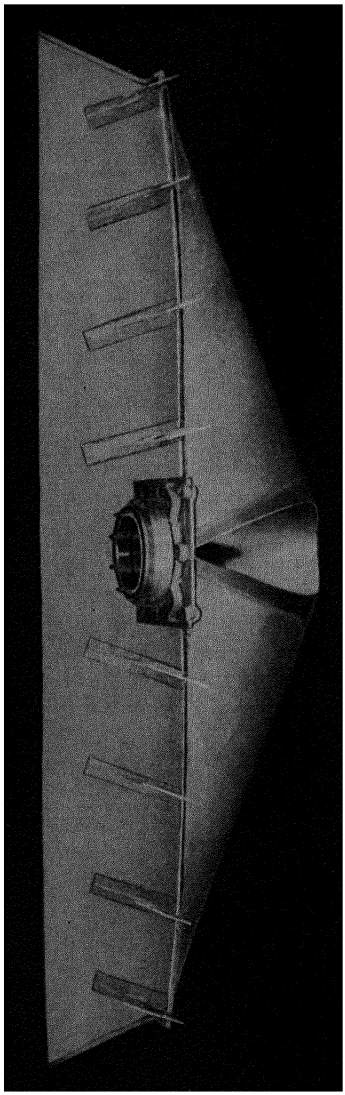

FIG. 2·17.—Inner surface of the Robinson scanning feed.

Inner Surface.—The inner portion of the scanning feed is shown in Fig. 2·17. The central portion is a machined aluminum casting which is called the "inner horse collar." A continuous sheet of aluminum is made fast to the inner horse collar with a series of closely spaced flush-head machine screws. The completely machined inner horse collar, but not the attached aluminum sheet, is shown at the left in Figs. 2·18 and 2·19. The edge of the inner horse collar is grooved so that the surface of the attached aluminum sheet will be flush with the surface of the horse collar. The cylinder that surrounds the rotating feed *H* is an integral portion of the inner horse collar.

Outer Surface.—The outer portion of the scanning feed is shown in Fig. 2·20. The central portion again consists of a machined aluminum casting, this one being known as the "outer horse collar." A continuous sheet of aluminum is made fast to this cast-

[1] This material was supplied by the Bell Telephone Laboratories.

ing in a manner similar to that described in the previous paragraph. The outer horse collar comprises not only the surfaces to which the outer aluminum sheet is made fast but also the inner core of the cylindrical portion of the scanning feed. The completely machined outer horse collar, but not the attached aluminum sheet, is shown at the right in Figs. 2·18 and 2·19.

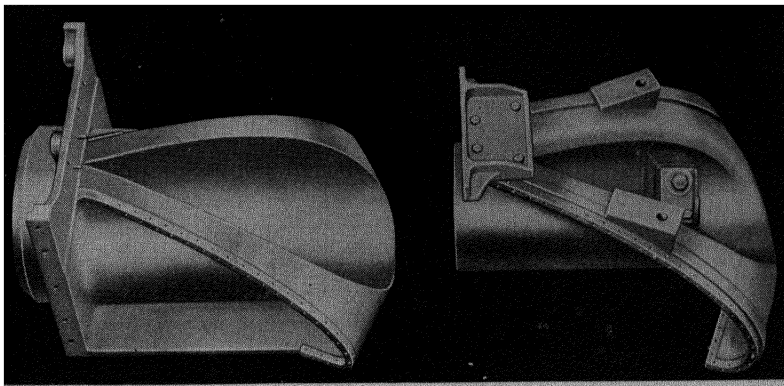

FIG. 2·18.—Inner and outer horse collars.

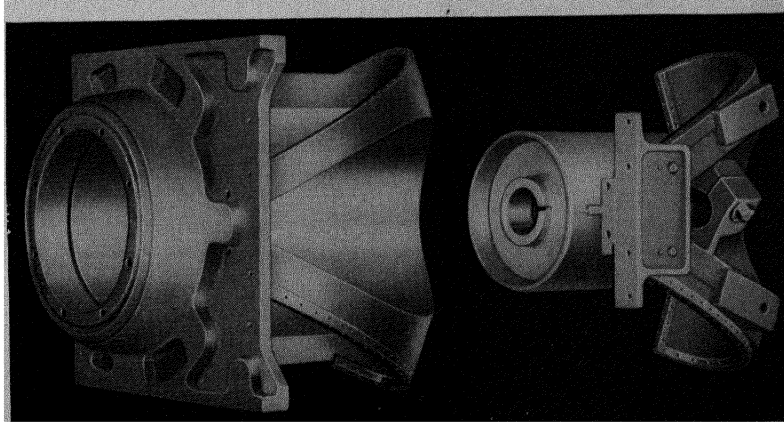

FIG. 2·19.—Inner and outer horse collars.

Assembly of the Inner and Outer Surfaces.—Figure 2·21 shows both the inner and outer members prior to final assembly. The complete inner member slides inside the complete outer member to form a folded trapezoid having a $\frac{3}{4}$-in. interspace. The edge of the inner horse collar is sharp or, at best, rounded slightly, and the machined metal surface beyond this sharp edge is a continuation of the contour of the rolled aluminum sheet. The most critical areas of the scanner are those where

the outer horse collar surface rolls over the sharp edge of the inner horse collar. The nominal distance between the two surfaces is $\frac{3}{4}$ in., but this dimension is slightly altered at the point where the outer surface rolls over the sharp inner surface. These alterations were incorporated in the design after a long series of experiments to produce an assembled scanner that would function without mismatching of the radiated energy. Accurate alignment at the sharply rolled section is secured by means of flat machined interfaces on the inner and outer horse collars. Figures 2·18 and 2·19 show these interfaces, which are doweled so that they can be bolted together firmly.

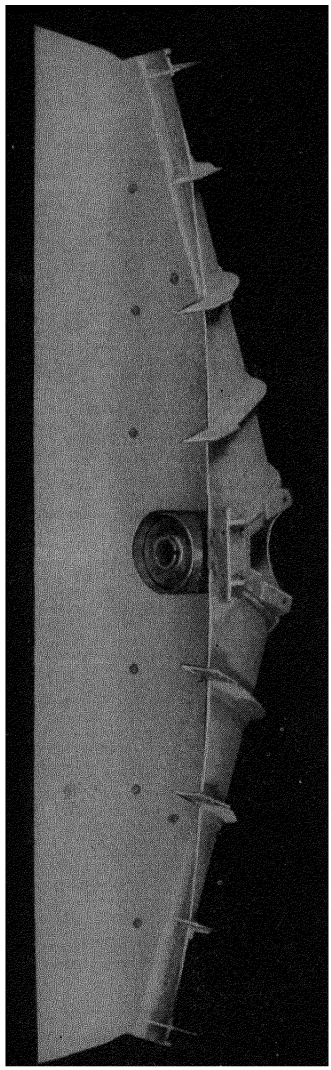

FIG. 2·20.- Outer surface of the Robinson scanning feed.

Spacing of the aluminum sheets is achieved by the insertion of studs $\frac{3}{4}$ in. in height, located throughout the length of the scanner. The studs in the lower portion of the outer member are visible in Fig. 2·21. The stud is not a simple mechanical post but is in itself a small choke joint, so that energy impinging on a stud will not be reflected to produce mismatching. The surfaces are stiffened by a series of machined webs. Figure 2·17 shows these machined webs placed inside the inner surface. The aluminum sheet is brazed to the machined surface of each of the web sections. A similar construction, shown in Fig. 2·20, has been employed to stiffen the outer aluminum sheet. After the inner and outer members have been pushed together for final assembly, the stiffening ribs are bolted together as illustrated in Fig. 2·22. Assembly is now complete, except for attaching the end sections and sealing the front of the flared section of the scanner with a strip of Fiberglas.

Machining of the Outer Horse Collar.—If a trapezoid comprised of a single sheet of thin metal is folded into the desired form, the contour of the sharp edge at the fold can be considered a "theoretical curve." The sharp edge of the inner horse collar corresponds approximately to this theoretical curve. The surface of the outer horse collar rolls over this theoretical curve in a manner that allows an interspace of approximately $\frac{3}{4}$ in. Figure 2·23 shows the relation between the theoretical surface and the inner and outer metallic surfaces. The inner horse collar is shown in

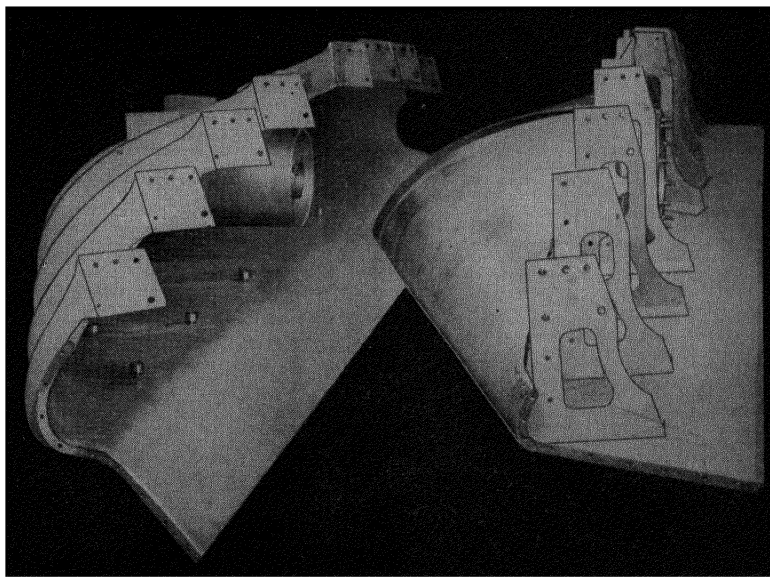

FIG. 2·21.—Assembly of the inner and outer surfaces of the Robinson scanning feed.

broken lines; the outer horse collar is shown in solid lines, and the theoretical surface is shown in dot-and-dash lines. It will be noted in the details *a* and *b* that the inner surface is displaced from the theoretical surface by the thickness of the metal and that the outer surface is displaced an additional $\frac{3}{4}$ in. The machining of the inner surface presents no very difficult problem, but the contouring of the curve where the outer surface rolls over the inner surface requires special tooling.

The machine built to do this special tooling is shown in Fig. 2·24. A cam corresponding to the theoretical curve is cut on a cylinder. The rough casting of the outer horse collar is mounted on a shaft concentrically with the cylindrical cam. The cylindrical cam and the work are rigidly bolted to a common arbor. Both the cam and the work are free to move as a unit longitudinally along the bed on which the arbor is mounted,

and both are free to rotate as a single unit. Any motion of the cam is therefore duplicated by the motion of the work. A ball cutter, revolving in a fixed location, is used as the finishing tool. The edge of the cam is moved over a roller guide that is fixed in position in relation to the cutting tool. The cam is held against the roller by a piston that is under air pressure to maintain an adequate force but that allows longitudinal movement as the cam and work are rotated. With each complete cut, which is made without alteration of the tool location, the shape of the cam is transferred in three dimensions to the finished surface of the work.

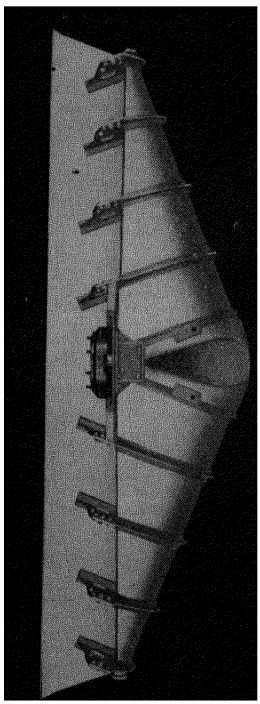

FIG. 2·22.—Side view of the Robinson scanning feed.

The rolled sections of the outer horse collar meet to form the sharp edge that is visible as a U-shape in Fig. 2·24. It is at this point that the power absorber is inserted. The metal is cut back until its thickness is equal to that of the power absorber, and the ceramic is held in place by suitably located grooves. Loose slots are employed to allow for thermal expansion of the power absorber.

The Complete Feed.—The complete Robinson scanning feed is shown in Figs. 2·25, 2·26, and 2·22. Castings are fabricated of 356HT6 aluminum; the formed aluminum sheets are SII aluminum; and the braces are 52S aluminum. The complete scanning feed is slightly over 8 ft long by 2 ft deep and weighs about 200 lb.

Resin-impregnated Fiberglas having been found to be an effective material for transmitting r-f energy (see Sec. 13·14), the window that seals the front of the flared horn is comprised of one continuous strip of Fiberglas approximately $\frac{1}{16}$ in. thick. A rubber gasket is employed as a seal between the Fiberglas and the aluminum, and rubber gaskets are also employed to seal the plates that close the extreme ends of the horn. With all of these precautions, it is still impossible to secure a completely watertight feed; or if the feed is completely watertight, water may still be accumulated because of condensation. Consequently, drain holes are suitably located in the horn and its associated equipment. In Fig. 2·16, a drain hole is shown located at point *C*. Drain holes are also drilled in the annular cavities that surround the rotating waveguide.

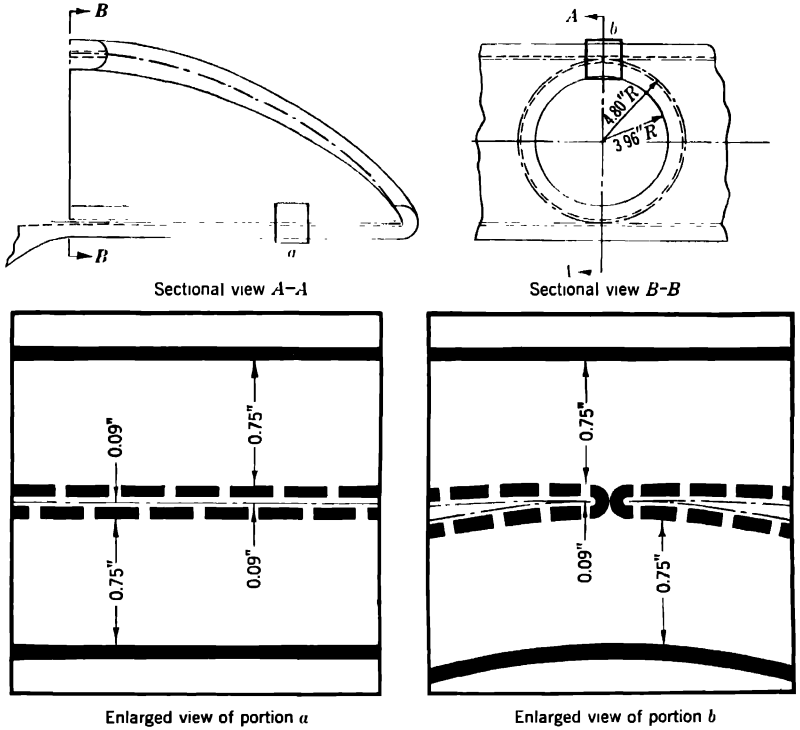

FIG. 2·23.—Diagram of the throat of the Robinson scanning feed. — — — — Inner horse collar. ———— Outer horse collar. —— – —— Theoretical surface.

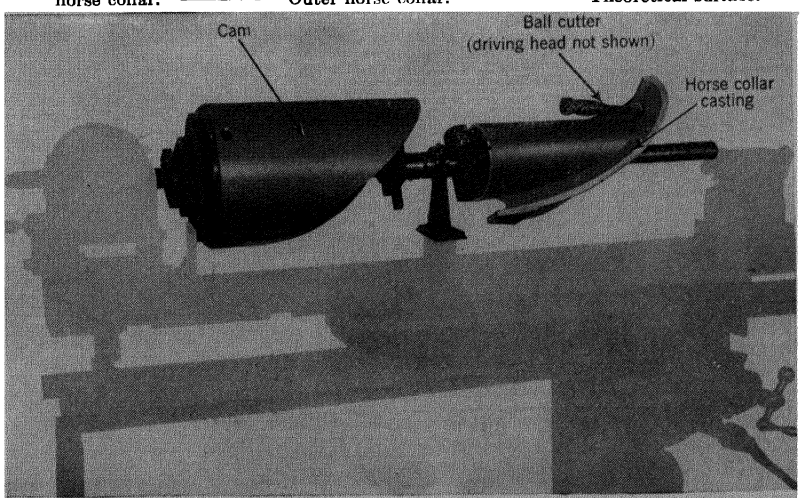

FIG. 2·24.—Machining of the outer horse collar.

Alternate Methods of Construction.—Experimental models of the Robinson scanning feed have been fabricated by casting and machining only the annular sections that surround the rotating waveguide. The

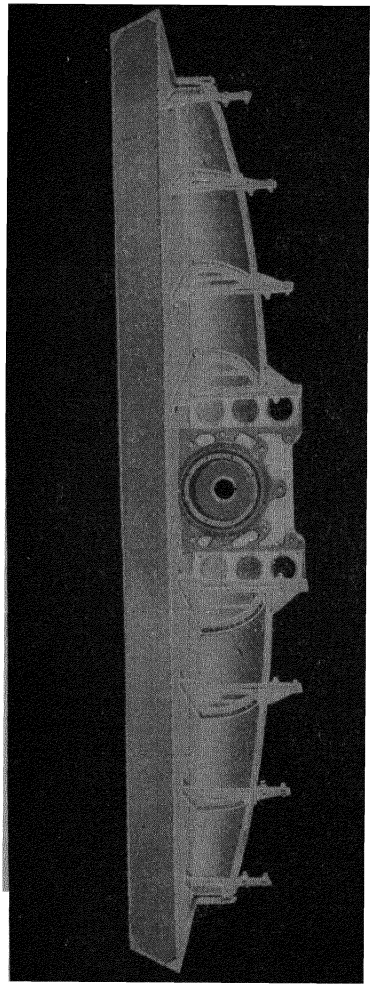

FIG. 2·25.

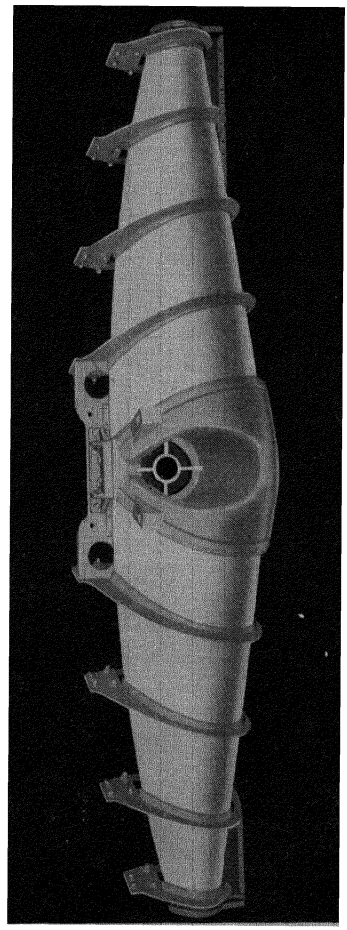

FIG. 2·26.

FIG. 2·25.—Front view of the Robinson scanning feed showing plastic window at left.
FIG. 2·26.—Rear view of the Robinson scanning feed.

entire inner member and the entire outer member are then made by the direct forming of aluminum sheets. This method of construction is fairly inexpensive and light, but the dimensions are not exact. Further-

more, the joint between the formed sheet metal and the cylindrical casting has little structural rigidity.

A third method of construction employs electroforming over suitably prepared molds. Small feeds for 3-cm radiation have been produced by electroforming methods, but the feed illustrated in this section would be inordinately heavy if made of any material other than aluminum or magnesium.

2·16. The Schwarzschild Scanning Feed.—Development of the Schwarzschild antenna system (see Fig. 2·27) was initiated to meet the

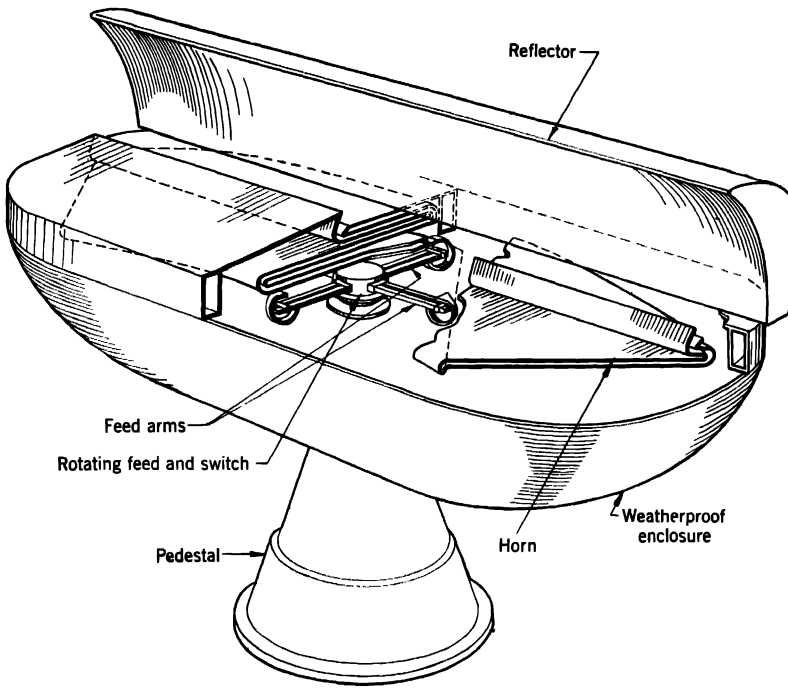

FIG. 2·27.—Perspective view of horn, reflector, and feed of the Schwarzschild scanner.

requirements for a position-finding radar to supply present-position data for seacoast fire control against surface targets. The technical requirements established for the system included an azimuthal accuracy of 0.05°. Because a rapid scan of a small sector was desired, it was decided to use an electrical scanner.

To secure the required gain and beamwidth in the azimuth direction, a system was designed with a radiator having effective dimensions 10½ ft in the horizontal direction and approximately 2 ft in the vertical. When such an aperture is properly illuminated with 3-cm radiation, the trans-

mitted beam dimensions at the half-power points measure approximately 0.6° horizontally and 3° vertically. To secure focusing in the vertical plane, a semiparabolic cylinder is used for a reflecting surface. This surface, as shown in Fig. 2·27, is illuminated by a line source $10\frac{1}{2}$ ft long, located at its focal line to produce a suitable vertical pattern. The line source produces a controllable uniform phase variation along its length, causing the beam to scan the required 10° sector. For this purpose, an optical system was designed for satisfactory performance over the required angular region. This system, in which energy is propagated between parallel plates, will be discussed at some length.

The desired scan could be obtained from a pillbox antenna feed if the feed horn were oscillated through the focus along a line parallel to the exit flaps. This method of scanning is satisfactory for a narrow scan sector. But because a scanning beam broadens when it is moved more than three or four beamwidths away from its normal position, the pillbox antenna feed is unsuitable for the purpose of finding position accurately.

A similar situation was encountered with astronomical reflecting telescopes: The focusing of the light from a star upon a photographic plate is imperfect if the star is too far away from the axis of the paraboloidal reflector. A well-known remedy, devised by Schwarzschild for this aberration (coma) in reflecting telescopes, was adapted to the radar-scanning problem. In a telescope a small secondary reflector is introduced between the main reflector and its focal point; the photographic plate is located between the reflectors and faces the secondary reflector. By proper curvature of the two reflecting surfaces of revolution, the system can be made perfect in the sense that any star in the field of view, even if off axis, gives a point image on a certain focal surface. The reflecting surfaces are not mathematically simple, but they can be conveniently described by polynomial equations. Within limits, for convenience of construction of the telescope the system can be designed with some choice of spacing of the surfaces.

The radar-scanning feed analogous to the Schwarzschild telescope is illustrated in Fig. 2·28. The parallel plates are folded as in Fig. 2·28*d*. In Fig. 2·28*c* is shown the median surface midway between the plates. The mathematical analysis applies to the geometry of the folds, which are analogous to the mirrors of a telescope. The exit flaps of the folded horn are shown at A; fold B corresponds to the primary reflector of the telescope; fold C is analogous to the secondary reflector; and curve D is the focal line.

The surfaces of the primary reflector fold B and secondary reflector fold C are calculated[1] according to the equations

$$x_1 = 0.5y^2 - 0.03125y^4 - 0.020y^6$$

[1] *Microwave Antenna Theory and Design*, Vol. 12, Chap. 15.

and

$$x_2 = 0.75y^2 - 5.96025y^4 + 40.53y^6$$

respectively. The coordinate x is parallel to the direction of the optical axis, and coordinate y is perpendicular to it. Figure 2·28*d* is an isometric schematic diagram of the plates, whereas Figs. 2·28*a*, *b*, and *c* show the

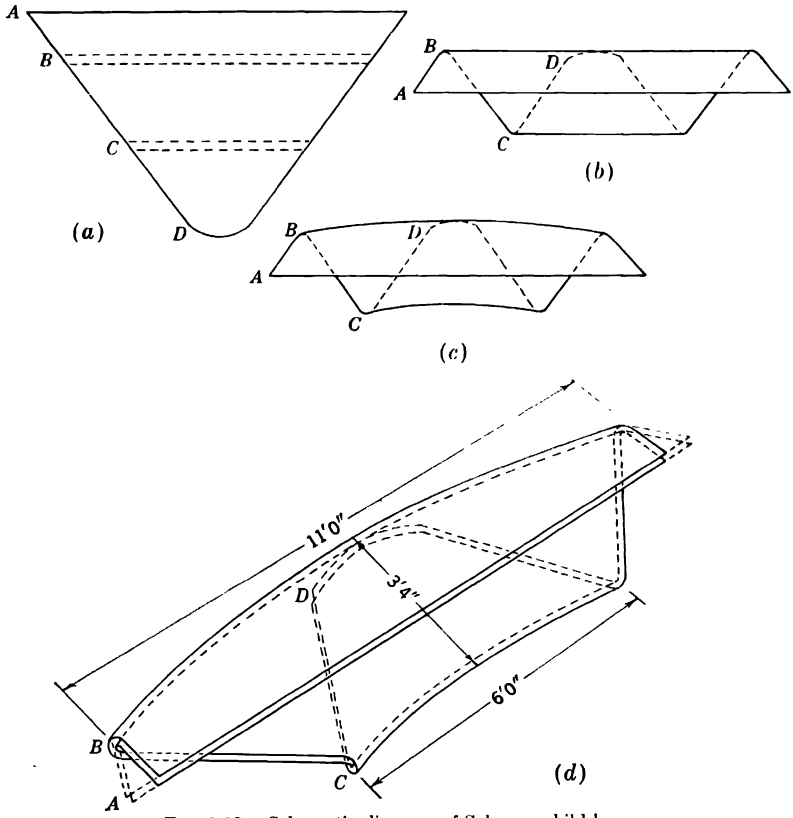

FIG. 2·28.—Schematic diagram of Schwarzschild horn.

median surface as imagined when folded and stretched at the folds. The horn is also shown in Fig. 2·27. An additional bend between *A* and *B*, not shown in Fig. 2·28 appears in Fig. 2·27. This bend has no effect on the focusing properties of the horn and is intended only as a means of compacting the design and directing the energy toward the external reflector. The focal length of the primary reflecting fold is 10 ft.

This antenna, like all modern radar antennas, depends on the principle of reversibility. The focusing of energy from a distant point in space to a

point on the focal curve has been discussed. Reciprocally, a point source of radiation at any position on the focal curve will produce a beam of energy well focused in space. By moving this point source along the focal curve, it is possible to scan the beam.

There is in the flared section an equivalent line where the radiation may be considered to originate. This line lies at the focus of the cylindrical semiparabolic reflector, as required for a satisfactory vertical pattern. The plates are flared at the exit gap. The flare dimensions are chosen to match the horn to space and to illuminate properly the external reflector.

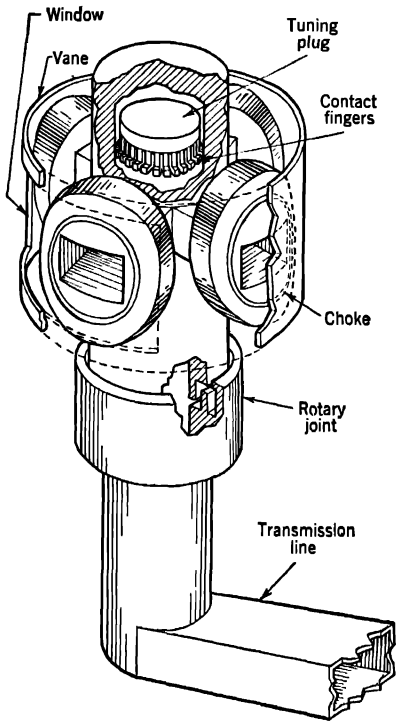

FIG. 2·29.—Phantom view of r-f switch.

The system is weatherproofed by a plastic closure of such dimensions that the reflections from the inner and outer surfaces cancel each other by destructive interference. The reflector is so disposed with respect to the flare section that no radiation is returned to the flare. Its presence, therefore, does not affect the match of the horn to space (see Fig. 2·27).

The Feed and Data System.—Fortunately, the focal curve may be approximated by a circular arc. The feed can thus be moved along this arc by rotation about a fixed axis. To reduce the fatigue of the operator, resulting from flicker of the scope, and to make the display as nearly continuous as may be practical, it is desirable to use a rapid rate of scan. An oscillating feed or a Robinson feed may be employed, but actually a four-arm steadily rotating feed is used, as illustrated in Fig. 2·29. An r-f switch is provided to direct the energy from the waveguide transmission line into whichever of the four rotating arms is momentarily looking into the edge D of the space between the parallel plates shown in Figs. 2·28 and 2·27. Figure 2·29, revealing a part of the switch, shows a rotary joint similar to the one shown in Fig. 6·8 with the exception of the four waveguides that are attached to the rotor. A cylindrical vane at all times prevents radiation of energy into the arms that are not opposite

the window in the vane. The window subtends an arc somewhat exceeding 90°, and its proportions are designed for a good r-f match. It is possible to keep the magnetron operating at a constant frequency during switching by a single setting of the line-stretcher[1] between the magnetron and the feed.

The arms shown in Fig. 2·27 rotate as a unit with the r-f switch. Each in turn carries the r-f energy to the entrance of the horn proper. Just beyond the entrance to the horn is a reverse bend to ensure clearance of the horn structure by the arms during their travel in the cutoff condition. The arms are flared in the horizontal plane to afford good illumination of the horn and a good radiation pattern. They are also slightly flared in the vertical plane to improve the match to the horn. The r-f switch includes a tuning plug with spring fingers in the tube above the four radial arms. This plug or cup can be adjusted, thus making possible the use of the feed over a frequency range of 8740 to 9170 Mc/sec. The plane of polarization is vertical.

The r-f switch energizes consecutively the four arms, which produce four scans of the field of view per rotation of the switch. The data-transmission system is geared to run at 4-speed with respect to the feed unit in order to maintain the same relationship to each of the four arms. The data-transmission system also includes a photoelectric gate generator that blanks the radar indicator between successive scans while the feed is switching. On the same shaft there is a photoelectric pip generator used to develop fiducial angle marks. The data take-off is a special variable condenser that in series with a fixed capacitor, constitutes a voltage divider across a 1-Mc oscillator. The divider output is detected and amplified to produce the azimuth sweep on the indicator tube.

Construction in Plywood.—The horn, as discussed previously, is designed to approximate the optical performance of a pair of mirrors. One step in making this unit behave as designed is to construct the horn so that the metallic surfaces are spaced less than one-half wavelength apart. All propagating modes are then polarized perpendicularly to the surfaces and have a constant wavelength in the horn equal to the free-space wavelength. Half a wavelength is about $\frac{5}{8}$ in.; but in practice, manufacturing specifications call for spacing of $\frac{1}{4}$ in. with a tolerance of $+\frac{1}{4}$ and $-\frac{1}{8}$ in. The variation of spacing must be gradual in terms of quarter wavelengths. This requirement is met more or less automatically when plywood is used in the construction. The reduced spacing also improves the approximation involved when the geometry of the centered surface is used for the geometry of the horn. The nondevelopable surfaces are held to a tolerance of $\pm\frac{1}{32}$ in.

[1] A device for making slight adjustments in the effective length of the transmission line.

The antenna system must be stout enough to withstand 80-mph winds, small enough to fit in the space available, and light enough to reduce the moment of inertia as much as possible. In addition to these specifications, the material used must be carefully chosen on the basis of freedom from warpage over a long term of extreme climatic conditions, since any deflection from the specified contours of the antenna is immediately felt in the electrical performance of the entire system.

Experiments proved that plywood, with its large flat surface, is excellent because it is approximately 12.5 times as rigid as an equal weight in either sheet aluminum or sheet steel. The double-curved surfaces at the folds can be made by molding, but early samples of this process were not altogether satisfactory. It is also feasible to form these surfaces by routing a laminated structure. Either process gives better results than forming the double-curved surfaces of sheet metal, although sheet metal was used successfully on one model. Figure 2·30 is a vertical section through one of the folds. In constructing the inner member, the $\frac{1}{4}$-in. plywood sheets are bonded to the spacing ribs. The nose-piece is bonded in place, and the composite structure is cut by a shaper to the semicircular section shown. The proper Schwarzschild curvature is obtained by guiding the work with a template. Copper sheets 0.003 in. thick, cut to size, and tinned along the edges can be made to conform to the surface when laid in place and bonded with Bostic Precoat and Cement (manufactured by BB Chemical Company, Cambridge, Mass.). Each piece is readily deformed to cover one-half of a nondevelopable surface. A lap joint is then formed by soldering the copper along the meridian section. Precautions must be taken to avoid overheating and damaging the neighboring copper bond. The construction of the outer member is similar to that of the inner member, the backing of the nondevelopable surface being shaped to a template from members $\frac{5}{8}$-in. thick, built-up of $\frac{1}{8}$-in. laminates and bonded along the curved edge of the central sheet. Copper foil cut to shape is bonded in place on each member.

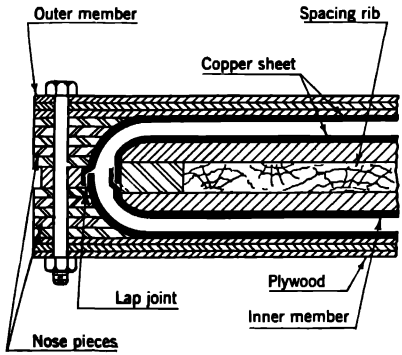

FIG. 2·30.—Vertical section through fold of Schwarzschild horn.

At the time of assembly, the inner and outer members are properly positioned by dowels in locating holes. Finishing strips are used to close the sides of the horn and tie the flat sheets together into a rigid unit.

The external reflector is built up from a series of plywood bulkheads

covered with a thin plywood skin, and the reflecting surface is formed by bonding copper to the parabolic cylindrical surface. Typical aircraft plywood construction is used throughout the construction of the horn, its supporting frame, and the plywood skin. All beams are box sections with plywood bulkheads and cutout lightening holes. The supporting frame, integral with the mounting yoke, is shown in Fig. 2·31. Several transverse ribs underneath the frame support the plywood skin. As illustrated in Fig. 2·27, the folded horn is bonded to several box members which run across the principal ring frame, thus making the horn an integral part of the structure that encloses it. The entire antenna unit is attached to its pedestal by means of a steel box-section frame bolted to the plywood yoke.

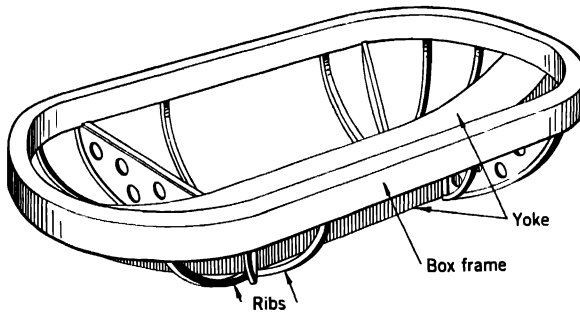

FIG. 2·31.—Plywood construction of the supporting frame and yoke of Schwarzschild antenna.

Weatherproofing the Plywood Structure.—All plywood laminations and nonlaminated pieces of stock used in the assembly are impregnated with or dipped in Celcure to increase their resistance to fungus, termites, and borers. All internal surfaces are painted with copper-flake paint and antifungus varnish.

To prevent water condensation in the antenna structure, an air-duct system fed by a heater and a blower is built into the set and circulates air through the entire antenna enclosure, with forced feed through the horn. While the system is in operation, the power dissipated by the feed motor, receiver, transmitter, and other components maintains the temperature of the enclosure a few degrees above the ambient temperature. When the set is not in operation, a thermostatic control on the heater system regulates the temperature of the enclosure.

MECHANICALLY SCANNING FEEDS

When a cyclic displacement is imparted to the entire antenna feed relative to the reflector in order to obtain a scanning beam of radiation, such a feed is called a *mechanically scanning feed.* Such feeds are

employed exclusively when a conical scan is desired. Either rotating or nutating feeds may be used for this purpose. At times, mechanically scanning feeds are also used to effect a scan oscillating through a small angle.

2·17. Rotating Feeds.—The azimuth and height of a single target can be accurately determined by tracking the target with a pencil beam. Tracking is usually accomplished by spinning the pencil beam so that it forms a conical scan of radiated energy in space, as shown in Fig. 2·32. If an echo received at the 0° reference point of the conical scan is of equal

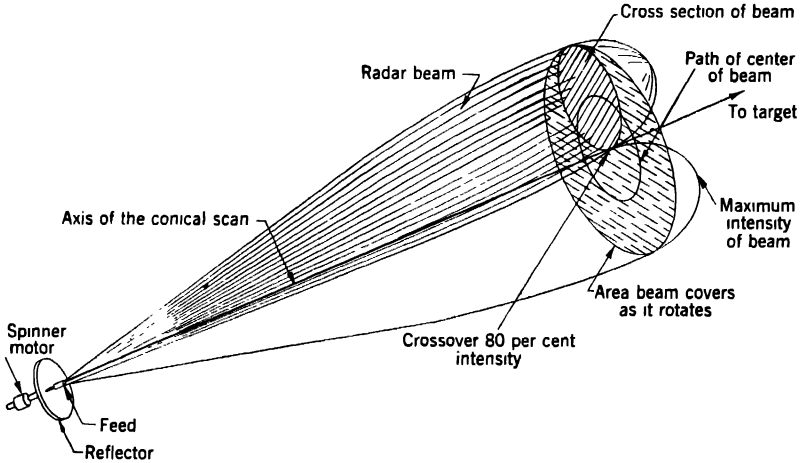

FIG. 2·32.—Conical scan. A section of the beam is illustrated at a point of crossover where the one-way power is 80 per cent of the maximum.

strength with the echo received at the 180° conical scan location, the target is centered on the antenna with respect to one reference plane. If, at the same time, equal echoes are received from the 90° and the 270° conical scan locations, the antenna as a whole is centered on the target. A reference generator is employed to pick off the signals received at the 0°, 90°, 180°, and 270° locations. To keep these signals equal in intensity, tracking can be accomplished by manual adjustment of a servomechanism or by automatic tracking such as that employed on gunlaying mounts. With this type of tracking, the antenna can be centered on a target with an accuracy limited only by the accuracy of servomechanisms on the azimuth and elevation axes.

A conical scan can be achieved by several combinations of feed or reflector rotations, although the majority of installations involve rotation of the feed alone. The usual speed of rotation for conical scanners is about 1800 rpm, which makes it impracticable to rotate paraboloids

that are over 2 ft in diameter. Except for some airborne scanners, therefore, fixed paraboloids and rotating feeds are characteristic of conically scanning antennas. The axis of rotation of the feed coincides with the axis of the paraboloid. At 1800 rpm, dynamic balance of rotating parts is essential. To minimize the mass that must be counterweighted, the offset of the beam can be obtained by a slight electrical unbalance of the dipole feed. Figure 2·33 illustrates such a rotating 10-cm dipole feed with an electrical offset used in the SCR-584 gunlaying antenna mount.[1]

The dipole feed is driven by a hollow-shaft direct-drive motor which eliminates all gearing and the accompanying problems of lubrication. In this unit the drive motor rotates at approximately 30 cps and is a three-phase 60-cycle 115-volt motor rated at $\frac{1}{6}$ hp. Mounted on the same hollow shaft is a reference generator that supplies two sine waves 90° out of phase that are the reference voltages for the elevation and azimuth servos. The stator of this generator must be readily adjustable for tracking alignment. This is easily accomplished by attaching a spur ring gear to the stator with an adjusting pinion mounted on a shaft that extends through the rear end bell. After being positioned, the adjusting shaft is held in place by a locknut.

The r-f requirements for this feed consist mainly of a high-speed rotating joint and proper seals for pressurization. The r-f transmission line is operated under a positive pressure of about 5 lb/in^2. To maintain pressure in the r-f line at the high-speed joint in the spinner motor, a special seal is provided. The seal consists of two superfinished steel rings spaced by a flat ring of carbon. One steel ring is fixed; the other is connected to a bellows which has an inner floating spring that takes up wear on the rubbing surfaces. The carbon-to-steel contacts require no lubrication.

Covering the dipole feed is a polystyrene cap furnishing necessary weather protection and allowing for proper pressurization of the line. Located at the end of the polystyrene cap is a bleeder cap to allow continuous flow of clean, dry air. To prevent r-f energy from reaching the front motor bearing, an r-f choke is located in the rear of the front end bell plate.

Because the mechanism rotates on the axis of the parabola at all times, necessary dynamic balancing is readily achieved. Dynamic unbalance of the rotating parts is held to within $\frac{1}{4}$ in.-oz. A special built-in motor concentric with the axis of rotation of the feed simplifies the drive mechanism but is not absolutely essential. Rotating feeds have been built with the motor mounted off-axis behind the reflector, driving the waveguide or rigid coaxial feed through a set of spur or helical gears.

[1] Sec. 9·12, *Radar System Engineering*, Vol. 1 of this series.

Mechanically offset feeds may take several forms. As the name implies, the radiating element is physically displaced from the axis of rotation. One arrangement (Fig. 3·8) utilizes a rotating bent waveguide of circular cross section. The emergent radiation is directed against a circular plate that is held stationary and normal to the axis of rotation and is reflected by this circular plate back into the main parabolic reflector. The coaxial lines may be bent to offset the dipole element, or the extension of the feed may coincide with the axis of rotation, and the dipole be offset by means of a short stub. Almost any type of simply terminated feed can be used for a mechanically offset arrangement.

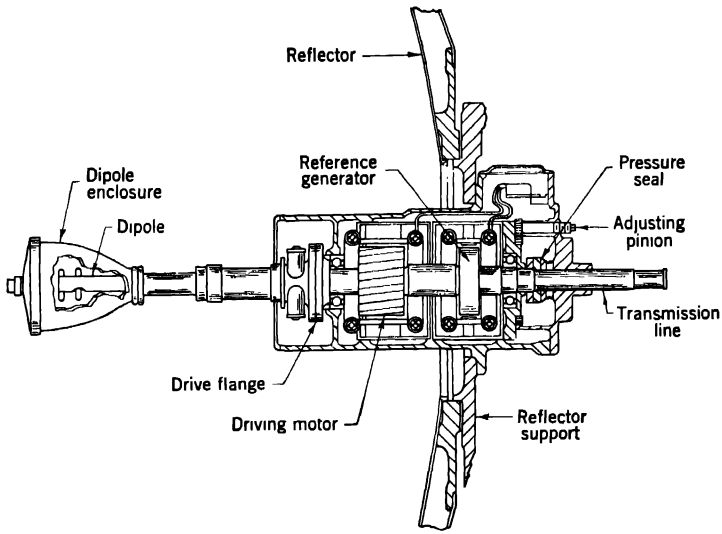

FIG. 2·33.—A rotating feed for the SCR-584.

2·18. Nutating Feeds.—If a dipole is used as the termination of the rotating feed, the simple rotating scan mechanism causes rotation of the plane of polarization of the emerging radiation, making this system unsuitable for some radar applications.

Nutating scanning feeds have the advantage of producing a constant (e.g., vertical) polarization; this allows better interrogation of radar beacons and affords a measure of protection against jamming by "window" or "chaff."[1] However, the mechanical complication of a nutating scan is considerable. Figure 2·34 presents as an example a nutating scan mechanism adapted for operation in the 3-cm band with a gunlaying radar set utilizing the SCR-584 pedestal.

[1] A generic term for material, such as metallized strips of paper, strewn from an airplane to produce spurious signals on indicator scopes.

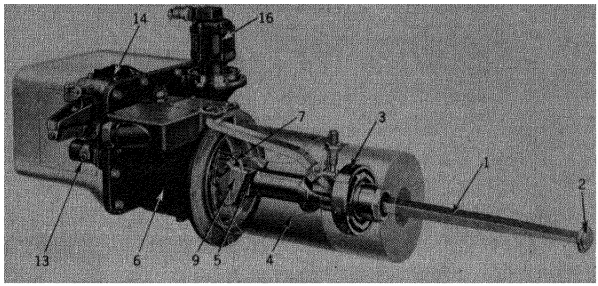

FIG. 2·34.—Nutating scan feed for the SCR-584. (*Courtesy of Palmer Bee Company.*)

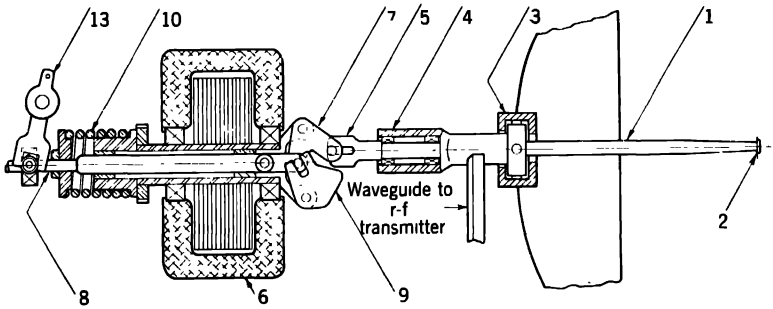

FIG. 2·35.—Schematic diagram of the nutating feed of Fig. 2·34.

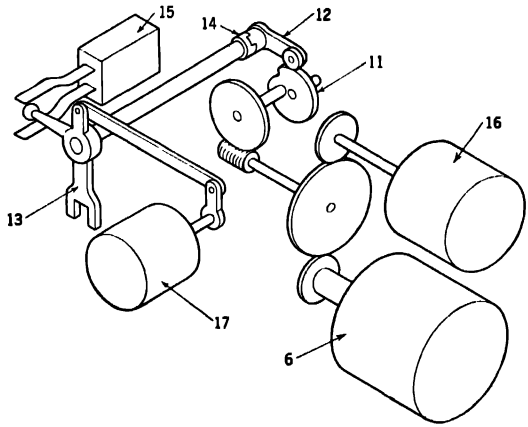

FIG. 2·36.—Cam mechanism of the nutating feed of Fig. 2·34. In Figs. 2·34, to 2·36: 1. Antenna waveguide. 2. Cutler feed. 3. Gimbal ring. 4. Antenna support. 5. Rotating crosshead shaft. 6. Three-phase hollow-shaft motor, $\frac{1}{6}$ hp. 7. Bell crank. 8. Pusher rod. 9. Counterweight. 10. Balancing spring. 11. Cam. 12. Cam follower. 13. Driving fork. 14. Solenoid operated clutch. 15. Timing switch. 16. Reference generator. 17. Synchro generator.

The 3-cm nutating scan mechanism illustrated is capable of three modes of scanning. These are

1. Conical scan, used for automatic following of the target. Nutation is about the axis of the parabolic reflector giving 0.8° crossover.
2. Spiral scan, used for finding targets. The mechanism nutates about the axis of the parabolic reflector and spirals from a 2° included tracking angle to a 12° included angle at 2 cps.
3. Palmer scan, used as another method of finding the target. The antenna feed continuously nutates about the axis of the parabolic reflector at the outer 12° included angle. The antenna mount moves either in azimuth or in elevation.

As seen in the preceding figure and in the schematic diagram (Fig. 2·35) the antenna waveguide (1), terminated by a Cutler feed (2), is mounted with its r-f wobble joint in a gimbal (3), fixed at the vertex of the parabolic reflector. The moving part of the wobble joint is attached to a hollow cylindrical support (4), carrying a rotary crosshead (5). A $\frac{1}{6}$-hp 1800-rpm hollow-shaft motor (6) drives a bell crank (7), linked to a reciprocating push-rod (8). As the bell crank oscillates, it deflects the support (4) together with the feed, back and forth with respect to the axis of rotation, causing the feed to nutate with a spiral scan. A moving counterweight (9) is linked with the bell crank to maintain the dynamic balance of the system. The resultant centrifugal force is balanced by the spring (10). The reciprocating push rod (8), which thus controls the angle between the antenna feed and the axis of the reflector, is positioned by a cam mechanism shown schematically in Fig. 2·36. A cam (11), geared through a spur and worm gear reduction to the feed-driving motor, actuates a cam follower (12), which in turn moves the driving fork (13), engaging the push rod (8). A solenoid-operated clutch (14) and a double contact switch (15) permit disengaging the fork (13) from the push rod (8), at the same time locking it in either of two positions: (1) providing a conical scan with 2° included angle for tracking or (2) providing a conical scan of 12° included angle which, in combination with the motion of the antenna mount, provides the Palmer search scan of the radar set.

A two-phase reference generator (16), geared 1/1 with the driving motor, provides reference voltage for automatic tracking by the antenna. A synchro generator driven through a linkage from the cam follower provides a reference voltage for indicating the angular position of the antenna feed.

In order to minimize the dynamic forces and reduce the size of the counterweight, the antenna feed (1) was made from a precision casting

of aluminum. A satisfactory light (0.020-gauge) fabricated stainless steel waveguide with an aluminum Cutler feed has also been used.

Other methods of obtaining conical scan by mechanical means as employed in some airborne scanners are outlined in Sec. 6·9.

2·19. Oscillating Feeds.—The generation of an oscillating scan by reciprocating the feed gives rise to two problems. The first is the electrical problem of obtaining adequate scanning amplitude without excessive distortion of the beam. The second is the mechanical problem of reciprocating the feed at a rapid rate.

It has been found experimentally that a point feed such as a horn feed or a dipole feed in a paraboloidal reflector can be displaced approximately four beamwidths from the axis before the pattern distortion becomes objectionable. Greater scanning amplitudes than this can be obtained by modifying the shape of the reflector to reduce the aberrations and distortions caused by the displacement of the feed from the focus. This approach has been investigated by means of the theory of geometrical optics, and an antenna has been built by Bell Telephone Laboratories with a 0.7° beamwidth that can be shifted ±25° without undue distortion.[1] Difficulties in fabrication resulting from requirement of the more complicated reflector surfaces have prevented widespread development along these lines.

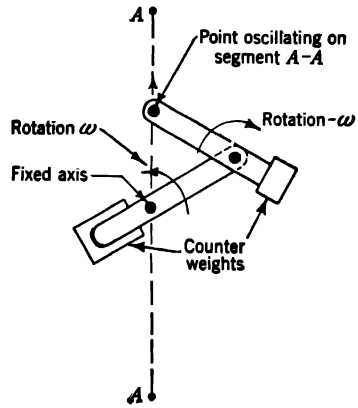

FIG. 2·37.—Diagram of experimental trammel mechanism.

The mechanical problem involved in designing reciprocating feeds has three aspects. The first is the problem of generating the motion, and the second is the problem of dynamic balancing. The third is both an electrical and a mechanical problem and concerns the transmission of r-f energy to the feed.

Although simple harmonic motion is not the best motion for producing desired electrical effects, it is the easiest to generate mechanically. Consequently, it is almost always the motion used in mechanically oscillated feeds. The four-bar linkage (including the crank and connecting rod) and the trammel linkage are perhaps the most common methods of generating this motion either accurately or approximately. The trammel

[1] "Use of Geometrical Optical Theory in Design of Mirror Shapes for Scanning Aerials," CSIR4662 Australian, Feb. 28, 1945; C. B. Feldman, "Rapid Scanning Radars," Bell Telephone Laboratories MM-42-160-151, Dec. 4, 1942.

linkage gives linear simple harmonic motion and is easy to balance dynamically. It is therefore a useful mechanism to employ to reciprocate a point feed on a straight line. Figure 2·37 schematically illustrates this linkage, which has been employed on an experimental system[1] of the Bell Telephone Laboratories. The method of mechanical resonance described in Sec. 6·12 may be cited in this connection.

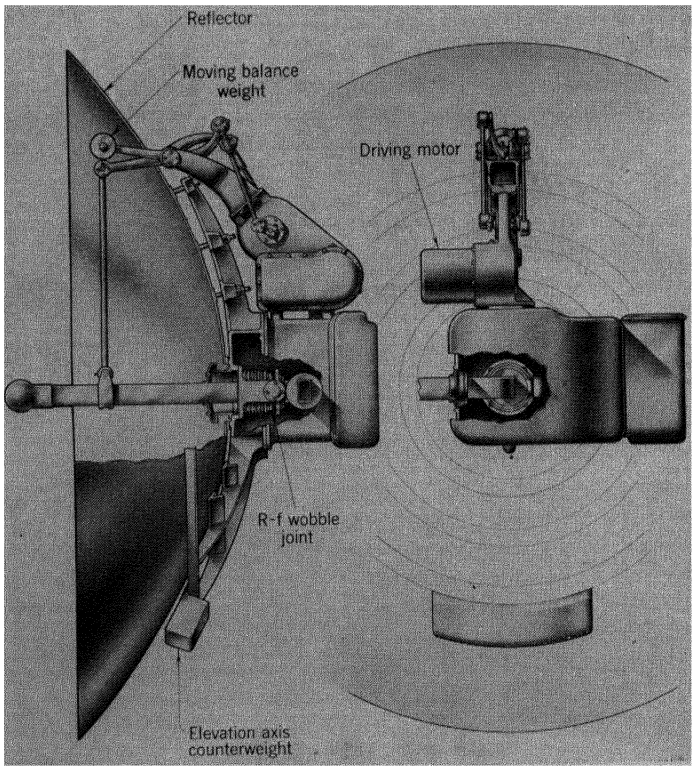

FIG. 2·38.—Oscillating feed assembly.

The dynamic balancing of crank and connecting rods has been extensively treated,[2] and the balancing of four-bar linkages may be treated in the same way. It need only be noted that in a four-bar linkage the oscillating link should be so proportioned that the system behaves as though all the mass of that link is concentrated at its junction with the end of the connecting rod. In practice this means that the connecting rod should be attached at the center of percussion of the oscil-

[1] Bell Telephone Laboratories MM-42-160-106, Sept. 4, 1942.

[2] Den Hartog, *Mechanical Vibrations*, McGraw-Hill, New York, 1940.

lating link. The oscillating feed in Fig. 2·38 consists of a 3- or 4-ft section of waveguide terminated in a double dipole feed that is balanced as described and is reciprocated with a crank and connecting rod.

The problem of transmitting the r-f energy to the feed is solved fairly easily when the feed is at the end of a long section of oscillating waveguide and when the angle of oscillation is small ($\pm 5°$ to $\pm 10°$). This requires an r-f wobble joint. If the angle of oscillation is larger, then either a rotary joint or a multiple wobble joint can be used. If the path of the feed must be linear, the design becomes more complicated and it is probable that more than one rotary r-f joint would be required.

CHAPTER 3

GROUND ANTENNA MOUNTS

By D. D. Jacobus

The shipborne or airborne antenna mount is a fixed installation on the ship or aircraft. The ground antenna mount, however, is ordinarily not permanently installed. If the mount is small, it can be truck-mounted to provide mobility. If it is large, means for its rapid assembly and disassembly are generally provided. Ground equipment must be built to withstand the rough handling and the exposure encountered in field service. These mounts may be broadly classified according to the function of the radar, as simple search and early-warning or height-finding; some are versatile and perform both of these functions.

SIMPLE SEARCH MOUNTS

The simple search ground antenna mount consists of an antenna and a supporting pedestal that provides azimuth rotation. A manually rotated turntable carrying a simple sighting device constitutes a primitive search set. With such a device, the direction of an observed echo can be noted by viewing the azimuth orientation of the mount. The limitations of visually determining the position of a mount at the precise moment of a signal return are too obvious to require elaboration. The ground antenna mount must therefore include a mechanism, either mechanical or electrical, for suitably displaying the azimuth position of each radar signal.

3·1. Scanning Requirements.—Some search equipments employ antenna systems that radiate "pencil" beams. A pencil beam can view all portions of the sky if the beam is gradually elevated (or lowered) while rotation is in progress. For full coverage, the ascending or descending spirals should not be spaced farther apart than the width of the beam of radiated energy. This process is tedious and, where attempted, has been found to be inadequate because of the time required for successive scanning cycles. In practice, the pencil beam is usually limited to search at the level of the horizon. On the other hand, a radiation pattern narrow in azimuth but of wide vertical extent permits search of a broad section of the sky by simple rotation. The search and early-warning antennas that will be discussed are all of this type.

The accuracies required of the data-transmitting system can be appreciated by consideration of a specific example, such as a reflector

with a 25-ft horizontal by 10-ft vertical projected aperture that operates on 10-cm radiation to produce a beam of reflected energy 0.8° wide. On a PPI(plan position indicator) display tube, the returned signal will have a length corresponding to approximately 0.8° of arc. The center of the visual signal that is displayed can be estimated with an accuracy of, at best, 1 part in 10, which represents 5 min of arc. Hence, our azimuth information, if these data are to be as good as the best that the eye can read, must be accurate to 5 min of arc. This accuracy, on a target viewed at 100 miles, represents an error in azimuth orientation of 250 yd. A mapping accuracy of this order at such extended range is, indeed, adequate for purposes of search and early warning and, in fact, represents the highest precision demanded of current search systems.

The PPI display tube is now almost universally used on ground systems to record the azimuth location of the antenna. The deflection coil in the PPI display tube is rotated in synchronism with the antenna, and the signals recorded on the face of the tube form a map of the surrounding area. The motion of the deflection coil is secured by means of synchronous electrical circuits between the rotating antenna and the rotating deflection coil. The most commonly used data-transmission system employs a synchro generator on the mount, mechanically linked to the rotating antenna. The generator is coupled electrically to a remotely located synchro control transformer, which in turn is geared to the servomotor that drives the deflection coil on the indicator display tube. A servoamplifier is used to control the rotation of the motor that drives the deflection coil. The *error voltages* in the circuit linking the synchro generator and the synchro control transformer are maintained at minimum values. The synchro generator on the antenna mount, in addition to keeping one or more PPI display tubes in phase, may at the same time be employed to energize a servomechanism for the control of the motor that drives the antenna mount.

Scanning may be accomplished by continuous rotation through 360° of horizon or by sweeping back and forth over a finite sector to secure more adequate coverage of a limited area. The motor drive and the gear trains of sector-scanning equipment must have power and torque characteristics adequate for reversing the motion of the antenna in the desired cyclic interval of time.

If a beam of radiation is swept rapidly past a target, the signal may be weaker than that which would be secured if the same target were viewed for a longer period of time. This diminution of signal strength is termed a "scanning loss." The maximum rapidity with which a beam can be swept past a target without incurring too high scanning losses is described in Sec. 3·4. In normal search equipment, the scanning losses are relatively low.

3·2. Component Parts.—An antenna mount cannot be designed until the position of the r-f components is determined. The following electronic or r-f components are sometimes located directly on the rotating portion of the antenna mount, or they may be located in an adjacent locality with provision for transmission of r-f energy to the antenna feed. The mechanism used to generate the pulse power is called the modulator. This pulse power, at a typical potential of 6000 volts, is conducted to a pulse transformer, where the potential may be raised to a typical value of 20,000 volts. The 20,000-volt pulse power then excites a magnetron that generates r-f radiation. Either a waveguide conductor or a coaxial conductor serves to carry this r-f radiation to an antenna feed, generally located at the focal point of the reflector. The return signal passes through the waveguide or coaxial conductor in the reverse direction of the generated signal and is deflected by the duplexer into the mixer, which is a part of the receiver. When it reaches the mixer, this r-f current, which may have a frequency of 3000-Mc/sec, is converted to a current having an intermediate frequency of perhaps 30-Mc/sec. In the same receiver, a second conversion reduces the currents to video currents of frequency spread 0 to 2-Mc/sec, which directly represent the echo intensity.

Blowers are needed to cool the magnetron, the pulse transformer, and the receiver. Of these three units, the magnetron requires the greatest amount of cooling.

From the standpoint of the antenna mount, our interest in these components is centered on the various frequencies of the currents that represent the returned signals. Currents of frequencies as high as 3 Mc/sec can be transmitted along a shielded wire and through standard slip rings without distortion. At the intermediate frequency of 30 Mc/sec, a coaxial cable is required. Therefore, if the receiver is placed on the rotating portion of an antenna mount, shielded wires and ordinary slip rings can be used to transmit the video signals to the display tube. A similar location for the r-f transmitter will also eliminate the necessity of an incoming r-f power transmission line.

An antenna mount can be classified as being in one of the following three categories, according to the position of the r-f components.

1. Modulator, transmitter, and receiver components are all on the rotating portion of the pedestal. With this arrangement, only conventional wiring is required through the torque tube of the azimuth axis. Neither a pulse rotating joint nor an r-f rotating joint is required.
2. The modulator is remotely located, and the transmitting and receiving r-f equipment are on the rotating portion of the pedestal. With this arrangement, no r-f waveguide is required through the torque

tube, but a high-voltage pulse rotary joint is required. The pulse rotary joint is a relatively simple device, requiring good contact between a set of brushes and a slip ring, with adequate insulation against potentials of about 6000 volts. The slip ring of the pulse joint is generally made of stainless steel. Tests have indicated that pulsed, high-voltage currents tend to pit silver or copper more readily than stainless steel. Brushes have been fabricated by the powder metallurgy technique of a 90 per cent silver, 10 per cent graphite mixture. A large number of small brushes are more effective than a single brush of equal total area.

3. No r-f generating and receiving equipment is located on the rotating portion of the pedestal. This arrangement requires an r-f transmission line through the center of the torque tube; the r-f rotary joint is generally located at the base of the torque tube. Figures 3·1 and 6·8 are characteristic drawings of two distinct types of r-f rotary joints. Figure 3·1 illustrates the "doorknob" coaxial type, and Fig. 6·8 shows the E_0-mode type.

Of the three arrangements discussed, the first or the second arrangement is used when a multiplicity of r-f systems is installed on an individual mount. On ground equipment it has become customary to carry the r-f transmitting and receiving components on the rotating portion of the mount in order to reduce the losses in the r-f transmission line. The remote location of the r-f components is usual on the shipborne antenna mounts, where access to the antenna is difficult.

Figure 3·2 illustrates the elements of a simple search antenna mount. The figure is diagrammatic; gear trains are represented as a single set of spur gears, and all retaining shoulders, locking devices, and structural details have been omitted from the diagram. The system used as an illustration is one where the r-f transmitting and receiving equipment is on the mount and where the azimuth axis is of the torque tube type. It is obvious that mounts may take a great multiplicity of forms, but this illustration will be an aid in clarifying the following discussion. As used in this discussion, *A*, *B*, *C*, etc., refer to similar notations on Fig. 3·2. The components are discussed in the order in which they might advantageously be considered in designing an antenna mount.

A. R-f Package.—The rectangle shown in Fig. 3·2 represents the r-f package, or r-f head, a waterproof enclosure containing the r-f transmitting and part of the receiving equipment. A junction box is usually installed between the r-f package and the mount so that the r-f package may be removed and another substituted by the simple procedure of disconnecting and reconnecting the wires to the electrical equipment.

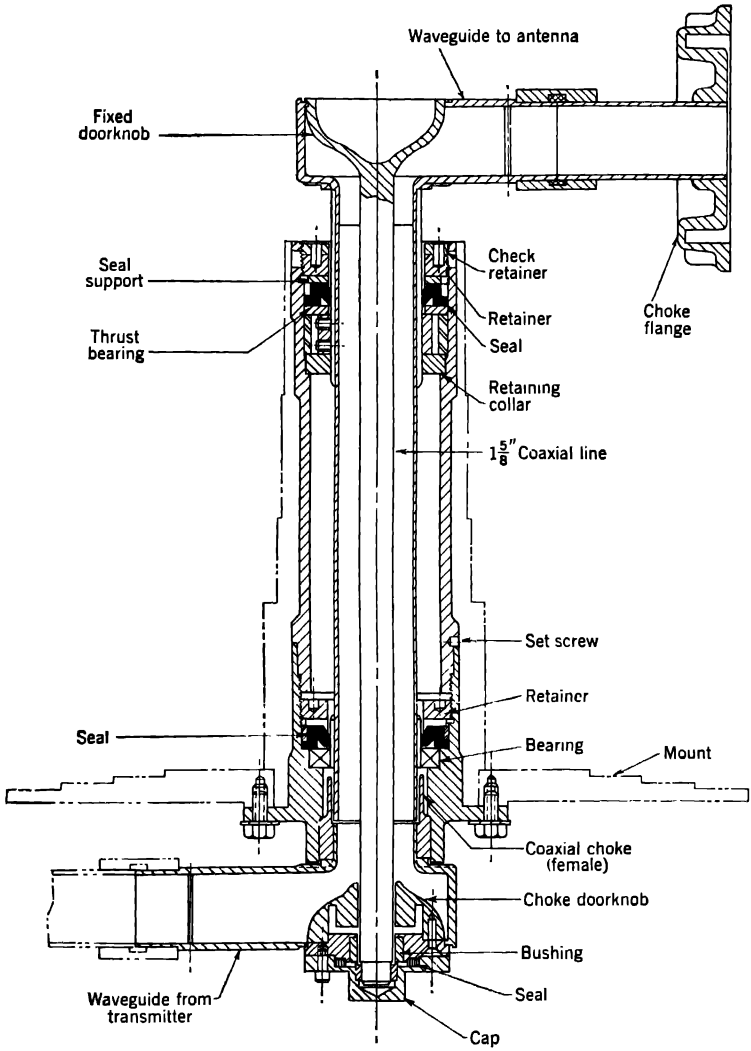

FIG. 3·1.—R-f rotary joint ("doorknob" type).

Figure 3·2 does not show this junction box, which for purposes of discussion can be considered a separable part of the r-f package.

B. Rotary Joint.—A rotary joint suitable for transmission of pulsed power at a potential of approximately 6000 volts is shown in outline in Fig. 3·2. If the r-f package did not rotate with the antenna, an r-f rotary joint of the type shown in either Figs. 3·1 or 6·8 would be used in

conjunction with an r-f transmission line. In either event, the azimuth torque tube *C* must have an internal bore of diameter sufficient to accommodate the type of rotary joint that is used. It is common practice to fasten one portion of the rotary joint rigidly to the bull gear at the base of

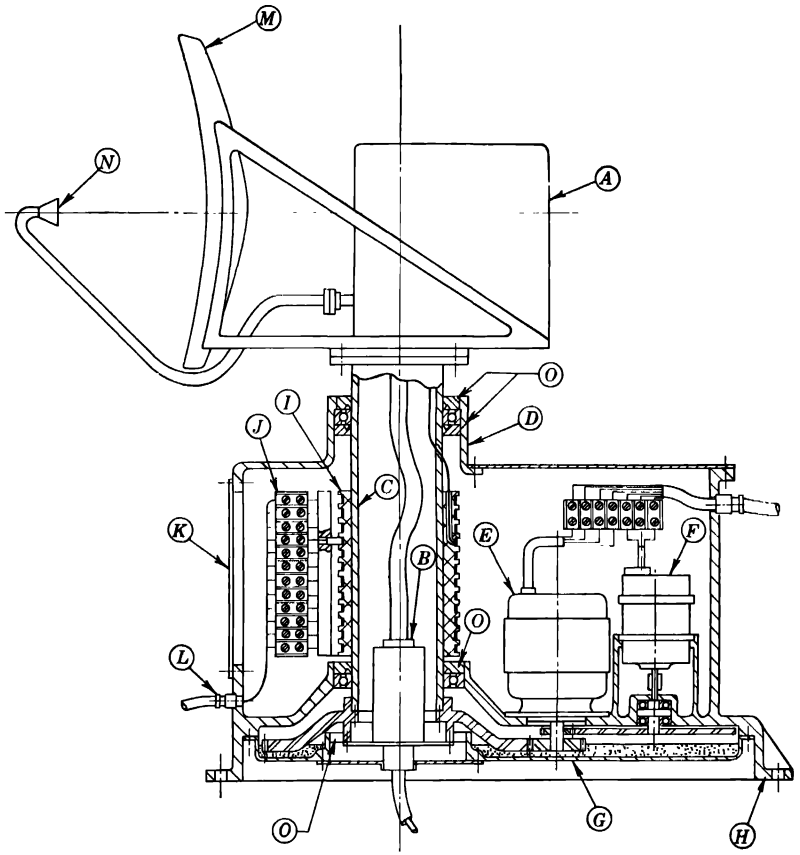

FIG. 3·2.— Schematic diagram of an antenna mount. *A*, R-f package; *B*, rotary joint; *C*, torque tube; *D*, azimuth housing; *E*, motor drive; *F*, synchro drive; *G*, gear case; *H*, footing; *I*, slip-ring assembly; *J*, brush terminal block; *K*, access door; *L*, stuffing gland; *M*, reflector and supports; *N*, antenna feed; *O*, oil seal.

the torque tube and to clamp the concentric rotating member on a device that is made fast to the gear case. This leaves the electrical conductor or the r-f transmission line free of strain. It is also worth noting that the electrical connector at the end of the high-voltage pulse line is of a special type requiring careful assembly. The entire passage between the pulse power terminal on the r-f package *A* and the access space at the base of

the torque tube C should therefore be made large enough in diameter to permit the free passage of the connector that terminates the pulse power cable.

C. Azimuth Torque Tube.—Figure 3·2 illustrates the use of a torque tube that is mounted between two sets of ball or roller bearings. This very common type of construction has the virtue of compactness. It also permits the construction of an enclosed gear box and provides space for inclusion of a slip-ring assembly I between the bearing supports. A roller-track bearing race may be employed as an alternate method of providing azimuth rotation. With the roller track, vertical stability is secured by using a bearing race of large diameter. This alternate method of construction requires the same essential elements as those illustrated in FIG. 3·2, but the physical appearance of the antenna mount is considerably altered. Examples of mounts on roller-track bearing races are the AN/TPS-10 mount, which employs a 30-in. roller-track bearing race weighing 65 lb (Sec. 3·6), and the mount of the V-beam radar, which employs a circular track with rotating two-wheel trucks weighing 2500 lb (Sec. 3·5).

D. Azimuth Housing.—The azimuth housing must support the azimuth bearings, the drive motor E, the synchro generator F, the gear case G, and the footings H. The slip-ring assembly I is generally mounted on the torque tube in a manner that will permit its being retracted for repairs. To make this possible, the inside diameter of the lower bearing supports is larger than the outside diameter of the slip-ring assembly. The motor and the synchro supports must be very accurately bored to maintain the proper gear centers. The housing must also support a terminal block J to hold the brushes that will contact the slip rings. The terminal tube L contains a stuffing gland that acts as a water seal around the entering electrical cable. The access panel K is large enough to permit the installation of electrical wiring and the periodic cleaning of the slip rings.

E. Motor Drive.—The gearing between the motor and the torque tube should be suitable for continuous 24-hr operation over long periods of time. The selection of a suitable motor requires no special treatment except in those cases where sector scanning or tracking is involved. Sector scanning necessitates rotating the mount backward and forward over a small portion of the horizon to secure more adequate coverage over a limited area. If tracking is desired, push-button control of the motor is highly unsatisfactory. Adequate tracking of a target requires a servomechanism that, controlled either manually or by the radar signal itself, can accurately control the rotation of the motor. Servomotors are ordinarily controlled in a manner that will permit the motor to develop 2.5 to 5 times the full-load rated torque when acceleration of the

mount is required. In selecting a motor, the maximum number of reversals that are required in a given period of time must be known in order that the rated horsepower loading will not be exceeded.

F. Synchro Drive.—A single synchro *F*, geared directly to the motor shaft, is shown in Fig. 3·2. The servomechanism that controls the motor drive is affected by the relative displacement of the drive motor *E* and the synchro *F*. Any play in the gear train between the drive motor and the synchro generator may be accentuated by the control system to produce "jitter." It is therefore essential that the gears be accurate and that the backlash between the servo-controlled motor and the associated synchro be reduced to a minimum. The following table records the tolerances that are considered acceptable for synchro gearing.

TABLE 3·1.—SYNCHRO GEAR SPECIFICATIONS

Item	Tolerances, in.	Remarks
Outside diameter	+0.000, −0.001	
Concentricity of OD with bore	0.001	Total indicator reading
Bore diameter	+0.0000, −0.0002	Hold to small side of tolerance
Taper of bore	0.0001 in 1.000 of length; not to exceed 0.0002 regardless of length	Must not be bell-mouthed
Finish of bore	F4	Must be smooth
Concavity of face of gear blank.	0.0002 per 1.000; not to exceed 0.0015 total	Mounting surface
Convexity of face of gear blank	0.0000	None allowed
Finishes of face of gear blank	F4	Must be smooth
Lateral runout	0.00025 at 1.000 radius; not to exceed 0.001 at 3½-in. radius	Total indicator reading
Pitch diameter runout	0.001	Total indicator reading

The unit static accuracy of a size 1G synchro generator is 1.5° maximum and 0.5° average, and that of a 5G and of larger sizes is 0.6° maximum and 0.2° average. The unit static accuracy of a size 1CT control transformer is 0.6° maximum and 0.2° average, and that of a size 5CT control transformer is 0.3° maximum and 0.1° average. These errors are inherent in the synchro units as such. It is therefore obvious that any data transmission by a single synchro generator traveling at the speed of the antenna is inadequate where high accuracy is required. Hence, a synchro generator is driven at some multiple of the speed of rotation of the antenna, often at 36-speed. The 1-speed synchro is retained to

record the absolute position of the antenna, and the 36-speed synchro controls the precise setting of the remote servomechanism (*cf.* Sec. 1·8).

G. Gear Case.—The gear case should be designed so that no joints or oil seals are below the oil level. The area below the central section of the torque tube must be left open to permit insertion of the rotary joint *B*. Suitable clamping devices for rotating the joint *B* must also be provided.

H. Footings.—The footings shown in Fig. 3·2 are suitable if the antenna mount is to be bolted onto a firm support. The illustrations in the latter portions of this chapter show the wide variety of footings that are used on ground antenna mounts.

I. Slip-ring Assembly.—The slip-ring assembly may be of the cylindrical type illustrated, or it may be of the concentric "pancake" type that is commonly used with searchlight equipment. The pancake type is more readily applicable where azimuth rotation is secured by means of a roller-track assembly.

Brushes are fabricated by the powder metallurgy technique of silver-graphite or copper-graphite mixtures. Silver is almost universally employed as the surface material of the ring. Small rings are often made entirely of silver, but larger rings have a silver band sweated onto a brass liner. The rings are spaced on molded plastic. Integrally molded slip-ring assemblies can be secured.[1] The use of individual annular spacers of molded plastic is more common, however; the slip-ring assembly is built up of the individual insulators interspaced with the silver rings. A stack built up in this manner is held together with rods that run longitudinally through the entire insulating pile. Grooves are provided through the stack of plastic insulators to permit the insertion of wires. A wire is generally soft-soldered to a stud on the inner diameter of each ring before the ring is assembled in the stack. After complete assembly of the stack of rings and insulators, the free ends of the wires are attached to suitable terminal boards.

Spare slip rings should always be provided in order to obviate the necessity of taking apart the slip-ring assembly in case of failure in any one of the circuits and also to anticipate possible future requirements for additional electrical units on the rotating part of the mount. In Fig. 3·2 the entire slip-ring assembly can be removed from the pedestal in the following manner: Remove the gear box *G*, the bull gear, and the lower bearing; disconnect the electrical leads from the slip rings at the upper terminal box; then withdraw the entire slip-ring assembly from the torque tube.

It is essential that slip rings carrying video currents be adequately shielded to prevent distortion of the signal information. This is usually

[1] Plastic Manufacturers, Inc., Stamford, Conn.

accomplished by providing a ground ring on each side of a ring that carries a video current. All wires carrying video currents are ordinarily shielded throughout their entire length, and this shielding is grounded to the pedestal.

J. Brush Terminal Block.—The brush terminal block *J* holds the slip-ring brushes in place. Each brush is accurately aligned with the center of the contacting ring. The screws that retain these brushes preferably should not be the same screws that hold the wiring in place. When a circuit is tested, a wire is often disconnected at the brush block, and it is desirable to do this operation without disturbing the brush setting.

K. Access Door.—This door should be large enough to permit installing the electrical wiring. It should also allow access for cleaning the slip rings at periodic intervals.

L. Stuffing Gland.—All cables entering waterproof enclosures pass through watertight seals of the type illustrated.

M. Antenna Reflector and Supports.—The antenna support *M* should combine a maximum of strength and rigidity with a minimum of weight. Rigidity is of particular importance if the antenna is to be sector-scanned.

N. Antenna Feed.—The r-f feed must be very rigidly supported, since any motion of this element will appear as an oscillating signal on the face of the display tube. If possible, the supports should be located outside the primary radiation pattern. This can usually be accomplished by diagonal braces that do not cross between the mouth of the feed and central portion of the reflector.

The foregoing general considerations can be applied to the design of shipborne antenna mounts, and the general aspects of shipborne mounts as outlined in Secs. 5·6 to 5·8 are, to a great extent, also applicable to the similar ground equipment.

3·3. Characteristics of Specific Mounts.—The characteristics of two widely different search and early-warning systems will be described. AN/TPS-1 is a portable lightweight set. It weighs approximately 2500 lb when packed for shipment and has a rather limited traffic-handling capacity. The other, a large ground-based radar is transportable by truck, weighs approximately 110 tons when packed for export shipment, and has a very long range and an enormous traffic-handling capacity. The latter is achieved by using separate PPI display tubes to cover limited sections of the horizon, with an operator assigned to each display tube. The information received from the separate operators is correlated on a large plotting board.

AN/TPS-1 Antenna Mount.—This search and early-warning set is shown in Fig. 3·3. Operating at about 25-cm wavelength, this mount produces a beam about 3° in width. The set is described in this section because of the unique nature of the antenna mount. The 200-mile range

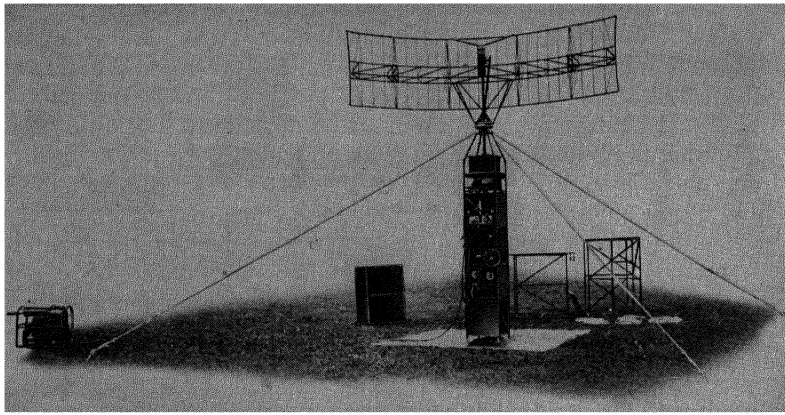

FIG. 3·3.—AN/TPS-1 antenna mount without shelter. (*Courtesy of Bell Telephone Laboratories.*)

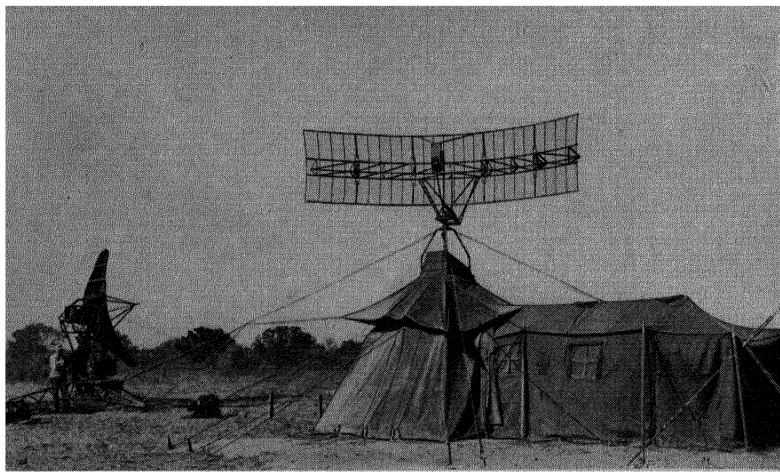

—**General** view of GCI station using AN/TPS-1 for search and AN/TPS-10 for height-finding. (*Courtesy of U.S. Army.*)

represents the limit at which targets can be viewed and is not a calibrated figure of the visibility of a specific plane. Portability has been a prime consideration in the design of all of the components. The set has been advantageously used in combination with the 3-cm AN/TPS-10 portable height-finder, as is illustrated in Fig. 3·4.

The antenna is a paraboloid grill of $\frac{1}{2}$-in. wire mesh 15 ft wide and 4 ft high, built in eight parts joined together by screw couplings and cowl

fasteners. The antenna can be rotated in either direction, by hand or by a motor acting through a belt and gear train. The motor is $\frac{1}{6}$ hp and operates at 1750 rpm on 27-volts direct current; it is shunt-wound, totally enclosed, externally fan cooled, and controlled from switches located at the indicator panel. Continuous rotation by motor is at a constant speed of about 6 rpm. When operated by hand, the motor can be uncoupled by means of a magnetic clutch. The handwheel is never uncoupled and at all times rotates with the motion of the antenna.

A 400-cycle synchro generator is geared to the antenna-torque tube at a speed ratio of 24/1. The synchro generator actuates a synchro motor at the deflection coil of a PPI display tube. A 60-cycle synchro generator at a speed ratio of 1/1 is also provided on the mount for the operation of remote PPI display tubes.

All of the components, both mechanical and electrical, are contained in waterproof cases that fit together to form a tower which serves as a support for the antenna. The separable portions of the tower, reading from the ground level upward, are shown in Table 3·2.

TABLE 3·2. AN/TPS-1 COMPONENTS

Tower section	Item	Weight, lb
1	Modulator	240
2	Indicator	207
3	Receiver, test equipment, manual drive	145
4	R-f transmitter	205
5	Antenna drive unit	195
	Antenna	185
		Total 1177

Microwave Ground Radar Antenna Mount.—This search and early-warning set is shown in Fig. 3·5. The radiation wavelength is in the 10-cm band. The antenna is rotated continuously at 1, 2, or 4 rpm. Echoes from large planes can be detected out to horizon range. The minimum height at which a plane can be viewed is thus a function of the curvature of the earth—a plane at 170 miles is not visible at elevations lower than 15,000 ft. Radiation from the set is in the form of two fan beams, each narrow in the horizontal and wide in the vertical sections. One beam covers the horizon and distant targets, is 3° high by 0.9° wide, and is centered approximately $1\frac{1}{2}$° above the horizon; the second beam covers high targets at close range, is approximately 30° high by 0.9° wide, and is centered approximately 15° above the horizon. The exact setting of both beams is conditioned by the character of the surrounding terrain and is fixed at the time of assembling. The set views all targets

within range once every revolution, with the result that an enormous amount of data is available if the set is located in an active area.

A single operator working with a single display tube would be unable to report all of the significant signals. The set therefore employs five separate PPI display tubes, one for 360° coverage and each of the remaining four covering a 90° sector of the horizon. These data are then correlated on a large plotting board in a room equipped to permit the

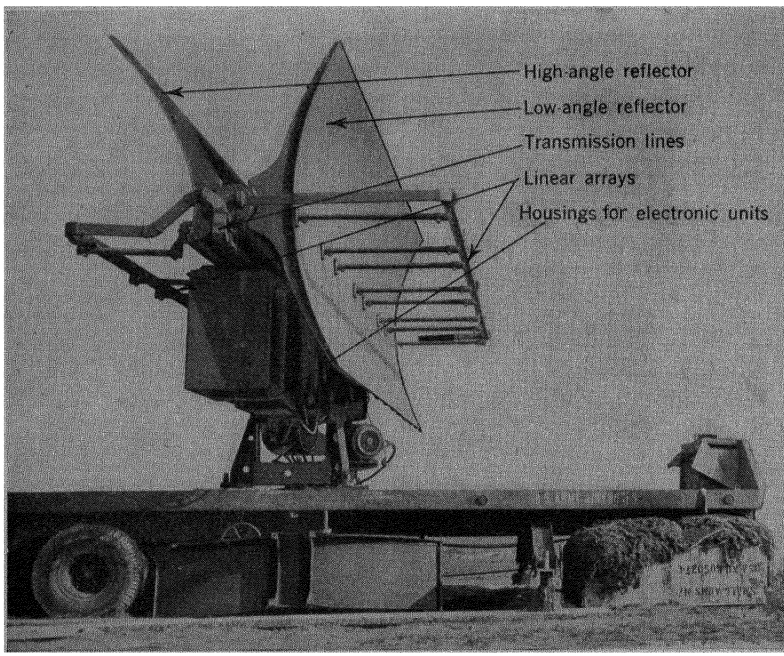

FIG. 3·5.—A ground radar antenna mount.

centralized control of all operations that are taking place within view of the set.

The modulator and two r-f transmitting and receiving components are carried on the rotating portion of the mount. Hence, all electrical currents can be transmitted through ordinary slip rings. The electrical equipment is built into individual waterproof boxes which are separately suspended from a cantilever beam as shown in Fig. 3·6. The same cantilever beam serves as a support for the two antennas. The low-angle beam is from a reflector 25 ft long by 8 ft high, and the high-angle beam from a reflector 25 ft long by 5 ft high. Both reflectors are parabolic cylinders mounted back to back. The reflectors are described in detail in Table 2·7 and the supplement thereto, Examples 1 and 2. The feeds

are linear arrays and are held in place by a series of tubular cantilever supports.

The entire superstructure, which consists essentially of the main cantilever supports and the equipment carried by these supports, is made fast to the top of the torque tube by means of a single cup-and-cone joint. Both sides of the central hub terminate in $15\frac{1}{2}$-in. diameter flanges that hold the ends of the main cantilever supports. An annular ring at the

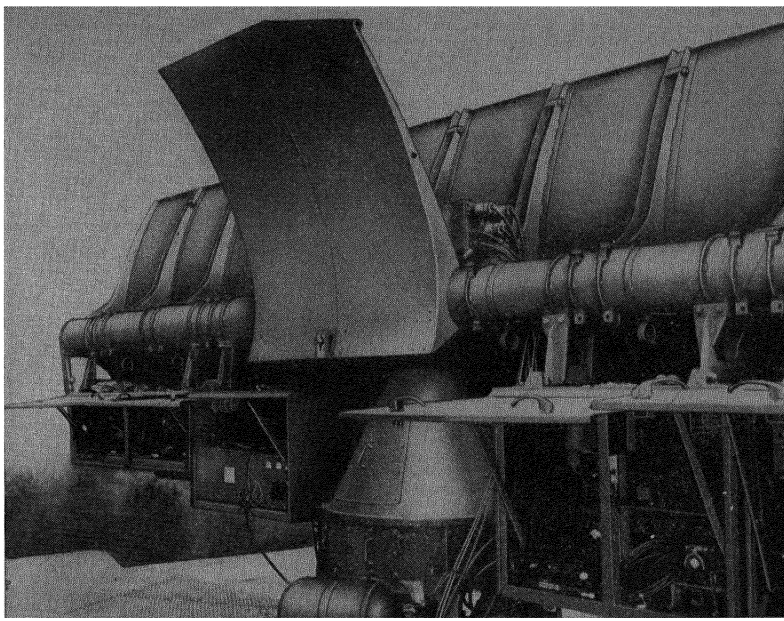

FIG. 3·6. Partially assembled antenna mount.

base of the hub seats against a flat shoulder, the two faces being pulled together by a disk that is bolted to the top of the torque tube. The wires from the slip rings pass upward through the center of the torque tube to a terminal box that is bolted directly to the top of the central hub.

The base, including the azimuth gear box, the motor drive, and the channels that form the supporting legs, is shown in Fig. 3·7. Bevel gears are used on the last reduction that drives the torque tube. For purposes of shipment, the gear box is made separable. Rotative power is supplied by a 3-hp 1760-rpm 208-volt three-phase 60-cycle totally enclosed fan-cooled motor. Data transmission is secured from a 1-speed 5G synchro and a 36-speed 5G synchro that are geared to the torque tube.

The weights of the separable portions of the antenna mount are shown in Table 3·3.

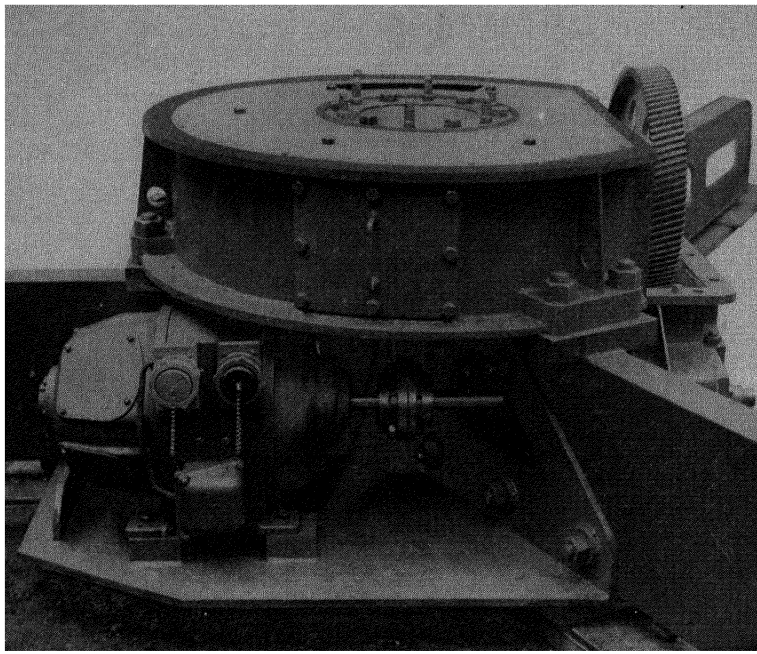

FIG. 3·7.—Base of the antenna mount, shown in Fig. 3·5.

TABLE 3·3.—WEIGHTS OF ANTENNA COMPONENTS

Item	Weight, lb
Footings (3 total)	600
Base and motor support	550
Motor and coupling	350
Lower gear box	200
Upper gear box	750
Torque tube, complete with slip-ring assembly, synchros, and cone shield	750
Central hub	100
Main cantilever supports (2 total)	900
Terminal box	70
8-ft reflector sections (11 total)	2,200
5-ft reflector sections (11 total)	1,650
Waveguide supports	100
Waveguide	300
Two r-f boxes complete with electrical equipment	1,800
One modulator complete with electrical equipment	900
Bolts, nuts, cables, etc	780
Total weight of the antenna mount	12,000

HEIGHT-FINDING

If an antenna reflects energy in the form of a fan beam having high vertical coverage, a signal from a high-flying plane can be identical with that received from a low-flying plane at the same range and azimuth position. When the antenna pattern is known, an estimate of height can be secured by observing at what range strong targets make their first appearance. This method is crude and at best has very serious limitations. Accurate height-finding is accomplished by the simultaneous measurement of range and elevation angle. One method involves direct tracking of a target with a conically scanning pencil beam on a two-axis mount. Another method employs the vertical oscillation of a beam of narrow vertical and wide horizontal dimensions and the simultaneous recording of the range and elevation angle of an echo from a specific target; a beam of this type is termed an "oscillating beavertail."

A third method, known as the "V-beam" system, employs a vertical plane of radiation and a plane of radiation slanted in space at an angle of 45°. These two planes bear a fixed relation to each other and are rotated in the azimuth plane around a common axis. Separate signal returns are received from the vertical beam and from the slant beam as the mount rotates. The angular displacement between the separate signals is coordinated with the range of the target to secure an accurate measure of height. The V-beam antenna mount employs this latter principle of height-finding.

3·4. Electrical Scanning.—A very rapidly oscillating beavertail scan is obtained by the use of any one of the electrical scanning feeds described in Secs. 2·15, 2·16, and 6·14. The rapidity with which the beam of radiation can be oscillated is limited by the necessity of securing an adequate r-f echo from the target. Microwave search sets have been built with pulse repetition rates ranging from 300 to 1200 cps, and high-resolution ultramicrowave systems for precision observation at short ranges may employ pulse repetition rates as high as 5000 cps. The time interval between successive pulses cannot be smaller than that required for the transmission of the r-f energy from antenna to target and its reflection, and hence a system of long range must employ a proportionately low pulse repetition rate. With the pulse repetition rate fixed by the foregoing considerations, the number of pulses of energy that are reflected from a target will be inversely proportional to the rate of scan. The reflection of a single pulse of energy can make itself apparent as an echo, but the image recorded on the display tube will be weak and unreliable unless a larger number of reflections are received. For example, the Robinson scanning mechanism is operated at a rate that will result in the reflection of about 10 energy impulses when the scanning beam sweeps past a target.

The elevation angle at which an echo is received is recorded by a data-transmission system that usually takes the form of a synchro generator geared to the moving portion of the electrical scanner. An electrical computer combines this datum with the simultaneously measured range to give a direct reading of the height of the target. The observed pip is made to appear on a display tube where the vertical coordinate represents range and the horizontal coordinate represents height.

Azimuth rotation should be at a rate that will allow some overlap between the patterns made by successive sweeps of the electrically scanning feed. A height-finder operated in this manner can also serve as a search set. The azimuth position of a target can be located with an accuracy no better than the width of the fan beam unless a separate search system is installed on the same antenna mount.

An important example of an electrically scanning height-finder is afforded by the ground control of approach, GCA, radar mentioned in Sec. 6·14.

3·5. Mechanical Scanning.—A beam wide in azimuth and narrow in its vertical aperture can be oscillated vertically by mechanical motion of the entire antenna. The inertia of the oscillating parts is too great to permit a rapidity of scan equal to that which can be secured with the electrical scanning feeds. As a result, mechanically oscillated beavertail scans must be rotated very slowly in azimuth if successive sweeps of the fan beam are to overlap. Hence, only a limited search coverage is provided or, at best, a search coverage that is slow. Sets of this type are therefore generally used in conjunction with a search set that is continuously rotated in azimuth, and targets in a limited portion of the horizon are viewed to determine their height. This operational procedure is more limited than that which can be secured either with the more rapid electrical scanners or with those of the V-beam type.

As stated in Sec. 2·17 the height of a single target can be obtained by tracking the target with a conically scanning antenna with a pencil beam. Height-finding methods other than direct-tracking are no more accurate than the display of the visual signal on the height-indicating tube. Antenna mounts, where extreme accuracy is required, universally employ tracking methods. On the other hand, the height-finding set that is limited to the tracking of a single target is severely handicapped if information on a multiplicity of targets is desired in a short interval of time.

Each of the antenna mounts described in the following portions of this section is an example of one of the three types of height-finder that employ mechanical scanning.

Two-axis Tracking Mount (SP-1M).—The SP-1M antenna mount is illustrated in Fig. 3·8. This mount operates in the 10-cm band. It can

be used for continuous search at any horizon level, or it can be used to determine height, range, and azimuth location of a single target.

The feed consists of a circular section of waveguide that is offset and is rotated at 1350 rpm to produce a conical scan (*cf.* Sec. 2·17). The r-f energy leaving the circular guide impinges on a splash plate and is in

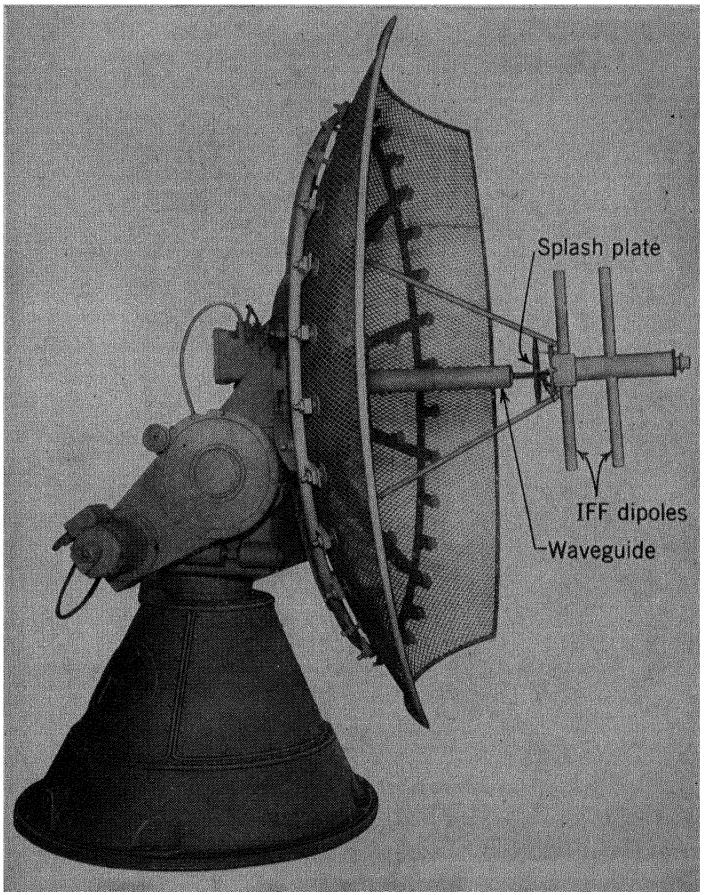

FIG. 3·8.—SP-1M antenna mount. (*Courtesy of General Electric Company.*)

turn focused by a paraboloid reflector 8 ft in diameter. The relative strengths of the signals received at the 0°, 90°, 180°, and 270° orientation points of the rotating offset waveguide are displayed by markers on the main control panel. An operator watches these markers and by manual control of two servomechanisms keeps the antenna centered on the target.

The servomechanisms actuate the motor drives on the azimuth and elevation axis.

The reflector is made of expanded steel and weighs in the neighborhood of 150 lb. It is supported on a series of studs. The studs in turn are threaded into an aluminum spider in a manner that permits the accurate setting of each stud at the true contour of the paraboloid surface. Nine

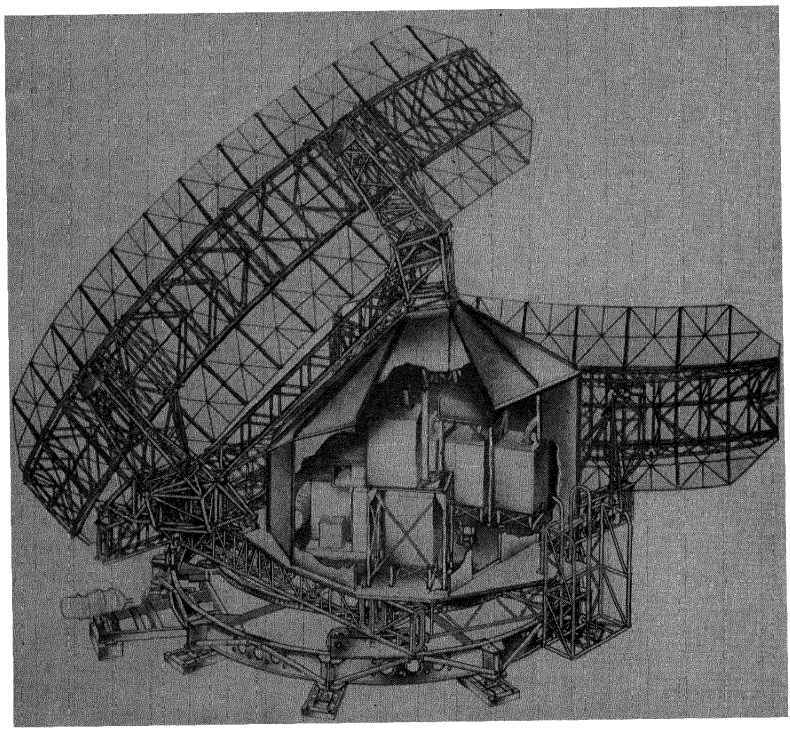

FIG. 3-9.—Cut-away perspective of the V-beam antenna mount.

inches of the lower section of the reflector are trimmed away to secure the necessary mechanical clearance, and the upper section is similarly cut away for mounting in a truck.

The active and the dummy dipoles that are located directly in front of the splash plate supply r-f energy in the band employed by the identification-of-friend-or-foe, IFF, system. The main reflector, in addition to its microwave functions, concentrates the IFF energy that is radiated by these dipoles.

The stationary portion of the pedestal and the azimuth and elevation axes, except for r-f waveguide, are identical with those of the SCR-584

mount.[1] One-half horsepower 3400-rpm motors are used on the azimuth and elevation axes. Maximum speeds of rotation are 6 rpm in azimuth and $3\frac{1}{2}$ rpm in elevation. Size 5 control transformers are used for data transmission at gear ratios of 1- and 36-speed in azimuth and 2- and 36-speed in elevation. The entire antenna mount weighs about 3000 lb.

V-beam Mount.—A 10-cm combined search and height-finding set designed for maximum coverage and for accurate height-finding on all targets up to 30,000 ft makes use of the V-beam principle. The antenna mount that is shown in Figs. 3·9 and 3·10 was designed to permit rapid field assembly of separable pieces of equipment. Five complete r-f transmitting and receiving systems and a single common modulator are carried on the rotating portion of the mount. Three of these systems supply r-f power through separate waveguides to a feed illuminating a paraboloidal reflector, 25 ft long by 10 ft high, that is used for search. The output of one r-f system is concentrated in the main search beam to secure coverage of long range targets, and the energy from the other two r-f systems is dispersed upward to secure coverage of high targets. The two remaining r-f systems supply energy through their respective waveguides to a 32- by 10-ft paraboloid reflector that is slanted at 45° for V-beam height-finding. All of this equipment is supported on four two-wheel trucks which rotate on a circular track 20 ft in diameter.

The V-beam principle involves a beam of radiation fanned in a vertical plane and one slanted in space at an angle of 45° to the vertical. If the two beams intersect to form a horizontal line at zero elevation, a target on the horizon in the common line of radiation will appear as a single pip on the face of the display tube. From an operational standpoint, it is desirable to know if a pip represents the single response from the vertical beam or if it represents the superimposed pips from the two separate beams. This is increasingly important in recording the height of low-flying planes, where separate pips are desired to give an accurate measure of height. To achieve this end, the slant antenna and the vertical antenna are located on the mount with a 10° displacement between the horizontal intercepts. As viewed by the vertical beam, a target on the horizon will then appear as a single pip; as viewed by the slant beam, the same target will appear as a pip displaced exactly 10° from the companion pip. A target above the horizon will produce two pips separated by an angle larger than 10°, where the increased angular displacement and the range are a measure of the height of the target.

The slant antenna is set on the mount at an angle of 45° with an accuracy of ± 5 min, and the 10° horizontal intercept between the two antennas is also constructed with an accuracy of ± 5 min. Figure 3·10 shows the feed support before installation of the feed and its associated

[1] Sec. 9·12, *Radar System Engineering*, Vol. 1 of this series.

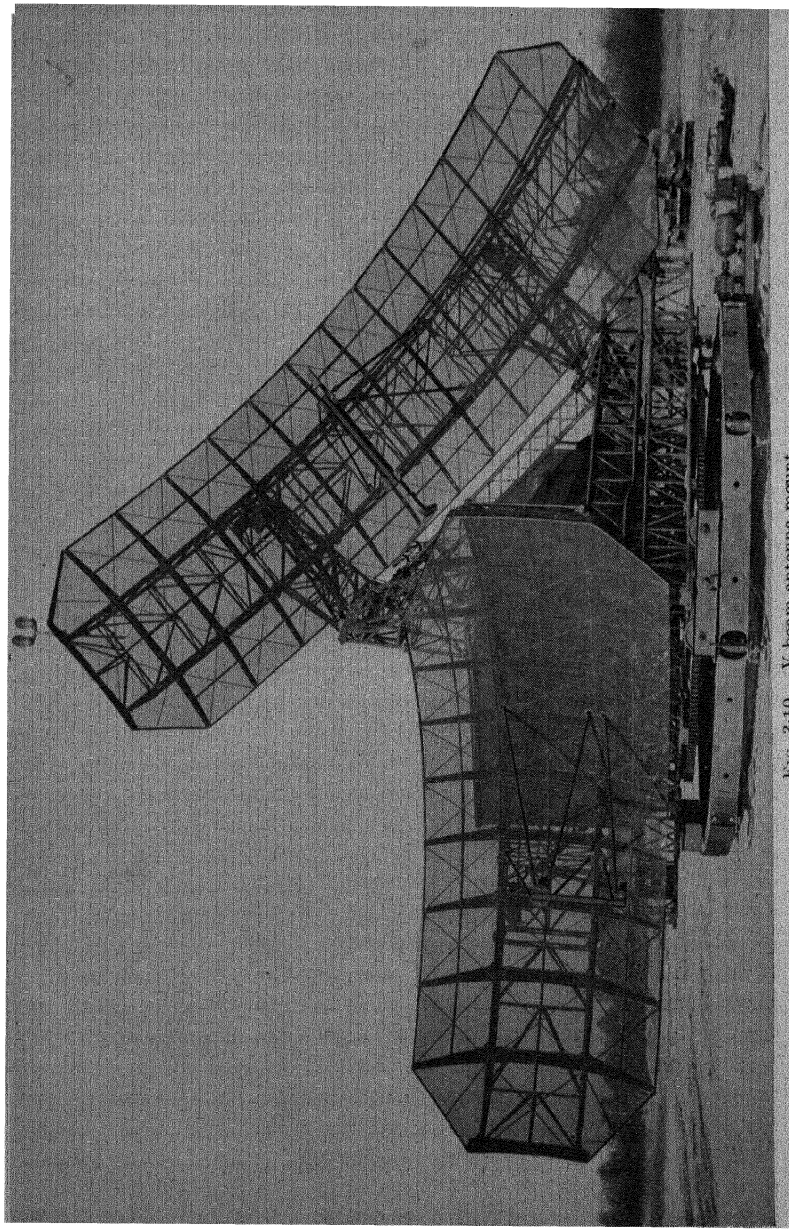

FIG. 3·10.—V-beam antenna mount.

waveguide. This feed support is provided with a device that will allow a small adjustment in the azimuth position of the vertical feed. The adjustment is for the purpose of final calibration, which is done by moving the feed location to produce on the display tube pips with an exact 10° spacing when a target at zero height is viewed. If the calibrated mount is to be accurate on all targets during 360° of rotation, the supporting track section must be level. This is accomplished by adjustment of the nine jack screws that support the separable track sections.

For the purpose of height-finding, the signals from the vertical beam and the slant beam are both recorded on a single display tube. The horizontal coordinate of the face of this height indicator is a measure of range, and the vertical coordinate is a measure of height. First the pip from the vertical beam will appear. Then the pip from the slant beam will appear directly above it, since the identical target will be at the same range after the mount has rotated 10° or more. The angular travel of the antenna mount determines the vertical distance between the two pips. If this vertical distance is to be an accurate measure of height, the servomechanism that governs the display tube must very accurately record the true azimuth location of the antenna mount. It is not essential that the mount be rotated uniformly, but it is essential that the azimuth position of the mount shall at all times be accurately transmitted to the servomechanism of the height indicator. This is accomplished with the slip-ring and synchro-unit assembly illustrated in Fig. 3·11.

The slip-ring and synchro-unit assembly is bolted as a complete unit onto a stationary hub. The electrical cables to the equipment on the mount pass through the center of the stationary hub and terminate in suitable electrical connectors. Figure 3·11 shows the top portion of the stationary hub, complete with connectors, bolted to the bottom of the slip-ring unit assembly. The use of electrical connectors between the slip-ring unit assembly and the stationary hub permits rapid assembly and disassembly of the equipment. Similar connectors are provided on the slip-ring unit assembly at the ends of the leads from the brushes. The entire slip-ring and synchro-unit assembly can be replaced, therefore, without disassembly of the mount and without disturbing the electrical wiring. All gearing on this unit is of precision manufacture. A 1-speed 6G synchro generator and a 36-speed 6G synchro generator transmit data. The lower portion of the slip-ring unit assembly is surrounded by a cylindrical can that performs the combined functions of a shield and a driving mechanism. This shield is fastened directly to the rotating member of the central hub.

The central hub is illustrated in Fig. 3·12. The stationary hub mentioned in the preceding paragraph forms the core of this unit. The inner races of a set of heavy bearings are mounted on the midsection of

the stationary core, which is held in central location with nine radial spokes that are made fast to the track sections. The lower electrical terminals are located directly above the sleeves that hold the radial spokes, and the upper electrical terminals are, of necessity, located above

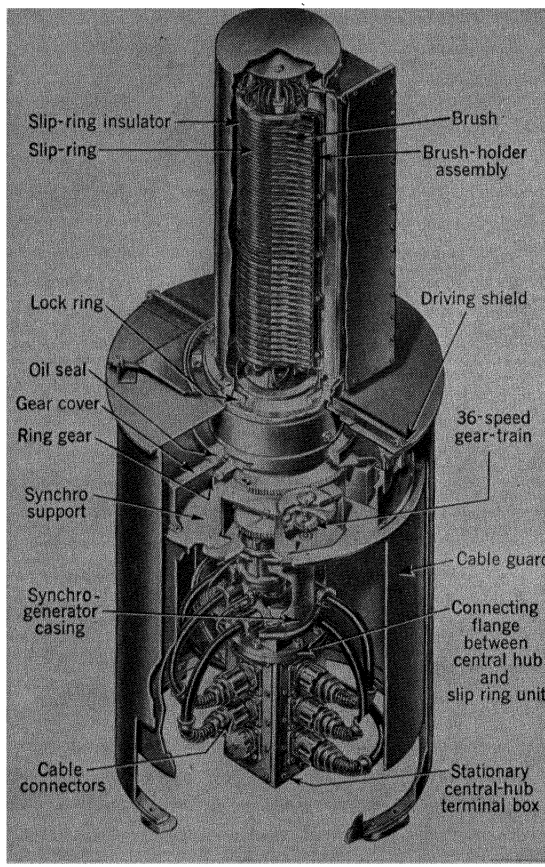

FIG. 3·11.—V-beam mount. Slip-ring assembly, cut-away view.

the central bearing. The outer bearing races are mounted in the cylindrical piece that also comprises the central section of the rotating platform. The driving shield of the slip-ring unit assembly is made fast to the rotating outer portion of the central hub. The top of the stationary hub is accurately machined to ensure that the axis of the slip-ring assembly and the axis of the central hub will be in true alignment.

The rotating portion of the mount, complete with equipment, weighs

approximately 23,000 lb and is held in a central location by means of the central hub. The use of flanged supporting wheels is avoided, as it is essential that the alignment between the slip-ring assembly and the axis of rotation of the mount be more accurately maintained than is possible

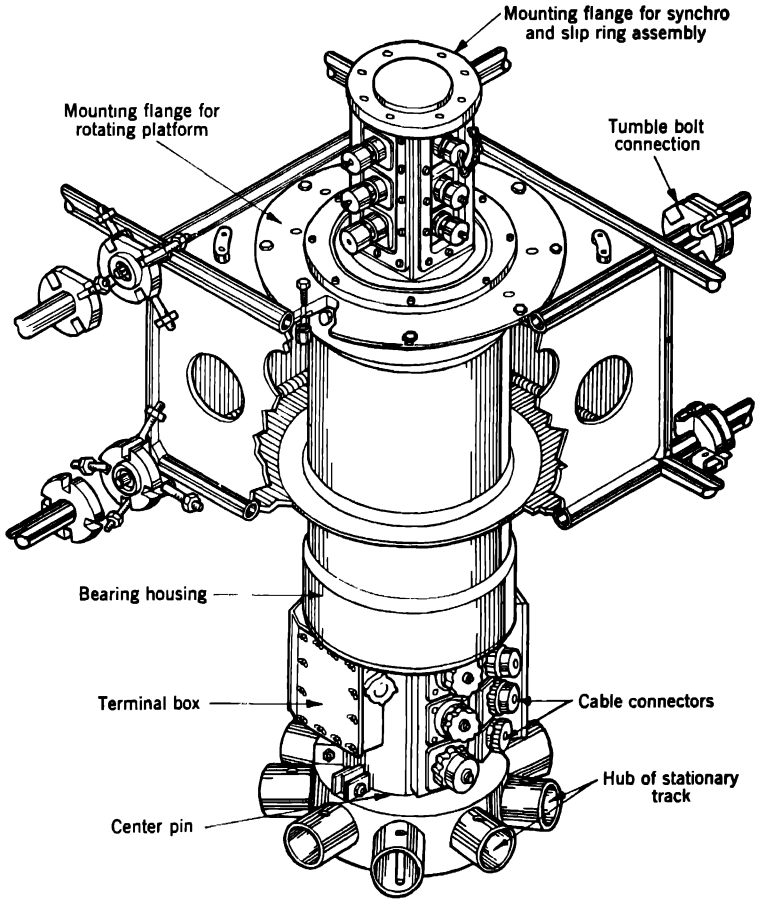

FIG. 3·12.—Central hub of the V-beam mount.

through the use of flanged wheels on a track of large diameter. The entire weight of all the rotating equipment is supported on four two-wheel trucks. The eight wheels are fabricated of cast steel, each of 15-in. diameter with 3-in.-wide beveled treads. A track $2\frac{1}{2}$ in. wide, of SAE 1040 to 1045 steel, is machined to a bevel matching that of the wheels and is flame-hardened. The tangent line from the wheel surface to the

intercept of the axis of the wheel with the axis of the central hub defines the angle at which true rolling contact takes place. A further requirement for true rolling contact is that the center line of each wheel intersect the center-line axis of the central hub. Relative wheel alignment is secured by jig-boring the wheel supports in each truck so that each set of two wheels is in accurate relative alignment. The alignment of a set of two wheels on the rotating platform is then secured by accurately locating the position of the truck. Each truck frame is carried on a stainless steel pin, 10 in. long, 2 in. in diameter, which acts as an equalizer. The pin is mounted in lubricated bronze bushings that permit the free movement of the truck around the axis of the pin and at the same time hold the truck in accurate alignment with the track.

A 5-hp 1760-rpm three-phase 208-volt totally enclosed induction motor drives the mount at a speed of 6 rpm. The gear-reduction mechanism that comprises the azimuth drive is usually a considerable fraction of the total weight of the mount. On this set, the weight limitation of 600 lb maximum was met by fabricating a bull gear of large diameter in separable sections. The gear consists of a series of hardened steel pins set into the webs of rolled structural-steel channels. A pinion meshes with this gear, and a loose tolerance is allowed between the teeth of the pinion and the steel pins of the bull gear. The play between the pinion drive and the bull gear is not objectionable, because the precision gearing on the slip-ring and synchro-unit assembly is independently mounted on the central hub and the motor is not controlled by a servomechanism. The pinion is connected to the motor drive through two sets of spur reduction gears.

Both antennas can be tilted in a manner that will raise or lower the beams of radiation without disturbing the angular relations between the two fan beams. This permits a nice adjustment of the radiated energy to horizon levels that will avoid "ground clutter." It is achieved by mounting each antenna in ball-and-socket joints and then controlling the position of the antenna through an extensible arm at each end of the supporting frame. A motorized mechanism such as is commonly used to open and shut gate valves is employed at the extensible arm on one end of the frame; a similar mechanism on the other end of the frame is kept in synchronism by means of a mechanical link that takes the place of the motor.

Each line of waveguide between a feed and the associated r-f components on the rotating platform is provided with a "wobble joint," as illustrated in Fig. 3·13. The blank flange can be tilted until its motion is limited by the opposing choke flange without disturbing the flow of r-f energy through the waveguide that terminates at the face of each flange. A rubber boot permits flexure and acts as a water seal. The

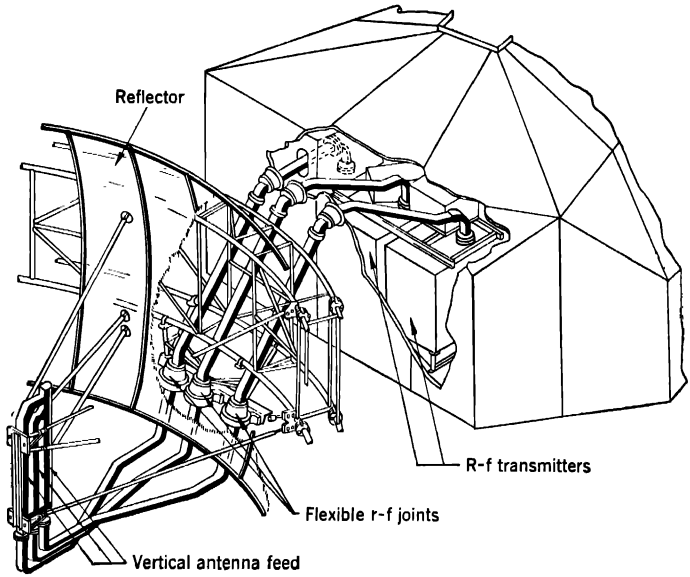

FIG. 3·13.—Feed and waveguide for the vertical beam of the V-beam radar set.

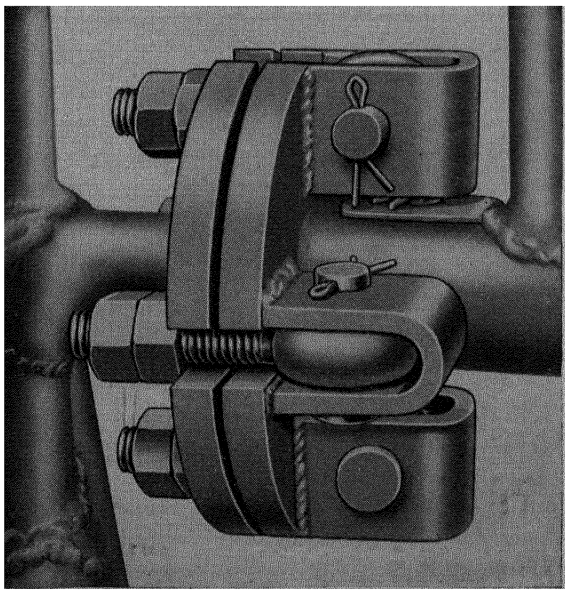

FIG. 3·14.—Typical tumble-bolt connection.

axes of the three flexible joints are in line with the ball joints on which the antenna is tilted. In Fig. 3·13 these joints appear at the lower portion of the illustration and should not be confused with the rubber boots that are used merely to seal the openings in the shelter at the points where the waveguides pass through the wall.

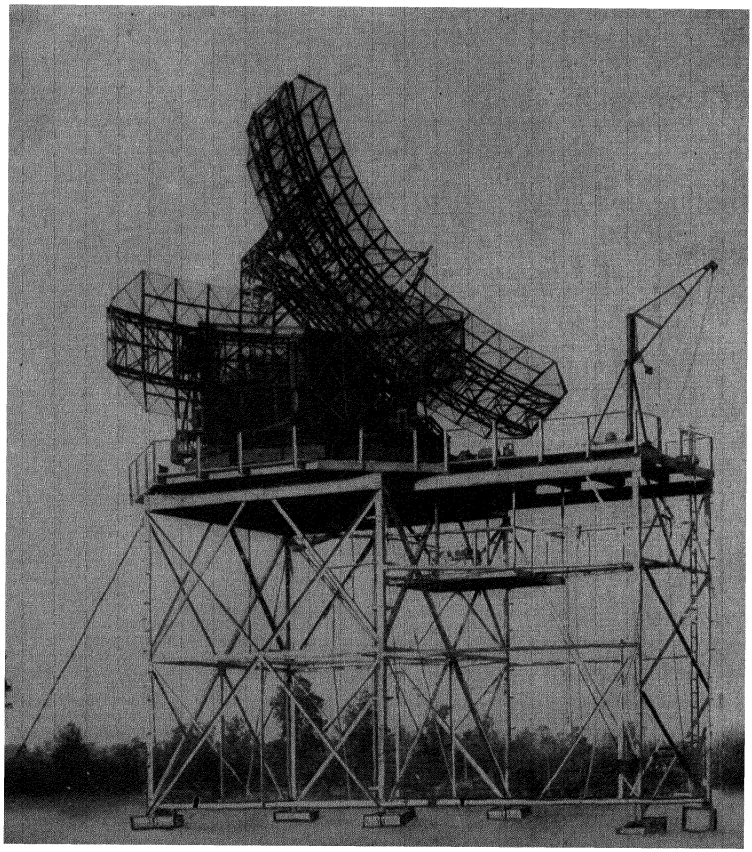

FIG. 3·15.—Antenna mount on a 25-ft tower.

The reflectors are described in Items 4 and 5 of Table 2·7. The track supports are fabricated of lightweight structural channels. All other structural members are builtup of SAE 1020 seamless steel tubing. Low-carbon steel is preferred to high-carbon steel, to facilitate welding operations. The ends of the large number of separate pieces of tubing required to fabricate the structural framework are machined to true fit prior to

welding. This procedure facilitates welding operations and produces a smooth, strong, welded joint. The separable portions of the mount, for the most part, are joined together with tumble-bolt flanged connections of the type illustrated in Fig. 3·14. Each flanged connection has a large, accurately machined center pin which fits into a hole in the mating section. No piece of the antenna mount is heavier than 600 lb. The walls of the shelter that houses the electrical equipment are Celotex heat-insulating slabs lined with sheet metal. Each wall section is held in place against a steel frame by means of thumbscrews. Cowling over all open seams makes the shelter watertight. The entire mount can be assembled by a skilled crew in approximately twelve hours.

The complete mount in operation on a 25-ft tower is shown in Fig. 3·15. The weights of the separate components are given in Table 3·4.

TABLE 3·4.—WEIGHTS OF ANTENNA MOUNT COMPONENTS

Components	Weight, lb
Track and stationary base	5,000
Trucks, wheels, and rotating platform	5,000
Structural supports for reflectors	2,600
32- by 10-ft reflector, feed and tilting mechanism	2,800
25- by 10-ft reflector, feed and tilting mechanism	2,100
Shelter and flooring	3,100
Electrical equipment in shelter	6,500
R-f feed and waveguide	1,000
Complete antenna mount	28,100

3·6. Oscillating Beavertail Mounts.—Several radar sets employ oscillating beavertail scans for height-finding. The antenna mount of a 10-cm set of this type uses a 20- by 5-ft reflector which is servo-controlled in azimuth to locate targets accurately at long ranges (Fig. 3·16).

The AN/TPS-10 is another set of this type. Its mount uses a 10- by 3-ft reflector with 3-cm radiation and is manually controlled for positioning in azimuth to keep the complexity and the weight of the set at a minimum. All parts are designed for manual portage and quick assembly. The mount will be described in some detail because of these features. Figure 3·17 shows an early model of the AN/TPS-10 mount with the r-f box located directly behind the midsection of the reflector; in subsequent models the r-f box was lowered to the roller-track level to make it easier of access.

The set has a beam of r-f energy that is 2° wide in the horizontal plane and 0.7° wide in the vertical plane. This beam oscillates in elevation from −2° to +23° at a rate of 60 to 75 cpm. When used as a search set, the mount rotates around the azimuth axis at $\frac{1}{3}$ rpm. This speed cannot be exceeded if successive sweeps of the beavertail scan are to cover all portions of the sector that is being scanned.

The total weight of the system is 1520 lb (2500 lb packed for shipment). This weight is distributed as follows: mechanical components (27 items), 865 lb, r-f and electrical components on mount (4 items),

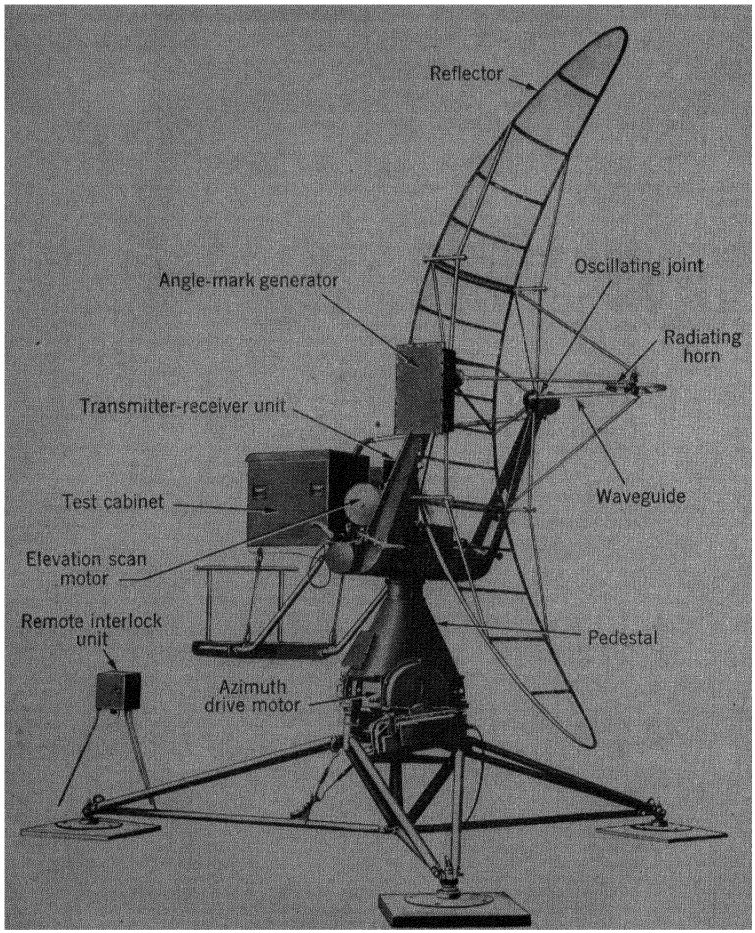

FIG. 3·16. - Beavertail antenna mount. (*Courtesy of Jordanoff Corporation.*)

260 lb, remote components and test equipment (9 items), 395 lb. The average weight of each item is 38 lb; the r-f box, which is the heaviest unit, weighs 130 lb. The power unit is an engine-driven generator weighing 128 lb. The generator supplies 1400 watts of power at 120 volts and 400 cycles and 400 watts of 24-volt d-c power. For convenience, the

design features of the mount can best be considered as details of the following three subsections: elevation driving mechanism, azimuth driving mechanism, and general construction.

Elevation Driving Mechanism.—Figure 3·18 is a left rear view of the mount and shows the details of the elevation drive. A $\frac{1}{3}$-hp 3000-rpm 24-volt d-c Eicor driving motor is contained within the waterproof cylindrical container with cooling fins (near the center of the figure). By

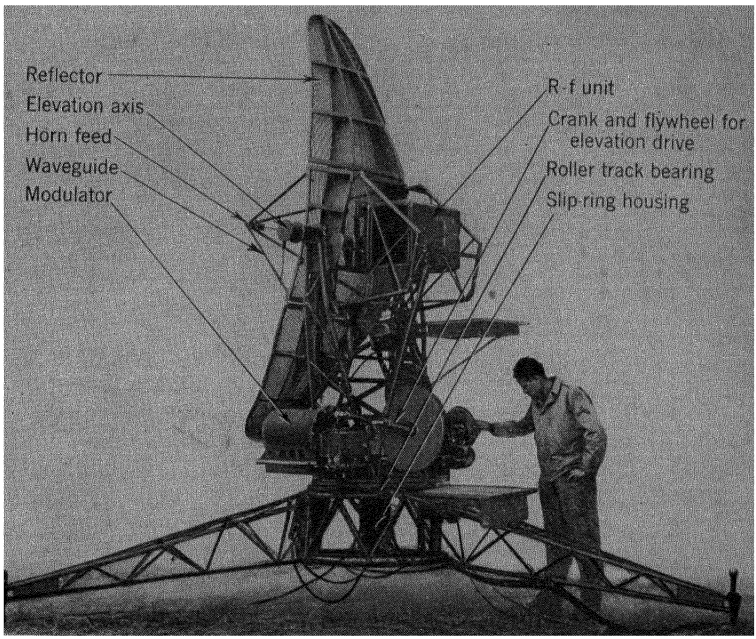

FIG. 3·17.—AN/TPS-10 antenna mount. (*Courtesy of U.S. Army.*)

changing the pulley on the motor, it is possible to vary the elevation scanning rate from 60 to 75 cpm. The pulley drives a 35-lb 15-in.-diameter flywheel through a "V" belt. The flywheel is keyed to the pinion shaft of a gear box. The slow-speed shaft of this gear box turns a crank arm that drives the reflector by means of the connecting rod. The inertia of the reflector is approximately 470 lb-ft^2. It should be noted that in any mechanism of this type, in which a part having a large inertia is oscillated at a rapid rate, a flywheel is ordinarily put on the crankshaft. Since, however, the crankshaft rotates at only 60 to 75 rpm, the weight of a flywheel on this shaft would be excessive. On the other hand, if the flywheel is removed by several stages of gearing from

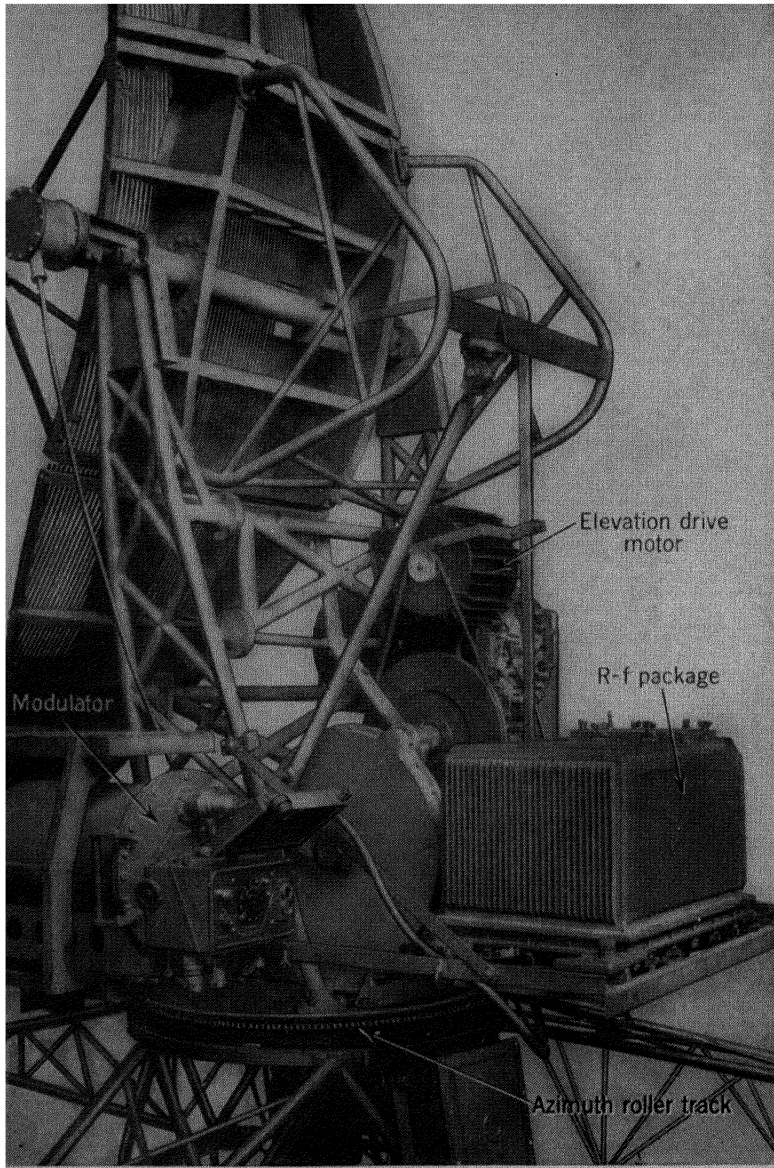

FIG. 3·18.—Elevation driving mechanism of the AN/TPS-10 antenna mount.

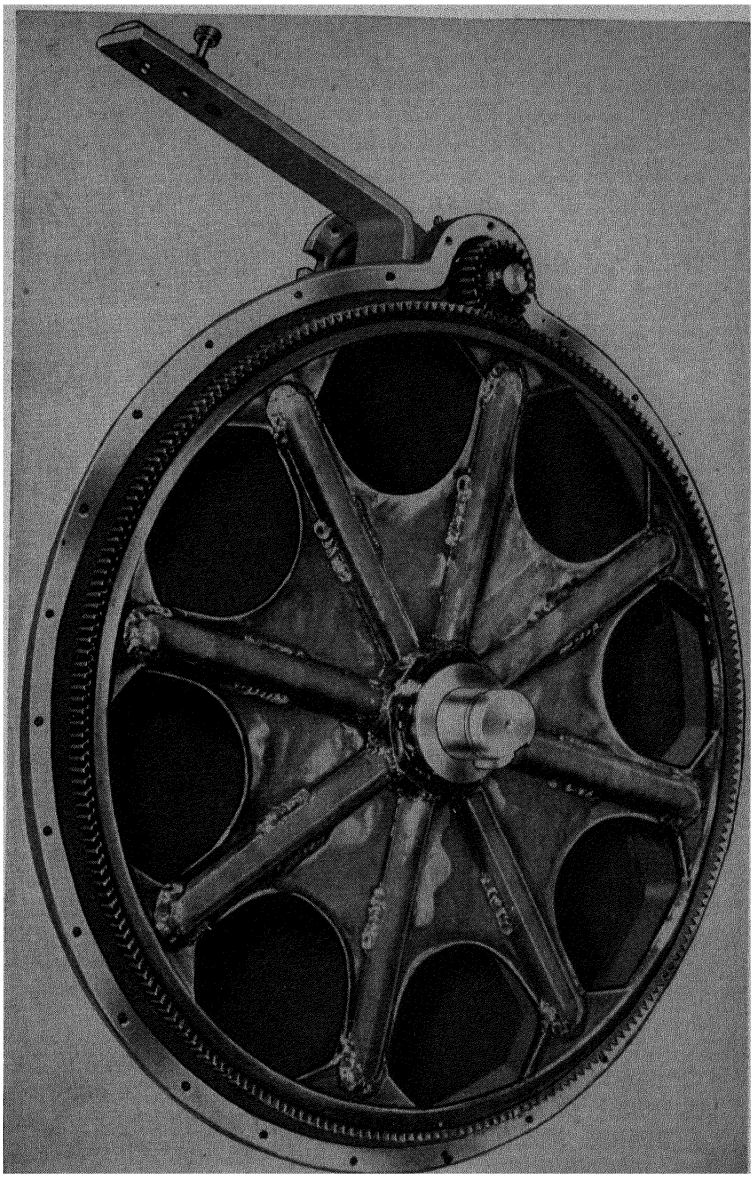

FIG. 3·19.—Elevation gear case of the AN/TPS-10 antenna mount.

the crankshaft, then cumulative backlash will induce pounding as the torque on the crankshaft reverses in direction. As a compromise, a single-stage 11.5/1 gear reduction is employed to reduce the backlash. Details of the construction of the large gear in this gear box are shown in Fig. 3·19. The spokes are steel tubes, each split on a diameter and welded to a sheet-metal web. A gear reduction with a minimum of weight and backlash has been produced by employing this type of construction.

Azimuth Driving Mechanism.—Figure 3·20 illustrates the azimuth drive. The gear box in the foreground contains a worm-gear train with

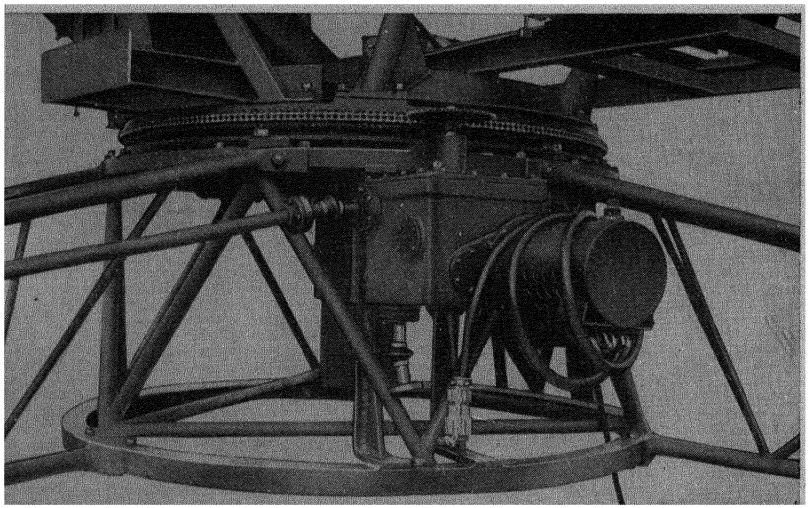

FIG. 3·20.—Azimuth drive of the AN/TPS-10 antenna mount.

2160-to-1 reduction, driven by a $\frac{1}{10}$-hp 27-volt d-c 6000-rpm Diehl motor. The sprocket on the vertical shaft projecting from the top of this gear box meshes with a chain gear 32 in. in diameter. The chain gear is made from ordinary roller chain mounted on the outer diameter of the 30-in. roller bearing with standard conveyor attachments. The rod that is attached to the universal joint on the shaft extends to a hand crank for use when manual tracking is desired. By means of a differential, the details of which are shown in Fig. 3·21, the hand crank can be used to supplement the rotation of the mount by the motor. If the motor is stopped, the gear reduction is self-locking and the hand crank can be used independently to turn the mount in either direction. The shaft and universal joint extending from the bottom of the gear box is an alternate hand-wheel attachment that is used when the mount is operated from a tower. The main azimuth bearing on this mount is a 30-in.

roller track, manufactured by General Bronze Corporation, Long Island City, N.Y. The bearing races are at an angle of 45° with the horizontal. One roller resists upthrust of the inner race, and alternate two out of every three rollers have their axes located at 90° to the axis of the first roller to resist downthrust. This bearing, including the chain gear, seals, etc., weighs 65 lb.

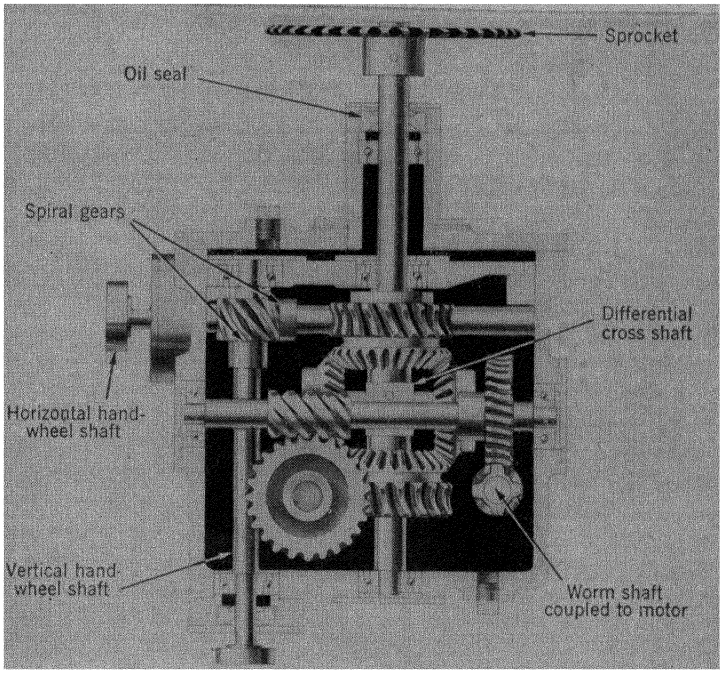

FIG. 3·21.—Azimuth gear box of the AN/TPS-10 antenna mount. (*Courtesy of U.S. Army.*)

General Construction.—Figures 3·17, 3·18, and 3·20 show some of the details of the structure of the mount. Except the aluminum reflector, which is described in Item 8, Table 2·7, most of the structure is built of welded steel tubing. The wall thickness of all tubing is 18 gauge. To facilitate rapid assembly of the various sections of the mount, captive screws are used wherever possible. The mount must be rigid to resist relatively large unbalanced dynamic loads. Consequently, all structural members are designed to load the individual elements only in tension or compression. During operation, the maximum deflection of the elevation axis from the normal position is less than $\frac{1}{32}$ in., which is well within the limits required on the basis of accuracy considerations.

CHAPTER 4

STABILIZATION OF SHIP ANTENNAS

By W. B. Ewing

PRELIMINARY CONSIDERATIONS

The earliest shipborne radar antennas projected beams of such ample dimensions that rolling and pitching of a ship did not ordinarily cause enough variation of beam direction to increase the difficulty of holding a target or to leave unscanned portions in the area of search. The problem of stabilizing antennas was born, then, with the development of microwave radar and the attendant need for close control of the direction of the beam in space if the full advantages of its sharpness and resolution were to be realized on ships at sea.

Stable reference data from gyroscopic devices have long been used in naval instruments to compensate, in part, for the unpredictable motions of the deck of the ship and thus provide for the steady aiming of the guns. It was hoped, at first, that radar antennas could be steadied against the roll and pitch of a ship by using similar methods and adapting stabilization equipment already in existence. To a limited extent, such a procedure was found to be possible. There are, however, four important differences between the problem of stabilizing a radar antenna and that of stabilizing a gun. These differences are

1. Preradar fire-control equipment was based on the sighting and holding of a target with optical sights that were partially stabilized by manually directed servomechanisms. The fact that no optical sight is held on a radar target introduces the need of automatically computed corrections to correspond to those usually provided by observers through the optical sights and servomechanisms of fire-control systems. These corrections are not directly obtainable from the true-vertical reference data provided by the gyroscopic equipment but must be computed from these and other known data by means of additional apparatus.
2. All gun-stabilizing and computing equipment is designed for gun mounts that have the gun proper attached to the deck by two supporting axes. Radar mounts can often utilize a different number or disposition of axes which require different functions for stabilization of the mounted antenna.

3. Gyro equipments providing vertical reference for fire control are not designed for continuous data output through the full cycle of rolls greater than 22° because it is possible to restrict firing of the guns to those parts of the periods when the roll is under 22°. Radar gear should be stabilized continuously, not intermittently, under such seaway conditions.
4. Some fire-control computers include elements that compute the data needed for some methods of radar-antenna stabilization. These elements, however, are inseparably associated with many others entirely extraneous to the radar, and they are designed for intermittent operation intended to total only a small fraction of the stand-by time. Radar stabilization gear, on the other hand, must be capable of continuous operation without undue wear.

The following discussion relates principally to stabilization considerations peculiar to radar antennas. More familiar equipments, such as gyroscopic stable elements, that have been used in radar-antenna stabilization are given only brief treatment.

BASIC TYPES OF STABILIZED ANTENNAS

Shipborne antennas are usually mounted on the mast or superstructure of a ship, as high above the deck as possible. Because it is important to keep the topside weight at a minimum, it becomes necessary to limit the weight of antenna mounts. In general, therefore, it is desirable to mount a stabilized shipborne antenna with the least number of supporting axes and servo drives that will provide satisfactory stabilization. The function and manner of use of the particular antenna should be considered, for they determine the necessary number of axes and their various arrangements.

Figure 4·1 schematically illustrates nine mounting arrangements, differing only in the number or disposition of the axes used. Although the four-axis mount requires no computers in addition to a stable-vertical reference and meets all the stabilization requirements of most radar sets, it is, unfortunately, relatively massive and heavy, for it has four servo-drive systems for controlling rotation about each of the four axes. The intermediate designs with two axes or an arrangement of three axes seem best suited to the needs of most shipborne antennas requiring stabilization. Each of the nine designs, however, is considered here from the viewpoint of stabilization.

4·1. The One-axis Pedestal.—The one-axis design (Fig. 4·1*a*) has a train axis only. It permits stabilization if the beam fans in a plane approximately perpendicular to the deck. It is stabilized only in the sense that a correction may be applied to rotation about the train axis to

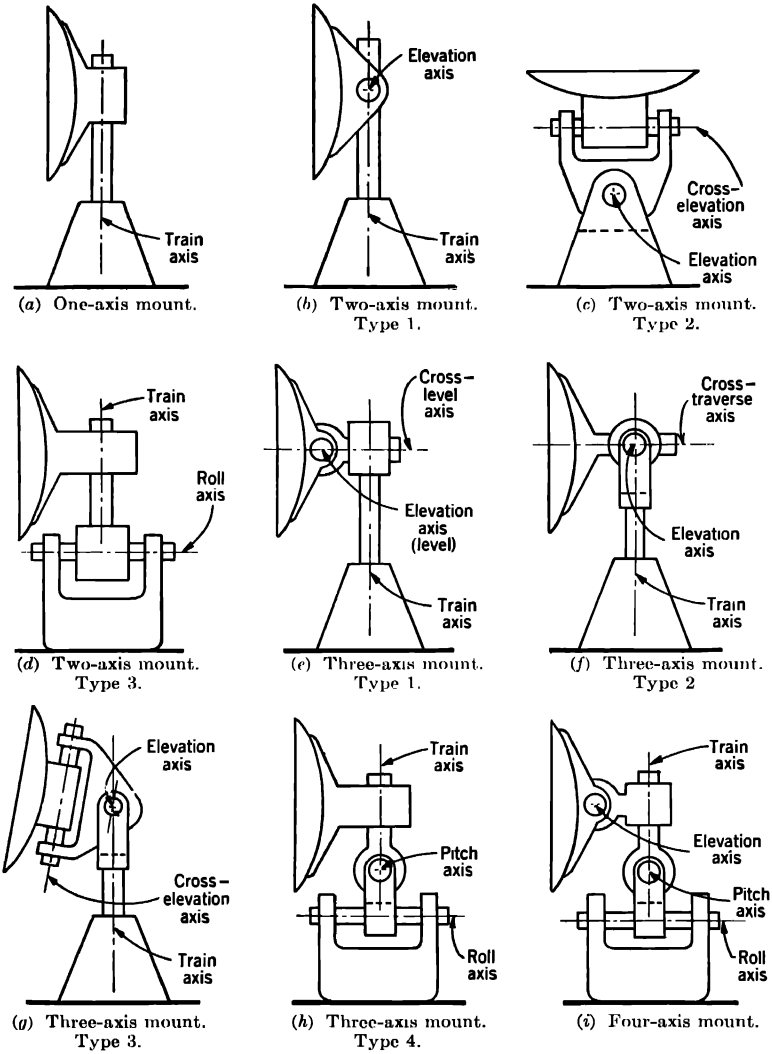

(*a*) One-axis mount.
(*b*) Two-axis mount. Type 1.
(*c*) Two-axis mount. Type 2.
(*d*) Two-axis mount. Type 3.
(*e*) Three-axis mount. Type 1.
(*f*) Three-axis mount. Type 2
(*g*) Three-axis mount. Type 3.
(*h*) Three-axis mount. Type 4.
(*i*) Four-axis mount.

FIG. 4·1.—Arrangements of axes for stabilized antenna mounts.

keep some portion of the fan beam at a known bearing angle. Figures 4·2*a*, *b*, *c*, and *d* indicate the space relationship among elements of the ship, target, and radar beam under consideration. The circular and sector planes shown are great-circle sections of a unit sphere. The cross-hatched sector shown in Fig. 4·2*a* represents a beam at relative bearing 45° on a ship that has, at the moment, neither pitch nor roll. The deck

plane is therefore in coincidence with the horizontal plane, and the mast line or train axis is in the true vertical. A very wide angle fan represents the central plane of the beam divided evenly above and below the deck.

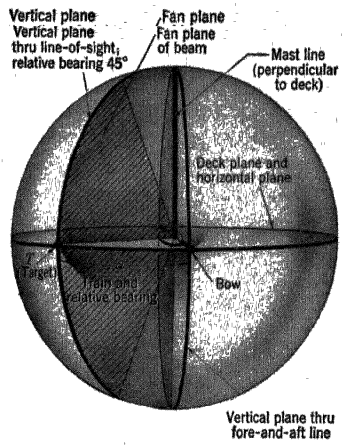

(*a*) Deck plane horizontal. Fan beam centered on horizontal target.

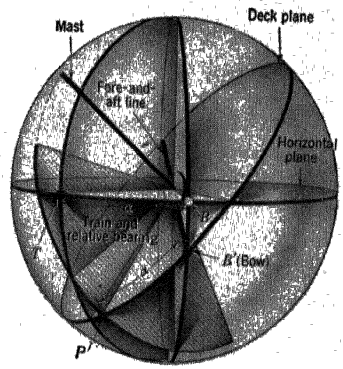

(*b*) Deck plane pitched 15° and rolled 45°. Antenna train angle uncorrected. Target unilluminated.

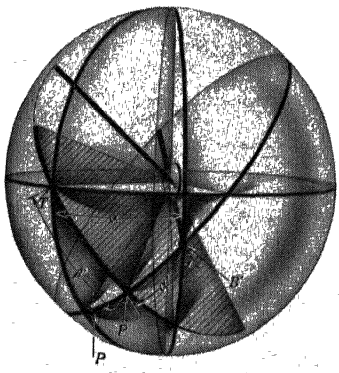

(*c*) Antenna train angle corrected for horizontal target deck-tilt error.

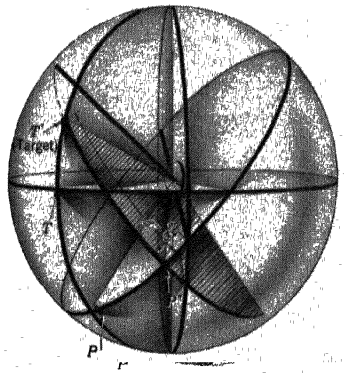

(*d*) Antenna train angle corrected for elevated target deck-tilt error.

FIG. 4·2.—One-axis and two-axis mounts. Elements of ship, target, and radar beam shown as space relationships of great-circle planes in a unit sphere.

It is clear that as long as the deck remains in this position, any given train angle at which the antenna may be rotated around the vertical train axis will be duplicated in the resulting bearing angle that is the intersection of the plane of the beam with the horizontal plane. This condition does not remain true, however, if roll and pitch angles are applied to the deck

plane, as shown in Fig. 4·2*b*. Here the fore-and-aft line has been displaced 15° in a vertical plane from B to B' (pitch), and the deck plane has been rotated 45° about the fore-and-aft line (roll). The train angle of the beam in the deck plane is unchanged from angle α. It is obvious, then, that the plane of the beam is wide of the target; and if it is again to include the target, it must be trained counterclockwise in the deck plane about 16° to point to P', as shown in Fig. 4·2*c*. The change in train angle required to retrain the beam on the target is the deck-tilt correction. It must be continuously and automatically computed and transmitted as an electrical signal controlling the train drive of the mount. The instantaneous values of the deck-tilt correction are found from the relationship[1]

$$\tan(\alpha' - \alpha) = \frac{\cos^2\alpha \sin R \sin P + \sin\alpha \cos\alpha (\cos R - \cos P)}{\sin^2\alpha \cos R + \sin\alpha \cos\alpha \sin R \sin P + \cos^2\alpha \cos P}, \quad (1)$$

(A·14)

where α = relative bearing of horizontal component of radar beam,
α' = train order for beam,
$(\alpha' - \alpha)$ = deck-tilt correction,
P = pitch angle,
R = roll angle.

Figure 4·3 presents graphs of the rates and accelerations imposed upon the train axis by the correction for the deck-tilt error when the horizon is being scanned at a uniform rate of 6 rpm in relative bearing. Later it is shown that these graphs apply also to the two-axis type 1 antenna when the beam is horizontally stabilized, and to the three-axis type 1 antenna, regardless of target elevation.

4·2. The Two-axis Type 1 Pedestal. *Two-axis Pedestal for Horizontal Beam.*—In the one-axis antenna, as shown in Fig. 4·2*a*, it is obviously impossible to maintain the central portion (nose) of the beam on the horizon or at any given elevation if the ship is rolling and pitching. Since the nose of the beam is normally the part with the highest intensity of radiation, it is desirable to hold the beam centered on the target or point of search. It is apparent that such centering can readily be accomplished by giving the antenna additional freedom through a second axis of support, as shown in Fig. 4·1*b*. Since this second axis is normal to the antenna beam and parallel to the deck, it enables the beam, as shown in Fig. 4·2*c*, to be elevated through arc $P'T = \beta'$. The beam center then illuminates the horizon; the plane of the fan and hence the antenna train remain unchanged. This use of the elevation axis is equally applicable to a pencil-beam antenna, since the plane traversed by the elevation of

[1] See Appendix A for the derivation of this equation and others that follow. The numbers preceded by A, such as (A·14) above, are the numbers of the equations in the appendix.

such a beam coincides with the plane of the fan beam. The fully stabilized two-axis surface-search antenna therefore requires not only the deck-tilt correction [Eq. (1)] but also a continuously corrected elevation angle or order β'. The latter is expressed by the equation

$$\sin \beta' = \cos \alpha \sin P \cos R - \sin \alpha \sin R. \qquad (2)$$
$$(A\cdot 16)$$

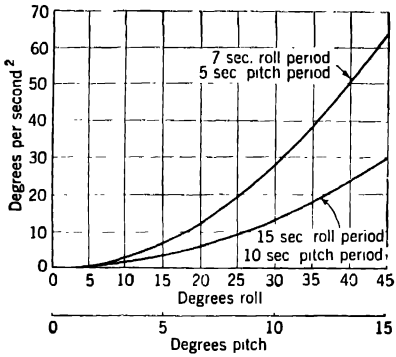

(*a*) Peak train acceleration. Scan rate of 6 rpm.

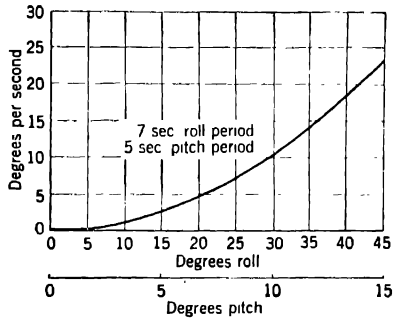

(*b*) Peak speed of deck-tilt error. Scan rate of 6 rpm.

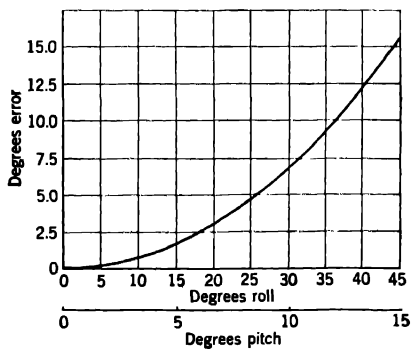

(*c*) Maximum values of deck-tilt error.

FIG. 4·3.—Characteristics of the deck-tilt error for stabilized three-axis mount (Type 1) and for two-axis mount (Type 1) with horizontal beam. Simultaneous values of pitch P and roll $R = 3P$ are assumed.

Two-axis Pedestal for Above-horizon Beam.—Because this two-axis pedestal has an elevation axis, the antenna beam center can be elevated not only to the horizon but also above it. It becomes possible, then, to direct the beam to any point in the sky by the proper combination of train and elevation angles. However, if the beam is to reach an elevated target position such as T', which has the same bearing as the horizontal target T (see Fig. 4·2*d*), the plane of the fan must be changed in train

still farther counterclockwise to point P''. This correction is the same for a one-axis pedestal if the elevated target is to be included in the fan beam. In either case, the value of the correction is dependent on the true elevation of the target. Equations (1) and (2) are inapplicable, being valid only for targets on the horizon. The new equation for train, in which β is target elevation and α' is train angle, is found to be

$$\tan \alpha' = \frac{\sin \alpha \cos R + (\cos \alpha \sin P + \tan \beta \cos P) \sin R}{\cos \alpha \cos P - \tan \beta \sin P}. \quad (3)$$

(A·15)

The equation for the corrected elevation angle or elevation order β' that the antenna will have to assume when the beam center is elevated to a target above the horizon is

$$\sin \beta' = (\cos \beta \cos \alpha \sin P + \sin \beta \cos P) \cos R - \cos \beta \sin \alpha \sin R. \quad (4)$$

(A·12)

Application of the above corrections results in high rates and excessive accelerations, especially in the train angle or order α' if the sum of the true target elevation angle β and the maximum inclination of the deck exceeds approximately 70°.[1] It is therefore impossible with the ordinary type 1 two-axis mount to maintain accurate beam control through a considerable region surrounding the zenith.

4·3. The Two-axis Pedestals, Types 2 and 3. *Two-axis Pedestal for Zenith Search.*—The type 2 trainless arrangement of two supporting axes for an antenna (see Fig. 4·1*c*) is a possible, but as yet unused, method by which only the zenith region may be searched without encountering impractical drive accelerations. In order to stabilize the antenna beam in a direct vertical plane, it must be assumed that the basic axis to be installed is parallel to the fore-and-aft line and that the angular displacements and accelerations required about the basic and second axes are, respectively, roll and pitch. To direct the beam elsewhere within the zenith cone, computed orders for each axis must be derived from the roll and pitch angles as well as from the known relative-bearing and true-elevation angles of the target or point of search.

Two-axis Roll Stabilization.—The two-axis type 3 pedestal (Fig. 4·1*d*) provides *roll stabilization*, which is only an approximate form of stabilization. It is, nevertheless, the method by which the most precise azimuth stabilization possible for a two-axis surface-search antenna is attained without involving computed orders. With the roll data from a stable vertical applied to the basic roll axis, the train axis becomes stabilized in respect to roll. Since the pitch angles are comparatively small, their

[1] H. M. James, "Train Rates in a Two-axis Director," RL Report No. 8, Sept. 18, 1943.

neglect is tolerable in certain applications. Thus, although an elevation error is equal at times to the pitch angle, the azimuth or deck-tilt error is reduced to a very low value which may be determined for a specific case by applying Eq. (1) with $R = 0$.

4·4. The Three-axis Type 1 Pedestal.—Although the two-axis antenna beam can be universally directed, it has been shown in Secs. 4·2 and 4·3 that with construction of this type it is impossible to get full coverage of the sky from an unstable base such as the deck of a ship. A further characteristic of any stabilized two-axis antenna mount is that the beam rotates about its central axis as changes occur in the angle of inclination of the elevation axis as a result of variations in the deck tilt. Such rotation is not permissible with a fan beam which, to fulfill its purpose, must be maintained in a vertical or horizontal plane.

In a single mount, if it is desired to provide for full hemispheric sky coverage or to eliminate rotation of the beam about its central axis, a third axis, as shown in Fig. 4·1*e*, may be added between the train and elevation axes of the type 1 two-axis mount. The elevation axis in a pedestal of this type is called the *level axis*. The additional axis, because it is disposed at right angles to the level axis, is called the *cross-level axis*. Since the cross-level order is always that which will maintain the level axis horizontal, and since the antenna is directly supported about the level axis, the beam is stabilized against rotation about its central axis. Thus, if the beam is fanned vertically in a manner similar to that in Fig. 4·4*a*, the cross-level order alone will keep it in the vertical plane after the ship has rolled and pitched to the position shown in Fig. 4·4*b*. The level order will serve to elevate and center the fan on the horizon or elevated target without changing its plane. The cross-level order alone, however, merely rotates the fan beam about its line of intersection with the deck plane without changing the position of the line in the deck. This line is shown in Fig. 4·4*a* as CT in the untilted deck plane and as CO' in the tilted deck of Fig. 4·4*b*. The angle α, the pedestal train angle, remains unchanged with respect to the fore-and-aft line, but the relative-bearing angle of the line CO' and consequently of the beam has obviously changed by the value of the arc TO. To include the target point T in the beam again, the pedestal must be rotated counterclockwise about the train axis through the arc $O'O''$ with a concomitant change in the cross-level order that will hold the fan plane vertical. A corresponding correction in level order is also required if the beam is to regain vertical centering of the target. In Fig. 4·4*c*, the beam is shown with corrections applied on all three axes. The change OT in train angle is the deck-tilt correction and is of exactly the same magnitude as arc PP', Fig. 4·2*c*. This arc is the deck-tilt correction [Eq. (1)] previously considered for horizontal targets for the one-axis pedestal and for the type 1 two-axis pedestal. It will be

noted that although the magnitude of the correction is the same, its phase relationship to the relative target bearing is shifted 90°. This shift may be attributed to the deck-tilt error arising from the tilting of an axis always parallel with a deck that is rolling and pitching. In the type 1

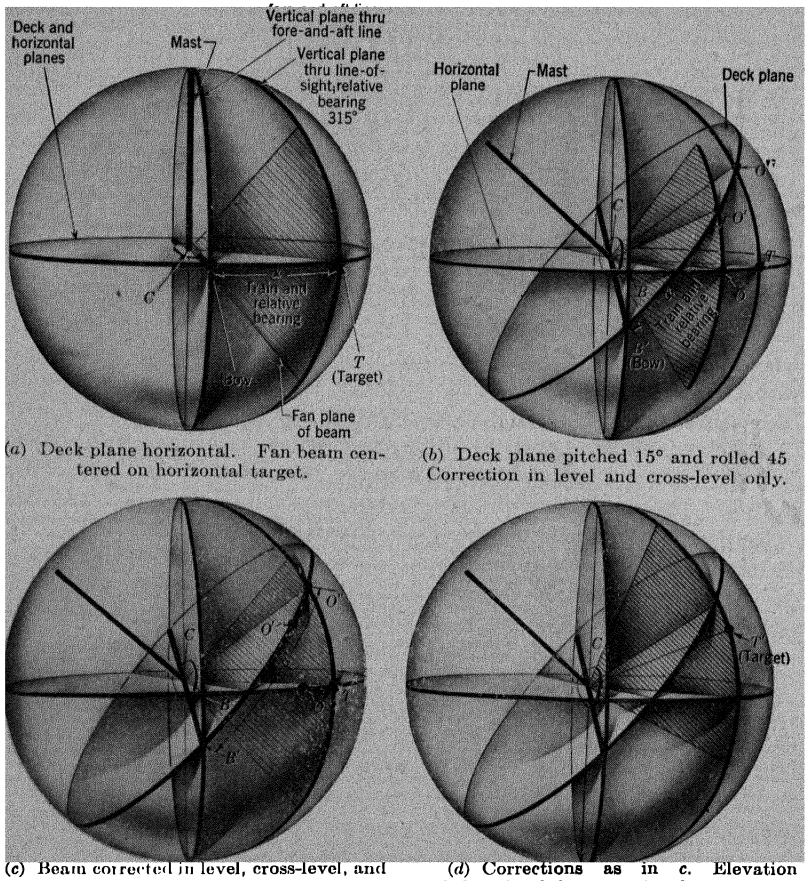

(*a*) Deck plane horizontal. Fan beam centered on horizontal target.

(*b*) Deck plane pitched 15° and rolled 45 Correction in level and cross-level only.

(*c*) Beam corrected in level, cross-level, and train.

(*d*) Corrections as in *c*. Elevation added to level for centering beam on elevated target.

FIG 4·4.—Three-axis mount. Elements of ship, target, and radar beam shown as space relationships of great-circle planes in a unit sphere.

three-axis mount this cross-level axis lies in a vertical plane including the line of sight, whereas in the two-axis mount the elevation axis lies in a vertical plane disposed at 90° to such a plane.

Since the plane of the fan beam (or the plane described by elevation of a pencil beam) in the three-axis type 1 antenna is kept vertical, it is

obvious that the beam can be centered on an elevated target having the same bearing as a horizontal target merely by adding the true elevation of the target to the level order, as shown in Fig. 4·4*d*. Thus, in a three-axis mount, target elevation is not a factor in determining level, cross level, or train as it is in one- and two-axis mounts.

The level and cross-level orders for a three-axis antenna mount may be developed directly by a properly trained stable element, which may be considered as a computer; or they may be developed and transmitted to the antenna mount by a stable vertical and a computing mechanism using roll, pitch, and train or relative-bearing data as inputs. These transformations are governed by the following relationships, where L is level and Z is cross-level orders:

$$\sin L = \sin P \cos \alpha' - \cos P \sin R \sin \alpha', \tag{5a}$$
(A·28)

$$\tan Z = \tan R \cos \alpha' + \tan P \sec R \sin \alpha', \tag{5b}$$
(A·24)

where train is available; or

$$\tan L = \tan P \cos \alpha - \tan R \sec P \sin \alpha, \tag{6a}$$
(A·38)

$$\sin Z = \sin R \cos \alpha + \cos R \sin P \sin \alpha, \tag{6b}$$
(A·40)

where relative bearing is available.

In problems where simultaneous values of level, cross-level, and train or relative bearing for any line of sight are known and employed as mechanical or electrical inputs to a proper computer, the values of roll and pitch may be obtained as computer outputs. These transformations,

$$\sin P = \sin L \cos \alpha' + \cos L \sin Z \sin \alpha', \tag{7a}$$
(A·30)

$$\tan R = \tan Z \cos \alpha' - \tan L \sec Z \sin \alpha', \tag{7b}$$
(A·29)

where train is available; or

$$\tan P = \tan L \cos \alpha + \tan Z \sec L \sin \alpha, \tag{8a}$$
(A·42)

$$\sin R = \sin Z \cos \alpha - \cos Z \sin L \sin \alpha, \tag{8b}$$
(A·41)

where relative bearing is available, are the converse of Eqs. (5) and (6). The roll and pitch outputs of such a computer may be used in place of outputs from a stable vertical.

Level, cross-level, and train orders can also be obtained from the data pertaining to the line of sight of another target *without* first converting to

pitch and roll, if both train and relative-bearing angles for the second line of sight are known. With L, Z, α, and α' as before and L_1, Z_1, α_1 and α'_1 the corresponding angles for the second line of sight, then

$$\tan L = \tan L_1 \cos(\alpha - \alpha_1) - \tan Z_1 \sec L_1 \sin(\alpha - \alpha_1), \quad (9a)$$

$$\sin Z = \sin Z_1 \cos(\alpha - \alpha_1) + \sin L_1 \cos Z_1 \sin(\alpha - \alpha_1), \quad (9b)$$

and

$$\tan(\alpha' - \alpha'_1) = \frac{\sin(\alpha - \alpha_1)\cos Z_1 + \cos(\alpha - \alpha_1)\sin L_1 \sin Z_1}{\cos(\alpha - \alpha_1)\cos P}. \quad (10)$$

In deriving Eq. (9) the level and cross-level angles pertaining to the second line of sight have been considered as pitch and roll angles associated with a reference line in the deck. This is not the fore-and-aft line—the normal reference line—but rather a new line at angle α_1 to the fore-and-aft line. The equations are derived by substituting $(\alpha - \alpha_1)$ for α, and L_1 and Z_1 respectively, for P and R in Eq. (6). Equation (10) is derived by making the same substitution into Eq. (A·13). The angle $(\alpha' - \alpha'_1)$ is a partial train order that applies to the substitute reference line; the train order α'_1 must be added to get the complete train order α'.

In a similar manner, data for any line of sight can be substituted for pitch and roll data in other foregoing equations, although the interlocking of data in this way is often undesirable in the construction of computer instruments.

4·5. The Three-axis Pedestals Types 2 and 3. *Train Axis Surmounted by Elevation and Cross-traverse Axes.*—Figure 4·1*f* illustrates an antenna support of a type that differs from the three-axis type 1 mount only in the 90° shift of the bearing angle of the antenna with respect to the axes. Since such an antenna requires the use of the two-axis train correction for elevation of the beam above the horizon, it is desirable to use it only where antenna elevation is not required or where some definite mechanical advantage accrues from the arrangement. Such an advantage was realized in the design of the 10-cm radar equipment (Sec. 5·9*d*) in which it was desired to mount two separate antennas on a common support, one antenna being used for search and the other for height-finding. Mechanical convenience was achieved by mounting the antennas at right angles to each other. Thus, one antenna has type 1 orientation, and the other has type 2 orientation.

The mount in Fig. 4·1*f* may also be considered as a two-axis type 1 pedestal with an added axis. This axis, parallel to the radiated beam, may be used to prevent rotation of the beam about its central axis, as noted in Sec. 4·4. When used in this manner, however, the third axis does not relieve the pedestal from the high train rates and accelerations required if the beam is to be elevated above the horizon.

Train Axis Surmounted by Elevation and Cross-elevation Axes.—The three-axis mount type 3 (Fig. 4·1*g*) is essentially the two-axis type 2 mount with a train axis added. The addition of a train axis produces a mount that is no longer restricted in operation to zenith coverage only but is also fully practicable for complete sky coverage. Application of this arrangement of axes has been made in experimental three-axis gun mounts. In radar design at present, however, it is of academic interest only as one of the possible and workable arrangements of three rectangularly disposed axes. Antennas of this type can be trained on the target with minimum rate or accceleration requirements on all axes, irrespective of the position of the target or motion of the deck. The solution for the required antenna orders would require a cumbersome equation solver or analytic computer, which might prove to be impracticable. These orders could be readily provided, however, by a constructive computer such as that discussed in Sec. 4·9.

4·6. The Stable-base Pedestals. *Three-axis Stable-base Pedestal.*—The disposition of three axes in the manner shown in Fig. 4·1*h* provides a stable-base mount in which a roll axis lies in a fixed position parallel to the fore-and-aft line of the ship. This axis carries the pitch axis that supports the train axis. Pitch and roll signals from a stable vertical are applied as servo inputs at the corresponding antenna axes. The result, unique to the stable-base type, is that the train axis is stabilized in the vertical and may therefore receive a direct order of relative bearing as a proper train order. Freedom from the requirement of a computed train order brings with it the corollary advantage of freedom from train accelerations due to roll and pitch. Hence, the antenna may be trained at constant rates higher than would be practicable with other pedestals requiring application of the variable deck-tilt correction.

The three-axis stable-base antenna has no elevation axis and is therefore limited to applications where it is acceptable to have a fixed angle of beam elevation with respect to the horizon. It is also limited in some instances by such considerations of mechanical design as windage and balance, specifically treated in Chap. 5.

Four-axis Stable-base Pedestal.—The four-axis antenna shown in Fig. 4·1*i* is a stable-base mount retaining the advantages of the simpler mount shown in Fig. 4·1*h*. Through the fourth axis, it gains the additional freedom required for variable angles of beam elevation. Having no train accelerations due to tilt of the deck and requiring no computers, it falls short of nearly universal applicability to stabilization problems only because of the mechanical difficulties cited in the preceding paragraph. These are accentuated in a four-axis mount.

Although an antenna of this type has been used experimentally, there has been no production of it as yet. Its eventual application will be

virtually mandatory, however, if the further progress of radar requires an antenna capable of training a beam at various elevation angles at high rates of scan.

STABILIZATION INSTRUMENTATION

4·7. Stable Elements and Stable Verticals.—The basic equipments furnishing data for stabilization are the gyro-pendulum devices called the "stable elements" or "stable verticals." These are gravity-sensitive instruments of various designs, but all operate on the principle of a pendulum. The pendulum, through an electrical or mechanical nonrigid coupling, tends to "erect" the gyroscope to a fixed position with respect to the ground, with the gyro axis usually at or near the vertical. A stable reference line that is maintained in a fixed relationship to a horizontal plane regardless of rolling and pitching is thus established within the ship.

There are no universally accepted definitions of the terms *stable element* and *stable vertical.* As generally applied, however, the stable element measures and transmits values of level and cross level for any bearing, whereas the stable vertical measures roll and pitch only. With the stable element oriented to bearing 0°, the level angle is equal and opposite to the pitch angle, and the cross-level angle equals the angle of roll.

So defined, the stable vertical is much the simpler of the two devices because the supporting axis of the primary gimbal member is fixed with respect to the deck. Since it is necessary to be able to train the corresponding axis in the stable element in the deck plane, mechanical complications are introduced. These become more involved as higher accuracies are sought through the incorporation of compensations for the precessing force (variable with latitude) due to the earth's rotation and also for the disturbing forces arising from changes in the course and speed of the ship. In one stable vertical developed for the Radiation Laboratory by General Electric Company it was possible to incorporate a "turn-corrector" method that was superior to turn-corrector methods previously used. However, it would have been practically inapplicable had a stable element been required.

The stable vertical for producing roll and pitch data is all that is needed below deck for precise stabilization of the four-axis antenna or the stable-base three-axis antenna. A stable element alone would serve as well, but its train axis, which is superfluous, would result in unnecessary weight and bulk.

Where simplification is worth the cost of lowered accuracy in gyro performance or where the errors of line-of-sight stabilization are not objectionable, modified stable verticals can be used successfully at or near

the antenna instead of below deck. When so stabilized, the position of the beam is corrected to hold the horizon, but the deck-tilt correction is ignored and an azimuth approximation is accepted. In its simplest form the gyro pendulum is mounted as "back-of-dish" equipment on a two-axis antenna mount. The antenna becomes the servo follow-up member and responds through its elevation axis to the output signals from the gyroscopic device.

A local gyro installation on the roll axis of the "roll-stabilized" two-axis antenna (Fig. 4·1*d*) can be used without resorting to computers. This method of stabilization introduces an elevation error but results in a good line-of-sight approximation. Theoretically, both azimuth and elevation errors may be eliminated by incorporating gyro controls locally in both the pitch and roll members of a stable-base antenna of either the three- or four-axis type. However, any gyro equipment that is carried on the mast as a part of the antenna mount or carried adjacent to it is subjected to disturbing lateral accelerations from roll and pitch and also to difficulties arising from atmospheric conditions encountered in such an exposed location.

COMPUTERS FOR STABILIZATION DATA

Upon an analysis of the virtues and weaknesses of various stabilization alternatives, the radar-system designer is confronted with the fact that he cannot attain in ideal combination the four things that he seeks: simplicity of equipment on the mast, simplicity of below-deck equipment, high accuracy, and avoidance of approximations. If his problem cannot afford the luxury of the stable-base antenna as a solution, the only precise and accurate alternative is the use of the two- or three-axis antenna mount on the mast and the necessary computer associated with the gyro equipment below deck.

Computers for radar stabilization are of two types, either of which can accurately achieve the precise solutions of the equations appropriate for the stabilization of any specific antenna. In the analytic type, the problem is analyzed, and interconnected mechanisms are used to solve successively each arithmetic and trigonometric step in the equations involved. The alternate type is the constructive computer, often referred to as the "constraint," "geometric," or "bail" computer, in which a miniature model of the elements of the problem is constructed and a solution produced without requiring more detailed analysis.

4·8. Mechanical Analytic Computers.—The first computer designed for radar stabilization was a complex aggregate of the conventional step-by-step mechanisms used in preradar fire-control computers. By using a chain of such devices, a solution can be partially worked out in which the rotation of the output shaft is a high multiple of the desired output angle.

This makes it possible to keep at a minimum errors that are due to mechanical and assembly inaccuracies in the gears, cams, and other component parts.

Although very high accuracy can thus be obtained by the analytic step-by-step method, the aggregate of mechanisms for the precise solution of a computation such as the deck-tilt error runs into considerable weight, bulk, and expense. A further disadvantage is the difficulty of designing mechanical analytic computers for continuous operation. As these devices have heretofore been constructed, they are not sufficiently wear resistant, and it would be difficult, if not impossible, to gain full continuous operation with them.

4·9. Constructive Computers.—The alternative to the analytic computer is the *constructive* or *mechanical constraint* computer, which in principle provides a precise solution of stabilization problems. A relatively compact and simple mechanical device can be made that will simultaneously provide data for three stabilization variables.

The constructive computer can be readily applied to solve any computation encountered in the stabilization of any type of antenna mount. The simplest view to take in the consideration of any such computer is that the device is essentially a miniature model of the space problem. The point of intersection of the various gimbal axes represents the location of the antenna. One system of gimbals and bails represents the elements of the problem of or associated with the horizontal plane. The other set of members represents the elements of the problem associated with the constantly moving deck plane. The two gimbal systems are joined through the elements that are always common to both planes. When the known angles of the problem are introduced through displacement of the appropriate members, the other members, representing the unknowns of the problem, are constrained to assume the only possible corresponding attitudes.

The conventional universal joint represents an excellent example of a mechanical constraint computer and provides the simple basis for a number of such devices. A shaft that is attached to such a universal joint and rotated at a constant speed will transmit a variable rate of rotation to a second shaft whose axis is at an angle to the axis of the first shaft. During parts of each revolution the driven shaft will alternately lead and lag behind the driving shaft. If the angular difference between the two shafts is expressed as an equation in terms of the bend angle through the joint and the rotation angle of the driver referred to a fixed point, the equation is one that requires an elaborate grouping of analytic mechanisms for solution. It is, in fact, the equation for the deck-tilt error of an antenna on a ship at some fixed angle of roll and pitch. Because this is so, the equations can be ignored as such and the solution

derived directly by the use of fixed references and the application of devices to measure the rotation of the driven shaft relative to these references and to the drive shaft. It is possible to go further and provide the means for changing the angle through the joint to represent other combinations of known values of roll and pitch and thus provide a continuous solution for the actual deck-tilt correction required.

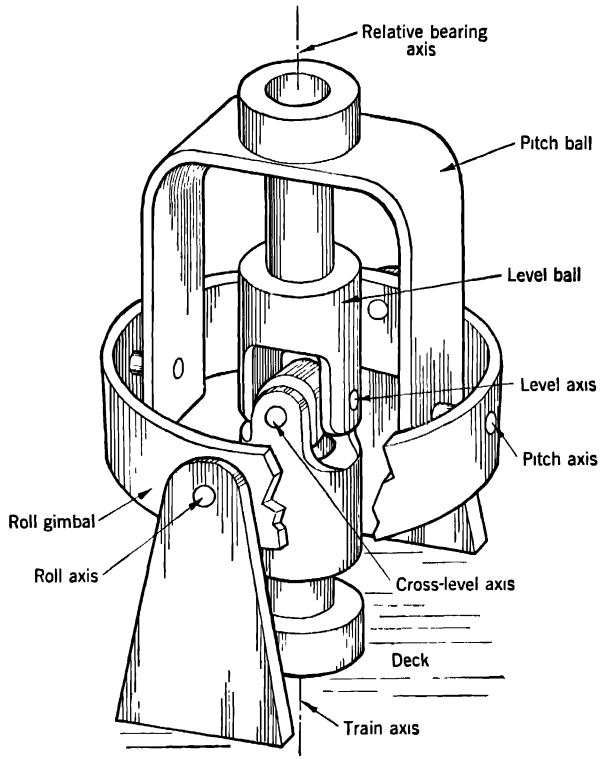

FIG. 4·5.—Constraint elements of a typical constructive computer. The synchros are not shown.

The universal joint must have one axis fixed in the ship and must be free to rotate about this axis while being located in the plane of a gimbal system that constitutes a similar second universal joint. The fixed axes of the two universal joints must be concentric and their pivotal axes must intersect at a central point. A union of two such concentric joints is represented schematically in Fig. 4·5.

In this figure the deck of the ship and a pair of trunnion supports form one shaft of the outer universal joint supporting the roll axis, which lies

parallel to the fore-and-aft line of the ship and about which the angle of roll is measured. If the angle of roll is applied to the roll gimbal in the proper direction, the roll of the ship will be canceled and the pitch axis will remain horizontal and parallel to the horizontal axis in the ship. If the angle of pitch is applied about the pitch axis in the proper direction, the pitch bail, representing the shaft of the outer universal joint, will be stabilized against both pitch and roll and the relative-bearing axis will be held vertical. The inner universal joint can be rotated with respect to the outer one if its shafts are concentrically supported by the corresponding parts of the outer joint.

The outer universal joint or gimbal system now provides the inner one with a means of controlling the angle of rotation through the joint between its shafts as a function of pitch and roll. It also provides these shafts with a reference base from which to measure the rotational departure of each, one in the deck plane and one in the horizontal plane, from its zero position.

The elements of a computer assembly required for stabilization of antennas are now evident. Such an assembly computes not only the train order including the deck-tilt correction [Eq. (1)] but also the level and cross-level orders [Eq. (6)]. It remains only to provide the means for putting in the known angular values at the driving members and for transmitting the computed values represented by the angular positions assumed by the driven members. For this purpose, servomechanisms receive roll and pitch signals from a stable vertical to drive the roll and pitch members R_m and P_m through their proper angles. A third servomechanism acts on target signals that are received from the radar operator's console and give relative bearing of the target, and applies this angle to displace the level bail relative to the pitch bail, shown in Fig. 4·5 at zero position. The induced relative rotation of the joined members around the level, cross-level, and train axes equals, respectively, the actual angles of level, cross-level, and train. These computed values may be transmitted to the stabilized equipment or wherever desired by synchro generators that are geared to the proper axes. By a relatively compact and simple mechanism, this geometric device can thus simultaneously compute three solutions that would otherwise require a formidable aggregate of component solvers for the arithmetic and trigonometric functions of the three equations.

It must be remembered, however, that a constraint computer is inherently a one-speed device that cannot take full advantage of geared-up synchros and that its accuracy in performance demands high quality of design and manufacture. Nevertheless, accuracies can be obtained that closely approach those possible with the analytic method and are adequate for high-precision radar stabilization. The slight loss of pos-

sible accuracy is more than offset by the great gain in simplicity, compactness, and adaptability to continuous operation without undue wear.

In the actual construction of a constraint computer, its essential basic elements are usually obscured by the interconnecting gear trains, motors, synchros, etc. It is difficult to recognize the simple members in the schematic sketch of an actual computer, but with sufficient study they can be traced.

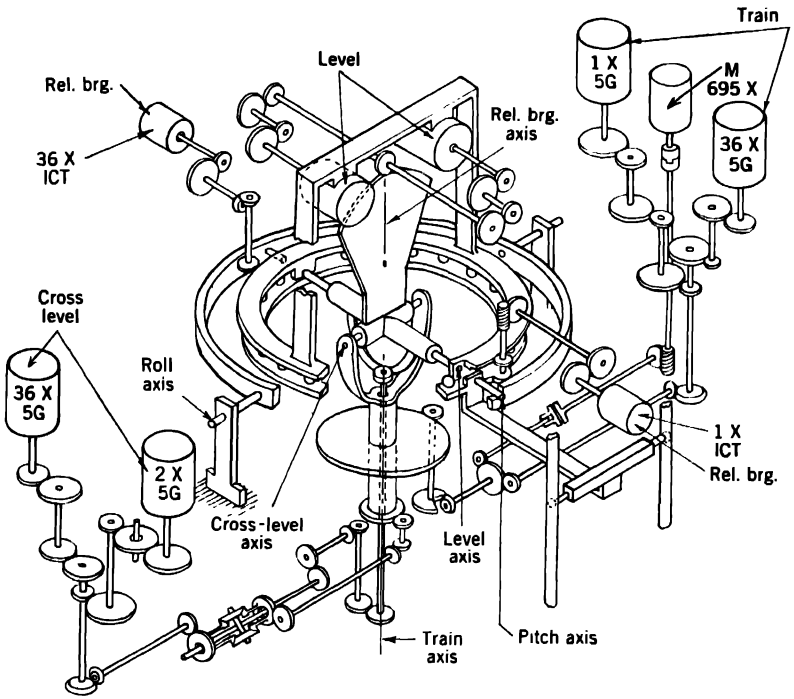

FIG. 4·6.—Schematic diagram of a constructive computer for three-axis stabilization.

Figures 4·6 and 4·7 present a developed schematic diagram and a photograph of computers evolved from the elementary schematic diagram of Fig. 4·5.

In spite of the relative simplicity of the geometric computer, highly accurate solutions are difficult to attain unless the greatest care is taken to assure the highest practical order of perfection in both design and machining specifications of all components. Such care is necessary, especially in the manufacture of precise low-speed gearing, of concentric gimbals and bails, and of high-quality servo follow-ups. Production techniques for precision gears and the performance characteristics of

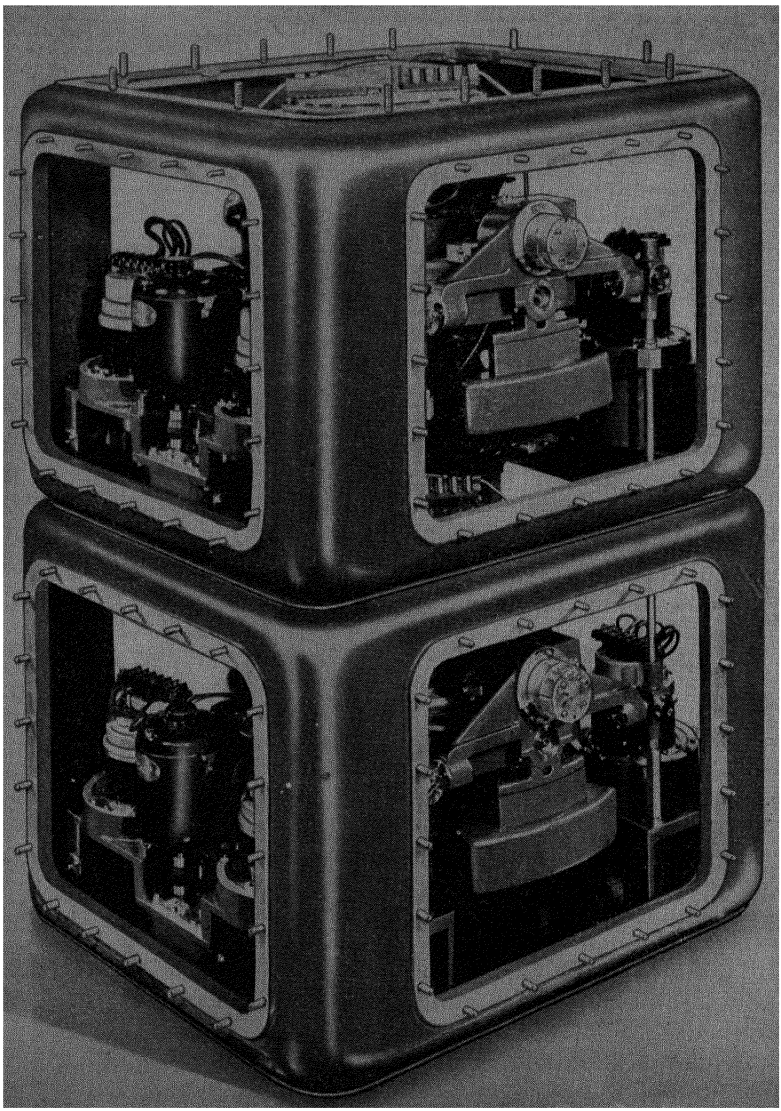

FIG. 4·7.—Computers for stabilization of three-axis (bottom) and two-axis (top) mounts with covers removed. (*Courtesy of International Business Machines Corporation.*)

instrument servomechanisms have so greatly advanced during the war that accuracies heretofore unattainable are now possible.

The stabilization of a three-axis mount by a stable vertical and constraint computer system was tested on a roll-and-pitch platform. The platform was made to roll with an amplitude of 15° at an 11-sec period and simultaneously to pitch with an amplitude of 5° at a 7-sec period. The weighted-average errors obtained at the antenna were 2′ in azimuth and 5′ in elevation, and the corresponding maximum errors were 5′ and 10′. Since these errors include gyro and antenna servo errors, the part of the error attributable to the computer is considerably smaller. These errors could possibly be reduced by a more advantageous arrangement of the gear trains and members in the computer; such an arrangement could be made by adopting for radar use the standard servo-synchro system of the Bureau of Ships. This system places the control transformer unit of the synchro tie at the stable-element, or computer, end of the system and thereby makes it practicable to use size 1 synchros in these instruments. This, in turn, by making rearrangements of parts possible, allows for more favorable gear and gimbal relationships without increasing the computer size.

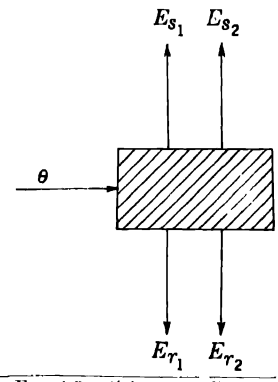

FIG. 4.8.—Schematic diagram of electrical resolver.

4·10. Electrical-resolver Computers.—The electrical resolver is a two-phase synchro differential, that is, a 1/1 two-phase transformer with a rotatable secondary. The two stator or primary windings are placed in space quadrature, as are the two secondaries. When a-c voltages E_{s_1} and E_{s_2} are applied to the stator windings and the rotor is displaced through an angle θ, the induced rotor voltages are, as indicated in Fig. 4·8,

$$E_{r_1} = E_{s_1} \cos \theta + E_{s_2} \sin \theta, \tag{11a}$$

$$E_{r_2} = -E_{s_1} \sin \theta + E_{s_2} \cos \theta. \tag{11b}$$

The angle θ is measured from a reference position of the rotor at which rotor coil 1 is in alignment with stator coil 1.

The electrical-resolver method of computing stabilization data is similar in some respects to both the analytic and the constructive methods of computation and may logically be considered as an adaptation of either. On one hand the equations of the problem may be broken down into a chain of subequations, each of which can be solved by one of a corresponding chain of electrical resolvers. On the other hand, study of the geometry shows that the problem can be solved constructively by a

sequence of rotations of the coordinate axes, each rotation being of the sort that can be represented by the action of a resolver. Such an analysis of the problem makes it possible to set up a suitable chain of electrical resolvers for solving the problem without the need for referring to the equations corresponding to each one of them.

The latter approach provides the simpler method of understanding the manner in which the resolvers may be applied to stabilization or similar angle-conversion problems. A vector having coordinates (x,y,z) in a right-hand system of coordinates is first considered. If the system is rotated about the z-axis through the angle θ, the coordinates of the vector in the displaced system will be

$$\begin{aligned} x' &= x \cos \theta + y \sin \theta, \\ y' &= -x \sin \theta + y \cos \theta, \\ z' &= z. \end{aligned}$$

It will be noted that these values of x' and y' are equivalent to the induced rotor voltages shown as outputs of the electrical resolver in Fig. 4·8. The function performed by the resolver is, therefore, the electrical counterpart of the rotation of axes in space. A series of such rotations can lead to the solution of most angle-conversion problems.

As an example, the computation of train and elevation orders for a conventional two-axis pedestal will be traced through the applicable resolver chain. It will be assumed that the true elevation and relative bearing of the target and the roll and pitch angles of the ship are known.

The general principle is to start with a system of coordinates with the x-axis along the line of sight and a unit reference vector in the same direction and then by successive rotations of the axes involving the angles of true elevation, true bearing, pitch, roll, bearing order, and elevation order to find the components of the unit vector in these successive sets of axes. The last two rotations must bring the axes back to their original position so that the final x component again has the value of 1, the y and z components again becoming zero. By this process it is found both mathematically and electrically what pair of values of the bearing and elevation orders is equivalent to any set of values of the other four angles. This problem is worked through mathematically in the first part of Appendix A, to which reference should be made.

If to the first resolver there are applied voltages $E_{s_1} = 1$ and $E_{s_2} = 0$, corresponding to $x = 1$, $y = 0$ of Eq. (A·1) and the rotor is turned through the angle β (β is the true elevation angle), the output voltages E_{r_1} and E_{r_2} will by Eqs. (11a) and (11b) be cos β and sin β, corresponding to x' and y' of Eq. (A·2). To the stator of the second resolver are then applied the voltages zero and cos β, respectively, and the rotor is rotated through the angle α. The output voltages will then be z'' and x'' of

Eq. (A·3). It will be noted that α can be varied continuously at a steady rate to correspond to steady scan in azimuth. The angles P and R obtained from a stable vertical can next be introduced by the third and fourth resolvers in an analogous manner so that voltages corresponding to Eq. (A·5) will be generated. These give the components of the reference vector in a system of coordinates in which the xz-plane is the deck plane, the x-axis pointing forward along the fore-and-aft axis of the ship,

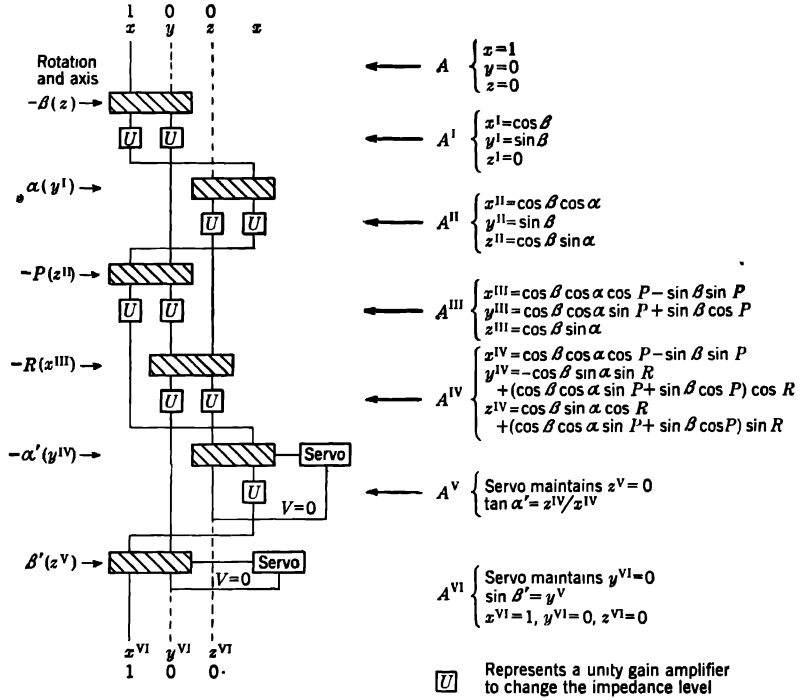

FIG. 4·9.—Schematic diagram of electrical-resolver chain in computer for two-axis stabilization.

the y-axis being perpendicular to the deck, and the z-axis pointing to starboard. This y-axis corresponds to the actual train axis.

The two final steps, which develop the solution angles, are readily accomplished in the last two resolvers by servomechanisms that drive the rotors of the resolvers representing the successive transformations involving α' and β' rotations so that zero voltages are maintained on the rotor outputs that correspond respectively to the z- and y-coordinates.

Figure 4·9 includes the equations for each step in the chain and designates the corresponding geometric transformations in the successive systems of coordinates.

Of all antenna-stabilization computers, the electrical-resolver type most nearly approaches the ideal of an aggregation of more or less standard component devices, and it may, therefore, provide the best possibility for minimizing computer manufacturing costs. The complete assembly of the synchro-and-resolver system with four servo systems and nine boosters (impedance-transforming amplifiers) becomes, however, a bulkier and particularly a heavier unit than might at first be expected from its mechanical simplicity. Also, the resolver computer, like the geometric bail computer, is a one-speed device and must therefore have highly precise gearing and servomechanisms if high accuracy is to be expected.

A single chain of resolvers can compute but two solution angles. This number is adequate for the two-axis mount, but three angular orders are required for the three-axis pedestal. If the three values are to be electrically computed, two chains are required, one having five resolvers and the other four.

Since the two-axis electrical computations are thus achieved more readily than three-axis computations, the situation encountered in the mechanical computers is reversed. This fact suggests that the resolver computer could logically be applied in two-axis antenna stabilization even though its weight and bulk may prevent its consideration for the three-axis mount.

4·11. Centralized vs. Individual Instrumentation.—The tendency through the war years was the continual addition to fighting ships of new radar, sonar, and other detection and communication equipments that, to be fully effective, require stabilization. The result has been the creation of problems of excessive weight and space allotment for the individual stable elements or stable verticals associated with these new systems.

The first approach to these problems was an attempt to avoid the duplication of gyroscopic instruments by tapping the train, level, and cross-level signals generated by and for the fire-control equipment and converting these data through appropriate computers to the orders necessary for stabilizing any other equipment. This approach was not approved by those responsible for ordnance stable elements because it was felt that interception of the vital output data for extraneous uses might adversely affect its validity for the original application. There were also the additional objections cited in the introduction to this chapter.

The second attempt at a solution was to make a single gyro equipment give the vertical-reference data for two or more of the new systems and thus reduce duplication. The result was an instrument, which combines the stable vertical with constructive computers as shown in Figs. 4·7 and

4·10. These computers are stacked upon the stable vertical and receive roll and pitch values from it through connecting rods. The stable vertical also produces synchro outputs of pitch and roll that are applicable to stable-base antennas and to any computers, either electrical or mechanical, that operate from pitch and roll data.

Various manufacturers have also given thought to reducing or eliminating the duplication of stable elements. The idea has gradually gained such general acceptance that it is no longer a question of whether or not

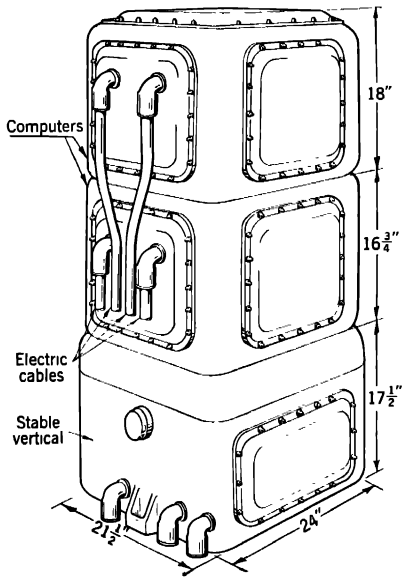

FIG. 4·10.—Stable vertical assembled with two computer units.

individual instrumentation should be abandoned but rather how far and along what lines should centralized instrumentation be pursued.

Four major alternatives may be considered:

1. Master stable vertical with electrical outputs for all purposes except main-battery fire control. All stabilized gear to be of stable-base design.
2. Same as (1), except with variously located individual computers to convert electrical pitch and roll data to data usable by nonstable-base equipments.
3. Master stable vertical in a ship to serve all stabilized gear in much the same manner as the course data of a ship are now supplied from the master gyro compass. Signals from main pitch and roll

buses to be converted individually to appropriate data for main-battery fire control and other nonstable-base gear.

4. Subdivision of the stabilized equipments of a ship into groups, each with one stable vertical providing mechanical and electrical pitch and roll data for the group.

Although Plan 1 offers the alternative requiring the simplest instrumentation, the gain in this direction does not appear great enough to offset the excessive weight of stable-base equipments (Sec. 4·6).

Plan 2 eliminates the question of main-battery participation and is perhaps the better for so doing. It is still open to the objection that stabilization problems other than main-battery fire control might benefit from prime data and that each computer for nonstable-base equipment requires duplicate roll and pitch servo systems.

Plan 3 possesses much merit but is open to the objection that the main battery is deprived of prime data. The conversion from pitch and roll to level and cross-level through a separate servo-driven computer necessarily introduces some error. The merit of the plan hinges largely on whether or not this error is tolerable. It is quite possible that it may ultimately be reduced to an acceptable value.

Plan 4 is exemplified by the Radiation Laboratory stable vertical and computer instruments and is a compromise between completely individual stable elements and complete centralization of gyro data. It has the possible disadvantage of requiring several gyro equipments in larger ships. It has, however, the advantages of solving at least two nonstable-base problems at each stable vertical with prime mechanical data and of eliminating pitch-and-roll servo duplication for each computer directly coupled to a stable vertical. In a great many ships there will not be more than two nonstable-base mounts to be stabilized, and these would be fully served by a single aggregate instrument. The more elaborate gyro-data requirements of other ships could be met by separate electrical or mechanical computers receiving electrical pitch and roll signals from the central instrument. As the number of stabilized equipments under this plan is increased, it would become desirable at some point to utilize a second stable vertical and a new group of dependent computers.

CHAPTER 5

SHIP ANTENNA MOUNTS

By R. J. Grenzeback and D. D. Jacobus[1]

The basic functions performed by shipborne radars are essentially no different from those of land-based radars. Scanning requirements, as set forth in Sec. 3·1, apply equally to land- or ship-based systems. In order to accomplish these functions fully, however, certain shipborne antennas must be compensated for the rolling and pitching of the ship.

The basic concepts of the stabilization of shipborne equipment are dealt with at length in Chap. 4. In the present chapter are discussed some of the mechanical features involved in the actual construction of mounts for ship antennas. Detailed descriptions of representative mounts are included at the end of the chapter.

5·1. Loading.—Intelligent design of an antenna mount requires consideration of all factors contributing to the loading of the apparatus. The relative importance of any factor is determined by the special requirements of the particular design. Military equipment, of course, is subject to much more violent loads than equipment intended for peacetime applications.

Wind forces constitute the largest single source of loading for ground and ship antenna mounts. The subject is discussed in Secs. 2·12 and 2·13 in some detail. The following discussion is concerned with the other factors contributing to the loading of an antenna mount.

The inertial loads are of paramount importance in the design of any antenna mount. They arise from two sources: accelerations due to forces acting upon the vehicle carrying the antenna mount, and accelerations imposed by the servo-driving system. Although these two inertial loading conditions have been defined separately, in practice they seldom occur separately. The severity of normal loads from the servo system varies with the purpose for which the radar is used. For instance, gun-laying mounts that must track moving targets rapidly experience much higher accelerations than mounts that perform simple search functions. Violent oscillations are not usually encountered under normal operating conditions, but the possibility of this occurrence during lining-up of the servo system must be allowed for in the design.

Shock loading may come from several sources and is usually more

[1] Section 5.9*d* is by D. D. Jacobus.

severe for shipboard installations than for ground antenna mounts. For the latter, road shock is probably the most severe of the normal loads encountered. These shocks occur primarily in the vertical direction and may cause maximum accelerations of 50 g. Since radar ground equipment is rarely operated while in transit, it is possible to provide stowing facilities that will prevent loads due to road shock from being transmitted to gear trains. Stowage as a means of protection against shock is not feasible for marine equipment.

Because of their location near the masthead, ship antenna mounts may experience accelerations of about 1.5 g as a consequence of rolling and pitching and of maneuvers of the ship. Motor torpedo boats are exceptional in that vertical shocks up to 15 g are encountered as a result of the motion of the vessel.

Maximum shocks that cause accelerations of 270 g, arising from gunfire, depth charges, and direct hits, may occur on warships. It is obviously impossible to build antenna mounts that can withstand loads of such magnitude and still comply with weight restrictions. Furthermore, the usual location of the antenna mount is such that shocks from the above sources will be largely absorbed by the structure of the ship. Generally speaking, design for 15 g vertically and 4 to 5 g horizontally will result in a serviceable unit. The foregoing design criteria will, of course, be modified whenever more specific information is available.

Shipborne and mobile ground equipments are subject to vibrations of widely varying frequencies. Damaging vibration frequencies are about 5 to 20 cps for most ships and 15 to 120 cps for motor torpedo boats. Suspensions that would isolate vibration at these low frequencies would offer very little resistance to severe shocks. The use of snubbers to limit the displacement under shock and to absorb the shock has been found to cause accelerations greater than those which would result through the use of stiffer suspensions with no abrupt changes in spring constant.

In view of the foregoing statements, it is currently considered good practice to use mountings that afford shock protection primarily but that are resonant above the range of damaging vibration frequencies in order to limit displacement. Rubber compression mounts having a resonant frequency at about 28 cps are recommended for ship installations. A high damping coefficient is desirable. Deflection under load of shock mounts used on ships should be about 0.010 to 0.015 in.

Generally speaking, since the antenna mount must maintain a fixed relationship to the ship upon which it is carried, pedestals are rarely supported by shock or vibration mountings but are fastened rigidly to the mast. Electronic equipment installed on the antenna mount, however, should be shock-mounted as discussed above. Most electronic equipment now being built will withstand low-frequency vibrations satis-

factorily if the vibration amplitude is not excessive. The rest of the antenna mount must be proportioned and reinforced so that it can withstand damage from vibration. As a rule, the reflector is the portion of the antenna mount that requires the most protection against damage from vibration. Critical points to watch are places of attachment, overhung tips, and local regions such as those between grid-element supports. Whenever possible, specific information should be obtained on vibrations that may be encountered in a proposed installation.

For small antenna mounts, structural weight loads are of minor consequence, but on larger mounts they are a considerable item. Accessories, in the form of special actuating devices, r-f components, etc., are a major source of dead weight. The designer must take into account the distribution of all these weights and evaluate their influence in combination with the dynamic loads.

One frequent cause of structural damage, not always apparent to the designer, is the variety of loads encountered in transporting and in moving the equipment into position during its installation. Damage that can be caused by careless personnel is considerable. It is impossible, of course, to anticipate and provide for all contingencies of this nature, but the designer can go a long way toward minimizing the chance for such damage. He should provide the equipment with judiciously placed and well-labeled handles or hoisting eyes. Projecting parts that might offer tempting handholds or footholds should be adequately reinforced if they cannot be eliminated. Fragile parts, if unavoidable, should be labeled with "Hands Off" warnings. Shielding, to prevent damage from dropped tools or other articles, should be liberal. These precautions should be observed even at the cost of a slight increase in weight.

Ice on the antenna structure will cause additional loading, and the problem of preventing its accumulation has, in the past, been a difficult one for designers of ground and ship antenna mounts. Various schemes have been proposed for dealing with ice by mechanical, thermal, or chemical means. Except for application of anti-icing fluid to radomes, none of these expedients has proved very practical in preventing ice or eliminating it once it has formed. Furthermore, prevention of ice formation on surface-based radomes has almost never been attempted operationally, and the trend in ground and ship installations is to eliminate radomes entirely.

The only remotely feasible means yet devised for preventing ice formation on exposed antennas is to apply heat to the structure. To accomplish this, especially with such an ideal heat radiator as a grid reflector, obviously requires large amounts of energy and is seldom practical. Actual experience with military equipment operating under all sorts of climatic conditions has proved that difficulties due to ice have

been less than anticipated. Only three or four instances of trouble from this source have been reported, and these were not serious.

Radar antennas intended for use in submarines require special designs. Both dynamic and static hydraulic loads are encountered. With due allowance made for differences in the applicable Reynolds number, the general remarks on wind loading (Secs. 2·12 and 2·13) apply in estimating dynamic loads on submerged reflectors. Reduction in total load is achieved by using a reflector of the grid type. Fortunately, from the standpoint of power demands, the antenna is not rotated while submerged. Sufficient power must be available, however, to overcome the friction of watertight packing glands and to permit operation in 60-knot winds.

The antenna must be capable of withstanding static pressures occasioned by operation of the submarine at great depths plus the pressure increment resulting from the explosion of depth charges near by. Impact loads from surface waves and the striking of floating objects must also be considered.

5·2. Antennas.—There are but few restrictions on the types of antennas that may find shipborne applications. Characteristics are set according to the intended use of the radar equipment, and the pedestal is then tailored to meet the demands of the antenna. In some instances, concessions can be made in the interest of mechanical simplification of the mount.

One example is the antenna mount[1] shown in Figs. 5·4 and 5·5. Whereas in elevation the feed and reflector are usually movable as a unit, in this mount only the reflector is tilted. The elevation axis passes through the vertex of the paraboloidal reflector, thus fixing this point with respect to the feed. Two advantages are realized by such an arrangement. (1) No rotary r-f joint is required for the elevation axis and (2) because of the geometric optics of the system, the radiant beam moves through approximately twice the angular movement of the reflector. There is a consequent saving in weight and space through the elimination of parts and the lowering of power requirements. The price paid for this simplification is a reduction in gain of the antenna. In the instance cited, this amounts to about 3 db (50 per cent) for beam deflections of 30°, but the loss is much less in moderate seas.

The major limitation imposed on the antenna design for nonstabilized mounts is that the vertical beamwidth must be at least 10° wide at the half-power point. This is the lower limit if the beam is not to rise above the horizon in moderate seas. If possible, the vertical beamwidth should

[1] *Cf.* T. J. Keary and J. I. Bohnert, "Shipborne Stabilized Radar Antenna for Sea Search," RL Report No. 659, Mar. 7, 1945; and "Line-of-Sight Stabilization of a Radar Beam by Reflector Tilt," RL Report No. 660, Feb. 19, 1945.

be not less than 15°. Sometimes this may be difficult to achieve. However, the problem is a matter of electrical, not mechanical, design. In the interest of high gain and good resolution the horizontal beamwidth is usually narrow.

There are no specific limitations on the type of reflector structure. In general, however, the open-grating type (*cf.* Sec. 2·7) is preferable for shipborne microwave equipment because of its sturdiness and low wind resistance. A secondary advantage is its optical semitransparency which serves to reduce blind spots. Specifications for most search antennas are that they shall be operative in winds up to 60 knots, i.e., about 70 mph, and that they shall not sustain damage in winds of 90-knot velocity.

Location of the reflector or reflectors with respect to the axes of rotation is determined primarily by consideration of wind loading, as discussed in Sec. 2·13. In addition to this requirement, an attempt should be made to maintain the center of gravity of the rotating parts as close to the axes of rotation as is feasible. Balancing about the train axis is important because as the ship rolls and pitches, this axis assumes a nonvertical position, thus forcing the power drive to lift any unbalanced loads against the force of gravity. Failure to take account of this in determining power requirements resulted in serious difficulties in early designs.

The speed at which the antenna rotates is set by operational requirements but generally will not exceed 24 rpm. For most shipborne search antennas a nominal speed of 6 rpm is maintained, with provision for variations of ± 4 rpm to cancel out the turning of the ship while maneuvering so as to hold a constant rate of rotation with respect to the surface of the earth.

5·3. Pedestals.—Of the various types of pedestals discussed in Chap. 4, only five have been generally used for shipborne service. These are the one-axis, the two-axis type 1, the three-axis types 1 and 2, and the stable-base pedestals. In each case, the choice has been determined on the basis of the simplest mechanical arrangement possible for adequate fulfillment of the operational requirements of the particular radar system.

Nonstabilized or single-axis mounts are intended to perform simple search functions and to aid in navigation. All remarks in Sec. 3·2 are applicable to shipborne units. Nonstabilized one-axis shipborne antenna mounts normally do not carry r-f equipment and hence do not require slip rings.

Line-of-sight stabilized two-axis antenna mounts for surface search perform exactly the same operational functions as the one-axis type, but with increased accuracy. The two-axis type 1 pedestals (Sec. 4·2), in conjunction with complex computers, are widely used with radars designed to aid in the control and direction of gunfire and are adequate

for tracking of the target. The two-axis pedestal is a good compromise when topside weight restrictions prohibit the use of the three-axis mounts that provide full stabilization of the radar beam.

In the three-axis stable-base antenna mount, the axis about which the antenna rotates is maintained in a vertical position at all times. The antenna, with its associated azimuth drive mechanism and data take-off, surmounts a gimbal system that allows limited rotation about each of two mutually perpendicular axes. These two axes are known as the "roll" axis and the "pitch" axis and may or may not lie in the same plane. The axes are named for those motions of the ship for which they compensate in maintaining the azimuth axis vertically. The roll axis is always parallel to the keel of the ship, and the pitch axis is always parallel to the surface of the earth.

Probably the worst feature of the stable-base mount is its top-heaviness. Even though the weight of the reflector and feed is small compared with that of the azimuth drive mechanism and data take-off, the necessary height of the center of gravity of the antenna above the gimbal axes makes the problem difficult. If the driving mechanism is lowered in an attempt to achieve equilibrium, the problem of clearances immediately becomes acute. From the standpoint of over-all weight, it is less expensive to keep clearances to the absolute minimum consistent with operational requirements and to increase the amount of power available for stabilization. The amount of total unbalance can be kept small for antenna mounts with light reflectors, and no practical difficulties result. For large antenna mounts that have relatively complex reflector and feed arrangements and the addition of r-f components on the stable platform, the limitations of the stable-base mount become more apparent, and employment of the three-axis type 1 pedestal is to be preferred. There is one requirement, however, that may dictate the use of the stable-base antenna mount despite its limitations. This mount sets no inherent limitation on the rate of rotation of the antenna about the azimuth axis. Where operations require high azimuth scanning rates, the only practicable solution is to employ a stable-base mount. A mount of the type in which the train axis is surmounted by cross-level and elevation axes has, in marine use, a practical upper limit of rotation about the train axis of about 9 rpm. Beyond this point the high accelerations that must occur about the level and cross-level axes for proper stabilization necessitate inordinately large and heavy power drives. Thus, the mount also becomes large and heavy and the weight advantage reverts to the stable-base mount. For equivalent systems, fewer slip rings will be required with a stable-base design.

It should be noted that the three-axis type 1 mount offers the lightest

construction for obtaining complete stabilization as well as permitting the antenna to be pointed at any elevation angle.

DRIVING MECHANISMS

5·4. Types of Driving Mechanisms.—Several methods can be employed to drive the axes of a shipborne antenna mount. The train or

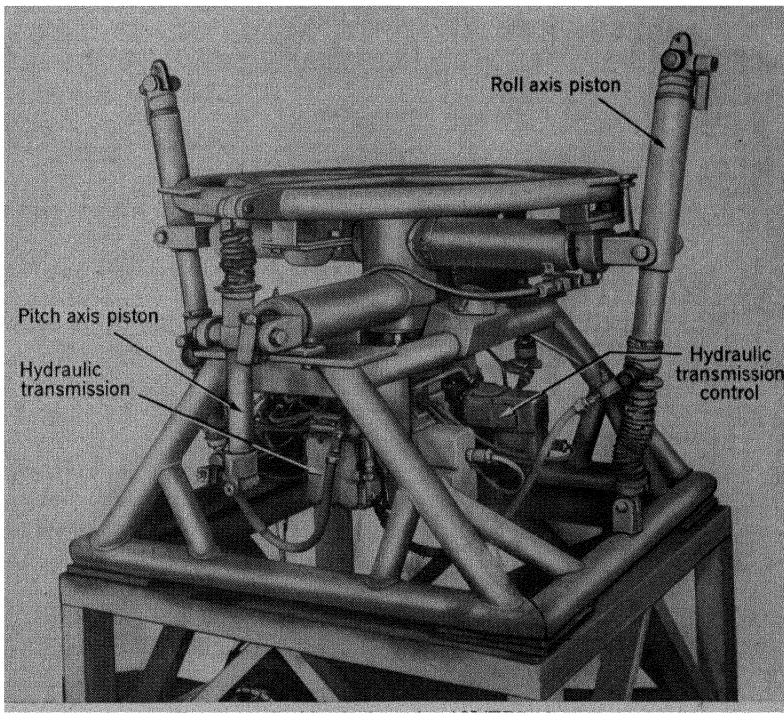

FIG. 5·1. Stable platform for AN/TPS-10 mount.

azimuth axis is almost invariably driven directly by an electric or hydraulic motor through a gear reduction. Similar direct-geared drive is also common on other axes of a pedestal. A motor-driven bell crank may be used to actuate the elevation axis of a two-axis mount.

The roll and pitch axes of a stable-base pedestal can be driven by (1) direct gearing from an electric or hydraulic motor, (2) electric motors driving lead screws, (3) crank-actuated push rods, and (4) hydraulic pistons. If hydraulic pistons or motors are used, an electric motor must be used to drive a high-pressure pump supplying the hydraulic drives.

The use of screws as actuating elements for the stabilizing axes has

been generally unsatisfactory, owing to their low efficiency of power transmission and the resulting heavy weight of such an installation.

In limited instances, crank-actuated push rods can be used advantageously to effect a lower center of gravity than can be had with direct gearing of motors to the stabilizing axes; the over-all arrangement, however, may require more space. Cranks have one merit in that the movements of the driven portions of the antenna mount are automatically limited by the throw of the crank. Thus, limit switches and mechanical stops can be eliminated. The disadvantage in cranks or push rods lies

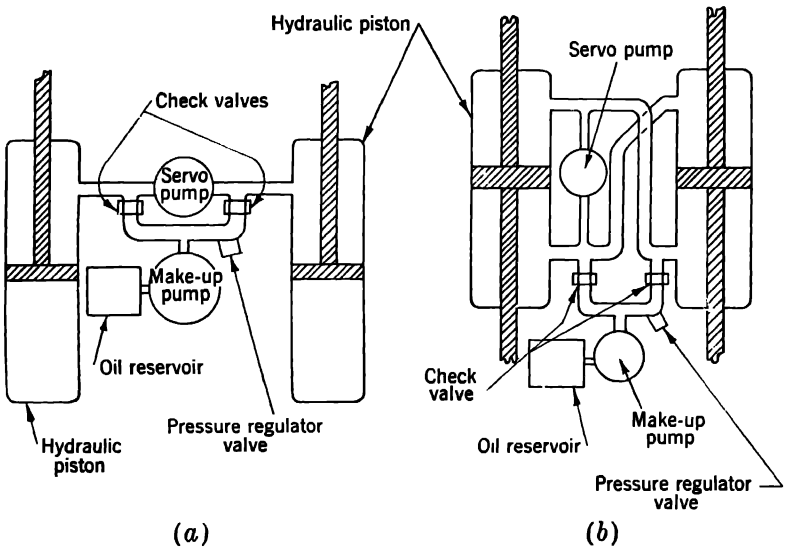

FIG. 5·2.—Hydraulic piston arrangements.

in their exposed position that makes them more susceptible to accidental damage than an enclosed directly geared drive.

The use of hydraulic pistons is shown in Fig. 5·1, illustrating the construction of a gyroscope-controlled stable platform maintaining a horizontal plane on a ship. A single 2-hp motor with a double-end shaft drives two servo-controlled hydraulic transmissions (Vickers #16801): one for the roll and one for the pitch axis of the platform. Each variable displacement pump of the hydraulic transmissions is connected by means of flexible tubing to two single-acting pistons on each axis. By reversal of the oil flow through the pump, oil is transferred from one piston into the other, thus retracting the first piston and extending the second. Replenishing gear pumps, driven directly by the drive motor, keep the servo valves under pressure and replenish the outputs of the system.

Synchro data take-offs located at the roll and pitch axes of the platform provide the controls for the servo valves.

Because of their availability, two pistons as shown in Fig. 5·2*a* have been used on each axis, connected as in the diagram. Since the total volume of oil in the two pistons varies because of unequal travel of the push rods at various pitch and roll angles, such a servo system may cause difficulties. It will operate properly only when the rate of change of the volume of oil in the servo loop is smaller than the leakage in the servo pump. Otherwise, failure may occur because of excessively high pressures that may build up in the system. Such a system cannot therefore be recommended as being too practical.

To counteract this deficiency, either one or two double-acting pistons of the type shown in Fig. 5·2*b* should be used for each pitch and roll axis, connected as shown in the diagram. It should be noted that the active areas of both faces of each piston are made equal. Pinned connections may be used at each end of all pistons if the roll pistons are fastened to the deck and the pitch pistons are fastened to members forming the roll axis, as in Fig. 5·1. When the platform is so constructed, there will be no interaction between the roll and pitch pistons as the deck changes its inclination. If it is desired to connect both the roll and pitch pistons to the deck, the roll pistons may be pinned at both ends, but universal or swivel-joint connections must be employed at the ends of the pitch pistons. A change of angular position of one axis in such a system will affect the displacement of the pistons on the other axis. The servo pump will automatically permit this readjustment when one set of pistons has three degrees of freedom of motion.

5·5. Motor-drive Selection.—Selecting the type of drive to be employed in any given antenna-mount design requires analysis of several factors. No inflexible specifications can be made for all contingencies. Each individual design necessitates separate study of the relative influence of the following interrelated items: (1) the intended operational function of the radar system, (2) the characteristics and limitations of the radar set as a whole, (3) the type or types of vessels for which the installation is contemplated, (4) the degree of stabilization necessary, (5) the weight allowances, (6) the type of servo control desired, (7) the physical sizes of available motors, (8) maintainance, and (9) the type of power available.

For example, for the stable-base mount, shown in Fig. 5·6, complete stabilization was desired but weight restrictions were severe. A hydraulic motor drive was selected for the stabilizing axes. The weight of the complete hydraulic installation at the mount was about the same as if two electric motors had been used to drive the axes directly. However, the very small physical size of the hydraulic motors, compared with an

equivalent electrical installation, resulted in a considerable over-all reduction of weight by permitting the use of a more compact gimbal. On the other hand, a three-axis type 1 pedestal (*cf.* Sec. 4·4) might not have benefited so much from the use of a hydraulic drive, since the pump unit could not be so conveniently housed on the cross-level axis.

Basic over-all power requirements are generally determined by the wind loading and the maximum accelerations that the mount will be required to attain. As a rule, wind loading will be the major determining factor for the roll, pitch, and train axes; the required accelerations are more important for level or cross-level axes. When the maximum speed at which the antenna must operate and the torque loads to which it will be subject are known, the horsepower of the driving motor can be determined. The loss of power within the gear train and from oil-seal friction must be allowed for. If the axes of an antenna mount are to be driven by servomotors, it may be noted that for most mounts the inertia (referred to the motor shaft) of the driven equipment is small when compared with the inertia of the motor itself. For practical design purposes, the inertia of small antennas can usually be neglected.

5·6. Gearing and Related Items.—Requirements for operational life of shipborne antenna mounts intended for search service are severe. The unit must be capable of continuous operation over long intervals of time; for naval service a normal life expectancy of 5 years is assumed. Allowing for some periods of stand-by, such as when the ship is in port, an estimated figure of 8000 hr per year is used as a basic design parameter. Gear dimensions and bearings must be selected on this basis.

Design of gears for the power drives is based upon wear and upon the stalling torque of the motor. Stalling torque is generally assumed to be four or five times the normal rated motor torque. If a hydraulic drive is used, relief valves serve to limit the maximum torque. Most gear reductions employed in antenna mounts require three to five stages of spur gearing. Designing for strength is the controlling factor only in the final stages; in initial stages gear proportions are determined entirely by consideration of wear.

Because the great majority of marine antenna power drives are servo-controlled, the reduction of backlash is imperative. This means that the gears must be accurately cut and of high quality. Over-all backlash of 6′ is considered a reasonable requirement for most gear trains employed in antenna-mount power drives; however, backlash of as much as 15′ is permissible in some cases.

Worm gearing should not be used in shipborne antenna-mount drives mainly because of its inherent shortcomings when subjected to servo control involving frequent and rapid reversals. The planetary type of gear reduction has had very limited use because of low efficiency

and the difficulties of proper manufacture. For general all-around reliability and ruggedness, the simple spur train is the most commendable. Also, the physical size of motors and the necessity for providing room close to the driving spindle for slip rings or other equipment often favor employment of a spur train to bridge the distance between the motor and output shafts.

Compactness of spur gearing can be achieved by cutting the gears in clusters and stacking them on shafts. Integral gears and shafts will also conserve space. For idling clusters, the use of a ball bearing at the larger end, combined with a needle bearing at the pinion end, will result in a design that is even more compact. When needle bearings are used, they should be of the precision type. Close tolerances must be maintained in their assembly, or the cluster will rock on the shaft and load up the ends of the needles, causing them to twist in their cases and become jammed. For maximum space-saving, hardened and ground shafts should be employed to act as inner races for the needle bearings. If these simple precautions are observed, a reliable and satisfactory mechanism will result without undue manufacturing difficulties.

Fits of splines and keys holding gears and shafts together must be held to tolerances as close as practicable without requiring too difficult an assembly job. A key or spline that is loose will rapidly get worse under conditions of servo operation.

The use of steel gears in aluminum gear boxes is entirely feasible when the gear boxes are small. Gears having pitch diameters over 8 in. should be made of high strength bronze in order to minimize changes in backlash due to differential thermal expansion of the aluminum case and the gears. Specifications generally call for equipment to be operated from $-40°$ to $+60°C$. If, to prevent interference, the minimum allowable backlash at $-40°C$ is taken as 0.0005 in., the backlash of the design in inches at $+20°C$ (68°F) for gears of 10 to 20 diametral pitch can be assumed as equal to 0.0005 in. plus one-half of the net change in center distance due to a temperature differential of 60°C. This amounts to backlash of approximately 2′ per stage for steel gears in aluminum cases if center distances are between 3 and 6 in. For practical purposes, a maximum over-all backlash of 2.5′ per stage for three- to five-stage trains may be assumed in allowing for temperature effects.

Aluminum is impractical for large gear boxes. Not only is thermal expansion a factor, but lack of rigidity in the aluminum box permits distortions that impair proper functioning of the gear train. Fabricated steel construction will weigh less than cast steel and has proved very satisfactory for large gear boxes when properly designed. A feature that is at times incorporated in large gear boxes is a bridge-type mounting of certain gears in the train, which allows adjustments to be effected in the

final assembly. This type of construction permits wider manufacturing tolerances while still fulfilling backlash requirements. For small gear boxes whose center distances normally do not exceed 6 or 8 in., accurate jig boring can be done without great difficulty; the adjustable feature is not needed. It may be utilized if desired but introduces unnecessary weight. Although not always possible, it is highly desirable to avoid blind assemblies. Inspection plates in gear boxes are of great assistance in the initial assembly and in trouble shooting.

The principal requirement of lubricants for shipborne antenna mounts is that they perform satisfactorily over a reasonably wide range of temperatures. Naval specifications usually indicate $-40°$ to $+60°C$, although for many purposes $-20°C$ would be a satisfactory lower limit. Oil equivalent to SAE 10 or 20 and a low-temperature grease such as Beacon M-285 should serve for almost all shipborne antenna mounts.

Large gear boxes require a sump with a small cam-driven pump of the plunger type, which distributes the oil through copper tubing to strategic points. Small gear boxes sometimes use this arrangement to minimize the head of oil over shaft seals, but splash lubrication is generally adequate. Oil leakage, a nuisance in general, has to be particularly guarded against in antenna mounts. In a radar system the whole operational performance can be seriously reduced because oil from gear boxes has leaked into the r-f waveguide or rotary joints or has fouled up slip rings, commutators, etc.

Truly effective sealing of rotating shafts against leakage of oil is difficult to accomplish practicably. Seals of the Garlock Klozure type are generally used but are seldom 100 per cent effective. At the bottom of vertical spindles, seals should be of the tandem type if space will permit. In the pedestal shown in Fig. 5·3 the motor is side-mounted and the main spindle enclosed in a well capped with a flinger, thus preventing the oil from getting to the lower main spindle bearing. Since main spindles rotate at low speed, the initial lubrication of the ball bearings is generally sufficient for the life of the unit. Seals, of course, are still necessary for the retention of this lubricant and exclusion of dirt and moisture.

Whether the motor is located on the top, bottom, or sides of the gear box will depend upon the design peculiarities of the mount under consideration. Whenever possible, however, the motor should be located on top of the gear box. The next choice is on the side; bottom mountings are the least desirable. This also applies to the location of the synchros. When motors must be mounted underneath the gear box, a flinger should be used above the motor shaft seal and the oil level should be kept below the seal when possible. A source of much trouble with leakage past oil seals is found in careless or ignorant handling of the seals during initial

assembly or removal and replacement of parts. The smallest nick in the sealing lip will make the seal ineffective. Hence, seals should never be installed without proper tools.

5·7. Power Distribution and Data Transmission.—Whenever electrical components are mounted behind the reflector, or whenever a pedestal has more than one axis of rotation, provision must be made for power distribution and data transmission between parts having relative motion. This is normally accomplished by the use of slip rings, flexible cables, rotary r-f joints, and, for hydraulic installations, flexible tubing. These are common expedients and do not differ from those discussed in Sec. 3·2.

With remotely located transmitters it is necessary, in the present state of development, to provide a rotary r-f joint for each axis of the mount. A piece of flexible waveguide would suffice at the stabilizing axes, but a waveguide of this type that will give entirely satisfactory service under conditions of continued flexing over long periods of time has not yet been developed.

The rotary r-f joint has considerable influence on the mechanical design of antenna mounts. Not only do the size and style have much to do with determining the physical dimensions of the pedestal, but the tolerances that must be maintained in the assembly of the parts will markedly affect the rest of the mount design. It is, therefore, of the utmost importance that the electrical designer and the mechanical designer have a mutual appreciation of their problems. Since the rotary r-f joint is an essential but sometimes temperamental part of the radar equipment, the design of its installation should be such as to permit easy removal and replacement. Savings brought about by improved design in rotary joints can be measured directly in terms of weight reduction and simplification of maintenance problems. The "mode absorber" waveguide rotary r-f joint[1] probably affords greater freedom in mount design than does any other joint, because it can be made in any arbitrary length and still give low standing-wave voltage ratios over a broad frequency band. Satisfactory joints up to 4 ft long have been built for the 3-cm band. This feature is especially helpful in designing a train axis that has a long torque tube.

In marine practice, the data-transmission devices for indicating angular position of the antenna differ in no respect from those already described in Sec. 3·2 for ground radar systems.

5·8. Corrosion, Thermal Effects, etc.—Shipborne antenna mounts are subject to severe weather conditions because of their exposed location. Their relative inaccessibility sometimes results in their being neglected by maintainance crews. Corrosion is bad for any equipment,

[1] Discussion of this type of rotary joint is found in Sec. 7·14 of *Microwave Transmission Circuits*, Vol. 9 of this series.

but with radar gear even slight fouling of small parts may be sufficient to impair the efficient performance of the entire set. Corrosion may arise from stack gases, salt spray, or electrolysis between dissimilar metals that are in contact. Condensation of moisture from the air inside the various pedestal enclosures is another common source of trouble. Because of the differences in heat capacity, steel parts within aluminum housings are especially likely to collect moisture, even though the ambient temperature change is only a few degrees. Entrance of rain water must be prevented by well-designed gasketing of all covers. Emergent shafts must also have proper seals to exclude dirt and moisture. Sealing elements should be of neoprene or other material that will not deteriorate under exposure to sunlight, oil, and temperature extremes.

Precautionary measures are simple but must be adhered to carefully. It is customary to provide pedestal compartments with thermostatically controlled heating coils. This will prevent condensation. All aluminum parts should be anodized, primed with one coat of zinc chromate, and finished with two coats of enamel paint. Interiors of aluminum gear boxes should receive one coat of Glyptal after anodizing. The liberal use of stainless steel is advised, expecially where parts are in rubbing contact. Adjacent parts made of dissimilar metals may corrode unless painted or plated or separated by a nonabsorbent gasket. Zinc plating is preferable to cadmium plating because it has less tendency to flake. Plated parts should not be used inside gear boxes or other places where flakes could cause damage.

Protection of the inner surfaces of brass waveguide and rotary joints is vital. Silver plating has been used extensively in the past few years but is being replaced for general use by the patented Ebonol,[1] which is a strongly oxidizing alkaline bath. It produces a finely etched black oxide surface that readily takes an external coat of paint.

CHARACTERISTICS OF SPECIFIC MOUNTS

The following descriptions of several shipborne antenna mounts designed to serve specific radar functions are included to indicate the diversity of form that the mounts may take. Some references to these mounts have been made throughout this text; main design and structural characteristics are presented here for convenience in tabular form.

5·9. Photographs and Tables. *a. Experimental 1-cm Antenna Mount.* The antenna mount shown in Fig. 5·3 is a nonstabilized one-axis mount for high-resolution search radars in the 1-cm band. In order to reduce the length of the transmission line the pedestal is bolted directly on top of the r-f package.

[1] Enthane Co., Waterbury, Conn.

The design and structural characteristics of this mount are as follows:

Service: shipborne surface search.
Type: one-axis, nonstabilized (*cf.* Sec. 4·1).
Total weight: 75 lb.
Over-all dimensions: diameter of sweep circle, 60.0 in.; height, 23.5 in.
Wind-load requirements: operational, 60 knots; structural, 90 knots.
Temperature requirements: to operate between −20° and 50°C.

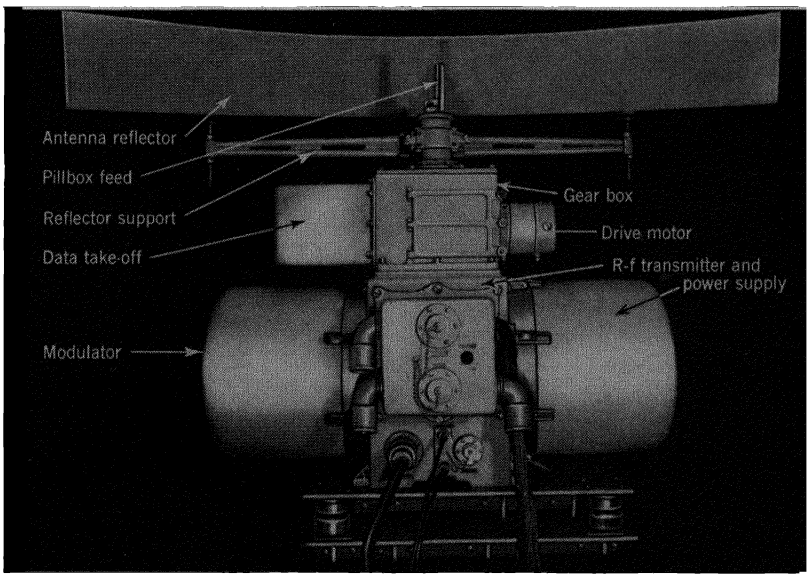

FIG. 5·3.—Antenna mount and r-f components of experimental 1-cm system. (*Courtesy of Sylvania Electrical Products, Inc., Boston.*)

Transmitting and receiving equipment: 1-cm band, adjacent to and directly beneath the antenna mount.

Train Axis:

Drive: $\frac{1}{10}$-hp 3600-rpm 115-volt d-c shunt motor.
Control: size 5 synchro generator at 1-speed.
Optional arrangements: size 6 synchro generator at 1-speed or size 5 synchro generator at 1-speed and size 5 synchro generator at 36-speed.
Gear reduction: 589/1 through 5 stages.
Allowable backlash: motor to 1-speed synchro, 12′ at 1-speed; motor to torque tube, 12′ at torque tube.
Stowing pin: none.

Antenna:

Feed: flared horn feeding half-parabolic pillbox.
Reflector: parabolic cylinder, solid surface, 58 × 7¼ × 14.5 in. focal distance.
Gain (abs): 36.5 db.
H-plane half-power width of beam: 10.3°.
E-plane half-power width of beam: 0.7°.
Polarization: horizontal.
Projected area: 2.92 ft².
Weight: 12 lb.

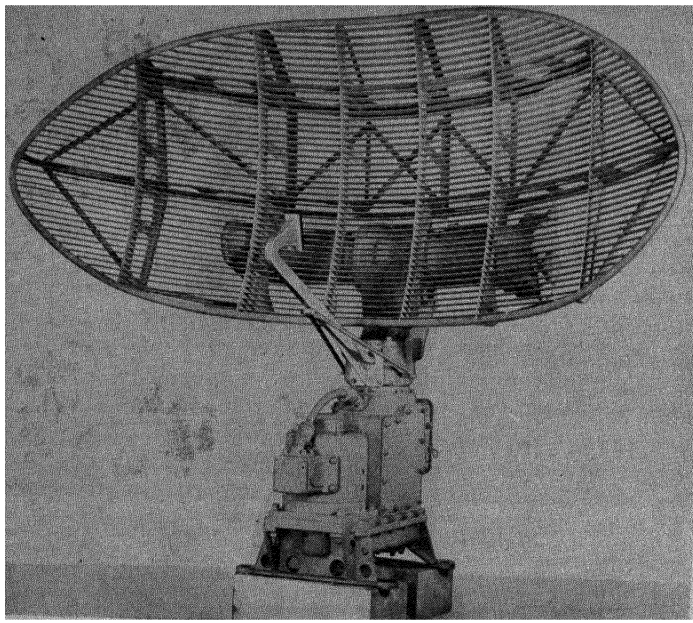

FIG. 5·4.—Line-of-sight stabilized antenna mount.

b. Experimental Line-of-sight Antenna Mount.—The two-axis line-of-sight antenna system (Figs. 5·4 and 5·5) was designed for the 3-cm band to fill the need for a lightweight shipborne radar that would provide stabilization adequate for surface search. When the beam is being stabilized on the horizon, only the antenna reflector is rotated about the elevation axis. The horn feed remains in fixed relation to the pedestal with the advantage, as stated in Sec. 5·2, that a smaller servomotor can be used and a rotary r-f joint at the elevation axis of the mount is eliminated.

When a size 6 synchro generator is used for data take-off, increased

size of the pedestal is required to house the larger synchro. This increase and provisions for captive screws at the access covers would increase the total weight of the antenna mount to 185 lb.

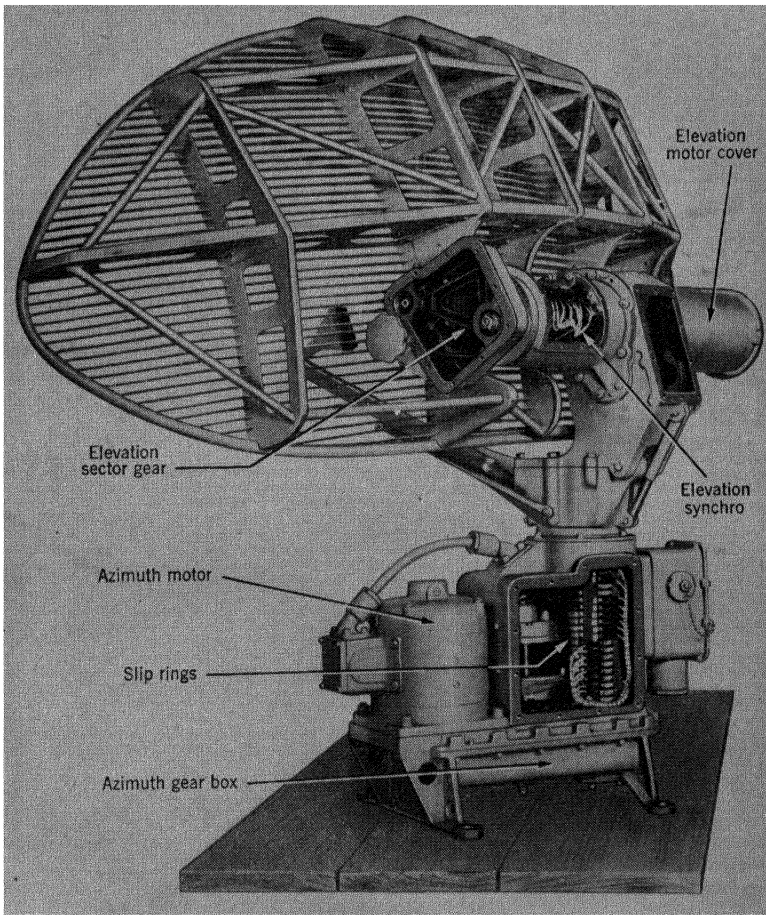

FIG. 5·5.—Antenna mount of Fig. 5·4 with covers removed to show elevation drive synchros and slip rings.

The characteristics of the experimental antenna mount are

Service: shipborne surface search.
Type: two-axis, type 1, stabilized (*cf.* Sec. 4·2).
Total weight: 151 lb.
Over-all dimensions: diameter of sweep circle, 66.0 in.; height 43.5 in.

Wind-load requirements: operational, 60 knots; structural, 90 knots.
Roll requirements:
Period of complete cycle: 6 sec.
Maximum angular displacement of radiant beam: 30°.
Pitch requirements:
Period of complete cycle: 4 sec.
Maximum angular displacement of radiant beam: 10°.
Azimuth scan rate (maximum): 10 rpm.
Maximum angular velocity in elevation: 0.73 rad/sec.
Maximum angular acceleration in elevation: 0.74 rad/sec^2.
Ratio $\frac{\text{beam tilt}}{\text{reflector tilt}}$: 1.78
Temperature requirements: to operate between $-20°$ and $+60°$C.
Transmitting and receiving equipment: 3-cm band, below deck.

Train Axis:

Drive: $\frac{1}{6}$-hp, 1725-rpm, d-c 250-volt armature, 125-volt field Amplidyne-controlled motor.[1]
Control: size 5 synchro generator at 1-speed.
Gear reduction: 139/1 through 4 stages.
Backlash: motor to 1-speed synchro, 10′ at 1-speed; motor to torque tube, 10′ at torque tube.
Stowing pin: none.

Elevation Axis:

Drive: $\frac{1}{20}$-hp 120-volt 4000-rpm split-field d-c motor.
Control: size 1 synchro generator at 2-speed.
Gear reduction: 1020/1 through 5 stages.
Allowable backlash: motor to 2-speed synchro, 8′ at 2-speed; motor to elevation shaft, 8′ at elevation shaft.
Stowing pin: to withstand 400 per cent of rated motor torque.
Stops: electrical limit stops set at $\pm 17°$ reflector tilt, $\pm 30°$ beam tilt. Mechanical limit stops to halt motion in the interval $\pm 17\frac{1}{2}°$ to $\pm 20°$ reflector tilt, with the electrical limit stops inoperative.

Antenna:

Feed: flared horn.
Reflector: slatted paraboloid, 54 × 24 × 14.5 in. focal distance.
Absolute gain: 36 db.
H-plane half-power width of beam: 3.7°.
E-plane half-power width of beam: 1.8°.
Polarization: horizontal.
Projected area: 7.69 ft^2.
Weight: 18 lb.

[1] General Electric Co.

c. Experimental Stable-base Antenna Mount.—This stable-base antenna mount (Figs. 5·6 and 5·7) for surface search radar in the 3-cm band provides full stabilization of the beam without any computers in the servo-loop system. Hydraulic drive, mounted inside the aluminum yoke casting, is used to actuate the roll and pitch axes of the mount for reasons outlined in Sec. 5·5. It is interesting to note that although the difference in weight of the reflectors of the two-axis, type 1 antenna mount (Sec.

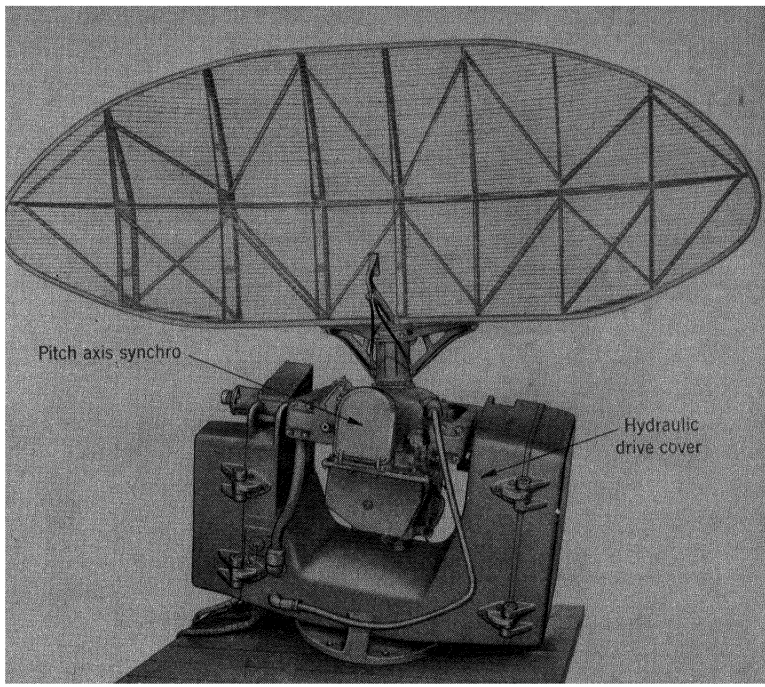

FIG. 5·6.—Stable-base antenna mount.

5·9*b*) and the reflector of the three-axis stable-base antenna mount (described in this section) is only 12 lb, the latter design is more than twice as heavy as the former. It would not be economical to use a smaller reflector on the stable-base mount, since the size of the pedestal could not be reduced any further and still provide for the specified limits of stabilization.

The characteristics of the 3-cm stable-base mount are

Service: shipborne surface search.
Type: three-axis stable base (*cf.* Sec. 4·6).
Total weight: 440 lb.
Over-all dimensions: diameter of sweep circle, 108 in.; height, 65 in.

Wind-load requirements: operational, 60 knots; structural, 90 knots.
Roll requirements:
Period of complete cycle: 6 sec.
Maximum angular displacement: 30°.
Maximum angular velocity (sinusoidal motion): 0.55 rad/sec.

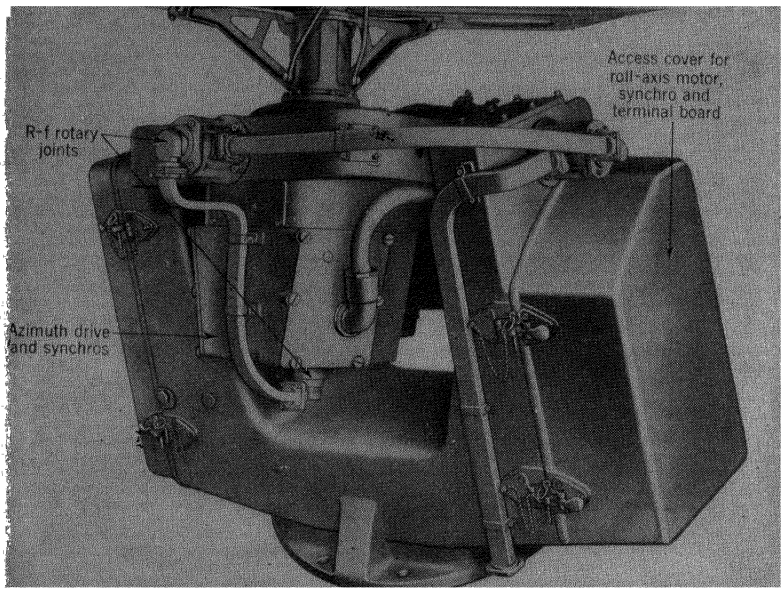

FIG. 5·7.—Stable-base antenna mount showing waveguide.

Pitch requirements:
Period of complete cycle: 4 sec.
Maximum angular displacement: 10°.
Maximum angular velocity (sinusoidal motion): 0.28 rad/sec.
Temperature requirements: to operate between −40° and +60°C.
Transmitting and receiving equipment: 3-cm band, below deck.

Azimuth Axis:

Drive: ¼-hp 1725-rpm d-c 250-volt armature, 125-volt field Amplidyne-controlled motor.
Control: size 5 synchro generator at 1-speed; size 5 synchro generator at 36-speed.
Gear reduction: 143/1 through 3 stages.

Allowable backlash: motor to 1-speed synchro, 8′ at 1-speed; motor to 36-speed synchro, 8′ at 36-speed; motor to torque tube, 6′ at torque tube.
Stowing pin: none.

Roll Axis:

Drive: Vickers MF 7-713-30 hydraulic motor. Maximum speed 1300 rpm when driven by Vickers AA-16850-B pump. Pump is a double unit supplying both roll and pitch motors. Pump is driven at 1650 rpm by a 115-volt 60-cycle 3-phase 3450-rpm Diehl electric motor rated $\frac{3}{4}$ hp for 0.9 time and 1 hp for 0.1 time.
Control: size 1 synchro generator at 2-speed.
Gear reduction: 247/1 through 3 stages.
Allowable backlash: motor to 2-speed synchro, 8′ at 2-speed; motor to roll shaft, 6′ at roll shaft.
Stowing pin: to withstand loads from simultaneous torques of 4500 in-lb at each of roll and pitch output shafts. Same pin used to stow both roll and pitch axes.
Stops: electrical stowing switches set at $\pm 31°$; electrical power cutoff switches to operate at $\pm 32°$ if stowing switches fail. Mechanical limit stops to halt motion in the interval $\pm 32°$ to $\pm 35°$.

Pitch Axis:

Drive: same as for roll axis.
Control: same as for roll axis.
Gear reduction: 493/1 through 4 stages.
Allowable backlash: same as for roll axis.
Stowing pin: see Roll Axis.
Stops: same as for roll axis, except limits are $\pm 11°$, $\pm 12°$, $\pm 12°$ to $\pm 15°$, respectively.

Antenna:

Feed: flared horn.
Reflector: slatted paraboloid, 78 × 30 × 21.6 in. focal distance.
Absolute gain: 39.4 db.
H-plane half-power width of beam: 2.7°.
E-plane half-power width of beam: 1.2°.
Polarization: horizontal.
Projected area: 13.24 ft^2.
Weight: 30 lb.

d. Experimental 10-cm Antenna Mount.—The fully stabilized 10-cm antenna mount (Figs. 5·8 and 5·9) is of the three-axis type and carries two

antennas. The radar set is designed to secure continuous information of the azimuth position, the range, and the height of all targets within a 50- to 100-mile radius at elevations up to 30,000 ft.

Height-finding is accomplished by electrical scanning at 600 cps by the use of the Robinson scanning feed described in Sec. 2·15. The feed illuminates the astigmatic reflector described in Sec. 2·9. With azimuth

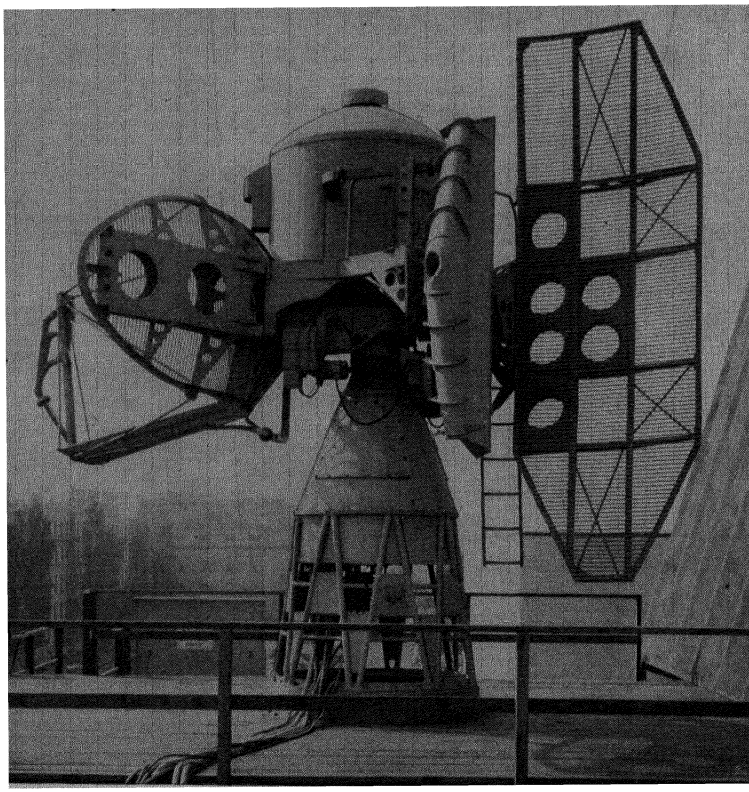

FIG. 5·8.—Combined search and height-finding equipment.

rotation at 4 rpm and a pulse repetition rate of approximately 1200 cps, airplane targets are viewed at ranges up to 50 miles; for targets at ranges in excess of 50 miles, the pulse repetition rate is lowered to approximately 400 cps and the rate of azimuth rotation is dropped to 2 rpm. This arrangement permits the height-finding sweep to secure an average of 10 pulse reflections as the electrical scanning beam sweeps past a target. Search information is secured from a fan beam narrow in azimuth and

wide in vertical pattern. A triple horn feed operating in the 10-cm band illuminates a 14- by 5-ft reflector.

The r-f transmitting and receiving equipment is located on the stabilized platform of the antenna mount. These components have been

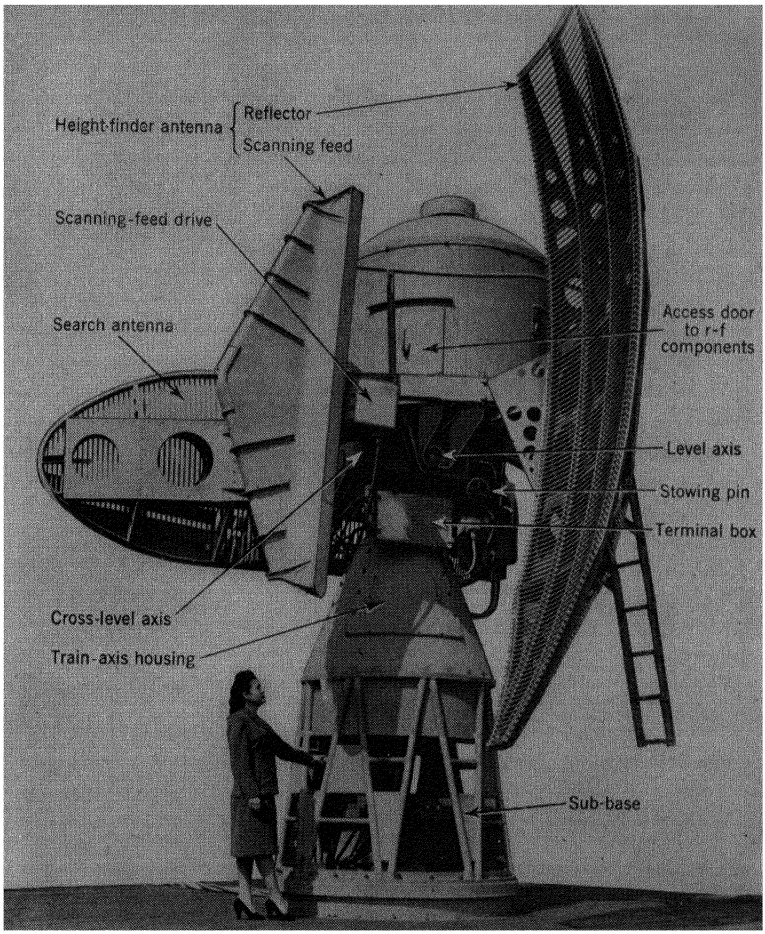

FIG. 5·9.—Antenna mount of combined search and height-finding equipment.

housed in an aluminum "igloo," with a ladder and an access door provided to permit easy access to the equipment for the periodic tuning and inspection required for peak efficiency and to permit adjustment of the receivers while the set is in operation. Sufficient space is provided inside

the igloo to allow the operator to make all adjustments from a comfortable sitting position.

Height-finding requirements demand that stabilization of the antenna be extremely accurate. The motors on all axes are controlled by servomechanisms from data transmitted by 1- and 36-speed synchros on the train axis and 2- and 36-speed synchros on the level and cross-level axes. All gearing is cut with great accuracy and set up with a minimum of backlash.

The weight limitations imposed because the antenna mount is located at the masthead have been met by fabricating the bulk of all structural parts of aluminum. The use of steel is limited to the torque tube, bearing plates, cross-level yoke, special alloy gears, and miscellaneous small parts. The antennas, which are subject to large wind forces, are centered as nearly as possible at the height of the level and the cross-level axes. In addition, the Robinson scanning feed, the associated height-finding reflector, and the search antenna are spaced around the azimuth axis so that there will be an approximate balance of the wind loads and thus a reduction of the resultant torques on the azimuth gear train.

All of the equipment is weatherproofed, and suitable drain holes are provided at all points where condensation can accumulate. Heaters are also provided to keep dry the double pulse rotary joint at the bottom of the torque tube, the slip-ring assembly and the electrical equipment inside the azimuth conical housing, and the r-f and associated electrical equipment in the igloo.

The full-load rated running current of the $1\frac{1}{2}$-hp azimuth drive motor is 5.4 amp at 210 volt. The current actually drawn by the azimuth motor with the mount running at 4 rpm and with no applied wind load is 1.0 to 1.2 amp.

The specific characteristics of the 10-cm antenna mount are given in the following list.

Service: shipborne search and height-finding.
Type: three-axis stabilized.
Weight:

Pedestal to stabilized support	3000 lb
Superstructure	1850 lb
r-f equipment	650 lb
Total	5500 lb

Over-all dimensions: diameter of sweep circle, 21 ft; height, 22 ft.
Wind-load requirements: operational, 60 knots; structural, 100 knots.
Roll (or pitch) requirements:
Period of complete cycle: 10 sec.

Maximum angular displacement: $\pm 19°$.
Maximum angular velocity (sinusoidal motion): 2 rpm.
Maximum angular acceleration (sinusoidal motion): 0.13 rad/sec^2.
Temperature requirements: to operate at $\pm 50°$C.
Transmitting and receiving equipment: two different wavelengths about 9 cm on the mount.

Train Axis:

Drive: $1\frac{1}{2}$-hp 3450-rpm 250-volt d-c Amplidyne-controlled motor.
Control: size 7 synchro generator at 1-speed; size 6 synchro generator at 36-speed.
Gear reduction: 3450 rpm to 6 rpm.
Backlash: motor to 36-speed synchro, 6′ at 36-speed; motor to 1-speed synchro, 5′ at 1-speed; motor to torque tube, 3′ at torque tube.
Stowing pin: to withstand 300 per cent of rated motor torque.

Cross-level Axis (level axis is identical):

Drive: $\frac{3}{4}$-hp 3450-rpm 250-volt d-c Amplidyne-controlled motor.
Control: size 5 synchro generator at 2-speed; size 5 synchro generator at 36-speed.
Gear reduction: 3450 rpm to 2 rpm.
Backlash: motor to 36-speed synchro, 6′ at 36-speed; motor to 2-speed synchro, 5′ at 2-speed; motor to cross level shaft, 3′ at CL-shaft.
Stowing pin: to withstand 300 percent of rated motor torque.
Stops: electrical limit stops set at $\pm 15°$. Mechanical limit stops to halt motion in the interval $\pm 15\frac{1}{4}°$ to $\pm 19°$, with the electrical limit stops inoperative.

Height-finding Scanner:

Drive: $\frac{1}{4}$-hp 1725-rpm 250-volt d-c Amplidyne-controlled motor.
Control: size 5 synchro generator at 1-speed.
Gear reduction: 1725 to 600 rpm.
Backlash: motor to 1-speed synchro, 5′ at 1-speed; motor to spinner, 3′ at spinner.

Materials of Construction:

Subbase: tubing, 61SW aluminum; cast footing, 40E aluminum (Frontier Bronze).
Drive gears: SAE 6145 steel forgings.
Synchro gears: stainless steel.
Structural fabrications: 61SW aluminum, SAE 1020 steel.
Cams, worm wheels: SAE 1112 steel.

Castings: 356-HT6 aluminum, cast steel.
Miscellaneous machined parts: 17SFM aluminum.
Slip rings: silver surface with bronze reinforcing.
Slip-ring brushes: 90 per cent copper, 10 per cent graphite.
High-voltage pulse joint rings: stainless steel.
High-voltage pulse joint brushes: 90 per cent silver, 10 per cent graphite.

CHAPTER 6

AIRBORNE SCANNERS

By W. M. Cady and R. M. Robertson[1]

By contrast to the surface-based antenna mounts discussed in Chaps. 3 and 5, airborne scanners are generally small and light. Except in special installations, the nature of the airplane[2] limits the width of the antenna to either 30 or 60 in. This limitation not only reduces the range performance [Eq. (1·4)] but also increases the beamwidth [Eq. (1·2)] of airborne radar. In order to improve the resolution, the shortest wavelengths are used: The 10-cm band is giving way to the 3-cm band, and the 1-cm band has been highly developed. The earlier airborne microwave radars, operating at about 10 cm, scanned with a 9° beam, but most current sets have beams from two to twenty times sharper.

The scanner installation is protected by a radome, a housing that is often in the form of a plastic blister external to the graceful shape of the airplane.[3] The installation is often inverted in comparison with surface-based mounts. This is almost universal in airborne radar for bombing or navigation, because in the very advantageous ventral location on an airplane, the antenna must be mounted below the base of the scanner.

To compensate the maneuvers and unsteady flight of an airplane, some scanners are stabilized (see Chap. 7).

The first part of this chapter is devoted to a general discussion of scanners. In Secs. 6·9 to 7·14 several typical scanners are described, these having been chosen for their diversity and because they exemplify particular characteristics. Other excellent designs are given only passing mention.

AIRBORNE ANTENNAS

Methods used in the construction of airborne microwave antennas are discussed in the following three sections, and the electrically important aspects of antenna design and specifications laid down in *Microwave Antenna Theory and Design*, Vol. 12 of the Radiation Laboratory Series, are briefly analyzed with reference to their reduction to airborne engineering practice.

[1] Sec. 6·14 is by R. M. Robertson.

[2] Although some airships carry radar, the overwhelming majority of airborne radar installations are carried by airplanes.

[3] See Part II.

6·1. Antennas with Paraboloidal Reflectors.—The earliest operationally important type of antenna for airborne radar operating at a wavelength of 10 cm or less consisted of a reflector in the form of a paraboloid of revolution, with a point source of energy at its focus. Although antennas of radically different design have since been developed, paraboloidal antennas are still the most widely used for airborne applications. In this and the following section the reflector and the point source, or antenna feed, are considered in turn.

Reflectors.—The most common parabolic reflectors of airborne radar have diameters of 13, 18, and 29 in. and 8 ft. A few intermediate sizes have also been produced. The three smaller sizes, which are of similar construction, are usually spinnings of 24ST aluminum alloy or similar material, 0.040 in. thick or less. For stiffness, the rim is turned back about $\frac{1}{2}$ in., either during or after the spinning process. Stampings of aluminum, magnesium, and steel have been used in place of spinnings; stamping is a convenient process, because the depth of a reflector is rarely as great as one-fourth of the diameter and a deep draw is therefore unnecessary. The reflector is screwed or riveted to a casting or other backing on the scanner; the screw heads or rivets in the face of the reflector do not harm the radiation pattern. Since airborne radar antennas are always housed, the wind forces that occur arise only from the motion of the antenna when it is scanning, and these are usually negligible. The reflector, therefore, in contrast to many of those in surface-based radars, is not perforated. For a paraboloidal reflector, the shape should be held locally to within $\pm\frac{1}{32}$ wavelength and to still smaller deviations over large areas.

Two of the chief functions of airborne radar are to aid navigation and to make blind bombing feasible. It is important that echoes be received not only from distant objects lying on the ground a very few degrees below the horizontal but also from closer objects at greater angles of depression; it is a great advantage if all like objects within range of the radar return echoes of equal strength. Figure 6·1 shows that a fan beam of radiation scanning the compass can fulfill these requirements. The energy must be dispensed frugally at the greater depression angles in order to avoid overillumination of the foreground. It can be shown that granting certain dubious assumptions as to the nature of the terrain, the energy should be transmitted in proportion to the square of the cosecant of the depression angle.[1] *Cosecant-squared* antenna beams are therefore specified for the most recent radars for air navigation. The beam may be thought of as a vertical fan of radiation of which the nose, or most intense portion, is nearest the horizon.

One method for producing a cosecant-squared beam is to use a dis-

[1] Vol. 1, Sec. 2·5, of Radiation Laboratory Series.

torted paraboloidal antenna. Several forms of distortion have been used as the art progressed and new energy distributions were required. One of the commonest of these is the 29-in. *barrel-stave* reflector (Fig. 6·2), so called because of an early experimental method of construction. To the upper half of the paraboloid there is added a false face, which merges with the paraboloid along the horizontal center line. The barrel-stave addition may be described by stating that (1) the intersection of the barrel with any plane that passes through the feed and is parallel to the horizontal diameter of the paraboloid is a parabola of which the feed

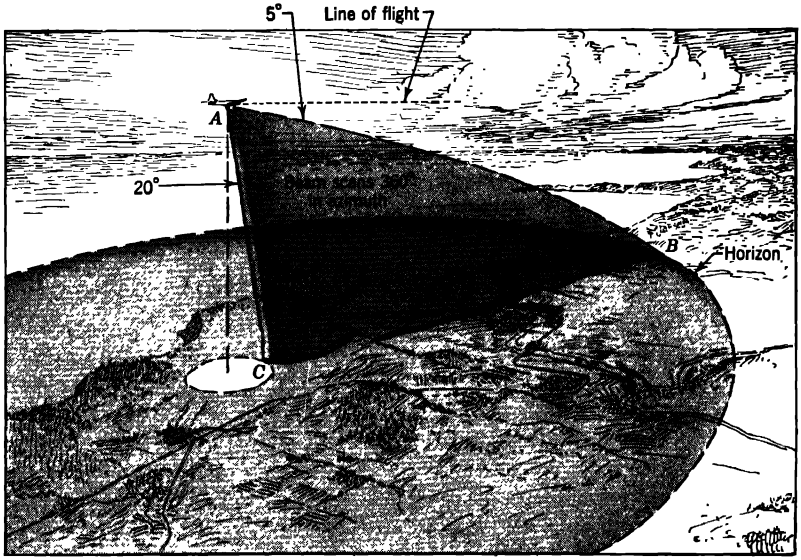

FIG. 6·1.—A fan beam that enables an airborne radar to scan the surface of the earth.

is the focus and (2) all these parabolas are identical. It follows that the part of the energy from the feed that falls on the barrel portion is reflected in a fan that is narrow in azimuth and wide in elevation. It also follows that the barrel is a surface of revolution and that the axis is a horizontal line crosswise through the feed. The barrel section is conveniently made by spinning; it is attached in two pieces to the paraboloid by bolts and braces. The tolerance on the shape of the reflector is about $\pm\frac{1}{32}$ wavelength.

The r-f transmission line to a paraboloid antenna terminates in the antenna feed at the focus of the paraboloid. The feed should be sufficiently directive so that nearly all of its radiation falls on the reflector and very little is propagated directly into space.

Feeds.—Most feeds for paraboloids can be classified as horns or vertex feeds. The horn feed is the flared ending of a waveguide transmission line. This type of feed is usually either an assembly of brass plates brazed to the end of standard brass guide or a single electroformed member. The transmission line to a horn feed is routed from the rotary joint past the upper edge of the paraboloid. In order to ensure proper utilization of the primary pattern the mouth of the horn must open

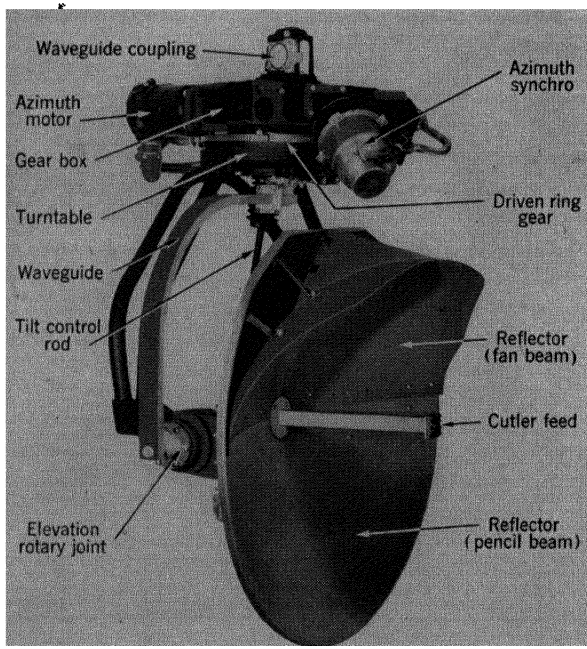

FIG. 6·2.—A barrel-stave antenna for producing a fan beam of radiation. It is shown mounted on a typical navigational pedestal. The wavelength is about 3 cm. (*Courtesy of U.S. Army, ACL, Wright Field.*)

toward the reflector. The aperture of a horn determines the primary pattern of the radiation: a paraboloid whose periphery is trimmed so that its width exceeds its height is best illuminated by a horn whose height exceeds its width. The horn may be hermetically sea'ed by means of a mica window or a plastic box or cup attached to a gasketed flange at the mouth of the flare.

Vertex feeds are point feeds that direct their radiation generally backward around the transmission line that they terminate. Such a feed is supported by the transmission line, which extends through a hole at the vertex of the paraboloid. These feeds also are ordinarily hermeti-

cally sealed. In one system, however, in which the transmission line that holds the feed spins rapidly, the entire spinning structure, including the spin motor, is within an airtight plastic envelope, thus removing the difficult requirement of sealing the high-speed rotary r-f joint.

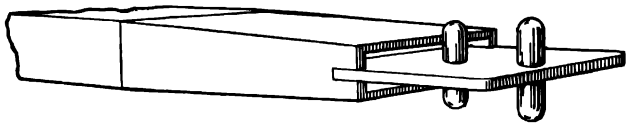

FIG. 6·3.—Two-dipole feed radiating toward the left.

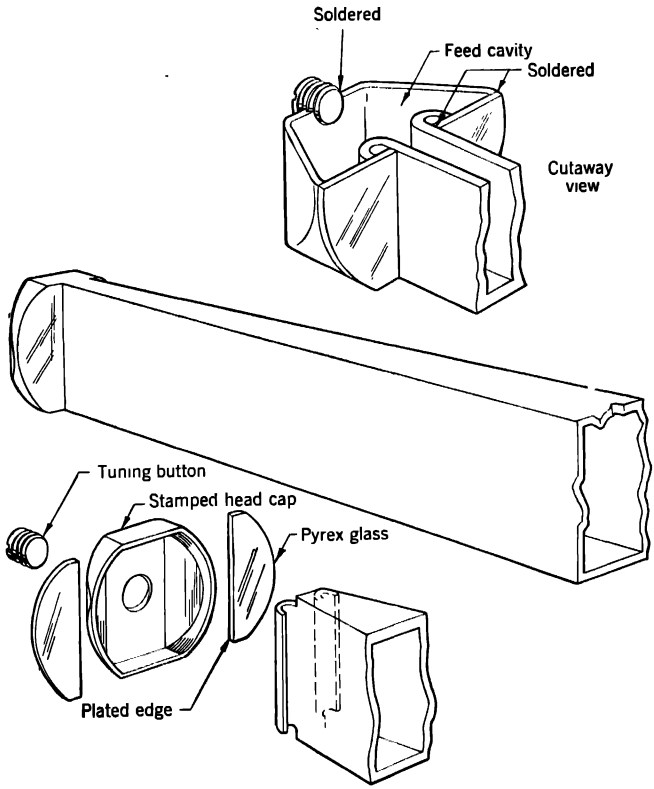

FIG. 6·4.—Modified Cutler feed. (*Courtesy of Dalmo Victor, Inc.*)

A two-dipole vertex feed, of a type commonly used at the 3-cm band, is shown in Fig. 6·3. An alternative design with similar properties has been developed by C. C. Cutler of the Bell Telephone Laboratories. The Cutler feed in one of its subsequent modifications is illustrated in Fig. 6·4. The electric vector and the narrow dimension of the wave-

guide for this feed are in the plane of the paper. The methods of construction will not be discussed at length, since the feeds present no unusual difficulties.

Vertex feeds are much used at the 3- and 10-cm bands, where the manufacturing tolerances are approximately $\pm\frac{1}{64}$ in. They have been made for the 1-cm band, but the tolerances have to be so close that horn feeds are preferred.

6·2. Antennas with Shaped Cylindrical Reflectors. *Reflectors.*—These antennas consist of a reflector and feed, as shown in Fig. 6·5, of

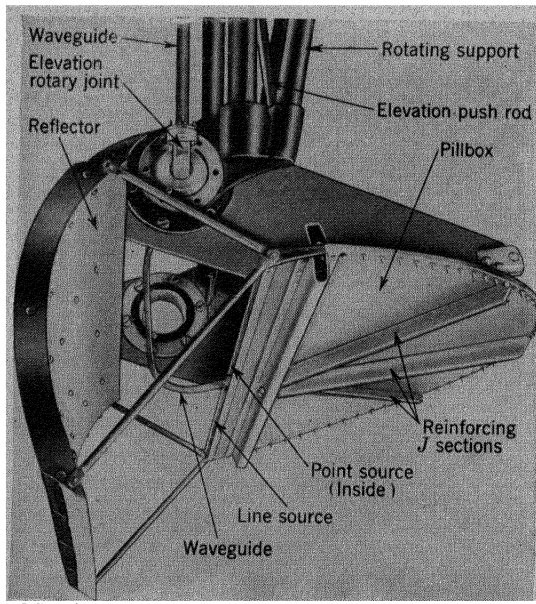

FIG. 6·5.—Antenna with a shaped cylindrical reflector for a 1-cm system.

design that is quite different from those described in Sec. 6·1. The reflector is a sheet in the form of a parabolic cylinder that has a horizontal generating line. Instead of a focal point, such a surface has a focal line; and instead of being concentrated at a point, the source of energy lies along this focal line. Since the feed is designed so that the r-f phase is at each instant the same at all points along its length, the radiation is propagated at right angles to its length. The radiation that falls on the reflector is thereby collimated in elevation and reflected into space as a sharp beam. The second antenna described in Sec. 3·3 is of this type.

The construction of typical shaped cylindrical reflectors is described in Secs. 6·11 and 6·12. In these examples, as always with antennas of this type, the upper part of the reflector is given excess curvature (shaped)

so that it reflects part of the energy earthward as the cosecant-squared fan.

Feeds.—The type of feed usually used with airborne shaped cylindrical reflectors is the pillbox. This is composed of two parallel metal sheets or plates that are straight on the front edge and connected by a metal strip forming a parabolic wall along the rear edge. The energy may be propagated between the plates in either the lowest *TE*-mode or the *TEM*-mode. When excited in the *TE*-mode, a pillbox radiates waves that are polarized parallel to its lips. The spacing between the plates must be uniform in order to prevent distortion of the wavefronts; slender metal posts may be used as spacers. With the *TEM*-mode the radiated energy is polar-

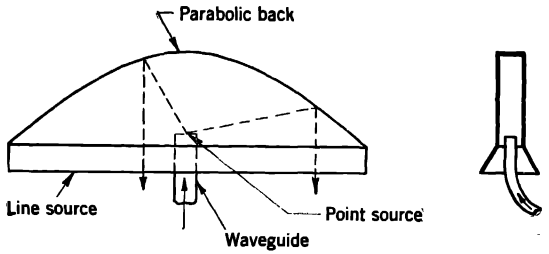

FIG. 6·6.—Energy propagation in a pillbox.

ized perpendicular to the lips. Simple spacer posts are forbidden, because in this mode the waves would be scattered by such obstacles. Fortunately, the spacing need not be uniform, and spacers are not a mechanical necessity.

In the pillbox shown in Fig. 6·6, two of the paths of the flow of energy (wave normals or rays) are indicated in dashed lines. Structural details of two pillboxes are discussed in Secs. 6·11 and 6·12.

6·3. Linear Array Antennas.—The elements of a linear array are dipoles (or slots) excited by energy tapped from the straight length of transmission line to which they are uniformly attached. The wavefronts from the individual dipoles are phased to form the resultant overall wavefront having the desired directivity.

The directivity is controlled by proper design and spacing of the dipoles. In one array, the energy is radiated in the end-fire direction. Such an array, acting as the entire antenna, has been used without a reflector. It projects a nonscanning beam forward from an airplane and enables determination of the distance to a target. The requirement for a broad pencil beam is best met by an end-fire array when considerations of aerodynamics or optical vision preclude an antenna that has any considerable cross section. One such design gives an end-fire beamwidth of 28°, is about 20 in. in length, and consists of 36 dipoles arranged 18

on each side of a $\frac{7}{8}$-in. coaxial transmission line. Each pair of dipoles is die-cast of an aluminum-silicon alloy as a single unit 2 in. in diameter and copper plated; it is then soldered in place on the transmission line, silver-plated, and finally gold-plated. Two probes, as shown in Fig. 6·7, penetrate slightly into clearance holes in the outer conductor of the transmission line. The 36 probes bleed out about 90 per cent of the power entering the antenna, and the residue is absorbed in a nonreflecting termination at the end of the line. Supported on metallic legs at either end and housed in a tubular plastic radome, this antenna is rugged enough to withstand the vibration and shock of combat service.

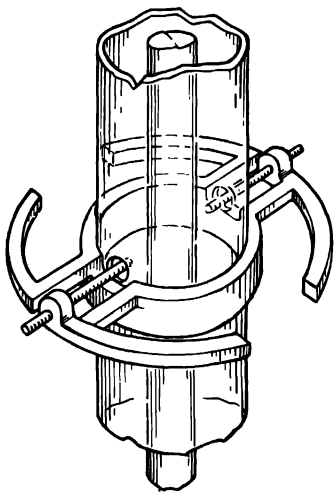

FIG. 6·7.—Two dipoles of an end-fire linear array, each energized by a probe.

A radically different array, also using no reflector, has a broadside pattern for airborne beacon use. It was designed for vertical mounting below the fuselage of an airplane. Its directivity is nearly uniform in all horizontal directions. The elements of the array are 18 vertical slots in three tiers, cut in the outer conductor of a coaxial line 1 in. in diameter. Two of these arrays are located in essentially the same tube. The inner conductor of the upper (transmitting) array is hollow and is in fact the outer conductor of the coaxial line that carries the energy from the lower (receiving) array to the beacon receiver. The electric polarization of each array is horizontal. The antenna, consisting of the two arrays housed in a streamlined radome, is mounted so that it extends 10 in. below the airplane. Neither this antenna nor the antenna previously described is used for scanning.

In place of a pillbox, a linear array with broadside radiation may be used for illuminating a shaped cylindrical reflector. Such an array, used with no reflector, is the basis of the Eagle scanner discussed in Sec. 6·14.

AIRBORNE ANTENNA MOUNTS

6·4. Conditions of Operation.—The ambient operating conditions of temperature, humidity, and pressure are often extreme for an airborne radar. The same set that must be ready for immediate use after standing in the desert sun must also perform satisfactorily at the low temperatures of the highest altitudes (*cf.* Table 6·1). The ambient temperature range

required for military service has been set by the Army and Navy at −55° to +71°C (−67° to +160°F) (*cf.* Table 6·1).

TABLE 6·1.—CONDITIONS IN A STANDARD ATMOSPHERE

Altitude, ft	Temperature, °F	Pressure, in. Hg
0	59 0	29.92
10,000	23.4	20.58
20,000	−12.3	13.75
30,000	−48.1	8.88
40,000	−67.0	5.54
50,000	−67.0	3.44

Operation under rapidly changing conditions of humidity is a contingency that must be given serious consideration. When an airplane makes a quick descent from a high altitude to a region of higher absolute humidity such as exists near the ground, accumulations of frost and dew form on mechanical and electrical parts. Furthermore, the condition known as sweating occurs when an airplane is left outdoors overnight, gets thoroughly cooled, and then condenses moisture from a humid atmosphere. This condensation may result in short circuits, corrosion, and impairment of the propagation of energy along internally wet transmission lines. Humid weather conditions favor the growth of fungus, even on circuit components. For airborne radars, the defense against humidity is to seal the transmission lines hermetically. For radars in tropical service it is further advisable to dip or spray all circuits with a fungusproof varnish.

The range of pressure in which radar must be operative is from atmospheric to perhaps $\frac{1}{3}$ atmosphere. The most notable effect of lowered pressure is arcing. This may occur in the transmission line, particularly at connectors and rotary joints or in the modulator or other circuits where high differences of potential exist. Arcing is prevented by careful design of the transmission line and particularly by pressurization. The transmission line, whether it is waveguide or coaxial conductor, can be hermetically sealed even at the rotary joints. It is common practice to maintain the pressure by a small air pump, on the realistic basis that true hermetic sealing is difficult and impracticable. In some radar systems, almost all of the equipment is sealed in an airtight "bomb."

An airborne radar set is subject to certain mechanical hazards. Vibration is one, and military specifications require that the scanner be able to withstand vibration of as much as a total excursion of 0.06 in. in any direction and at any frequency between 10 and 60 cps. This severe requirement has been relaxed for some antennas, because airplanes normally vibrate less than these figures imply. Most of the chassis

housing the electronic components are shock-mounted, but the scanner is generally rigidly attached to the airframe. The shock of a rough landing can cause damage to the radar. Shock mounts, however, are probably not effective in cushioning a hard landing, since their total unrestricted motion scarcely exceeds ¼ in., an insignificant figure by comparison with the landing-gear shock-absorbing mechanism, which has a travel of several inches. Extra ruggedness must be planned for the scanner, since inexpert handling is probably even more destructive than vibration and shock.

The weight in pounds of an airborne scanner[1] is about one-tenth of the square of the width of the reflector in inches. Rapid scanners and stabilized scanners are generally heavier than this, and some more recent scanners are lighter.

The angular motions of an airplane are severe enough to require consideration in scanner design (see Chap. 7). Of the voluntary maneuvers, banking involves larger angles than climbing or gliding. It has been variously estimated that small bombers rarely exceed bank angles of 15° to 30° and that the rate of banking of a large bomber rarely exceeds 6°/sec. The angle of attack of an airplane flying at a constant altitude varies when the indicated air speed is varied and is also dependent on the gross weight of the airplane. Within the range of speeds, loads, and altitudes of practical concern, the angle of attack varies by no more than about 5°, the nose-high attitude being characteristic of low speed, heavy load, or high altitude.

The involuntary angular motions of the airplane in rough air are almost ten times more severe in roll than in pitch or yaw. In the usual variety of flying weather, an airplane of medium size is probably disturbed about 5 per cent of the time by gusts that induce bank angles exceeding 10° or angular rates of banking that exceed 2°/sec.

6·5. Airborne Scanner Installation.—One of the problems in planning a scanner installation is the choice of its location. For successful operation, the radar must have unobstructed vision, and the antenna should be so installed that it may be housed in an aerodynamically acceptable radome. A very common requirement is circular vision of the ground well out toward the horizon. The only good location for mounting the scanner is then below the fuselage. The problems of such a location are discussed in Chap. 14. If rearward vision is not required, an antenna with circular scan may be mounted just behind and below the nose of the airplane, where the radome may be completely faired in. Scanning of only a forward sector is possible if the antenna is mounted in the nose. Such a location is impossible in an airplane that has a single tractor pro-

[1] W. L. Meyers, "Weight Analysis of Airborne Radar Sets," RL Report No. 340, Jan. 1, 1945.

peller; in that case an external housing becomes necessary. Aerodynamically, perhaps the best external site is at a wing tip, although a blister faired in to the leading edge of a wing has been widely used. For maintenance reasons, easy replacement of the set is desirable, and this has been effected in one instance by packaging the greater part of the set in a bomb suspended under one wing. The scanners of aircraft interception, AI, radars in night fighters are installed in locations that allow vision in all generally forward directions. They may be mounted in any of the positions that are fit for sector scanners. Scanners for protective fire control in bombers are located in a special rearward nacelle or on the turret guns, where they can search for and track enemy fighters approaching from the rear or sides.

Accurate orientation of the scanner installation in relation to the airplane is important. In a ground-mapping radar set, malorientation will cause falsification of the azimuth of all signals; in this event it is usual to secure faithful mapping by adjusting ("zeroing") the azimuth data transmitter rather than the entire scanner. The AN/APS-10 scanner is mounted in such a way that it allows compensation in flight for a changing angle of attack (*cf.* Sec. 7·4). Scanners for fire control must be oriented (*bore-sighted*) as a whole. Thus, for point-blank fire, where the axis of the conical scan must be parallel to the bore of the gun, specially designed adjustments are provided for aligning the scanner.

6·6. The R-f Transmission Line.—Although the r-f transmitter is never revolved with the antenna of an airborne radar, it is often so close to the scanner that as much as half of the transmission line is within the scanner. It is desirable to avoid the use of long lines because (1) the attenuation per meter of line is appreciable, (2) instability of the magnetron transmitter may result from the long-line effect, (3) the installation and cleaning of a long line is troublesome, and (4) weight is at a premium.

To facilitate the design and production of microwave transmission lines, sizes have been standardized. Almost all of those listed in Table 1·1 have been useful in airborne systems.

The most critical parts of a transmission line are often the rotary joints. Figure 6·8 shows one that was designed for use at the 3-cm band. Energy from the transmitter reaches the rotary joint in a rectangular waveguide. A transition is then made from this guide to a circular guide, so designed that in the latter the waves propagate in the TM_{01}-mode, which has axial symmetry about the center line. The gap between the stationary parts and the rotating parts is in the circular guide. The parts that rotate are the lower rectangular waveguide, the circular waveguide below the gap, and the sleeve immediately surrounding the latter. At a second transition, the waves again enter a rectangular guide into which certain internal structures have been introduced to eliminate

standing waves and to ensure the lowest possible *TM*-mode in the circular guide. As at the fixed couplings, a choke, or wave trap, is included at the gap. This eliminates the necessity for good and continuous contact between adjoining parts of the waveguides. The rotary joint may

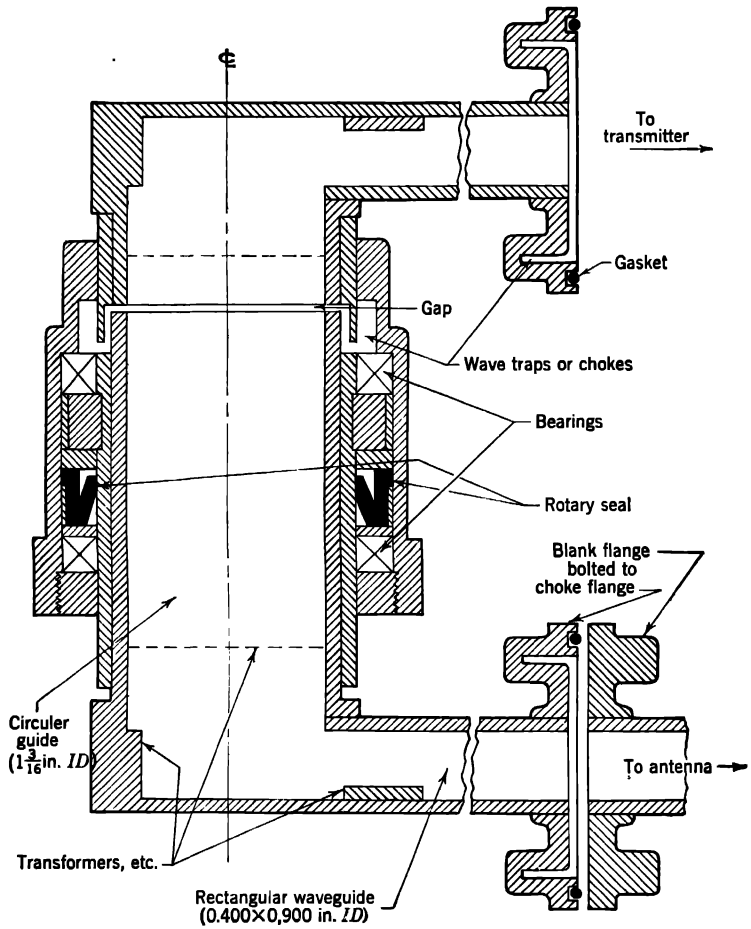

FIG. 6·8.—Schematic diagram of a typical waveguide rotary joint.

be hermetically sealed with a rubber-compound ring, as illustrated in Fig. 6·8.

Among the other types of rotary joints there is one that enables relative rotation of two sections of coaxial line, since the energy in this case propagates in a symmetrical mode. In a coaxial line a choke can be incorporated in the inner as well as the outer conductor. It is possible

to make a transition from a rectangular guide to a coaxial line. By the use of two such transitions and a rotary joint in the coaxial line, relative rotation of two segments of rectangular guide is possible, as shown in Fig. 3·1. Recent airborne waveguide practice favors the TM_{01}-mode joint for the 3-cm band and the coaxial joint for the 10-cm band.

A choke-to-flange coupling, as illustrated, permits considerable misalignment in both linear and angular displacement without causing severe standing waves. Very simple "wobble joints" that allow a total motion of 20° have been made by the use of such couplings. These may be sealed by means of a corrugated rubber-compound tube.

As it is extremely difficult to make a perfect seal in a joint, special pumps have been produced (Zenith Associates, Newton, Mass.) to supply dried air to the transmission line. These pumps weigh about 3 lb. They are automatically controlled to keep the pressure in the line at about sea-level value when the airplane is at high altitudes. Pressurization of transmission lines is now almost universally specified in airborne design.

6·7. Data Transmission.—A radar yields data not only on the distance to an echoing object but also on its angular position. It is therefore obviously necessary to know the direction of the beam of radiation whenever echoes are observed. This information can be made available to the operator in the form of scale readings, but other means are also used in all operational systems. The general practice is to generate at the scanner certain voltages dependent on the angular position of the beam and to use these voltages at the indicator to control the display on the cathode-ray screen.[1] The source of this voltage is termed a *take-off* or *data transmitter*. In airborne radar the principal use of scale readings to indicate the angular data transmitted from a take-off is to show the depression angle of the beam radiated from a ground-mapping radar.

It is sometimes required to set the position of an airborne antenna by means of a servomechanism. The data take-offs necessary for this are discussed in several sections of the next two chapters.

Among the many types (*cf.* Vol. 17, Radiation Laboratory Series) of data transmitters that have been used, the most common is the rotary inductor, or synchro, whose rotor is often geared to the antenna through 1/1 gearing and turns as the antenna turns. Transmitters, weighing from 1 to 3 lb each, are available under the trade names of Selsyn, Autosyn, Diehlsyn, and others. Usually, the stator contains three coils connected in Y and spaced 120° apart. The rotor is excited by a 115- or 26-volt 400-cps supply and excites the stator coils. The voltages so induced may be applied to the indicator. In the AN/APQ-13 radar system these voltages are applied to a synchro motor that orients

[1] The circuits involved are described in Chap. 3 of *Cathode-ray Tube Display Circuits*, Vol. 22, Radiation Laboratory Series.

the deflection coil of the cathode-ray tube. If, as in this method, appreciable torque is demanded of the synchro motor, both the generator and the motor must be sufficiently large and may weigh about 5 lb. The torque of such a synchro is about 0.4 oz-in. per degree. For most airborne synchros the accuracy is 0.5° to 0.8°.

Another method of operating a PPI display tube is to employ two fixed deflection coils in place of a single rotating deflection coil. The fixed coils are at right angles to each other and are excited in a manner that will produce a rotating magnetic field, an effect equivalent to that of a single rotating coil. The energizing of the two deflection coils is proportional to the sine and cosine, respectively, of the relative azimuth of the beam. This proportionality is realized if the data take-off is a sine-cosine resolver that is energized by the saw-tooth voltage from the sweep circuit. Such a resolver resembles a synchro in form and mounting.

Potential dividers, commonly called potentiometers, are frequently used to transmit angular data. The motion of the potentiometer brush is synchronized with the motion of the antenna. Usually the winding is toroidal, and the motion of the brush is rotary. Potentiometers are most often used to indicate angles that vary less than 360°, for example, the tilt angle of an antenna or the azimuth angle in a sector scan. Since the life of even a specially constructed potentiometer is limited to one or two million cycles of smooth and accurate operation, potentiometers are not used for rapid scans. Occasionally, a potentiometer may have more than one brush or more than two leads to the winding.

It is often important that the potentiometer be linear, in the sense that the resistance be a linear function of the angular position of the brush. A typical figure for the linearity of a good new potentiometer is 0.1 per cent; the linearity deteriorates slightly in one million cycles of operation. The resistance may be specified as high as 100,000 ohms or as low as 100 ohms, the wire diameter being 0.0015 to 0.010 in. The radius of the brush arm is commonly $\frac{3}{4}$ to $2\frac{1}{2}$ in. Potentiometers are sometimes built by winding the wire on an insulating strip that is then bent into the shape of a ring. If the brush must rotate through 360°, however, the winding must be toroidal, with no gap between the first and last turns.

Another data take-off that should be mentioned here is the "pipper," or heading marker. This is a switch closed by a cam on the azimuth axis of some scanners at the instant the beam is directed straight ahead, i.e., at zero relative azimuth. The closing of this switch intensifies the trace on the cathode-ray tube, thereby providing the operator with a heading marker. For other data take-offs, see Secs. 6·9 and 6·13.

6·8. Mechanical Components.—In this section there is a general discussion of the construction of airborne mechanical scanners. A com-

ponent common to all scanners is the drive motor. It is mounted on the scanner base, which is rigidly attached to the airframe, and is often a high-speed (6000 rpm) compound-wound 27-volt d-c motor in order to keep the weight at a minimum. Instead of grounding one terminal of the motor to the airframe, a ground return lead from the motor is usually provided. In a few systems, an explosionproof feature has been considered necessary. More generally, the ends of the motor are partially open to allow ventilation, which may be forced. The power rating of the motor, for continuous duty, usually ranges from $\frac{1}{8}$ to $\frac{1}{2}$ hp. It has often been necessary to protect the communications equipment in the airplane from the electrical noise produced at the commutators of motors employed in the radar system; this is effected by means of filters in the motor leads.

Since the speed of the motor usually exceeds the desired rate of scan, a gear reduction is necessary. The scan rate is usually in the range of from 6 to 30 rpm for circular scanners, 30 cpm or more for sector scanners, and up to 2400 rpm for the fastest spiral and conical scanners. For antennas that must "track" another airplane, a rate as fast as 120°/sec should be available. Spur gearing is usually desirable for the speed reduction. Because of the humidity, dust, sand, and salt spray to which scanners are often subjected, the gearing in most designs is enclosed as completely as possible. Another design problem is imposed by the temperature requirements. The differential expansion of the gears, shafts, and gear case, which are commonly all of different materials, must be anticipated in order to avoid binding or excessive backlash at extreme temperatures. This problem is aggravated by the unequal temperatures of the various parts.

The lubrication of a gear train presents obvious difficulties because of the great temperature range. An oil bath is sometimes used but is often undesirable because it requires tight seals where shafts pass through the gear case and because the starting torque is high at low temperatures. More commonly, a small amount of grease smeared on the gears is considered sufficient. The Beacon M-285 grease has proved valuable.

In addition to the motor, the scanner base carries one or more data take-offs. Since the gearing for these take-offs must be as free from backlash as possible, it is good practice to use a special gear train between the take-offs and the main shaft of the scanner rather than to depend on the drive gear train for this purpose. The data gear train often has spring-loaded split gears whereby the gear teeth are kept always "on the same side of the backlash." When two take-offs are required, it is sometimes possible to simplify the data train by coupling one take-off to each end of a single shaft instead of providing a separate shaft for each. For greater accuracy, one of the data take-offs is sometimes geared to turn, for

example, just ten times faster than the antenna. That this practice can lead to a 10-fold ambiguity in the angular indication of the antenna is obvious, but the ambiguity is removed by providing on the antenna a contact that closes once every revolution.

The function of the drive gearing is to rotate the main shaft of the scanner. Commonly, this shaft supports at its extremity a yoke, or fork, with two equal arms equipped with bearings for mounting the antenna. In most scanners the antenna may be made to tilt or nod a few degrees in relation to the yoke. The power for this rotation is transmitted to the antenna in one of two ways, either through a gear train powered by a motor that is mounted on the yoke and to which current is brought through slip rings on the main shaft or through a mechanical linkage. Such a linkage consists of three elements: a motor and gear train on the scanner base, providing a linear output motion parallel to the main axis of the scanner; a thrust bearing concentric with the axis and moved along it by the gearing; and revolving with the reflector, a push rod or cable connecting the reflector with the revolving race of the thrust bearing. In some instances, use of the mechanical linkage has resulted in a lighter and more satisfactory scanner. In this way, a scanner has been designed weighing only 13 lb as compared with the original 20 lb for the AN/APS-10 scanner.

No matter how the power for antenna tilt is transmitted, it is necessary to provide a data take-off to indicate the tilt angle. It is convenient to locate the take-off on the same structure as its corresponding motor.

In almost all scanners, the main shaft is a torque tube that is hollow to allow insertion of the transmission line. Sometimes this tube itself serves as a waveguide, but more often the transmission line is distinct from the structural parts of the scanner and is supported by them. The shaft diameter is always determined by the size of the transmission line at the rotary joint. The most compact designing seldom allows reduction of the inside diameter of the main ball bearings below $1\frac{1}{2}$ in. for scanners at the 3-cm band. It is less than this for the 10-cm band because $\frac{7}{8}$-in. coaxial line may then be used.

Ball bearings are used throughout in almost all scanners. On the main shaft one bearing is often clamped and the other left free to slide longitudinally as differential expansion requires. Differential expansion also may be accommodated by the use of one ball bearing and one needle bearing. Bearings of porous alloy impregnated with oil have been used for low-speed shafts, but these tend to become stiff under service conditions. In exposed positions, shielded or grease-sealed ball bearings are generally used; but in protected locations and especially on high-speed shafts, it is preferable to use open bearings and thereby reduce friction.

EXAMPLES OF AIRBORNE SCANNERS

6·9. AN/APG-15.—The 7-lb unit shown in Fig. 6·9 was designed by General Electric Company. The smallest and simplest of the airborne scanners, it is part of an aircraft gun sight, AGS, radar.[1] It is attached to a cannon in a tail turret and enables the gunner to aim directly at an attacking fighter, regardless of visibility conditions.

The AGS antenna consists of a 13-in. paraboloidal reflector that collimates the 10-cm energy from a dipole-and-disk vertex antenna feed and

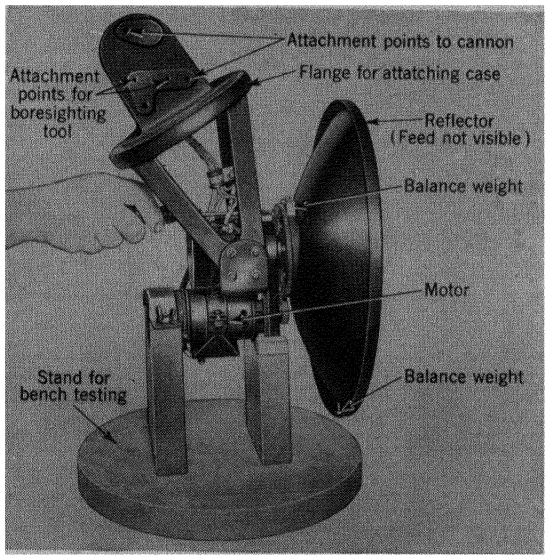

FIG. 6·9.—A conically scanning unit. (*Courtesy of General Electric Company.*)

produces a beam 25° to 30° wide that moves in a conical scan at 2400 rpm. The feed is the termination of a coaxial transmission line with an outside diameter of $\frac{1}{2}$ in. Although the line is not pressurized, there is no tendency toward arcing at high altitudes, because the power level of the transmitter is low. The axis of the feed and scan is parallel to the gun barrel.

Generally speaking, there are at least three distinct possible mechanizations of conical scan (*cf.* Secs. 2·17 and 2·18) by rotation of parts of an antenna:

1. The feed may be held fixed while the reflector, which is slightly tilted to one side, spins about an axis through the feed.

[1] Bert W. Weber, "Preliminary Instruction Manual for AN/APG-15," RL Report No. M-178B, Jan. 3, 1945.

2. The paraboloid may be held fixed while the feed, which is located slightly to one side of the axis of the paraboloid, spins in a circle about this axis.
3. The feed may be permanently located at the focus of the paraboloid, and the entire antenna spun about an axis slightly displaced in angle from the axis of the paraboloid.

The AGS scanner, or spinner, exemplifies the first of these motions, the spinning reflector being tilted about 4°, producing a beam nearly 8° off axis. This method of conical scan has the advantage of needing no rotary joint in the transmission line.

The reflector is manufactured by spinning a 0.040-in. sheet of Dowmetal FS-1 magnesium alloy. Its rim is turned back about $\frac{1}{2}$ in. for the sake of rigidity. It is supported only by being bolted to a slightly tilted collar that is 3 in. in diameter and mounted on the main shaft. Suitable weights attached to the collar and to the rim of the reflector remove the dynamic unbalance caused by the tilted attitude of the reflector.

The spinning shaft is hollow so that it can take the transmission line. It turns in two ball bearings and is driven by a $\frac{1}{6}$-hp 3800-rpm d-c motor. A ground return is used, a return lead being considered unnecessary for so small a motor. The two 32-pitch steel gears, although noisy, have a longer life than the nonmetallic pinions of the earlier models of this scanner. By means of a commutator on the main shaft, voltages that are applied to the indicator signify within which quadrant is the attitude of the spinning reflector. The commutator carries four slip rings made of coin silver—one continuous, the other three broken—and is molded in a single piece by the polymerization and solidification of the plastic cylinder that supports the rings. The brushes are made of silver graphite and are easily replaceable.

The aluminum-alloy base of the scanner supports the motor parallel to the main shaft. The base is mounted to a cast support arm, hung on the yoke that carries the cannon. The scanner is enclosed in a spherical case, one hemisphere of which is steel; the other is the radome, made of Fiberglas laminated with a resin. The r-f line leading to the scanner is a flexible coaxial cable which allows relative motion between the gun and the transmitter-receiver unit of the radar.

6·10. Large (10-cm) Experimental Scanner.—The largest airborne mechanical scanner so far used is simple. The axis of the beam does not have to be elevated or depressed; the scanner merely revolves at 6 rpm. The scanner is shown in Fig. 6·10. Its weight is about 190 lb.

The reflector is a paraboloid 8 ft in diameter and is trimmed to a roughly elliptical shape 3 ft high to permit streamlining the radome and to allow clearance of the ground in landing. Radiation of about 10-cm wavelength is used, resulting in a beamwidth of 3.5° in azimuth and 8° in

elevation. The reflector is illuminated by horizontally polarized waves that issue directly from the end of a rectangular waveguide flared into a rectangular horn 1.751 in. wide and 8.474 in. high at the mouth.

The face of the reflector is a single sheet of 0.040-in. 24ST aluminum alloy that has been stretch-formed to shape. It is made rigid by means of a 0.051-in. 61SW aluminum alloy backing sheet into which a waffle pattern has been indented in a hydropress. The softer alloy is required in

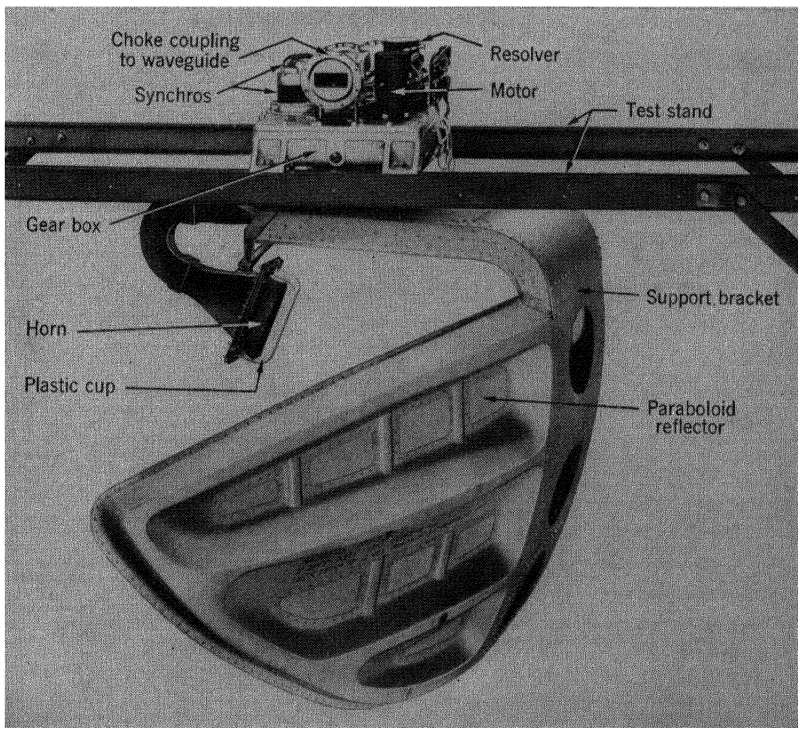

FIG. 6-10. - Large airborne scanner with an 8-ft reflector.

order to avoid tearing the metal in forming the indentations, which are $2\frac{1}{2}$ in. deep. The concave side of the backing sheet has the same curvature as the rear of the reflector sheet to which it is riveted. For convenience, the backing sheet is made in three sections. The center section forms a part of the box beam made of curved sheet aluminum alloy that serves as the support bracket. The mechanical design, tooling, and manufacture of this reflector were carried out by the aircraft industry, in close collaboration with the Radiation Laboratory. The weight is 43 lb, or slightly over 2 lb/ft^2.

The feed horn is formed by electroplating. A precision casting of a base alloy, Cerrobase, is first heavily plated with iron. The base is then melted away, leaving a strong iron shell that is internally smooth and precisely in the shape of the feed and associated waveguide. To prevent corrosion of the feed, a coating of nickel is electrodeposited both before and after the deposition of the iron. A Cerex (Monsanto Chemical Company) plastic cup, bolted to an external flange on the horn, hermetically seals the feed.

The two ball bearings in which the main shaft of the scanner turns are fastened to the scanner base, which is an aluminum gear box 16 by 22 by 4 in., that has a cover and four feet for mounting. The $\frac{1}{3}$-hp 7500-rpm d-c motor and the data take-offs are mounted on the cover. Steel spur gearing is used throughout, except that the gear that meshes with the motor pinion is of fiber. There are four pairs of gears. The first three are calculated for resistance to wear, and the fourth, for strength at the maximum expected load. The assembly is blind but not troublesome. The lubricant is a low-temperature oil, splashed for distribution to the upper bearings and sealed against leakage at the lower main bearing by means of a leather ring seal reinforced with steel springs. The proposed use of magnesium in place of aluminum as the material of the gear box will reduce the weight of the scanner by about .14 lb.

In addition to the circular scan at 6 rpm, there is provision for sector scan whose position is controllable and whose width may be selected at any value between 15° and 150°. The oscillating motion through the sector is produced by the reversal of a motor that is controlled by a voltage generated in a synchro geared to rotate in synchronism with the antenna. The synchro gear is split and spring-loaded to prevent backlash. The shock of starting and reversing the motor is softened by a resistor that is connected in series with the motor each time the circuit closes and then automatically cut out after a suitable time delay.

Instead of coaxial line which is usual in 10-cm airborne systems, waveguide is used because of the higher transmitted power that might cause arcing in a coaxial line. To enable rotation of the antenna, a coaxial rotary joint of the type illustrated in Fig. 3·1 is provided at the main axis of the scanner. The joint can pass about 1.5 Mw of r-f pulse power without arcing. Two pressure seals in series give double assurance of hermetic sealing of the rotary joint. Each depends on the sliding contact between a ring of rubber compound and the outside of a cylindrical member of polished steel. The rings rotate with the antenna, and the steel member is attached to the stationary part of the outer conductor of the coaxial portion of the transmission line.

On the cover of the gear box, in addition to the synchro already mentioned there is an Arma resolver whose armature also rotates at single

speed, its gear being split and spring-loaded, and a 10-speed synchro. A spare location for an additional single-speed data take-off is provided for unforeseen needs.

6·11. AN/APQ-13 (60-in.).—This scanner (Fig. 6·11) is part of a 3-cm radar set used for navigation and bombing. It is mounted under the wing spar of a B-29 airplane between the bomb bays. The 60-in. antenna is a recent development. The scan can be circular at about 24

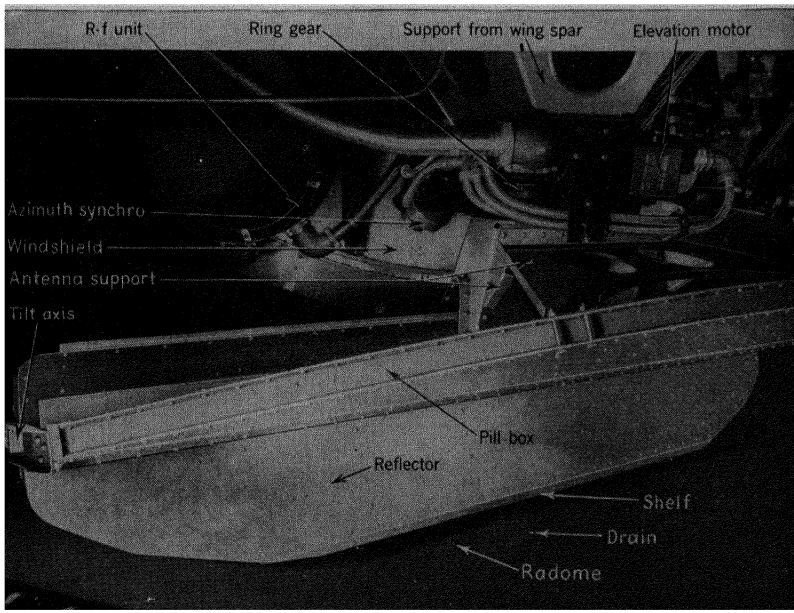

FIG. 6·11.—Installation of 60-in. antenna on a B-29. The antenna protrudes only 4 in. below the keel line but was later lowered to 7 in. to reduce interception of the beam.

rpm or in a 45° sector at 55 cpm. The sector scan is controlled electronically, the center of the sector being adjustable from −70° to +70° relative azimuth.

In an older version,[1] shown in Fig. 6·2, there was a 29-in. paraboloid, distorted to produce a cosecant-squared beam. This was replaced on the same pedestal by the present 60-in. antenna.

A shunt-wound main motor drives the antenna through a worm and spur gear train at about 24 rpm. As viewed from above, the rotation is clockwise. The gearing is enclosed and greased, with the exception of the last pair, which is open. The exposed bronze ring gear suffers excessive wear under some conditions. In sector scanning, the motor is

[1] "Preliminary Instructions for Radar Set AN/APQ-13," *War Training Book* WTB-38.

dynamically braked before each reversal by means of a resistor shunted across the armature for a short time. Although most of the transmission line is waveguide, the azimuth rotary joint is a coaxial section that is hermetically sealed as described in Sec. 6·10. A heater that surrounds the rotary joint prevents the rubber from leaking or frosting to the steel at low ambient temperatures.

The ring gear drives two azimuth data take-offs. One of these is a synchro generator geared to rotate at ten times the antenna speed. This generator actuates a synchro motor and a 1/10 gear reduction at the indicator to rotate the deflection coils[1] of the cathode-ray tube in synchronism with the antenna. With AN/APQ-13, as with several other systems, two such indicators are provided. The other take-off, used to control the sector scan, is a toroidally wound potentiometer with brushes that rotate in synchronism with the antenna.

The nose of the cosecant-squared fan beam of radiation can be tilted between 10° above the horizontal and 30° below. A motor and gear train mounted on the scanner base supply the power for this adjustment. Also attached to the scanner base is a unit that transmits the elevation data of the beam angle to the operator's station. This unit is a toroidally wound potentiometer with three equally spaced taps. Current is supplied by diametrically opposed brushes, one of which is grounded and the other held at 27.5 volts direct current. The sensitive element in the control panel is a permanent magnet, connected to a pointer, which takes a position that depends on the currents in three identical coils connected in Δ to the taps of the transmitting potentiometer.

Slip rings are provided on the scan axis in order to supply power to the AN/APA-15 line-of-sight stabilization attachment (Sec. 7·10) when this attachment is required.

The pedestal, as thus far described, supports either the old antenna (Fig. 6·2) or the new shaped cylindrical antenna (Fig. 6·11). The 60-in. reflector for this antenna is a curved aluminum sheet with a vertical aperture of 12 in. As seen from the end, this sheet is roughly parabolic, although the upper portion of it is curved more than a parabola so that some energy can be distributed in the cosecant-squared fan below the nose of the beam. A horizontal aluminum shelf 1½ in. wide, attached along the lower edge of the reflector, improves the uniformity of the ground echoes. The lower corners of the reflector are trimmed to permit good aerodynamic design of the radome.

The reflector is illuminated by the horizontally polarized radiation from a pillbox 60 in. long. At the focus of the pillbox is the end of a waveguide that directs the microwaves in the *TE*-mode toward the parabolic rear wall of the pillbox. This waveguide, which is made flexible to

[1] *Cathode-ray Tube Displays*, Vol. 22, Chap. 10, Radiation Laboratory Series.

facilitate installation, is connected to the azimuth rotary joint. Its termination is hermetically sealed by a mica window and a gasket. The beamwidth, which is determined by the pillbox and unaltered by the reflector, is 1.3°. In elevation, the beam is roughly cosecant-squared between depression angles of 5° and 70°.

The reflector is a sheet of 24ST aluminum alloy 0.040 in. thick. It is accurately stretch-formed and then held to the correct curvature by being riveted to six identical accurately stamped flanged ribs. A second sheet with large flanged lightening holes is riveted to the ribs to form the back of a box beam. The ends of this beam are supported in ball bearings that allow the tilt link to control the depression angle of the radiation.

The two parallel sheets of the pillbox are also of 24ST aluminum alloy 0.040 in. thick. They are spaced 1.23 in. ($\pm$0.010 in.) apart by means of 36 aluminum posts $\frac{3}{16}$ in. in diameter. Since, with the *TE*-mode used, the electric field in the pillbox is horizontal, almost no r-f current is excited in the posts and they have little electrical effect. The pillbox does not tilt with the reflector but is held by the same sheet metal support that is bolted to the revolving member of the pedestal and holds the bearings for the reflector.

The original scanner weighed 75 lb, and the support for mounting it on a B-29 weighed 14 lb. An earlier mechanism that allowed partial retraction of the scanner and radome weighed 133 lb. With the present antenna, the scanner weighs 83 lb, and its support weighs 36 lb. A vertical aluminum windshield that is installed immediately behind the forward bomb bay of the B-29 extends from the skin of the fuselage to the wing spar and protects the scanner from the wind when the bomb bays are open. Two favorable features of the new antenna are that its beamwidth is less than half that of the older one and, because it is only 12 in. high, its protrusion below the keel of the airplane need not exceed 7 in.

6·12. Experimental Stabilized Scanner for 1-cm Radar.—This example of scanner design, shown in Fig. 6·12, differs in several respects from those discussed in preceding sections. It is a stabilized sector scanner designed for 1-cm band operation. Because compactness is required, the r-f head that contains the receiver and part of the transmitter is rigidly mounted to the scanner directly behind it. The scanner is therefore shock-mounted. The weight of the scanner system and stabilization servomechanism is about 70 lb, exclusive of the gyro and r-f head. The castings for the mounting base are of Dowmetal H magnesium alloy. The ball bearings are pressed directly into these castings, with the expectation that no serious electrolytic corrosion will ensue. The antenna consists of a shaped cylindrical reflector and pillbox and resembles that of AN/APQ-13 described in Sec. 6·11.

The scanner is mounted in a forward location, housed in a radome that is 24 in. in diameter and symmetrical about a fore-and-aft axis. The reflector is only 17 in. wide and 10 in. high, because within the 24-in. nacelle the antenna must have sufficient scanning clearance, with due allowance made for vibration. The face of the reflector is a sheet of $\frac{1}{16}$-in. aluminum alloy rolled to the correct curvature, made rigid by bulb section extrusions that reinforce the upper and lower edges and by

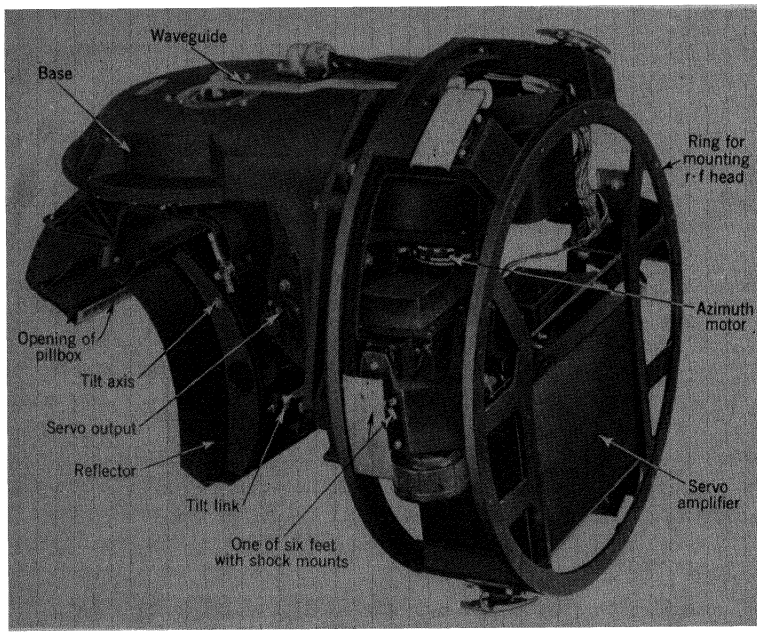

FIG. 6·12.—A stabilized sector scanner for the 1-cm band. The reflector is 10 in. high. (*Courtesy of Philco Corporation.*)

two wide stamped flanged ribs that are riveted to the back edge. A wide flanged tube to which the bulb sections and the ribs are riveted serves as a torsion box to prevent warping of the reflector. Since the pillbox emits radiation that is polarized perpendicularly (*TEM*-mode) to its sheets and cannot therefore contain spacer posts, these sheets must be accurately flat and parallel; they are made of $\frac{1}{16}$-in. aluminum alloy reinforced externally with bulb sections. The termination of the waveguide at the focus of the pillbox is hermetically sealed with a glass window whose platinized edges are soldered to the brass edges of the termination. The beam is 1.7° wide in azimuth and is a cosecant-squared fan in elevation. Stabilization is achieved by tilting the reflector about an axis

that is parallel to its length and just above and behind its center. This tilting is actuated through a crank arm and link by a servomechanism controlled by a gyroscope located near the scanner. Since the pillbox does not tilt, no rotary joint is needed at the elevation axis. The reflector tilts $\pm 18°$, causing a beam tilt of $\pm 30°$, the ratio of reflector tilt to beam tilt being fixed by the choice of tilt axis.

The azimuth motor, rated at about $\frac{1}{4}$ hp, drives the antenna through an enclosed and greased train of spur gears. Sector scanning is accomplished by reversing the motor with no attempt made to soften the shock. The antenna scans through its sector at the rate of 20 rpm or, alternatively, $7\frac{1}{2}$ rpm if the resistance in series with the armature is increased. The 150° sector is scanned forty-two or twelve times per minute, appreciable time being required for reversal. A 60° sector, which can be oriented at will, may be scanned at ninety-seven or thirty times per minute.

The vertical dimension of the main bearing in this scanner is reduced by replacing the more usual pair of bearings with a single 10-in. disk whose edge is supported by three equally spaced rollers. (A similar roller bearing is described in Sec. 3·6 under "Azimuth Driving Mechanism.") Power is supplied to the tilt servomotor and its spur gear train, which are mounted on the sector-scanning portion of the assembly, through ten concentric slip rings that are attached to the main bearing disk. The spring-loaded gear train that drives the data take-offs is mounted on Oilite bearings in the main gear case.

The scanner is equipped with two synchros for take-offs, and a place is provided for an additional take-off. One of the synchros, previously described in Sec. 6·7, is used as a resolver for controlling the sweep voltages in the indicator. A sine-cosine resolver, whose rotor turns with the antenna, is also provided for the stabilization system. A further discussion of the stabilization of this scanner will be found in Sec. 7·11.

The Mechanical Resonant Scanner.—A novel approach to the problems of a sector scanner resulted in the development of the mechanical resonant scanner, MRS.[1] It has a scan rate of nearly 6 cps (or 12 "looks" per second). The sector of scan is centered in the direction of flight, and its width can be adjusted continuously between 10° and 155°. The 17-in. antenna is essentially as described above. During operation, the reflector can be tilted to elevate the nose of the cosecant-squared beam from 20° below to 10° above the horizon. The data transmitter is a resolver. The total weight is 35 lb. Only one model, illustrated in Fig. 6·13, has been constructed.

A tuned spring system that exerts a torque on the azimuth axis, thereby tending to hold the antenna at the center of the sector to be

[1] D. B. Nichinson, "Mechanical Resonant Scanner," RL Report No. 782, Mar. 13, 1946.

scanned, produces the high rate of scan. By reversing at the resonant frequency of the antenna and spring system, a motor that is geared to the azimuth torque tube supplies energy to the oscillating antenna and sustains the amplitude of its scan. Two coiled springs, connected at one

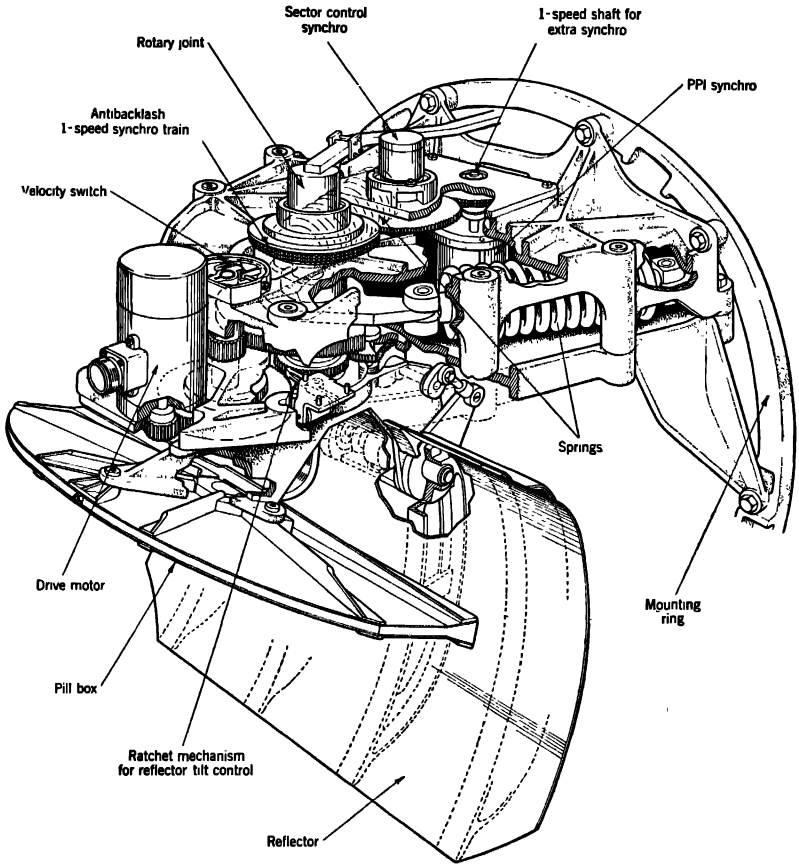

FIG. 6·13.—Cut-away perspective view of mechanical resonant scanner.

end to arms attached to the torque tube and at the other end to the scanner base, are so located as to provide a good approximation to simple harmonic motion.

The reversals of the motor occur just as the extremes of the sector scan are reached and are controlled by a single-pole single-throw velocity switch that is actuated through a light slip clutch by the angular velocity of the antenna. The switch controls a reversing relay in the d-c power line to the motor and assures proper timing of the power reversals. A

synchro that is geared to the resolver previously mentioned provides azimuth information to a control box that cuts off the current to the motor as the antenna approaches the end of each half swing and reenergizes it for reversal after the backswing has started. In this way, the motor is protected against stall currents, and the motor current is off each time the reversing relay is thrown. The angle at which the current is cut off can be adjusted by means of a potentiometer in the control box, thus permitting variation of the amplitude of the scan. Typically, the

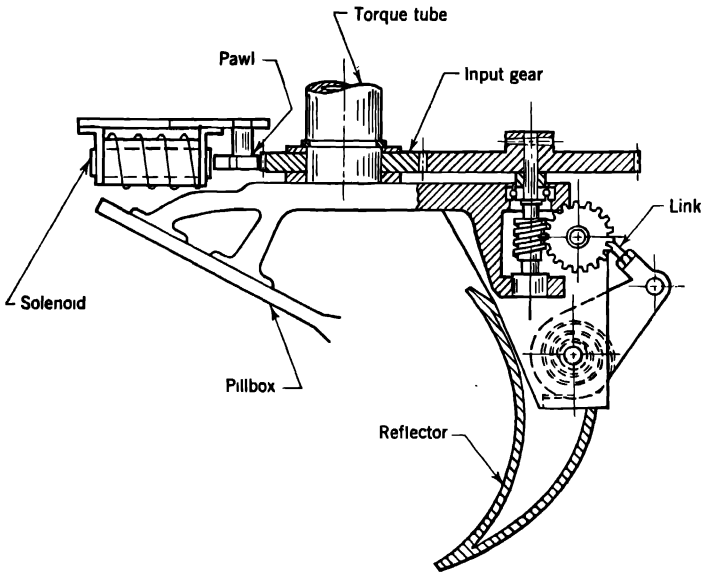

FIG. 6·14.—Partial schematic layout of mechanical resonant scanner showing elevation mechanism.

duty ratio of the motor is about 50 per cent, and its average power output is about 50 watts.

A very simple motorless method of elevation control is illustrated in Fig. 6·14. The elevation gear train and connecting link are carried on the lower end of the torque tube. The input gear of this train is concentric with the torque tube, friction preventing its easy rotation in relation to the oscillating torque tube. On the scanner base there is a pawl that prevents clockwise rotation when it is pressed against the gear by a solenoid but allows counterclockwise movement in relation to the base as the antenna oscillates. Another pawl, similarly controlled, alternatively prevents counterclockwise rotation. Thus, the reflector can be elevated or depressed by energizing one or the other solenoid. A

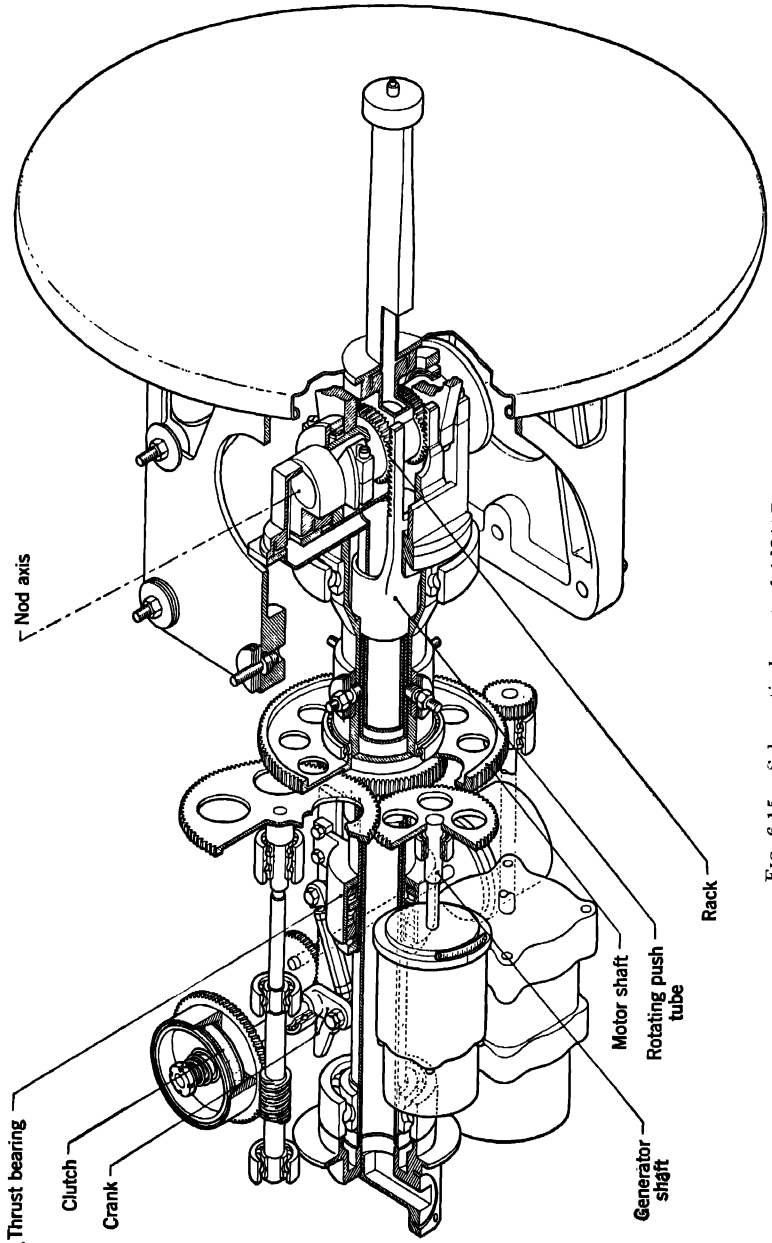

FIG. 6·15.—Schematic layout of AN/APS-6 scanner.

tilt potentiometer take-off, with its leads connected to pigtails in lieu of slip rings at the azimuth axis, is mounted on the oscillating structure.

Backlash is eliminated from the gear train by splitting and spring-loading critical gears. With this scanner, as with all sector scanners, a simpler arrangement would be to load the last gear of the train with a coil spring, which would remove backlash from the entire train.

6·13. AN/APS-6.—The AN/APS-6 scanner, shown in Figs. 6·15 and 6·16, is mounted in a forward-looking location. It is used for locating enemy airplanes and determining their range, relative azimuth angle,

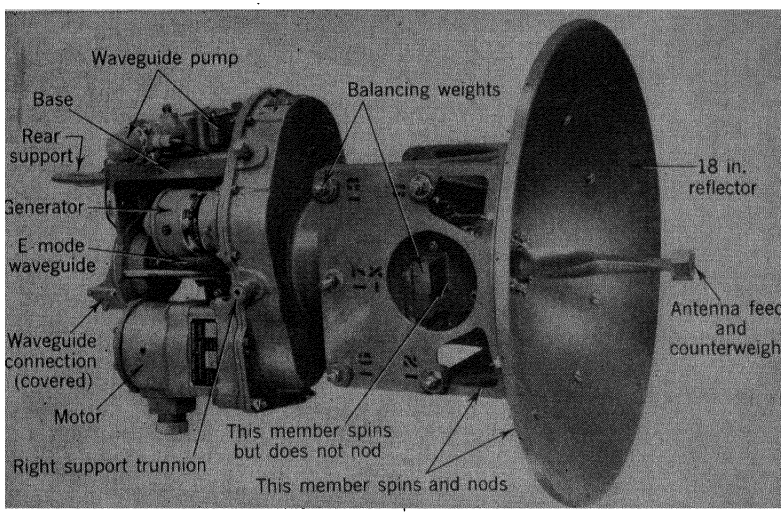

FIG. 6·16.—A scanner with an 18-in. antenna, shown looking straight forward. This scanner directs its beam spirally to cover a 120° cone centered in the direction of flight. (*Courtesy of Dalmo Victor, Inc.*)

and relative elevation angle. A spiral scan is used; the axis of spin is nearly parallel to the direction of the fixed guns of the airplane. One turn of the spiral is described in $\frac{1}{20}$ sec. In 1 sec the entire circular field is solidly covered from its center dead ahead to its perimeter at 60° up, right, down, and left. A 5° beam at the 3-cm band is formed by a $17\frac{1}{2}$-in. paraboloid. The scanner, engineered by Dalmo Victor, Inc., weighs about 50 lb.

A motor, whose power output is rated 400 watts at 6000 rpm, is mounted on the aluminum scanner base and spins the antenna through a 5/1 steel spur gear reduction. The gear case is oil filled and has oil seals that absorb over 100 watts of the mechanical power. A small two-phase permanent-magnet sine-wave generator, driven synchronously with

the antenna, provides voltages that indicate the spin angle.[1] A push tube that is concentric with the spin axis is driven longitudinally with harmonic motion by a crank and worm gearing, also actuated by the motor. The time for a complete cycle of this motion is 4 sec. An exposed rack that is carried at the forward end of the push tube engages a pinion to which it imparts an oscillatory motion about the nod axis that intersects the spin axis at a right angle. The antenna is mounted so that it rotates through $\pm 60°$ in relation to the nod axis, and it oscillates harmonically through this angular range because of its rigid attachment to the pinion.

Because the push tube spins but the mechanism actuating its motion does not spin, a thrust bearing is provided at the rear of the push tube. A rack attached to the mechanism actuating the push tube engages a pinion on the shaft of the toroidally wound potentiometer that serves as the data take-off for the nod angle of the antenna.

The r-f transmission line necessarily has two rotary joints; these use the TM_{01}-mode of propagation. The use of coaxial joints is avoided because of the difficulties encountered in their manufacture. The spin axis is hermetically sealed by the sliding contact between a ring of polished carbon and one of polished steel, the carbon ring being spring-loaded against the steel ring. This type of seal is advantageous for high speed. Although the rotary joint at the nod axis spins bodily at 1200 rpm, the relative motion of its parts is slow. The carbon-on-steel type of seal is therefore not necessary at the nod joint, and use is made of a simpler type, similar to those with a single rubber ring, as described in Sec. 6·10. The r-f line passes through the vertex of the paraboloid and ends at the focus in the hermetically sealed antenna feed (*cf.* Fig. 6·4) that directs the radiation back toward the paraboloid. The $17\frac{1}{2}$-in. diameter paraboloid is spun from aluminum of $\frac{1}{32}$-in. thickness and has a supporting structure $11\frac{1}{2}$ in. in diameter.

In addition to spiral scan, AN/APS-6 also affords conical scan. For conical scan it is necessary only to halt the nodding motion when the antenna is about 3° away from the straight-ahead position. This is accomplished by actuating a solenoid, which introduces an obstruction to the oscillation of the push tube. The slip clutch provided in the gear train that rotates the crank mentioned above is necessary in order to prevent breakage when the solenoid is energized.

A part of the power developed in the motor is dissipated by windage as the antenna spins. A test conducted in an altitude chamber at room temperature showed current requirements of 24.5 amp at sea level and

[1] The indicator circuits for the three-dimensional display on the oscilloscope are described in *Cathode-ray Tube Displays*, Vol. 22, Sec. 14·2, Radiation Laboratory Series.

22 amp at a pressure equal to that at an altitude of about 21,000 ft. The losses due to windage are reduced when the scanner is installed in a closely fitting symmetrical radome on the leading edge of an airplane wing.

It is obvious that the rotating part of the AN/APS-6 scanner must be well balanced. This requirement could be met easily were it not that the slow nodding of the antenna constitutes an internal motion within the spinning assembly that must be compensated to assure balance, regardless of the nod angle of the antenna. Briefly, the assembly consisting of the nodding antenna and the parts that are rigidly attached to it must be dynamically equivalent to a solid of revolution whose axis is the axis of nod. If, then, the entire structure, which rotates at 1200 rpm, is in dynamic balance when the antenna is at some one nod angle, it will be in balance for all other nod angles. A step-by-step routine for balancing the scanner was developed in collaboration with Gisholt Machine Company, which has produced balancing machines for this specific purpose, and with Dalmo Victor, Inc., which has since further refined the balancing routine. The scanner is designed so that there are 18 points of attachment for special lead washers; the balancing machine is calibrated in terms of their weight.

Dalmo Victor, Inc., is now developing a scanner that meets performance specifications similar to those for AN/APS-6 but is more versatile, draws less power, and weighs several pounds less than the AN/APS-6 scanner.

6·14. AN/APQ-7 (Eagle).—One method of obtaining high resolution in an airborne radar set is to use a long, narrow scanner fitted into the leading edge of a wing or carried in a streamlined auxiliary vane mounted transversely below the fuselage. Such a scanner must employ a method of scanning that does not require the entire antenna structure to be moved.

The Eagle scanner,[1] which is mounted in a streamlined vane beneath the fuselage of a medium bomber, as shown in Fig. 6·17, represent a successful device of this type. By the end of the war, over 2000 Eagle scanner units had been produced under Western Electric Company, Inc., contract at Ex-Cell-O Corporation and American Machine and Foundry Company. About 300 were installed in B-24's, B-17's, and B-29's during the war. The research and early development work were done at the Radiation Laboratory; later development and production engineering were carried on jointly by the Bell Telephone Laboratories and the Radiation Laboratory. The streamlined vane was engineered and produced by Douglas Aircraft Company, Inc.

[1] L. W. Alvarez, "Microwave Linear Radiators," RL Report No. 366, July 31, 1942; R. M. Robertson, "Variable Width Waveguide Scanners for Eagle and GCA," RL Report No. 840, Apr. 30, 1946.

Figure 6·18 shows the Eagle scanner, its array of 250 dipoles fed by a waveguide of variable width. At about 3 cm, the operating wavelength of the Eagle system, the full width of the beam at half power is 0.4° to 0.5° in azimuth. The beam is wide in elevation (full width at half power is

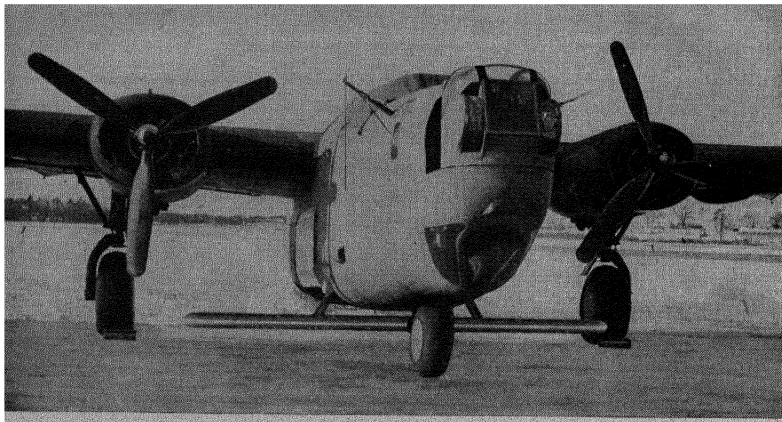

FIG. 6·17.—Eagle scanner mounted on a B-24.

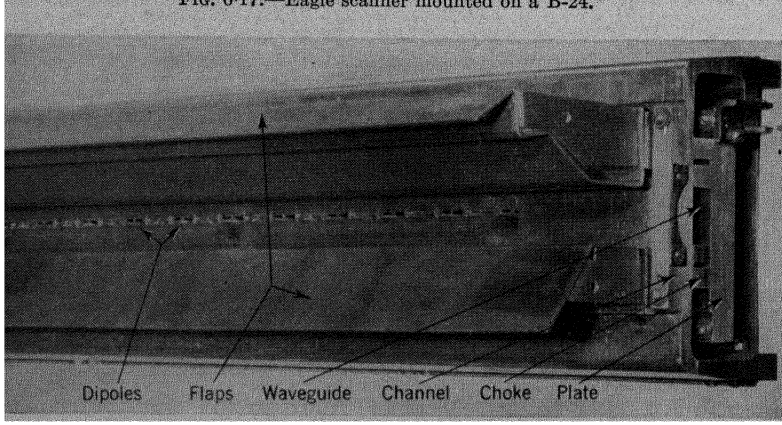

FIG. 6·18.—Left end view of an Eagle scanner.

about 30°) and is shaped to give approximately uniform return from ground targets.

The formation of a narrow beam of radiation by the dipole array is similar to the action of an ordinary broadside antenna array and to the diffraction of a beam of light by a flat diffraction grating. The beam radiated by the Eagle scanner lies at an azimuth determined by the spacing of the dipole radiators and by the common r-f phase difference between successive dipoles. The dipoles shown in Fig. 6·19 are mounted on a

16-ft length of waveguide, and each one is energized by a probe that penetrates slightly into the guide. Alternate dipoles are reversed by 180° to give a spacing less than the wavelength in air and hence to eliminate higher order lobes in the pattern. (Despite this reversal, adjacent dipoles radiate approximately in the same phase because their spacing S is approximately half the wavelength of the energy in the variable guide.) The beam can be made to scan in azimuth if the relative phases of the

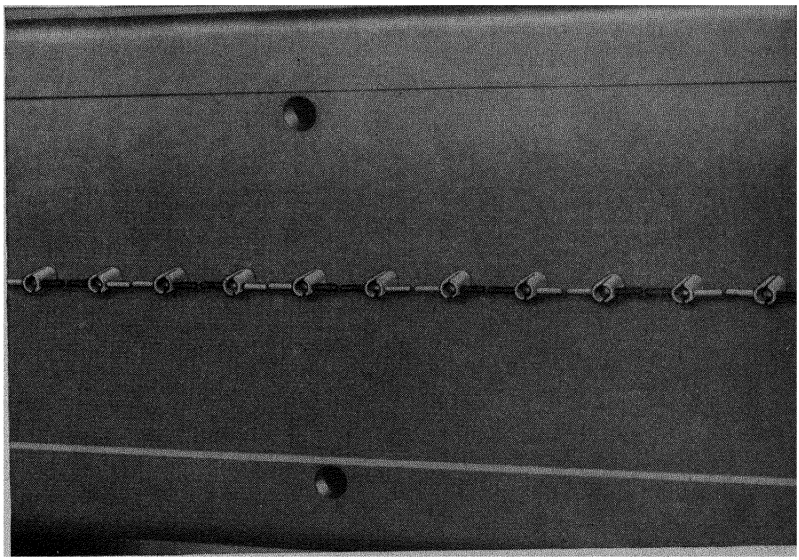

FIG. 6·19.—Dipoles mounted on an Eagle scanner.

dipoles are varied. In the Eagle scanner this is effected by changing the width a of the waveguide. The azimuth angle θ is determined by the relation

$$\sin \theta = \sqrt{1 - \left(\frac{\lambda}{2a}\right)^2} - \frac{\lambda}{2S},$$

where λ is the wavelength in free space and θ is positive when the beam is in the end-fire direction.

If all the dipoles are excited in the same phase, the beam is broadside to the array and directed straight ahead of the airplane. With the dipole spacing and wavelength used, this occurs when the inside width of the guide is 1.200 in. If the guide is narrowed to 0.660 in., the beam moves 30° toward the back-fire direction. When the energy is propagated in the waveguide from left to right, then as the width of the waveguide is decreased between the limits mentioned and is increased again, the beam

scans from straight ahead to 30° to the left and back again. When the waveguide carries the energy from right to left, the scan extends for 30° to the right of the center line of the airplane. By feeding energy into the alternate ends of the waveguide, a total scanning range of 60° is realized in the Eagle scanner.

The waveguide of variable width consists fundamentally of two L-shaped sections that fit together to form a rectangle. A longitudinal system of chokes (see cross section in Fig. 6·21) prevents the energy from leaking out at the breaks in the wall of the waveguide. The total loss in the guide before insertion of dipoles is less than 0.5 db per meter.

Two scanners similar to the Eagle scanner are used together in the AN/MPN-1 (ground control of approach, GCA) system[1] for precision location of aircraft in azimuth and elevation. The 14-ft height-finding scanner has a beamwidth of about 0.5° in elevation, and the 8½-ft azimuth scanner has a beamwidth of about 0.8°.

When the Eagle scanner was being developed, there was a reasonable doubt that a long scanning array of this kind was practicable. Fortunately, many of the anticipated difficulties did not materialize, and those which did were successfully overcome. It was found, for example, that the principal problem in realizing satisfactory azimuth radiation patterns was to obtain correct r-f phasing of the dipole array. Random phase errors occurring over lengths of a few dipoles had a negligible effect as compared with systematic phase errors occurring over a considerable fraction of the length of the array. Attention was therefore focused on the problem of preventing or correcting systematic errors such as those caused by a uniform taper in the width of the guide or by a difference in the spacing of the dipoles in different parts of the array.

The problem of maintaining the parallelism of the 16-ft waveguide to a tolerance of a few thousandths of an inch was difficult for production men. It was found impossible to attain the required freedom from error on the first assembly; therefore means had to be developed for trimming the width after assembly. The method has been further extended so that width adjustment can now be used to optimize the radiation pattern. In this "optimum pattern" method, width adjustment is used to compensate other phase errors such as those caused by inaccuracies in the dimensions of the long r-f chokes. The technique resulted in the virtual elimination of scanner rejections in production and in a generally improved product.

Width adjustment is provided at each toggle point by the mechanism shown in Fig. 6·20. The effectiveness of the method depends on the

[1] A ground radar used in conjunction with radio communication to direct aircraft into landing position. It was produced by Gilfillan Bros., Inc., Bendix Aviation Corporation, and Federal Telephone and Radio Corporation.

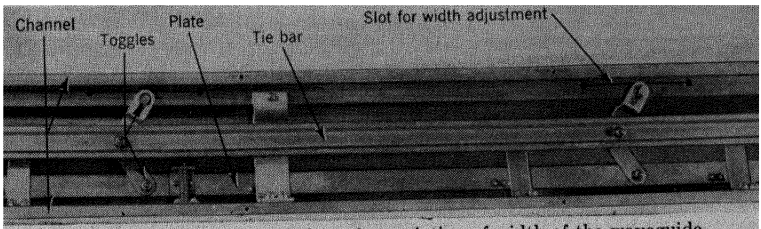

FIG. 6·20.—Parallel bar linkage for variation of width of the waveguide.

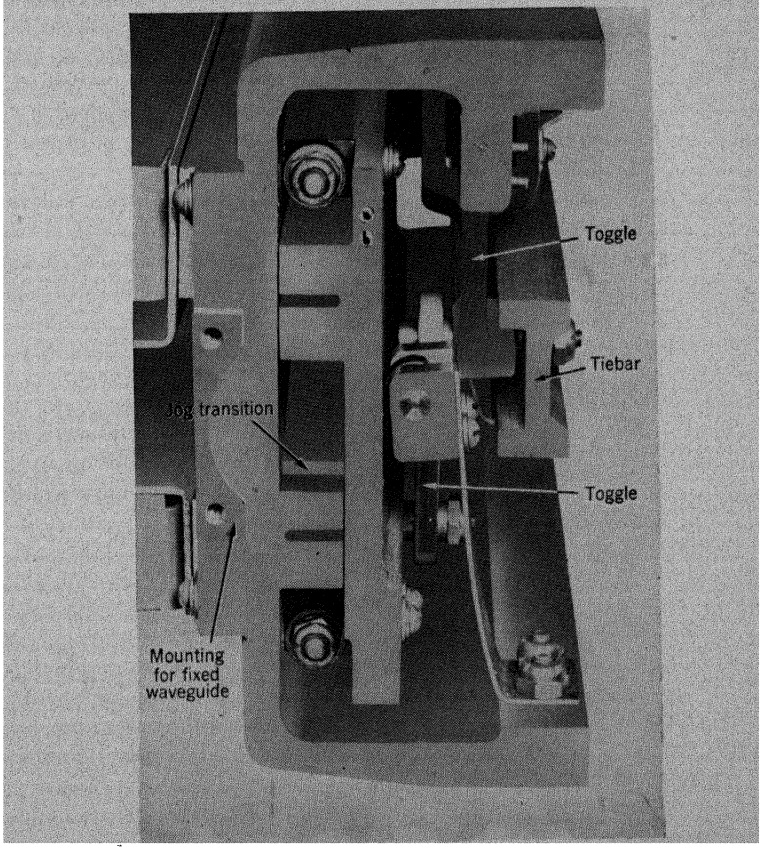

FIG. 6·21.—Detail of the left end of the Eagle scanner.

fact that almost all of the nonuniformities along the width of the guide in production scanners are in the form of long curves and tapers. In the Eagle scanner there are nine adjustment points spaced $20\frac{5}{8}$ in. apart. The technique used in making the optimum pattern adjustment is as

follows. The guide width is set at its narrowest point, since it is then that the pattern is most susceptible to phase errors. (This susceptibility is one reason why it is not practical to scan more than $\pm 35°$ with a device of the Eagle type.) Using the scanner as a receiver, it is oriented to receive maximum power from a distant transmitter. Each toggle is adjusted in turn until one is found that causes the power to rise sharply. That toggle is then adjusted for maximum power. Side lobes and beamwidths are then checked; if further improvement is required, the adjustment procedure is repeated. If it is desired to reduce a side lobe, the scanner is oriented to the maximum of the lobe and the adjusting point found that reduces it. Always, a final over-all check is required. An average scanner can be adjusted in less than half an hour.

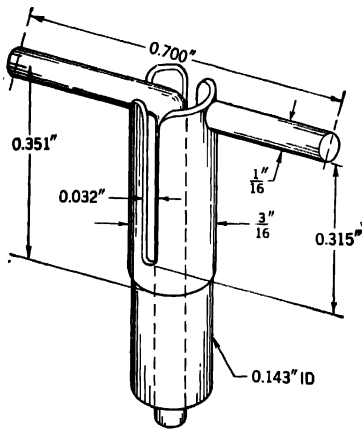

FIG. 6·22.—Construction of dipoles used in the Eagle antenna.

The complete production scanner assembly weighs 165 lb, and the housing vane, including the motor and gear box for the scanner, weighs 247 lb. Thus, the entire assembly exclusive of mounting struts weighs 412 lb.

In the production scanner the principal structural member is an extruded channel, made of 61ST aluminum alloy and machined on the critical surfaces. The dipoles are pressed into holes in the channel and held in place by friction, their probes extending into the variable waveguide. Half of the waveguide is provided by the channel, as shown in Fig. 6·21, and the other half by an extruded "plate" of 61ST aluminum alloy, also machined on the critical surfaces and attached to the channel by a system of toggle linkages connected by a tie bar, as shown in Fig. 6·20. Contact between the channel and plate is prevented by a roller system which provides an air gap, called the *b*-clearance, between the opposing surfaces. Hardened steel inserts prevent the ball-bearing rollers from wearing into the softer aluminum.

An individual dipole is illustrated in Fig. 6·22. More than half a million such dipoles were used in production scanners. They were manufactured of aluminum alloy by the "lost wax" precision casting technique or alternatively by individual fabrication with assembly by aluminum brazing. Both methods were satisfactory, and the cost was about the same for each, although the individually fabricated dipole had greater strength.

The vertical radiation pattern is shaped by means of a set of reflectors, "flaps," visible in Fig. 6·18, attached to the front of the channel. The modified horn formed by the flaps was designed largely by empirical methods to produce the required pattern. The flaps are manufactured by a continuous rolling process, in which a flat aluminum sheet is fed through a series of rollers. A difficult problem arose when it was found that scattering of the radiation by the sharply curved plastic leading edge of the vane caused serious interference with the radiation pattern of the fan beam, especially in the lower portion, 60° to 70° below the horizontal. This meant that until an arrangement could be worked out which was less sensitive to such reflections, the leading edge had to be

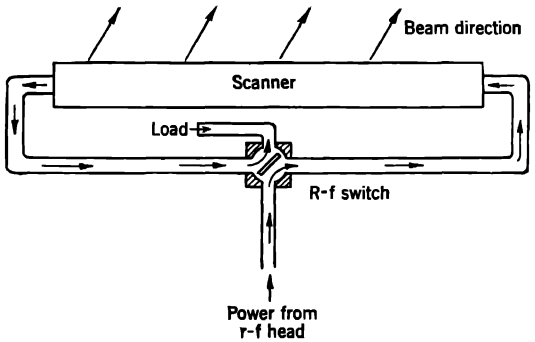

FIG. 6·23.—Energy flow in a waveguide.

considered a part of the reflector system. As a result, it was necessary to impose strict tolerances on the location of the scanner in the vane with respect to the leading edge. Experiments have shown, however, that flaps can be designed to give a pattern that is not seriously affected by the leading edge.

Angular information is obtained from the scanner by means of a synchro and cam arrangement. The cam is mounted on one of the toggle arms and is so cut that a follower arm mounted on the synchro shaft turns through the beam angle as the scanning takes place.

Energy is fed into alternate ends of a waveguide of variable width by means of a simple r-f switch mounted on the scanner. Figure 6·23 shows the routing of the energy from the transmitter through this switch and into one or the other end of the scanner; the residue not radiated is led via the switch into an absorbing termination. Figure 6·24 is a diagram of the switch. A relay system actuated by the drive shaft causes reversal of the switch each time that the waveguide reaches its maximum width.

The apparently difficult problem of feeding a waveguide of variable width from a waveguide of fixed width was solved by engineers of the

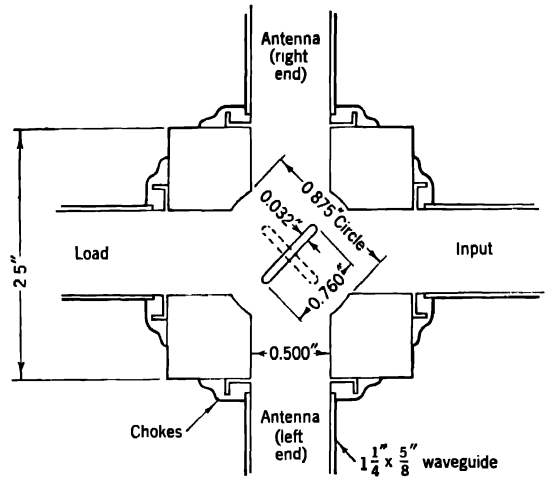

FIG. 6·24.—Detail of r-f switch.

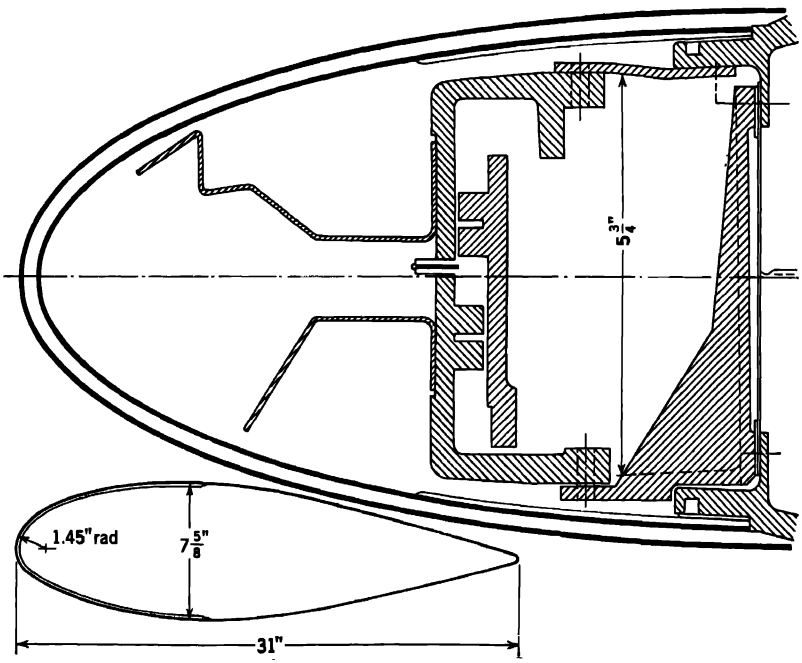

FIG. 6·25.—Cross section of Eagle vane.

Bell Telephone Laboratories. A simple matching transformer cut into the fixed side of the waveguide, visible in Fig. 6·21, gives a good match over a wide range of guide widths.

Mounted in the vane, behind the main spar, are the motor and gear box for driving the scanner. The scanner drive shaft actuates the moving plate by means of a steel box cam that drives a ball-bearing follower mounted directly on the plate. The rotation speed is 90 rpm, which produces a scanning rate of 60° in $\frac{2}{3}$ sec. The drive is powered by a $\frac{1}{8}$-hp 24-volt d-c 5000-rpm motor. The scanner is mounted on two U-shaped brackets fastened to the main spar of the vane at the points where the vane is attached to the airplane, thus avoiding distortions of the scanner by air load deflections of the vane. The mounting points are spaced 90 in. apart in production vanes.

Figure 6·25 shows a cross section of the Eagle scanner in the vane, together with one of its two attachment brackets. The vane is mounted to the fuselage by two struts (see Fig. 6·17), which are faired in to reduce drag. Electrical connections and hot-air ducts are led to the vane through the strut fairings.

Standard aircraft construction is used throughout, except for the leading edge that serves as the radome for this scanner. The leading edge is a double-walled plastic sandwich of laminated glass cloth, each skin consisting of seven layers of Fiberglas ECC-11-128 laminated with Laminac X-4000 resin (see Chap. 13). The construction is double-walled to provide for deicing by the circulation of hot air between the walls and to minimize the radiation reflections from the radome. Prototypes of leading edges were made by Douglas Aircraft Company, Inc.; the major production source was the General Electric Company at Lynn, Mass.

The section of the wing that contains the scanner may also be pressurized to prevent arcing. Pressurization, however, is found to be unnecessary for altitudes up to 40,000 ft at the power level of about 50 kw used in the Eagle system.

CHAPTER 7

STABILIZATION OF AIRBORNE ANTENNAS

By R. Sher[1]

Airplanes, like ships, pursue a course that is not always straight and level; this introduces serious errors and shortcomings in airborne radar presentation. If the radar transmits a "pencil" beam, the worst effect encountered is a shortening of the range to both sides when the airplane is banking. This effect is illustrated in Fig. 7·1. If the transmitted beam has a cosecant-squared pattern, the illumination of the desired area is nonuniform and there is a loss of range.

For best results, provision for stabilization must be incorporated into the design of a scanner. The weight added by stabilization components is likely to be 25 lb or more. Partly for this reason and partly because

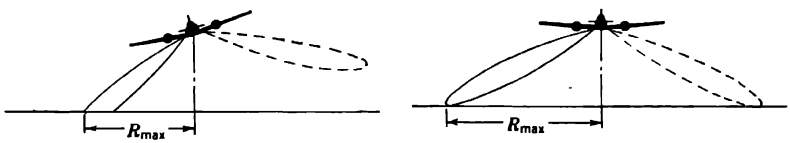

FIG. 7·1.—Loss of range resulting from use of an unstabilized scanner in nonlevel flight.

the technique of stabilizing airborne scanners is new, most installations are still not stabilized.

Two methods of stabilization may be used. By stabilizing the antenna, the elevation of the beam in space may be maintained regardless of variations in attitude of the aircraft; in a limited number of instances the data displayed on the radar indicator may be altered to suit circumstances. Stabilization of the data is an electrical circuit problem; a detailed discussion of it is beyond the scope of this book (see Vol. 22 of this series).

In antenna stabilization, a gyroscope and a servomechanism automatically tilt the beam of radiation to counteract the pitching or rolling of the airplane. This prevents the scan from being disturbed by limited maneuvers of the airplane and ensures against impairment of the presentation of the kind shown in Fig. 7·1. The angular limits within which stabilization will function have been variously set from $\pm 15°$ to $\pm 30°$; accuracy of stabilization to within $\pm 1°$ is a typical requirement.

[1] Some material first written by F. B. Lincoln was used in writing Secs. 7·5, 7·7, and 7·10.

It should be noted that the usual practice in designing airborne stabilization equipment is to compensate only *controlled* nonlevel flight conditions, such as climbs, glides, and banks made at the pilot's discretion. Few attempts are made to compensate all nonlevel flight conditions caused by rough air.

TYPES OF ANTENNA STABILIZATION

7·1. Stable-base Stabilization.—Kinematically, the most nearly perfect airborne stabilization scheme is the one in which the scanner is mounted on a gimbal system[1] that maintains the axis of scan truly vertical. The gyroscope is a stable vertical. A separate servomechanism that is connected to each axis keeps the scanner in such a position that its gimbals are parallel to those of the gyroscope. This type of stabilization is known as stable-base stabilization because the entire platform, or base, of the scanner is stabilized. The two axes chosen are parallel to the roll and pitch axes of the aircraft.

7·2. Roll Stabilization.—In some airborne radar applications the pitch deviation of the aircraft is so small that little harm results from leaving the pitch axis of the scanner unstabilized. Adjustment for the actual angle of attack of the airplane may, however, be combined with roll stabilization. Automatic stabilization about the roll axis is obtained like stable-base stabilization, except that a gyroscope with a take-off on the roll-gimbal axis only is used.

7·3. Line-of-sight Stabilization.—An entirely different approach to the problem is represented by line-of-sight, or tilt, stabilization, illustrated in Fig. 4·1*b*. In this method no effort is made to mount the scanner on a partially or completely level platform. Instead, as the antenna rotates, it is tilted about the elevation axis by the stabilizing servomechanism. The tilt is controlled so that the angle between the "nose" of the beam (i.e., the direction of greatest energy transmission) and the horizon is kept constant at a predetermined value,[2] which depends on both the attitude of the aircraft and the heading of the scanner. When a pencil beam is at the zero depression angle, theoretically complete stabilization can be effected in this way.

The mechanisms of airborne line-of-sight stabilization systems have

[1] *Cf.* Chap. 4, Fig. 4·1*h*, *i*.

[2] Equation A·16 of Appendix A gives the exact expression for the tilt angle that is required to keep the beam horizontal. It can be written

$$\sin D = \sin \alpha \sin R - \cos \alpha \sin P \cos R,$$

where R = roll of the aircraft, positive if roll is to the left,
P = pitch of the aircraft, positive if the nose is depressed,
D = depression required for line-of-sight stabilization [$D = -\beta'$ of Eq. (A·16)],
α = heading of the scanner clockwise from the forward direction.

taken two general forms. In one system, the gyro is a stable element mounted on the scanner and rotates with the antenna in azimuth; in the other, it is a stable vertical, remotely located from the scanner. In the former system, a synchro is placed at the outer gimbal axis of the gyro, the axis being parallel to the elevation axis of the antenna, as in

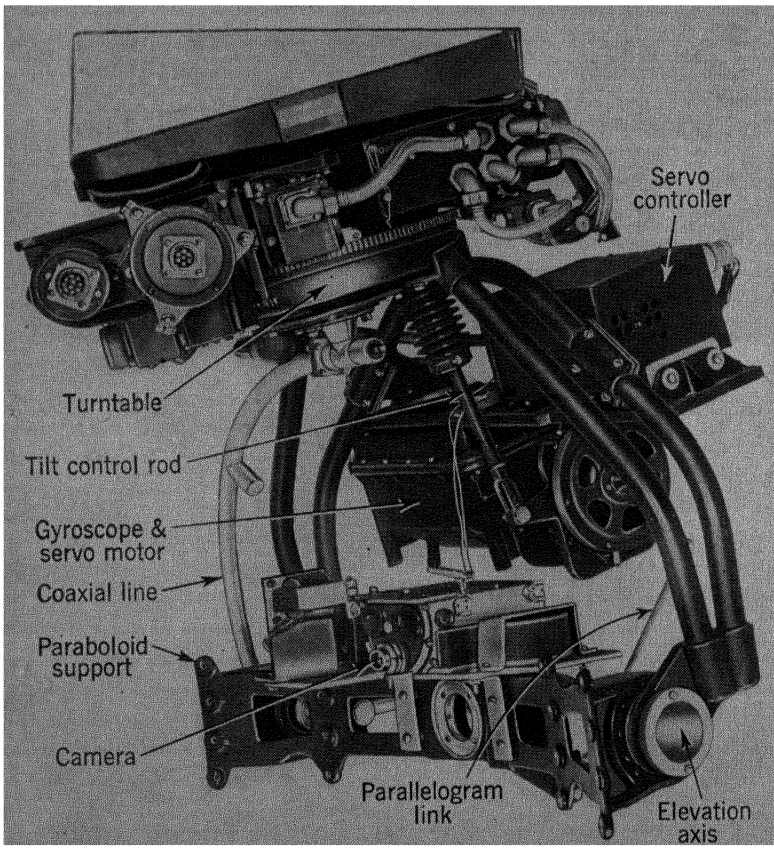

FIG. 7·2.—AN/APA-15 stabilizer mounted on an AN/APS-2 scanner. The inclined attitude of the scanner base simulates an aerial maneuver.

Fig. 7·2. A servo system then constantly keeps the antenna in the proper position as it scans. An example may make the principle clearer. When an airplane is in a simple glide and the antenna is looking straight ahead, the beam must be elevated by an amount equal to the glide angle; when the antenna is looking aft, the beam must be depressed by the same amount; when it is looking to either side, no compensation is necessary.

There are two serious disadvantages in the method of line-of-sight stabilization that makes use of a stable element mounted on the scanner, and both occur because the rotation of the gyro is in azimuth whereas the gyro is so mounted that its spin axis is not parallel to the azimuth axis of the scanner. (1) The inertia and complex motion of the gimbals give rise to a force that precesses the gyro rotor, resulting in a false indication of the vertical axis. This error, discussed in Sec. 7·7, is a function of the tilt angle, gimbal inertia, speed of scan, speed of rotation of the gyro rotor, duration of the nonlevel attitude of the aircraft, etc., and has been observed in the Radiation Laboratory to be as high as 5° for a 20° angle of simulated climb or glide. (2) A gyro that is mounted on the scanner will topple if the scanner is sector-scanning at certain headings for more than a few minutes.

One method of improving the performance of a gyro employed as an airborne stable element, successfully applied by Sperry Gyroscope Company, is to use a servo system to keep the gyro housing in position so that the plane of the gimbal axes remains horizontal. This eliminates the error due to inertia of the gimbals and prevents toppling of the gyro when the scanner is sector-scanning. In the gyro housing a synchro is mounted at each gimbal axis, and the voltages generated by these synchros control the servo channels that keep the housing level. The elevation angle of the antenna is controlled by a parallelogram linkage with the gyro housing; an additional control enables the operator to adjust the angle at which the beam is stabilized. In the gimbal system supporting the gyro housing, one gimbal axis lies in the vertical plane through the nose of the beam; a synchro on this axis measures the tilt of the antenna in respect to cross traverse which is needed for data stabilization.

In a simpler method, the gyro that acts as a stable vertical is rigidly attached to the aircraft, and special synchros and a resolver are used to obtain the necessary angular information. This system is discussed in Sec. 7·11. The output voltage from the resolver can be made proportional to the quantity $D_a = R \sin \alpha - P \cos \alpha$, which is the approximation[1] used for the tilt angle. This voltage is the input to a servomechanism that tilts the scanner about its elevation axis. The errors resulting from these approximations are not so serious as those attributable to the precession caused by the inertia of the gimbals in a stable element; toppling due to sector-scanning does not occur at all. Recent designs have

[1] When values calculated from this expression are compared with those obtained by use of the expression given in the preceding footnote, they are found to be nearly equal; the geometrical error $D - D_a$ has a maximum value of about 1.5° for $R = 30°$, $P = 10°$, the maximum deviations from level flight that may normally be expected. Since this is the maximum error and is encountered only in fairly vigorous maneuvers, it is tolerable.

therefore specified the line-of-sight stabilization systems with gyros that are remotely located.

A novel means of obtaining line-of-sight stabilization, which requires a level platform, has recently been considered. In this system, schematically illustrated in Fig. 7·3, a ring or swash-plate *a-a* is kept horizontal by a two-axis gyro-servo combination similar to that used in stable-base stabilization. One arm *BC* of a parallelogram linkage *ABCD* rides around the ring on a roller as the scanner rotates in azimuth. By this means, the tilt of the reflector is adjusted so that the angle between the beam and the horizontal plane of the swash-plate is kept constant. In Fig. 7·3, the scanner is shown with the antenna looking forward while the aircraft is in a climb.

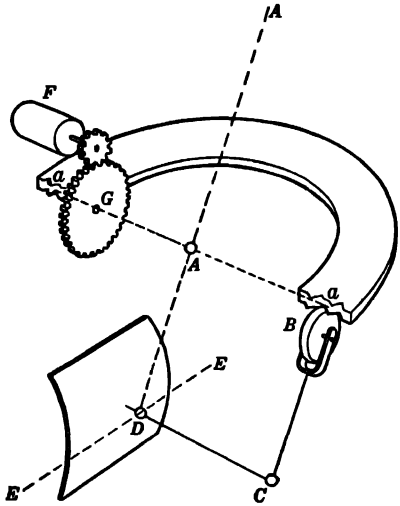

FIG. 7·3.—"Swash-plate" method of line-of-sight stabilization. *A-A*, main axis of scanner (airplane not level); *a-a*, leveled ring (swash-plate); *ABCD*, parallelogram linkage; *E-E*, tilt axis of reflector; *F*, roll (or pitch) servomotor; *G*, gear train.

7·4. Pitch Stabilization.—Although momentary pitch deviations are generally small by comparison with roll deviations, the "angle of attack" of an aircraft may gradually alter over a range of about 5° during flight because of fuel consumption and changes of load, speed, and altitude. Pitch stabilization is designed to compensate for these variations. It resembles roll stabilization in that it is patterned after the stable-base method.

In one light installation, AN/APS-10, it was considered desirable to stabilize the pitch axis only. In the proposed version, it would have taken on a form completely different from any of the types of stabilization heretofore discussed. Instead of a gyro, the gravity-sensitive element was to be a mercury switch mounted on the scanner base. When the aircraft changed its attitude, flying nose high or low, the mercury switch was to energize relays to furnish armature voltage to a small motor. This motor would then move the scanner so that the azimuth axis would remain vertical with respect to pitch. The accuracy of stabilization was calculated to be about $\pm 2°$, and the weight of the rudimentary servomechanism under 1 lb.

A mercury switch or any other control element quickly responsive to gravity cannot be used in roll stabilization because the effective, or

dynamic, gravity present when an airplane is turning is not the same as true gravity but is the resultant of true gravitational forces and those arising from the centrifugal acceleration of the turn.

7·5. Comparison of Stabilization Methods.—Pitch stabilization will not be discussed further, as it has been proposed for only one airborne application. Stable-base stabilization also needs no additional exposition because the advantage of its greater accuracy in comparison with roll stabilization is outweighed by its extra requirements for weight and power and because the same considerations that apply to roll stabilization will, with few exceptions, also apply to stable-base stabilization. The discussion in this section will therefore be limited to roll and line-of-sight stabilization.

Size and Weight.—In both roll and line-of-sight stabilization it is necessary to have a gyro and a servo system. The gyros differ only in the number of take-offs required. A servo system for roll stabilization is considerably heavier than one for line-of-sight stabilization. Since the whole scanner, rather than just the antenna, must be moved in a roll stabilization scheme, the servomotor must be more powerful; and since the output speed is low, a greater gear reduction must be used.

The scanner as a unit will normally be heavier in a roll-stabilization system because of the special construction used for keeping the scanner base in a level position. In the only American system having a roll-stabilized scanner, the weight is about 100 lb; an unstabilized scanner with a reflector of the same size is likely to weigh at least 25 lb less. For a line-of-sight stabilized scanner, the mechanism that is needed for the continual tilting of the antenna about its elevation axis would probably weigh less than 25 lb because the load presented by the antenna alone is less than that of the whole scanner.

Servo Systems.—The servo system used in a roll-stabilized scanner must have high static accuracy but need not have high dynamic accuracy, because it operates only while the aircraft is actually *changing* its attitude. Such changes are infrequent and last for only a very few seconds. When the aircraft is at a constant attitude, level or nonlevel, the servo system merely holds the scanner at its desired position. A line-of-sight servo system, on the other hand, must continuously readjust the elevation of the antenna except when the aircraft is in perfectly level flight. Indeed, it periodically changes the position of the antenna at a rate equal to that of the azimuth scan, which may be as high as 30 rpm, and must therefore have fast response and good dynamic accuracy. Typical maximum angular velocities characteristic of the systems are 10°/sec for roll stabilization and 70°/sec for line-of-sight stabilization. The lighter weight and smaller rotor inertia of the line-of-sight servomotor make it easier to realize the required dynamic accuracy.

Swept Volume.—A serious disadvantage of platform- or roll-stabilized scanners is the increase in the volume of the radome needed to house the scanner and equipment for even a few degrees of stabilization and results from the relative displacement of the scanner and the aircraft, as illustrated in Fig. 7·4. Even if it is mounted in the more compact way shown in Fig. 7·7, a roll-stabilized scanner for circular scanning requires a larger ventral radome than a line-of-sight stabilized scanner with an antenna of the same size. The roll-stabilized scanner shown has a 42- by 10-in. reflector and was stabilized for $\pm 26°$; the size of the radome is 75 by 54 by 23 in.

It should be noted, however, that roll-stabilized sector scanners do not give this trouble, since they are almost always designed to fit into a

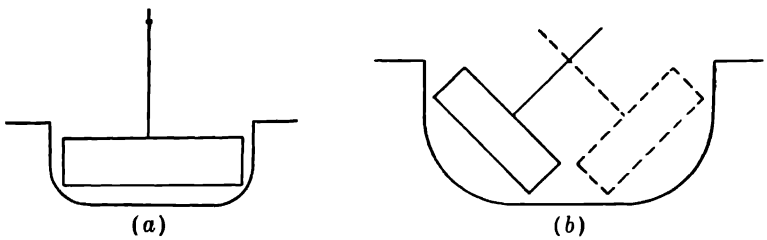

FIG. 7·4.—Diagram showing increase of size of radome required for roll stabilization, (*a*) unstabilized; (*b*) stabilized.

radome that is symmetrical about the roll axis. They may be stabilized by rotation about the axis of the radome and will not require a larger radome.

Indicator Distortions.—A drawback of line-of-sight stabilization is the distortion that appears on the plan position indicator (PPI) screen. When the axis of rotation is not vertical, the plane of a fan beam will be tilted away from the vertical by an amount equal to the cross-traverse angle (*cf.* Fig. 4·1). This tilting is dependent on the heading of the scanner and the attitude of the aircraft and causes the beam to intersect the ground along a line different from the one desired. The error is serious. If an airplane flying at an altitude of 30,000 ft banks at an angle of 6° to the right, for example, an object on the ground directly ahead of the airplane will appear to be displaced more than 3000 ft to the right.

There are two ways of correcting this distortion. One is by the use of a three-axis scanner of the type shown at either *e* or *f* of Fig. 4·1. The cross-level or cross-traverse motion of a wide antenna so mounted would, however, require such a large radome that it seems impractical to try to keep the plane of a cosecant-squared beam vertical in line-of-sight stabilization. The other method is to stabilize the data displayed on the PPI by applying to the indicator voltages that prevent the image from

shifting as the airplane maneuvers. Data stabilization of this type is not used at present in any airborne radar.

REQUIREMENTS FOR ACCURACY

7·6. Stabilization Tolerances.—The purpose of stabilizing airborne antennas is to preserve the range performance and uniform intensity of the display in nonlevel flight.[1] In deciding the accuracy requirements, various factors, such as the shape of the beam and the operational function of the radar system, must be considered.

It is found that if the beam moves up or down because of maneuvers of the aircraft or poor stabilization, the signal from a target at the nose of the beam will fade. Quantitatively, if a pencil beam moves up or down by one-half its beamwidth, a range reduction of 29 per cent can be expected. The range will be reduced by 10 per cent if the beam varies from the stabilized position by 0.28 beamwidth and by 5 per cent if it varies by 0.19 beamwidth. If a range reduction of 10 per cent is considered the maximum allowable in a navigational radar, the beam must be stabilized so that it remains within 0.28 beamwidth of a completely stabilized position (*cf.* Table 7·1 for the stabilization tolerance of a pencil beam radar).

TABLE 7·1.—STABILIZATION TOLERANCES FOR NAVIGATIONAL RADARS

Radar	Type of beam	Nose depression, degrees	Beamwidth in elevation, degrees	Tolerance, ± degrees
AN/APS-2, SCR-717	Pencil	Variable	9.0	2.5
AN/APQ-13, AN/APS-15	Fan	8	7.0	1.4
AN/APQ-13 (60 in.)	Fan	6	10.0	1.7
Experimental	Fan	3	8.0	1 2
Experimental	Fan	4	4.5	0.8

When a cosecant-squared beam is used, the presentation of targets at maximum range is the one that suffers the most from poor stabilization. If the nose of the beam tilts below such a target, the illumination falls off in a proportion that depends on the beamwidth as measured in the elevation plane, as discussed in the preceding paragraph. If the nose of a cosecant-squared beam tilts upward by one-tenth of θ_0, which is its usual depression angle, a 10 per cent decrease in range performance is to be expected. Thus, the upper and lower limits of the depression angle of the beam, between which the range performance is essentially optimum, determine the tolerances for the stabilization accuracy of fan-beam navi-

[1] W. M. Cady, "Stable Scanners and Unsteady Airplanes," RL Report No. 701, Feb. 21, 1945.

gational radars. These tolerances are calculated as being one-half the total permissible travel in the elevation of the beam (see Table 7·1).

Figure 6·1 shows a cosecant-squared fan beam which provides signals of equal strength from equal objects on the ground, regardless of their distance. When such a beam is tilted slightly downward, targets at intermediate distances are illuminated more than targets nearer the vertical; upward tilting of the beam produces the reverse effect. These effects being undesirable, especially in a radar system that is used for bombing, an arbitrary figure of ± 4 db has been set as the greatest tolerable uniform radial variation in signal strength[1] that may be allowed to result from incorrect tilting of the fan beam. The restriction makes it necessary to stabilize the beam within a tolerance of $0.23\theta_0$.

In practice, weight considerations in aircraft make it quite difficult to realize stabilization accuracies high enough to satisfy these tolerances for the various types of beams and radars. Future development of gyros and servomechanisms will lead to greater accuracy and lighter weight in stabilized airborne scanners.

7·7. Gyros. *Erection Mechanisms and Rates.*—Some mechanism must be built into the gyro system to control the position of the rotor in order to prevent it from wandering away from true vertical. Such devices are erection mechanisms. They are built in various forms, depending on the error tolerances and the size of the rotor. The static accuracies of airborne gyros now in use range from $\pm\frac{1}{4}°$ to $\pm\frac{1}{2}°$.

The vertical gyro that is made by the Pioneer Instrument Company incorporates a simple mechanical erection device in which a ball slowly rolls around a race concentric with the gyro axis and attached to the inner gimbal ring. When the gyro axis is not vertical, the rotation of the ball is nonuniform; that is, the ball moves slower on the ascending side of the race than it does on the descending side. This action slowly erects the gyro. When the gyro axis is vertical, the rotation of the ball is uniform. The rate of erection cannot be varied at will.

A more complex electrical erection device employs pendulums on the roll and pitch axes. Pickup coils are mounted on the pendulums. When the rotor begins to precess during roll or pitch, a voltage is generated and fed through amplifiers to the erection motors, thus bringing the rotor back to vertical.

Some of the gyros designed and built by the Sperry Gyroscope Company are equipped with a liquid-level mechanism. The liquid is enclosed in a flat container mounted on the inner gimbal ring. When the ring is

[1] This allowance for a gradual tapering of the signals is more liberal than is permitted for fluctuations in the cosecant-squared distribution, because a 2-db ripple in the fan causes an objectionable ring on the PPI whereas a gradual falling off of 2 db in the pattern is not noticeable.

tilted, the closing of contacts by the conducting liquid energizes erection motors that level the rotor. The erection mechanism can be operated at any desired speed.

The erection rate of a gyro is the rate in degrees per minute at which the axis of the rotor approaches true vertical when the erection mechanism is brought into play. Because the rate varies as the rotor approaches the vertical, the rate is often given in degrees per minute per degree off vertical. Rates of 1°/min to 8°/min per degree off vertical are typical. An erection curve is illustrated in Fig. 7·5.

Errors Inherent in Airborne Gyros.—As a result of tactical maneuvers such as banks, climbs, glides, and turns, gyroscopes in airborne stabilization equipment often indicate false verticals. The two most important errors created are the turn error and the gimbal inertia error.[1]

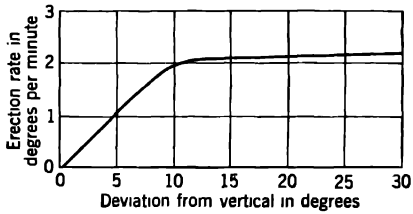

FIG. 7·5.—Characteristic of the erection mechanism of the Pioneer Instrument Company's airborne gyro.

The turn error occurs when the aircraft performs a turn, and is caused by the erection of the gyro rotor toward a dynamic "vertical" instead of the true vertical. This "vertical" is the resultant of the vectors that represent gravity and the centripetal acceleration, $v\omega$, of the turn. In a coordinated turn the effective or dynamic vertical is inclined to the true vertical by the angle given by $R = \tan^{-1} v\omega/g$, where R is also the angle of bank of the airplane, as in Fig. 7·6. As the airplane rolls into a turn, the gyro immediately begins to erect toward the effective vertical. The effective vertical rotates about the true vertical with an angular velocity ω, the angular velocity of the turning aircraft. This causes the gyro to precess about the true vertical. The magnitude of the precessional error is a function of the duration of the turn, until a maximum constant error is approached if the turn lasts for several revolutions.

In order to eliminate this error, some control over the erection mechanism of the gyro is necessary. The gyro used in the C-1 autopilot employs an electromagnetic device that completely cuts out the erection mechanism during turns. This solves the turn-error problem, but the gyro becomes free-running and wanders away from true vertical. In some

[1] *Cf.* H. M. James, "Effect of Gimbal Inertia on a Rotating Stable Vertical," RL Group Report No. 43, May 23, 1944, for a theoretical investigation of these errors.

systems, however, the wandering error is negligible by comparison with the turn errors that would have occurred had the erection mechanism been retained during the turn. A compromise between retaining the erection system in a turn and completely cutting it out is to provide the gyro with a two-speed erection device that allows a high rate of erection for normal level flight and a low rate of erection for turns.

The gimbal-inertia error is encountered when the gyro system is rotated about the scan axis whenever that axis is not parallel to the gyro axis. When this occurs, the gyro housing and gimbal rings exert a torque upon the rotor, causing it to precess about the scan axis of the antenna.

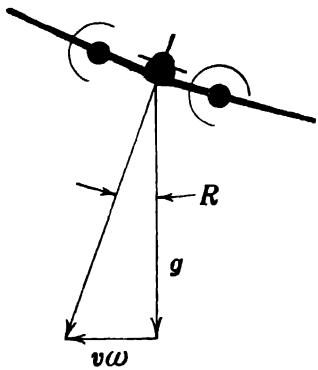

FIG. 7·6. Resolution of dynamic vertical. g, Vertical acceleration of gravity; R, roll angle of aircraft; $v\omega$, horizontal or centripetal acceleration.

Such a precession is found in the line-of-sight stabilizer AN/APA-15. A gyro with one take-off is mounted on the rotating part of the pedestal and ordinarily revolves at a rate of 12 or 24 rpm. In a climb or glide when the angle D between the gyro axis and axis of scan is small, the rate of precession will be roughly proportional to D. For moderately large values of D, however, the rate varies more nearly as the cube of D. The expression for the precessional rate of the airborne stable vertical made by the Pioneer Instrument Company for use in the AN/APA-15 stabilizer is

$$\omega_p = (0.182 \sin D + 1.35 \sin^3 D + \cdots +) \frac{\omega_s}{\omega_G} \omega_s,$$

where ω_p = speed of precession of gyro wheel,
ω_G = speed of rotation of gyro wheel = 20,000 rpm,
ω_s = speed of rotation of stable element.

The constants depend upon the physical characteristics of the gyro and gimbal system. If, for example,

$$D = 18° \quad \text{and} \quad \omega_s = 24 \quad \text{rpm},$$

then

$$\omega_p = (0.062 + 0.038)10.4°/\text{min} = 1.04°/\text{min}.$$

If

$$D = 30° \quad \text{and} \quad \omega_s = 24 \quad \text{rpm},$$

then

$$\omega_p = (0.100 + 0.160)10.4°/\text{min} = 2.7°/\text{min}.$$

The precession continues until the erection mechanism counterbalances it, at which time the gyro maintains a false vertical. By comparing this

precession rate with the erection rate of the gyro, it can be seen that the error in the vertical will be 5.2° for a tilt angle of 18°. This agrees closely with the value observed in a bench test of the system.

7·8. Servo Systems.—The gyro in an airborne stabilization system is merely an indicating device and does not stabilize the scanner by its own torque. In order that the scanner or antenna may be put in the desired attitude, a servo system or some other follow-up must be employed to amplify the torque of the gyro.

It has been pointed out in Sec. 7·5 that the most important difference between a servomechanism for a roll-stabilized system and one for a line-of-sight system is that the roll-stabilization servo system must be statically accurate whereas the line-of-sight system must be dynamically accurate. The precise form that the servo system takes, then, depends on the type of stabilization employed. In general the system consists of synchros mounted on the appropriate axes of both the gyro-gimbal system and the scanner, and of servoamplifiers, servomotors, gear trains, and sometimes linkages. For some systems, potentiometer data transmission can be used instead of synchros.

The output from the synchros represents the error between the actual position of the scanner and its desired position as indicated by the gyro. This error signal is amplified and used to control the motor that adjusts the position of the scanner so that the error is reduced to zero. A detailed discussion of the servo systems employed in stabilization is postponed until the following chapter.

Almost exclusively, the servo systems used in airborne stabilization equipment have been of the continuous-control type. Recently, however, it has been felt that contactor (on-off) servo systems could be employed profitably for this work because of lighter weight and simplification of design. The possibility of using multiple-speed data transmission, as discussed in Sec. 8·6, has not yet been fully explored. The fact that scanners are not stabilized for more than $\pm 20°$ or $\pm 30°$ means that multiple-speed data transmissions up to at least 6-speed could be used without ambiguity.

EXAMPLES OF AIRBORNE STABILIZED SCANNERS

7·9. GEI Roll-stabilized Scanner.—A roll-stabilized scanner for use in a bombing and navigational 1-cm radar was conceived at the Radiation Laboratory, and several models were built by the General Electronics Industries in 1944. The scheme was to mount the reflector, azimuth motor and drive, and r-f head on a "wagon" that could be driven along a circular section of track so that the azimuth axis would be kept vertical with respect to roll, with the track rigidly attached to the aircraft. A simplified schematic diagram of this arrangement is shown in Fig. 7·7.

The wagon is driven along the track by a mesh between a pinion geared to the servomotor and a large sector gear that is part of the wagon. Figure 7·8 shows this arrangement in a close-up view. The total gear ratio between the motor and scanner is 3600/1. The scanner weighs about 100 lb, including the pillbox and a 42- by 10-in. reflector. The gyro and servo components add about 35 lb.

The stable-vertical gyro mounted on the airframe is manufactured by the Pioneer Instrument Company. Its erection mechanism has been described in Sec. 7·7. One synchro is mounted on the roll axis of the gyro-gimbal system, and another in the servo gear box on the scanner.

Mounted near each end of the track ($\pm 23°$ away from the center), the scanner has a microswitch that acts as a limit switch by cutting out the error voltage at the input to the amplifier and replacing it by a few volts of the opposite phase, received from a filament transformer. Thus, when the scanner is driven into a limit switch, it is immediately driven out again and oscillates about the switch until the gyro comes back into the working region. A rubber-cushioned mechanical stop is located a few degrees beyond each switch.

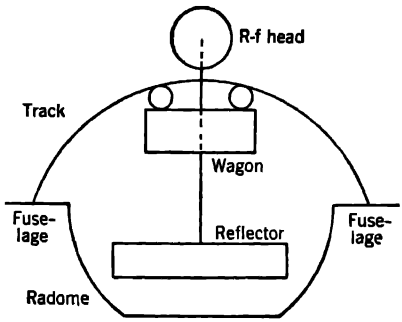

FIG. 7·7.—Simplified schematic diagram of GEI roll-stabilized scanner.

The gear train gives a 144/1 reduction from the servomotor to the pinion that drives the large sector gear. The ratio between the pinion and the sector gear is 25/1, so that the over-all ratio of the train is 3600/1. A separate gear train consisting of two meshes, with a total ratio of 25/1, goes from the pinion shaft to the synchro and causes it to rotate at 1-speed (scanner speed). Precision spur gearing is used throughout the train to avoid excessive backlash and friction.

The results of tests made on the scanner at the Radiation Laboratory show that the average static error for a series of different effective roll angles is 0.2°; the maximum error does not exceed 0.4°. The overshoot observed when an abrupt change of angle of roll is made is approximately equal to the magnitude of the change, and the scanner reaches its steady-state error after a damped oscillation of 1 or 1.5 cycles. Dynamically, the maximum error encountered is a transient of 1° when the roll rate is 5°/sec, and the steady-state dynamic, or velocity, error is considerably less. The resonant frequency of the servo system is about 1.5 cps. It should be pointed out that in this application static accuracy is more

important than dynamic, since the servomotor is driving only when the aircraft is actually changing its attitude.

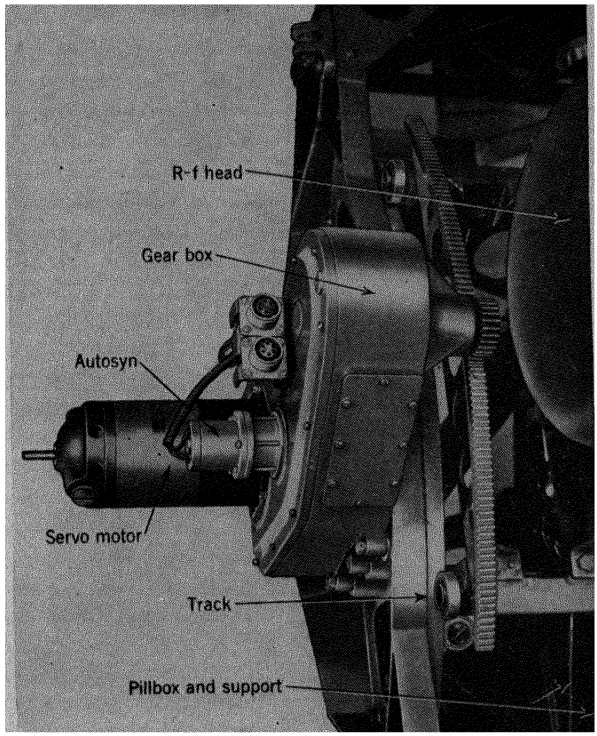

FIG. 7·8.—Servomotor, synchro, and gear box of roll-stabilized scanner. (*Courtesy of Maguire Industries, Inc.*)

7·10. AN/APA-15 Line-of-sight Stabilization Attachment.—AN/APA-15 is an attachment for AN/APS-2, AN/APQ-13, and AN/APS-15 radars designed to maintain a line-of-sight stabilized beam. One of the earliest stabilization equipments, it is built by the Pioneer Instrument Company as three units: the gyro unit, the servocontroller, and the inverter. The gyro unit is a single-axis transmitter that includes a gyro, synchro, servomotor, and a reduction gear train. The inverter delivers 0.5 amp of three-phase 400-cycle 115-volt alternating current from an input of 12-amp 24-volt direct current. The entire attachment, with the exception of the inverter, rotates with the antenna. It should be noted that in Fig. 7·2, which shows the mounting arrangement on an AN/APS-2 scanner, the reflector has been removed from the installation

photographed; the motion-picture camera is not normally part of the scanner but was specially mounted for test purposes. The gyro unit and amplifier together weigh about 20 lb.

A parallelogram linkage connects the gear train with the reflector, thus enabling the motor to drive the reflector about its elevation axis. The linkage is schematically presented in Fig. 7·9. The arm *OF* from the base of the scanner to the structure supporting the antenna is the tilt-control arm, normally present in AN/APS-2 or AN/APS-15. This arm is removed and replaced by the shorter arm *OE* when AN/APA-15 is installed. Changing the length of *OE* will change the fixed angle of depression of the beam. The control is manual and is used at the discretion of the operator. In the diagram it is assumed that a fixed angle has been chosen, and the parallelogram is formed by *ABCD*. The arms *EA* and *AB* are on a differential at the output of the servo gearing, as seen in Fig. 7·2. The use of this linkage makes it convenient to put the servomotor and gear train in the same housing as the gyro, with a consequent saving in space and weight.

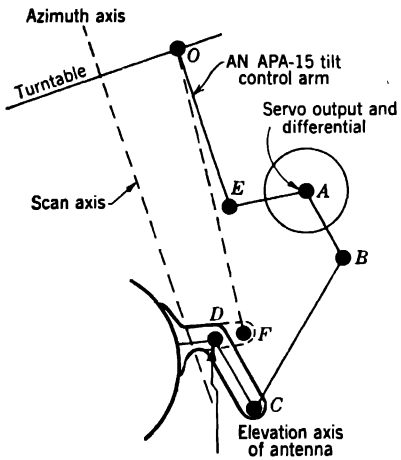

FIG. 7·9.—Schematic diagram of parallelogram linkage system of AN/APA-15 stabilizer. The points *ABCD* form a parallelogram. *OF* represents the tilt-control arm when there is no stabilizer mounted on the scanner.

There are many flaws in the AN/APA-15 system. It suffers from the gimbal inertia error. The erection mechanism cannot be disconnected while the aircraft is turning. Sector-scanning during nonlevel flight is impossible because the angular tilt and the accelerations encountered at the sector extremities cause the gyro to topple. The erection mechanism being of the gravity type with a ball that rotates clockwise (described in Sec. 7·8), the only method that can be used to change the erection rate to combat the turn errors is to control the direction and rate of scan. This is done by counterclockwise scanning which decreases the rotational speed of the erection mechanism with respect to the airplane. The decreased rotational rate results in an increased erection rate and a larger turning error. If clockwise scanning is utilized, however, the rotational rate is increased and the erection rate is decreased, thus producing a smaller turning error.

Flight observations of an AN/APA-15 system showed that because

of the introduction of turn and gimbal inertia errors the stabilization error was increased from about $\pm 2°$ to $\pm 10°$ after a 10° bank of 4-min duration. The test method used is the only one that has been found to give reliable quantitative results. It employs a motion-picture camera mounted in place of the reflector. Both the camera and scanner are enclosed in a special optically transparent radome. Photographs of the horizon at sea are taken while the scanner is operating during flight and can be analyzed to give information about the stabilization system.

7·11. Experimental Stabilization System.—Because of the excessive size and weight of the roll-stabilized scanner and the poor performance of

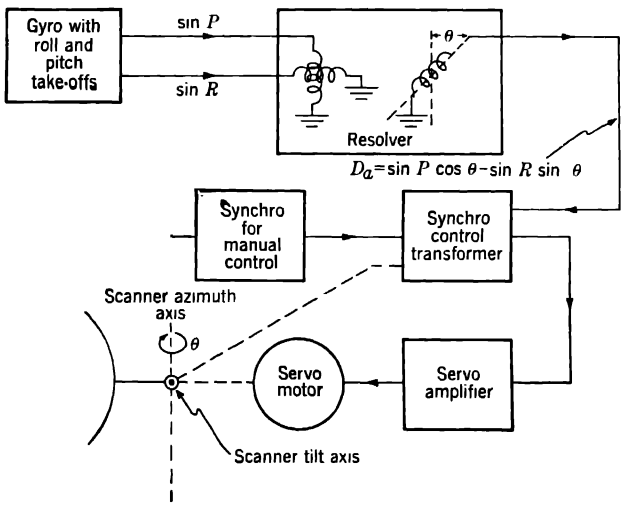

FIG. 7·10.—Block diagram of line-of-sight stabilization system using a remote gyro.

the AN/APA-15, neither of these stabilization systems described in Secs. 7·9 and 7·10 is in current use.

Improved stabilization equipment has recently been designed. The antenna is line-of-sight stabilized by means of a stable-vertical gyro that is rigidly attached to the airframe near the scanner. The scanner is shown in Fig. 6·12, and the servo system is schematically illustrated in Fig. 7·10. Voltages proportional to the sines of the roll and pitch angles are obtained from take-offs on the gyro. These are fed into the stator of a two-phase resolver[1] mounted on the scanner. The relative azimuth θ of the scanner is introduced as the mechanical rotation of the resolver shaft. The output voltage from the rotor winding of the resolver represents the approximate desired tilt angle of the antenna. This is added to

[1] The resolvers discussed in Sec. 4·10 are similar but have two output voltages. As used here, the resolver might better be termed a "synthesizer" (*cf.* Sec. 7·3).

the output of a manually controlled synchro with which the fixed depression angle of the beam may be controlled. The resultant voltage is amplified to control the tilt angle of the antenna.

The entire stabilization system weighs about 50 lb, the servoamplifier, gyro, and power inverter accounting for 35 lb. The accuracy of stabilization has been measured on the bench at $\pm 1\frac{1}{2}°$ for roll and pitch angles up to 15°.

CHAPTER 8

SCANNER CONTROL MECHANISMS

By J. K. McKendry and R. Sher[1]

SERVOMECHANISM PRINCIPLES

Devices for remote control of the angular position of radar scanners can be classified broadly in two categories, according to the anticipated use of the radar set. In the first, if operational requirements are satisfied by having the radar beam scan continuously in azimuth or through some other predetermined pattern, the control mechanism will normally be in the form of a relatively simple motor speed controller. In the second category, where operational considerations require that the radar beam traverse varying patterns, which are, in general, unpredictable except as

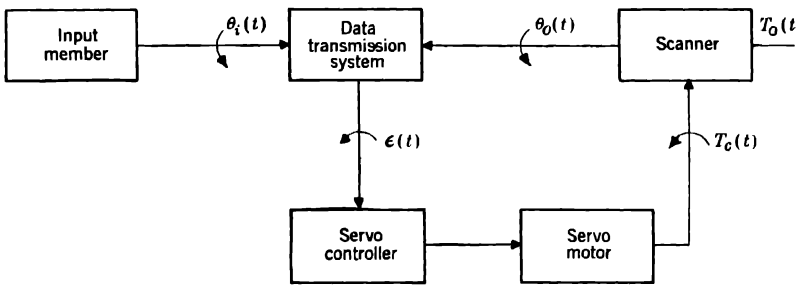

FIG. 8·1.—The servo loop.

to their limits, a "closed-cycle controller" or "servomechanism" is usually required.

This chapter is devoted largely to the discussion of servomechanisms, although examples of the simpler controllers are mentioned. Its purpose is to acquaint the mechanical designer with only the broad outlines of servomechanism design and, in particular, with the effect of mechanical design factors on the quality of servomechanism performance. The scope and minuteness of detail are limited accordingly. For a more complete treatment of the subject the reader is referred to *Theory of Servomechanisms*, Vol. 25, Radiation Laboratory Series.

8·1. The Servo Loop.—The distinguishing characteristic of a scanner servomechanism, as contrasted to simpler controllers, is the closed cycle

[1] Secs. 8·9, 8·10, and 8·12 are by R. Sher.

or loop, shown schematically in Fig. 8·1, which permits the continuous comparison of the input and output angles and establishes a controlling torque as a function of the angular difference or error.

The diagram includes the essential servomechanism components and indicates their functional relationship. A complete scanner control system may consist of several such loops functioning interdependently, but for purposes of this discussion the simple loop diagram may be considered completely representative.

The following definitions specify the physical nature of the various components of the servo loop and to some extent indicate their interaction.

$\theta_i(t)$ = input angle or desired scanner angle as a function of time.
$\theta_o(t)$ = output angle or actual scanner angle as a function of time.
$\epsilon(t)$ = angular difference between $\theta_i(t)$ and $\theta_o(t)$.
$T_c(t)$ = controlling torque exerted by the servomotor.
$T_o(t)$ = disturbing torques on the scanner, e.g., wind forces.
J_o = moment of inertia of the rotating scanner mechanism.
f_o = coefficient of viscous friction of the scanner mechanism (frictional force proportional to velocity).

In brief outline, the sequence of operation of the servo loop components is as follows. The input member is caused to assume an angular position θ_i, the desired angular position of the scanner. This angle is fed into the data-transmission system which instantaneously computes an algebraic quantity ϵ, the angular difference between θ_i and the actual scanner angle θ_o. This difference, or error quantity, ϵ is transmitted to the servo controller whose response causes the servomotor to apply a torque T_c to the rotation axis of the scanner. The scanner rotation resulting from this torque is in such a direction as to produce a value of θ_o equal to θ_i and consequently to reduce ϵ to zero. If θ_i remains fixed, the scanner eventually comes to rest with $\theta_o = \theta_i$ unless restrained by some disturbing torque T_o.

In general, this operation of the control mechanism is not an isolated event but is one of a continuing series. For purposes of a useful analysis of the system, θ_i must be regarded as a variable function of time, and all other quantities dependent on θ_i are then also functions of time. They are so labeled in the diagram and will be treated as such in the following discussion.

8·2. Basic Servo Equations.—To arrive at any useful understanding of the operation of the servo loop it is necessary to express the functional relationships of the various components in mathematical form.[1] Refer-

[1] Based on the derivation given in "Dynamic Behavior and Design of Servomechanisms," by Gordon S. Brown and Albert C. Hall. *Paper* No. 45-A-20, contributed by the Instruments and Regulators Division for presentation at the November 1945 annual meeting of the American Society of Mechanical Engineers in New York City.

ring to the loop diagram and the definitions previously given, the following expressions can be stated immediately.

$$\epsilon(t) = \theta_i(t) - \theta_o(t). \tag{1}$$

$$T_c(t) = J_o \frac{d^2\theta_o}{dt^2} + f_o \frac{d\theta_o}{dt} + T_o(t). \tag{2}$$

$$T_c(t) = k\epsilon + m\frac{d\epsilon}{dt} + n\frac{d^2\epsilon}{dt^2} + s\int_0^t \epsilon\, dt. \tag{3}$$

Equation (2) states that the controller torque $T_c(t)$ applied to the rotating mechanism of the scanner is consumed in accelerating the system and in overcoming the viscous friction of the mechanism and any disturbing torques applied to it. Equation (3) expresses the controller torque as a function of the error angle ϵ. The reason for the particular form of this expression is not immediately obvious and will be discussed in some detail in later paragraphs. It should be noted at this point that Eq. (3) is idealized in the sense that it is not physically possible to produce a controlling torque that is a function of the exact derivative and integral functions of ϵ as expressed in the equation. Commonly used means of approximating these functions will also be described later.

To facilitate the further manipulation of the loop equations it is convenient to use the operational notation and procedures. In this form, the symbol p is understood to represent the operation $d(\ )/dt$, p^n represents $d^n(\ )/dt^n$, and $1/p$ represents $\int_0^t (\ )\, dt$. Through application of these conventions, Eqs. (2) and (3) become

$$T_c(t) = (J_o p^2 + f_o p)\theta_o(t) + T_o(t), \tag{2a}$$

$$T_o(t) = \left(k + mp + np^2 + \frac{s}{p}\right)\epsilon(t), \tag{3a}$$

or

$$T_c(t) = G_c(p)\epsilon(t), \tag{3b}$$

where $G_c(p)$ represents the entire operator of Eq. (3a).

Since the quantity $\epsilon(t)$ is a measure of the accuracy with which the scanner reproduces the input motion, an explicit expression for $\epsilon(t)$ in terms of design quantities is useful in predicting the performance of the servomechanism or in establishing desirable values for the design quantities. Such an expression can be derived as follows:
From Eqs. (2a) and (3b)

$$G_c(p)\epsilon(t) = (J_o p^2 + f_o p)\theta_o(t) + T_o(t). \tag{4}$$

Combining Eqs. (1) and (4), we find

$$G_c(p)\epsilon(t) = (J_o p^2 + f_o p)[\theta_i(t) - \epsilon(t)] + T_o(t), \tag{5}$$

or

$$[G_c(p) + J_o p^2 + f_o p]\epsilon(t) = (J_o p^2 + f_o p)\theta_i(t) + T_o(t), \tag{6}$$

Let us now consider a system for which $\epsilon(t)$ is a solution of Eq. (6) and impose on it a sudden shift of the input angle corresponding to a step function; i.e., the input angle is made to undergo a sudden discontinuous finite change $\Delta\theta_i$, and thereafter to maintain the values that it would have had without the shift, except that they are all shifted by this amount. Since Eq. (6) is a *linear* differential equation, the solution for ϵ will be the sum of the original one and another solution that corresponds to the shifting of θ_i by the step function. For the step function the right-hand side of Eq. (6) is zero, since the derivatives of θ_i are zero after the shift has been made, and there has been no addition to $T_o(t)$. The additional solution for ϵ to be added to the original one in this assumed single case is thus the solution of the complementary equation of Eq. (6), obtained by putting the right-hand side equal to zero:

$$[G_c(p) + J_o p^2 + f_o p]\epsilon(t) = 0. \tag{7}$$

The further treatment of this equation is entirely analogous to the one that is familiar in various problems of damped oscillatory motion. A function of the form

$$\epsilon(t) = Ae^{rt},$$

in which A and r are constants, is obviously a solution. Substituting it into Eq. (7) we find the equation giving the values of r that will give such solutions:

$$G_c(r) + J_o r^2 + f_o r = 0. \tag{8}$$

Any root of Eq. (8) gives a possible solution of Eq. (6). When G_c has the full generality expressed by Eqs. (3*a*) and (3*b*), Eq. (8) will be a cubic equation having roots r_1, r_2, and r_3. The solution corresponding to the assumed shift of θ_i will be the sum of the three separate solutions corresponding to the three roots:

$$\epsilon(t) = A_1 e^{r_1 t} + A_2 e^{r_2 t} + A_3 e^{r_3 t}. \tag{9}$$

The values of the constants A_1, A_2, and A_3 are to be determined from the initial conditions for ϵ, $d\epsilon/dt$, etc., at the time at which the shift $\Delta\theta_i$ is made.

If the coefficient s of Eq. (3) is zero, Eq. (8) is a quadratic, there are only two terms in Eq. (9), and the whole solution reduces to the familiar one of damped harmonic motion.

All of these preceding general remarks also apply if the step function expresses a discontinuous change of $T_o(t)$ rather than of θ_i. Equation (6) then becomes one that has a constant on the right-hand side, but the solutions are of the same form.

The nature of the transient response of the system is specified by the nature of the roots r_1, r_2, etc. If the roots are real and negative, the response will be stable and aperiodic; if complex with negative real parts, the response will be a damped oscillatory motion. Two equal negative real roots correspond to the boundary condition of critical damping. Positive real roots or positive real parts of complex roots indicate an inherently unstable system.

In Eq. (3) the controller torque $T_c(t)$ is expressed as a function of ϵ, the first and second time derivatives of ϵ, and the time integral of ϵ. All these terms were included for the sake of generality, but in many types of controllers one or more of the coefficients may be zero. In the simplest basic controller, all coefficients except k are zero. Since $G_c(p)$ is then equal to k, Eq. (8) reduces to

$$J_o r^2 + f_o r + k = 0, \tag{10}$$

and the roots are

$$r_1, r_2 = -\frac{f_o}{2J_o} \pm \sqrt{\frac{f_o^2}{4J_o^2} - \frac{k}{J_o}}. \tag{11}$$

From this it is seen that the system will be stable, since f_o and J_o are inherently positive; it will be aperiodic if $f_o^2/4J_o^2 > k/J_o$ and oscillatory if $f_o^2/4J_o^2 < k/J_o$. Significant relationships in these roots are the "damping ratio" $f_o/2\sqrt{J_o k}$, which is the ratio of the actual damping to the damping that would cause aperiodic system response [the value of $f_o/2J_o$ that would make the radical of Eq. (11) = 0] and the "undamped natural frequency" $\sqrt{k/J_o}$, which gives the oscillation frequency in radians per second when $f_o = 0$ and no damping exists. The limitations of such a simple controller are made more obvious by deriving the expression for the steady-state error of the system for a constant velocity input. Setting $G_c(p)$ in Eq. (6) equal to k, and substituting ω_i for $p\theta_i(t)$, we find

$$(J_o p^2 + f_o p + k)\epsilon(t) = (J_o p + f_o)\omega_i + T_o(t). \tag{6a}$$

For constant values of ω_i and T_o, all terms involving p eventually become equal to zero, and the value of ϵ in the steady state ϵ_{ss} is given by

$$\epsilon_{ss} = \frac{f_o\omega_i + T_o}{k}. \tag{6b}$$

It is then obvious that to maintain a small error under constant velocity conditions k must be large with respect to f_o (disregarding the effect of T_o). However, examination of the expression for the damping ratio shows that its magnitude is reduced if k is increased relative to f_o. The effect of this reduction is to permit transient oscillations to persist for a longer time. Selection of the value of k must then be a compromise

between a high steady-state velocity error and poorly damped transient oscillations. The usefulness of the simple controller is also limited, because true viscous friction is seldom present to any significant degree in scanner mechanisms. Then k must be made so small for satisfactory damping that any constant disturbing torques T_o on the scanner will result in large constant errors.

These conditions can be improved by the use of a controller function having time-derivative terms. Equation (10) then becomes

$$J_o r^2 + f_o r + k + mr + nr^2 = 0 \tag{12}$$

or

$$(J_o + n)r^2 + (f_o + m)r + k = 0, \tag{12a}$$

and the roots are

$$r_1, r_2 = \frac{-(f_o + m)}{2(J_o + n)} \pm \sqrt{\frac{(f_o + m)^2}{4(J_o + n)^2} - \frac{k}{(J_o + n)}}. \tag{13}$$

With this type of controller it is possible, by varying the values of m and n, to make the real parts of the roots as large as desired, thereby damping out transient oscillations quickly while maintaining a high value of k with resulting high steady-state accuracy. The function of an integral term in the controller output is to reduce the constant velocity error. The value of $s \int_0^t \epsilon \, dt$ eventually becomes so large as t increases that the controller will maintain a constant velocity with ϵ reduced to zero.

The preceding mathematical treatment has been general and does not necessarily represent the best approach to the problem of designing a specific servomechanism. For example, in some types the time lag in the servomotor response may be negligible in comparison with time lags in the controller; in this case the quantities J_o and f_o must be redefined to represent the equivalent quantities in the controller. In other types, both servomotor and controller may have time lags of the same order of magnitude; both must therefore be included in the analysis. Not only the basic definitions but also the form of the servo equations may be altered by such considerations. The solutions, however, will normally be found in forms similar to those given. Special treatment for particular types of servomechanisms will be indicated in following sections.

In order to specify the performance of an actual servomechanism completely and to include the effects of all time lags and energy storage elements in the system, it is sometimes found that Eq. (8) must be of cubic or higher order. Since the solutions for transient response become progressively more laborious as the order of the equation increases, it is sometimes preferable to base the design of a system on the relatively simple calculations of response to steady-state sine-wave inputs over a

range of useful frequencies.[1] Transient response can be correlated with the results of these computations; in many applications the sinusoidal steady-state error is of much greater weight than the transient error.

8·3. The Input Member.—In the introductory paragraph of this chapter it was stated that servomechanisms are generally used where the angle of the required position of the scanner cannot be predicted as a function of time except with regard to its limits. In order to establish these limits it is necessary to know the nature of the input member of the servo loop. In common radar practice this member may take the form of a handwheel, which may be positioned manually by the radar operator or driven in continuous or oscillatory motion by a control motor. The input member may be a gyroscopic stable vertical, a stabilization computer, or a gyrocompass, or it may be a target aircraft or surface craft that the radar is tracking automatically. Frequently the complete input member may be made up of a series of such members with their outputs combined to produce θ_i in the servo loop. The limiting characteristics of the input element that must be known in order to establish a basis for servomechanism design are its maximum angular velocity and acceleration and the range of frequencies present in its motion.

It is more difficult to predict limits of velocity and frequency for a control handwheel that is manually positioned by a radar operator than for any other usual type of input member. For the operator's convenience the control member should be easily operable; but if this principle is carried to extremes, there is no significant limit to the motions that may be fed into the servomechanism. On the other hand, if the motion of the input member is restricted by such factors as inertia or friction, the proper functioning of the radar system may be hampered. The best solution of this difficulty appears to be the use of an input member that can be easily manipulated in the manner required by any imaginable operational conditions. The other servomechanism components can then be designed to limit the actual response to meet only the operational requirements, regardless of excessive input velocities and accelerations applied by the operator.

For the second type of input member, as exemplified by the stabilization devices and compasses mentioned above, the input limits can be defined fairly well. Since the relative motion of these components is generally the negative equivalent of, for example, the angular motion of the deck plane of a ship or the displacement from true north of the fore-and-aft line of a ship, it can readily be calculated from the values and natural periods of maximum roll, pitch, and yaw angles and maximum

[1] A. C. Hall, "The Analysis and Synthesis of Linear Servomechanisms," Ph. D thesis, M.I.T., 1943.

turn rates. These quantities are known for most types of naval surface craft and for aircraft.

A great deal of study has been expended on the functioning of a radar target as the input member of a servomechanism. In general, the limits of velocity and acceleration of such a member can be predicted with good accuracy and constitute only a minor factor in the servomechanism associated with an automatic-tracking radar.

It should be noted that the limits of velocity and acceleration that can be assigned to the input member do not necessarily represent the maximum transient values that can be applied to the controller. If the system is suddenly energized, with a large value of error present the effect is the same as for an applied step function of input, and the full transient torque will be developed. Thus, the strength of the design must be based on the analysis of transients (including saturation effects) even though the accuracy of the performance is predicted for steady-state conditions.

8·4. The Servomotor.—The characteristics of the servomotor, or torque-producing component of the servo loop, will usually constitute a major factor in setting the ultimate limits of performance of the servomechanism. Since the servomotor is normally torque-consuming as well as torque-producing, it influences every term of both operators of Eq. (7) to some extent. Conversely, the important considerations in the selection of a servomotor for a specific application can be derived from examination of the basic servo equations. The effect of the motor constants on the performance of the servomechanism can be demonstrated most clearly if it is assumed that the servo controller is of the simplest type, producing a controller output directly proportional to the error angle; $G_c(p)$ is then equal to k.

Equation (11), which gives the roots of the transient equation for this type of controller, shows that the transient behavior depends on the relative values of f_o, J_o, and k.

As previously stated, true viscous friction seldom occurs to any important extent in scanner mechanisms, and an equivalent term must be inserted in the controller in order to obtain quickly damped response. Controller design is considerably simplified, however, if the servomotor has a characteristic that produces an effect similar to viscous friction. This is the case if the motor torque decreases as its speed increases under constant input conditions. If the torque-speed characteristic of the servomotor is of this type, and if the decrease in torque per unit increase in speed is reasonably constant over the operating range of the motor, the damping may be satisfactory for many applications without the use of a first derivative term in the controller output.

The term J_o has previously been defined as the moment of inertia of the rotating system and must include that of the servomotor. In com-

mon types of scanner servomechanisms the inertia of the servomotor may constitute considerably more than one half of the total value of J_o because the motor is usually geared up from the scanner axis and its inertia is effectively multiplied by n^2, n being the motor-to-scanner gear ratio.

The effect of the inertia term on the response of the servomechanism is seen by examination of the expressions for the damping ratio and the natural frequency. With other terms held constant, increasing J_o reduces the damping ratio and the natural frequency of the system. Transient oscillations will then be of longer duration; i.e., the response will be slower.

In the preceding discussion it has been tacitly assumed that k is a pure constant. This assumption is necessary if the performance of the servomechanism is to be expressed in the form of a linear differential equation. Variation of k with ϵ results in a differential equation of higher degree, which will usually be more difficult to solve. This suggests that the torque developed by the servomotor should be a linear function of the controller output, since it is generally easier to design a controller whose output is a linear function of input than it would be to introduce nonlinearity of the controller to compensate for nonlinearity of the servomotor. Servomotors are never precisely linear in response, but those in common use are sufficiently so to make compensation of the controller unnecessary. The restriction to approximate linearity applies only over the range of speeds and torques required by the particular application. Any servomotor will respond nonlinearly if sufficiently overdriven. The criterion for the calculation of the required servomotor rating is, accordingly, that the motor must have sufficient rated torque to control the inertia of the scanner and motor in accordance with any velocity and acceleration within the operating range of the input member. Use of the rated torque in this calculation usually allows a comfortable margin of safety before the nonlinear region is reached.

Three general types of servomotors have had wide application in servomechanisms for scanner control. These are the polyphase a-c electric motor, the d-c electric motor, and the hydraulic motor. Each has basic merit, and for a particular application the choice will frequently be governed purely by engineering considerations or even by the personal prejudice of the designer.

In many respects the hydraulic motor approaches the characteristics of the ideal servomotor more nearly than does any other available type. The motor is usually controlled by regulating the delivery rate of the pump that feeds it. With this type of system the motor response can be an accurately linear function of the setting of the pump regulator within the operating range. Furthermore, the torque-speed slope can be made very steep and constant, giving a large constant damping factor. The

torque/inertia ratio of the hydraulic motor is likewise favorable. To be weighed against these advantages are the relative mechanical complexity and the high precision required in manufacture. The repair and maintenance of hydraulic systems have not been so satisfactory as with systems using electric motors, presumably because of the greater familiarity of radar maintenance personnel with electric motors. Another disadvantage is that the smallest available hydraulic systems are too heavy for lightweight airborne radars.

The d-c electric motor, as used in scanner servomechanisms, is usually operated with fixed-field excitation and is controlled by regulation of the armature voltage. (An exception is the field-controlled d-c servomotor described later in this chapter.) With properly designed compensating field windings the motor with armature control has good torque-speed characteristics and reasonably linear response to the control voltage, except that the coulomb friction[1] of the brushes and commutator causes a discontinuity in the control at zero speed. This is not of importance except in very small sizes where the torque resulting from brush friction may be comparable in magnitude to the rated torque of the motor. The torque/inertia ratio is not so high as in the hydraulic motor but has been found adequate for even the most precise scanner control requirements.

The ideal mechanical simplicity of the polyphase induction motor gives it a strong advantage in other applications, but as a servomotor it has been less widely used than either the d-c electric or hydraulic motors because of its torque-speed curves, which have a slope varying from a high positive value near synchronous speed to a negative value nearly as large at low speeds. To produce characteristics useful in a servomotor, it is necessary to use rotor conductors of higher resistance than those in standard types of induction motors. Rotor losses are consequently high, and the problem of heat dissipation becomes very troublesome. Recent advances in the design of polyphase motors have increased the torque/inertia ratio and improved the cooling arrangements; some very good motors are now available in ratings up to 1 hp.

8·5. The Servo Controller.—The function of the servo controller is basically the transformation of the error quantity $\epsilon(t)$, usually a voltage, into some other quantity suitable for application to the servomotor to produce a positioning torque. As indicated in Eq. (3), the controller output is not, in general, simply proportional to the error quantity but may have components proportional to the time integral and time derivatives of the error quantity. The controller, therefore, will customarily have an output stage designed to furnish a controller quantity specifically suited to the particular type of servomotor, a proportional amplifier,

[1] Coulomb friction is a force that is substantially independent of velocity and always in opposition to the direction of rotation.

and an "equalizing network" that computes the integral and differential terms and combines them in the proportions necessary to assure satisfactory performance. These three components may not be clearly defined in any given controller, but for purposes of analysis they can be considered as being separate.

The nature of the output stage of the controller determines to a considerable extent the form in which the defining equations must be expressed in order to represent the actual servo performance to the best approximation. For example, if the controller output is best represented as a voltage to be impressed on the armature of a d-c servomotor, the characteristics of the motor that are important in the defining equations are its inertia and its viscous-friction component. If, on the other hand, the controller is regarded as impressing a current on the armature, the motor can be regarded as having an inertia term but no viscous friction. In either case, certain factors, such as the electrical impedance of the output stage and the armature, will be present and their importance will be minimized or accentuated by the choice of the form in which the controller function is stated. Normally, the form of this expression should be chosen to permit lumping of system constants with consequent reduction of the order of the operational expressions for the servo performance.

In servomechanisms using d-c armature-controlled electric motors, the commonest type of controller output stage is a constant-speed d-c generator whose output voltage is proportional to the current that produces an exciting field. Since it is desirable to control the current of the exciting field with low-power vacuum tubes, the generator must have a high ratio of output power to power of the control field. This has been accomplished by using a two-stage generator or an Amplidyne (manufactured by the General Electric Company). In the Amplidyne, excitation of the control field causes a current flow through a pair of short-circuited brushes on the commutator. This relatively high current in the armature induces a strong field, which in turn excites a high voltage between the output brushes that are located in quadrature with the short-circuited brushes. A power gain of about 1000 can easily be obtained in this way. If the current of the control field is regulated by a pair of pentodes, the time lag in the Amplidyne is usually negligible.

Another method of armature control for d-c servomotors utilizes a pair of thyratrons connected to furnish rectified current to the armature. The polarity of the rectified current depends on which thyratron is turned on. This method has not been widely used in scanner servomechanisms.

Thyratrons have also been used to control polyphase servomotors, usually in circuits similar to that shown in Fig. 8·2. The a-c supply voltage is impressed between the common terminal c of L_1 and L_2, the

field coils of a two-phase motor, and the common connection d of T_1 and T_2, a pair of saturable core transformers. If the thyratrons are not conducting, the primary impedance of transformers T_1 and T_2 is so high that only a small fraction of the line voltage appears across L_1 and L_2. If only V_1 is made conducting, the rectified current through the secondary of T_1 saturates its core and reduces its primary impedance with the result that a larger fraction of the line voltage appears between terminals a and c. A current due to this voltage flows in L_1, and a current shifted 90° ahead in phase flows through the series combination of L_2 and C. The rotating field produced by these currents causes the rotor to revolve in the same direction. If V_2 is made conducting, the result is the same

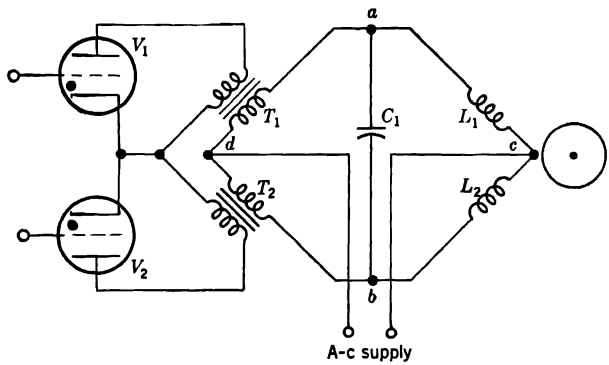

FIG. 8·2.—Thyratron controller for polyphase motor.

except that the current in L_2 is then in phase with the line voltage and the current in L_1 is 90° ahead. Rotation of the field and the rotor is thus opposite to that produced by allowing V_1 to conduct.

In hydraulic systems the output stage of the controller normally consists of a variable displacement pump together with the mechanism for controlling its displacement. This mechanism may consist of one or more hydraulic amplifiers and some sort of electromechanical torque motor. In some cases the response of a hydraulic motor to variations in pump displacement is so rapid that the time lag of the motor is negligible in comparison with the time lag in producing the variations in displacement. The response of the servomechanism is then mainly determined by the characteristics of the output stage of the controller.

The process of computing time derivative and integral functions of the servo error is ordinarily performed by the use of electrical circuits that produce a close approximation to the desired function over the required range of input frequencies. Figure 8·3 shows two basic circuits frequently used for such purposes. In circuit A, if e_i is an input voltage, the output e_o will consist of a term proportional to e_i and a term propor-

tional to the time derivative of e_i. The output of circuit B contains terms proportional to e_i and to the time integral of e_i. This is true over a considerable range of frequencies, and the outputs bear a useful resemblance to these functions even for a step function of input voltage.

In some controllers it is necessary to preserve the carrier frequency of the data-transmission system for application to the servomotor; it follows that equalizing networks must operate directly on the amplitude-modulated carrier. Circuits that have been used for this purpose include the Wien bridge, the bridged T and parallel T, and the carrier-resonant *RLC*-circuit.

Another method of equalization that has been used frequently with d-c servomotor controllers is based on the degenerative feedback into the

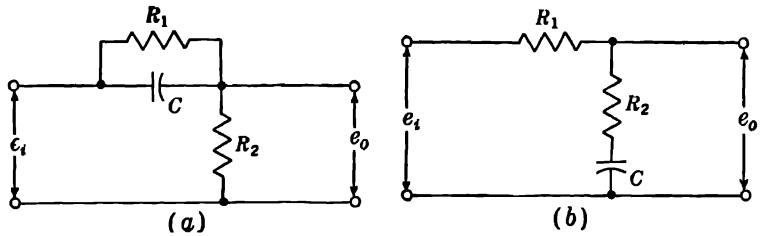

FIG. 8·3.—Equalizing networks. In each circuit e_i is the input voltage and e_o is the output voltage of the network.

controller of a voltage proportional to the acceleration of the servomotor. The effect is a reduction of response over a critical range of frequencies.

All of the servomechanisms previously discussed have been assumed to be of the "continuous control type," in which the controlling torque is a linear function of ϵ and its time derivatives and time integral. There exists, however a very useful and popular class of servo controller that has an output stage consisting of electrically operated relays. With this type of controller, restoring torque is applied as a step function of ϵ (in more complex circuits, a series of step functions), and the previously derived equations are consequently not valid. The general considerations are nevertheless much the same. Relay control can be applied to both a-c and d-c servomotors and also to hydraulic controllers. It has been widely used in low-accuracy applications.

8·6. Data-transmission Systems.—The function of a data-transmission system in the servo loop is, as previously mentioned, to compare continuously the actual scanner angle with the desired angle and to compute a quantity proportional to the error. Since the scanner is usually not at the same place as the input member, the commonest and most convenient types of data-transmission systems are electrical, usually consisting of a pair of synchros, as shown in Fig. 8·4.

The synchro generator or transmitter is very similar in construction to an ordinary three-phase electrical generator. It has a two-pole rotor with a single electrical winding and a stator with three equally spaced windings connected in Y or Δ. When an alternating voltage of rms value E_G is applied between the rotor terminals R_1 and R_2 (with the rotor held stationary with respect to the stator), the rms voltages induced between the pairs of stator terminals S_1, S_2, and S_3 are given by the following expressions:

$$E_{(S_1-S_2)} = KE_G \sin(\theta_i - 120°). \tag{14a}$$

$$E_{(S_2-S_3)} = KE_G \sin(\theta_i + 120°). \tag{14b}$$

$$E_{(S_3-S_1)} = KE_G \sin \theta_i. \tag{14c}$$

In these equations K is a fixed transformation ratio and θ_i is the angular displacement of the axis of the rotor pole from an arbitrarily established

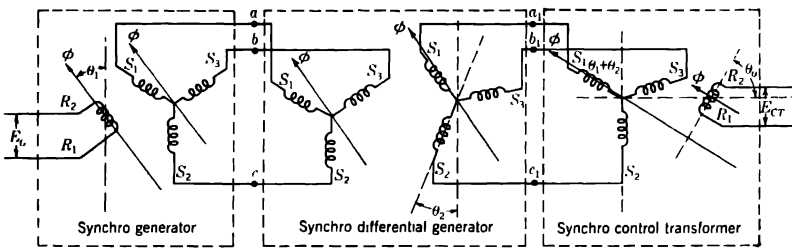

FIG. 8·4.—Synchro data transmission. The system shown here computes $E_{CT} = K'E_G \sin(\theta_1 + \theta_2 - \theta_o)$. With rotor positions as shown, $\theta_o = \theta_1 + \theta_2$ and $E_{CT} = 0$. Vectors labeled ϕ represent the direction of the magnetic field in each instrument. With the differential generator omitted, and connections a to a_1, b to b_1, and c to c_1, the system computes $E_{CT} = \sin(\theta_1 - \theta_o)$.

"electrical zero" position. (In this instance, the shaft of the synchro generator is assumed to be mechanically coupled to the input member, and θ_i therefore represents the input angle of the servomechanism as hitherto.)

Stator terminals S_1, S_2, and S_3 are electrically connected to the respective S_1, S_2, S_3 terminals of the synchro receiver, or control transformer CT, which is substantially identical in construction with the synchro generator except that its coil windings are of higher impedance. The shaft of the CT is mechanically coupled to the rotation axis of the scanner, and its angular position θ_o, therefore, represents the scanner angle. The stator voltages transmitted by the generator then produce a magnetic field in the CT, and the angular position of the axis of this field with respect to the stator windings of the CT is exactly the same as that of the rotor of the generator with respect to its own stator windings. If then the CT rotor is turned through varying values of angular position θ_o, the voltage between its terminals can be expressed by the formula

$$E_{(CT)} = K'E_G \sin(\theta_i - \theta_o), \tag{15}$$

where K' is an over-all transformation ratio. Since in practice the error angle $(\theta_i - \theta_o)$ is of small amplitude, the voltage $E_{(CT)}$ can be regarded as directly proportional to $(\theta_i - \theta_o)$ and is therefore suitable for use as the input to the servoamplifier. It should be noted that a synchro-transmission system can be used in the reverse order from that indicated by the above discussion. The CT can be positioned by the input member, and the generator then represents θ_o. By the use of a third type of synchro, a differential generator, it is also possible to set up a transmission system to perform computations such as

$$E_{(CT)} = E_G K' \sin (\theta_1 + \theta_2 - \theta_o). \tag{16}$$

The accuracy specified for construction of synchros of the military type permits over-all errors of nearly 1° of rotation in the performance of the angular additions and subtractions indicated by Eqs. (15) and (16). To minimize this error, it is common to gear up synchros from the axes of the scanner and input member. A standard gear ratio is 36/1; 1° of error in the synchro is equivalent to $\frac{1}{36}$° of error in the position of the scanner. It should be noted, however, that in Eq. (15) $E_{(CT)}$ will then vary through 36 complete cycles for one revolution of θ_i (θ_o constant). It is therefore necessary to use a one-speed transmission system in addition to the geared-up system to prevent the scanner from being stably positioned at some value of θ_o equal to $(\theta_i + n10°)$, where n is any integer from 1 to 35. An automatic switch in the servoamplifier connects the geared-up system only when $\theta_i - \theta_o$ is less than 10°.

Nearly the same results can be achieved by the use of specially wound potentiometers. Potentiometers are generally not so durable as synchros, however, and they are not so frequently used.

In automatic-tracking radars, the data-transmission system is composed of the radar transmitter, the reflecting surfaces of the target, and the radar receiver with its associated circuits. The error quantity measured is the displacement angle between the principal axis of the antenna and the line from antenna to target. This system is subject to a variety of disturbances not encountered in other types. Among these are periodic fading of the signal, thermal noise in the receiver, and interfering signals. Filtering of the data from this transmission system has been one of the major problems in the development of automatic tracking systems.

MECHANICAL DESIGN FACTORS

8·7. Linear Factors.—In the mathematical treatment of Sec. 8·2 servomechanisms behavior is expressed in the form of a linear differential equation with constant coefficients. If coefficients that are not constant but are functions of the variables are introduced, the equation is no

longer linear and the difficulty of solution is correspondingly greater. A rigorous analysis of any servomechanism usually does introduce terms having variable coefficients but in a well-designed system these terms can usually be made negligible. Design factors that can be expressed as constant coefficients have here been termed *linear factors*. Quantities that must be expressed as variable coefficients in a precise analytical study are discussed in Sec. 8·8 as *nonlinear factors*.

The only linear factor over which the mechanical designer can exert any appreciable control is the term J_o, the moment of inertia of the rotating mechanism. It has been shown that the effect of increasing J_o is to slow up the transient response by causing poorly damped oscillations of long period. It has also been shown that the maximum possible acceleration is inversely proportional to J_o. It is then obvious that low inertia is a desirable feature in a scanner mechanism, and this fact should certainly be considered as a guiding principle in the mechanical design. It is also true, however, that the principle can be followed beyond the limits of sound economic return. There is, for example, no strong incentive for reducing the inertia of the scanner below a value that permits satisfactory acceleration and transient response unless the reduction is large enough to permit the use of a smaller standard size of servomotor.

As indicated in the previous discussion (Sec. 8·2), true viscous friction is seldom found in any appreciable amount in radar scanner mechanisms, and an equivalent term must therefore be found in either the controller or the servomotor. It is, of course, possible to design a true viscous damping device for a scanner servomechanism, but such a device can hardly be recommended because of the power loss represented and the high steady-state error that it would cause and because equivalent results can be obtained much more simply and inexpensively by electrical circuits. Mechanical dampers consisting of inertia coupled through viscous friction to the servomotor have been used extensively in instrument servomechanisms, but not to any considerable extent in radar scanners.

8·8. Nonlinear Factors.—The term $T_o(t)$ has been defined as disturbing torque on the output member. From Eq. (7) it will be seen that a step or discontinuity in $T_o(t)$ will produce an error transient basically similar to that produced by a step function of input angle and that a constant value of $T_o(t)$ will cause a constant displacement error. Certain mechanical design factors, which would necessitate the introduction of variable coefficients in an exact mathematical analysis of a servomechanism, can be studied, at least qualitatively, by representing them as disturbing torques on the output member.

Coulomb friction is such a factor. It can be represented by a step of torque applied each time that the motor reverses direction. This may be further complicated if the static value is greater than that with

the mechanism in motion. At best, the net effect is to produce a lag in response at reversal and to excite transient oscillations immediately thereafter. The effect of irregularities of gear teeth may be regarded as a variation, with time or displacement, in the value of coulomb friction. The effect may be simply a slow periodic change in the steady-state error or the production of transient oscillations, depending on the nature of the irregularity.

Backlash in the gearing of scanner mechanisms may give a variety of effects on behavior of servomechanisms, all undesirable. Again, as in the case of coulomb friction, the least objectionable condition that it can create is a lag in response at reversal and transient oscillations thereafter. In addition, it may make stabilization of the system extremely difficult. A servomechanism that is otherwise quite stable may have a strong tendency to oscillate through the amplitude permitted by the backlash. To some extent, elasticity in the gearing can produce effects similar to those produced by backlash.

The use of worm gears in scanner mechanisms warrants special mention. A reversible worm-gear assembly, that is, one that can be driven equally well from either end, is no different in behavior from an equivalent spur-gear assembly and is also desirably compact by comparison. The presence of coulomb friction, however, makes practical worm-gear assemblies something less than ideal in this respect. When there is an inertial load that must be rapidly reversed or accelerated, the result is discontinuity in the load applied to the motor. Furthermore, cumulative wear on the gears and bearings soon produces rough and erratic performance of the servomechanism. The use of worm gearing is justified only where the inertial load is extremely light and should therefore probably never be considered for radar scanner mechanisms.

The effect of a fixed static unbalance around the axis of rotation of the scanner is a constant unidirectional error in the servomechanism. If the unbalance varies with position, the error will vary correspondingly. Since the unbalance must be compensated by a torque from the servomotor, a frequent result is that the motor is subjected to a high static load, which leads to excessive heating. A special case of unbalance is produced by unsymmetrical distribution of wind resistance about the axis of rotation. This, of course, varies not only with position but with wind velocity.

DESIGN SPECIFICATIONS

The engineering design of a practical servo system cannot be accomplished by attention to only the purely electromechanical considerations discussed in the preceding sections. Every scanner servomechanism must meet certain design specifications, basically determined by the

function of the radar system for which it is intended. These specifications include limitations on weight and space for airborne and shipborne sets and the degree of accuracy demanded by the operational needs of the system. Also to be considered are special requirements for tropicalization, rustproofing, shock-mounting, etc. Such factors are variable and difficult to take into account, but they should be considered as much as possible in determining the final design of the equipment.

8·9. Accuracy.—The accuracy of a servo system may be defined by the maximum permissible steady-state and transient errors. Depending on the particular needs of radar sets, the accuracy required of their servo systems may vary from a few mils to several degrees. For airborne stabilization equipments (*cf.* Chap. 7), accuracy to better than 1° or 2° is seldom necessary. Fire-control servo systems, on the other hand, must be far more accurate, whether they are low-power computer servo systems or high-power gun-mount drives. Under some conditions permissible static errors may be much larger than permissible dynamic errors; in other circumstances the reverse may be true.

The problem of the design of a servo system is greatly simplified if the system need not have high accuracy. In a low-accuracy servo system with tolerances of 1° or more, far less effort need be expended in refinements such as precision gearing, antihunt devices, etc., than in a

TABLE 8·1.—SERVOMECHANISMS FOR AIRBORNE SYSTEMS

System	Type	Accuracy, degrees	Weight of controller, lb	Estimated total weight of the servo system, lb
Experimental	Continuous control	±1 to 2½	.....	50
AN/APA-15	Continuous control (a-c)	±0.5 to 1.0	6	15 (excludes gyro rotor and gimbals)
GEI roll-stabilized scanner	Continuous control (d-c)	±0.25	19	45 (excludes gyro rotor and gimbals)
NOSMO (AN/APS-15)	Contactor (d-c)	±0.25	11.5	15 (uses motor already on scanner)
AN/APG-1	Continuous control (d-c)	±0.15	65, 2 channels (includes amplifier and 2 Amplidynes)	75–80
AN/APG-14	Contactor (d-c)	±4.0	8 (2 channels) (not a production model)	20

servo system of high accuracy. Where accuracy requirements are low, contactor (on-off) servo systems and potentiometer data-transmission systems may often be used to advantage because of their saving in weight and size, although they may also be used to obtain high accuracy.

In considering the accuracy of a servo system, care must be taken to allow for errors that arise from sources such as the input member and the data-transmission systems. Generally, as the requirements for accuracy of a servo system are relaxed, the design may be simplified and the equipment made lighter and less cumbersome. The accuracies actually realized in the servomechanisms of some airborne scanners are listed in Table 8·1. The first three systems are for antenna stabilization; the fourth enables the operator to train an antenna at will; and the last two can be used in airborne fire-control systems.

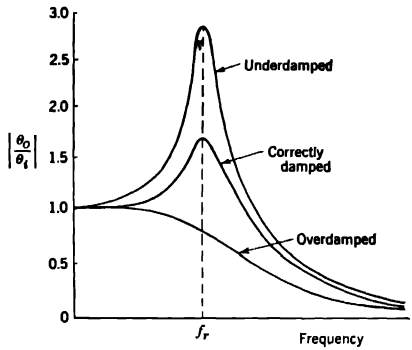

FIG. 8·5.—Response of a servo system to a sinusoidal input.

8·10. Speed.—Usually, there is no way of strictly specifying the input and output velocities of a servomechanism. These quantities vary from one application to another and even within a single application may cover a wide range of values, although from a knowledge of the proposed uses of the radar the maximum speed may often be specified. For example, a servo system for roll-stabilizing an airborne scanner need never move the scanner faster than the maximum rate of roll of the aircraft, which may be determined from flight and aerodynamic data. A B-17, for example, rarely rolls faster than 10°/sec in a coordinated turn. The servo system, therefore, need not be designed to operate at higher speeds. Knowledge of the average and maximum speeds required directly aids in determining the choice of the motor and gear train for a particular servomechanism.

It is possible to correlate the speed of response of a servo system (as distinguished from its speed) with its frequency characteristics. That is, if the input member is oscillated at constant amplitude (the amplitude

being small enough to avoid saturation effects that may be produced in the controller) and the absolute value of the ratio of output amplitude to input amplitude is plotted as a function of frequency, a curve similar to one of those in Fig. 8·5 is obtained.

Unless the servo system is overdamped, a peak will be observed at some frequency f_r. When the peak is present, f_r is the resonant frequency of the servo system, usually in the range of 1 to 10 cps.

If a servo system is to have a high speed of response and small dynamic errors at large velocities, the resonant frequency must be as high as possible. The peak value of the ratio of amplitudes should not be higher than 2. This is an empirical result based upon the observation that higher peaks are usually associated with underdamped or unstable servo systems. It is extremely important that servo members be sufficiently rigid so that they cannot vibrate naturally at the resonant frequency of the servo system.

REPRESENTATIVE SCANNER SERVOMECHANISMS

8·11. Ship and Ground Applications.—The control mechanisms for radar scanners discussed in the following pages have been selected as representative of the principal types now in wide use by the United States Army and Navy. They are classified into four groups that correspond roughly to the degree of complexity of the design problem; the tabulations present the important factors of design and performance. All figures for inertias and torques are referred to the servomotor shaft, and inertia values include those of the servomotors. Motor torques are computed on the basis of rated horsepower and rated speed. Acceleration values are given for rated torque applied to the inertia of the system. Values given for acceleration are related to the axis of the scanner, since this figure is of more immediate interest than the acceleration of the motor.

Continuous-scan Type.—As previously mentioned, control of a radar having a fixed, predetermined pattern of scan is normally accomplished by the use of an open-cycle control mechanism. Representative of this type is a land-based microwave early warning set having a 10- by 25-ft reflector, described in Sec. 3·3. Its chief functions are air search and ground control of aircraft, in the performance of which it is normally required to rotate continuously in azimuth at speeds up to 4 rpm. In the preproduction models the scanner was driven by a 5-hp separately excited d-c motor. A motor generator supplied d-c power to the drive-motor armature, and speed of scan was controlled over a range of 0 to 4 rpm by adjustment of the field current of the generator. Production models use a three-phase induction motor with a pole-switching arrangement to give synchronous speeds of 450, 900, and 1800 rpm or speeds of

scan of 1, 2, and 4 rpm. The motor rating is $\frac{3}{4}$, $1\frac{1}{2}$, and 3 hp at the respective speeds.

Manual-control Type.—The principal requirements for manually controlled scanner servomechanisms are usually a very low static error and a quickly damped response to positioning orders. Ordinarily, the amplitude of transient errors and steady-state following errors is of secondary importance. This follows from the method by which precise information is obtained with such radar sets. The angular position of the scanner is adjusted manually until an indicator device shows that the principal antenna axis is precisely on the target. While the scanner is staionary, the angular coordinates are then read from dials connected to the control handwheel. The scanner may be driven through a continuous search pattern most of the time, but accurate information is not required under this condition.

In this category, SCR-615 may be cited. This set was developed specifically as a ground control of interception, GCI, radar and furnished precise information as to bearing, range, and height. Its operation was as described in the preceding paragraph. The azimuth and elevation axes were controlled by identical servomechanisms utilizing two-phase induction motors and controller circuits of the type shown in Fig. 8·2.

TABLE 8·2.—SERVOMECHANISM FOR SCR-615

Motors	$\frac{1}{6}$-hp 2-phase 360-volt 1600-rpm
Gear ratios	250/1 in azimuth, 400/1 in elevation
Inertias	12 in.²-lb in azimuth, 10 in.²-lb in elevation
Motor torque	7 in.-lb
Viscous friction	$\frac{1}{4}$ in.-lb/rad per sec
Maximum acceleration	0.9 rad/sec² in azimuth, 0.6 rad/sec² in elevation
Equalization	Derivative network and tachometer feedback
Static accuracy	±0.03° in azimuth, ±0.01° in elevation
Data transmission	1- and 33-speed synchros

The service record of this control mechanism was unsatisfactory. The performance was unpredictable, possibly because of aging effects in the control thyratrons. Frequent breakdowns were caused by overheating of the motors to the point where cracks occurred in the rotor and rings. The worm gearing was also a source of trouble and required frequent replacement. Production models in the SCR-615 series did not use this servomechanism.

Shipborne Stabilized Scanners.—In order to obtain precise angular information about a target, referred to fixed coordinates from a shipborne radar, it is necessary to compensate in some way for the rolling and pitching of the ship and for changes in its heading. The various methods of computing stabilization of ship antennas and their specific applications are covered in Chap. 4 of this book.

It will be seen that in this type of antenna mount the dynamic errors of the servomechanisms are just as important as the static errors, since rotation of the axes of the pedestal will be required a large part of the time even though the radar beam is kept stationary in space.

One of the first stabilized antenna mounts put in service was CXBL, designed by the Radiation Laboratory as a prototype for the Navy SM radar. The salient features of the hydraulic servomechanisms used in this pedestal are covered in Table 8·3.

TABLE 8·3.—SERVOMECHANISM FOR CXBL

Drive motors	1½-hp 3-phase
Pump	Variable displacement
Servomotor	Constant displacement, 2000 rpm
Torque limit*	120 in.-lb
Gear ratio	252/1 in train
Inertia	11 in.²-lb in train
Maximum acceleration	16.7 rad/sec² in train
Viscous friction coefficient	28.9 in.-lb/rad per sec
Wind torque	48 in.-lb
Velocity error constant	240°/sec per degree
Equalization	Derivative and integral network

* Relief valve setting.

To determine the effect of wind torques on their performance, the servomechanisms were tested with a coulomb-friction torque of 48 in.-lb. With a sine-wave input of 15° amplitude and 9-sec period, the effect of the frictional load was to increase the maximum error from 3.5′ to 4′. With a 20°/sec constant velocity input, the error was increased from 5′ to 5.75′ by addition of the frictional load.

The servomechanisms for a newer experimental radar presented a problem in design similar to that of CXBL. In this case the final design

TABLE 8·4.—SERVOMECHANISM FOR EXPERIMENTAL RADAR

Motors	3450-rpm separately excited d-c 1½-hp in train, 3450-rpm separately excited d-c ¾-hp in elevation and cross level
Gear ratios	600/1 in train, 1736/1 in elevation and cross level
Inertias	39 in.²-lb in train, 13 in.²-lb in elevation and cross level
Rated torques	27.6 in.-lb in train, 13.8 in.-lb in elevation and cross level
Maximum acceleration	0.45 rad/sec² in train, 0.24 rad/sec² in elevation and cross level
Windage and unbalance torque	48 in.-lb in train, 8.9 in.-lb in elevation and cross level
Equalization	Motor voltage feedback
Data transmission	Synchros: 1- and 36-speed in train, 2- and 36-speed in elevation and cross level
Performance	5′ error for sine-wave inputs of 10° amplitude and 10-sec period

utilized Amplidyne-controlled electric motors in place of a hydraulic system. Some of the values given in Table 8·4 are preliminary estimates used in original computation and are subject to considerable error.

Because of the high computed value of wind torque and unbalance, the train servomechanism was originally designed to use two $1\frac{1}{2}$-hp motors. The systems, however, were originally assembled with only one motor and have operated without overloading in winds up to 40 knots.

Fire-control Scanners.—The precision of performance demanded of servomechanisms for fire-control radars is higher than it is of those previously described. The system in the following tabulation represents an advanced development in automatic tracking.

TABLE 8·5.—SERVOMECHANISM FOR THE SCR-584

Motors*	3600-rpm d-c separately excited, $\frac{1}{2}$-hp
Controller	Amplidyne
Gear ratios	480/1 in train, 1000/1 in elevation
Inertias	21 in.²-lb in train, 13 in.²-lb in elevation
Rated torques	8.7 in.-lb
Maximum accelerations	0.33 rad/sec² in train, 0.26 rad/sec² in elevation
Coefficient of the viscous friction	0.15 in.-lb/rad per sec
Velocity error constant	150°/sec per degree
Data transmission	Automatic target-tracking
Equalization	Motor voltage feedback

* *Cf.* Sec. 3·13.

8·12. Airborne Applications.—The following discussion emphasizes the design considerations peculiar to the scanner control mechanism for an airborne radar system. The particular examples cited are broadly representative of types now in common use.

Sector Scanning.—Sector scanning presents a control problem that can sometimes be solved by the use of a servo system. The problem is to control one or more of the scan variables, which are amplitude, position of the center of the scan, and frequency.

A bell crank or similar mechanism can be used with a continuously rotating azimuth motor to provide a sector scan. This method commonly affords a choice of only one or two sector angles and no control over the center position of the scan.

Limit switches and cams can be mounted on the scanner to furnish greater flexibility in controlling the relays that determine the direction of rotation of the azimuth motor. With slightly more complex switching circuits, stepwise control of both the amplitude and the center position has been achieved.

A more flexible electronic control can, if necessary, afford continuous control of the amplitude and the center position of the scan. It may be a servo system, with a separately excited synchro in series with the control transformer. The synchro is rotated continuously by a small

motor, causing the input voltage to the servoamplifier to oscillate at the frequency of rotation and drive the azimuth motor back and forth. The amplitude of the scan is a function of the excitation voltage of the synchro. The center position of the scan is determined by the alignment of the original synchros of the servo system.

A simpler electronic control can be made if a *CT* synchro, whose voltage output controls the bias of a vacuum tube that operates latching relays, is geared to the azimuth axis. Each time the synchro voltage reaches a critical value, the motor reverses. This synchro is used in conjunction with a differential synchro on the operator's control panel, thereby permitting adjustment of the center of scan. A switch allows sector scans of either 60° or 150°.

D-c Continuous-control Type.—The continuous-control servomechanism used in the experimental roll-stabilized airborne scanner mentioned in Sec. 7·9 was designed for higher accuracy than has proved to be essential. It is unnecessarily heavy but will serve as a good example of a system of this type.

The roll stabilization is accomplished by mounting the r-f head, azimuth gear box, and antenna on a section of circular track that is fastened to the aircraft structure. The unit is driven along the track, until it is in the true vertical position, by the servomotor that receives input information from a stable-vertical gyro (made by Pioneer Instrument Company). An Autosyn on the gyro acts as a roll-data take-off, and another Autosyn mounted at one-speed on the servo gear box of the scanner is the control transformer. These Autosyns (also built by the Pioneer Instrument Company, No. Ay-100D) have a sensitivity of about 0.3 volt (400 cps) per degree of error. The error signal is fed into an amplifier that controls an Oster ES-1-1 $\frac{1}{20}$-hp d-c split-field motor. The split field enables direct control of the motor from the vacuum-tube power amplifiers and thus eliminates the need for either contactors or an Amplidyne. Figure 8·6 is a block diagram of the servo loop.

The maximum operating velocity expected of this servo system is about 10°/sec. The use of the Oster motor, with its maximum speed of about 6000 rpm, dictates a gear ratio of 3600/1 from the motor to the scanner. The inertia of the scanner and r-f head when referred to the motor shaft is negligible compared with the inertia of the armature of the motor, which is approximately 4.0 in.^{2}-oz.

From considerations of the inertia of the system and the torques acting on the system as a result of gravity and centrifugal force, it can be seen that the maximum load torque that the motor must overcome is approximately 8.5 in.-oz at the motor shaft. The constant of the motor is about 0.5 in.-oz/ma of field difference current; hence, to obtain a static accuracy of 0.25°, an amplifier gain of 68 ma per degree of error is required.

The amplifier gain is actually 125 ma per degree, and the predicted accuracy is therefore 0.14°. The actual static errors, however, are higher because of coulomb friction and inaccuracies of the synchro.

The amplifier input is the 400-cps error signal from the synchros. This is applied to an a-c amplifier and cathode follower, having an over-all voltage gain of 4. The output of the cathode follower is then applied through a step-up transformer to a triode phase-sensitive detector. The output from the detector is smoothed by an *RC*-filter that has a time constant purposely kept low to avoid lags. The over-all gain of the a-c

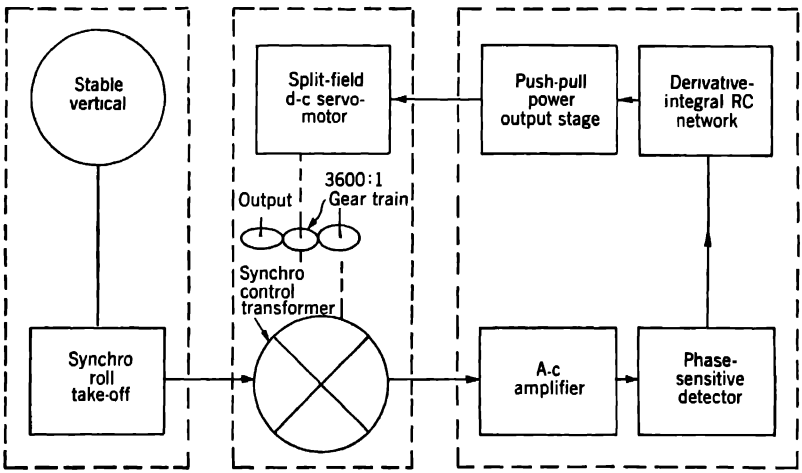

FIG. 8·6.—Block diagram of the servo loop of the GEI roll-stabilized scanner.

amplifier and detector is 400 volts direct current per degree of error in its linear region.

The voltage is then used as the input to an integral-derivative equalizing network for improved transient response, and the output from the network is impressed on the grids of the push-pull power-output tubes. The motor fields are the plate-load resistances of these tubes; the field currents are unbalanced when there is an error signal coming into the amplifier, and the polarity and magnitude of this unbalance are such that they tend to drive the system to zero error. The resistance of each field is approximately 1500 ohms, and the balance current at zero signal is approximately 40 ma.

A-c Continuous-control Type.—Because two-phase a-c induction motors can be made with low-inertia rotors, they have become popular for servomotor use. They are generally small, however, and in airborne practice have been used most commonly for instrument and low-power

work. Recent designs have produced good a-c antihunt circuits, overcoming most of the difficulties previously experienced.

A light a-c scanner servomechanism of the continuous-control type was developed as an attachment (AN/APA-15) for AN/APS-15 and AN/APS-2 for the purpose of obtaining line-of-sight stabilization. In this system, the error signal is again obtained from synchros mounted on one axis of a vertical-gyro gimbal assembly.

The amplifier receives the error signal, amplifies it, and impresses it on a two-phase induction motor in a manner similar to that described in Sec. 8·5. In this system, however, hard tubes are used instead of thyratrons, and the supply voltage is applied in a different manner, one winding being constantly excited with a fixed voltage. The maximum amplifier gain is 1000, and the constant relating the output torque to the alignment error is about 25 in.-lb per degree of error at the output shaft.

The servoamplifier described in this section amplifies the error voltage caused by the misalignment between the gyro gimbals and the housing and applies it to one winding of a two-phase a-c induction motor. The other winding of this motor is constantly excited from one phase of the three-phase 400-cycle line. When the error signal is zero, the amplifier impresses no voltage across the first winding, and hence there is no torque on the motor. If the error is in one direction, the voltage on the variable winding is roughly proportional to the error and leads the phase of the voltage on the fixed winding by approximately 90°. If the error is in the other direction, the amplified voltage lags behind the fixed voltage by the same amount. The motor thus turns in the direction that reduces the error and actuates the torque arms, thereby positioning the antenna by means of a parallelogram linkage (see Figs. 7·2 and 7·9).

It is difficult to give quantitative estimates of the accuracy of this servo system, because a large part of the error of the system arises in the gyro and it is not easy to isolate gyro errors from servo errors. However, it is conservatively estimated that the system can position to an accuracy better than 0.5°.

Contactor (On-off) Type.—In radar engineering, although a contactor servomechanism is infrequently used for purposes of high accuracy at medium or high power, one was designed for use with the "Nosmo" attachment on the AN/APS-15 scanner (similar to that shown in Fig. 6·2) to fill the need for an accurate and stable servo system to provide for manual positioning in azimuth. In this application, relays are used to control the armature current of the standard AN/APS-15 scanner motor. Data transmission is obtained from a pair of synchros, one mounted on the scanner at the one-speed shaft, and the other in the operator's control box. The error signal is amplified and put through a phase-sensitive detector similar to the one used in the GEI scanner servoamplifier. It

then goes through integral-derivative networks and is impressed on the grids of a twin-triode voltage amplifier whose loads are the coils of two special relays.[1] The relays have make-and-break coil currents of approximately 5 or 6 ma and are therefore easily controlled by vacuum tubes. Their contacts are sealed in an inert gas, with a pool of mercury to keep them clean. Circuits are incorporated in the amplifier to "buzz" the relays (i.e., oscillate the relay leaf so as to eliminate friction and dead space in the relay and to give an average current in the motor roughly proportional to that of the error signal) and to protect the contacts against surges of the current in the motor.

The system is capable of positioning the AN/APS-15 scanner to within 0.25°. The amplifier weighs about 11.5 lb.

For contactor servo systems requiring less accuracy, the circuits may often be considerably simplified, and the relay coils made a part of the plate load of the phase-sensitive detector. An experimental system of this type was built to control the motions of a light scanner in azimuth and elevation. For this purpose low-power two-phase induction motors controlled by relays were used. The control circuits, including the relays, for both the azimuth and elevation drives were built into one amplifier chassis weighing 8 lb. The system positioned the scanner in either coordinate to within 4° and had a maximum follow-up speed of about 120°/sec.

Fire-control Servo Systems.—The scanner control systems of AN/APG-1 and AN/APG-2 are two similar systems employing almost idential servomechanisms. The AN/APG-1 radar[2] is an automatic gun-laying set designed for aircraft search. To enable blind firing, the antenna automatically tracks a selected target and feeds information about its range and direction to the gun computer.

The scanner of AN/APG-1 has three motors. One motor drives it in elevation about a horizontal axis; another drives it in azimuth about a vertical axis; and the third spins the feed in a conical scan. Thus the scanner can be made to point anywhere in space within the total limits of its motions in azimuth (170°) and elevation (80°).

The control box for the scanner contains three input circuits, allowing a choice of the functions of search, manual tracking, or automatic tracking.

Figure 8·7 is a block diagram of the control box. In any of the tracking functions, the error signal is introduced into the power amplifiers: in manual tracking, from synchros; and in automatic tracking, as a voltage from the signal audio amplifier. In automatic tracking, these error signals, one for elevation and one for azimuth, are put into phase-sensitive detectors. When the system is automatically tracking, the reference

[1] Relay No. D-168479, manufactured by Western Electric Company.

[2] *Handbook of Maintenance Instructions for Radio Set AN/APG-1*, Bell Telephone Laboratory Manuals 557, 558.

voltages for the detectors are obtained from a two-phase generator mounted on the shaft of the motor that spins the feed. The output of the detectors is then fed into push-pull power amplifiers that in turn excite the field windings of a pair of Amplidynes. The Amplidynes deliver power to the azimuth and elevation motors. Antihunt feedback voltage from the outputs of the Amplidynes is introduced to the screen

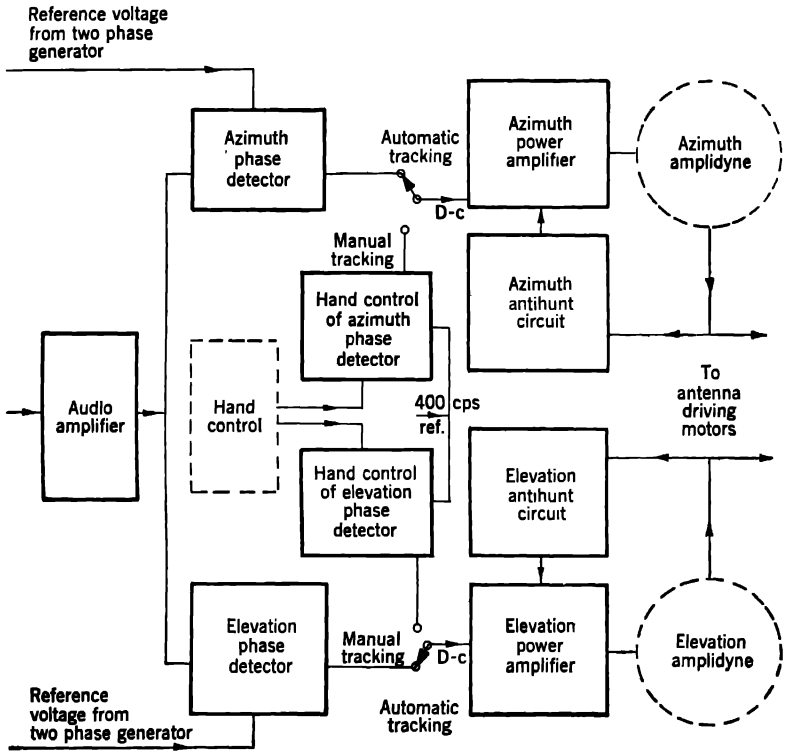

FIG. 8·7.—Block diagram of the AN/APG-1 scanner control box. (*Courtesy of Bell Telephone Laboratories.*)

grids of the power amplifiers through a d-c amplifier and an RC-network. The tracking accuracy is $\pm 0.15°$ in azimuth and in elevation.

The control box contains a total of 16 tubes for the two channels and weighs 30 lb. It is shock-mounted and easily removable for inspection. Including its mounting, it is 9 in. high, 23 in. long, and about 10.5 in. wide.

The two motor generators (Amplidynes), especially designed for aircraft use, are each 8 in. wide, 6 in. high, and $11\frac{3}{8}$ in. long and weigh 17.5 lb. Each can deliver about 150 watts to one of the drive motors.

PART II

RADOMES

CHAPTER 9

GENERAL SURVEY OF THE RADOME PROBLEM

By H. Leaderman[1]

The installation of a microwave radar scanner or beacon antenna in a ground location, on shipboard, or in an airplane involves not only mechanical but also electrical problems. Difficulty is sometimes experienced with an airborne radar antenna because aerodynamic requirements dictate that it be mounted close to the metal structure of the airplane. Such an antenna must be provided with a rigid housing to protect it from large aerodynamic loads and to avoid disturbance of the control of the airplane. A ground or shipborne antenna may also require a housing for protection against wind forces. When gridded or perforated reflectors are used with ground-based or shipborne radar sets, however, protection is usually not required.

These housings for microwave antennas are called *radomes* (radar domes). Since the wall thickness of a radome is of the same order of magnitude as the wavelength of the radiation involved, there is appreciable reflection and absorption of r-f energy by a radome. Its design must therefore comply with certain electrical requirements as well as with structural and mechanical ones. If the radome is for an airborne antenna, aerodynamic considerations are important. It is the aim of this second part of the book to present and discuss all of the principal factors that enter into the design of radomes. The remainder of this chapter treats the general problem; Chaps. 10, 11, and 12 are devoted to further development of the electrical considerations; Chap. 13 discusses the mechanical, thermal, and electrical properties of the materials most useful for radomes and gives some information about fabrication and testing; Chap. 14 discusses different actual radomes in the light of the principles developed in the preceding chapters. More emphasis is put on the electrical aspects[2] of the problem than on the others, not because these are more important but because there is no readily available treatment of this part of the subject. The aerodynamic aspects are touched on only briefly because they are part of a much larger subject that is beyond the scope of this work.

[1] This chapter includes some material on pulling of magnetrons written by W. Ellis and illustrative material supplied by E. B. McMillan.

[2] For a summary of the electrical aspects, see R. M. Redheffer, "An Outline of the Electrical Properties of Radomes," RL Report No. 483-2, December 1943.

9·1. Types of Installation.—The nature of an antenna installation and the design of a radome depend in general upon the intended use of the radar. A radome for a ground or ship radar installation may often be a cylindrical shell of dielectric material, as shown in Fig. 9·1. Other radomes for such use are shown in Figs. 9·2, 9·3, and 9·4. When gridded or perforated reflector structures are ground-based or shipborne, however,

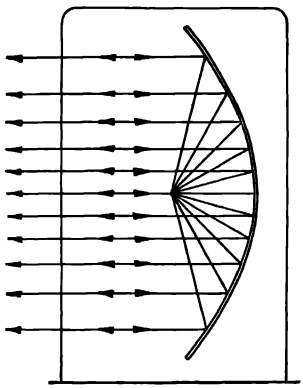

FIG. 9·1.—Cylindrical wall radome.

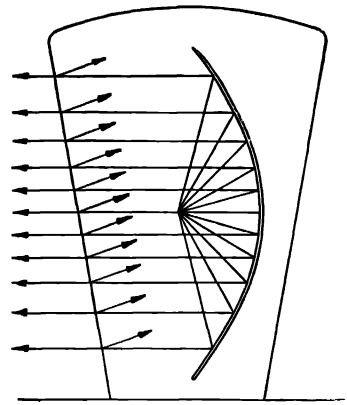

FIG. 9·2.—Conical wall radome.

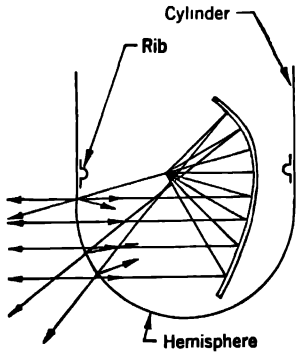

FIG. 9·3.—Cylindrical-hemispherical radome.

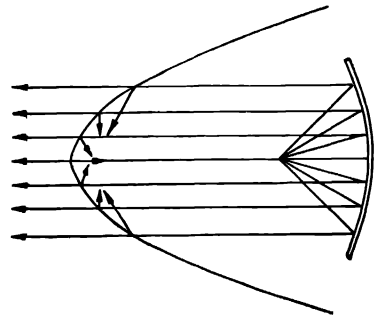

FIG. 9·4.—Nose-type radome.

they do not usually require the protection of a radome. In this and the succeeding chapters, therefore, the principal topic will be radomes intended for airborne use. Because the design of airborne radomes cannot be intelligently discussed without considering the installation of antennas in airplanes, this problem will also be considered.

Figure 9·5 is a composite illustration of some possibilities for airborne antenna installations. The antenna at *A* is an installation of the "nose" type and has forward vision, with limited vertical and horizontal scan.

The "tail" installation at B permits rearward vision for the antenna. The installation shown at C has possibility of a 360° scan, with the extent of vision below the horizontal depending upon the geometry of both the installation and the airplane. Installations shown at D and E are used in conjunction with a cosecant-squared antenna when uniform illumination of the ground is required. For such an antenna, permanent

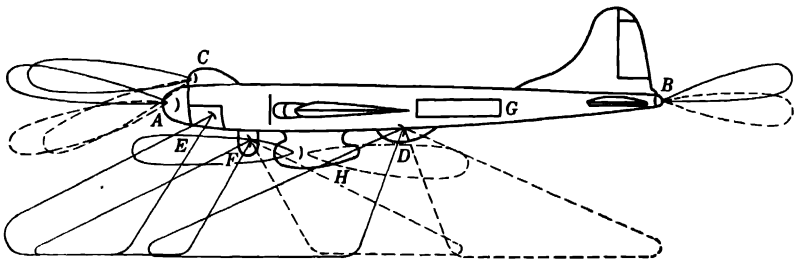

FIG. 9·5. - Possible installations of radar scanners on a fuselage.

partial retraction within the contour line of the airplane is possible. With the installation shown at D, 360° vision is possible. The installation shown at E, like that at A, is such that the radome need not project beyond the skin line of the airplane, thereby eliminating additional wind resistance. This type of installation is usually restricted to 180° vision (or less) in the forward direction and imposes certain restrictions on the design of the antenna, radome, and airplane. The installation shown at

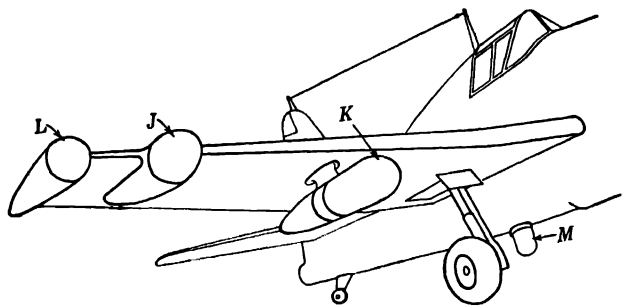

FIG. 9·6.—Possible installations of radar scanners on a small airplane.

F is capable of 360° vision of either ground or airborne targets; however, it causes a large additional drag. Represented at G is a linear array that is arranged along the side of the fuselage for giving lateral vision by electrical scan.

The beamwidth of an antenna in the azimuthal plane depends upon the horizontal aperture of the scanner; when the width of the fuselage is insufficient to accommodate a reflector having the necessary aperture,

the scanner may be mounted beneath the airplane fuselage in a streamlined bulge, as at H. If only limited sector scan in the forward direction is required, an electrically scanning linear array may be mounted beneath the fuselage in a streamlined vane as in the Eagle (AN/APQ-7) system. The leading edge of the vane thus forms the radome (*cf.* Sec. 6·14).

The possibilities for antenna installation in an airplane wing are shown in Fig. 9·6.

The installation shown at J in Fig. 9·6 is housed in a nacelle faired into the wings, whereas at K the scanner is carried in a separate streamlined housing. For both installations, the forward portion of the housing forms the radome. Aerodynamically, the wing-tip installation shown at L is preferable to those shown at J and K. Linear-array microwave beacon antennas are usually mounted beneath the wing or fuselage as shown at M. Such antennas require housings that may be regarded as miniature radomes (Sec. 6·3).

9·2. Electrical Requirements.—The chief electrical factors that affect the antenna installation and the design of the radome are reflection of r-f energy from the internal and external surfaces of the airplane and from the radome wall; diffraction effects due to discontinuities in the r-f field, such as ribs in the radome; and absorption of r-f energy by the radome wall and by material purposely inserted for absorption of stray r-f energy.[1] Discontinuities and reflections may cause distortion of the antenna pattern and variation of the magnetron frequency that will change as the scanner rotates. Reflection and absorption by the radome wall must be kept to the lowest possible values in order to avoid loss of transmitted power that would lead to a reduction in the range of the radar set.

The effects of reflection by the radome on the performance of a radar set should first be considered. The most obvious one is the loss in range that results from a reduction of the radiated power and also of the strength of the received echo. Even though the material of a radome may absorb very little energy, the radome may reflect as much as 20 per cent of the incident power. The range on a given target would then be reduced to 89 per cent of what it would be without the radome.

Reflection of energy by the radome may be small enough to be unimportant so far as range is concerned but still large enough to have other serious consequences. Reflection of energy by the radome usually results in the presence of reflected power and standing waves in the r-f transmission line of the system. This would be most serious if a flat sheet were to be placed perpendicular to the axis of a paraboloid. The effective reflection is somewhat less when a concave sheet of the same construction

[1] R. M. Redheffer, "Radomes and System Performance," RL Report No. 483-6, November 1944.

is used instead of a flat one. If the sheet is tilted with respect to the axis of the paraboloid, the reflection into the line is much reduced. In installations such as at A and C in Fig. 9·5, the reflection into the line would consequently be expected to vary widely with antenna scan. In installations such as D, most of the radiation makes such a large angle of incidence with the radome wall that the reflection of energy into the line is usually small.

Reflection of energy into the transmission line changes the magnetron frequency; this phenomenon is known as "pulling." If the local oscillator is tuned to a fixed frequency, the beat frequency will be varied by the reflection into the line. If this variation exceeds the bandwidth of the i-f amplifier, no received signals will be amplified; hence, the regions producing excessive reflection during the scan yield blank sectors in the screen when the type of presentation used is PPI. The results of such pulling caused by a radome are shown in Fig. 9·7. Illustration (a) shows the PPI presentation of a radar set with no radome, situated on the roof of a laboratory for test. When the radome that was originally designed for an airborne installation was used, (b) was obtained; the disappearance of signals in some sectors is marked. The presentation when a newer double-walled radome was used is shown at (c); the lost signals are recovered. The radar was an early airborne 10-cm set, ASG (AN/APS-2), that did not include automatic frequency control, AFC. The original radome had a single wall that was later found to reflect 4.5 per cent of the incident power. A cylindrical shape had been used in an attempt to keep the distance uniform from the scanner to the wall of the radome, but it was found impracticable to control the centering of the scanner with sufficient accuracy to keep the distance adequately uniform. Both radomes are described in Sec. 14·4.

A streamlined radome was designed for the same radar set for installation in a different airplane. Figure 9·8 shows the effect of this radome on the performance. The simulated direction of flight is to the left. With no radome, the pattern of echoes was as shown in (a). When the radome was used, pattern (b) was obtained. Targets have disappeared in at least two sectors on each side of the forward direction. Pattern (c) was obtained after the radome had been modified to have a reflectionless double wall in the forward direction. The original radome and its modification are described in Sec. 14.5.

As previously noted, reflections from a radome into the transmitting line are significant only when the transmitted wave is incident nearly normally upon the radome wall. Hence, the following discussion is of importance primarily in connection with normal-incidence radomes. Pulling resulting from reflections into the line is dependent upon the magnitude (voltage standing-wave ratio) and position (phase) of the

is used instead of a flat one. If the sheet is tilted with respect to the axis of the paraboloid, the reflection into the line is much reduced. In installations such as at A and C in Fig. 9·5, the reflection into the line would consequently be expected to vary widely with antenna scan. In installations such as D, most of the radiation makes such a large angle of incidence with the radome wall that the reflection of energy into the line is usually small.

Reflection of energy into the transmission line changes the magnetron frequency; this phenomenon is known as "pulling." If the local oscillator is tuned to a fixed frequency, the beat frequency will be varied by the reflection into the line. If this variation exceeds the bandwidth of the i-f amplifier, no received signals will be amplified; hence, the regions producing excessive reflection during the scan yield blank sectors in the screen when the type of presentation used is PPI. The results of such pulling caused by a radome are shown in Fig. 9·7. Illustration (a) shows the PPI presentation of a radar set with no radome, situated on the roof of a laboratory for test. When the radome that was originally designed for an airborne installation was used, (b) was obtained; the disappearance of signals in some sectors is marked. The presentation when a newer double-walled radome was used is shown at (c); the lost signals are recovered. The radar was an early airborne 10-cm set, ASG (AN/APS-2), that did not include automatic frequency control, AFC. The original radome had a single wall that was later found to reflect 4.5 per cent of the incident power. A cylindrical shape had been used in an attempt to keep the distance uniform from the scanner to the wall of the radome, but it was found impracticable to control the centering of the scanner with sufficient accuracy to keep the distance adequately uniform. Both radomes are described in Sec. 14·4.

A streamlined radome was designed for the same radar set for installation in a different airplane. Figure 9·8 shows the effect of this radome on the performance. The simulated direction of flight is to the left. With no radome, the pattern of echoes was as shown in (a). When the radome was used, pattern (b) was obtained. Targets have disappeared in at least two sectors on each side of the forward direction. Pattern (c) was obtained after the radome had been modified to have a reflectionless double wall in the forward direction. The original radome and its modification are described in Sec. 14.5.

As previously noted, reflections from a radome into the transmitting line are significant only when the transmitted wave is incident nearly normally upon the radome wall. Hence, the following discussion is of importance primarily in connection with normal-incidence radomes. Pulling resulting from reflections into the line is dependent upon the magnitude (voltage standing-wave ratio) and position (phase) of the

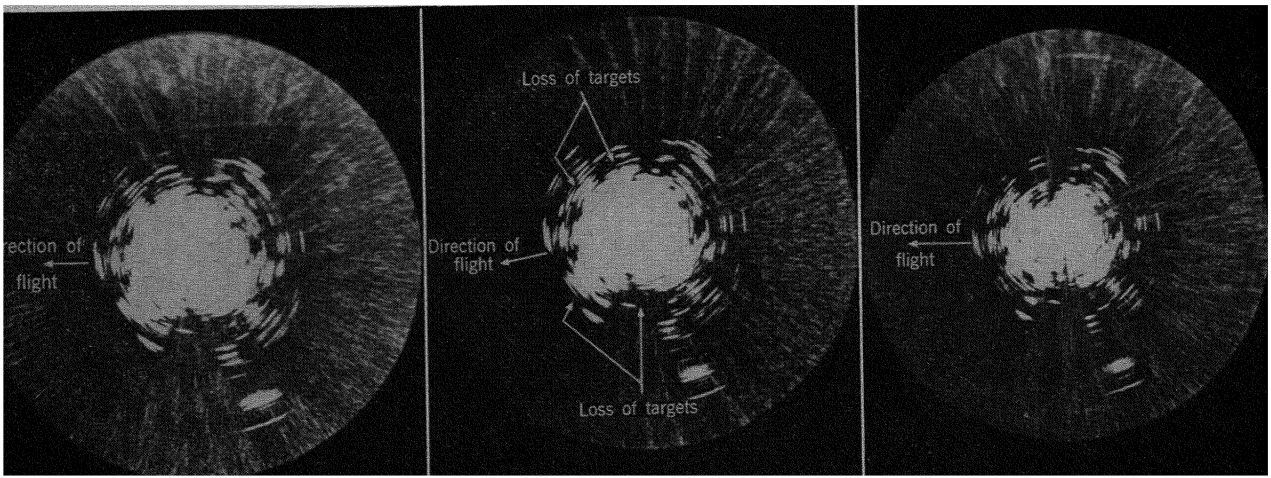

(*a*) Without radome. (*b*) With single-walled streamlined radome. (*c*) With streamlined radome having double wall over forward half.

FIG. 9·8.—Loss of signals resulting from pulling. AN/APS-2 radar. (*Courtesy of Bureau of Aeronautics, U.S. Navy.*)

standing waves. Change of phase is important as well as change of magnitude. Cases have been observed[1] in which a high reflection $(VSWR)^2 = 9$ that was fairly constant in magnitude and phase produced a nearly constant pulling of only about $\frac{1}{2}$ Mc, whereas in other cases, a reflection of maximum value $(VSWR)^2 = 1.2$, but with varying phase, produced pulling of about 4 Mc; the latter case is more nearly typical.

In order to evaluate the pulling caused by a given radome or to estimate that which may reasonably be expected to be caused by a proposed radome, it is necessary to study the pulling characteristics of the transmitting source used in the system. Standard methods of making such studies for magnetrons are given in Sec.1·9 of *Microwave Magnetrons* and Sec. 2·11 of *Microwave Transmission Circuits*, Vols. 6 and 9 respec-

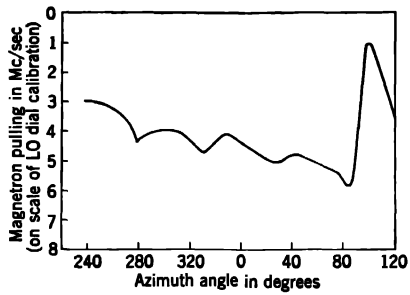

FIG. 9·9.—Dependence of magnetron pulling on position of the scanner.

tively, of the Radiation Laboratory Series where the Rieke diagram, Smith chart, and pulling figure are discussed in detail.

To plot the pulling attributable to a radome in an actual installation, measurement can be made by means of a wavemeter or otherwise of the frequency of the transmitter for various orientations of the antenna with respect to the system. A typical curve obtained by this procedure is shown in Fig. 9·9. Since, in operation of a system, scanner position is a function of time, an experimental curve of pulling vs. time should be drawn for the entire scan.

The pulling that may be caused by a proposed radome can be estimated by proceeding as suggested, using properly fabricated radome samples of appropriate size and shape and correctly located so as to simulate the pertinent sections of the radome. A more sophisticated procedure has been described by Redheffer, *loc. cit.* It involves the Rieke diagram and the pulling figure of the magnetron but replaces the magnetron by a low-power continuous-wave transmitter and the frequency-measuring equipment by a device for measuring complex reflection.

[1] R. M. Redheffer, "Dependence of Magnetron Pulling on Radome Shape and Orientation," *RL Radome Bull.* 483-18.

Variation of the magnetron frequency, caused by radome reflection or otherwise, may be compensated by variation of the *LO*-frequency with AFC. However, the response of the AFC is not instantaneous; it involves a time constant. If the magnitude of the reflection changes very rapidly with time, as it does whenever an antenna scans over a radome rib, a large momentary reflection may be produced. When this occurs, the change in *LO*-frequency may be produced too late to compensate for the pulling but will persist after it has disappeared. The net result is equivalent to a prolongation of the frequency shift, so that system performance can actually be reduced by the use of AFC.

Power reflected from the radome can also cause an apparent shift in the angular position of targets that have not been obliterated. This effect[1] can cause angular errors as large as 2.5°, resulting from the variation of the transmitted frequency as the antenna scans. Since the arc representing the target on the PPI may be shortened at one end by sudden pulling, the resulting apparent shifting of the target can be studied by varying the beat frequency. It was found that errors of considerable magnitude occurred in practical systems. Further discussion of the effect of pulling and of its relation to apparent beam direction can be found in Sec. 17·8 of Vol. 12, *Microwave Antenna Theory and Design*, and in Radome Bulletin No. 18, "Dependence of Magnetron Pulling on Radome Shape and Orientation," RL Report No. 483-18, Mar. 1, 1946, by R. M. Redheffer. The important thing to do practically is to eliminate the causes of sudden changes of impedance.

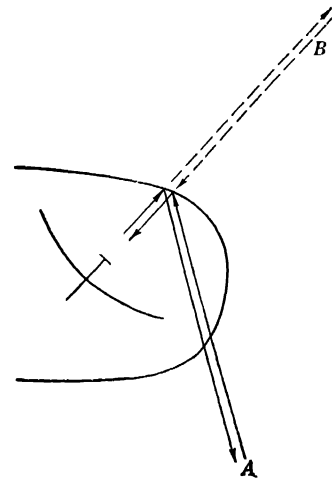

FIG. 9·10.— Reflection of energy from a radome. *A* is the actual target; *B* is the apparent target.

Shifting of the apparent bearing of targets can also result from reflection and focusing of an appreciable amount of power to a focus at a point about halfway between the center of curvature of the radome surface and the surface itself if the beam is thereby shifted off-axis. Extremely high reflected power has been encountered in radomes actually in service, as, for example, an early radome for the AN/APS-6 wing nacelle. The effect of this radome on the beam direction is not known. An effect of such refocusing in a spherical-ended radome was observed, however, with the AN/APS-4 radar.

[1] S. C. Hight, Bell Telephone Laboratories Report No. MM-44-170-12.

Serious distortions of the antenna pattern may arise as a result of reflection of r-f energy by the radome or by the skin of the airplane.

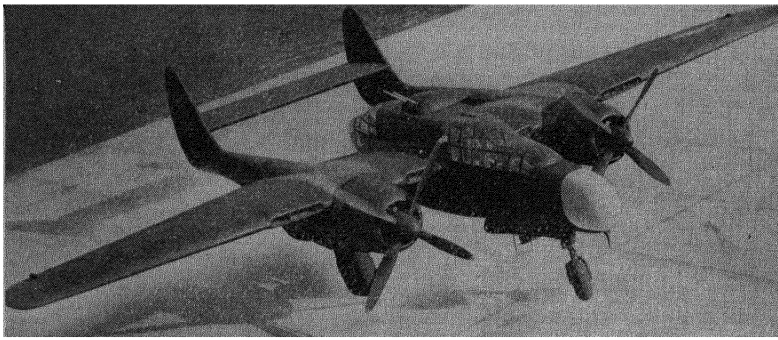

FIG. 9·11. P-61 airplane with nose radome.

The radome reflection may occur either from some portion of the wall or merely from a rib. Such reflections may cause the appearance of large side lobes with beams of the pencil type. Figure 9·10 shows how reflection from the radome can produce a strong side lobe, with the result that a target situated at A appears to be located at B. For example, in an airborne search radar, undesired reflections from the ground ("clutter"), as at A, can obscure desired signals from an airborne target B. This effect was found to be the cause of a serious obscuration of targets by echoes from the ground directly below the airplane in certain installations of the SCR-720 radar. This was a 10-cm airborne set designed for detection of other aircraft. Figure 9·11 shows a P-61 aircraft in which this radar was installed. The white portion of the nose is the radome. Figure 9·12 indicates the way in which metal shielding was installed to eliminate ground return that was supposed to come from side lobes of the antenna. The original radome had been

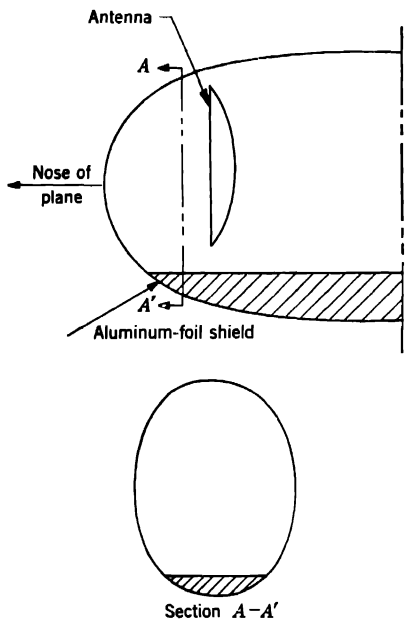

FIG. 9·12.—Shielding in the nose of the P-61.

made thick because of doubts about the strength of the plastic material. It was later found to reflect 8 per cent of the power at normal incidence. Analysis of the structure showed that the thickness could be reduced by one-third to reduce the reflection to 2.8 per cent without danger. The thinner radome was made and tested. Figure 9·13 shows the results of tests. Mere rotation of the plane of polarization by 90° to make it vertical helped considerably. Since the reflection is less for parallel polarized

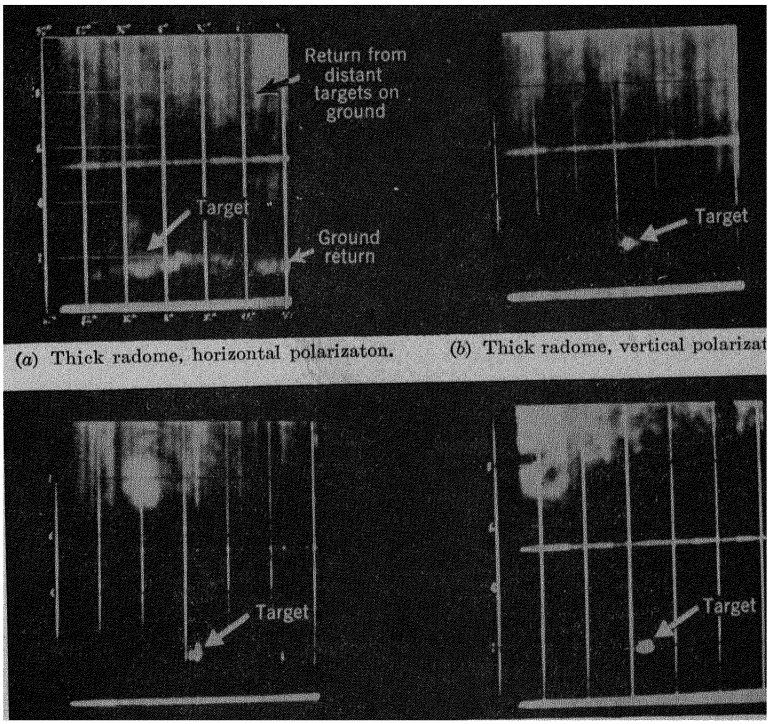

(*a*) Thick radome, horizontal polarizaton. (*b*) Thick radome, vertical polarizat

(*c*) Thin radome, horizontal polarization. (*d*) Thin radome, vertical polarization.

FIG. 9·13.—Ground return resulting from reflection in nose radome. Range vertical, azimuth horizontal.

radiation, there is less energy reflected toward the ground when the plane of polarization is vertical. Use of the thinner radome resulted in further improvement.

Any reflection of an appreciable amount of energy in the direction of the direct beam will result in interference between the two beams; closely spaced holes in the pattern can be produced by mutual cancellation. An example of how this can occur is shown in Fig. 9·14. Energy reflected from the skin of the airplane and from the radome, as at A, is parallel to

energy radiated directly from the antenna as at B. Another possibility involving reflection from only the skin of the airplane is shown in Fig. 9·15. Here, interference takes place between energy radiated along the path A and that first radiated along path B but then reflected from the skin of the airplane.

This effect is most pronounced with cosecant-squared antennas if a part of the energy from the intense part of the beam is reflected in the

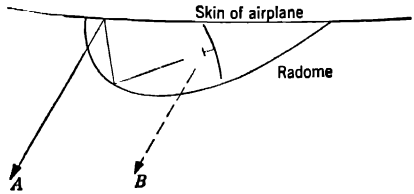

FIG. 9·14.—Reflection of energy from a radome and the skin of an airplane.

direction of the weaker portion. Figure 9·16*a* is a PPI picture that shows this effect. It was obtained with an AN/APQ-13 3-cm radar with the original 29-in. scanner in a B-29 airplane flying at 8000 ft above Fort Myers, Fla. The top of the picture is north, and the aircraft was headed east-southeast. The interference minima are most noticeable at steep angles of depression in the azimuths of the wings of the airplane. Figure 9·16*b* shows the same terrain viewed from 20,000 ft with an AN/APQ-13 radar equipped with the newer 60-in. antenna.

Reflection of energy from the radome thus not only causes reduction in range but may also cause further serious impairment of the performance of the radar set. Consequently, it must be minimized. Methods

FIG. 9·15.—Reflection from the skin of an airplane.

for doing this are discussed in detail in Chaps. 10 and 11. In the installation of an antenna care must also be taken to avoid strong reflection from any parts of the airplane. For any proposed installation the pattern of the antenna and radome in a mockup of the adjacent metal surfaces of the airplane should be studied carefully if there is a possibility of interference taking place. A detailed discussion of the procedure is given in Chap. 14.

A radome can have still other deleterious effects on the performance of a radar system. One is variation of the phase of the transmitted radiation over the radome, causing angular distortion of the beam;

another is diffraction by a rib or other discontinuity on the radome, resulting in distortion or interference. Since ribs may cause pattern distortion, pulling, or both, such ribs cannot be allowed in any portion of the radome where the r-f intensity is high at any time during the scan. This restriction makes it all the more difficult to achieve adequate structural strength.

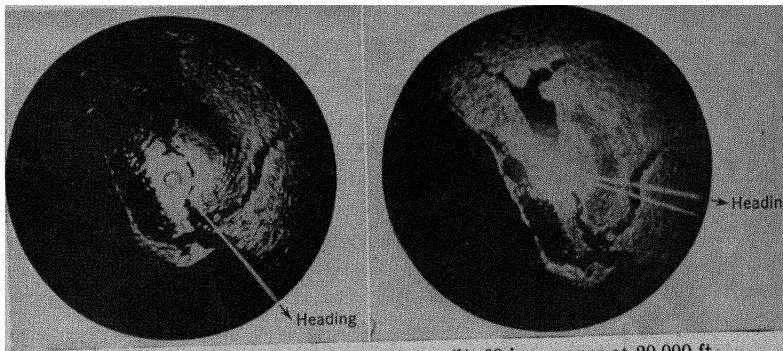

(*a*) 29-in. scanner at 8000 ft. (*b*) 60-in. scanner at 20,000 ft.

FIG. 9·16.—Interference effects with AN/APQ-13 radar over Fort Myers, Fla.

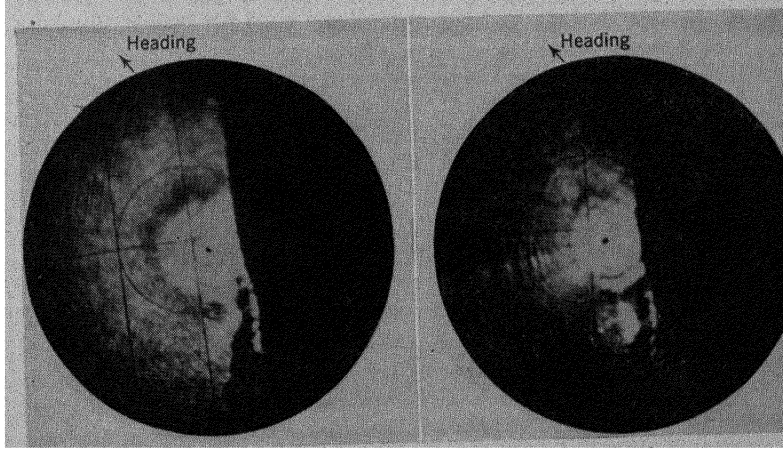

(*a*) Tilt −5°. (*b*) Tilt 0°.

FIG. 9·17.—Diffraction effects with AN/APQ-13 (60-in.) radar over Miami, Fla.

It is preferable from the aerodynamic viewpoint that an antenna installation such as *D* in Fig. 9·5 be retracted as much as possible within the contours of the fuselage. The amount of retraction, however, is limited by diffraction at the edge of the antenna cavity and by requirements for adequate radar vision. Figure 9·17 shows PPI pictures of Miami, Fla., taken from an aircraft at an altitude of 20,000 ft on a

northerly heading. The radar was AN/APQ-13 with the 60-in. antenna. In *a* the tilt was $-5°$ as in normal operation; in *b* it was 0°. With the tilt at 0° the radiation from the upper 4 in. of the reflector are intercepted by the fuselage of the airplane. The fore-and-aft range is reduced, and a dark band appears in the pattern below the center. These changes are attributable to the weakening and distortion of the pattern by the interception and diffraction of part of the beam. To the left are interference fringes similar to those of Fig. 9·16.

9·3. Mechanical Requirements.—For any given type of antenna installation, many radome designs that meet the electrical requirements are possible. These designs may differ considerably, however, in strength, stiffness, weight, ease of fabrication, and general serviceability. In general, when the mechanical requirements for strength and stiffness are minimal, as with cylindrical radomes for small linear-array beacon antennas, a relatively simple design will meet both electrical and mechanical requirements. When the mechanical specifications are severe, as for large radomes for scanning antennas in fast airplanes, it often becomes difficult to find a design that is satisfactory both mechanically and electrically. Under such circumstances, it may be necessary to relax the electrical specifications to some extent.

Strength.—Structural failure of the radome must not take place under the maximum anticipated aerodynamic or other loads. For an airborne radome the loads can be estimated fairly well and the adequacy of its structural strength can be determined by test. Some radomes that are strong enough to withstand aerodynamic loads may be fragile and require great care in handling. Because it may sometimes be necessary to remove the radome to check or adjust the antenna, it is important that the radome be sufficiently rugged to withstand reasonably rough handling.

In the event of a forced landing of an airplane on water ("ditching"), it is highly desirable that no radome failure take place, in order that buoyancy of the aircraft be maintained as long as possible. It can be seen that in installations like those at *E*, *D*, and *F* (Fig. 9·5) the radome is subject to direct impact whereas for an installation such as that at *A*, impact shock may cause failure in the radome shell or at the attachment points. The ditching load may be much larger than the aerodynamic load.

Finally, in some systems, it may be desirable to pressurize the radome instead of merely the r-f transmission line. Stresses due to the differential pressure between the inside and outside of the radome may then be greater than those due to the aerodynamic load and therefore dictate the strength requirement.

Stiffness.—We have seen that supporting ribs cannot be placed in any portion of the radome wall through which high r-f energy is to be transmitted, that is, in what may be called the "electrical portion" of the

radome. Minimization of the reflection of energy from the radome imposes upon the design of the radome wall certain restrictions that may necessitate a thin wall over a large unstabilized area. Under such circumstances, elastic instability may occur either locally ("oil-canning") or throughout the entire radome. Even if elastic instability should not occur, the deflections of the radome under maximum aerodynamic load may be such as to interfere with the scanning motion of the scanner; hence, stiffness, as well as strength, of radomes and radome materials is important.

Heat and Cold Resistance.—Many materials useful for radome construction have limited resistance to heat. Radomes fabricated of these materials may be adequate in some installations, as, for instance, under the center section of the fuselage, where the radome is well protected by the fuselage and wings from direct sunlight. On the other hand, if such a radome is mounted in the nose position, the direct rays of the sun may cause thermal collapse, especially if the radome is painted a dark gray or black. These radomes are also subject to failure if stored under poor conditions without free circulation of air.

Some materials that are tough at moderate temperatures become extremely brittle at low temperatures. Their use should be avoided if extremely low temperatures are anticipated in service.

To summarize, the selection of a radome material must be based on service requirements; extremes of temperature may rule out many materials that are otherwise satisfactory.

Absorption of Water Vapor and Water.—When exposed to air at a high temperature and high relative humidity many plastic materials absorb appreciable amounts of water. Absorption of this kind, which occurs, for example, under tropical conditions, results in an increase in both the dielectric constant and loss tangent of the material. Such changes in electrical properties of the material in a radome are generally undesirable. In regions where high absolute humidity occurs for a relatively brief period of the year, the entry of moisture into a radome containing hygroscopic material (cotton, for example) can be appreciably retarded by a suitable protective coating. Such protection is likely to be merely temporary, however, and inadequate where high absolute humidity occurs for extended periods.

It is possible for plastic materials, even though nonhygroscopic, to absorb water on immersion; this may occur if they are porous or cellular or contain voids or capillary paths. Consequently, radomes containing such materials are likely to absorb water when exposed to rain and therefore should have a suitable protective coating.

Abrasion.—Abrasion of radome materials can occur when dust and stones are thrown up from gravel and coral runways by propellers and

nose wheels or when hail and water droplets in the atmosphere pelt against the plane. To allow for such abrasion it may be necessary to have a radome structure that is heavier than would otherwise be required or one that is provided with an abrasion-resistant coating; both solutions may be undesirable electrically.

9·4. Normal-incidence Radomes.—Electrically, a radome is an obstacle of dielectric material in front of the antenna, of arbitrary shape and wall section. Predictions as to its influence on the pattern and gain of the antenna are generally impossible. It is therefore necessary to resort to an approximation that will usually be adequate for most problems. If the validity of geometrical optics is assumed, rays may be traced from the center of the antenna feed to the reflector dish where they are specularly reflected and then to the radome. Since in most radomes the radius of curvature is large compared with the wavelength, it may be assumed that each small element of the radome area is independent of the adjacent areas. This is justifiable when the properties of the radome do not change too rapidly from point to point and ribs and other discontinuities are absent.

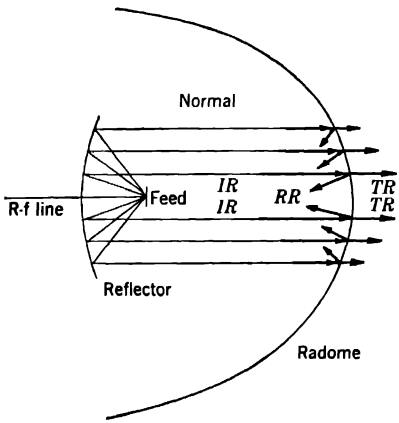

FIG. 9·18.—Normal incidence radome. *IR*, incident rays; *RR*, reflected rays; *TR*, transmitted rays.

A representative type of antenna and radome arrangement is illustrated in Fig. 9·18. The radome may be cylindrical or hemispherical; a paraboloidal reflector is assumed, together with a pencil beam. The rays incident upon the radome are denoted by *IR*; the rays reflected from the radome, by *RR*; and the transmitted rays, by *TR*. The relative lengths of the lines in Fig. 9·18 are intended to give some representation of the relative power involved; the transmitted power at any point is less than the incident power because of reflection and absorption. In a radome such as that depicted in Fig. 9·18, the angle of incidence is usually less than 30°. Under these circumstances the percentages of reflected, absorbed, and transmitted power closely approach those for normal incidence. This may therefore be called a *normal-incidence* radome. The power-transmission coefficient for any point of the radome is defined as the ratio of the transmitted power to the incident power at that point, and the power-reflection coefficient, as the ratio of the reflected power to the incident power. These ratios will be denoted by $|T|^2$ and $|R|^2$, respec-

tively. Most radome walls have uniform electrical properties from point to point; and as far as transmitted power is concerned, they are equivalent to plane sheets of like material upon which radiation is incident normally. The transmission of any normal-incidence radome may be predicted, therefore, from the known behavior of a corresponding plane sheet of dielectric toward a normally incident plane electromagnetic wave. Similarly, the reflection by a radome of any given wall construction is closely approximated by that from a plane panel made of the same material.

9·5. Streamlined Radomes.—The problems in a typical streamlined radome,[1] such as is depicted in Fig. 9·19 may now be analyzed. The

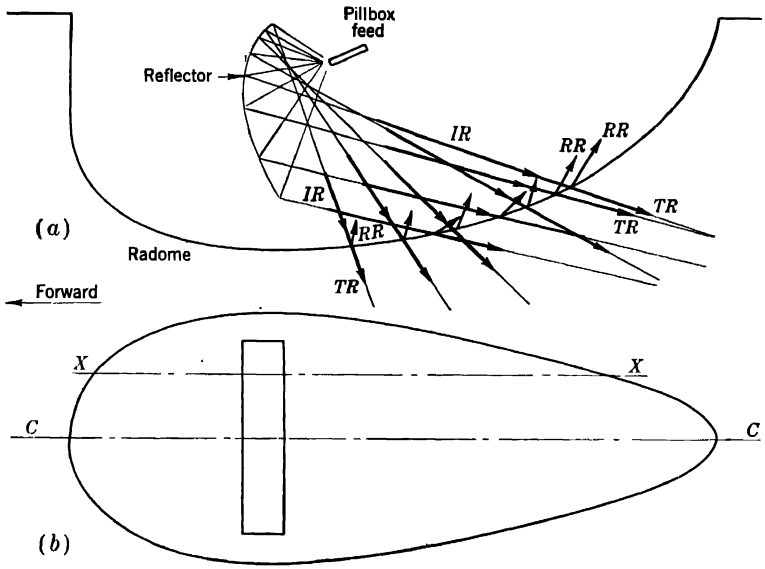

FIG. 9·19.– Streamlined radome. (*a*) Elevation view; (*b*) plan view. *IR*, incident rays; *RR*, reflected rays; *TR*, transmitted rays.

plan view of the radome and antenna is shown at *b*, with the antenna reflector looking aft. At *a* a section through the longitudinal plane *CC* in *b* is shown in elevation. The ray diagram of a typical pillbox-type cosecant-squared antenna is also shown. The steep low-intensity ray is seen to be incident on the radome wall almost normally, whereas for the almost horizontal ray the angle of incidence is large. If, for example, a feed were polarized horizontally, the radiation at any point of the radome

[1] Many of the nose-type radomes for airborne use may be *streamlined* from the aerodynamical viewpoint and still be considered *normal-incidence* radomes from the electrical point of view.

in the vertical plane *CC* in Fig. 9·19 would be polarized perpendicularly to the plane of incidence.

Consideration of other vertical sections, such as *XX* in Fig. 9·19, shows that for some positions of the antenna there are rays that have a large angle of incidence with respect to the radome wall but with the polarization parallel to their plane of incidence. Other rays can be found for which the angle of incidence is large, and both parallel and perpendicular components are comparable in amplitude. For any given angle of incidence, both the power transmitted and the phases of the reflected and transmitted radiation depend upon the polarization. The incident ray at any point, therefore, must be separated into two components—one polarized perpendicular to and the other parallel to the plane of incidence —and the two components considered separately.

Reflection from a streamlined radome into the r-f line is likely to be small, as illustrated in Fig. 9·19, making it unnecessary to reduce the reflection coefficient of the radome wall to a very low value. It is desirable, however, to keep the reflection over the radome wall as a whole to as low a value as possible—(1) to avoid loss in range and (2) to avoid possible pattern distortion resulting from large amounts of r-f power randomly reflected from inside the radome enclosure. In order to design wall constructions suitable for streamlined radomes, it is necessary to know the transmission behavior of a plane panel of the dielectric material for a plane wave incident at any angle, with the plane of polarization also arbitrary. Such an analysis shows that the reflection and transmission characteristics of wall constructions suitable for radomes of the normal-incidence type do not vary appreciably for angles of incidence ranging from 0° to 30°.

CHAPTER 10

ELECTRICAL DESIGN OF NORMAL-INCIDENCE RADOMES

By H. Leaderman

10·1. Introduction.—A normal-incidence radome is defined as one in which the radiation from the antenna falls almost normally upon the radome wall. If the angle of incidence is less than 30°, the percentage of the incident power reflected by the radome is nearly the same as for normal incidence on a plane panel of the same wall construction (see Sec. 11·3). The power reflected into the line by the radome and the phase of the reflected wave depend upon the geometry of the antenna and radome; for any given geometrical configuration, the power reflected into the r-f line by the radome is proportional to the power-reflection coefficient of the equivalent plane panel with respect to a normally incident plane wave. Where magnetron pulling determines the design of the radome, the allowable power-reflection coefficient of the equivalent plane panel is known either from experience or by calculation from the magnetron characteristics and the geometry of the system. Hence, for a normal-incidence radome the transmission and reflection of a normally incident plane wave by a plane panel of the same wall construction as the radome are of primary interest.

In general, where radomes are used for ground and ship systems they are of the approximate normal-incidence type, as shown in Figs. 9·1 and 9·2. The purpose of the conical wall of the radome of Fig. 9·2 is to reduce the reflection of energy into the r-f line.

Figures 9·3 and 9·4 show two types of radomes for airborne use. The former consists of a cylinder capped with a hemisphere and is shown with a cosecant-squared antenna. With this installation, radiation falls nearly normally on the radome wall, passing mostly through the hemisphere. It would be expected that a rib or other discontinuity placed as shown in Fig. 9·3 would be in a region of such low power level that it would have only a slight effect on the pattern. In Fig. 9·4, which shows a nose-type radome for a very fast airplane, the angle of incidence is large over most of the electrical area of the radome; from the electrical point of view the radome is therefore streamlined and not one of normal incidence.

The simplest construction of the radome wall consists of a single dielectric sheet either of uniform thickness or with variations in thickness

much smaller than the wavelength. The design of such normal-incidence radomes will be considered first. More complicated constructions, involving layers of material with different dielectric properties, possess certain advantages over the homogeneous wall construction in strength, stiffness, and weight; they will be discussed subsequently.

Some of the r-f energy is absorbed by the radome wall owing to dielectric losses in the material. Because of the short path in the dielectric, however, extremely low-loss material is not required as it is for coaxial transmission lines. Even so, reasonably low-loss material should be used to prevent excessive absorption of r-f energy. It will be found that in the range of allowable absorption, the *reflection* of a panel or radome is only slightly affected by the loss properties of the radome materials but the *transmission* may be reduced considerably.

10·2. Plane Lossless Sheet, Normal Incidence.—When radiation is incident normally on the surface of a plane sheet of dielectric material, part of it is reflected at the front surface; the remainder enters the sheet and is partially reflected at the back surface. Some of this wave that is reflected at the back surface reemerges at the front surface and is directly superposed on the originally reflected portion; part of it undergoes multiple reflection in the sheet and further contributes to the resultant reflection. In general, the resultant reflection from the back wall would be expected to be equal in magnitude but opposite in phase to that from the front wall and thus cancel it. If this were not so, there would be a sudden discontinuous jump from no reflection for no sheet to an appreciable one of finite value for a sheet that is infinitesimally thin. Such discontinuities are rarely found. The expectation is confirmed by the electromagnetic theory of the reflection: the amplitude-reflection coefficients for the two surfaces are equal in magnitude but opposite in sign, and the amplitude of the resultant reflected wave approaches zero for a sheet of infinitesimal thickness (see Secs. 12·4 and 12·5).

When the thickness of the sheet of dielectric material equals one quarter wavelength, the wave reflected from the back surface will have traveled a half wavelength more than the wave that is reflected at the front surface and will be in phase with it. For this thickness and also for those of $\frac{3}{4}\lambda_s$, $\frac{5}{4}\lambda_s$, etc., the reflection should be a maximum.

For a sheet whose thickness is an integral multiple of a half wavelength in the material, however, the waves should again be out of phase and give a resultant reflection value of zero. All of this is expressed by Eq. (12·77), giving the power-reflection coefficient

$$|R|^2 = \frac{4r_{ab}^2 \sin^2 \phi}{(1 - r_{ab}^2)^2 + 4r_{ab}^2 \sin^2 \phi}. \tag{1}$$

In this equation r_{ab} is the amplitude-reflection coefficient at the front surface, and

$$\phi = 2\pi \frac{d}{\lambda_0/n} = 2\pi \sqrt{\frac{\epsilon}{\epsilon_0}} \frac{d}{\lambda_0} \tag{2}$$

$\phi/2\pi$ being the electrical thickness of the sheet, where

d = thickness of the sheet,
λ_0 = free-space wavelength,
n = index of refraction = $\sqrt{\epsilon/\epsilon_0}$,
ϵ = dielectric constant of the material,
ϵ_0 = dielectric constant of free space,
ϵ/ϵ_0 = specific dielectric constant,
λ_0/n = wavelength in the dielectric.

It is apparent that $|R|^2 = 0$ for $\phi = N\pi$. (N is any integer, including 0.) For such values of ϕ, d is given by

$$d_{\min} = \frac{N}{2}\left(\frac{\lambda_0}{n}\right). \tag{3}$$

As d is varied, the maximum value of the power-reflection coefficient is found to be

$$|R|^2 = \frac{4r_{ab}^2}{(1 + r_{ab}^2)^2} \qquad \text{for} \qquad \phi = \left(N + \frac{1}{2}\right)\pi; \tag{4}$$

this maximum is realized at any value of d satisfying the relation

$$d_{\max} = \left(N + \frac{1}{2}\right)\frac{1}{2}\left(\frac{\lambda_0}{n}\right).$$

For calculating actual values, we use

$$r_{ab} = \frac{n - 1}{n + 1} = \frac{\sqrt{\frac{\epsilon}{\epsilon_0}} - 1}{\sqrt{\frac{\epsilon}{\epsilon_0}} + 1} \tag{5}$$

from Eq. (12·39a). When the value of r_{ab} from Eq. (5) is put into Eq. (4), the maximum value of the power-reflection coefficient is given by

$$|R|^2_{\max} = \frac{(n^2 - 1)^2}{(n^2 + 1)^2} = \left(\frac{\frac{\epsilon}{\epsilon_0} - 1}{\frac{\epsilon}{\epsilon_0} + 1}\right)^2. \tag{6}$$

Curves of the power-reflection coefficient $|R|^2$ plotted against d/λ_0 for various values of ϵ/ϵ_0 are given in Fig. 10·1.

In the curves plotted in Fig. 10·2 the ordinates give the absolute values of the amplitude-reflection coefficient $|R|$ for various values of ϵ/ϵ_0. The

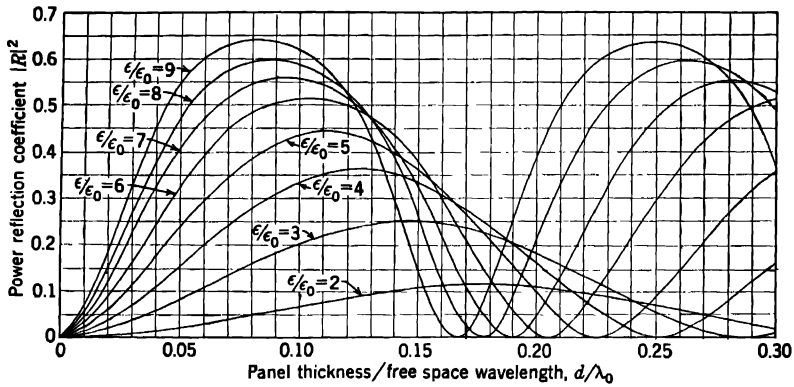

FIG. 10·1. Power-reflection coefficient of a lossless dielectric sheet.

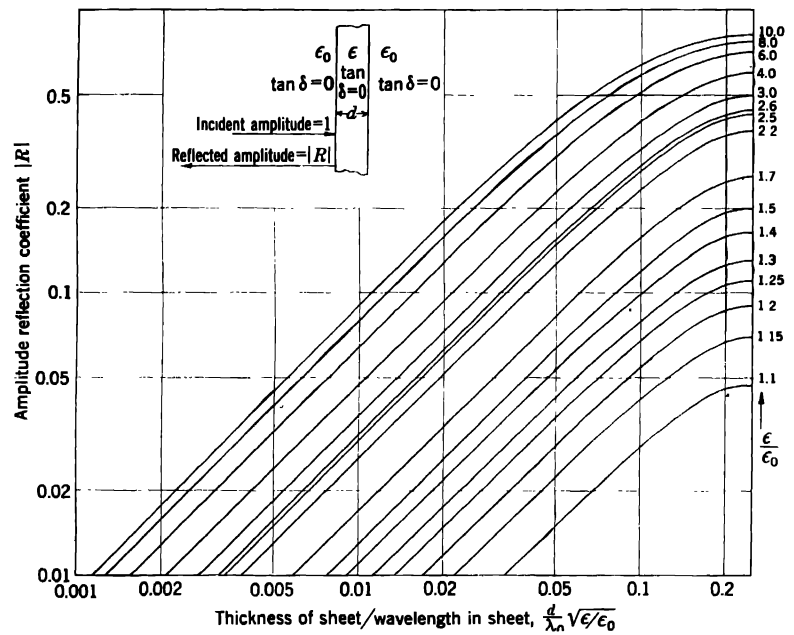

FIG. 10·2.—Amplitude-reflection coefficient of a lossless dielectric sheet.

abscissas are values of the ratio of the thickness of the panel d to the wavelength in the panel, $\lambda_0/\sqrt{\epsilon/\epsilon_0}$. This ratio, which is equal to $\phi/2\pi$ [Eq. (2)] represents the electrical thickness of the panel. The curves extend from $\phi/2\pi = 0$ to $\phi/2\pi = 0.25$. To find the reflection of a panel that has a greater electrical thickness, the difference between the actual

electrical thickness and the nearest half-integer is taken for the abscissa in Fig. 10·2.

To minimize the reflection, then, the panel or radome should have a thickness that is just equal to an integral number of half wavelengths in the dielectric. In Table 10·1 the half-wavelength thicknesses for several values of λ_0 and ϵ/ϵ_0 are given in centimeters. These thicknesses are too great for the longer wavelengths (say 10 to 25 cm) to be practicable for radomes; their use, however, is reasonable in the 1-cm band and possible in the 3-cm band.

TABLE 10·1.—HALF-WAVELENGTH THICKNESSES OF DIELECTRIC SHEETS

$\frac{\epsilon}{\epsilon_0}$ (specific dielectric constant)	λ_0 (free-space wavelength), cm			
	25	10	3	1
10	3.95	1.58	0.47	0.158
4	6.25	2.50	0 75	0.250
2	8.84	3 54	1.06	0.354

In practice, it is not possible to make a panel or radome of the exact thickness that will be nonreflecting at a given frequency. What can be specified, however, is the maximum power- (or amplitude-) reflection coefficient that the panel or radome may have and still possess satisfactory electrical properties. The allowable value of $|R|^2$ thus determines the limits of thickness above and below the half-wavelength thicknesses given in Table 10·1. Let us assume that the thickness of a panel deviates by a small amount Δd from the half-wave thickness so that

$$d = \frac{N\lambda_0}{2n} + \Delta d$$

(N is an integer). By Eq. (2),

$$\phi = \frac{\frac{2\pi N\lambda_0}{2n}}{\frac{\lambda_0}{n}} + \frac{2\pi\,\Delta d}{\frac{\lambda_0}{n}}, \tag{7}$$

or

$$\phi = N\pi + \Delta\phi \tag{8}$$

if

$$\Delta\phi = 2\pi\frac{\Delta d}{\frac{\lambda_0}{n}}. \tag{9}$$

For $\Delta\phi \ll 1$, $\sin(N\pi + \Delta\phi) = \sin\Delta\phi \approx \Delta\phi$. After substituting this and $r_{ab} = \dfrac{\sqrt{\epsilon/\epsilon_0} - 1}{\sqrt{\epsilon/\epsilon_0} + 1}$ in Eq. (1), it can be reduced to give

$$|R|^2 \cong \left[\left(\frac{\epsilon}{\epsilon_0} - 1\right)\pi\frac{\Delta d}{\lambda_0}\right]^2. \tag{10}$$

The values of $\Delta d/\lambda_0$ corresponding to different choices of ϵ/ϵ_0 and $|R|^2$ can be calculated from Eq. (10). Such values of $\Delta d/\lambda_0$ are given in Table 10·2.

TABLE 10·2.—TOLERANCES IN HALF-WAVELENGTH THICKNESSES OF HOMOGENEOUS PANELS

$\frac{\epsilon}{\epsilon_0}$	Values of $\frac{\Delta d}{\lambda_0}$, cm		
	$\|R\|^2 = 0.01$	$\|R\|^2 = 0.02$	$\|R\|^2 = 0.04$
2	0.033	0.047	0.069
4	0.011	0.015	0.022
10	0.004	0.005	0.007

In the region of $\lambda_0 = 1$ cm, where the half-wavelength panel has a practicable thickness, the tolerances are reasonable when the dielectric constant is low but decrease rapidly as the dielectric constant increases. This result is apparent also from Fig. 10·1.

Even though a radome with a wall of half-wavelength thickness has been designed for a given wavelength λ_0, it will probably be used for a definite band of wavelengths that may extend ± 2 per cent from the center of the band. Thus, appreciable reflection may arise not only because of variations in thickness within manufacturing tolerances but also because of variations in frequency.

Thin Panels and Radomes.—From Fig. 10·1 it can be seen that a panel of lossless dielectric has low reflection if its thickness is small in comparison with the free-space wavelength. Equation (10) and the calculated values of $\Delta d/\lambda_0$ of Table 10·2 also apply for such actual deviation from zero thickness. For relatively large values of λ_0 (say, 10 to 25 cm), reasonable values of d, now Δd, correspond to small values of $|R|^2$. For wavelengths in the 3-cm range, these thicknesses are smaller, while in the 1-cm range the thicknesses for small values of $|R|^2$ are usually too small to be practicable. For any particular radome, the choice of material for the wall must depend not only upon the dielectric constant of the material but also upon its mechanical properties and the mechanical requirements for the radome.

Panels with Low Dielectric Constant.—From Eq. (6) it is clear that the maximum reflection at normal incidence of a lossless panel decreases rapidly with a decrease in dielectric constant. Table 10·3 gives values of the maximum power-reflection coefficient for various values of ϵ/ϵ_0. Thus, if the maximum allowable power-reflection coefficient is 0.040, any thickness of panel necessary for mechanical reasons can be used, provided that $\epsilon/\epsilon_0 \leqq 1.5$. Since actual materials are not lossless, the

TABLE 10·3.—REFLECTION OF PANELS WITH LOW DIELECTRIC CONSTANT

$\frac{\epsilon}{\epsilon_0}$	$\lvert R\rvert^2_{\max}$
1.7	0.067
1.6	0.053
1.5	0.040
1.4	0.028

absorption may be large if the panel is a large number of wavelengths thick; thus the transmission may be low even though the reflection is small. This situation, however, seldom arises with radomes. If the specific dielectric constant is slightly higher than 1.5 (say, 1.6 or 1.7), then it is necessary merely to keep somewhat away from the region of odd multiples of the quarter-wavelength thickness in order to keep the power-reflection coefficient below the specified value of 0.040.

Summarizing the results so far, we see that it is possible to make homogeneous panels or radome walls giving low reflection, provided that one of the following three conditions is satisfied:

1. The thickness is small compared with the wavelength [Eq. (10)].
2. The thickness is very nearly equal to an integral multiple of the half-wavelength thickness [Eq. (3)].
3. The dielectric constant is low [Eq. (6)].

10·3. Plane Lossy Sheet, Normal Incidence.—Actual dielectrics are always somewhat lossy,[1] so it is in order to consider how the results of the preceding section are modified when the losses of energy are taken into account.

In general, it can be stated that the same considerations are relevant, but with the modifications that are obviously necessary because of the attenuation of any wave that is propagated in the lossy material. The transmitted power is less because each emerging partial wave has traversed the sheet of dielectric once or more. The waves reflected from the back surface, which combine with the primary reflected wave from the

[1] For a detailed account of the properties of lossy sheets see R. M. Redheffer, "Reflection and Transmission of Single Plane Sheets," RL Report No. 483-4, July 1944; also "Transmission and Reflection of Parallel Plane Sheets," RL Report No. 483-12, January 1945.

front surface, will have made at least two traversals of the sheet. Their resultant will therefore be smaller than in a lossless medium and will never be great enough to cancel the primary reflected wave completely. The reflection, therefore, for thicknesses of material that are integral multiples of the half wavelength, will be expected merely to have minimum values rather than to become zero.

These expectations are in accord with the quantitative results that are derived in Sec. 12·5. In order to discuss some of those results, it is necessary to define the quantities customarily used in describing lossy mediums.

A lossy medium is often characterized by a dielectric constant that is a complex number. It may be written

$$\epsilon = \epsilon' - j\epsilon'', \tag{11}$$

or

$$\epsilon = \epsilon'(1 - j \tan \delta). \tag{12}$$

The specific dielectric constant is ϵ/ϵ_0, ϵ_0 being the dielectric constant of free space, so

$$\frac{\epsilon}{\epsilon_0} = \frac{\epsilon'}{\epsilon_0}(1 - j \tan \delta). \tag{13}$$

The quantity $\tan \delta$ is the loss tangent and equals ϵ''/ϵ'.

In optical theory, dielectric materials are characterized by an index of refraction n and an absorption coefficient κ. The present considerations are mixed, since they deal with the optical behavior of materials whose properties are determined by electrical measurements. The relationships among these various quantities are developed in Sec. 12·2. Here it should suffice merely to quote the results. The equations [see Eqs. (12·16*a*)] are

$$\begin{aligned} n &= \sqrt{\frac{\epsilon'}{\epsilon_0}}\sqrt{\frac{\sqrt{1 + \tan^2 \delta} + 1}{2}}; \\ \kappa &= \sqrt{\frac{\sqrt{1 + \tan^2 \delta} - 1}{\sqrt{1 + \tan^2 \delta} + 1}}. \end{aligned} \tag{14}$$

For $\tan^2 \delta \ll 1$, these reduce to

$$\begin{aligned} n &= \sqrt{\frac{\epsilon'}{\epsilon_0}}\left(1 + \frac{\tan^2 \delta}{8}\right); \\ \kappa &= \frac{\tan \delta}{2}\left(1 - \frac{\tan^2 \delta}{4}\right); \end{aligned} \tag{15}$$

or to a first approximation to

$$\begin{aligned} n &\approx \sqrt{\frac{\epsilon'}{\epsilon_0}}; \\ \kappa &\approx \frac{\tan \delta}{2}. \end{aligned} \tag{16}$$

The wavelength of the radiation in the dielectric material λ_s equals λ_0/n. From Eq. (15) it is clear that λ_s decreases if tan δ increases for a given value of ϵ'/ϵ_0. The half-wavelength thickness of a lossy panel is thus slightly less than that of a lossless one having the same value of ϵ'/ϵ_0.

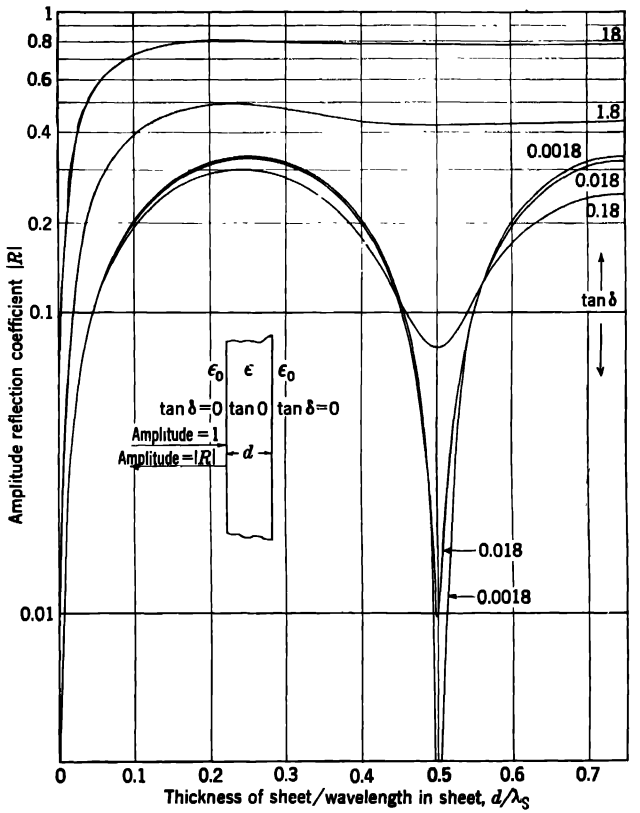

FIG. 10·3.—Reflection of a plane lossy sheet. The dielectric constant is $2\epsilon_0$.

Equation (12·81) gives the expression for the power-reflection coefficient. It seems preferable to present the results graphically here rather than to define all the quantities appearing in that equation and to analyze it in detail. The absolute value of the amplitude-reflection coefficient $|R|$ is plotted against d/λ_s for different values of tan δ. Figures 10·3 and 10·4 show such curves for $\epsilon'/\epsilon_0 = 2$ and $\epsilon'/\epsilon_0 = 4$, respectively. It is seen that if tan δ is small, the reflection is slightly less than for a lossless sheet, except in the region of the half-wavelength thickness. At the half-wavelength thickness the reflection does not become zero but is small

when tan δ is small, so that it can be neglected. When tan δ is large, this is not true; the transmission of such materials, however, is so small for appreciable values of d/λ_s that they are of no use for construction of radomes. With useful materials, the reflection at normal incidence is practically what it would be if they were lossless.

Equation 12·82 gives the corresponding expression for the power-transmission coefficient $|T|^2$. It is also plotted against d/λ_s for different

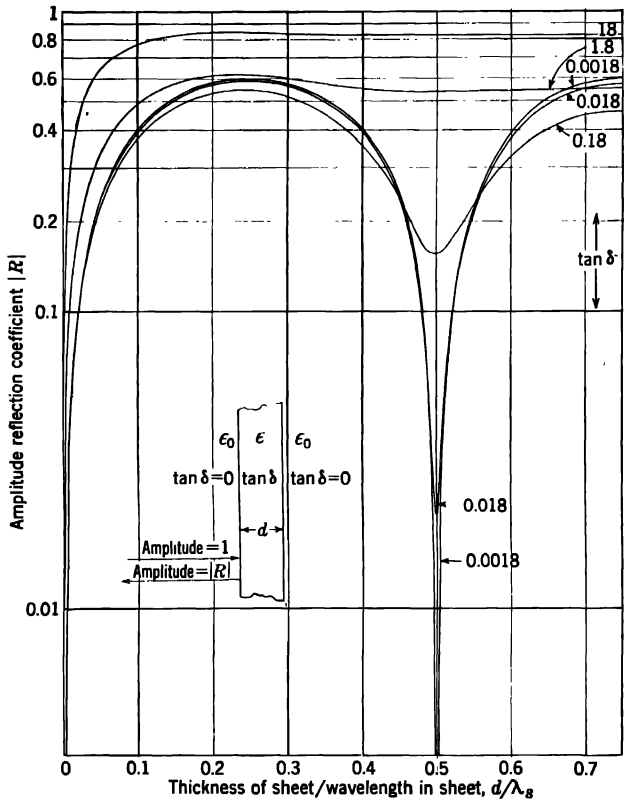

FIG. 10·4.—Reflection of a plane lossy sheet. The dielectric constant is $4\epsilon_0$.

values of tan δ for values of ϵ'/ϵ_0 equal to 2 and 4 in Figs. 10·5 and 10·6, respectively. It is seen that the transmission depends significantly upon the loss tangent, except when d/λ_s is extremely small. The transmission of a sheet whose thickness is a half wavelength falls off rapidly with an increase in tan δ; for any value of tan δ other than zero the optimum transmission occurs at a thickness slightly less than $\lambda_s/2$.

In actual practice, the materials useful for making homogeneous walls

for radomes in the range of wavelengths from 1 to 10 cm are low-loss materials for which tan δ is less than 0.1. At the lower end of the wavelength range the half-wavelength thickness is practicable for radome construction, but tan δ must be small because the transmission depends on it markedly. Alternatively, materials of very low dielectric constant have been used in thicknesses of several half-wavelengths; the reflection

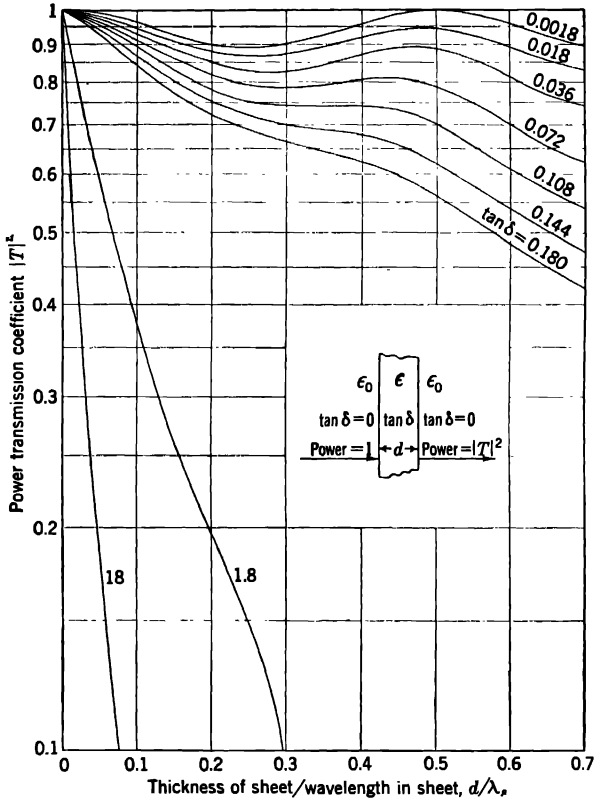

FIG. 10·5.—Transmission of a plane lossy sheet. The dielectric constant is $2\epsilon_0$.

is then low and the transmission is high if the loss tangent is small enough. At the upper end of the wavelength range it is feasible to use materials of high strength in sheets that are thin compared with λ_s. It is nevertheless desirable to keep ϵ'/ϵ_0 as low as possible in such "thin-walled" radomes or panels in order that the reflection may be as small as possible. The materials of lower dielectric constant usually also have low values of the loss tangent.

Equation 12·85 is an approximate expression for the power-transmission coefficient for N-half-wavelength panels. If we substitute $n_b = \sqrt{\epsilon'/\epsilon_0}$ and $\kappa_b = \tan \delta/2$ into it, it becomes

$$|T|^2 \approx \frac{16 \frac{\epsilon'}{\epsilon_0} e^{-N\pi \tan \delta}}{\left[\left(\sqrt{\frac{\epsilon'}{\epsilon_0}} + 1\right)^2 - \left(\sqrt{\frac{\epsilon'}{\epsilon_0}} - 1\right)^2 e^{-N\pi \tan \delta}\right]^2}. \tag{17}$$

In Fig. 10·7 the transmission loss $(1 - |T'|^2)$ has been plotted for a panel

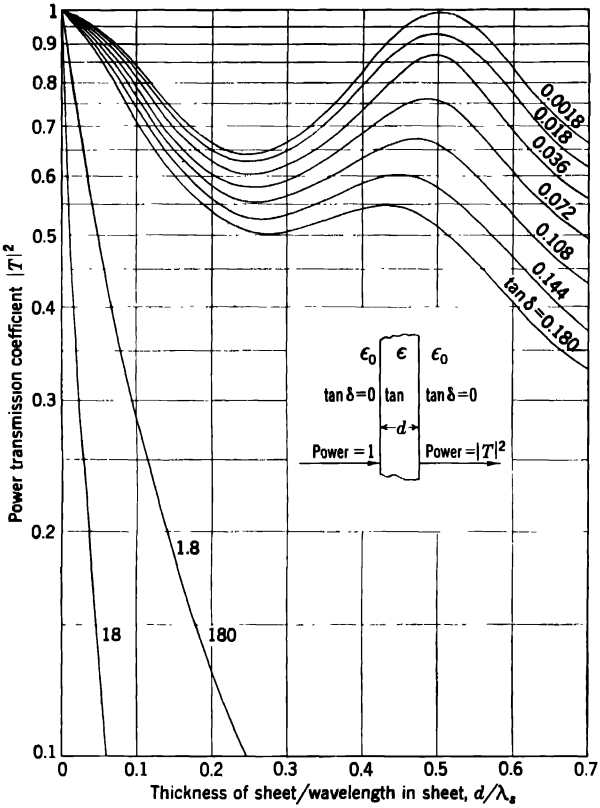

FIG. 10·6.—Transmission of a plane lossy sheet. The dielectric constant is $4\epsilon_0$.

of half-wavelength thickness for various values of ϵ'/ϵ_0 and tan δ. The curves are computed from the exact equation [Eq. (12·82)], and the points are computed from the approximate equation [Eq. (17)]. It can be seen that the latter expression is sufficiently accurate for all practical purposes.

In many cases, the value of the loss tangent is known only approximately, and it is desired to obtain a preliminary idea as to the transmission loss in a single or multiple half-wavelength sheet designed for normal incidence. If $N\pi \tan \delta$ is small, Eq. (17) can be reduced to

$$1 - |T|^2 \approx \frac{\frac{\epsilon'}{\epsilon_0} + 1}{2\sqrt{\frac{\epsilon'}{\epsilon_0}}} N\pi \tan \delta. \tag{18}$$

Thus, the transmission loss of a panel N half wavelengths thick is seen to be approximately equal to $N\pi \tan \delta$ for many materials. For a panel

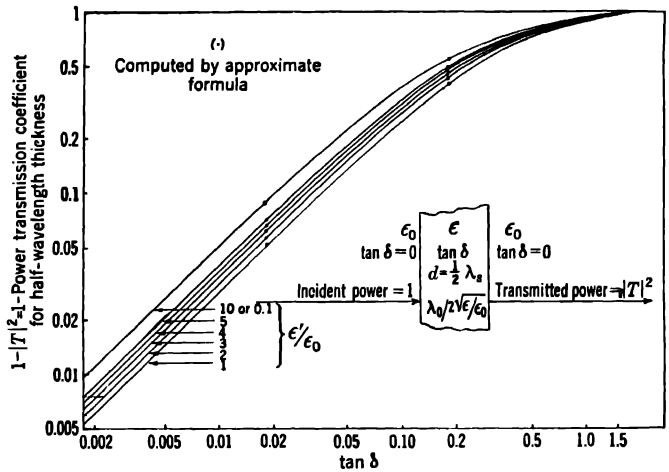

FIG. 10·7.—Transmission loss of a lossy sheet of half-wavelength thickness.

one half wavelength thick, for which ϵ'/ϵ_0 is equal to 4 and tan δ is equal to 0.015, the loss in transmission is almost entirely due to absorption and is about 5 per cent of the incident power. If the tolerances can be maintained so that the transmission loss due to reflection is less than 5 per cent, a transmission of 90 to 95 per cent of the incident power can be expected. In this case it is hardly worth while to use materials of lower loss tangent in order to reduce the transmission loss, especially because such materials are usually less desirable because of lower strength, stiffness, and heat resistance.

Materials with high loss tangents should not be used for single or multiple half-wavelength radomes. For example, a material for which $\epsilon'/\epsilon_0 = 4$ and tan $\delta = 0.1$ has a transmission of only 64 per cent for a single half-wavelength thickness. The transmission loss of 36 per cent

of the incident power is almost entirely due to absorption in the dielectric. Likewise, materials that are likely to absorb appreciable amounts of water under operating conditions should not be used for radomes because absorption of water causes an increase in dielectric constant (with a resulting increase in reflection) and also in an increase in loss tangent.

In panels or radomes that are thin compared with the half wavelength, there is even less reason to use materials of very low loss tangent than there is with half-wavelength constructions. Examination of Eqs. (12·69) to (12·72) inclusive shows that the absorption factor is one that has d/λ_0 in the exponent. As an instance, with the material considered two paragraphs back, for which ϵ'/ϵ_0 is 4 and tan δ is 0.015, we find that when $d/\lambda_0 = 0.025$ and $(d\sqrt{\epsilon'/\epsilon_0})/\lambda_0 = 0.05$, the loss by absorption is less than 1 per cent, to be compared with a reflection loss of 5 per cent. Even if the loss tangent were to be 0.10 instead of 0.015, the absorption would be only 5 per cent. We conclude that in thin-walled radomes designed for longer wavelength antennas (10 to 25 cm) it is not necessary for the loss tangent to be low if $(d\sqrt{\epsilon'/\epsilon_0})/\lambda_0$ is small.

It is sometimes necessary to provide a housing for an antenna of longer wavelength, say 100 cm. In this case, the thickness that is necessary for structural reasons may be small enough to be only a few thousandths of the wavelength. Under these circumstances it is not necessary to use material having either a low dielectric constant or a low loss tangent, nor is it necessary to use a material with low water absorption, because large values of these factors will be more than compensated for by the small value of d/λ_0.

10·4. General Characteristics of Double-wall and Sandwich Radomes. The reflection and transmission characteristics of a single plane sheet of dielectric were considered in Sec. 10·3. In spite of the variety of available materials of various electrical and mechanical properties, it is often impossible to design a satisfactory normal-incidence radome made of a single homogeneous sheet of dielectric. The impediment may be inadequate mechanical strength, stiffness or weather resistance of materials otherwise electrically suitable, excessive weight, or impossible tolerances. For example, let us assume that it is desired to fabricate a normal-incidence radome using a material of dielectric constant $4\epsilon_0$, the loss in transmitted power resulting from reflection to be less than 4 per cent. From Fig. 10·2, it is found that the electrical thickness $(d/\sqrt{\epsilon'/\epsilon_0})/\lambda_0$, corresponding to the allowed amplitude-reflection coefficient of 0.2, must be less than 0.044 or must lie within the range 0.500 ± 0.044.

A half-wavelength radome wall would thus be more than eleven times as thick and heavy as one corresponding to the smaller electrical thickness; its strength and stiffness would be approximately one hundred thirty and fifteen hundred times as great, respectively, as for the thin-wall

design.[1] The ratios depend, of course, upon the smaller thickness determined by the allowable reflection coefficient. It may happen that a thin-wall design has insufficient strength or stiffness while the half-wavelength design is excessively heavy and unnecessarily strong and stiff. The half-wavelength design may be entirely too heavy for an airborne radar set. The double-wall and sandwich constructions that will now be discussed are more flexible, in that low reflection can be obtained without necessarily involving excess weight, strength, or stiffness.

As shown in the preceding section, the minimization of the reflection by a single-wall radome results from mutual cancellation of the reflections from the front and rear interfaces of the dielectric sheet. This suggests that similar cancellation can be obtained by the use of two thin sheets separated by an air space: the *double-wall* construction. More generally, the space between the two sheets is filled with a second dielectric medium; this is the *sandwich construction*.

It will be recalled that the reflection coefficient for a wave incident upon a sheet of dielectric material is equal in magnitude but opposite in sign to the reflection coefficient for the wave incident on the rear interface of the sheet. For this reason cancellation is obtained for vanishing thickness and for thicknesses that are integral multiples of a half wavelength in the dielectric, so that the retardation in one round trip in the sheet is an integral number of whole wavelengths. If two like thin sheets separated by an air space are to be used, the reflection coefficient will be the same for each. The reversal of phase necessary for the cancellation will have to be produced by spacing the sheets either one quarter wavelength or an odd multiple of a quarter wavelength apart.

There is a related case for the single dielectric sheet that is of interest, although so far it has not been of much practical consequence. If a sheet of dielectric is put between two different mediums and has a dielectric constant that is the geometric mean of those of the two mediums, the reflection coefficients for both entering and emerging waves will be equal both in magnitude and in sign. This is discussed in detail at the end of Sec. 12·5. Under such circumstances, zero reflection will again be obtained if the sheet has a thickness of a quarter wavelength or some odd multiple of that thickness.

The double-wall construction can have greater mechanical strength than a single sheet, and the space between the walls can be used as a duct for hot air in order to prevent the formation of ice on the radome. A disadvantage, however, is that a large number of spacers is required to maintain the spacing within tolerable limits; such spacers are likely to distort the pattern.

When the space between two sheets is filled with a core of some dielec-

[1] *Cf.* Sec. 13·15.

tric other than air, the reflection coefficients at the surfaces of the core are no longer either in the same phase or in exactly the opposite phase. The latter condition is rapidly approached, however, as cores of increasing dielectric constant are used. The spacing for minimum reflection will rapidly increase and approach an integral multiple of a half wavelength. The sandwich becomes a half-wavelength sheet slightly modified by the presence of the thin skins.

When the skins that are to be used have an electrical thickness that is appreciable compared with a half wavelength, the problem is more complicated: The thickness of the sheets also contributes to the relative displacement in phase. The theory of such sandwich or double-wall construction is developed in Sec. 12·6. The general result is that when the sandwich or double-wall is symmetrical, i.e., has skins of the same material and thickness, there is a set of values for the thickness of the core that will reduce the reflection to zero. These values differ by one half wavelength in the material of the core.

A great improvement in mechanical properties is obtained when the air space of the double-wall construction is replaced by a core of material that has a low dielectric constant (say, less than $1.7\epsilon_0$) and low density (6 to 20 lb/ft^3), while material of high strength and density is used in the faces or skins. With this type of construction, high ratios of strength to weight and of stiffness to weight are obtained for any desired electrical performance; this is especially important for airborne radomes. Distortion of the pattern is not likely to arise except where excessive variation in the dimensions of the sandwich wall occurs in a distance that is a wavelength or less.

The sandwich with high-density faces and low-density core is not the only one electrically possible; there are other arrangements that are not so satisfactory from the standpoints of strength/weight and stiffness/weight ratios but may be preferable electrically under some circumstances.

The general expression for the thickness of the core of a lossless symmetrical radome that will have a power-reflection coefficient of zero for normal incidence [see Eqs. (12·102) and (12·100) of Sec. 12·6] is

$$(d_c)_N = \frac{\lambda_0}{2\pi\sqrt{\alpha_c}} \left[N\pi - \tan^{-1} \frac{2(\alpha_s - 1)\sqrt{\alpha_s\alpha_c}\sin 2\phi_s}{(\alpha_s + 1)(\alpha_c - \alpha_s) + (\alpha_s - 1)(\alpha_s + \alpha_c)\cos 2\phi_s} \right], \quad (19)$$

where N = integer, the order of the sandwich,
$(d_c)_N$ = thickness of the core of the sandwich of order N,
λ_0 = free-space wavelength,
α_c = specific dielectric constant of the core material = ϵ_c/ϵ_0,
α_s = specific dielectric constant of the skin material = ϵ_s/ϵ_0,
ϕ_s = $2\pi \times$ electrical thickness of the skin [*cf.* Eq. (2)].

If the actual thickness of the core deviates from the optimum by an amount Δd_c, the power-reflection coefficient [see Eq. (12·103)] is given by

$$|R|^2 \approx \frac{4|\rho|^2 \sin^2(\Delta\phi_c)}{(1-|\rho|^2)^2 + 4|\rho|^2 \sin^2(\Delta\phi_c)} \tag{20}$$

in which

$$\Delta\phi_c = \frac{2\pi\sqrt{\alpha_c}}{\lambda_0}\Delta d_c.$$

In Eq. (20), $|\rho|$ is the absolute value of amplitude-reflection coefficient for

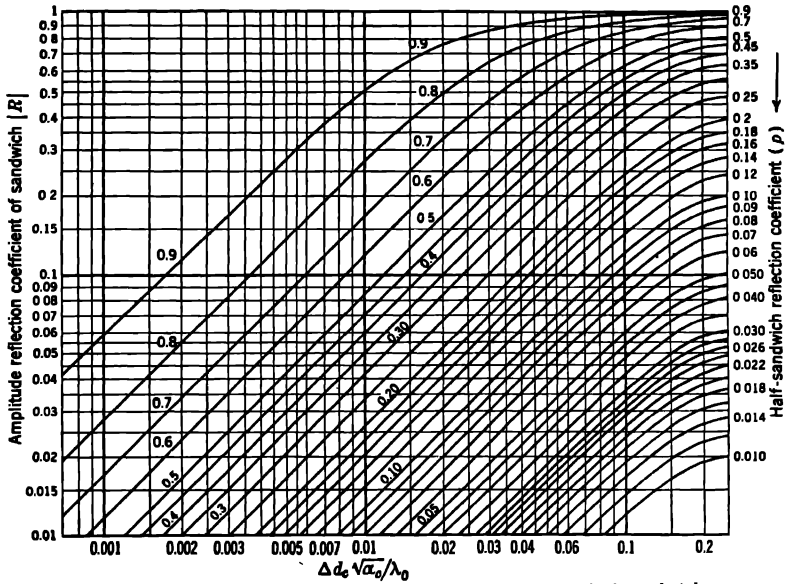

FIG. 10·8.—Chart for computation of reflection of symmetrical sandwiches.

a wave incident on the skin from the core (or on the core from the skin). It has a value [see Eq. (12·101)] given by

$$|\rho|^2 = \frac{\alpha_s(\sqrt{\alpha_c}-1)^2 - (\alpha_s-1)(\alpha_c-\alpha_s)\sin^2\phi_c}{\alpha_s(\sqrt{\alpha_c}+1)^2 - (\alpha_s-1)(\alpha_c-\alpha_s)\sin^2\phi_c}. \tag{21}$$

In Fig. 10·8, $|R|$ is plotted against $\Delta d_c\sqrt{\alpha_c}/\lambda_0$ for different values of $|\rho|$. It is seen that when $|\rho|$ is small, large changes in core thickness result in relatively small variations in reflection of the sandwich; when $|\rho|$ is large, the variations in reflection will be large.

In Sec. 12·6 it is shown that the minimum value for the power-reflection coefficient cannot be zero if the two skins of the sandwich have different thicknesses. Such unsymmetrical sandwiches, however, may

sometimes be desirable for structural reasons. Even with the asymmetry the minimum values of $|R|^2$ can be quite small if $|\rho_1|$ and $|\rho_2|$ do not differ greatly. It is also shown in Section 12·6 that in such a case the optimum value for the thickness of the core is the average of the two values that would be appropriate for symmetrical sandwiches having the two thicknesses of the skin of the actual unsymmetrical sandwich.

10·5. Electrical Design of Normal-incidence Double-wall Radomes.—So far we have been considering the general electrical properties of the

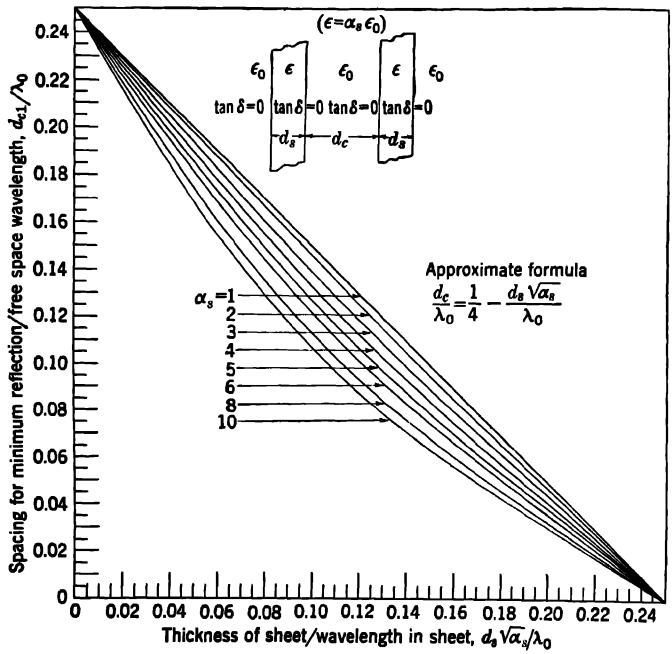

FIG. 10·9.—Optimum spacing between walls for a symmetrical double-wall normal-incidence radome.

lossless sandwich construction at normal incidence. Let us now consider in detail some special results that apply to the design of double-wall radomes,[1] restricting ourselves to a discussion of the symmetrical double-wall construction with lossless sheets. The thickness of the inner and outer walls is denoted by d_s; the dielectric constant of the sheets, by $\alpha_s\epsilon_0$; and α_c is equal to unity. The separation between the sheets is given by d_c, and the free-space wavelength of the radiation is λ_0. If

[1] R. M. Redheffer, "Electrical Properties of Double-wall and Standard Radomes," RL Report No. 483-11, February 1944. J. B. Birks, "Dielectric Transmission and Scanner Nacelle Design," TRE Report No. T1677, and "Dielectric Transmission and Scanner Nacelle Design," Part 2, TRE Report No. T1769, December 1944.

$(d_c)_N$ is the spacing for zero reflection, Eq. (12·102) becomes

$$\frac{(d_c)_N}{\lambda_0} = \frac{N}{2} - \left(\frac{1}{2\pi}\right) \tan^{-1} \frac{2\sqrt{\alpha_s}}{1+\alpha_s} \cot \frac{2\pi d_s \sqrt{\alpha_s}}{\lambda_0} \tag{22}$$

where N is a positive integer as before. The quantity $(d_c)_N$ is plotted against $d_s\sqrt{\alpha_s}/\lambda_0$ for the first-order spacing ($N = 1$) in Fig. 10·9 for values of α_s from 1 to 10; the curves are plotted for a range of values of $(d_c)_1/\lambda_0$ and $d_s\sqrt{\alpha_s}/\lambda_0$ from zero to 0.25. These curves can be used to cover all values of spacing and thickness of the walls if we use, instead of the actual values of $(d_c)_1/\lambda_0$ and $d_s\sqrt{\alpha_s}/\lambda_0$, the differences between each quantity and the nearest half-integer.

It is seen that if the walls of a double-wall radome have a very small value of electrical thickness $d_s\sqrt{\alpha_s}/\lambda_0$, the spacing is equal to $\lambda_0/4$. In general, the first-order spacing lies between this value and zero. (A wall of quarter-wavelength thickness would require zero spacing, becoming a half-wavelength panel.) An approximate formula for the optimum first-order spacing is given by

$$(d_c)_1 = \frac{\lambda_0}{4} - d_s\sqrt{\alpha_s}. \tag{23}$$

Since it is impossible to manufacture double-wall radomes with exactly the spacing given by Eq. (22), we have to determine the spacing tolerance Δd_c corresponding to a specified value of power-reflection coefficient $|R|^2$ for a plane wave normally incident on a plane double-wall arrangement. The power-reflection coefficient of each wall can be determined by means of Eq. (21) or, more easily, by using Fig. 10·2. With the value of $|\rho|^2$ thus obtained, the power-reflection coefficient of the double-wall arrangement with spacing $d_c \pm \Delta d_c$ is obtained from Fig. 10·8. If the amplitude-reflection coefficient $|\rho|$ of a skin of a symmetrical double-wall arrangement is less than 0.25, the amplitude-reflection coefficient of the whole arrangement is given approximately

$$|R| \approx \frac{4\pi|\rho|\,\Delta d_c}{\lambda_0}, \tag{24}$$

derived from Eq. (20).

10·6. Electrical Design of Normal-incidence Sandwich Radomes.— Three types of construction have been used or considered for sandwich radomes. The most important type has thin skins of high-strength material separated either by a core of "expanded" or "foam" plastic or by some cellular construction. As remarked in Sec. 10·4, the low-density core makes it possible to construct a light radome that has satisfactory strength and stiffness. The dielectric constant of the skins ranges usually from about $3\epsilon_0$ to $4.5\epsilon_0$, while the dielectric constant of the core ranges from $1.1\epsilon_0$ to $1.7\epsilon_0$. For the wavelength range from 1 to 10 cm,

the electrical thickness $d_s \sqrt{\alpha_s}/\lambda_0$ of the skins of such normal-incidence radomes is usually less than 0.1. The discussion in this section is devoted principally to this type of sandwich construction.

The second sandwich construction is one mentioned briefly in Sec. 10·4. The dielectric constant of its core is equal to the square of the dielectric constant of the skins; the skins have an electrical thickness of one quarter wavelength and give zero reflection. There is therefore no restriction on the thickness of the core. Such a sandwich can be constructed by using an expanded dielectric for the faces and full-density high-strength material for the core. Alternatively, high-strength material of dielectric constant $3\epsilon_0$ to $4.5\epsilon_0$ can be used for the faces and special material of high dielectric constant for the core. This type of construction has possibilities for the fabrication of streamlined radomes but is of little practical importance for normal-incidence application.

The third type of sandwich construction utilizes a core of a full-density or nearly full-density thermoplastic having a thickness of slightly less than a half wavelength. Materials that can be used include polystyrene ($\epsilon/\epsilon_0 = 2.56$), polymethyl methacrylate ($\epsilon/\epsilon_0 = 2.66$), and microporous expanded polystyrene obtained by molding polystyrene fibers ($\epsilon/\epsilon_0 \approx 2.2$ for a specific gravity of 0.85). The flexural strength of half-wavelength thicknesses of such materials is somewhat limited, especially in the 1-cm band. An appreciable improvement in flexural strength and stiffness is obtained by cementing a single layer of glass fabric to each surface of the thermoplastic sheet, the thickness of which is suitably reduced below the half-wavelength value so that the sandwich as a whole has zero reflection. This type of construction is of value chiefly for streamlined radomes.

Symmetrical Sandwiches with Cores of Low Dielectric Constant.—We consider first the effect of the dielectric constant of the core and the thickness of the skin on the optimum core thickness for a symmetrical lossless sandwich with skins of given dielectric constant. Curves that are plotted in Fig. 10·10 show the ratio of the core thickness to free-space wavelength against the ratio of skin thickness to free-space wavelength for values of α_c from 1.0 to 2.0 and for a value of α_s of 4.0. They have been computed from Eq. (19). For vanishing skin thickness, the core thickness in Fig. 10·10 is seen to approach the half-wavelength value $\lambda_0/2\sqrt{\alpha_c}$, except when the core dielectric constant is equal to unity, in which case the core thickness approaches the quarter-wavelength value $\lambda_0/4\sqrt{\alpha_c}$. Thus, except when α_c equals unity (double-wall case), a sandwich with very thin skins behaves like a half-wavelength thickness of core material. On the other hand, when the skins are relatively thick (say $d/\lambda_0 = 0.05$), the optimum thickness of the core of a sandwich is not markedly affected by the dielectric constant of the core.

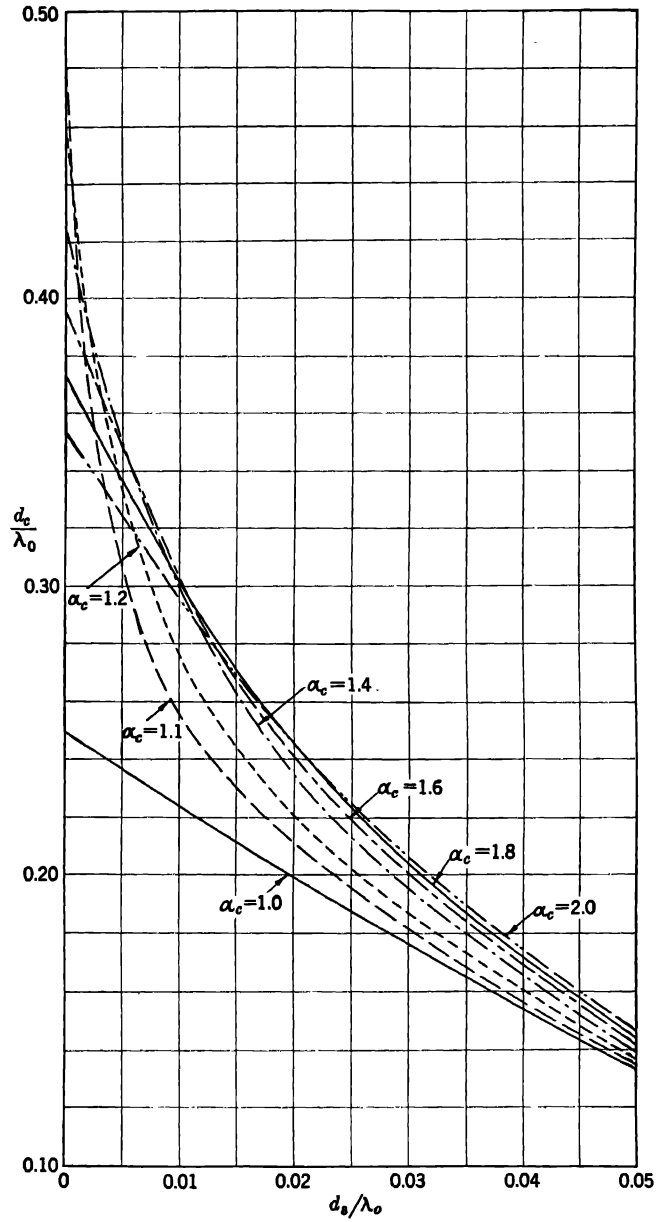

FIG. 10·10.—Optimum core thickness for a symmetrical normal-incidence sandwich radome. The dielectric constant of the skin is $4\epsilon_0$.

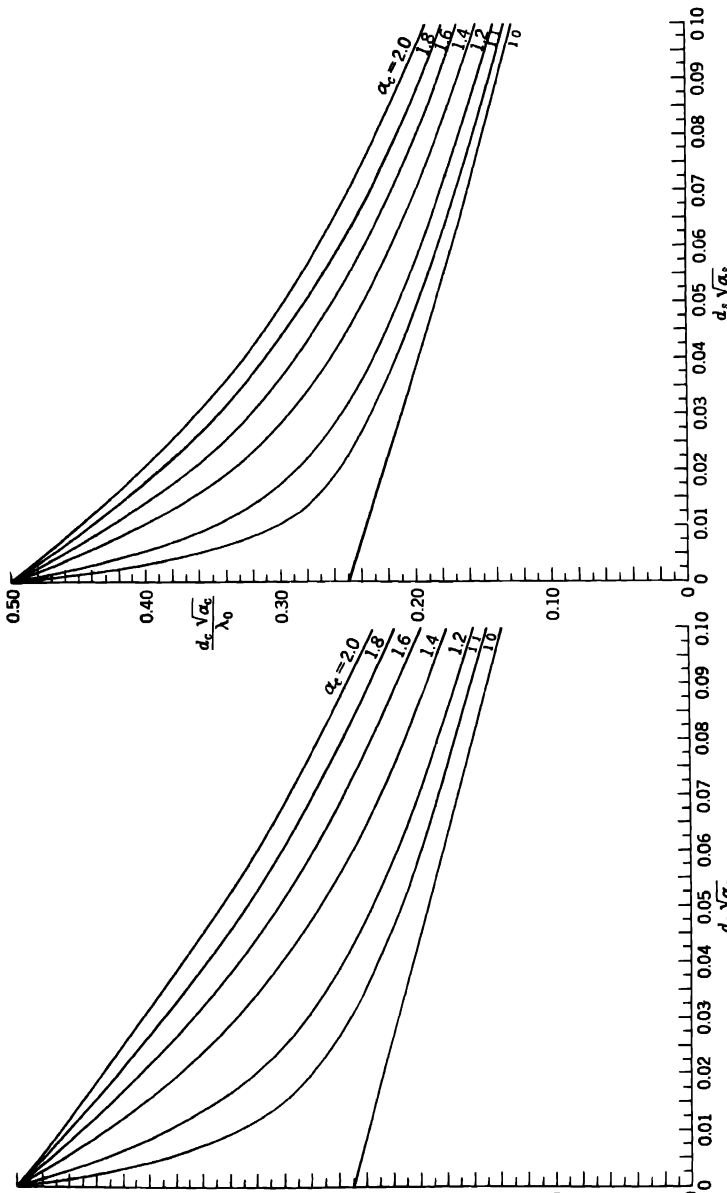

FIG. 10·11.—Optimum core thickness for a symmetrical normal-incidence sandwich radome. The dielectric constant of the skin is $3\epsilon_0$

FIG. 10·12.—Optimum core thickness for a symmetrical normal-incidence sandwich radome. The dielectric constant of the skin is $5\epsilon_0$.

Figure 10.10 also shows that when the skins are thin, the core thickness for zero reflection varies critically with skin thickness and also with the dielectric constant of the core; the reflection, however, does not usually vary critically with the core thickness. The requisite tolerances of spacing are therefore not difficult to maintain in production. Low-density foam materials are variable in density and dielectric constant, but this variability is not serious for the type of construction under consideration. On account of the wide tolerances, it is possible to design a sandwich construction that is nearly a first-order sandwich at a given wavelength and, at the same time, a second- or higher-order sandwich at some shorter wavelength.

In Figs. 10·11 and 10·12 electrical core thickness $d_c\sqrt{\alpha_c}/\lambda_0$ is plotted against electrical skin thickness $d_s\sqrt{\alpha_s}/\lambda_0$ for values of α_s of 3 and 5, respectively. The core spacing for zero reflection at normal incidence for any given skin thickness can be obtained by interpolation from Figs. 10·10 to 10·12 when the dielectric constant of the skin lies between $3\epsilon_0$ and $5\epsilon_0$.

When the skins are very thin compared with the wavelength, Eq. (19) reduces to

$$(d_c)_N = \frac{N\lambda_0}{2\sqrt{\alpha_c}} - 2d_s\left(\frac{\alpha_s - 1}{\alpha_c - 1}\right). \tag{25}$$

Hence, for very thin skins, we see that the difference between the half-wavelength thickness and the actual thickness of the core is approximately proportional to the thickness of the skins, other things being equal. Equation (25) is equivalent to replacing the curves of Figs. 10·11 and 10·12 by the tangent at the axis of ordinates.

Actual and Effective Skin Thickness.—So far we have considered only the skin and core of a sandwich. In practice there is a third component to be taken into consideration, namely, the bond between the skin and core. In the type of construction so far considered, in which the core is a low-density foam material, the nature of the bond is in general as indicated in Fig. 10·13. Immediately under the skin of dielectric constant $\alpha_s\epsilon_0$ is found a layer of adhesive; then a layer consisting of core material, with the pores more or less filled by cement; and next, core material of dielectric constant $\alpha_c\epsilon_0$. Presumably, the behavior of such a sandwich would be different from one with the same skin thickness and core thickness but without cement.

In an actual sandwich there are two quantities that can be measured easily, namely, the over-all thickness h and the power-reflection coefficient $|R|^2$ at normal incidence. Since reflection does not depend very much upon the loss tangents of the skin and core if these loss tangents are small, for any given skin and core dielectric constants we can compute

the reflection $|R|^2$ as a function of skin thickness d_s and over-all thickness h. For example, in Fig. 10·14 contours of constant power-reflection coefficient (at normal incidence) are plotted as a function of h and d_s for a skin dielectric constant of $3.7\epsilon_0$ and for a core dielectric constant of $1.4\epsilon_0$. If the skin thickness of a sandwich is obtained from measured values of h and $|R|^2$, using such a chart for the appropriate values of α_s and α_c, it is

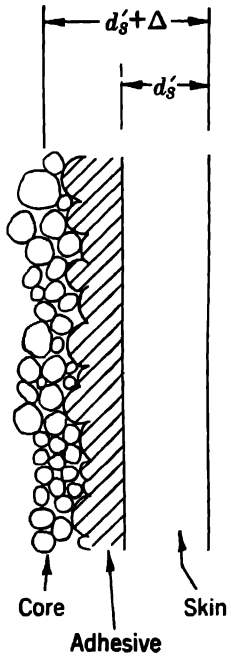

FIG. 10·13.—Actual and effective skin thickness.

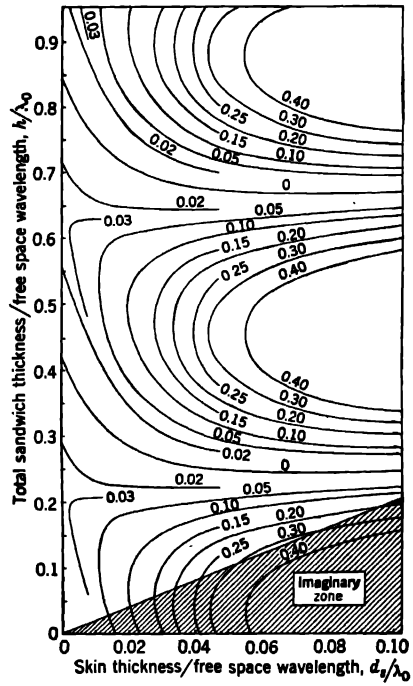

FIG. 10·14.—Power reflection as a function of sandwich thickness (h) and skin thickness (d_s); $\alpha_s = 3.7$, $\alpha_c = 1.4$.

found that this derived skin thickness is greater than the physical thickness of skin because of the adhesive.[1] When there is a heavy glue line of adhesive of high dielectric constant and there are large pores in the core, the *effective* skin thickness d_s determined in this way may easily be double the *actual* skin thickness denoted by d_s'. The difference $d_s - d_s' = \Delta$ may be called the glue-line thickness.

Figure 10·14 shows, however, that neglect of the effect of adhesive should not result in more than a small reflection by a sandwich designed to have zero reflection at normal incidence.

[1] E. R. Steele, "Some Electrical Aspects of Microwave Sandwich Radome Design," RL Report No. 483-16, May 1945.

Where the reflection at normal incidence has to be held closely to zero or any other special value, it is necessary to estimate the value of d_s' for the combination of materials and the technique of fabrication to be used. This is best done by fabricating a sandwich with the proposed construction but with its over-all thickness in the region where $|R|^2$ varies most critically with d_s, that is, in the region where the reflection contours are approximately vertical. For $\alpha_s = 3.7$, $\alpha_c = 1.4$, and

$$\frac{d_s}{\lambda_0} = 0.04,$$

Fig. 10·14 shows that h/λ_0 should be about 0.45 in order to get the most accurate determination of the effective skin thickness from measurements of $|R|^2$ and h.

It is apparent from Fig. 10·14 that if the electrical thickness of the skin $d_s \sqrt{\alpha_s}/\lambda_0$ is small at any particular wavelength λ_0, then the core thickness may have values very much less than that corresponding to zero reflection, without resulting in very much reflection of the sandwich. This core thickness may correspond to zero reflection at some shorter wavelength. This has a practical consequence, as shown by the following example. If a first-order sandwich radome that is constructed with moderately thick skins and the correct core thickness for the 3-cm wavelength is used at 10 cm, say, the skins are much thinner electrically. If $|\rho|$ is small at the longer wavelength, the reflection of the sandwich as a whole at the longer wavelength is likely to be small. Similar remarks apply to a sandwich radome designed to have zero reflection at normal incidence at a wavelength of 1 cm that is used in the 3-cm band.

10·7. Sandwiches with Low-loss Skins and Cores.—The results for single homogeneous sheets show that it is undesirable to use materials with large values of loss tangent (0.1 or greater) for microwave radomes because the loss in transmission becomes excessive. The same is obviously true for sandwiches.[1] If the squares of the loss tangents of the materials are much smaller than unity, the methods of calculation in Sec. 10·3 can be used. To this degree of approximation, all interface reflection coefficients are unchanged in absolute value, but the phase shift on reflection is changed [*cf.* Eq. (12·49)].

The optimum core thickness of a sandwich with low-loss skins and core for maximum transmission is not the same as for minimum reflection; the thicknesses, however, are almost the same; whenever such a sandwich is spaced for maximum transmission, the reflection is very small. The core thickness for maximum transmission of a low-loss sandwich is not quite the same as for an equivalent lossless sandwich [Eq. (19)]. The

[1] For a discussion of sandwiches with low-loss skins and cores, see Yael Dowker, "Transmission of Lossy Sandwiches," RL Report No. 483-22, January 1946.

difference, however, is slight and is usually much less than the tolerance in core thickness; hence Eq. (19) may be used to design a normal-incidence sandwich radome with low-loss skins and core.

Let the power-transmission coefficient of a lossless sandwich of arbitrary spacing be given by $|T|_0^2$ and the power-transmission coefficient by $|T|_1^2$ for a sandwich that is identical except that the skins and core are of low-loss materials. In both cases the specific dielectric constants of the skins and core will be taken to be α_s and α_c, respectively; in the second case the loss tangents of the skins and core will be represented respectively by tan δ_s and tan δ_c. We then have to a first approximation [see Eq. (12·115)]

$$\frac{|T|_0^2 - |T|_1^2}{|T|_0^2} \approx 4Q_s + 2Q_c, \tag{26}$$

in which

$$Q_s = \frac{\pi d_s \sqrt{\alpha_s}}{\lambda_0} \tan \delta_s,$$

$$Q_c = \frac{\pi d_c \sqrt{\alpha_c}}{\lambda_0} \tan \delta_c.$$

When the skins are thin, the greater part of the absorption is likely to take place in the considerably thicker core. The thickness of the core is then close to a half wavelength in the material, $\lambda_0/2\sqrt{\alpha_c}$, and the fractional absorption $2Q_c$ equals approximately π tan δ_c [*cf.* Eq. (18)].

From the discussion of actual and effective skin thickness in Sec. 10·6, it can be seen that when the bond between the skin and core is a heavy glue line of cement with a high dielectric constant, such as resorcinol-formaldehyde, it has the effect of an additional thickness of skin. Unless this additional thickness is allowed for in the spacing of the sandwich, increased reflection will result. Even in extreme cases, however, the reflected power is relatively slight and may be about 2 per cent of the incident power. Nevertheless, with many such sandwich constructions using cold-setting or warm-setting resorcinol-formaldehyde cements, the transmission may be as low as 80 per cent of the incident power; hence, nearly 20 per cent of the incident power is absorbed in the sandwich. From Eq. (26) it appears that only a small part of this loss in transmission can be attributed to absorption in the skins and core; the cement must be the cause of the high absorption. Thus, for electrical reasons, many cements that are extremely effective mechanically when applied in sufficient amount cannot be used.

On the other hand, sandwiches bonded with rubber-base cements of low loss and low dielectric constant have almost zero reflection at normal incidence when designed with optimum spacing. The absorption is very small, since the transmission coefficient of the sandwich is nearly unity;

such cements are thus adequate electrically. These cements, however, do not give an adequate mechanical bond between the skins and core.

Techniques that have been developed and put into practice give results that are satisfactory both electrically and mechanically; they involve use of the laminating resin of the skins as the adhesive. The absorption of sandwiches made by this technique is but little greater than the absorption due to the skins and core alone, and the bond between the skin and core is excellent. These techniques are described in Sec. 13·6.

CHAPTER 11

ELECTRICAL DESIGN OF STREAMLINED RADOMES

By H. Leaderman, W. Ellis, and L. A. Turner[1]

11·1. Introduction.—Chapter 10 deals with radomes for use where the radiation falls normally or nearly normally upon the radome wall. These include all radomes of ground-based and shipborne radar sets and some airborne radomes as well. It is frequently necessary, however, and almost always desirable to streamline the radome of a radar set installed in a speedy aircraft. A normal-incidence design, such as shown at *F* in Fig. 9·5, can introduce drag that cannot be tolerated. For this reason, the horizontal cross section of an airborne beacon housing must be streamlined rather than circular, even though a very large lateral lift and torque on such a streamlined beacon housing is to be expected in sideslips and rolls. Streamlined radomes that are a part of the nose of the fuselage, as at *E* in Fig. 9·5, will be subjected to very large aerodynamic loads (see Sec. 14·1).

The electrical requirements are somewhat different from those for a normal-incidence radome (see Sec. 9·5) because the angle of incidence of the radiation on the wall of the streamlined radome may vary over a large range for any particular position of the scanner and the angle of incidence at any particular point of the radome is likely to change with the scan. Usually, it is not practical to vary the wall design from point to point so that it can have the optimum construction for the angle of incidence at that point or, with scanning antennas, for the range of angles of incidence. The problem is to design a streamlined radome that will have a wall of uniform thickness and be satisfactory electrically as well as aerodynamically and mechanically.

The range of angles of incidence is usually from close to 0° up to 70° or more. The linearly polarized radiation falling at a high angle of incidence upon the radome wall may have its polarization make any angle with the plane of incidence. Since only a small part of the energy is reflected back to the antenna, it is no longer necessary that the reflection at normal incidence be reduced to a small value for the purpose of avoiding pulling. It is desirable, however, that the reflection over a

[1] The parts of Sec. 11·12 that describe the experimental apparatus and method are by W. Ellis; Sec. 11·13 is by L. A. Turner; the major part of the chapter is by H. Leaderman.

large range of angles of incidence be minimized in order to obtain maximum transmission of power and to reduce the possibility of distortion of the pattern by parasitic reflections. This requirement must usually be satisfied over a range of frequencies; that is, the radome must be *broad-banded.*

The results for reflection and transmission of radiation incident at an arbitrary angle of incidence θ_0 can be obtained very simply from those

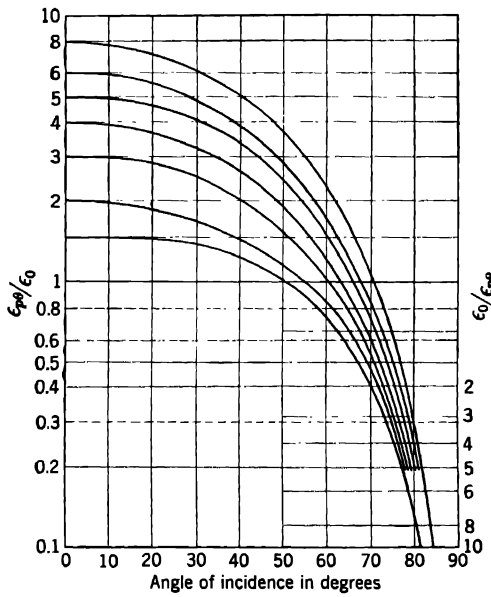

FIG. 11·1.—Effective dielectric constants (parallel polarization).

already given in Chap. 10 for waves incident normally. It is shown in Sec. 12·4 that the expression for the reflection coefficient for normal incidence can be used, provided that in place of the ratios of indices of refraction or specific dielectric constants there be substituted equivalent or fictitious values that depend on the angle of incidence. For parallel polarized waves (electric vector in the plane of incidence) the effective dielectric constant to be used, represented by $\epsilon_{p\theta}$, is given by

$$\frac{\epsilon_{p\theta}}{\epsilon_0} = \frac{\left(\frac{\epsilon_b}{\epsilon_a}\right)^2}{1 + \frac{\left(\frac{\epsilon_b}{\epsilon_a}\right) - 1}{\cos^2 \theta_0}}, \tag{1}$$

[see Eq. (12·43*b*)]. The ratio $\epsilon_{p\theta}/\epsilon_0$ is to be used for a wave incident at angle θ_0 in place of the ratio of the actual dielectric constants of the two mediums, ϵ_b/ϵ_a. Similarly, the appropriate value to be used for perpendicularly polarized radiation (electric vector perpendicular to the plane of incidence) is

$$\frac{\epsilon_{s\theta}}{\epsilon_0} = 1 + \frac{\frac{\epsilon_b}{\epsilon_a} - 1}{\cos^2 \theta_0} \tag{2}$$

[see Eq. (12·44*b*)]. Figures 11·1 and 11·2 show $\epsilon_{p\theta}/\epsilon_0$ and $\epsilon_{s\theta}/\epsilon_0$ as a function of θ_0 for different values of ϵ_b/ϵ_a. Figure 11·3 shows the amplitude-

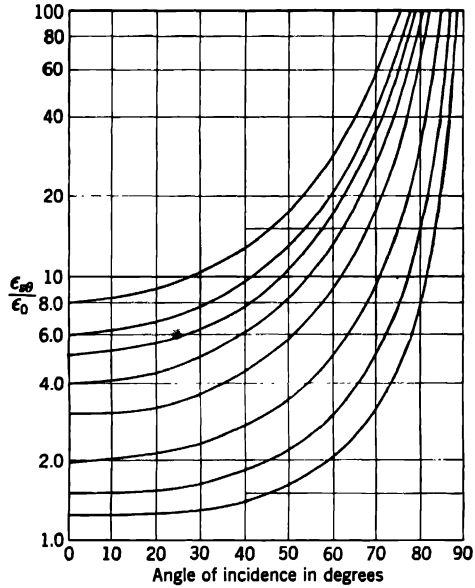

FIG. 11·2.—Effective dielectric constants (perpendicular polarization).

reflection coefficient as a function of the effective dielectric constant. It is computed from Eq. (12·39) and is of aid in making further computations.

If either $\epsilon_{p\theta}/\epsilon_0$ or $\epsilon_{s\theta}/\epsilon_0$ becomes equal to 1, the reflection coefficient for the correspondingly polarized radiation at the interface will become equal to zero [*cf.* Eqs. (12·39*a*) and (12·39*b*)]. It is apparent from Eq. (2) and Fig. 11·2 that there is no angle for which $\sqrt{\epsilon_{s\theta}/\epsilon_0} = 1$ if $\epsilon_b/\epsilon_a > 1$; there is, therefore, no angle of incidence for which the reflection of perpendicularly polarized radiation at the surface of a sheet of material in air drops to zero. If we set $\epsilon_{p\theta}/\epsilon_0 = 1$, however, a value for θ that is designated as θ_B, is given by

$$\left.\begin{aligned} \tan \theta_B &= \sqrt{\frac{\epsilon_b}{\epsilon_a}} \\ \text{or} \qquad \theta_B &= \tan^{-1} \sqrt{\frac{\epsilon_b}{\epsilon_a}}. \end{aligned}\right\} \tag{3}$$

This familiar result is known as Brewster's law, and θ_B is known as the Brewster angle. Parallel polarized radiation incident at angle θ_B is not reflected at all.

Comparison of the variation of the power-reflection coefficient for parallel polarized radiation $|r_{(Hp)ab}|^2$ with that for perpendicularly polar-

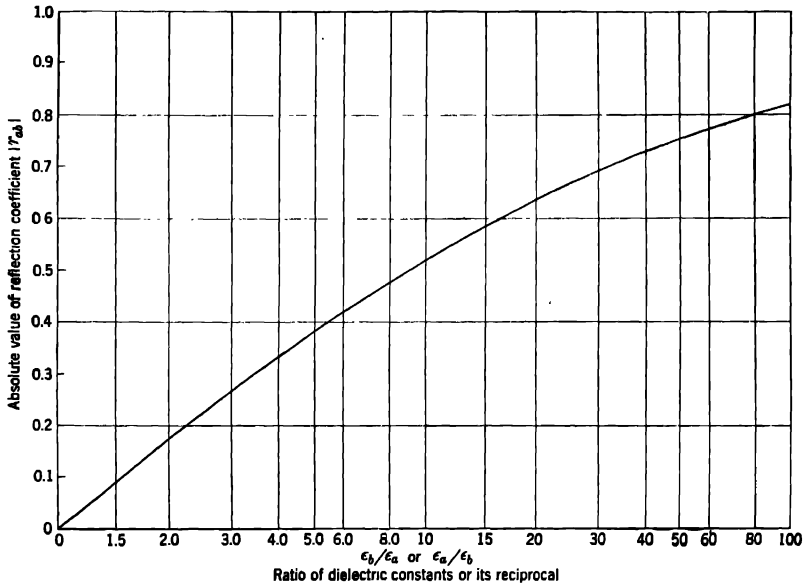

FIG. 11·3.—Amplitude-reflection coefficients.

ized radiation $|r_{(Es)ab}|^2$ as θ varies from 0° to 90° is instructive. Where $n_b^* = \sqrt{\epsilon_b/\epsilon_0}$ is real and $n_a^* = 1$ (air), both $r_{(Hp)ab}$ and $r_{(Es)ab}$ are real and there is no longer any distinction between the squares of the absolute magnitudes and the squares of the quantities themselves. The quantity $|r_{(Hp)ab}|^2$ starts at $\left(\dfrac{\sqrt{\epsilon_b/\epsilon_0} - 1}{\sqrt{\epsilon_b/\epsilon_0} + 1}\right)^2$ for $\theta = 0$, drops to zero for

$$\theta_B = \tan^{-1} \sqrt{\frac{\epsilon_b}{\epsilon_0}} \text{ (Brewster angle)},$$

and then increases rapidly to a value of unity for $\theta = 90°$. The quantity

$|r_{(E\theta)ab}|^2$ begins at $\left(\frac{\sqrt{\epsilon_b/\epsilon_0}-1}{\sqrt{\epsilon_b/\epsilon_0}+1}\right)^2$, rises slowly at first, and then rises more rapidly to unity for $\theta = 90°$. Curves for $\epsilon_b/\epsilon_0 = 4$ are plotted in Fig. 11·4. They are typical. It is apparent that for all angles of incidence, parallel-polarized radiation is reflected to a lesser degree than is perpendicularly polarized radiation.

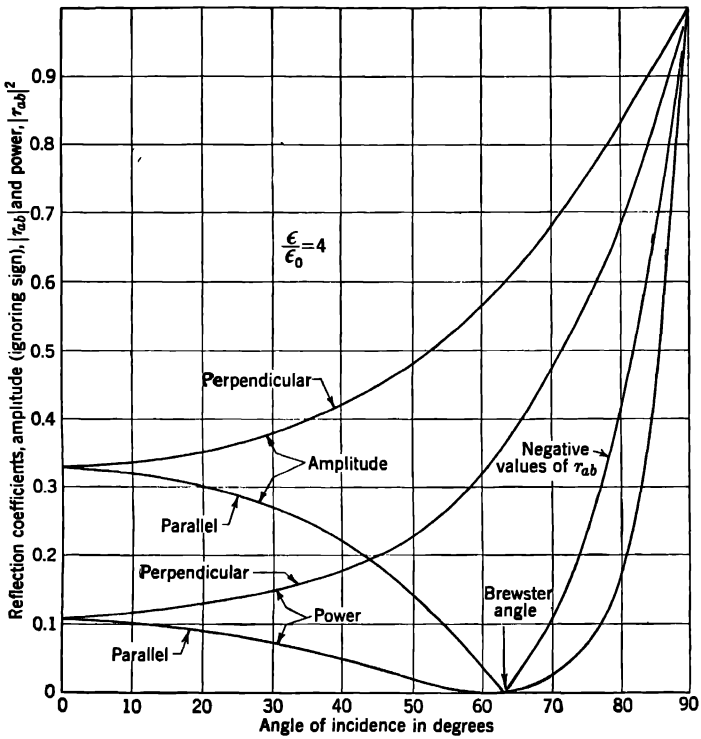

FIG. 11·4.—Reflection at oblique incidence.

The design of a streamlined radome depends, therefore, upon the plane of polarization of the radiation that is to be incident on the wall. Because perpendicularly polarized radiation is always reflected more than parallel-polarized radiation, it is more difficult to design a radome that will give good transmission of perpendicularly polarized waves over a wide range of angles of incidence. For the sandwich construction with low-density core poorer electrical behavior is obtained with thicker skins, skins of higher dielectric constant, and higher-order spacing, i.e., with all the features of design that lead to better mechanical properties. If satisfactory transmission of perpendicularly polarized radiation is to be

obtained, a streamlined sandwich radome must be designed with not too great a factor of safety for strength. When the radiation is parallel polarized, the design for normal incidence is often satisfactory up to fairly high angles; extremely good transmission is frequently obtained from 0° up to high angles with single-wall radomes having the thickness of approximately a full wavelength and with sandwiches of modified second-order spacing.

Actually, the polarization of the wave may be complex, or it may be plane, with the plane of polarization making an arbitrary angle with the plane of incidence. In either case, the radiation can be analyzed into parallel- and perpendicularly polarized components to be treated separately. It must be remembered, however, that they will not necessarily remain completely separate in a radar. When the plane of polarization makes an arbitrary angle with the plane of incidence, components of both polarizations will be emitted and returned as echoes, to be recombined by the receiving antenna. The targets may have depolarizing properties, giving echoes polarized in the plane at right angles to that of the transmitted wave. Furthermore, a relative displacement of phase of the two components may be produced in the radome (see Sec. 11·13).

In dealing with sheets of material of finite thickness, it is also necessary to take account of the change of electrical thickness that results from change of the angle of incidence. In Sec. 12·5, it is shown that the general expression for ϕ, which is 2π times the electrical thickness, is

$$\phi = \frac{2\pi d}{\lambda_0} \sqrt{\frac{\epsilon'}{\epsilon_0} - \sin^2 \theta_0} \tag{4}$$

in a medium having a real dielectric constant ϵ' and a thickness d [*cf.* Eq. (12·71*b*)]. The angle θ_0 is the angle of incidence of an incident wave assumed to be in a medium for which $\epsilon'/\epsilon_0 = 1$ and λ_0 is the wavelength in that medium. Equation (4) shows that the effective thickness of a sheet decreases with increasing angle of incidence.

For low-loss material, the factor A that expresses the decrease of amplitude of the wave as it travels once through the sheet [*cf.* Eq. (12·71*a*)] becomes

$$A = e^{-\frac{\pi d}{\lambda_0} \frac{\left(\frac{\epsilon'}{\epsilon_0}\right) \tan \delta}{\sqrt{\frac{\epsilon'}{\epsilon_0} - \sin^2 \theta}}} \tag{5}$$

From this it appears that the attenuation becomes greater with increasing angle of incidence.

The behavior of sheets and sandwiches with respect to waves incident at an arbitrary angle can now be deduced if the quantities calculated from Eqs. (1), (2), (4), and (5) are used in the various expressions of Chap. 10, applied there to waves that are incident normally.

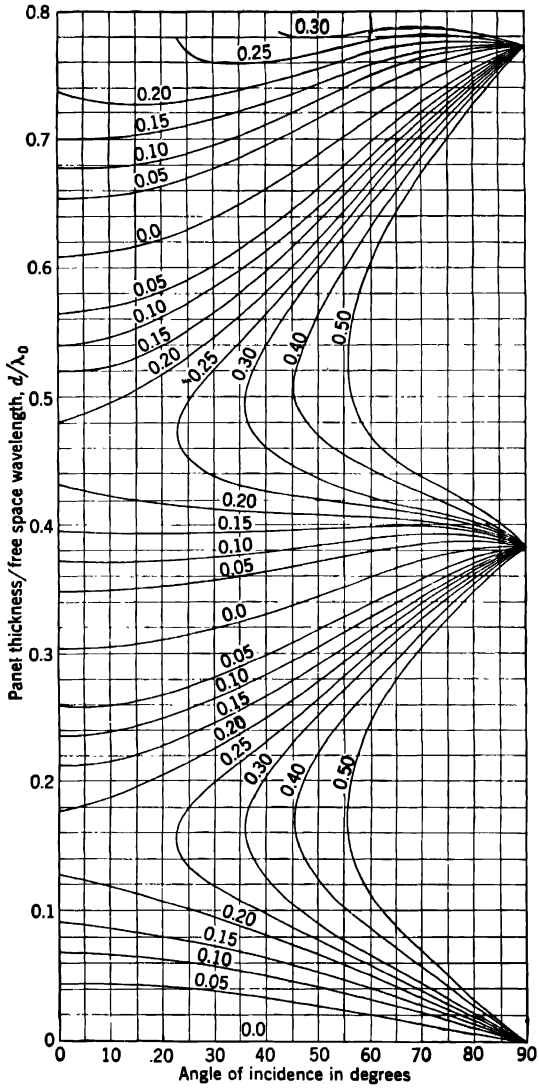

FIG. 11·5.—Contours of constant power reflection (perpendicular polarization, dielectric constant = $2.7\epsilon_0$).

11·2. Plane Lossless Sheets, Arbitrary Incidence.—At normal incidence, the reflection of a low-loss sheet is almost the same as that of an equivalent lossless sheet, but the transmission is less; the same is true for arbitrary incidence. As with normal incidence, the first problem is to

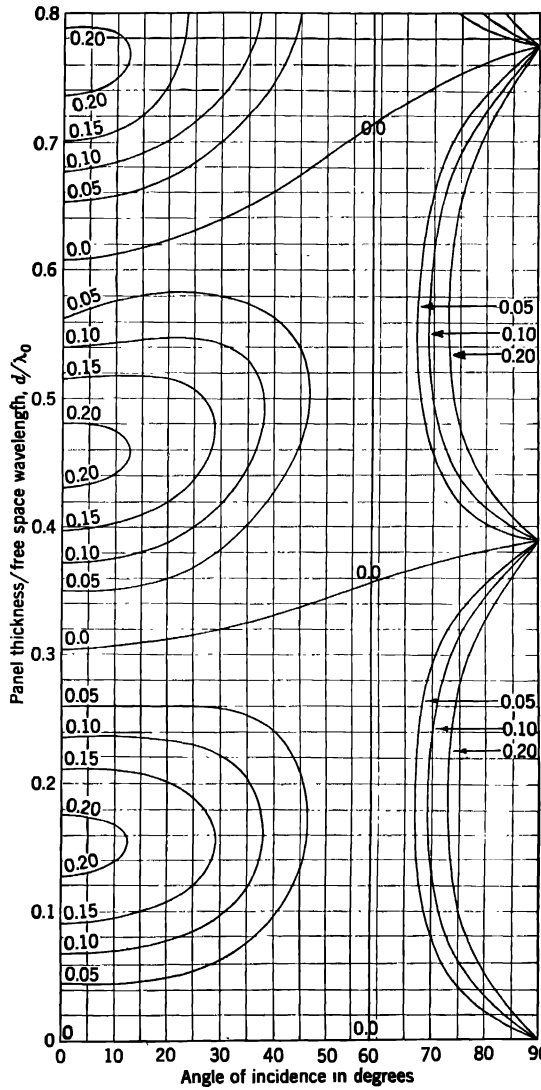

FIG. 11·6.—Contours of constant power reflection (parallel polarization, dielectric constant = $2.7\epsilon_0$).

find how transmission loss due to reflection can be minimized; the additional transmission loss due to absorption by low-loss materials can be considered later.

First, it is desirable to examine the reflection of plane sheets of arbi-

trary thickness over the range of angles of incidence from 0° to 90° for both polarizations. It is useful to plot the panel thickness against the angle of incidence for various percentages of reflected power[1] for every value of the dielectric constant that is of interest. Figures 11·5 and 11·7 show such reflection contours for materials of dielectric constant $2.7\epsilon_0$ and $10\epsilon_0$, respectively.[2] These are for perpendicular polarization. Figures 11·6 and 11·8 present the corresponding results for parallel polarization.

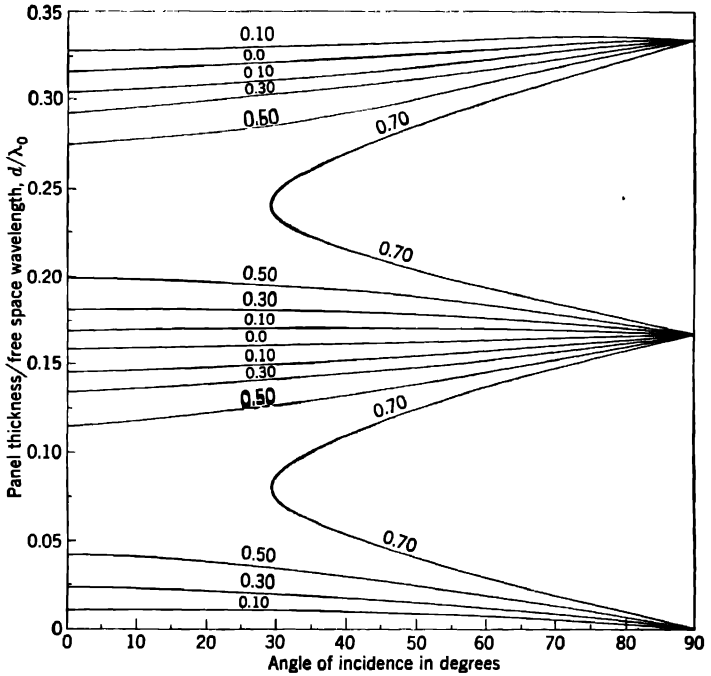

FIG. 11·7.—Contours of constant power reflection (perpendicular polarization, dielectric constant = $10\epsilon_0$).

The charts can be computed from those previously given. The equivalent dielectric constants for different angles of incidence can be obtained from Figs. 11·1 and 11·2 (pages 287 and 288), and the corresponding values of the interface reflection coefficient r, taken from Fig. 11·3 (page 289). Figure 10·8 (page 275) can now be used to find the electrical thickness corresponding to any such values of r and $|R|^2$ that are of inter-

[1] J. B. Birks, "Dielectric Transmission and Scanner Nacelle Design," TRE Report No. T1677.

[2] For such contour charts covering a range of dielectric constants $1.2\epsilon_0$ to $10\epsilon_0$ see E. M. Everhart, "Radome Wall Reflections at Variable Angles of Incidence," RL Report No. 483-20, January 1946.

est. The value of r for the interface here plays the same role as does $|\rho|$ for the half sandwich in the computations for which Fig. 10·8 was devised while the abscissa scale gives values of $\phi/2\pi$ from which d may be computed [Eq. (4)]. The values of the electrical thickness thus obtained are correct in the neighborhood of zero thickness, so the corresponding contours are called "zero-order contours." Formally, they can be

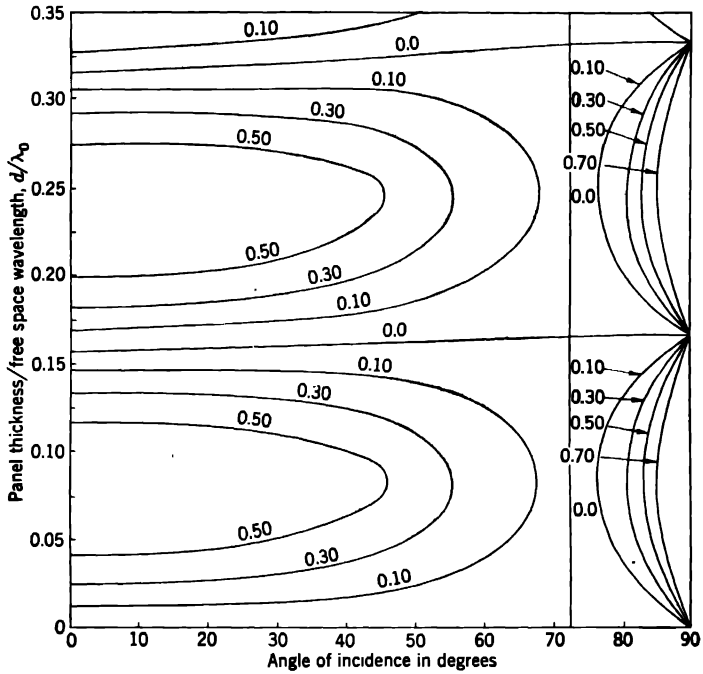

FIG. 11·8.—Contours of constant power reflection (parallel polarization, dielectric constant = $10\epsilon_0$).

extended to negative values of d with symmetry about the axis for $d = 0$; these hypothetical negative branches are of help in developing the charts further. The first-order contours are obtained from those of zero order by adding to every ordinate the appropriate value of the thickness of what is called the modified half-wavelength panel $\dfrac{\lambda}{2\sqrt{\epsilon'/\epsilon_0 - \sin^2\theta_0}}$, derived from Eq. (4). It is the thickness of the sheet that gives the value of π to the angle ϕ of Eq. (4) to be used in Eq. (10·1) and, therefore, zero reflection of radiation incident at angle θ_0. For second-order contours twice this thickness is to be added, and so on for higher orders.

While the contour charts of reflection (Figs. 11·5 to 11·8 inclusive)

are seen to be basically similar, characteristic differences will be noted. For parallel polarization, the reflection goes to zero for the Brewster angle $\tan^{-1}\sqrt{\epsilon'/\epsilon_0}$. Its values are 58.6° and 72.4° for $\epsilon'/\epsilon_0 = 2.7$ and 10, respectively. From the information presented in charts of this nature, design procedures for streamlined radomes consisting of a single homogeneous low-loss dielectric sheet can now be developed.

11·3. Lossless Panels at Perpendicular Polarization. *Panels of Approximate Half-wavelength Thickness.*—Figure 11·9 shows the reflection

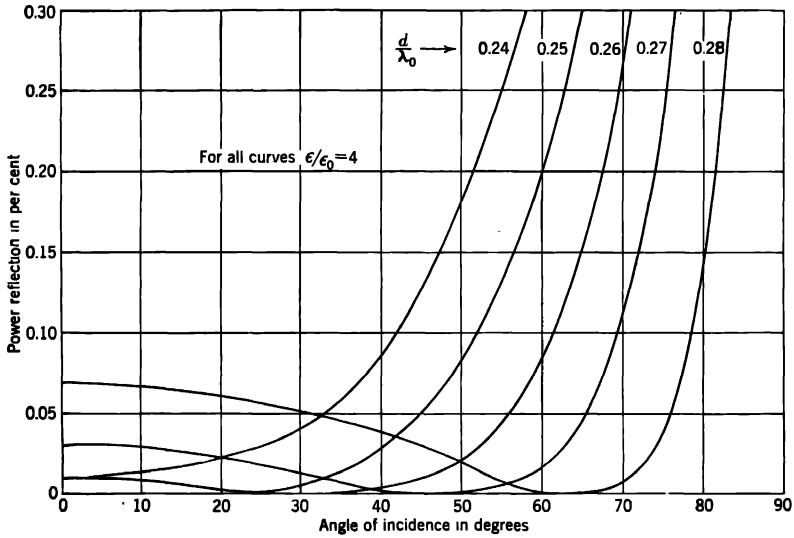

FIG. 11·9.—Power reflection of plane panels (perpendicular polarization).

coefficient $|R|^2$ as a function of the angle of incidence for plane panels of dielectric constant $4\epsilon_0$ and of approximate half-wavelength thickness; the polarization is perpendicular to the plane of incidence. Since $\epsilon' = 4\epsilon_0$, the index of refraction equals 2 and the wavelength in the panel is half that in air. The thickness of the half-wavelength panel is thus $0.25\lambda_0$. For this panel the reflection first increases slowly with angle of incidence; at 30° incidence it is still small (less than 1 per cent in power), but it begins to increase rapidly thereafter and is large at 60° incidence (20 per cent in power).

If next we consider the reflection from a panel that is 4 per cent thicker than the previous one ($d = 0.26\lambda_0$), we find that the reflection at normal incidence is 1 per cent in power. The reflection falls slowly with increase of angle of incidence and is zero at 33° incidence; thereafter it rises rapidly. We note that for this thicker panel the reflection is the same at 45° incidence as at 0° incidence and conclude that to minimize reflection loss

at perpendicular polarization over a range of angles of incidence from 0° to 45° with a panel of dielectric constant $4\epsilon_0$, we use a panel of such thickness that reflection is zero at 33° incidence. The maximum reflection over the range is 1 per cent in power.

Similarly, to minimize reflection loss over a range of angles of incidence from 0° to 63° we choose a panel whose thickness d is 8 per cent greater than the half-wavelength thickness ($d = 0.27\lambda_0$). The maximum reflection over the range of angles of incidence is now 3 per cent in power, and the reflection of the panel is zero for 50° incidence. For a thickness that is 12 per cent greater than the half-wavelength thickness ($d = 0.28\lambda_0$) the reflection is less than 7 per cent in power over a range of angles of incidence from 0° to 77°. We see from Fig. 11·9 that for a thickness less than the half-wavelength thickness (for example, $d = 0.24\lambda_0$), the reflection is

TABLE 11·1.—OPTIMUM THICKNESSES AND MAXIMUM POWER-REFLECTION COEFFICIENTS OF PLANE PANELS AT PERPENDICULAR POLARIZATION

Dielectric constant, ϵ	Range of angles of incidence, degrees	Ratio of optimum thickness to full-wavelength thickness	Maximum power-reflection coefficient $\lvert R\rvert^2$ corresponding to optimum thickness and range of angles of incidence
$2\epsilon_0$	0–40	0.535	0.006
	0–60	0.590	0.032
	0–70	0.630	0.058
	0–80	0.672	0.084
	20–60	0.594	0.032
	40–80	0.673	0.062
$4\epsilon_0$	0–40	0.516	0.006
	0–60	0.536	0.026
	0–70	0.551	0.048
	0–80	0.565	0.084
	20–60	0.538	0.023
	40–80	0.566	0.053

greater than for the half-wavelength panel. This is obviously true for all values of the dielectric constant, since a modified half-wavelength panel is always thicker than a true half-wavelength panel [see Eq. (4)]. For $\theta > 0$ the radical is less than $\sqrt{\epsilon'/\epsilon_0}$, so d must be increased to get $\phi = \pi$.

We will assume that the optimum wall thickness for a radome is one in which the greatest reflection for any angle in a given range of angles of incidence is reduced to a minimum value by suitable choice of wall thickness. We shall refer to this value of reflection as the *minimized maximum* reflection; *other things being equal,* the construction with the lowest minimized maximum reflection is likely to be the preferred one.

Table 11·1 gives the optimum panel thickness in terms of the half-

wavelength thickness and the corresponding values of the maximum power-reflection coefficient for ϵ equal to $2\epsilon_0$ and $4\epsilon_0$, respectively.[1] Comparison of the first four entries in each section of the above table shows that increase in the range of angle of incidence increases the maximum power lost by reflection. When the first entry is compared with the last two entries in each section of the table, it is seen that the maximum reflection loss increases as a given range of angles of incidence is moved toward higher angles of incidence.

Results for the behavior of homogeneous plane sheets at perpendicular polarization can be summarized as follows:

1. The reflection of a sheet that is a half wavelength thick

$$\left(d = \frac{\lambda_0}{2\sqrt{\epsilon'/\epsilon_0}}\right)$$

   is small up to about 30° incidence but increases fairly rapidly thereafter.
2. The reflection of a full-wavelength sheet ($d = \lambda_0/\sqrt{\epsilon'/\epsilon_0}$) increases more rapidly with angle of incidence than the reflection of a half-wavelength sheet.
3. In order to minimize reflection loss over a given range of angles of incidence, the thickness should be somewhat greater than the half-wavelength thickness. With increasing angle of incidence, the reflection falls gradually from its value at the lower end of the range of angles of incidence, becomes zero, and then rises rapidly to its initial value at the upper end of the range. The angle of incidence corresponding to zero reflection lies nearer to the upper end of the range of angles of incidence than to the lower end.
4. The minimized maximum value of reflection loss depends upon the range of angles of incidence, being greater with greater range of angle.
5. The minimized maximum value of reflection loss for a given range of angles of incidence increases with the number of half-wavelengths in the sheet. This effect is less important with materials of higher dielectric constant. If $\epsilon' = 10\epsilon_0$, as in Fig. 11·7, a thickness that is a little greater than $\lambda_0/\sqrt{\epsilon'/\epsilon_0}$ can be used.

Tolerances for Modified Half-wavelength Panels.—It appears from Table 11·1 that if the thickness of a panel (or radome) is held exactly to a specified thickness, the reflection loss can be kept to a small value over the whole range of angles of incidence, even if the range of angles of incidence at perpendicular polarization is large. We know that in prac-

[1] R. M. Redheffer, "Reflection and Transmission of Single Plane Sheets," RL Report No. 483-4, July 1944.

tice, however, the wall thickness of a radome cannot be held exactly at a specified value; only by consideration of tolerances can the practical worth of any type of construction be evaluated.

As a basis for computing tolerances, assume that the power-reflection loss is to be less than 10 per cent over a range of angles of incidence from 0° to 70°. From a chart giving power-reflection contours for each dielectric constant, we can immediately obtain the range in allowable wall thicknesses and the tolerances consistent with this assumed maximum reflection of 10 per cent. The upper and lower limits of panel thickness d_1/λ_0, d_2/λ_0 and the tolerances $\pm(d_1 - d_2)/2\lambda_0$, expressed in terms of the free-space wavelength, are given for several values of dielectric constant in Table 11·2. It is seen that the tolerances are smallest at about the

TABLE 11·2.—PANEL THICKNESSES AND TOLERANCES FOR LESS THAN 10 PER CENT REFLECTION IN POWER, INCIDENCE RANGE 0°–70°, PERPENDICULAR POLARIZATION

$\frac{\epsilon}{\epsilon_0}$	$\frac{d_1}{\lambda_0}$	$\frac{d_2}{\lambda_0}$	$\frac{d_1 - d_2}{2\lambda_0}$
1.7	0.587	0.505	0.041
2.2	0.444	0 407	0.019
3.7	0.290	0 288	0.001
10.0	0.169	0.160	0.005
10.0	0.327*	0.326*	0.0005*

* Second order.

middle of the range of dielectric constant. Because the materials in this range are usually the easiest to control, both as to thickness and dielectric constant,[1] it is possible to construct panels and radome walls of approximate half-wavelength thickness to have less than 10 per cent reflection in power at perpendicular polarization over the range of angles of incidence from 0° to 70°; the tolerances are, however, such as to require considerable care in fabrication.

Reflection of Panels of Low Dielectric Constant.—It will be recalled that a radome wall can be designed to have a low reflection at normal incidence if a material of very low dielectric constant and of arbitrary thickness is used for the wall (Sec. 10·2). For example, if the material has a dielectric constant of $1.7\epsilon_0$, then the maximum reflection at normal incidence is only 6.7 per cent of the incident power; this is often small enough to be unimportant, especially if automatic frequency control, AFC, is used. For streamlined radomes, where radiation that is polarized perpendicular to the radome wall is incident upon it at a high angle of incidence, the effective dielectric constant becomes large and very large reflection coefficients may result; careful electrical design is then required. For

[1] For information concerning the variability in dielectric constant of radome materials, see Secs. 13·13 and 13·14.

example the effective dielectric constant $\epsilon_{s\theta}$ at normal incidence, corresponding to an angle of incidence of 70° at perpendicular polarization for a material of dielectric constant $1.7\epsilon_0$, is $7.0\epsilon_0$ (see Fig. 11·2). The maximum power-reflection coefficient corresponding to this dielectric constant is thus 0.56 [Eq. (10·6)]. It is clear that both the dielectric constant and the thickness of the wall of a radome made of material having a low dielectric constant must be controlled within close limits to avoid excessive reflections at high angles of incidence. Such control is not often possible with materials of low dielectric constant.

Reflection of Thin Panels.—A third method by which the reflection loss of normal-incidence radomes is kept low is the use of a wall whose thickness is small compared with the wavelength. Streamlined radomes for scanning antennas are of necessity usually large; for example, for an antenna that has a reflector with a diameter of 18 in., a radome about 4 ft long may be required. In general, the aerodynamic load on a radome of this type requires a strong and stiff construction such as is obtained with a modified half-wavelength or sandwich construction. On the other hand, linear-array antennas for microwave beacons in high-speed aircraft require much smaller streamlined housings; it is mechanically feasible to make such housings or radomes of dielectric materials that are thin compared with the wavelength. The cross section of such a radome may possibly be a streamlined section only about 2 in. wide and 8 in. long. Such beacon antennas must radiate in all directions in the azimuthal plane with the greatest uniformity possible; a poor streamlined housing can distort the pattern badly.

If the radiation from the linear array is polarized parallel to the axis of the array, the radiation falling on the streamlined housing at a high angle of incidence will be polarized perpendicular to the plane of incidence. In Figs. 11·5 and 11·7, it can be seen that at perpendicular polarization, for values of d that are not near the half-wavelength thickness, the reflection increases especially rapidly above 30° incidence. If, for example, we assume that the angle of incidence at perpendicular polarization varies from 0° to 70° in a linear-array housing and that the power-reflection coefficient must not exceed 0.10 for a material of dielectric constant $4\epsilon_0$, we find that d/λ_0 cannot exceed 0.012 for a thin-wall design. Thus, if λ_0 is 10 cm, d is 0.12 cm or 0.047 in.; mechanically, such a thickness might be satisfactory in some cases. On the other hand, if λ_0 is 3 cm, d becomes 0.036 cm or 0.014 in., a thickness that is clearly inadequate structurally. The solution of the problem of designing a streamlined housing for a 3-cm beacon with a vertically polarized antenna is discussed in Sec. 14·11.

11·4. Lossless Panels at Parallel Polarization. *Panels of Approximate Half-wavelength Thickness.*—A characteristic of parallel polarization

is that the reflection of a panel, irrespective of the thickness, is always zero when the angle of incidence is equal to Brewster's angle, $\tan^{-1}\sqrt{\epsilon'/\epsilon_0}$. At perpendicular polarization, the reflection of a panel of half-wavelength thickness increases rapidly with angle of incidence from its value of zero at normal incidence. At parallel polarization, however, the reflection of such a panel is less than 1 per cent for all angles up to Brewster's angle but increases rapidly at higher angles of incidence. In Fig. 11·10 the amplitude-reflection coefficient $|R|$ of a lossless half-wavelength sheet at

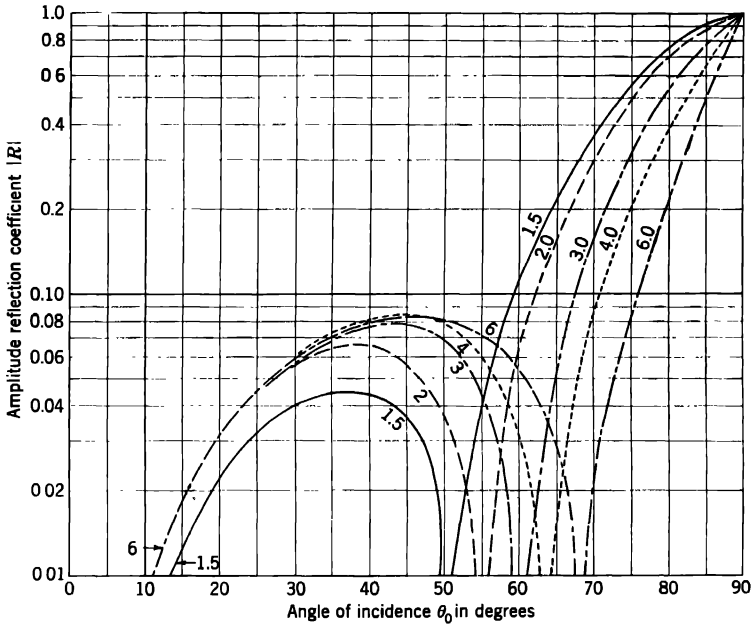

FIG. 11·10.—Amplitude-reflection coefficient of half-wavelength panels (parallel polarization).

parallel polarization is shown for different values of the dielectric constant. It is seen that for half-wavelength thickness, the reflection is satisfactorily low if the maximum angle of incidence is not much greater than Brewster's angle. Hence, for a panel of half-wavelength thickness, materials of higher dielectric constant are preferable because Brewster's angle is greater for these materials.

If the maximum angle of incidence is appreciably in excess of Brewster's angle, the reflection behavior can be improved by making the thickness slightly greater than the half-wavelength value. The reflection at normal incidence is then a little more than zero, but the reflection falls to zero as the angle of incidence is increased to that given by Eq. (4)

for $\phi = \pi$. Thereafter, the reflection rises with increase of angle of incidence and again falls to zero at Brewster's angle. For higher angles of incidence the reflection again increases with angle of incidence, but more slowly than for the half-wavelength panel. This general behavior is shown by Figs. 11·6 and 11·8. Panels of low or moderate dielectric constant of modified half-wavelength thickness can thus be designed with low reflections at parallel polarization over a wide range of angles of incidence to beyond Brewster's angle. In Table 11·3 examples are given of values of optimum thicknesses to minimize the maximum reflection over a given range of angles of incidence, together with the maximum power-reflection coefficient corresponding to the range of angles of incidence and thickness.[1] A comparison of Table 11·3 with Table 11·1 shows that the minimized maximum reflection for a given range of angles of incidence is always lower with parallel polarization than it is with perpendicular polarization.

Furthermore, the tolerances for a design of a panel of modified half-wavelength thickness are, in general, wider for a given requirement when

TABLE 11·3.—MINIMIZATION OF REFLECTION AT PARALLEL POLARIZATION

Dielectric constant ϵ	Range of angles of incidence, degrees	Ratio of optimum thickness to full-wavelength thickness	Power-reflection coefficient
$2\epsilon_0$	0–40	0.521	0.002
	0–60	0.525	0.003
	0–70	0.582	0.029
	0–80	0.648	0.073
	20–60	0.541	0.002
	40–80	0.675	0.013
$4\epsilon_0$	0–40	0.506	0.001
	0–60	0.511	0.003
	0–70	0.516	0.006
	0–80	0.541	0.036
	20–60	0.514	0.005
	40–80	0.559	0.009

the polarization is parallel to the plane of incidence. Examples of the panel thicknesses and tolerances for less than 10 per cent reflection of the incident energy when the range of angles of incidence is from 0° to 70°, given in Table 11·4, should be compared with those in Table 11·2. In the region of wavelengths where the modified half-wavelength design is practicable, the tolerances in the last column of Table 11·4 are obtainable without any extraordinary care in fabrication.

[1] R. M. Redheffer, *op. cit.*

Reflection of Thin Panels.—Except in the region of the half-wavelength thickness, the reflection at parallel polarization of a plane panel generally decreases steadily with increasing angle of incidence to a value of zero at Brewster's angle and then increases to a value of unity for the reflection coefficient at 90° incidence. For a given dielectric constant, the reflection of a plane panel at a given angle of incidence increases with thickness if the thickness is less than one quarter wavelength in the panel (*cf.* Figs. 11·6 and 11·8). We have seen that the use of a radome that is thin compared with the wavelength is limited in practice to small streamlined housings for antennas of microwave beacons; materials useful for this purpose have dielectric constants that range from $2.2\epsilon_0$ to $10\epsilon_0$. If

TABLE 11·4.—PANEL THICKNESSES AND TOLERANCES FOR LESS THAN 10 PER CENT REFLECTION IN POWER, INCIDENCE RANGE 0°–70°
PARALLEL POLARIZATION

$\frac{\epsilon}{\epsilon_0}$	$\frac{d_1}{\lambda_0}$	$\frac{d_2}{\lambda_0}$	$\frac{d_1 - d_2}{2\lambda_0}$
1.7	0.722	0.401	0.160
2.2	0.444	0.311	0.067
3.7	0.290	0.232	0.029
3.7	0.549*	0.502*	0 024*
10.0	0.169	0.147	0.011
10.0	0.327*	0.306*	0.011*

* Second order.

the radiation is polarized perpendicular to the axis of the beacon antenna, the radiation that falls at a high angle of incidence on the radome wall is polarized parallel to the plane of incidence. The power reflection can then be less than 10 per cent from 0° up to at least 70° incidence. For example, a panel of material that has a dielectric constant of $4\epsilon_0$ and a thickness of $0.036\lambda_0$ will give less than 10 per cent reflection over this range of angles. This thickness is just three times the thickness allowable under the same conditions for perpendicular polarization (see end of Sec. 11·3). Obviously, it is easier to design a mechanically satisfactory thin-walled, streamlined housing for a microwave linear array when the electric vector is transverse to the axis of the array.

Reflection of Panels of Low Dielectric Constant.—Even with parallel polarization and a material of low dielectric constant, the reflection coefficient becomes large at high angles of incidence. Certain ranges of thickness must be avoided if the reflection of a panel made of such material is to be kept low.

11·5. Homogeneous Panels with Finite Loss at Arbitrary Incidence.—It is shown in Sec. 10·3 that the loss tangent of the material affects both

the reflection and the transmission at normal incidence.[1] For low values of the loss tangent, the reflection is negligibly affected by the finite loss except that it goes to small finite minima rather than to zero for critical thicknesses; the transmission, however, can be appreciably reduced. Equations (12·81) and (12·82) from which these results are derived apply for incidence at arbitrary angles provided that the correct values of $|r_{ab}|$, χ (the shift of phase), ϕ and A are used. It is shown in Section 12·4 that the magnitude of the reflection coefficient $|r_{ab}|$ for low-loss materials is negligibly different from what it is for lossless materials having the same dielectric constant and that the shift of phase at reflection χ is small although different from zero. For any particular case the values for $|r_{ab}|$ and χ can be obtained from Eqs. (12·47) and (12·48), using the equivalent index of refraction and the absorption coefficient from Eqs. (12·51) and (12·52). The values of A and ϕ appropriate for oblique incidence are given by Eqs. (12.71*a*) and (12.71*b*) and can be written

$$A = e^{-\frac{\pi d}{\lambda_0}\frac{\left(\frac{\epsilon'}{\epsilon_0}\right)\tan\delta}{\sqrt{\frac{\epsilon'}{\epsilon_0}-\sin^2\theta_0}}} \tag{6}$$

and

$$\phi = \frac{2\pi d}{\lambda_0}\sqrt{\frac{\epsilon'}{\epsilon_0}-\sin^2\theta_0}, \tag{7}$$

ϕ being the same as for the lossless sheet [Eq. (12·64)]. The general result is the same as for normal incidence—an unimportant change of the reflection of the panel and an appreciable reduction of the transmission.

The reduction of the transmission is greater for oblique incidence than it is for normal incidence, because the exponent in the expression for A is proportional to the ratio

$$\frac{\frac{\epsilon'}{\epsilon_0}}{\sqrt{\frac{\epsilon'}{\epsilon_0}-\sin^2\theta_0}}.$$

Equation (6) can also be put in the form

$$A = e^{-\frac{\phi\tan\delta}{2}\frac{\left(\frac{\epsilon'}{\epsilon_0}\right)}{\left(\frac{\epsilon'}{\epsilon_0}-\sin^2\theta_0\right)}} \tag{8}$$

from which it is apparent that the reduction of the transmission with increasing angle of incidence is even greater if sheets of equal electrical thickness are compared rather than sheets of equal thickness of material.

[1] R. M. Redheffer, "Transmission and Reflection of Parallel Plane Sheets," *Radome Bull.* 12, RL Report No. 483-12, January 1945; Yael Dowker, "Transmission of Lossy Sandwiches," RL Report No. 483-22, January 1946.

For modified half-wavelength panels, Eq. (12·84) gives the expression for the corresponding maximum values of the transmission. It is

$$|T|^2_{\text{lossy(max)}} \approx A_N^2 \left(\frac{1 - |r_{ab}|^2}{1 - A_N^2 |r_{ab}|^2} \right)^2. \tag{9}$$

When $|r_{ab}|^2$ is small the A_N^2 factor is the principal one; but when $|r_{ab}|^2$ becomes comparable with unity, the second factor is also of importance and contributes to a further reduction of $|T|^2_{\max}$. Since $|r_{ab}|^2$ is greater for perpendicular polarization than for parallel polarization and A_N^2 is the same for both, $|T|^2_{\max}$ will always be less for perpendicular-polarized radiation incident at any given angle than it will be for parallel-polarized radiation incident at the same angle. At perpendicular polarization the decrease is particularly marked at large angles of incidence for which $|r_{ab}|^2$ gets fairly large.

Some representative values for modified half-wavelength panels of one particular dielectric are given in Table 11·5. The panels of Table

TABLE 11·5.—TRANSMISSION LOSS OF MODIFIED HALF-WAVELENGTH PANELS

$\frac{\epsilon'}{\epsilon_0} = 4; \quad n = 2; \quad \tan\delta = 0.02; \quad \kappa = 0.01$

Angle of incidence, degrees	$\frac{d}{\lambda_0}$	A	Perpendicular polarization			Parallel polarization		
			$\frac{\epsilon_{s\theta}}{\epsilon_0}$	$\lvert r_{ab}\rvert$	$1 - \lvert T\rvert^2$	$\frac{\epsilon_{p\theta}}{\epsilon_0}$	$\lvert r_{ab}\rvert$	$1 - \lvert T\rvert^2$
0	0.250	0.97	4	0.33	0.08	4.00	0.33	0.08
60	0.277	0.96	13	0.56	0.14	1.20	0.03	0.08
75	0.286	0.96	46	0.73	0.23	0.35	0.25	0.11

11·5 are ones that have very small reflection at the given angles of incidence; the transmission loss results almost entirely from absorption. The absorbed power increases rapidly with angle of incidence at perpendicular polarization, especially at the higher angles of incidence, whereas at parallel polarization there is no marked change in absorption with angle of incidence.

These results for panels of modified half-wavelength thickness may be generalized as follows. The reflection by a panel of low-loss material under given conditions is almost the same as for an equivalent lossless panel. The absorption increases significantly with angle of incidence for perpendicular polarization but does not change noticeably for parallel polarization. The extent of the change depends upon the dielectric constant and loss tangent of the material; as a rough rule, the transmission loss due to absorption at 70° incidence is about three times the loss

at normal incidence. If an appreciable amount of the power radiated from an antenna is to be transmitted through a radome at angles of incidence greater than 70° at perpendicular polarization, absorption may become an important factor in limiting the transmitted power. Thus with half-wavelength or modified half-wavelength radomes, moderately lossy materials ($\tan \delta \leqq 0.05$) may be used, provided radiation does not fall at a high angle of incidence at perpendicular polarization. Minimization of both reflection and absorption is more difficult for perpendicular polarization than for parallel polarization.

TRANSMISSION AND REFLECTION OF SANDWICHES

11·6. General Considerations.—Ordinarily, a designer tries to plan constructions that meet mechanical and electrical requirements and are at the same time as light as possible. The sandwich consisting of thin high-strength faces and a low-density core of gridded construction or expanded plastic is of this kind. Since streamlined radomes for scanning antennas are large and sometimes subject to high aerodynamic loading, sandwich constructions that are stiff and strong are desirable. It may also be required that the radome have a high value of the transmission coefficient over a wide range of angles of incidence either at parallel or perpendicular polarization or at both polarizations.

These electrical and mechanical requirements severely limit the possibilities for design of sandwich constructions with thin high-strength skins and low-density cores, especially at the shorter wavelengths. Where this conventional type of sandwich construction cannot be employed, it is necessary to use a homogeneous sheet of modified half-wavelength thickness or alternative types of sandwich construction; these constructions are heavy compared with conventional sandwich constructions of the same strength and stiffness. Some of the alternative types of construction are considered in Secs. 11·9 and 11·10. The mechanical properties of this type of construction are considered in Sec. 13·10.

Sandwiches for the 10-cm band can be designed with skins that are electrically thin compared with the wavelength. Such sandwiches have excellent strength and stiffness and a reflection coefficient that is low over a wide range of angles of incidence. In the 3-cm band the skins that are required for mechanical reasons are thicker electrically. In order that the reflection coefficient remain low over a wide range of angles of incidence at perpendicular polarization, no spacing greater than the first-order spacing can be used. In the 1-cm band the construction with thin skins and low dielectric-constant core is of limited strength and stiffness when the incidence covers a wide range of perpendicular polarization. A sandwich with skins that are of the order of the half-wavelength

thickness is strong and has good electrical characteristics over a wide range of angles of incidence.

There is no difficulty in getting low reflection over a wide range of angles of incidence when the polarization is parallel to the plane of incidence; normal-incidence designs with first- or second-order spacing are often entirely satisfactory. The more difficult problems arise when the polarization is perpendicular to the plane of incidence. It is then necessary to make the core thicker than for normal incidence so as to minimize the maximum reflection over a given range of angles of incidence (*cf.* Sec. 11·3). The angle of incidence corresponding to zero reflection for such a sandwich lies nearer to the upper than to the lower limit of the range of angles of incidence, as with homogeneous panels. A sandwich in which the core spacing is thus modified to obtain optimum transmission characteristics over a given range of angles of incidence at perpendicular polarization usually has good transmission characteristics at parallel polarization. For given values of skin thickness and skin and core dielectric constants, at perpendicular polarization the minimized maximum reflection increases with increase of range of angles of incidence; for a given range of angles of incidence, it is greater for a second-order sandwich with optimum core thickness than for a similar first-order sandwich. In all these respects the behavior of a sandwich at both parallel and perpendicular polarization is analogous to that of a homogeneous dielectric sheet. For a given range of angles of incidence and values of skin and core dielectric constants, the reflection at perpendicular polarization with the optimum core thickness depends very much upon the thickness of the skins; they must be kept as thin as possible if the best transmission characteristics are to be obtained over a wide range of angles of incidence. In this connection it should be pointed out that the strength and stiffness of the sandwich construction are mainly attributable to the skins (*cf.* Sec. 13·10).

It was shown in Sec. 10·6 that the presence of an adhesive layer between the skin and core can be taken into account electrically by assuming an *effective* value of skin thickness d_s in excess of the actual skin thickness d'_s by an amount Δ depending upon the materials used and the technique of the fabrication. The design of the sandwich construction for a streamlined radome should be based upon the effective skin thickness and not the actual one; otherwise, the electrical transmission may be adversely affected, especially when good transmission is required over a range of angles of incidence at perpendicular polarization.

For the transmission of sandwiches with low-loss skins and cores, at parallel polarization the additional transmission loss resulting from finite loss in the skin and the core does not vary greatly with angle of incidence. At perpendicular polarization, the transmission loss due to absorption

increases markedly with increase of angle of incidence, especially above angles of incidence of about 60°. Lossy materials such as cellulosic substances cannot therefore be used for streamlined radomes where radiation is incident perpendicular to the plane of incidence at a large angle of incidence. Materials that are used in the "electrical" portion of the radome must, for the same reason, be as nearly nonhygroscopic as possible. The requirement that a radome be used with perpendicularly polarized radiation incident over a wide range of angles of incidence involves losses of transmitted power resulting from both reflection and absorption and thus restricts the design.

11·7. Lossless Sandwiches at Arbitrary Incidence.—By use of the equivalence relationships discussed in Secs. 11·1 and 11·2, the electrical behavior[1] of a lossless sandwich, at any particular angle of incidence and polarization, may be represented by the electrical behavior of a hypothetical equivalent sandwich at normal incidence. For the hypothetical sandwich the effective dielectric constants of the skin and core given by Eqs. (1) and (2) are functions of the angle of incidence, of the polarization, and of the actual dielectric constants of the skin and core. Similarly, the electrical thicknesses of the skin and core of the hypothetical sandwich are functions of those of the actual sandwich and of the angle of incidence, as per Eq. (4). With these values, the core thickness that will give zero reflection can be computed for any given skin construction, angle of incidence, and polarization. The change in core thickness corresponding to any given reflection coefficient of the sandwich can also be computed. Hence, for a given skin construction and a given dielectric constant of core, reflection contours of constant power-reflection coefficient can be obtained on charts where the core thickness is plotted as the ordinate and the angle of incidence as the abscissa.

Symmetrical Lossless Sandwiches.—Proceeding as for normal incidence, we see that a lossless sandwich can have zero reflection only when it is symmetrical. If $(d_c)_N$ is the core thickness corresponding to zero reflection, then for perpendicular polarization[2]

$$\phi_c = N\pi - \tan^{-1}\left[\frac{2(\alpha_s' - 1)\sqrt{\alpha_s'\alpha_c'}\sin 2\phi_s}{(\alpha_s' - 1)(\alpha_s' + \alpha_c')\cos 2\phi_s + (\alpha_c' - \alpha_s')(\alpha_s' + 1)}\right] \quad (10)$$

where

$$\phi_c = \frac{2\pi(d_c)_N}{\lambda_0}\sqrt{\alpha_c - \sin^2\theta_0}, \qquad \phi_s = \frac{2\pi d_s}{\lambda_0}\sqrt{\alpha_s - \sin^2\theta_0},$$

[1] R. M. Redheffer, "Electrical Properties of Double-wall and Sandwich Radomes," RL Report No. 483-11, February 1944; J. B. Birks, "Dielectric Transmission and Scanner Nacelle Design," TRE Report No. T1677, and Part 2, TRE Report No. T1769, December 1944.

[2] The quantities α_s' and α_c' are the *effective* specific dielectric constants of the skin

and similarly for parallel polarization [*cf.* Eq. (10·19)]. If the core has an arbitrary thickness d_c that equals $(d_c)_N + \Delta d_c$, then the power-reflection coefficient of the sandwich as a whole is given by

$$|R|^2 = \frac{4|\rho|^2 \sin^2\left[\dfrac{2\pi(\Delta d_c)\sqrt{\alpha_c - \sin^2\theta}}{\lambda_0}\right]}{(1 - |\rho|^2)^2 + 4|\rho|^2 \sin^2\left[\dfrac{2\pi(\Delta d_c)\sqrt{\alpha_c - \sin^2\theta_0}}{\lambda_0}\right]} \tag{11}$$

where $|\rho|^2$ has the value corresponding to the angle of incidence θ_0 and the appropriate polarization. $|\rho|^2$ is obtained from Eq. (10·21) by replacing α_s and α_c by α_s' and α_c' and using the above expression for ϕ_c. Just as for the plane dielectric sheet at arbitrary incidence (Sec. 11·2), Fig. 10·8 can be used for the construction of reflection contour charts. Here, however, the abscissa represents values of $\pm(\Delta d_c/\lambda_0)\sqrt{\alpha_c - \sin^2\theta_0}$. Thus, by the use of expressions derived for the case of normal incidence, for arbitrary incidence we can compute the reflection coefficient for the skin backed by the core material, the core thickness for zero reflection, and the reflection for arbitrary spacing.

Contours of Constant Reflection.—As with the single homogeneous sheet, the first object is to find the conditions under which loss due to reflection is minimized over a given range of angles of incidence. The reflection of any actual sandwich is nearly the same as for a lossless sandwich made of materials having the same dielectric constants. For any given set of values of skin thickness d_s, skin dielectric constant ϵ_s, and core dielectric constant ϵ_c, it is first necessary to calculate the core thickness d_c corresponding to a given power-reflection coefficient $|R|^2$ as a function of angle of incidence. If for each value of $|R|^2$ we plot the core thickness against the angle of incidence, we get a chart of reflection contours, as before. In order to present information on the behavior of single homogeneous sheets at arbitrary incidence, a large set of contour diagrams for each polarization is needed, one for each value of the dielectric constant. For the sandwich construction, the presentation of the corresponding information necessitates a threefold set of charts for each polarization, covering all values of skin thickness, skin dielectric constant, and core dielectric constant. The most valuable types of construction, however, have high-strength skins, for which α_s ranges from 3.0 to 5.0, and cores of air, low-density plastic, or thermoplastic material, with α_c ranging from 1.0 to 2.7. A study of diagrams of reflection contours for perpendicular polarization shows the desirability of restricting the electrical skin thickness to values either less than about 0.10 or close to 0.50. The behavior of sandwiches with thin skins and cores of low dielectric constant

and core for radiation incident at angle θ_0 in air; α_c and α_s in the expressions for ϕ_c and ϕ_s are the actual specific dielectric constants.

becomes apparent after study of a small number of charts giving reflection contours.[1]

In Figs. 11·11 and 11·12 typical reflection contours are shown for perpendicular and parallel polarization respectively. The ordinate represents the ratio of core thickness d_c to the free-space wavelength λ_0; the

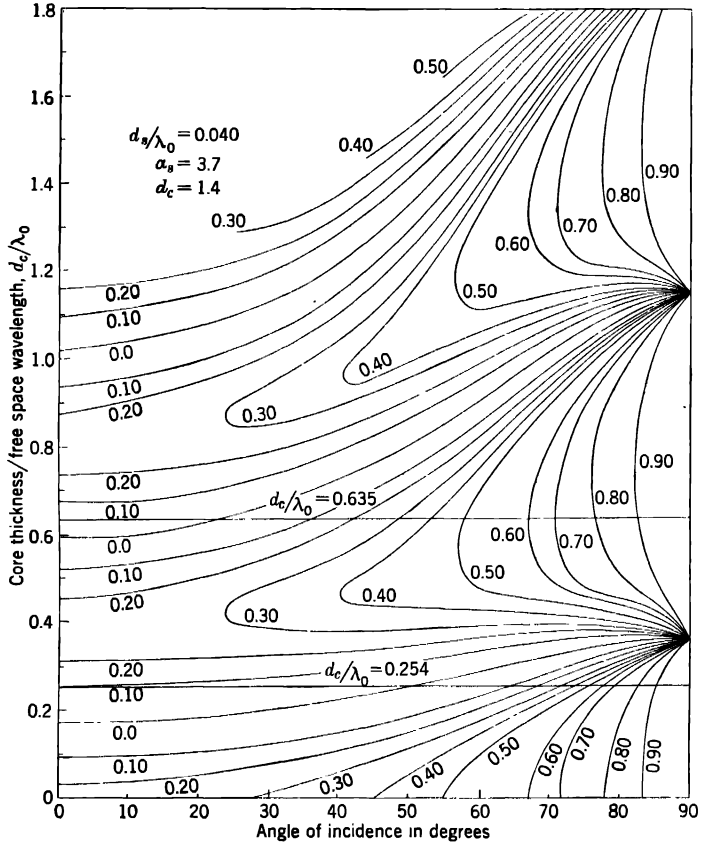

FIG. 11·11. – Power-reflection contours for a sandwich (perpendicular polarization).

percentage of reflected power is marked on each contour. The charts are computed for a skin dielectric constant of $3.7\epsilon_0$, a core dielectric constant of $1.4\epsilon_0$, and a skin thickness of $0.040\lambda_0$. Figure 11·11 shows that the core thickness for zero reflection increases with the angle of incidence, as does the thickness of a modified half-wavelength panel. The second-

[1] For charts of a large number of typical sandwich constructions, see E. M. Everhart, "Radome Wall Reflections at Variable Angles of Incidence," RL Report No. 483-20, January 1946; see also RL Report No. 483-8, December 1944.

order core thickness for zero reflection is obtained from the first-order thickness by increasing d_{c1}/λ_0 by an amount $1/(2\sqrt{\alpha_c - \sin^2\theta_0})$. Thus, the second-order contour for zero reflection is steeper than the first-order contour. The contours for 10 per cent reflection are observed to be equally spaced above and below the corresponding zero reflection con-

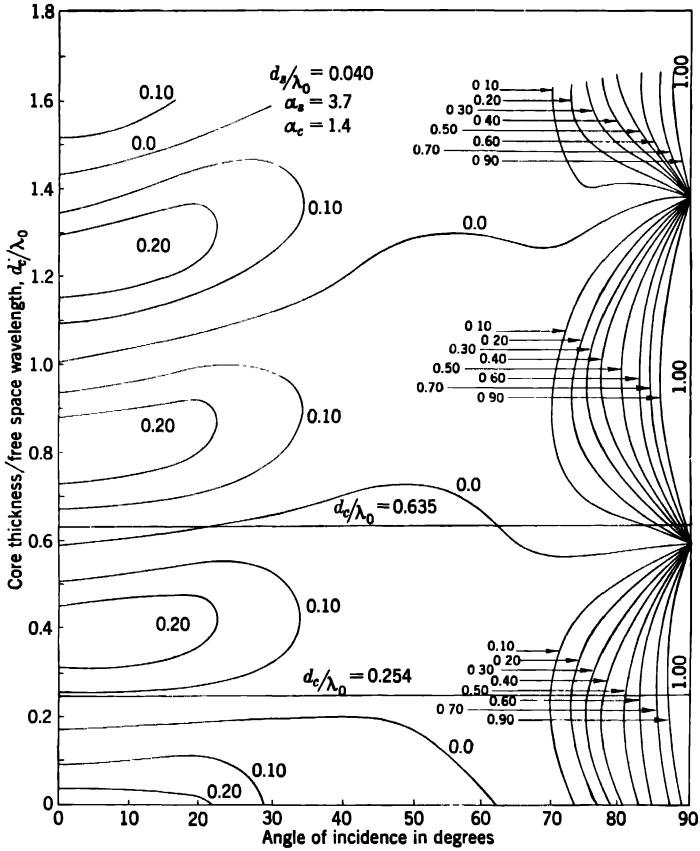

FIG. 11·12.—Power-reflection contours for a sandwich (parallel polarization).

tour, as are the contours for other amounts of reflection. In this way it is possible to construct the contour diagram from computations made for the first-order spacing only. From Figs. 11·11 and 11·12 it can be seen that the zero reflection contours for parallel polarization are different from the zero reflection contours for perpendicular polarization. The contour diagrams for a family of sandwiches differ in this respect from those for plane dielectric sheets of given dielectric constant (Sec. 11·2).

A sandwich that has zero reflection at some particular angle of incidence at perpendicular polarization does not usually have zero reflection at the same angle of incidence at parallel polarization, and vice versa. As with perpendicular polarization, the second-order reflection contours for parallel polarization are obtained from the first-order contours by increasing the core thickness for any given angle of incidence θ_0 by an amount $\lambda_0/(2\sqrt{\alpha_c - \sin^2\theta_0})$. Since Brewster's angle for the air-skin interface is different from Brewster's angle for the core-skin interface, there is no angle of incidence for which the reflection is always zero, except, of course, in the special case of the double-wall construction. If we denote the angle of incidence corresponding to Brewster's angle for the air-skin interface by θ_B (equal to $\tan^{-1}\sqrt{\alpha_s}$), the reflection of the whole sandwich at this angle of incidence is the same as if the skins had been removed and only the core remained. Thus we see that the core thickness for zero reflection at an angle of incidence θ_B at parallel polarization is equal to an integral multiple of $\lambda_0/(2\sqrt{\alpha_c - \sin^2\theta_B})$.

11·8. Lossless Sandwiches with Thin Skins.—The electrical behavior of lossless sandwiches can be studied most easily with the aid of charts of constant reflection contours, as discussed in the preceding section. In this section we consider the effect on transmission as the core thickness of a sandwich with given skin construction is varied, the effect of the skin thickness on the transmission of lossless sandwiches with optimum core thickness, the effect of the adhesive layer between the skins and the core, and the tolerances required in the fabrication of streamlined sandwich radomes.

Effect of Core Thickness on Reflection. Perpendicular Polarization.—As a typical example, let us assume dielectric constants of $3.7\epsilon_0$ and $1.4\epsilon_0$ for the skin and core respectively and a skin thickness of $0.040\ \lambda_0$ corresponding to an electrical thickness of 0.148. This is a reasonable value of electrical skin thickness in the 3-cm wavelength band; it is high for the 10-cm band and too low for a construction of appreciable strength in the 1-cm band. The results found will be qualitatively valid for other values of electrical skin thickness and for other dielectric constants of the skin and core, although the quantitative results may be far different.

From the charts in Figs. 11·11 and 11·12 we find that the first-order core thickness corresponding to power-reflection coefficients at normal incidence of zero, 0.05, 0.10, and 0.15 are $0.175\lambda_0$, $0.230\lambda_0$, $0.254\lambda_0$, and $0.278\lambda_0$, respectively. Curves of the power-reflection coefficient as a function of angle of incidence can be plotted from these contours. Such curves for perpendicular polarization are presented in Fig. 11·13. It is seen that the set of curves for different thicknesses of the core of a sandwich is similar to the corresponding set for different thicknesses of a panel (see Fig. 11·9). Just as for the panels, it is advantageous that the thick-

ness of the core be made greater than that for a normal-incidence design of a sandwich. The optimum core thickness depends upon the range of angles of incidence and the permissible values of the reflection or transmission coefficients at each end of the range of angles of incidence. The specification adopted depends upon engineering judgment in any particular case;[1] in this discussion it will be assumed, as before, that *the optimum*

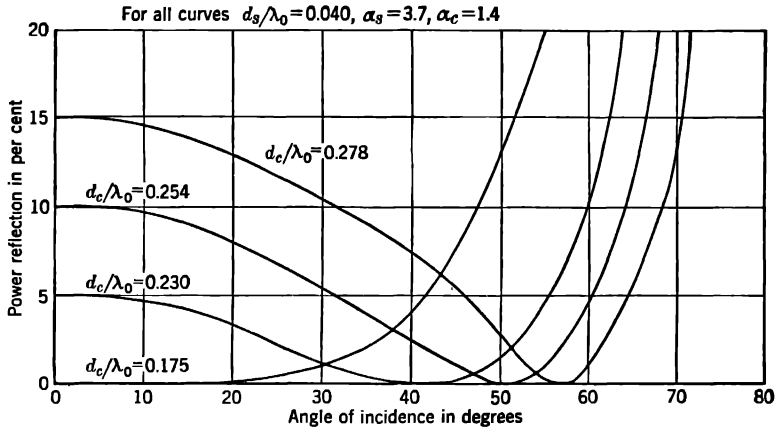

FIG. 11·13.—Effect of core thickness on the reflection of lossless sandwiches (perpendicular polarization).

core thickness is the one for which the greatest value of reflection is minimized over the given ranges of angles of incidence. If we assume that the lower end of the range of angles of incidence is at normal incidence, then the

TABLE 11·6.—REFLECTION BEHAVIOR OF LOSSLESS SANDWICHES
$\alpha_s = 3.7$; $\alpha_c = 1.4$; $d_s/\lambda_0 = 0.040$

$\frac{d_c}{\lambda_0}$	$\lvert R\rvert^2$ at normal incidence	Range of angles of incidence for which $\lvert R\rvert^2$ is less than normal-incidence value, degrees	Angle of incidence for which $\lvert R\rvert^2 = 0$, degrees
0.230	0.05	0–56	42
0.254	0.10	0–64	51
0.278	0.15	0–71	57

ranges of angles of incidence corresponding to values of $|R|^2$ of 0.05, 0.10, and 0.15 are as given in Table 11·6 together with the angle of incidence

[1] E. R. Steele, "Some Electrical Aspects of Microwave Sandwich Radome Design," RL Report No. 483-16, May 1945.

for zero reflection. It is seen that the minimized maximum value of reflection coefficient increases with increase in range of angles of incidence and the angle of incidence for zero reflection lies near the upper end of the range of angles of incidence.

From Fig. 11·13 it is apparent that the reflection by a sandwich with a given skin construction changes rapidly with change in core thickness, especially at the upper end of the angle of incidence range. In practice, therefore, the core thickness must be held to a specified value within a close tolerance in order to obtain given reflection characteristics.

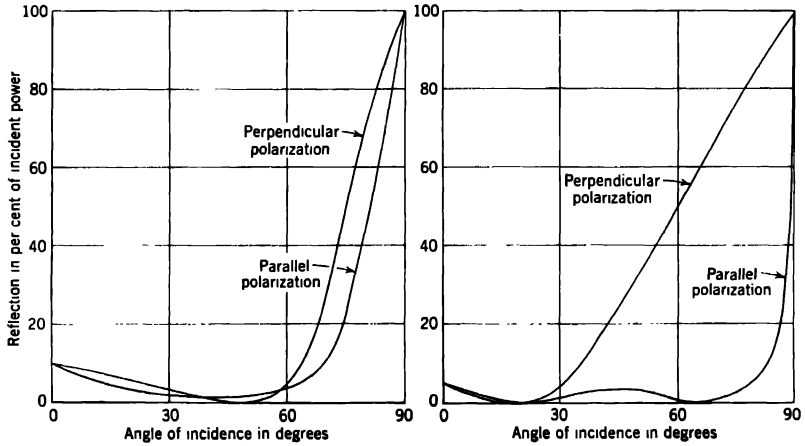

(*a*) First-order spacing.
Skin thickness = $0.040\lambda_0$.
Core thickness = $0.254\lambda_0$.
$\alpha_s = 3.7$; $\alpha_c = 1.4$.

(*b*) Second-order spacing.
Skin thickness = $0.040\lambda_0$.
Core thickness = $0.635\lambda_0$.
$\alpha_s = 3.7$; $\alpha_c = 1.4$.

FIG. 11·14.—Power reflection of a sandwich.

Since the second- and higher-order contours are steeper than those for the first order in the reflection contour chart, the second-order spacing is less suitable electrically for use in a streamlined radome where the radiation is incident over a wide range of angles at perpendicular polarization. For example, the reflection of two sandwiches for which $\alpha_s = 3.7$, $\alpha_c = 1.4$, $d_s = 0.040\lambda_0$, and $d_c = 0.254\lambda_0$ and $0.635\lambda_0$, respectively, is shown in Fig. 11·14 at perpendicular and at parallel polarization as a function of angle of incidence. In the second-order sandwich, the reflection at perpendicular polarization is seen to be large except over a narrow range of angles of incidence.

Effect of Core Thickness on Reflection. Parallel Polarization.—In general, the power-reflection coefficient of a sandwich with thin skins and core of low dielectric constant designed for zero reflection at normal incidence is less than 0.10 from normal incidence up to an angle of inci-

dence of 70° at parallel polarization.[1] It is apparent from Fig. 11·12, for example, that the core thickness can be increased appreciably without marked increase in reflection coefficient of the sandwich. Good transmission characteristics at parallel polarization are therefore to be expected of a sandwich that has been designed for optimum transmission of perpendicularly polarized radiation (*cf.* Fig. 11·14*a*). Usually there is a range of values of second-order core thickness for which the transmission

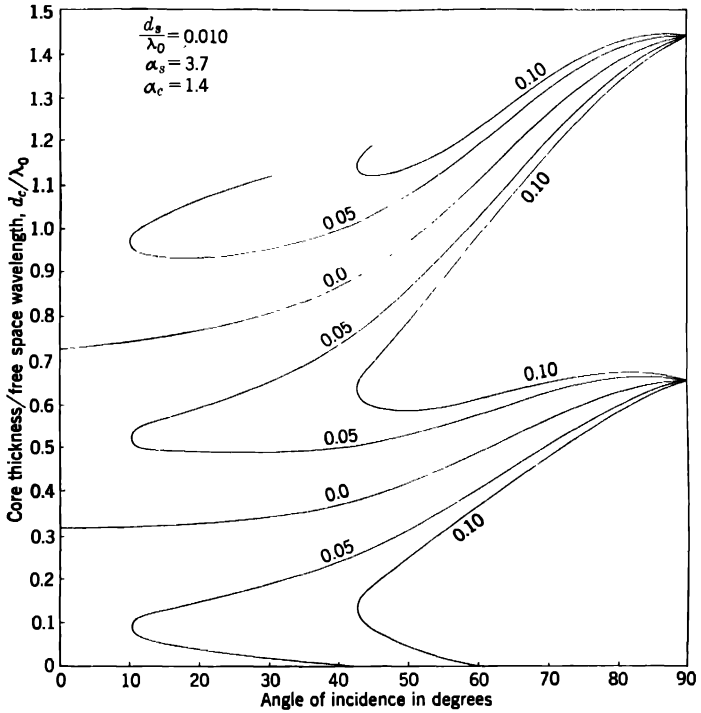

FIG. 11·15.—Power-reflection contours for a sandwich (perpendicular polarization).

of sandwiches for parallel polarization is good from normal incidence up to angles of incidence in excess of 80°. This, too, is evident from Figs. 11·12 and 11.14*b*.

Effect of Skin Thickness on Optimum Core Thickness.—For the most part, the required mechanical strength can be obtained with a thick enough skin. The thickness of the core must be adjusted accordingly. The thickness of the skin cannot be too great, however, if perpendicularly

[1] *Cf.* E. M. Everhart, "Radome Wall Reflections at Variable Angles of Incidence," RL Report No. 483-20, January 1946.

polarized radiation is to be incident over a wide range of angles, because the minimized maximum reflection with optimum core spacing may become very large as the skin thickness increases.

This can be illustrated by an example. Again taking the same values of dielectric constant of the skin and core as before ($3.7\epsilon_0$ and $1.4\epsilon_0$) and assuming that the reflection has to be minimized over a range of angles of incidence from normal incidence to 70°, we will assume values of skin

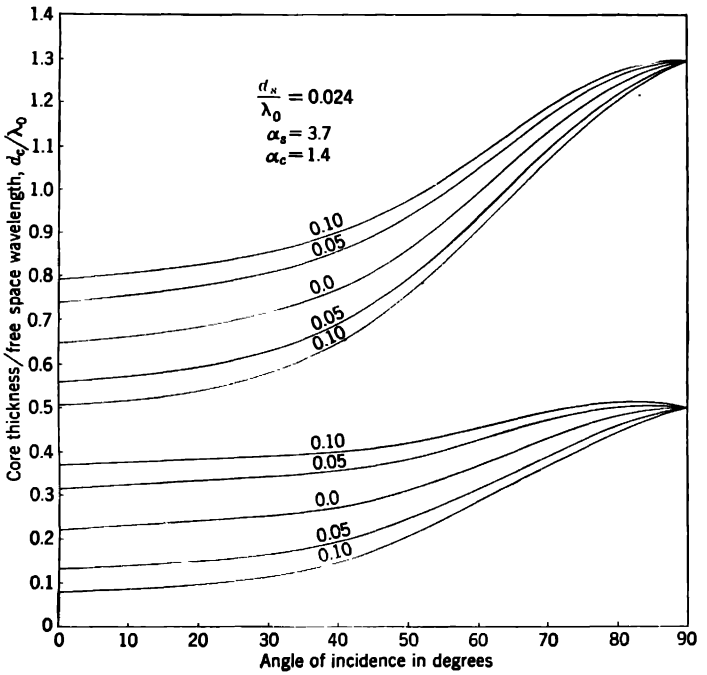

FIG. 11·16.—Power-reflection contours for a sandwich (perpendicular polarization).

thicknesses equal to $0.010\lambda_0$, $0.024\lambda_0$, and $0.040\lambda_0$, corresponding to the reflection contour charts in Figs. 11·15, 11·16, and 11·11, respectively. The optimum first-order core thicknesses obtained from these reflection contour charts are found to be approximately $0.500\lambda_0$, $0.373\lambda_0$, and $0.278\lambda_0$, respectively. Transmission curves as a function of angle of incidence for lossless sandwiches corresponding to these thicknesses are given in Fig. 11·17.

In Table 11·7 are given values of the optimum core spacing $d_{c(\text{opt})}$, of the corresponding total sandwich thickness h (equal to $d_{c(\text{opt})} + 2d_s$), of the angle of incidence for which the reflection is zero, and of the maximum reflection over the range of incidence from 0° to 70° for each value of skin

thickness; all dimensions are given in terms of the free-space wavelength. It is observed that with increase in skin thickness there results a marked increase in the maximum reflection; the angle of peak transmission decreases slightly while the optimum core thickness and optimum overall sandwich thickness diminish. There is, therefore, a practical restric-

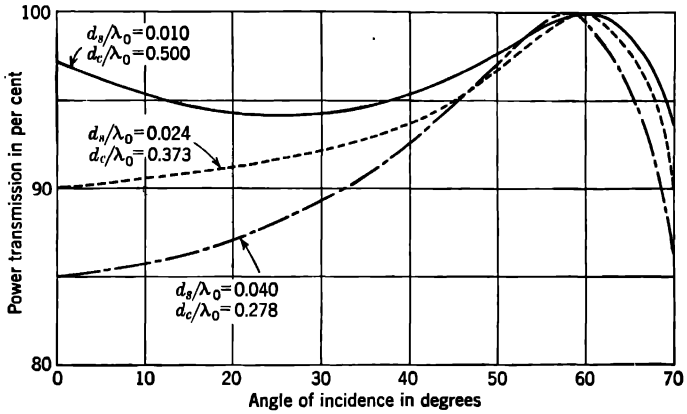

FIG. 11·17.—Effect of skin thickness on the transmission of lossless sandwiches (perpendicular polarization).

tion on the skin thickness of such sandwiches that depends upon the desired range of angles of incidence.

Other things being equal, the flexural strength and stiffness of sandwiches with thin skins and low-density cores can be considered as being approximately proportional to $\lambda_0^2(d_s/\lambda_0)(d_c/\lambda_0)$ and $\lambda_0^3(d_s/\lambda_0)(d_c/\lambda_0)^2$,

TABLE 11·7.—EFFECT OF SKIN THICKNESS ON MINIMIZED MAXIMUM REFLECTION ($\alpha_s = 3.7$; $\alpha_c = 1.4$)

$\frac{d_s}{\lambda_0}$	$\frac{d_{c\,(\mathrm{opt})}}{\lambda_0}$	$\frac{h}{\lambda_0}$	Angle of zero reflection, degrees	Max. percentage reflected power with optimum core spacing, approx.
0.010	0.500	0.520	61.0	6
0.024	0.373	0.421	60.5	10
0.040	0.278	0.358	57.5	15

respectively (Sec. 13·10). Thus, for a given electrical behavior at perpendicular polarization, the strength and stiffness should vary as the square and the cube of the free-space wavelength, respectively. In the 10-cm band, d_s/λ_0 may be kept sufficiently small so that the reflection

remains low over the range of angles of incidence, the strength and stiffness of a radome being adequate. In the 3-cm band, the same requirements for strength and stiffness will necessitate a higher value of d_s/λ_0 with consequent impairment of transmission characteristics at perpendicular polarization. Any unnecessary strength or rigidity of a radome will degrade its electrical characteristics.

In the 1-cm range, the strength and stiffness become quite small for certain values of d_s/λ_0 and d_c/λ_0 because of the λ_0^2 and λ_0^3 coefficients in the expressions for strength and stiffness. Unless the mechanical requirements are modest, the thin-walled sandwich cannot be used for this wavelength region when the angle of incidence covers a wide range at perpendicular polarization. Furthermore, since the actual skin thickness in a radome is somewhat less than the value to be used in the electrical design, because of the presence of the adhesive layer, the strength and stiffness of a sandwich designed for given electrical behavior fall off even more rapidly as λ_0 is reduced.

When the aerodynamic loading on a radome is primarily in one sense (inward or outward), asymmetrical sandwiches may be of advantage in the 3-cm band. If the thickness of one skin is reduced while that of the other is increased correspondingly, with but a slight change in over-all thickness, there is no significant change in transmission but there is a significant increase in flexural strength when the thicker skin is in compression (Sec. 13·10).

Effect of Adhesive.—The value of the thickness of the skin that must be used in computing the design of a sandwich is not the actual thickness but an effective thickness that is greater because of the properties of the core-skin bond (*cf.* Sec. 10·6). The consequence of neglecting this increase of thickness is much more serious for streamlined radomes, because the tolerances on the thickness of the skin are not so liberal as they are for normal-incidence radomes. Drastic impairment of the behavior of the radome may result if the effect of the layer of adhesive is ignored. Experimental results[1] indicate that the value of the effective thickness appropriate for oblique incidence is the same as that for normal incidence. Let us denote the actual skin thickness by d_s' and the effective skin thickness by d_s as in Sec. 10.6 In the 10-cm band, both d_s/λ_0 and $(d_s - d_s')/\lambda_0$ are likely to be small. Thus, the effect of the adhesive layer should be very small if it is allowed for; it may be neglected without serious impairment of transmission. In the 3-cm band, d_s/λ_0 and $(d_s - d_s')/\lambda_0$ are usually larger; the technique of fabrication that results in the minimum value of $(d_s - d_s')$ is preferred, and the design must be based upon the effective skin thickness. In the 1-cm band, the value of $(d_s - d_s')/\lambda_0$ is so large that the allowable value of actual skin thickness d_s'

[1] E. R. Steele, *op. cit.*

is very small when good transmission characteristics are required. The best value of $d_s - d_s'$ obtainable when the "wet lay-up" technique described in Sec. 13·6 is used appears to be about 0.010 in.; lower values can be obtained, but with the sacrifice of an adequate bond. For radomes made by cementing prefabricated skins, as described in Sec. 13·6, $d_s - d_s$ may become as high as 0.030 in.

As would be expected, the variation of the reflection as the thickness of the skins is changed is found to be much less serious with parallel polarization than with perpendicular polarization. It will not be treated in detail here. The design that is best for perpendicular polarization can be expected to be satisfactory for parallel polarization as well. It should, of course, be based on d_s, the effective skin thickness, rather than on d_s', the actual skin thickness.

Tolerances for Sandwiches with Thin Skins and Low Dielectric Constant Cores.—The practicability of any given design for radome construction depends upon whether or not the manufacturing tolerances necessary to maintain satisfactory electrical properties can be realized in practice. Variation is possible in all four parameters: thickness of skin and core and dielectric constant of skin and core. Variation of the dielectric constant of a core made of expanded plastic may result from chemical variations or from variations in density (Sec. 13·13). Variation of the dielectric constant of laminates used to form the skin may be large (Sec. 13·14); and when the fabrication of the radome takes place simultaneously with the cure of the skin, it is difficult to determine accurately the thickness and dielectric constant of the skin so formed.

A study has been made, for typical cases of sandwich construction, of the effect of variation of the parameters on the reflection at arbitrary incidence.[1] Some of the results for perpendicularly polarized radiation will be presented here.

Tolerances in Core Thickness.—At perpendicular polarization the transmission over a range of angles of incidence depends upon the skin thickness and also upon the core thickness, which is difficult to control closely in practice. In most streamlined radomes, the lower end of the required range of angles of incidence is nearly zero, while the upper end of the range depends upon the design. It is important to know how the upper end of the range is affected by variation of skin thickness and core thickness in order to specify tolerances. Figure 11·18, showing this range for particular values of dielectric constant of skin ($3.7\epsilon_0$) and of core ($1.4\epsilon_0$), is based on the assumption that the power-reflection coefficient is not to exceed 0.10. It is seen that the upper end of the range of angles of incidence is in excess of 70° only when the skin is made very thin and the core thickness is held to a narrow tolerance.

[1] E. M. Everhart, *op. cit.*

Tolerances in Dielectric Constant of the Core.—The effect of variation of the dielectric constant of the core can be determined by analysis of reflection contour charts for sandwiches with the same skin construction but with different dielectric constants of the core. In practice it will be found that variation of the dielectric constant of the core that is due to variation in density of commercial core material has but slight effect on the reflection characteristics of sandwiches.

Tolerances in Thickness of the Skin.—In a series of sandwich panels made by the same process with the same materials, both the effective

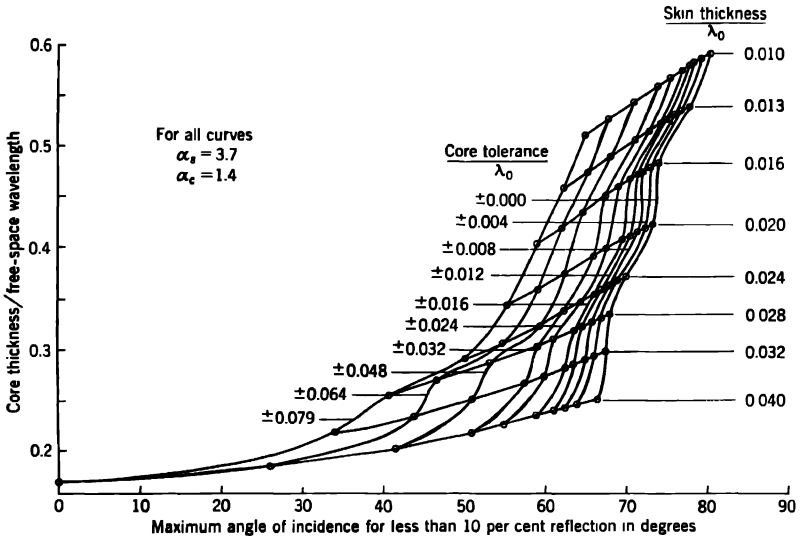

FIG. 11·18.—Allowed range of angles of incidence (perpendicular polarization).

skin thickness and the core thickness will be found to vary. From reflection contour charts we can find the result of variation of effective skin thickness when an assumed variation in core thickness occurs simultaneously. Obviously, the effects can be either compensatory or cumulative. As an example, let us consider a sandwich construction for a streamlined radome in which the skin and core dielectric constants are respectively $3.7\epsilon_0$ and $1.4\epsilon_0$ and in which the maximum power-reflection coefficient is to be kept at less than 0.10. The core tolerances are assumed to be equal to $\pm 0.016\lambda_0$, and the core thickness is such as to give optimum electrical behavior at perpendicular polarization for a skin thickness of $0.028\lambda_0$. If the skin thickness is changed, the range of angles of incidence for which the reflection is less than 10 per cent in power is changed. The shaded area in Fig. 11·19*a* shows the effect of change in skin thickness on this range. Increase in effective skin thick

ness is seen to result in improved behavior at large angles of incidence at the price of poorer behavior at small angles of incidence. Figure 11·19*b* shows the effect on the range of angles of incidence for the same conditions, except that the core thickness is now assumed to have the

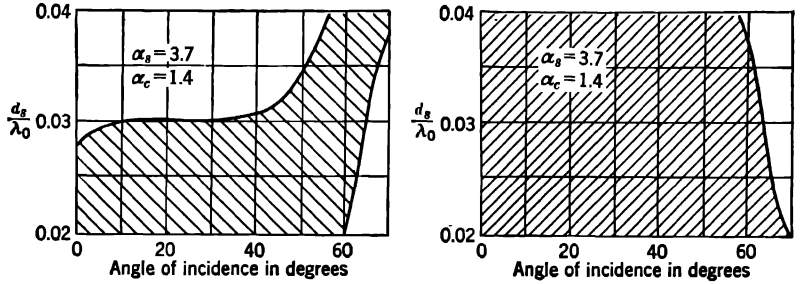

(*a*) *Constant* core thickness. Core tolerance $= \pm 0.016\lambda_0$. (*b*) *Optimum* core thickness. Core tolerance $= \pm 0.016\lambda_0$.

FIG. 11·19.—Effect of variation in skin thickness (perpendicular polarization). Shaded area represents range of angles of incidence for which the reflection is less than 10 per cent.

optimum value for each skin thickness; in this case the upper end of the range of angles of incidence for less than 10 per cent reflection is seen to decrease gradually with increase in effective skin thickness.

Tolerances in Dielectric Constant of the Skin.—A similar behavior is observed in the reflection characteristics of a typical sandwich at per-

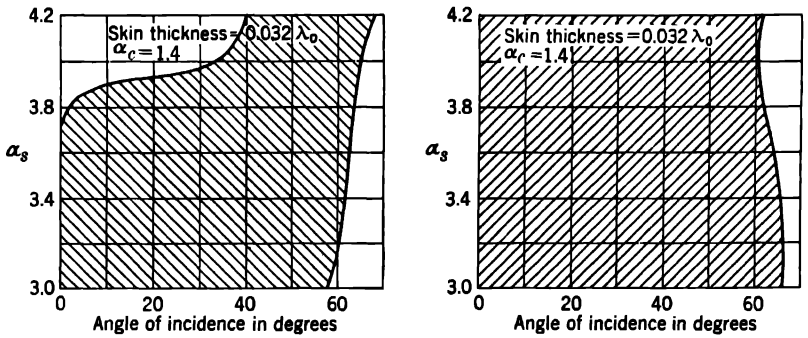

(*a*) *Constant* core thickness. Core tolerance $= 0.016\lambda_0$. (*b*) *Optimum* core thickness. Core tolerance $= 0.016\lambda_0$.

FIG. 11·20.—Effect of variation in dielectric constant of the skin (perpendicular polarization). Shaded area represents range of angles of incidence for which the reflection is less than 10 per cent.

pendicular polarization if the dielectric constant of the skin is assumed to vary while the skin thickness remains unchanged. In Fig. 11·20*a* are curves showing the range of angle of incidence for less than 10 per cent reflection in power for a sandwich in which $\alpha_c = 1.4$, $d_s = 0.032\lambda_0$, core

tolerance = $\pm 0.016\lambda_0$, and the core thickness has the optimum value for a skin dielectric constant of $3.7\epsilon_0$. In this case, variation between $3.5\epsilon_0$ and $3.9\epsilon_0$ appears allowable in the dielectric constant of the skin, other factors remaining constant. This represents a reasonable range of variation of dielectric constant of certain skin materials in use at present.

If the core thickness is adjusted to take care of variation in the dielectric constant of the skin, it then appears that within reasonable limits the reflection behavior of a given sandwich construction is not markedly affected by variations in the dielectric constant of the skin. The range of angles of incidence for less than 10 per cent reflection in power is nearly as great for a skin with a dielectric constant of $4.2\epsilon_0$ as it is for a skin with a dielectric constant of $3.7\epsilon_0$, provided that suitable change is made in the thickness of the core (Fig. 11·20*b*).

11·9. Reflection of Sandwiches with Skins of Modified Half Wavelength.—The sandwich construction with core of low dielectric constant and electrically thin skins is of limited use for streamlined radomes for perpendicular polarization in the 1-cm band because its strength and stiffness are small. It is therefore desirable to consider the electrical properties of the sandwich made of modified half-wavelength skins, as it is strong and stiff.

Assume that the skins of a sandwich are of such thickness that by themselves they would each have zero reflection at either perpendicular or parallel polarization at a given angle of incidence, say θ_s. The skin thickness is then given by $\lambda_0/2\sqrt{\alpha_s - \sin^2\theta_s}$, where α_s is the specific dielectric constant of the skins. When θ_0 equals θ_s, the reflection of the whole sandwich is equal to the reflection of the core alone at an angle of incidence θ_s and is thus a function of θ_s, the core thickness d_c, and the dielectric constant of the core α_c. For example, if the dielectric constant of the core is equal to $1.4\epsilon_0$ and θ_s is equal to 45°, the maximum power-reflection coefficient of such a sandwich at that angle at perpendicular polarization is 0.08. Table 11·8 gives, similarly, the maximum possible value of $|R|^2$ for the whole sandwich when the angle of incidence θ_0 is

TABLE 11·8.—MAXIMUM POWER-REFLECTION COEFFICIENT AT ANGLE OF INCIDENCE θ_s FOR THICK-SKINNED SANDWICHES

α_c	$\theta_s = 30°$		$\theta_s = 45°$		$\theta_s = 60°$	
	Perpendicular polarization	Parallel polarization	Perpendicular polarization	Parallel polarization	Perpendicular polarization	Parallel polarization
1.4	0.04	0.01	0.08	0	0.20	0.02
1.2	0.01	0	0.03	0	0.08	0.01

equal to θ_s, for values of θ_s equal to 30°, 45°, and 60° and for values of α_c equal to 1.4 and 1.2 respectively. It is observed from Table 11·8 that if α_c is equal to 1.4 and θ_s is less than 45° or if α_c is equal to 1.2 and θ_s is less than 60°, the reflection of the sandwich at perpendicular polarization at an angle of incidence equal to θ_s is not greater than 8 per cent in power

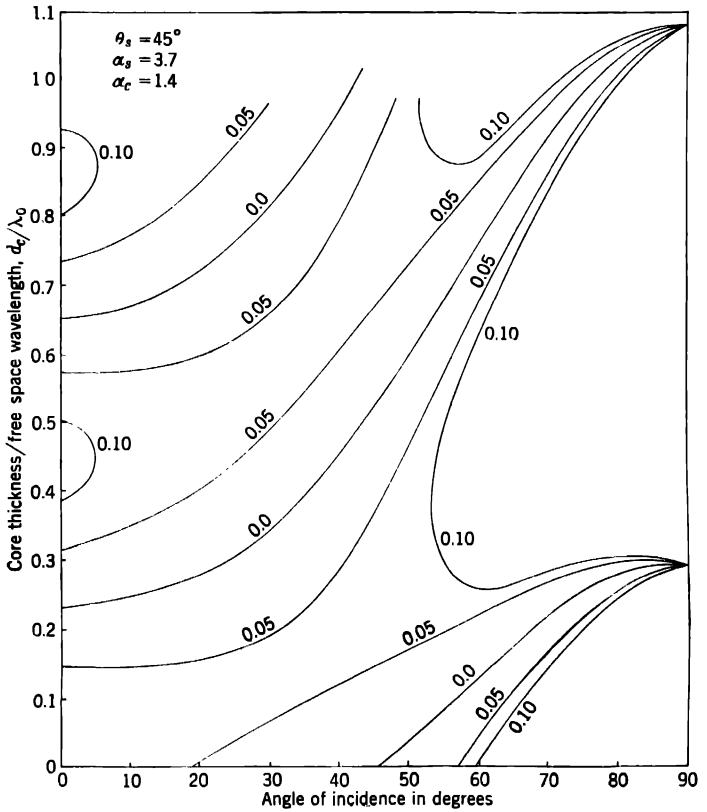

FIG. 11·21.—Power-reflection contours for a thick-skinned sandwich (perpendicular polarization).

for all values of core thickness. If the core thickness chosen is such that the reflection of the sandwich as a whole is zero (at perpendicular polarization) at some other angle of incidence θ_c, the reflection of the sandwich over the whole range of angles of incidence from θ_s to θ_c can be made small.

The reflection contours[1] for perpendicular polarization of such sand-

[1] For reflection contour charts for similar sandwiches in which the dielectric constant of the skin is equal to $3.0\epsilon_0$, see E. M. Everhart, *op. cit.*

wiches, for which $\alpha_s = 3.7$ and $\alpha_c = 1.4$, are shown in Fig. 11·21. The skin thickness is equal to $0.280\,\lambda_0$, corresponding to a value of θ_s equal to 45°. From Fig. 11·21 it is seen that at perpendicular polarization if θ_c is equal to 14°, corresponding to a first-order core thickness of $0.258\lambda_0$, the

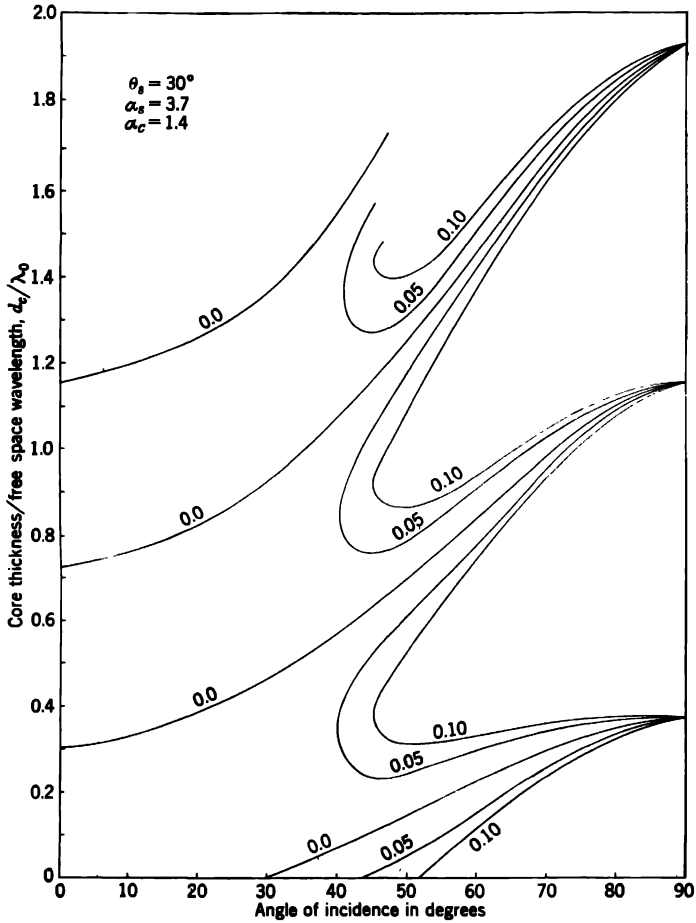

FIG. 11·22.—Power-reflection contours for a thick-skinned sandwich (perpendicular polarization).

reflection is less than 10 per cent in power from normal incidence up to 82° incidence. If θ_c is equal to 35°, corresponding to a second-order core thickness of $0.871\lambda_0$, the reflection is less than 10 per cent in power from 5° to 72° incidence. Under these circumstances the reflection of the whole sandwich is zero at 35° and 67° incidence, while at 45° incidence

the reflection cannot be greater than 8 per cent in power for any core thickness.

Figure 11·22 shows the reflection contour diagram for perpendicular polarization for a family of sandwiches similar to those in Fig. 11·21 except that the skin thickness is reduced to $0.269\lambda_0$, corresponding to a

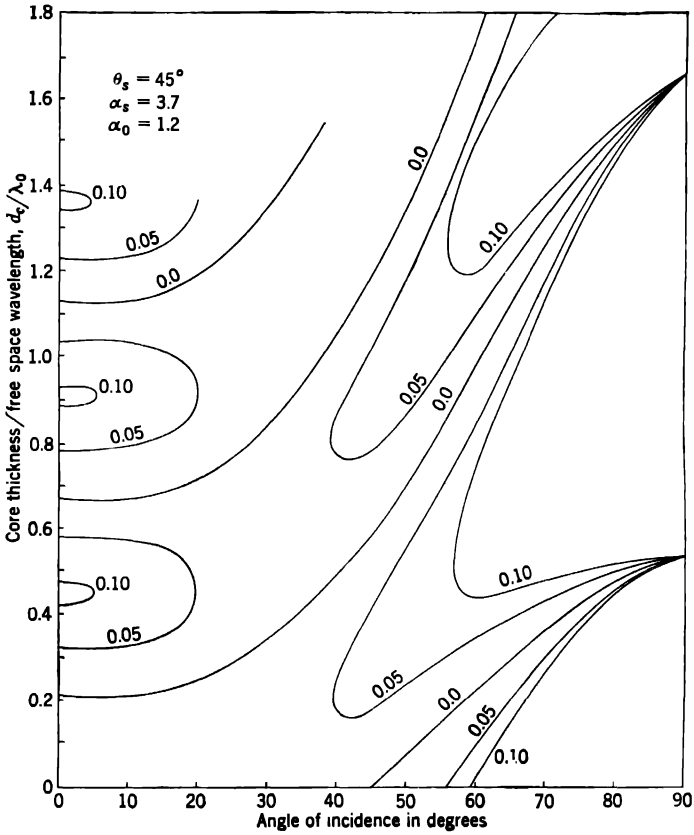

FIG. 11·23.—Power-reflection contours for a thick-skinned sandwich (perpendicular polarization).

value of θ_s equal to 30°. By a comparison of Fig. 11·21 with Fig. 11·22 it is seen that if good transmission characteristics over a wide range of angles of incidence at perpendicular polarization are required and α_c is constant, the tolerance of the skin thickness is a rather small percentage whereas the tolerance of the core spacing is large. Corresponding reflection contours show that for parallel polarization the reflection is always less than 10 per cent in power below 68° incidence.

When the dielectric constant of the core is reduced to $1.2\epsilon_0$ but the thickness and dielectric constant of the skin are unchanged from the values of Fig. 11·21, the power-reflection contours for such sandwiches for perpendicular polarization are as given in Fig. 11·23 and are appreci-

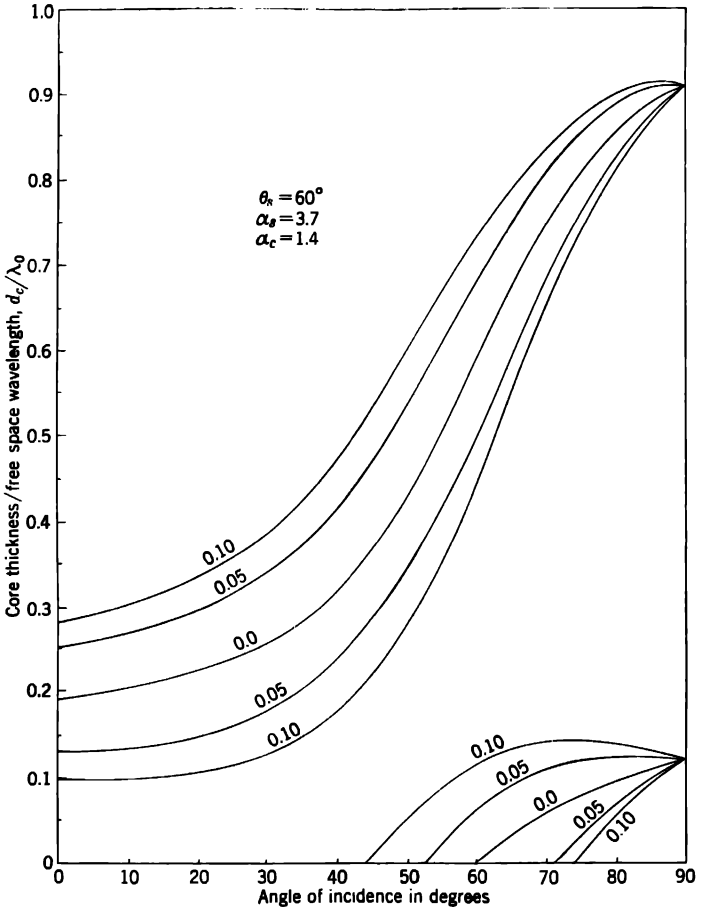

FIG. 11·24.—Power-reflection contours for a thick-skinned sandwich (perpendicular polarization).

ably different from those of Fig. 11·21. It appears, therefore, that the dielectric constant of the core is critical for this type of sandwich.

In Fig. 11·24 reflection contours are plotted for perpendicular polarization for a family of sandwiches differing from that of Fig. 11·21 in that the skin thickness is equal to $0.292\lambda_0$, corresponding to a value of θ_s of 60°. They show that for no value of core thickness of even the first order

does a sandwich with these skins possess satisfactory electrical behavior over a wide range of angles of incidence at perpendicular polarization. The loss in transmission resulting from reflection is practically the same in a real sandwich as in a lossless sandwich, but the transmission loss due to absorption may become important in sandwiches for which the electrical thicknesses of both skin and core are large (see Sec. 11·11). For such sandwiches it may be necessary to use materials having lower loss tangents than are satisfactory for use with thin-skinned first-order sandwiches. It appears that the tolerance requirements are more severe for sandwiches with skins of modified half-wavelength thickness than they are for sandwiches with thin skins.

Another sandwich construction which seems to have interesting possibilities for use at perpendicular polarization in the 1-cm band is one in which the faces are themselves each first-order sandwiches with thin skins, with a core of such thickness that each individual "face sandwich" has zero reflection at some particular angle of incidence θ_s. The face sandwiches are assembled into a sandwich separated by a core of such thickness that the reflection of the whole assembly is zero at another angle of incidence θ_c. With suitable choice of θ_s and θ_c it should be possible to design such a sandwich with a low reflection coefficient over a wide range of angles of incidence at perpendicular polarization. The strength, stiffness, and weight of such a construction should be intermediate between those of the thin-skinned sandwich considered in Sec. 11·8 and those of the sandwich with modified half-wavelength skins.

11·10. Reflection of Sandwiches with Cores of High Dielectric Constant.—The reflection of a sandwich is zero for all thicknesses of the core when the dielectric constant of the core is equal to the square of the dielectric constant of the skin and the thickness of the skin is equal to an odd multiple of one quarter wavelength in the skin (Secs. 10·6 and 12·5). In order to design a sandwich wall so that the reflection for all values of core thickness is zero at a given angle of incidence (θ_s, say), we substitute for the actual dielectric constants ϵ_s and ϵ_c of skin and core respectively the corresponding equivalent values $\epsilon_{(s\theta)s}$ and $\epsilon_{(s\theta)c}$ (for perpendicular polarization) or $\epsilon_{(p\theta)s}$ and $\epsilon_{(p\theta)c}$ (for parallel polarization), as per Eqs. (1) and (2). The skin thickness at either polarization for the arbitrary incidence case [*cf.* Eq. (4)] is given by

$$\frac{d_s}{\lambda_0}\sqrt{\alpha_s - \sin^2\theta_s} = \frac{2N+1}{4}, \tag{12}$$

where N is zero or a positive integer. If the core thickness is now chosen so that the reflection of the sandwich as a whole is zero at some other angle of incidence (θ_c, say), then for the given polarization, there will be at least two angles of incidence for which the reflection of the sandwich is

zero. Although this type of design has not been studied in detail, it seems reasonable to believe that with a suitable choice of materials and of θ_s and θ_c, a low reflection over a wide range of angles of incidence might be obtained. One possible combination of values for the dielectric constants of the skin and core is given by $\theta_s = 0°$, $\alpha_s = 3.0$, $\alpha_c = 9.0$. This arrangement requires a core material of high dielectric constant; such materials are discussed in Sec. 13·13. Another set of values for perpendicular polarization is $\theta_s = 30°$, $\alpha_s = 1.7$, $\alpha_c = 3.0$. This requires a conventional high-strength laminate for the core with an expanded material of low dielectric constant for the faces (see Sec. 13·13). This construction can be generalized by having three or more types of material symmetrically arranged, with the material of lowest dielectric constant on the outside and a layer of the material of highest dielectric constant in the center of the sandwich, or by using material whose dielectric constant varies continuously from a low value at each surface to a maximum value at the center. Such an arrangement is analogous to a broad-banded transformer in a transmission line.[1] Favorable strength/weight and stiffness/weight ratios, as are obtained with sandwiches with high-density faces and low-density cores, should not be expected from any of these arrangements which have cores of dielectric constant higher than that of the skins.

11·11. Transmission of Lossy Sandwiches.—The theory of the transmission of power by lossy sandwiches[2] is developed in Sec. 12·6, Eq. (12·112) giving a good approximation for the maximum transmission of the symmetrical lossy sandwich. As a basis for general discussion we can take the somewhat rougher approximation given by Eq. (12·115). It is

$$\frac{|T'|_0^2 - |T'|_{\text{lossy}}^2}{|T'|_0^2} \approx 4Q_s + 2Q_c, \tag{13}$$

in which

$$Q_s = \frac{2\pi d_s}{\lambda_0} \frac{n_s^2 K_s}{\sqrt{n_s^2 - \sin^2\theta_0}} = \frac{\pi d_s \alpha_s \tan\delta_s}{\lambda_0 \sqrt{\alpha_s - \sin^2\theta_0}},$$

$$Q_c = \frac{2\pi d_c}{\lambda_0} \frac{n_c^2 K_c}{\sqrt{n_c^2 - \sin^2\theta_0}} = \frac{\pi d_c \alpha_c \tan\delta_c}{\lambda_0 \sqrt{\alpha_c - \sin^2\theta_0}}.$$

In all practical cases the loss in transmission will be a little greater than the value given by Eq. (13).

In the sandwich having thin skins the thickness of the core is approximately a half wavelength in the material of the core, $\lambda_0/2\sqrt{\alpha_c}$. For such sandwiches $Q_c \approx (\pi/2)(\tan\delta_c \sqrt{\alpha_c}/\sqrt{\alpha_c - \sin^2\theta_0})$, so the fractional absorption attributable to the core $2Q_c$ is about $\pi \tan\delta_c$ for inci-

[1] *Cf.* J. C. Slater, *Microwave Transmission*, McGraw-Hill, New York, 1942, p. 57.

[2] For a more detailed treatment of this subject see Y. N. Dowker, "Transmission of Sandwiches with Low-loss Skins and Cores," RL Report No. 483-22, 1945.

dence close to normal. Q_s and Q_c both increase with increasing angle of incidence, the relative increase being greater for materials of low dielectric constant.

The increase of loss in transmission with increasing angle of incidence is also greater for perpendicular polarization than for parallel polarization; this increase appears in the secondary factors of Eq. (12·112) that express the effects of multiple reflection. As with homogeneous sheets (*cf.* Sec. 11·5), these factors become important for high angles of incidence, particularly for perpendicular polarization.

11·12. Experimental Results on the Transmission of Typical Sandwiches.—The theory of the transmission of homogeneous panels and of sandwiches has been discussed in preceding sections of this chapter.

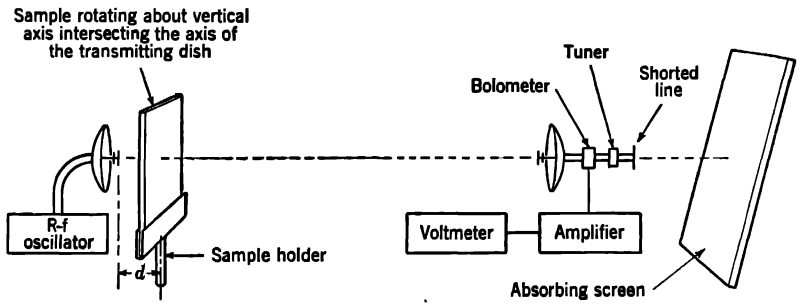

FIG. 11·25.—Equipment for free-space measurement of transmission of panels at arbitrary incidence.

Although the theory seems to be correct and is useful as the basis for design, it is nevertheless desirable to have an experimental method for studying the transmission. This is especially important for sandwiches because of the variability of their dielectric constants, loss tangents, and thicknesses and the difficulty of making proper allowance for the skin-core bond. The experimental test on a plane panel is a necessary intermediate step between the study of theoretical contour charts and the actual design, fabrication, and testing of a streamlined sandwich radome.

Experimental Methods.—Apparatus in which samples of the materials under test can be inserted into transmission lines, particularly waveguides, has been found to be of limited usefulness, principally because of the smallness of the area tested in any one sample and because of the difficulties of preparing an adequate number of representative test samples of the material. The free-space method to be described has therefore been developed.

Figure 11·25 shows the equipment used for such measurements. The transmitting and receiving antennas, each with paraboloidal reflectors, are arranged with their axes horizontal and coincident and their separa-

tion D about 12 to 16 ft. The distance d from the transmitting antenna to the panel ranges from 12 to 15 in. It must be great enough to allow the panel to be tilted through the desired angles without interfering mechanically with the transmitting antenna. Arrangements for altering both d and D by $\lambda_0/4$ are provided. The axis about which the sample holder rotates is vertical and intersects the common axis of the antennas. Absorbing screens are placed around the equipment to reduce the effects of reflection of stray radiation.

In order that voltmeter readings may be proportional to received power, a square-law detector is used. The receiving line is tuned for the maximum value of received power with no sample in place; and by altering the attenuation in the transmitting line or the gain on the amplifier, the voltmeter needle is set in about the middle of its scale.

For a chosen polarization, voltmeter readings are taken for each of four settings of d and D, at each of a reasonably large number of values of the angle of incidence. The four pairs of values of d and D used at each angle of incidence are (1) d_0, D_0; (2) $d_0 \pm \lambda_0/4$, D_0; (3) $d_0 \pm \lambda_0/4$, $D_0 \pm \lambda_0/4$; (4) d_0, $D_0 \pm \lambda_0/4$, where d_0 and D_0 are the initial values of the distances d and D shown in Fig. 11·25. Varying the distances d and D by a quarter wavelength and taking the averages of the readings so obtained serve to nullify the effects of extraneous reflections, varying thicknesses of the panels, and nonintersection of the axes of the antennas and the axis of rotation of the panel. The power output of the transmitter is checked by occasional reading of the voltmeter at $\theta = 20°$, $d = d_0$, $D = D_0$. It has been found sufficient to take readings at $\theta = 10°$, 20°, 30°, 40°, 50°, 55°, 60°, 65°, and 70°. Voltmeter readings taken at $\theta = 0°$ are unreliable and are not used because reflection into the transmitting line results in pulling. To obtain power transmission in per cent for a given value of θ, we divide each of the four voltmeter readings at that value of θ by the no-sample reading and take the arithmetical mean of the quotients. The results are plotted graphically and connected by a smooth curve. The process is repeated for the other polarization, and the resulting graph superimposed on the first. Since the transmission at $\theta = 10°$ does not differ significantly from that at $\theta = 0°$, the two curves can be extrapolated to a common value for $\theta = 0°$. Figures 11·28 and 11·29 show such curves. Numerous experiments show that such transmission measurements are reproducible to within 2 per cent by different observers and different equipment, even without extreme care being taken in the alignment of the axes of the antennas and the axis of rotation of the sample. The apparatus has been further developed to give autographic records of transmission.

The Thin-skinned Sandwich with Low-density Core.—The type of sandwich panel that has been studied in greatest detail is one upon which

the specifications for a saucer-shaped streamlined radome for the Boeing B-29 airplane have been based; the radome (Fig. 14·1) houses the scanner with the 60-in. reflector of the AN/APQ-13 system (Sec. 6·11). This sandwich panel consists of skins of four layers of ECC-128 Fiberglas cloth bonded with low-pressure resin (Laminac X-4000 of the American Cyanamid Company) and a core made of a fine-cell GR-N synthetic hard rubber foam with a density of about 12 lb/ft³. The fabrication tech-

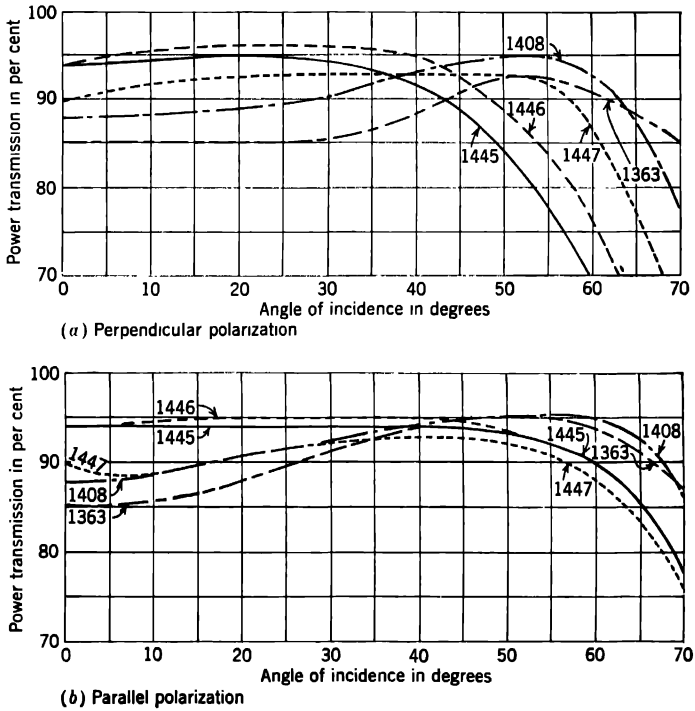

FIG. 11·26.—Effect of over-all thickness on transmission of sandwiches with Fiberglas skins.

nique is the "single-stage wet lay-up" procedure.[1] The actual thickness of the skin is about 0.030 in., and its effective thickness is about 0.040 in. The tests were made at a wavelength of 3.2 cm. Figures 11·26*a* and 11·26*b* show curves of power-transmission coefficient at perpendicular and at parallel polarization, for a series of such plane sandwich panels made by the same fabricator; the panels differ only in over-all thickness. The power-transmission coefficient $|T'|^2$ at normal incidence for the sandwiches is obtained by extrapolating the transmission curves for parallel and perpendicular polarization back from 10° incidence to a common

[1] See Sec. 13·6.

value at 0° incidence. In Table 11·9 are given the values of $|T|^2$ and $|R|^2$ for normal incidence and the values of $|T|^2$ at the peak transmission and at 70° incidence for each polarization. In general, $|T|^2$ is less than $1 - |R|^2$ because of absorption of power in the panel.

TABLE 11·9.—TRANSMISSION CHARACTERISTICS OF SANDWICH PANELS
$\lambda_0 = 3.2$ cm

Panel No.	Over-all thickness, h, in.	Normal incidence		$\|T\|^2$ at peak value		$\|T\|^2$ at 70° incidence	
		$\|T\|^2$ by extrapolation	$\|R\|^2$	Parallel polarization	Perpendicular polarization	Parallel polarization	Perpendicular polarization
1445	0.317	0.940	0.002	0.94	0.95	0.78	0.47
1446	0.354	0.940	0.006	0.95	0.96	0.78	0.54
1447	0 407	0.900	0.011	0.93	0.94	0 77	0.66
1408	0.407	0.880	0.069	0.96	0.95	0.87	0.78
1363	0.425	0.850	0.092	0.95	0.92	0.87	0.86

The measured transmission of these panels agrees in a general way with theoretical considerations. Panel 1445 is seen to be almost a normal incidence design; the reflection at normal incidence is very small, while the transmission at parallel polarization is very good up to about 55° incidence and thereafter falls off sharply. The transmission at perpendicular polarization, however, begins to fall off at about 30° incidence. Panel 1446 is slightly thicker than Panel 1445; the behavior at perpendicular polarization is slightly improved. Panel 1447 is still thicker; its transmission at parallel polarization is slightly poorer than that of the preceding panels, while the transmission at perpendicular polarization is now uniformly good up to about 60° incidence. Panel 1408 is seen to have the same thickness as 1447 but a higher value of $|R|^2$ at normal incidence, suggesting that the first-mentioned panel has a greater value of effective skin thickness. The transmission of Panel 1408 at perpendicular polarization is nearly as good as at parallel polarization. Finally, for the thickest panel in the series, 1363, the transmission at 70° incidence for both polarizations is the same as at normal incidence; this panel may be considered as representing a construction having optimum transmission characteristics for many streamlined radomes.

Effect of Skin Resin.—Resins used in sandwich construction differ appreciably in dielectric constant and loss tangent, ease of manipulation in fabrication, cost, and resistance to weathering. Experiments with different resins indicate that there is not too much difference in characteristics of sandwich transmission if the over-all sandwich thickness

h is reduced slightly when resins of higher dielectric constant are used. Tests were made on sandwiches with the following resins used in the skins: Laminac X-4000 polyester-styrene resin (American Cyanamid Company), Bakelite BRS 16631 polyester-styrene resin (Bakelite Corporation), Plaskon 911 resin (Plaskon Corporation), Styramic HT dichlorostyrene resin (Monsanto Chemical Company), and Bakelite BV17065 phenolic resin (Bakelite Corporation). The electrical characteristics of these panels are summarized in Table 11·10. All appear to be suitable where good transmission over a range of angles of incidence from normal incidence to 70° is required at both polarizations; the transmission is approximately the same at both ends of this range of angles of incidence. Information concerning the mechanical properties of this type of sandwich construction is given in Sec. 13·10.

TABLE 11·10.—TRANSMISSION CHARACTERISTICS OF SANDWICH PANELS
$\lambda_0 = 3.2$ cm

Resin	Panel No.	Panel thickness h, in.	Normal incidence		$\|T\|^2$ at peak value		$\|T\|^2$ at 70° incidence	
			$\|T\|^2$ by extrapolation	$\|R\|^2$	Parallel polarization	Perpendicular polarization	Parallel polarization	Perpendicular polarization
X-4000	1363	0.425	0.850	0.092	0.95	0.92	0.87	0.86
X-4000	1074	0.450	0.845	0.096	0.96	0.94	0.85	0.85
BRS 16631	1508	0.457	0.860	0.086	0.94	0.94	0.83	0.84
BRS 16631	1509	0.462	0.825	0.123	0.94	0.93	0.82	0.84
BRS 16631	1122	0.455	0.830	0.120	0.93	0.92	0.83	0.87
Pl. 911	1077	0.444	0.850	0.105	0.96	0.95	0.85	0.82
Pl. 911	1277	0.423	0.835	0.072	0.96	0.91	0.84	0.79
Styramic HT	1549	0.455	0.900	0.079	0.98	0.98	0.87	0.83
BV17065	1547	0.431	0.870	0.068	0.97	0.92	0.83	0.76

Asymmetrical Sandwiches.—Asymmetrical sandwiches were fabricated as discussed above, except that instead of using four layers of Fiberglas fabric to form each skin, one skin was fabricated from three layers of fabric and the other from five layers. The resin used was Bakelite BRS 16631. The electrical characteristics of such Panels 1318 and 1319 are summarized in Table 11·11.

It appears that Panel 1318 represents a satisfactory construction where good transmission over a range of angles of incidence is required at parallel polarization. Panel 1319 has good transmission characteristics at both polarizations from normal incidence to 70° incidence. Comparing

this panel with the corresponding symmetrical Panels 1508, 1509, and 1122, it is seen that all these panels are equally satisfactory electrically. Mechanical properties of these asymmetrical sandwich panels are discussed in Sec. 13·10.

TABLE 11·11.—TRANSMISSION CHARACTERISTICS OF ASYMMETRICAL SANDWICH PANELS
$\lambda_0 = 3.2$ cm

Panel No.	Panel thickness, h, in.	Normal incidence		$\|T\|^2$ at peak value		$\|T\|^2$ at 70° incidence	
		$\|T\|^2$	$\|R\|^2$	Parallel polarization	Perpendicular polarization	Parallel polarization	Perpendicular polarization
1318	0.407	0.920	0.052	0.98	0.95	0.86	0.75
1319	0.482	0.865	0.104	0.95	0.93	0.87	0.88

Honeycomb Core Construction.—A series of sandwich panels has been fabricated using Fiberglas "honeycomb" (hexagonal grid) core, the core and skins being impregnated with Plaskon 911 resin. This series of panels is of interest in showing the effect of both skin thickness d_s' and over-all sandwich thickness h on transmission behavior. The electrical characteristics of these honeycomb core sandwich panels are listed in Table 11·12, and their mechanical properties are discussed in Sec. 13·10.

TABLE 11·12.—ELECTRICAL CHARACTERISTICS OF SANDWICH PANELS WITH HONEYCOMB CORES
$\lambda_0 = 3.2$ cm

Panel No.	Skin thickness d_s', in.	Panel thickness h, in.	Normal incidence		$\|T\|^2$ at peak value		$\|T\|^2$ at 70° incidence	
			$\|T\|^2$	$\|R\|^2$	Parallel polarization	Perpendicular polarization	Parallel polarization	Perpendicular polarization
1514	0.040	0.340	0.930	0.034	0.96	0.95	0.90	0.63
1515	0.040	0.405	0.840	0.133	0.95	0.93	0.93	0.79
1425	0.040	0.436	0.760	0.186	0.91	0.91	0.81	0.85
1424	0.040	0.479	0.730	0.224	0 94	0.90	0.88	0.88
1517	0.030	0.455	0.860	0.123	0.96	0.96	0.88	0.84
1400	0.030	0.470	0 830	0.134	0.97	0.94	0.89	0.87
1427	0.030	0.532	0 780	0.128	0.95	0 91	0.89	0.89
1426	0.020	0.489	0.965	0.032	0.99	0.99	0.93	0.84

The power-transmission coefficients of the sandwich panels whose skin thickness is equal to 0.040 in. are plotted in Fig. 11·27; the transmission

characteristics of the other sandwich panels given in Table 11·12 are shown in Fig. 11·28.

Panels 1514 and 1426 are seen to be nearly of normal-incidence design; these panels have good transmission characteristics at parallel polarization between normal incidence and 70° incidence. This is especially true for Panel 1426 which also has fairly good transmission at perpendicular polarization; such behavior is attributable to its extremely thin skins. Panel 1515 (skin thickness equal to 0.040 in.) corresponds

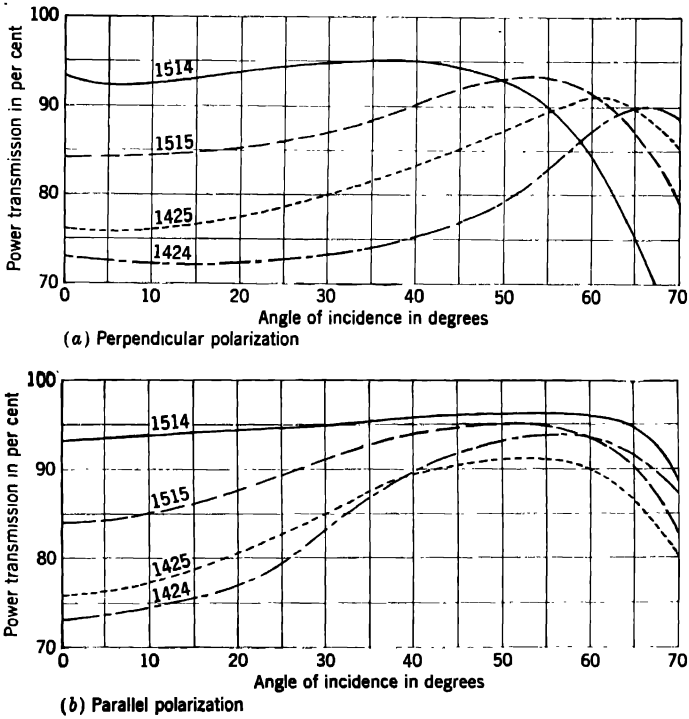

FIG. 11·27.—Transmission characteristics of sandwiches with honeycomb cores.

roughly to Panels 1517 and 1400 ($d_s' = 0.030$ in.). These panels represent satisfactory designs where good transmission characteristics are required from normal incidence to 70° incidence at perpendicular polarization. A decrease of 0.010 in. in skin thickness is seen to correspond to an increase of about 0.050 in. in over-all sandwich thickness. In Fig. 11·27*a* it is seen clearly that in accord with theory, increase in sandwich thickness at first increases the transmission at perpendicular polarization at high angles of incidence without too greatly reducing the transmission at low angles of incidence. As the thickness of the sandwich is further

increased, the transmission at low angles of incidence is decreased without very much improvement in the transmission at 70° incidence. With increase in sandwich thickness, the angle of incidence corresponding to

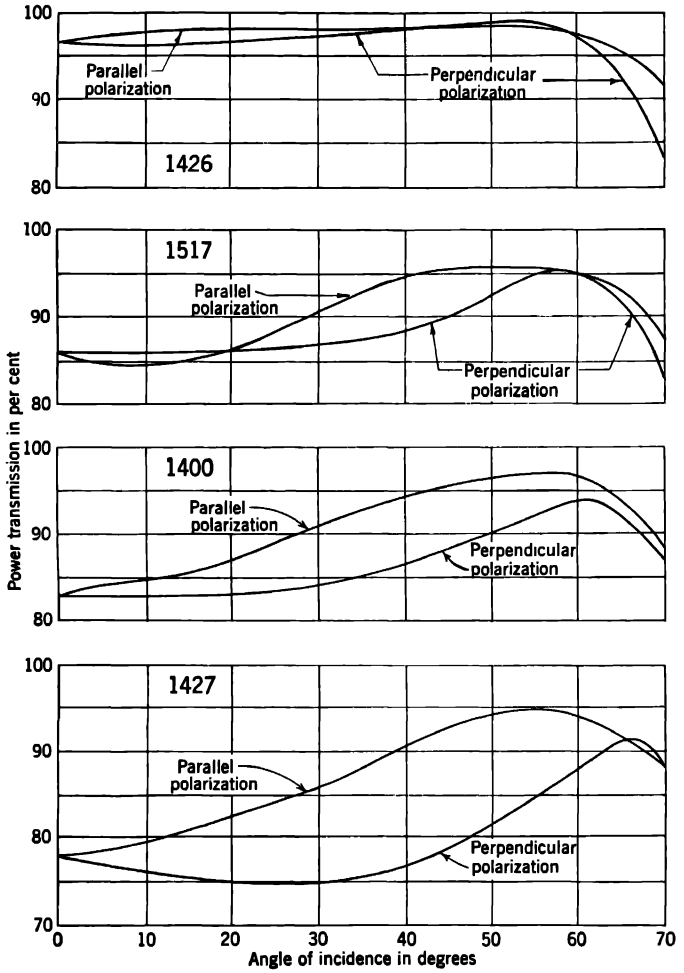

FIG. 11·28.—Transmission characteristics of sandwiches with honeycomb cores.

peak transmission at perpendicular polarization increases. At the peak transmission the reflection is presumably very small. As the thickness of the sandwich is increased the peak transmission falls off as it moves to higher angles of incidence. This is presumably due to the increase in absorption with angle of incidence at this polarization.

Sandwiches with Fiber-A Skins.—Fiber-A fabric is of interest for the construction of radomes, especially of streamlined radomes, on account of its low moisture absorption; laminates of Fiber-A with the usual low-pressure resins have lower dielectric constants and loss tangents than laminates of Fiberglas fabric with the same resins (*cf.* Sec. 13·14). Sandwich panels with skins of Fiber-A fabric laminated with Bakelite BRS 16631 resin have been made with cores of synthetic rubber foam. The three sandwich panels listed in Table 11·13 have skins 0.039 in. thick.

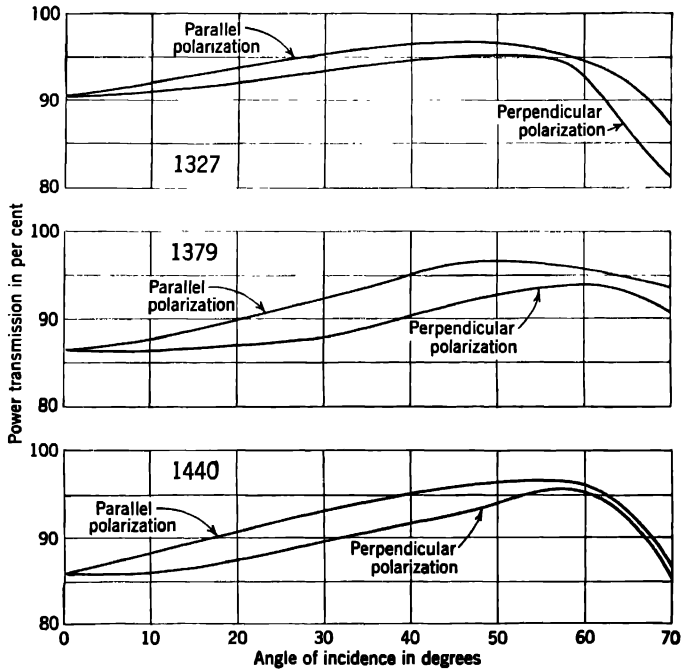

FIG. 11·29.—Transmission characteristics of sandwiches with Fiber-A skins.

The table gives the electrical characteristics of these panels; their mechanical properties are discussed in Sec. 13·10. Transmission curves for the above three sandwich panels are given in Fig. 11·29 for comparison with the transmission behavior of Fiberglas sandwich panels.

Sandwiches with Cotton Fabric Skins.—In view of the availability and cheapness of cotton fabric and the ease of fabrication of sandwiches with skins of this material, one might think that it could be used for radomes. In order to have the same flexural strength as Fiberglas skins, cotton fabric skins must be thicker (*cf.* Sec. 13·9). This requirement, together with the high loss tangent that cotton laminates have under ordinary

conditions, leads to excessive electrical absorption. This absorption becomes worse under extreme conditions of temperature and humidity, as experienced in tropical climates. The use of this fabric for microwave radomes is therefore inadvisable.

TABLE 11·13.—ELECTRICAL CHARACTERISTICS OF FIBER-A SANDWICH PANELS
$\lambda_0 = 3.2$ cm

Panel No.	No. of fabric plies in each skin	Panel thickness h, in.	Normal incidence		$\|T\|^2$ at peak value		$\|T\|^2$ at 70° incidence	
			$\|T\|^2$	$\|R\|^2$	Parallel polarization	Perpendicular polarization	Parallel polarization	Perpendicular polarization
1327	3	0.475	0.905	0.045	0.97	0.95	0.87	0.81
1379	3	0.525	0.865	0.099	0.97	0.94	0.93	0.91
1440	6	0.532	0.860	0.052	0.96	0.95	0.86	0.85

11·13. Elliptical Polarization.—When a plane polarized wave passes through a panel at oblique incidence, it suffers a retardation in phase that is different for parallel and perpendicular polarizations. If the plane of polarization lies at an angle between parallel and perpendicular, the wave can be thought of as consisting of two such polarized components. These components will undergo a relative shift of phase in passing through the panel, and the emerging resultant wave will be elliptically polarized. The theory of this effect is discussed in Sec. 12·7, wherein it is shown that the result is always a weakening of the radar signals.

The designer of radomes needs to know whether or not this effect is ever serious and, if so, under what circumstances. The answer appears to be that it will not be serious for well-designed radomes that are otherwise satisfactory. It is difficult, however, to make a general argument that will apply to all cases. All proposed radomes should be carefully scrutinized to see whether or not they are likely to give trouble on this account. The calculations required can be laborious; it will often be easier to investigate the effect experimentally. Apparatus similar to that described in Sec. 11·12 and illustrated in Fig. 11·25 can be used. If a reflecting sheet of metal is placed so as to reflect the transmitted wave back through the sheet into the transmitting antenna, standing waves will be produced in the r-f line from the oscillator to the antenna. The shift of phase of the reflected wave can be determined from the shift of the pattern of standing waves that is observable in a slotted section of the r-f line.

Before the importance of this effect can be judged, it is necessary to

set up a criterion of satisfactory performance. Let us make the conservative assumption that a radome will be satisfactory if the variation between maximum and minimum received power is no more than 1 db as the plane of polarization is rotated. This condition is to be satisfied at every angle of incidence in the range for which the radome was designed.

When the received signals for the two principal polarizations are equal (assuming equal reflection by the target), the minimum power will be received at settings of the plane of polarization of 45°, 135°, etc., and have a value that is $(1 + \cos \delta)/2$ times the maximum [see Eq. (12·119); $\sin \psi = \cos \psi = \sqrt{2}/2$]. The angle δ is the relative shift of phase resulting from two traversals of the radome. One decibel is equivalent to a ratio of 0.79, so we have $1 + \cos \delta = 2 \times 0.79$, or $\cos \delta = 0.58$. If, however, we assume that the received power at perpendicular polarization is just 0.79 times that at parallel polarization, we have to find the limiting value of $\cos \delta$ that will give no further decrease of power at any other value of ψ. By Eq. (12·121) and its discussion, this is seen to be $\cos \delta = \sqrt{0.79} = 0.89$. This second value for $\cos \delta$ is more restrictive and will therefore be taken as the one to be used. The corresponding value of δ is 27°. By this criterion, any radome that gives a maximum relative phase displacement of 13·5° or less in one traversal should be considered satisfactory.

The phase shifts in sheets of dielectric material can readily be calculated. It is necessary to take some upper limit for the allowed reflection. A value of 0.11, corresponding to a loss of 1 db for two traversals of the radome, is consistent with the previously chosen criterion for allowable shift of phase. For materials of dielectric constant less than about $5\epsilon_0$ the thickness must be enough greater than a half wavelength to give this value of reflection at normal incidence. The reflection goes to zero at a larger angle of incidence and then rises rapidly (see Fig. 11·9). As the dielectric constant approaches $5\epsilon_0$, the angle of incidence for which the reflection becomes zero approaches 90°. For higher values of the dielectric constant the appropriate thickness is the one that corresponds to $\phi = 180°$ either for grazing incidence or for the largest angle of incidence that will be encountered in practice. The general principle for keeping δ small is to make the departures from the modified half-wavelength thickness small for the higher angles of incidence, for which the interface reflection is large. [Equations (12·117) and (12·118) show that it is desirable to keep $\tan \phi$ small for large values of r^2.] The power-reflection coefficient at normal incidence is less than 0.11 for all such sheets of dielectric constant above $5\epsilon_0$ and has still lower values at intermediate angles. If the shifts of phase are calculated for an array of such panels, it is found in all cases that the shifts are less than the allowable 13.5° when the power-reflection coefficient for a perpendicularly

polarized wave is less than 0.11. Larger shifts of phase will be found for panels that reflect more energy; but if this increased reflection is permissible, the restriction on the shift of phase can be relaxed. The general conclusion is that the shift of phase is negligible for any well-designed radome.

The same general conclusion may be expected to be valid for symmetrical sandwich radomes. The shift of phase and the minimization of the reflection are different effects of the multiple reflection that is fundamentally the same both for homogeneous sheets and for sandwiches. The relation between the two effects should therefore be much the same in both.

CHAPTER 12

THEORY OF THE REFLECTION AND TRANSMISSION OF ELECTROMAGNETIC WAVES BY DIELECTRIC MATERIALS

By H. Leaderman and L. A. Turner

Many questions that arise in the design of radomes can be answered by reference to the theory of reflection and transmission of plane electromagnetic waves by infinite sheets of dielectric material. The basic theory is developed in the standard textbooks[1] on optics and electromagnetic waves. This chapter presents a brief review of the fundamentals, a selection of some of the familiar results that are needed for the discussion, and further development for special cases of interest in connection with radomes.[2] These cases were not of much interest in the past and in the standard books are not treated so fully as is desirable for present purposes.

12·1. Plane Electromagnetic Waves.—As is well known, Maxwell's equations for the electric and magnetic fields in space can be manipulated to yield the following differential equation

$$\frac{\partial^2 M}{\partial x^2} + \frac{\partial^2 M}{\partial y^2} + \frac{\partial^2 M}{\partial z^2} = \epsilon\mu \frac{\partial^2 M}{\partial t^2}. \tag{1}$$

In this equation M can represent any one of the three components of the electric field or any one of the three components of the magnetic field, ϵ is the dielectric constant of the medium, and μ is its permeability. One solution of this equation has the form

$$M = f\left(\alpha x + \beta y + \gamma z - \frac{t}{\sqrt{\epsilon\mu}}\right), \tag{2}$$

where f is any analytical function of the quantity in the parentheses. For this expression for M to be a solution of Eq. (1), it is necessary that

$$\alpha^2 + \beta^2 + \gamma^2 = 1. \tag{3}$$

When the quantities α, β, and γ are real numbers, they are the direction cosines of the common normal to a set of parallel planes, each of these

[1] P. Drude, *Theory of Optics*, Longmans, New York, 1939; J. A. Stratton, *Electromagnetic Theory*, 1st ed., McGraw-Hill, New York, 1941.

[2] The applications to radomes have been worked out in great detail in numerous reports of the Radiation Laboratory, principally by R. M. Redheffer, and in similar reports from TRE (Telecommunications Research Establishment) in England, principally by J. B. Birks.

planes being represented by the equation $\alpha x + \beta y + \gamma z = p$. The planes differ in their values of p, which, it may be recalled, represents the distance of such a plane away from the origin, as measured along the normal to the plane. Equation (2) represents a plane wave, since at every point on a plane having the equation $\alpha x + \beta y + \gamma z = p$ the component M has the same value

$$M = f\left(p - \frac{t}{\sqrt{\epsilon\mu}}\right). \tag{4}$$

At the instant $t = 0$, Eq. (4) reduces to $M = f(p)$, the simplest expression for the form of the whole wave. Since $f(p)$ is an entirely arbitrary function of p, the wave may be of any shape. It is sinusoidal if $f(p)$ is a sine or cosine function, but it may be a pulse, a saw tooth, or any other sort.

That Eqs. (2) and (4) represent plane waves traveling in the direction of increasing p with a velocity of $1/\sqrt{\epsilon\mu}$ is readily seen as follows. Equation (4) shows that if M has a certain value for $p = p_0$ and $t = t_0$, it will have the same value at the later time $t = t_0 + \Delta t$ over a plane further out for which $p = p_0 + (\Delta t/\sqrt{\epsilon\mu})$; the quantity in the parenthesis keeps the same value if both these changes are made in it. This means that the whole configuration of values of M existing at a time $t = t_0$ will again be found at the later time $t = t_0 + \Delta t$ but at a distance that is increased by $\Delta t/\sqrt{\epsilon\mu}$. The rate at which this configuration travels out, i.e., the velocity of the wave, is given by the distance traveled $\Delta t/\sqrt{\epsilon\mu}$ divided by the time in which it was traversed Δt; so the velocity of the wave is $1/\sqrt{\epsilon\mu}$.

One form of Eq. (2) that is of use for present purposes is

$$M = Ae^{C\left(\alpha x + \beta y + \gamma z - \frac{t}{\sqrt{\epsilon\mu}}\right)}, \tag{5}$$

in which both A and C are arbitrary constants that may be complex numbers. In particular, if we let C take the value $-2\pi j\sqrt{\epsilon\mu}/T$, Eq. (5) takes the more familiar and useful form

$$M = Ae^{2\pi j\left[\frac{t}{T} - \frac{(\alpha x + \beta y + \gamma z)\sqrt{\epsilon\mu}}{T}\right]} \tag{6}$$

Remembering that $e^{j\theta} = \cos\theta + j\sin\theta$, we see that the real part of the right-hand side of Eq. (6) represents a sinusoidal plane wave. The imaginary part also represents a sinusoidal wave. The complete expression is a linear combination of the two that is often used because it is simple to handle mathematically. The quantity T that appears in Eq. (6) is the period of the oscillation, since M takes the same value whenever t is increased by the amount T. The reciprocal of T is the frequency. Similarly the space period, or wavelength, λ is $T/\sqrt{\epsilon\mu}$, since M has the same value for all values of p that differ by this amount.

It is convenient to change the expression by introducing a new quantity that becomes the ordinary index of refraction in simple cases. As shown, the velocity of the waves is $1/\sqrt{\epsilon\mu}$. In vacuum this has the value $c = 1/\sqrt{\epsilon_0\mu_0}$, ϵ_0 and μ_0 denoting the values of ϵ and μ for free space. (The numerical values depend on the system of units used.) Let us define the constant n^* characterizing a medium as the ratio of the velocity in free space to the velocity in the medium.

$$n^* = c\sqrt{\epsilon\mu} = \frac{\sqrt{\epsilon\mu}}{\sqrt{\epsilon_0\mu_0}}. \tag{7}$$

In the following sections we shall be dealing only with mediums for which $\mu = \mu_0$, so that from now on n^* will be taken as equal to $\sqrt{\epsilon/\epsilon_0}$, the square root of the *specific* dielectric constant ϵ/ϵ_0. For those mediums for which ϵ is a real number, n^* is the ordinary optical index of refraction. In absorbing mediums, however, for which ϵ is a complex quantity, n^* is no longer the index of refraction in the ordinary sense but, as will be shown below, also expresses the absorbing properties of the medium.

If from Eq. (7) $\sqrt{\epsilon\mu} = n^*/c$ is substituted into Eq. (6) and λ_0 set for cT, we get

$$M = Ae^{2\pi j\left[\frac{t}{T} - \frac{n^*(\alpha x + \beta y + \gamma z)}{\lambda_0}\right]} \tag{8a}$$

or

$$M = Ae^{2\pi j\left[\frac{t}{T} - \frac{n^* p}{\lambda_0}\right]}. \tag{8b}$$

The product cT or λ_0 is the distance traveled in free space by the wave in one period of duration T; that is, it is the wavelength in free space. The quantity λ_0/n^* is the space period or generalized wavelength in the medium characterized by the constant n^*.

As mentioned above, the constant A can be a complex number. It can be represented by $a + jb$, in which a and b are both real numbers. It will be remembered that the complex number $a + jb$ can also be written as $Re^{j\psi}$ if $R = \sqrt{a^2 + b^2}$ and $\psi = \tan^{-1}(b/a)$. If for A, $Re^{j\psi}$ is substituted into Eq. (8b), it is clear that R is the real amplitude of the M-wave and the angle ψ that combines with the other exponent is a phase angle. The complex amplitude A thus expresses both amplitude and phase.

12·2. Absorbing Mediums.—(This section and the following one can be omitted by any reader who does not wish to go into the complications of the behavior of waves in absorbing mediums, without prejudice to his understanding of the further considerations of lossless dielectrics.)

As is discussed at length elsewhere,[1] the behavior of lossy dielectrics

[1] For example, A. von Hippel and R. G. Breckenridge, "The Interaction between Electromagnetic Fields and Dielectric Materials," NDRC 14–122, January 1943.

can be described by attributing to them a complex dielectric constant

$$\epsilon = \epsilon' - j\epsilon'' \tag{9a}$$

or

$$\epsilon = \epsilon'(1 - j \tan \delta). \tag{9b}$$

where $\tan \delta = \epsilon''/\epsilon'$.

Let us now consider the implications of Eq. (8*b*) in a case for which α, β, and γ are still real numbers but ϵ is complex. We have

$$n^* = \sqrt{\frac{\epsilon}{\epsilon_0}} = \sqrt{\frac{\epsilon'}{\epsilon_0}}\sqrt{1 - j \tan \delta}; \tag{10}$$

n^* is thus a complex number if ϵ is complex. If we put it equal to $g - jh$, where g and h are real positive numbers, we then have

$$n^* = g - jh = \sqrt{\frac{\epsilon}{\epsilon_0}}\sqrt{1 - j \tan \delta}. \tag{11}$$

By squaring, equating real and imaginary parts on the two sides of the resulting equation, and then solving for g and h, we find

$$g = \sqrt{\frac{\epsilon'}{2\epsilon_0}(\sqrt{1 + \tan^2 \delta} + 1)} \tag{12a}$$

and

$$h = \sqrt{\frac{\epsilon'}{2\epsilon_0}(\sqrt{1 + \tan^2 \delta} - 1)}. \tag{12b}$$

When $\tan \delta$ is small compared with unity, as it is for most useful dielectric materials, the quantities under the radicals in the exact expression for g and h can be developed by the binomial theorem. By dropping off all powers of $\tan \delta$ above $\tan^2 \delta$, we obtain the approximate expressions

$$g = \sqrt{\frac{\epsilon'}{\epsilon_0}}\left(1 + \frac{1}{8} \tan^2 \delta\right), \tag{13a}$$

$$h = \sqrt{\frac{\epsilon'}{\epsilon_0}}\frac{\tan \delta}{2}. \tag{13b}$$

If now the complex expression for n^*, $g - jh$, is put into Eq. (8*b*), it becomes

$$M = Ae^{-\frac{2\pi hp}{\lambda_0}} e^{2\pi j\left(\frac{t}{T} - g\frac{p}{\lambda_0}\right)}. \tag{14}$$

Equation (14) represents an attenuated plane wave traveling in the direction of increasing p. The effective index of refraction in the ordi-

nary sense is g, the real part of n^*. The factor $e^{-\frac{2\pi hp}{\lambda_0}}$ expresses an exponential decrease of the amplitude of the wave as it travels in the direction of increasing p. Both the amplitude and the phase of M are constant over the plane corresponding to any particular value of p.

Because there may appear to be discrepancies between this and other treatments of the subject, it is desirable to put in a word of caution about care in the choice of the sign of the imaginary part of complex quantities. The wave represented by the real part of Eq. (8*b*) can just as well be represented by the real part of the conjugate complex expression Eq. (15).

$$M = Ae^{-2\pi j\left(\frac{t}{T}-\frac{n^*p}{\lambda}\right)} \tag{15}$$

that differs from Eq. (8*b*) only in the sign of the exponent. The real parts of Eqs. (8*b*) and (15) are identical. If now $n^* = g - jh$ is put into Eq. (15), there is obtained a real factor $e^{+\frac{2\pi hp}{\lambda_0}}$ that represents a steady increase of amplitude as the wave progresses, an unlikely occurrence. The apparent difficulty has its origin in an inappropriate choice of the sign of the imaginary term in the expression for the dielectric constant. If we arbitrarily choose to represent the wave by Eq. (15), the complex conjugate of Eq. (8*b*), it is necessary to use the conjugate expression for the dielectric constant, $\epsilon' + j\epsilon''$, instead of $\epsilon' - j\epsilon''$. Similarly, we must use $g + ih$ for n^*. The wrong sign for the imaginary term ascribes to the medium the impossible property of developing energy rather than absorbing it, but just which sign has to be used to avoid this absurdity depends on the form chosen for representation of the wave. A similar difficulty may be encountered when a shift of phase is to be expressed by a complex number. From this point on Eqs. (8*a*) and (8*b*) will be used to represent a plane wave, and the minus sign will be used in the expression for the dielectric constant.

In many of the books on physical optics n^* is set equal to $n(1 - j\kappa)$, n being the real index of refraction and κ the damping or absorption coefficient. This is to be equated to $\sqrt{\epsilon'/\epsilon_0}\sqrt{1 - j\tan\delta}$ to get expressions as per Eqs. (13)

$$\left.\begin{aligned} n &= \sqrt{\frac{\epsilon'}{\epsilon_0}}\sqrt{\frac{\sqrt{1+\tan^2\delta}+1}{2}}, \\ n\kappa &= \sqrt{\frac{\epsilon'}{\epsilon_0}}\sqrt{\frac{\sqrt{1+\tan^2\delta}-1}{2}}, \\ \kappa &= \sqrt{\frac{\sqrt{1+\tan^2\delta}-1}{\sqrt{1+\tan^2\delta}+1}}. \end{aligned}\right\} \tag{16a}$$

For $\tan^2 \delta \ll 1$ these reduce to

$$\left.\begin{aligned} n &= \sqrt{\frac{\bar{\epsilon}'}{\epsilon_0}}\left(1 + \frac{\tan^2 \delta}{8}\right), \\ n\kappa &= \sqrt{\frac{\bar{\epsilon}'}{\epsilon_0}}\frac{\tan \delta}{2}\left(1 - \frac{\tan^2 \delta}{8}\right), \\ \kappa &= \frac{\tan \delta}{2}\left(1 - \frac{\tan^2 \delta}{4}\right) \end{aligned}\right\} \tag{16b}$$

or, to the first approximation,

$$\left.\begin{aligned} n &\approx \sqrt{\frac{\bar{\epsilon}'}{\epsilon_0}}, \\ \kappa &\approx \frac{\tan \delta}{2} \end{aligned}\right\} \tag{16c}$$

Since λ_0/n is the wavelength in the ordinary sense in the absorbing medium the damping ratio is $e^{-2\pi\kappa}$ per wavelength in the medium, or $e^{-\frac{2\pi n\kappa}{\lambda_0}}$ per unit distance.

12·3. Hybrid Plane Waves.—As noted above, Eq. (8*b*) is a solution of Maxwell's equations provided that $\alpha^2 + \beta^2 + \gamma^2 = 1$. If α, β, and γ are all real, they form a set of direction cosines. In general, however, they may be complex and subject only to the restriction that the sum of their squares equals unity. The general properties of waves that correspond to complex values of α, β, and γ have been discussed at length by Fry,[1] who calls them "hybrid waves."

If α, β and γ are complex, we can write

$$\left.\begin{aligned} \alpha &= a' + ja'', \\ \beta &= b' + jb'', \\ \gamma &= c' + jc'', \end{aligned}\right\} \tag{17}$$

in which a', a'', etc., are all real numbers. The condition

$$\alpha^2 + \beta^2 + \gamma^2 = 1$$

gives

$$(a'^2 + b'^2 + c'^2) - (a''^2 + b''^2 + c''^2) = 1 \tag{18}$$

and

$$a'a'' + b'b'' + c'c'' = 0.$$

If the values for α, β, and γ of Eqs. (17) are put into Eq. (8*a*) and $n = g - ih$ used,

$$M = Ae^{+\frac{2\pi}{\lambda_0}[(a''g - a'h)x + (b''g - b'h)y + (c''g - c'h)z]} \cdot e^{+2\pi j\left[\frac{t}{T} - \frac{(a'g + a''h)x + (b'g + b''h)y + (c'g + c''h)z}{\lambda_0}\right]}. \tag{19}$$

[1] T. C. Fry, *Jour. Optical Soc. Am.*, **15**, 137 (1927), and **16**, 1 (1928).

If we let

$$(a'g + a''h)^2 + (b'g + b''h)^2 + (c'g + c''h)^2 = S^2 \tag{20}$$

and set

$$\left.\begin{aligned} \frac{a'g + a''h}{S} &= l, \\ \frac{b'g + b''h}{S} &= m, \\ \text{and} \\ \frac{c'g + c''h}{S} &= n, \end{aligned}\right\} \tag{21}$$

then l, m, n can be a set of direction cosines, since their sum is unity. Likewise p, q, and r can be a set of direction cosines if

$$(a''g - a'h)^2 + (b''g - b'h)^2 + (c''g - c'h)^2 = R^2 \tag{22}$$

and

$$\left.\begin{aligned} \frac{a''g - a'h}{R} &= p, \\ \frac{b''g - b'h}{R} &= q, \\ \text{and} \\ \frac{c''g - c'h}{R} &= r. \end{aligned}\right\} \tag{23}$$

Equation (19) becomes

$$M = Ae^{+\frac{2\pi R}{\lambda_0}(px+qy+rz)} e^{2\pi j\left[\frac{t}{T} - \frac{S(lx+my+nz)}{\lambda_0}\right]}. \tag{24}$$

The hybrid wave is thus a plane wave with the normal to the surfaces of constant phase having direction cosines l, m, n, and its velocity being such as to correspond to an index of refraction S. The amplitude is not constant over these planes. There are, however, plane surfaces of constant amplitude, and the direction cosines of their normal are p, q, and r. The planes of constant amplitude are not parallel to those of constant phase.

As will be seen later, waves of this type are set up in a lossy medium into which an ordinary plane wave enters across a boundary between two mediums. The wave that is set up in the less dense medium when radiation undergoes total internal reflection also belongs to this group. These waves are not so familiar as some other types but are no less real or important.

12·4. Reflection and Refraction of a Plane Electromagnetic Wave at the Boundary between Mediums.—Assume a plane electromagnetic wave being propagated in a medium a, to be incident upon an infinite plane boundary between medium a and a second medium b. The boundary plane can be taken as the xy-plane, and the yz-plane can be taken so as to

contain a normal to the wave, without loss of generality. The direction cosines of the incident wave are α_a, β_a, and γ_a. When coordinate axes are chosen so that the normal is in the yz-plane, α_a becomes zero. In the following treatment only isotropic mediums will be considered, so for reasons of symmetry it is apparent that all reflected and transmitted waves will also lie in the yz-plane, there being nothing to cause a deviation to either side of it (see Fig. 12·1). Since $\alpha_a = 0$, our Eq. (8a) becomes

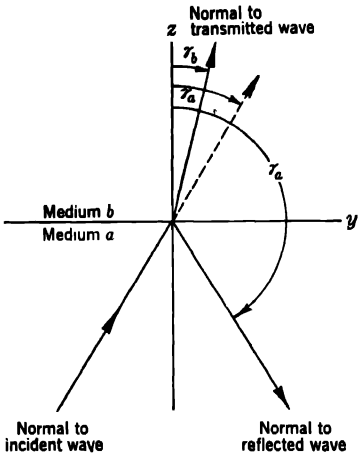

FIG. 12·1.—Reflection and refraction at a plane interface between two dielectric mediums.

$$M = A_a e^{2\pi j\left[\frac{t}{T} - \frac{n_a^*(\beta_a y + \gamma_a z)}{\lambda_0}\right]}. \quad (25)$$

As is shown in the standard treatments of this subject (see footnote on page 341) the boundary conditions can be satisfied if an additional wave is present in medium a (the reflected wave) and also a wave in medium b moving away from the boundary (the refracted wave). The reflected wave can be represented by

$$M' = A'_a e^{2\pi j\left[\frac{t}{T} - \frac{n_a^*(\beta'_a y + \gamma'_a z)}{\lambda_0}\right]}, \quad (26)$$

and the refracted wave by

$$M_b = A_b e^{2\pi j\left[\frac{t}{T} - \frac{n_b^*(\beta_b y + \gamma_b z)}{\lambda_0}\right]}. \quad (27)$$

The mere existence of boundary conditions to be satisfied at all times over the whole boundary requires that T and λ_0 have the same value for all three waves and that

$$n_a^*\beta_a = n_a^*\beta'_a = n_b^*\beta_b \quad (28)$$

or

$$\beta'_a = \beta_a = \sin\theta_0 \quad (29)$$

and

$$\beta_b = \frac{n_a^*}{n_b^*}\beta_a. \quad (30)$$

Since $\beta_a^2 + \gamma_a^2 = 1$ and $\beta_a'^2 + \gamma_a'^2 = 1$ (each is the sum of the squares of a set of direction cosines; α_a and α'_a equal 0), we have

$$\gamma_a = \sqrt{1 - \beta_a^2} = \cos\theta_0$$

and γ'_a also equals $\sqrt{1 - \beta_a^2}$.

Since γ'_a cannot be equal to γ_a and still be associated with a distinguishable wave, opposite signs of the square root must be used for γ'_a and γ_a.

Thus, in general,

$$\gamma_a' = -\gamma_a = -\cos\theta_0. \tag{31}$$

This equation, of course, merely expresses the familiar law of reflection.

In similar fashion, when both n_a and n_b are real, Eq. (30) expresses Snell's law, $\sin\theta_0/\sin\theta_r = n$. The sine of the angle of incidence, $\sin\theta_0$, equals β_a; the sine of the angle of refraction, $\sin\theta_r$, equals β_b; the relative index of refraction, n, equals n_b/n_a. Since $\gamma_b = \sqrt{1-\beta_b^2}$, we have by Eq. (30)

$$\left.\begin{aligned} \gamma_b &= \frac{\sqrt{n_b^{*2} - n_a^{*2}\cdot\beta_a^2}}{n_b^*} \\ \text{or} \qquad \gamma_b &= \frac{\sqrt{n_b^{*2} - n_a^{*2}\sin^2\theta_0}}{n_b^*}. \end{aligned}\right\} \tag{32}$$

In Eq. (32) the positive sign must be taken for the square root in order for the wave to be one traveling away from the boundary into medium b.

If the relations of Eqs. (29) to (32) are substituted into the expressions for the reflected and refracted waves, they will then be expressed in terms of the angle of incidence and the properties of the mediums.

Equation (26) for the reflected wave becomes

$$M' = A_a' e^{2\pi j\left[\frac{t}{T} - \frac{n_a^*}{\lambda_0}(y\sin\theta_0 - z\cos\theta_0)\right]}, \tag{33}$$

and Eq. (27) for the refracted wave becomes

$$M_b = A_b e^{2\pi j\left[\frac{t}{T} - \frac{(n_a^* y\sin\theta_0 + z\sqrt{n_b^{*2} - n_a^{*2}\sin^2\theta_0})}{\lambda_0}\right]}. \tag{34}$$

It is apparent from expressions (30) and (32) for β_b and γ_b that if either medium is absorbing so that n_a^* or n_b^* is complex, both β_b and γ_b will be complex and the refracted wave will be a hybrid wave of the type discussed in Sec. 12·3. For the particular case that medium a is lossless, medium b is lossy, and the incident wave is an ordinary plane wave, Eq. (34) shows that the y term of the refracted wave has a pure imaginary coefficient (since n_a^* is real). This means that there will be only changes of phase but no change of amplitude over any plane of constant z (i.e., parallel to the boundary between the mediums). The coefficient of the z term, however, is complex; its imaginary part expresses changes of phase, and its real part gives the variation of amplitude with change of z. Closer inspection reveals that there is an exponential decrease of the amplitude with increasing z. The surfaces of constant amplitude are not parallel to those of constant phase as they were for the wave expressed by Eq. (14) above but are parallel to the boundary.

The actual values of the amplitude coefficients of reflection and refraction are obtained as in the familiar treatments of this subject by setting

up the expressions for the boundary conditions at the surface and combining them to eliminate superfluous variables. This treatment will not be repeated in detail here; the results useful for present purposes are the following. For an incident wave polarized parallel to the plane of incidence (electric vector in the plane of incidence, magnetic vector perpendicular to it and therefore tangential to the boundary surface), Eq. (19) of page 494 of Stratton's book (*op. cit.*) becomes in our notation

$$r_{(Hp)ab} = \frac{H'_x}{H_x} = \frac{n_b^{*}\gamma_a - n_a^{*}\gamma_b}{n_b^{*}\gamma_a + n_a^{*}\gamma_b} = \frac{n_b^{*2}\cos\theta_0 - n_a^{*}\sqrt{n_b^{*2} - n_a^{*2}\sin^2\theta_0}}{n_b^{*2}\cos\theta_0 + n_a\sqrt{n_b^{*2} - n_a^{*2}\sin^2\theta_0}}. \tag{35}$$

The expression $r_{(Hp)ab}$ is the amplitude-reflection coefficient.

Similarly, the amplitude-reflection coefficient for the perpendicularly polarized wave is given by Eq. (36). It is convenient for present purposes to express this for the electric vector, the one that is now tangential to the surface. The subscript s indicates perpendicular polarization. Equation (14) of page 492 of Stratton's book can be written

$$r_{(Es)ab} = \frac{E'_x}{E_x} = \frac{n_a^{*}\gamma_a - n_b^{*}\gamma_b}{n_a^{*}\gamma_a + n_b^{*}\gamma_b} = \frac{n_a^{*}\cos\theta_0 - \sqrt{n_b^{*2} - n_a^{*2}\sin^2\theta_0}}{n_a^{*}\cos\theta_0 + \sqrt{n_b^{*2} - n_a^{*}\sin^2\theta_0}}. \tag{36}$$

It is apparent from Eqs. (35) and (36) that

$$r_{(Hp)ba} = -r_{(Hp)ab}$$

and

$$r_{(Es)ba} = -r_{(Es)ab} \tag{37}$$

if the rays are reversed, i.e., if the incident wave approaching the boundary from within medium b does so at an angle of incidence that is equal to the angle of refraction when the radiation is incident on the boundary from within medium a.

The values for the amplitudes of the transmitted waves can be written in similar fashion. The point of dealing only with the tangential components is that the continuity of tangential components across the boundary requires that

$$\left.\begin{aligned} t_{(Hp)ab} &= 1 + r_{(Hp)ab,} \\ t_{(Es)ab} &= 1 + r_{(Es)ab,} \end{aligned}\right\} \tag{38}$$

whereas the relations between the coefficients for components normal to the boundary are more complicated. If tangential components only are used, the later developments apply to both parallel and perpendicularly polarized waves.

In the special case of normal incidence, $\sin\theta_0 = 0$ and $\cos\theta_0 = 1$; Eq. (35) then becomes

$$r_{H(\text{norm})ab} = \frac{\dfrac{n_b^*}{n_a^*} - 1}{\dfrac{n_b^*}{n_a^*} + 1} = \frac{n_{ba}^* - 1}{n_{ba}^* + 1}, \tag{39a}$$

and Eq. (36) becomes

$$r_{E(\text{norm})ab} = -\frac{\dfrac{n_b^*}{n_a^*} - 1}{\dfrac{n_b^*}{n_a^*} + 1} = -\frac{n_{ba}^* - 1}{n_{ba}^* + 1}, \tag{39b}$$

$(n_b^*/n_a^*) = n_{ba}^*$ being the generalized index of refraction of medium b with respect to medium a. Remembering that $\mu_a = \mu_b$, Eq. (7) gives

$$n_{ba}^* = \sqrt{\frac{\epsilon_b}{\epsilon_a}}. \tag{40}$$

The difference of sign in Eqs. (39a) and (39b) does not indicate any difference in the reflection but is a consequence of the relative orientation of the E and H vectors in the waves. A reflection with no change of sign of the H vector necessitates a reversal of the E vector, and vice versa. Such a change of sign could not be of more than formal significance, since the concepts of parallel and perpendicular polarization lose their meaning for normal incidence, for which there is no particular plane of incidence.

Equations (35) and (36) can be thrown into another form that is of practical usefulness. They become

$$r_{(Hp)ab} = \frac{\dfrac{(n_{ba}^*)^2}{\sqrt{1 + [(n_{ba}^*)^2 - 1]/\cos^2\theta_0}} - 1}{\dfrac{(n_{ba}^*)^2}{\sqrt{1 + [(n_{ba}^*)^2 - 1]/\cos^2\theta_0}} + 1} \tag{41}$$

and

$$r_{(Es)ab} = -\frac{\sqrt{1 + \dfrac{(n_{ba}^*)^2 - 1}{\cos^2\theta_0}} - 1}{\sqrt{1 + \dfrac{n_{ba}^* - 1}{\cos^2\theta_0}} + 1}. \tag{42}$$

These are now of the same form as Eqs. (39a) and (39b) but with more complicated expressions in place of the simple ratio $n_{ba}^* = n_b^*/n_a^* = \sqrt{\epsilon_b/\epsilon_a}$. Thus, for reflection of parallel polarized waves at angle θ the expression

$$n_{(p\theta)ba}^* = \frac{(n_{ba}^*)^2}{\sqrt{1 + \dfrac{(n_{ba}^*)^2 - 1}{\cos^2\theta_0}}} \tag{43a}$$

becomes an effective index of refraction. It can be substituted for n_{ab}^* in all expressions obtained for normal incidence in order to derive the corresponding ones for incidence at angle θ. The corresponding effective specific dielectric constant is given by

$$\frac{\epsilon_{(p\theta)ba}}{\epsilon_0} = \frac{\left(\frac{\epsilon_b}{\epsilon_a}\right)^2}{1 + \left[\left(\frac{\epsilon_b}{\epsilon_a}\right) - 1\right] \Big/ \cos^2 \theta_0} \tag{43b}$$

Similarly, for perpendicularly polarized waves we have

$$n_{(s\theta)ba}^* = \sqrt{1 + \frac{n_{ba}^{*2} - 1}{\cos^2 \theta_0}} \tag{44a}$$

and

$$\frac{\epsilon_{(s\theta)ba}}{\epsilon_0} = 1 + \frac{\frac{\epsilon_b}{\epsilon_a} - 1}{\cos^2 \theta_0}. \tag{44b}$$

It will be noted that

$$n_{(p\theta)ba}^* \, n_{(s\theta)ba}^* = n_{ba}^{*2}$$

or

$$\frac{\epsilon_{(p\theta)ba}}{\epsilon_0} \frac{\epsilon_{(s\theta)ba}}{\epsilon_0} = \left(\frac{\epsilon_b}{\epsilon_a}\right)^2. \tag{45}$$

When medium a is air for which $n_a^* = 1$ and $n_b^* = n(1 - j\kappa)$, Eq. (39a) becomes

$$r_{H(\text{norm})ab} = \frac{n - 1 - jn\kappa}{n + 1 - jn\kappa}. \tag{46}$$

This can be put into the form

$$r_{H(\text{norm})ab} = \sqrt{\frac{(n-1)^2 + n^2\kappa^2}{(n+1)^2 + n^2\kappa^2}}\, e^{-j\chi}, \tag{47}$$

where

$$\chi = \tan^{-1}\left[\frac{2n\kappa}{n^2(1 + \kappa^2) - 1}\right]. \tag{48}$$

For $n^2\kappa^2 \ll n^2 - 1$ $\left[\text{or } \tan^2 \delta \ll \frac{4(\epsilon'/\epsilon_0 - 1)}{\epsilon'/\epsilon_0}\right]$, this reduces to

$$r_{H(\text{norm})ab} \approx \left(\frac{n-1}{n+1}\right) e^{-j \tan^{-1}\left(\frac{2n\kappa}{n^2-1}\right)}. \tag{49}$$

For lossless mediums, Eq. (39a) and Eqs. (46) to (49) inclusive reduce to

$$r_{H(\text{norm})ab} = \frac{n-1}{n+1}. \tag{39a}$$

Comparison of Eqs. (39a) and (49) shows that for a low-loss medium the absolute magnitude of the reflection coefficient is practically the same as

for a lossless medium having the same dielectric constant; the phase of the reflected wave can, however, be appreciably different from what it is for a lossless medium.

The respective coefficients for reflection of power are equal to the squares of the absolute values of the amplitude coefficients $|r_{(Hp)ab}|^2$ and $|r_{(Es)ab}|^2$. Their behavior as a function of the angle of incidence is discussed in Sec. 11·1. The amplitude coefficient $|r_{(Hp)ab}|^2$ goes to zero for $\theta = \tan^{-1} n_{ba}^*$; for $n_{ab}^* > 1$ there is no angle for which $|r_{(Es)ab}|^2$ has a value of 0.

Similar results are obtained for oblique incidence. Again consider the case for which $n_a^* = 1$ and $n_b^* = n(1 - j\kappa)$. Substitution of these values into Eqs. (43*a*) and (44*a*) yields complex expressions for the effective indices of refraction. If we write these as

$$\left.\begin{aligned} n_{(p\theta)}^* &= n_{(p\theta)}[1 - j\kappa_{(p\theta)}] \\ n_{(s\theta)}^* &= n_{(s\theta)}[1 - j\kappa_{(s\theta)}] \end{aligned}\right\} \tag{50}$$

and compare the terms with those of the complex expressions obtained from the substitution, we get

$$\left.\begin{aligned} n_{(p\theta)} &= \frac{n^2}{\sqrt{1 + \dfrac{n^2 - 1}{\cos^2 \theta_0}}}, \\ \kappa_{(p\theta)} &= \left(\frac{n^2 - 2\sin^2 \theta_0}{n^2 - \sin^2 \theta_0}\right)\kappa, \end{aligned}\right\} \tag{51}$$

$$\left.\begin{aligned} n_{(s\theta)} &= \sqrt{1 + \frac{n^2 - 1}{\cos^2 \theta_0}}, \\ \kappa_{(s\theta)} &= \frac{n^2\kappa}{n^2 - \sin^2 \theta_0}. \end{aligned}\right\} \tag{52}$$

If now either pair of these effective constants of the material is substituted in Eq. (46), the general result will be that obtained for normal incidence by the comparison of Eqs. (39*a*) and (49); the magnitude of the reflection by the low-loss material is but slightly different from what it would be for a lossless material having the same index of refraction, but there is a relative shift of phase. At the Brewster angle for which $\tan \theta_B = n$, $n_{(p\theta)} = 1$, and $\kappa_{(p\theta)}$ becomes $(n^2 - 1/n^2)\kappa$, $|r_{(Hp)ab}|$ takes the small value of $\kappa_{(p\theta)}/\sqrt{4 + \kappa_{(p\theta)}}$ instead of zero, according to Eq. (47). Equation (48) shows that χ then becomes $\tan^{-1}(2/\kappa)\, n^2/(n^2 - 1)$, an angle close to $\pi/2$. Such large values for χ are found only for angles of incidence very close to the Brewster angle, for which angles $\kappa_{p\theta}$ is not small compared with $n_{p\theta} - 1$. Thus, in lossy mediums the 180° change of phase that occurs in passing through the Brewster angle takes place quickly but continuously, rather than discontinuously, as it does in lossless mediums at that angle.

12·5. Reflection and Transmission by a Sheet of Dielectric Material. The next problem of interest is that of the reflection and transmission of a plane wave by an infinite sheet or slab of dielectric material of uniform finite thickness. Assume the original plane wave to be present in medium a, the sheet to be made of medium b and bounded on the far side by a third medium c. Assume the a-b boundary to be in the xy-plane and the b-c boundary to be a parallel plane at $z = d$. Also, assume the normal to the incident plane wave to be in the yz-plane, so that the x direction cosine of all waves will be 0, as before (see Fig. 12·2).

The original plane wave will give rise to reflected and transmitted waves at the a-b boundary, and the wave transmitted into medium b will then undergo multiple reflection back and forth as in Fig. 12·2. At each such reflection at the b-a boundary a transmitted wave will emerge and be traveling in the same direction in medium a as the originally reflected wave. The amplitude of the resultant wave in this direction is the vector sum of the amplitude of all these lesser waves. Similarly, at every reflection at the b-c boundary, a wave emerges into medium c. These will all be traveling in the same direction and combine to give a resultant transmitted wave.

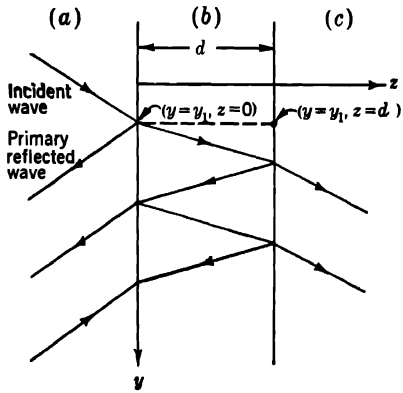

FIG. 12·2. Internal reflections in a dielectric sheet.

The amplitudes of the reflected and transmitted waves can be calculated as follows. Let the reflection coefficient of the amplitude of the wave incident on the a-b surface be represented by r_{ab} and the transmission coefficient by t_{ab}. The corresponding coefficients for a wave approaching that boundary in medium b are r_{ba} and t_{ba}; r_{bc} and t_{bc} are the corresponding quantities for a wave in b that is incident on the b-c boundary. Also, let F_b represent the ratio of the amplitude at $z = d$, $y = y_1$ to that at $z = 0$, $y = y_1$ for a wave in b traveling toward c. For the amplitudes of the successive waves traveling in the direction of the reflected wave in medium a, at a given point on the boundary, we get the following, assuming the incident wave to have an amplitude of unity,

$$
\begin{aligned}
r_0 &= r_{ab}, \\
r_1 &= t_{ab}F_b r_{bc}F_b t_{ba}, \\
r_2 &= t_{ab}F_b r_{bc}F_b r_{ba}F_b r_{bc}F_b t_{ba}, \\
&\text{etc.}
\end{aligned}
$$

The sum $r_{a\to c}$ is given by

$$r_{a\to c} = r_{ab} + t_{ab}t_{ba}F_b^2 r_{bc}[1 + F_b^2 r_{bc}r_{ba} + (F_b^2 r_{bc}r_{ba})^2 + \cdots +].$$

Since $1 + x + x^2 + x^3 + \cdots + = 1/(1 - x)$,

$$r_{a\to c} = r_{ab} + \frac{t_{ab}t_{ba}F_b^2 r_{bc}}{1 - F_b^2 r_{bc}r_{ba}}. \tag{53}$$

Similarly, for the amplitude of the transmitted waves, partial and resultant, at a point directly opposite the one considered for the reflection

$$\left.\begin{aligned} t_1 &= t_{ab}F_b t_{bc}, \\ t_2 &= t_{ab}F_b r_{bc}F_b r_{ba}F_b t_{bc}, \\ &\text{etc.} \\ t_{a\to c} &= t_{ab}F_b t_{bc}[1 + (F_b^2 r_{ba}r_{bc}) + \cdots +], \\ t_{a\to c} &= \frac{F_b t_{ab}t_{bc}}{1 - F_b^2 r_{ba}r_{bc}}. \end{aligned}\right\} \tag{54}$$

If now attention is confined to components of the incident wave that are perpendicular to the plane of incidence, these expressions can be simplified by using the relations

$$r_{ba} = -r_{ab}, \tag{37}$$

$$\left.\begin{aligned} t_{ab} &= 1 + r_{ab}, \\ t_{ba} &= 1 + r_{ba} = 1 - r_{ab}. \end{aligned}\right\} \tag{38}$$

Making these substitutions Eqs. (53) and (54) become

$$r_{a\to c} = \frac{r_{ab} + F_b^2 r_{bc}}{1 + F_b^2 r_{ab}r_{bc}}, \tag{55}$$

$$t_{a\to c} = \frac{F_b(1 + r_{ab})(1 + r_{bc})}{1 + F_b^2 r_{ab}r_{bc}}. \tag{56}$$

The same results can be derived somewhat more formally by assuming the existence of one resultant wave in medium c, two in medium b, and two in medium a and then calculating the amplitudes required to satisfy the boundary conditions.

From the symmetry, it can be seen that

$$r_{c\to a} = -\frac{r_{bc} + F_b^2 r_{ab}}{1 + F_b^2 r_{ab}r_{bc}}, \tag{57}$$

$$t_{c\to a} = \frac{F_b(1 - r_{ab})(1 - r_{bc})}{1 + F_b^2 r_{ab}r_{bc}}. \tag{58}$$

When the medium is the same on both sides of the sheet,

$$r_{a\to c} = r_{c\to a} = R = \frac{r_{ab}(1 - F_b^2)}{1 - F_b^2 r_{ab}^2}, \tag{59}$$

$$t_{a\to c} = t_{c\to a} = T = \frac{F_b(1 - r_{ab}^2)}{1 - F_b^2 r_{ab}^2}. \tag{60}$$

It must be emphasized that expressions (55) to (60) inclusive are valid only for *transverse* components, that is, for the magnetic vector of a wave polarized in the plane of incidence and the electric vector of a wave polarized perpendicular to the plane of incidence.

It is now desirable to examine the quantity F_b more closely. By reference to Eq. (27) we find

$$F_b = e^{\frac{-2\pi j n_b^* \gamma_b d}{\lambda_0}}. \tag{61}$$

Substituting for γ_b from Eq. (32) this becomes

$$F_b = e^{-2\pi j \sqrt{n_b^{*2} - n_a^{*2} \sin^2 \theta_0} \frac{d}{\lambda_0}}. \tag{62}$$

It is convenient to express F_b as

$$F_b = A e^{-j\phi}, \tag{63}$$

in which A and ϕ are real numbers. A is the amplitude of the wave as it is about to emerge from medium b, if its value as it enters medium b is taken as 1; ϕ is the shift of phase angle. When medium a is air for which $n_a = 1$ and medium b is lossless, with $n_b^* = n_b = \sqrt{\epsilon_b/\epsilon_0}$,

$$A = 1$$

and

$$\phi = \frac{2\pi d}{\lambda_0} \sqrt{n_b^2 - \sin^2 \theta_0}. \tag{64}$$

For normal incidence for which $\sin \theta_0 = 0$ this becomes

$$\phi = 2\pi \frac{n_b d}{\lambda_0} = 2\pi \frac{d}{\lambda_0/n_b}. \tag{65}$$

The ratio $n_b d/\lambda_0$, or $\sqrt{\epsilon_b/\epsilon_0}\ (d/\lambda_0)$, is called the electrical thickness of the sheet of dielectric. It is the ratio of the actual thickness of the sheet to the wavelength in the material: λ_0/n_b or $\lambda_0 \sqrt{\epsilon_b/\epsilon_0}$. For oblique incidence at angle θ_0 the electrical thickness becomes $\sqrt{n_b^2 - \sin^2 \theta_0}\ (d/\lambda_0)$.

When medium a is air with $n_a^* = 1$, but medium b is lossy with $n_b^* = n_b(1 - j\kappa_b)$, F_b becomes

$$F_b = e^{-2\pi j \sqrt{n_b^2(1 - j\kappa_b)^2 - \sin^2 \theta} \frac{d}{\lambda_0}}. \tag{66}$$

The complex radical of Eq. (66) can be expressed as

$$\sqrt{C}\ \sqrt{1 - jB}, \tag{67}$$

in which

$$\left.\begin{aligned} C &= n_b^2(1 - \kappa_b^2) - \sin^2 \theta_0, \\ B &= \frac{2n_b^2 \kappa_b}{C}. \end{aligned}\right\} \tag{68}$$

The complex product of Eq. (67) can be handled the same way as was the corresponding one of Eq. (11) to give

$$F_b = e^{-\frac{2\pi d}{\lambda_0}\sqrt{\frac{C}{2}}\sqrt{\sqrt{1+B^2}-1}} e^{-j\frac{2\pi d\sqrt{C/2}}{\lambda_0}\sqrt{\sqrt{1+B^2}+1}}. \tag{69}$$

When $\kappa_b \ll 1$, $B \ll 1$ and Eq. (69) reduces to

$$F_b = e^{-\frac{2\pi d}{\lambda_0}\frac{n_b^2\kappa_b}{\sqrt{n_b^2-\sin^2\theta_0}}} e^{-j\frac{2\pi d}{\lambda_0}\sqrt{n_b^2-\sin^2\theta_0}}. \tag{70}$$

Thus, for the case of a sheet of low-loss dielectric material

$$A = e^{-\frac{2\pi d}{\lambda_0}\frac{n_b^2\kappa_b}{\sqrt{n_b^2-\sin^2\theta_0}}} \tag{71a}$$

and

$$\phi = \frac{2\pi d}{\lambda_0}\sqrt{n_b^2-\sin^2\theta_0}, \tag{71b}$$

ϕ being the same as for the lossless sheet [Eq. (64)]. It should be noted that these expressions for A and ϕ are independent of the polarization. For normal incidence, these become

$$A = e^{-\frac{2\pi d n_b\kappa_b}{\lambda_0}} \tag{72a}$$

and

$$\phi = \frac{2\pi\, dn_b}{\lambda_0}. \tag{72b}$$

Thus, A of Eqs. (71) and (72) expresses the decrease of the amplitude of the wave as it passes through the lossy sheet once between the front and rear faces.

The values of A for sheets that have effective thicknesses of an integral number of half wavelengths are of particular interest. If ϕ of Eq. (71b) is set equal to $N\pi$, N being an integer, the resulting value of d will be the thickness of the sheet corresponding to N half wavelengths. Let us call it d_N. We find that

$$d_N = \frac{N}{2}\frac{\lambda_0}{\sqrt{n_b^2-\sin^2\theta_0}}. \tag{73}$$

If d_N now is substituted for d in Eq. (71a), it will give the value of A for the sheet of N half wavelengths, A_N, which is

$$A_N = e^{-\pi N\kappa_b\frac{n_b^2}{(n_b^2-\sin^2\theta)}}. \tag{74}$$

For normal incidence

$$A_N = e^{-\pi N\kappa_b}. \tag{75}$$

Having examined the quantity F_b in some detail, we may now continue consideration of the reflection and transmission by various sheets

of dielectric material. When medium a is air and medium b is lossless, $A = 1$ [Eq. (71a)], so that Eq. (59) becomes

$$R = \frac{r_{ab}(1 - e^{-2j\phi})}{1 - r_{ab}^2 e^{-2j\phi}}. \tag{76}$$

In Eq. (76), r_{ab} is a real number [*cf.* Eqs. (41) and (42) for the real value of r_{ab} for $n_{ba}^* > 1$]. Because of the $e^{-2j\phi}$ terms, however, $R_b$is, in general, complex. The reflection from a sheet of dielectric material of finite thickness involves a shift of phase. The value of the reflection coefficient for power $|R|^2$ is obtained by multiplying R by its complex conjugate. This gives

$$|R|^2 = \frac{4r_{ab}^2 \sin^2 \phi}{(1 - r_{ab}^2)^2 + 4r_{ab}^2 \sin^2 \phi}. \tag{77}$$

$|R|^2$ goes to zero for $\phi = 0, \pi, 2\pi$, etc., and has a maximum value of $4r_{ab}^2/(1 + r_{ab}^2)^2$ for $\phi = \pi/2, 3\pi/2$, etc. Thus, the reflection is very small for any sheet having an equivalent electrical thickness that is either small compared with a wavelength in the medium or close to any integral multiple of a half wavelength in the medium.

If we let $\phi = n\pi + \Delta\phi$,

$$\sin \phi \approx \Delta\phi. \tag{78}$$

To this approximation Eq. (77) becomes

$$|R|^2 \approx \frac{4r_{ab}^2(\Delta\phi)^2}{(1 - r_{ab}^2)^2}. \tag{79}$$

The expression for the power-transmission coefficient obtained by developing Eq. (58) in a similar way is

$$|T|^2 = \frac{(1 - r_{ab}^2)^2}{(1 - r_{ab}^2)^2 + 4r_{ab}^2 \sin^2 \phi}. \tag{80}$$

The sum of $|R|^2$ and $|T|^2$ from Eqs. (77) and (80) equals 1, as it should, since there is no loss in the sheet of dielectric material.

When the dielectric is a low-loss material, F_b has a value $Ae^{-j\phi}$ in which A is less than unity, as given by Eq. (71a), and ϕ has nearly the same value as for the lossless medium. As discussed in the preceding section, $|r_{ab}|_{\text{lossy}}$ has almost the same value as for a lossless material but is multiplied by a phase-shifting factor that we may express as $e^{-j\chi}$, in which $\chi \ll 1$ for low-loss mediums for nearly all angles (see page 352). Using these expressions for $(r_{ab})_{\text{lossy}}$ and $(F_b)_{\text{lossy}}$, Eq. (59) yields

$$|R|_{\text{lossy}}^2 = \frac{|r_{ab}|^2[(1 - A^2)^2 + 4A^2 \sin^2 \phi]}{(1 - A^2|r_{ab}|^2)^2 + 4A^2|r_{ab}|^2 \sin^2 (\phi + \chi)}, \tag{81}$$

and from Eq. (60) we get

$$|T|^2_{\text{lossy}} = \frac{A^2[(1 - |r_{ab}|^2)^2 + 4|r_{ab}|^2 \sin^2 \chi]}{(1 + A^2|r_{ab}|^2)^2 + 4A^2|r_{ab}|^2 \sin^2 (\phi + \chi)}. \tag{82}$$

From Eq. (81) it is apparent that minimum values for $|R|^2_{\text{lossy}}$ are also found for values of ϕ close to $N\pi$. The minima do not occur at precisely these angles because of the presence of the angle χ in the denominator; χ, however, is usually small enough to be ignored. The actual minimum values of $|R|^2_{\text{lossy}}$ are not zero but are given by

$$|R|^2_{\text{lossy min}} \approx \frac{|r_{ab}|^2 (1 - A_N^2)^2}{(1 - |r_{ab}|^2 A_N^2)^2} \tag{83}$$

(χ having been taken as equal to zero for the approximation). Similarly, Eq. (82) becomes

$$|T|^2_{\text{lossy max}} \approx A_N^2 \left(\frac{1 - |r_{ab}|^2}{1 - A_N^2|r_{ab}|^2}\right)^2, \tag{84}$$

for $\phi = N\pi$, instead of becoming 1 as it does for lossless sheets. For most materials at incidence close to normal the A_N^2 factor is the important one since the one in parentheses decreases with decreasing A_N much more slowly than A_N^2 does.

For angles of incidence close to the Brewster angle, however, it is not legitmate to assume that $\chi \ll 1$. For such angles of incidence, the thicknesses for minimum reflection and maximum transmission are different, but the maximum possible value of the reflection given by Eq. (81) is negligibly small because of the low value of $|r_{ab}|$. For the same reason the transmission will be given by $|T|^2_{\text{lossy}} \approx A^2$ for all thicknesses, the factors of Eq. (82) containing $|r_{ab}|$ reducing to unity.

For normal incidence, for which $r_{ab} = (n_b - 1)/(n_b + 1)$ and

$$A_n = e^{-\pi N \kappa_b} \qquad \text{[See Eq. (75)]}$$

Eq. (84) becomes

$$|T_N|^2_{\text{lossy max}} \approx \frac{16n_b^2 e^{-2\pi N\kappa_b}}{[(n_b + 1)^2 - (n_b - 1)^2 e^{-2\pi N\kappa_b}]^2}. \tag{85}$$

The properties of the half-wavelength sheets that we have been discussing can be stated in a different way, in terms of Eq. (55),

$$r_{a\to c} = \frac{r_{ab} + F_b^2 r_{bc}}{1 + F_b^2 r_{ab} r_{bc}}. \tag{55}$$

The sheets just discussed are those for which $r_{bc} = -r_{ab}$ and

$$F_b^2 = e^{-j2N\pi} = 1,$$

so that the numerator in Eq. (55) vanishes. Another simple case of interest in connection with sandwich radomes is that in which $r_{bc} = +r_{ab}$

and $F_b^2 = -1$; i.e., $F_b^2 = e^{-j2(N+\frac{1}{2})\pi}$. The numerator of Eq. (55) also goes to zero for these conditions. They are realized if

$$\left.\begin{aligned} \frac{n_c^*}{n_b^*} &= \frac{n_b^*}{n_a^*} \\ \text{or} \\ n_b^{*2} &= n_a^* n_c^* \\ \text{or} \\ \epsilon_b^2 &= \epsilon_a \epsilon_c \end{aligned}\right\} \tag{86}$$

[*cf.* Eqs. (39*a*) and (39*b*)], and if the thickness of the sheet of dielectric *b* is an odd multiple of a quarter wavelength in that material. Such a quarter-wavelength sheet of dielectric material, having a dielectric constant that is the geometric mean of those of the two bounding mediums, is the analogue of the quarter-wavelength transformer used for matching two transmission lines having different values of the characteristic impedance.

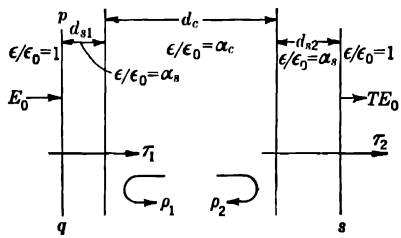

FIG. 12·3.—Diagram of sandwich.

12·6. Reflection and Transmission by Sandwiches.—For reasons discussed in Chap. 9, it has been found useful to make radomes of several layers of different materials. This section develops the theory of the reflection and transmission by panels of such construction.

A construction of generality sufficient for present purposes is illustrated in Fig. 12·3. The ambient medium *a* will normally be air, for which $n_a^* = 1$. The thickness of the two skins, both made of material *b*, are d_{s1} and d_{s2}, respectively; the thickness of the core, made of material *c*, is d_c.

Here again we shall deal only with components of the waves that are tangential to the boundary planes between the mediums. Let τ_1 represent the amplitude-transmission coefficient of the left-hand skin for a wave incident on it from the left ($t_{a\to c}$ of the notation used on page 355); τ_2 is the amplitude-transmission coefficient of the second skin for a wave incident on it from the left ($t_{c\to a}$ for skin 2). Let ρ_1 and ρ_2 be the reflection coefficients for waves incident on the core-skin interfaces from within the core (values of $r_{c\to a}$ for the two skins.). Further, let T represent the amplitude-transmission coefficient of the whole sandwich for a wave incident on it from the left. By the same argument that led to Eq. (54) for the transmission coefficient of the single sheet ($t_{a\to c}$) we find

$$T = \frac{\tau_1 \tau_2 F_c}{1 - \rho_1 \rho_2 F_c^2}, \tag{87}$$

in which F_c has the same significance now for the core as F_b had for the sheet of the earlier considerations.

For simplicity, let us deal with sandwiches made of lossless materials. We can then write $F_c = e^{-j\phi_c}$ as before, where ϕ_c now equals

$$2\pi \sqrt{n_r^2 - \overline{\sin^2 \theta_0}} \left(\frac{d}{\lambda_0}\right).$$

The coefficients ρ_1 and ρ_2 can be replaced by $|\rho_1|e^{-j\psi_1}$ and $|\rho_2|e^{-j\psi_2}$ in which ψ_1 and ψ_2 are real phase angles. Making these substitutions in Eq. (87) and multiplying it by its complex conjugate, we derive the expression for the power-transmission coefficient,

$$|T|^2 = \frac{|\tau_1|^2|\tau_2|^2}{(1 - |\rho_1||\rho_2|)^2 + 4|\rho_1||\rho_2| \sin^2\left(\phi_c + \frac{\psi_1 + \psi_2}{2}\right)}. \tag{88}$$

This equation shows that the power-transmission coefficient has its maximum value when

$$\sin\left(\phi_c + \frac{\psi_1 + \psi_2}{2}\right) = 0. \tag{89}$$

The values of ϕ_c for maximum transmission of power are, of course, also the ones for minimum reflection. For given thicknesses of the skins that determine the values of ψ_1 and ψ_2, there is therefore a set of values of ϕ_c corresponding to a set of cores of different thicknesses that can be determined from the condition expressed by Eq. (89), that will make sandwiches having minimum reflection.

When Eq. (89) is satisfied, Eq. (88) becomes

$$|T|^2_{\max} = \frac{|\tau_1|^2|\tau_2|^2}{(1 - |\rho_1||\rho_2|)^2}. \tag{90}$$

This can be simplified by introducing a relationship that exists between the $|\rho|$'s and $|\tau|$'s. It is

$$|\tau_1|^2|\tau_2|^2 = (1 - |\rho_1|^2)(1 - |\rho_2|^2). \tag{91}$$

Equation (91) can be derived as follows. Since we are dealing with lossless mediums, the sum of the values of the energy flux of a reflected and transmitted wave must equal the energy flux of the incident wave. In terms of our earlier notation, this gives for the reflection by skin 1 of a wave incident from medium a

$$C_a|r_{a\to c}|^2 + C_c|t_{a\to c}|^2 = C_a. \tag{92}$$

The terms C_a and C_c are constants that have to be included because the relation between the energy flux and the square of the amplitude depends on the medium. It is not necessary to give further detailed attention to this aspect of the matter here. From Eqs. (55) and (57) we get $|r_{a\to c}|^2 = |r_{c\to a}|^2$, so Eq. (92) can be written

$$C_a|\rho_1|^2 + C_c|\tau_1|^2 = C_a. \tag{93}$$

In the same way, for the wave reaching skin 2 from within the core we get

$$C_c|\rho_2|^2 + C_A|\tau_2|^2 = C_c. \tag{94}$$

If Eqs. (93) and (94) are now solved for $|\tau_1|^2$ and $|\tau_2|^2$ and multiplied together, Eq. (91) results. Putting this into Eq. (90) gives

$$|T|^2_{\max} = \frac{(1 - |\rho_1|^2)(1 - |\rho_2|^2)}{(1 - |\rho_1||\rho_2|)^2}. \tag{95}$$

The corresponding value for the minimum power-reflection coefficient is given by $|R|^2_{\min} = 1 - |T|^2_{\max}$. (Both waves are in the same medium so that C_a drops out.) Thus, from Eq. (·5), we find

$$|R|^2_{\min} = \left(\frac{|\rho_1| - |\rho_2|}{1 - |\rho_1||\rho_2|}\right)^2. \tag{96}$$

When $|\rho_1| = |\rho_2|$, $|R|^2_{\min} = 0$ and $|T|^2_{\max} = 1$; $|\rho_1| = |\rho_2|$ for a symmetrical sandwich for which the two skins are alike.

For the symmetrical sandwich $\psi_1 = \psi_2 = \psi$ and $\rho_1 = \rho_2 = \rho$, so that Eq. (88) becomes [also using Eq. (91)]

$$|T|^2 = \frac{(1 - |\rho|^2)^2}{(1 - |\rho|^2)^2 + 4|\rho|^2 \sin^2 (\phi_c + \psi)}. \tag{97}$$

and

$$|R|^2 = 1 - |T|^2 = \frac{4|\rho|^2 \sin^2 (\phi_c + \psi)}{(1 - |\rho|^2)^2 + 4|\rho|^2 \sin^2 (\phi_c + \psi)}. \tag{98}$$

The condition for zero reflection by the sandwich is thus $(\phi_c)_N + \psi = N\pi$ or

$$(\phi_c)_N = N\pi - \psi. \tag{99}$$

Lossless Sandwich Normal Incidence.—The actual thicknesses of core for zero reflection can be obtained by putting the appropriate values of $(\phi_c)_N$ and ψ into Eq. (99). For normal incidence

$$\phi_c = 2\pi \frac{d_c n_c}{\lambda_0},$$

and ψ can be calculated from Eq. (57) if we remember that

$$r_{c\to a} = \rho = |\rho|e^{-j\psi},$$

$$r_{bc} = \frac{\dfrac{n_c}{n_s} - 1}{\dfrac{n_c}{n_s} + 1},$$

$$r_{ab} = \frac{n_s - 1}{n_s + 1}.$$

[*cf.* Eq. (39*a*)]
and

$$F_b^2 = e^{-j2\phi_s}.$$

[*cf.* Eq. (63)]
Making these substitutions we get a cumbersome complex expression that can be rationalized and reduced to give

$$\tan\psi = \frac{2n_c n_s(n_s^2 - 1)\sin 2\phi_s}{(n_c^2 - n_s^2)(n_s^2 + 1) + (n_s^2 - 1)(n_c^2 + n_s^2)\cos 2\phi_s} \tag{100}$$

and

$$|\rho|^2 = \frac{n_s^2(n_c - 1)^2 - (n_s^2 - 1)(n_c^2 - n_s^2)\sin^2\phi_s}{n_s^2(n_c + 1)^2 - (n_s^2 - 1)(n_c^2 - n_s^2)\sin^2\phi_s}. \tag{101}$$

Equation (99) becomes

$$(d_c)_N = \frac{\lambda_0}{2\pi n_c}(N\pi - \psi), \tag{102}$$

ψ being given by Eq. (100).

Successive integral values of N give corresponding values of $(d_c)_N$, the core thicknesses for nonreflecting sandwiches. They differ in thickness by a half wavelength in the material of the core.

If the thickness of the core deviates by an amount Δd_c from the ideal thickness $(d_c)_N$ for the nonreflecting sandwich, this will correspond to a value of $(\phi_c + \psi + \Delta\phi_c)$ for the angle of Eq. (96), $\Delta\phi_c$ being equal to $\pm 2\pi(\Delta d_c/\lambda_0)n_c$. Equation (98) becomes

$$|R|^2 \approx \frac{4|\rho|^2\sin^2(\Delta\phi_c)}{(1 - |\rho|^2)^2 + 4|\rho|^2\sin^2(\Delta\phi_c)}. \tag{103}$$

This can be solved for $\Delta\phi_c$ to give

$$\sin\Delta\phi_c = \pm\frac{(1 - |\rho|^2)}{2}\sqrt{\frac{|R|^2}{1 - |R|^2}}, \tag{104}$$

from which corresponding values of Δd_c may be calculated for given $|\rho|^2$ and allowable $|R|^2$.

For the unsymmetrical sandwich $|R|^2_{\min}$ does not equal zero [Eq. (96)]. The thickness for minimum reflection and maximum transmission, how-

ever, will be given by

$$[\phi_{c(1+2)}]_N + \frac{\psi_1 + \psi_2}{2} = N\pi. \tag{105}$$

For symmetrical sandwiches having skins characterized by ψ_1 the condition is

$$(\phi_{c1})_N + \psi_1 = N\pi, \tag{106}$$

and for those having skins of a second thickness it is

$$(\phi_{c2})_N + \psi_2 = N\pi. \tag{107}$$

From Eqs. (105) to (107) we see that

$$[\phi_{c(1+2)}]_N = \frac{(\phi_{c1})_N + (\phi_{c2})_N}{2}. \tag{108}$$

Equation (108) means that the core thickness required to give minimum reflection from an unsymmetrical sandwich is the average of the two values that would be appropriate if it were made symmetrical first with one thickness of skin and then with the other thickness.

Transmission Losses.—The transmission of a sandwich made of low-loss materials can be estimated most readily by comparing it with the corresponding lossless sandwich. If τ_{10} be used for the transmission of the skin of the lossless sandwich and τ_1 for the lossy one and similarly for the other quantities, and if we write $F_c = A_c e^{-j\phi_c}$ in accord with Eq. (63), Eq. (87) can be written

$$T = \frac{\tau_{10}\tau_{20}e^{-j\phi_c}}{1 - \rho_{10}\rho_{20}e^{-j2\phi_c}} A_c \left(\frac{\tau_1\tau_2}{\tau_{10}\tau_{20}}\right)\left(\frac{1 - \rho_{10}\rho_{20}e^{-j2\phi_c}}{1 - A_c^2\rho_1\rho_2 e^{-j2\phi_c}}\right). \tag{109}$$

The first factor of Eq. (109) is seen to be what we would have for the lossless sandwich.

Since the general principles are made clear by considering the symmetrical sandwich, the following discussion will be limited to that case for the sake of avoiding extremely cumbersome expressions. Letting $F_s = A_s e^{-j\phi_s}$, Eqs. (56) and (58) give

$$\frac{\tau_1\tau_2}{\tau_{10}\tau_{20}} = A_s^2\left(\frac{1 + r_{ab}r_{bc}e^{-j2\phi_s}}{1 + A_s^2 r_{ab}r_{bc}e^{-j2\phi_s}}\right)^2, \tag{110}$$

assuming r_{ab} and r_{bc} to be the same for the lossy mediums as for the lossless ones. Putting this into Eq. (109) and multiplying by the complex conjugate we get

$$|T|^2_{\text{lossy}} = |T|_0^2 \cdot A_s^4 A_c^2 \left[\frac{(1 + r_{ab}r_{bc})^2 - 4r_{ab}r_{bc}\sin^2\phi_s}{(1 + A_s^2 r_{ab}r_{bc})^2 - 4A_s^2 r_{ab}r_{bc}\sin^2\phi_s}\right]^2 \cdot \left[\frac{(1 - |\rho_0|^2)^2 + 4|\rho_0|^2\sin^2(\phi_c + \psi_0)}{(1 - A_c^2|\rho|^2)^2 + 4A_c^2|\rho|^2\sin^2(\phi_c + \psi)}\right]. \tag{111}$$

For sandwiches with very thin skins or modified half-wavelength skins, $\sin^2 \phi_s$ is small and the terms containing it can be ignored. The $\sin^2 (\phi_c + \psi)$ and $\sin^2 (\phi_c + \psi_0)$ terms can also be ignored for sandwiches made with the proper thicknesses of the core for maximum transmission, ψ and ψ_0 being nearly equal.

Thus, for a thin-skinned low-loss sandwich at maximum transmission,

$$|T'|^2_{\text{lossy}} = |T_0|^2 A_s^4 A_c^2 \left(\frac{1 + r_{ab} r_{bc}}{1 + A_s^2 r_{ab} r_{bc}}\right)^4 \left(\frac{1 - |\rho_0|^2}{1 - A_c^2 |\rho|^2}\right)^2. \tag{112}$$

By Eq. (71*a*)

$$A_s = e^{\frac{-2\pi d_s}{\lambda_0} \frac{n_s^2 \kappa_s}{\sqrt{n_s^2 - \sin^2 \theta_0}}},$$

$$A_c = e^{\frac{-2\pi d_c}{\lambda_0} \frac{n_c^2 \kappa_c}{\sqrt{n_c^2 - \sin^2 \theta_0}}}.$$

By Eqs. (39)

$$r_{ab} = \pm \frac{n_s - 1}{n_s + 1}, \qquad r_{bc} = \pm \frac{n_c - n_s}{n_c + n_s}.$$

From Eq. (57) by rationalizing and ignoring terms containing $\sin^2 \phi_s$, we have

$$|\rho|^2 = \left(\frac{r_{bc} + A_s^2 r_{ab}}{1 + A_s^2 r_{ab} r_{bc}}\right)^2 \tag{113}$$

and

$$|\rho_0|^2 = \left(\frac{r_{bc} + r_{ab}}{1 + r_{ab} r_{bc}}\right)^2. \tag{114}$$

The factors A_s^4 and A_c^2 are the principal ones that would be obtained if the wave merely passed through the sandwich once without multiple reflection. The other factors express the additional attenuation that results from the multiple reflection.

For values of A_s and A_c not much less than unity they may be expressed as e^{-Q_s} and e^{-Q_c} and expanded to give $1 - Q_s + \cdots +$, and $1 - Q_c + \cdots +$, with

$$Q_s = \frac{2\pi d_s}{\lambda_0} \frac{n_s^2 \kappa_s}{\sqrt{n_s^2 - \sin^2 \theta_0}},$$

and

$$Q_c = \frac{2\pi d_c}{\lambda_0} \frac{n_c^2 \kappa_c}{\sqrt{n_c^2 - \sin^2 \theta_0}}.$$

To this degree of approximation, the effects of the multiple reflection are ignored, and Eq. (112) yields the expression

$$\frac{|T|_0^2 - |T|^2_{\text{lossy}}}{|T|_0^2} \approx 4Q_s + 2Q_c. \tag{115}$$

12·7. Elliptical Polarization.—If the plane of polarization of linearly polarized radiation impinging on a sheet or sandwich does not lie either in the plane of incidence or perpendicular to it, the wave can be resolved into two components in those planes. For oblique incidence, the emergent transmitted wave compounded from the component waves will not, however, be linearly polarized, because the phase of the perpendicularly polarized component will no longer be the same as that of the parallel-polarized component. The retardation in phase in passing through the panel is, in general, different for the two components. The emergent radiation will be elliptically polarized.

The magnitude of the relative shift of phase produced by a homogeneous sheet can be derived by further consideration of Eq. (60),

$$T = \frac{F_t(1 - r_{ab}^2)}{1 - F_b^2 r_{ab}^2}. \tag{60}$$

As before F_b can be set equal to $Ae^{-j\phi}$, and T itself can be written as $|T|e^{-j\Pi}$. In the rest of this development, the subscripts a and b of r_{ab} will be omitted. If the denominator of Eq. (60) is rationalized and the resulting expression for T compared with $T = |T|(\cos \Pi - j \sin \Pi)$,

$$\tan \Pi = \left(\frac{1 + A^2r^2}{1 - A^2r^2}\right) \tan \phi. \tag{116}$$

The value of Π for perpendicular polarization Π_s will be greater than that for parallel polarization Π_p, since r_s for perpendicular polarization is always greater than r_p for parallel polarization (*cf.* Sec. 11·1) and A is the same for both polarizations [Eq. (71)]. Using the expression for the tangent of the difference between two angles, we get

$$\tan (\Pi_s - \Pi_p) = \frac{\left[\left(\frac{1 + A^2r_s^2}{1 - A^2r_s^2}\right) - \left(\frac{1 + A^2r_p^2}{1 - A^2r_p^2}\right)\right]}{1 + \left(\frac{1 + A^2r_s^2}{1 - A^2r_s^2}\right)\left(\frac{1 + A^2r_p^2}{1 - A^2r_p^2}\right) \tan^2 \phi} \tan \phi. \tag{117}$$

Inspection of Eq. (117) shows that $\tan (\Pi_s - \Pi_p)$ goes to zero for $\phi = N\pi$ and $\phi = (N + \frac{1}{2})\pi$. It also vanishes for all values of ϕ at normal and grazing incidence because at those angles of incidence $r_s = r_p$. The condition $\phi = N\pi$ is also the one for zero reflection by a panel, so the shift of phase should be small at angles of incidence near the one for which the reflection vanishes. The calculations of $\Pi_s - \Pi_p$ for cases of practical interest are discussed in Sec. 11·13.

An analogous treatment of sandwiches would be complicated in detail. The behavior of symmetrical sandwiches having thin skins or half-wavelength skins would be expected to be nearly the same $|\rho|^2$ taking the place or r^2.

The radar signal received by a linearly polarized antenna may always be thought of as the resultant of two separate but coherent signals. One of these is produced by the component plane-polarized wave that is polarized parallel to the plane of incidence on the radome; the other is produced by the perpendicularly polarized component. If these two components of the received signal are in phase, the amplitude of the resultant signal is the *arithmetic* sum of the amplitudes of the two component signals. If, however, there has been a relative shift of phase, the resultant amplitude will be the *vectorial* sum of the amplitudes. Such a vectorial sum can never exceed the arithmetic sum, so relative shifts of phase produced by a radome always weaken the received signals. The extent of the weakening depends both on the amount of the shift of phase and on the angle between the plane of incidence on the radome and the plane of polarization of the wave.

Let A_p represent the amplitude of the received signal when the plane of polarization is the same as the plane of incidence, and let A_s represent the amplitude when the plane of polarization is at right angles to the plane of incidence. Also, let it be assumed that the cross section of the radar target is the same for all polarizations. (In general, this is not true for actual radar targets.) The angle that specifies the plane of polarization ψ is taken as 0° for perpendicular polarization and 90° for parallel polarization. The amplitude of the component of the signal that can be ascribed to the perpendicularly polarized component of the wave is $A_s \cos^2 \psi$. One of the cos ψ factors results from the resolution of the transmitted wave into perpendicular and parallel components; the second cos ψ factor is introduced by the resolution of the returning perpendicularly polarized wave into components in and at right angles to the plane of polarization of the antenna, the latter component contributing nothing to the received signal. Similarly, the amplitude of the signal from the parallel polarized component is $A_p \sin^2 \psi$. The shift of phase δ is twice the angle $\Pi_s - \Pi_p$ previously discussed, because of the two traversals of the radome. The amplitude of the received signal A, the vectorial sum of the component signals, is given by

$$A^2 = A_p^2 \sin^4 \psi + A_s^2 \cos^4 \psi + 2A_pA_s \sin^2 \psi \cos^2 \psi \cos \delta \quad (118)$$

or

$$P = P_p \sin^4 \psi + P_s \cos^4 \psi + 2\sqrt{P_p}\sqrt{P_s} \cos^2 \psi \sin^2 \cos \delta. \quad (119)$$

The P's are the signal powers. Upon differentiating P with respect to ψ to get the maxima and minima we find that the derivative vanishes when

$$\sin 2\psi = 0 \quad (120)$$

or

$$\tan^2 \psi = \frac{P_s - \sqrt{P_s}\sqrt{P_p} \cos \delta}{P_p - \sqrt{P_s}\sqrt{P_p} \cos \delta}. \quad (121)$$

For $\tan^2 \psi$ of Eq. (121) to be positive, the conditions $\cos \delta < \sqrt{P_s/P_p}$ and $\cos \delta < \sqrt{P_p/P_s}$ must be satisfied—$\cos \delta$ must be less than the ratio of the smaller of $\sqrt{P_s}$ and $\sqrt{P_p}$ to the greater. When this condition is satisfied, P has maximum values of P_s and P_p at $\psi = 0°$, 90°, 180°, etc., corresponding to the condition expressed in Eq. (120). The values of ψ of Eq. (121) are those of the intermediate minima. In particular, when $P_s = P_p$ these minima come at $\psi = 45°$, 135°, etc. For values of $\cos \delta$ that make $\tan^2 \psi$ negative, no real conditions are given by Eq. (121). The signal power P then has minimum values of amount P_s for $\psi = 0°$, 180°, etc., and maximum values of P_p for $\psi = 90°$, 270°, etc. (or vice versa, if $P_s > P_p$). The limiting condition $\cos \delta = \sqrt{P_s/P_p}$ (assuming $P_s < P_p$) gives the value of δ for which P just fails to take minimum values less than P_s. For this value of δ and all smaller ones the received power will be equal to or greater than P_s for all values of ψ.

CHAPTER 13

RADOME MATERIALS AND METHODS OF FABRICATION

By H. Leaderman[1]

13·1. Fabrication of Radomes.—The materials that are useful for radome construction are those having adequate mechanical strength and low loss tangents. Certain organic and inorganic high polymers are found to be satisfactory; of the inorganic, the only form that has been used so far is a fabric woven of an extremely fine yarn of continuous glass filaments. Organic high polymers are usually divided arbitrarily into resins, rubbers (elastomers), and fibrous materials, all useful for radomes. Molded plywood was used for some early radomes but proved to be unsatisfactory, principally because it is hygroscopic.

The organic plastics are more or less rigid resin- or elastomeric-base materials that are commercial products. Filled plastics contain different fillers to give them various desired properties; these fillers may be powders (wood flour, glass powder, or mica powder), fibers (glass floss or flax), or sheets (cotton, rayon, nylon, glass fabric, or paper). The sheet form is used in the laminated plastics. Because of the ordered fibrous filler, the laminated plastics are generally the strongest and stiffest of these materials.

For the small quantities of radomes needed, the usual method of fabricating plastics by high-pressure molding would be prohibitively expensive because of the elaborate molds and molding presses that would be required. Fortunately, during the past few years, two other methods of fabricating large plastic objects have been developed. One is a drawing operation, in which large flat sheets are formed to the required shape. In the other, the elements are bonded together under low pressure; it is known as "low-pressure molding" or, more correctly, as "impression molding," since one surface of the molded object (usually the outside surface) is made to conform to the contours of the mold but the other surface is not directly controlled. Suitable forms or molds for both of these methods of fabrication are relatively easy to make, and the plant equipment required (ovens and autoclaves) is relatively inexpensive. The life of the mold is satisfactory for the usual small production runs.

13·2. Drawn Thermoplastic Materials. *Polymethyl Methacrylate.*—Polymethyl methacrylate (acrylic plastic) either with or without plasticizer

[1] F. J. Mehringer assisted in the editing of this chapter.

is marketed under the trade names of Lucite (E. I. duPont de Nemours and Company) and Plexiglas (Rohm and Haas Company). It is also manufactured under the name of Perspex in England by the Imperial Chemical Industries. Corresponding grades of these materials are practically identical. Many materials such as this acrylic plastic are rigid at room temperature but pass through a leathery stage when heated and finally become rubberlike on further heating. If a sheet of this material is heated to the rubbery stage, bent over a mold to a given shape, and then allowed to cool on the mold, the "high-elastic" deformation will be "frozen in," so that the sheet conforms essentially to the shape of the mold. If the formed object is reheated, the material will reassume its original plane form if the first process has merely been one of bending. When there has been any appreciable stretching, as occurs in a deep-drawing operation, some nonrecoverable flow has taken place, and the original plane form will not be entirely regained. Because the molecular arrangement in the bent or drawn sheet is not in true equilibrium but is under internal stress, the formed object tends to reassume its original plane form at a significant rate at a temperature that is below the original forming temperature. Thus, the ASTM heat distortion temperature,[1] and not the forming temperature, is a measure of the upper limit of temperature for serviceability of a radome fabricated from sheets of acrylic plastic.

Polystyrene cannot be used for making this type of radome because of various practical difficulties involved. Compression-molded sheets of polystyrene of limited size would have to be used, since this material cannot be cast in a reasonable time because of the slow rate of polymerization of the monomer. Furthermore, the range of temperatures for forming polystyrene is much narrower than it is for acrylic plastics. The loss tangent of polymethyl methacrylate is higher than that of polystyrene (*cf.* Sec. 13·12), but it is low enough to limit the absorption by streamlined radomes of modified half-wavelength thickness to a tolerable value (Sec. 11·5). The procedures for making acrylic plastic radomes are essentially the same as for making transparent aircraft enclosures; these have been frequently described.[2]

Because reinforcing ribs cannot be used for nose radomes, a heavy wall thickness (about $\frac{1}{2}$ in.) may be necessary for structural reasons. In the 10-cm band this wall thickness may result in too high a reflection of r-f energy. In the 3-cm band, the thickness needed for mechanical strength is close to the desired modified half-wavelength thickness. Serious variations in thickness are, however, to be expected in structures

[1] American Society for Testing Materials, "Tentative Method of Test for Heat Distortion Temperature of Plastics," D 648-45T.

[2] See, for example, *Modern Plastics Encyclopedia*, 1946, p. 812.

such as deep-drawn radomes where appreciable double curvature is present. The variations may exceed permissible tolerances.

A technique has been developed in England for construction of acrylic plastic radomes having a uniform wall thickness. The radome is fabricated from several transverse strips formed by a bending operation that causes but slight change in thickness. A paste, or dough, consisting of a mixture of polymer, monomer, and catalyst is then made and inserted between the butted strips. The polymerization of the dough joint is accelerated by exposure to ultraviolet light. In this way a streamlined radome of modified half-wavelength thickness with excellent electrical properties is obtained. It will be shown later, however, that a sandwich radome having just as good electrical and mechanical properties can be built with much less weight and greater heat stability (see Sec. 13·10). In the design of mounting attachments for acrylic plastic radomes great care must be exercised to prevent concentrations of stress that may produce cracks and have disastrous consequences.

Cyclized Rubber.—A second type of drawn thermoplastic radome uses an expanded plasticized material made from cyclized rubber. This material is a rigid plastic having a low dielectric constant, a low loss tangent, and a low absorption of moisture, all desirable properties for a radome material. Cyclized synthetic rubber also has essentially the same properties. Both natural and GR-S cyclized rubbers are marketed by the Marbon Corporation under the names Marbon B and Marbon S. Radomes are fabricated from sheets of material formed by milling Marbon B (or Marbon S) with natural rubber (or GR-S) and an expanding agent. When a sheet of this material is heated in an oven, an expansion takes place that results in a foam having a density somewhere between 8 and 33 lb/ft^3. To make a radome, the sheet is removed from the oven during the process of expansion and is drawn over a wooden male mandrel, or "plug," and allowed to cool before being removed. The density of material suitable for this process is 33 lb/ft^3 (corresponding to a dielectric constant of about $1.7\epsilon_0$). At this density, at room temperature the material is leathery rather than rigid. Because of the low loss tangent and low dielectric constant, however, a massive wall thickness can be used in order to obtain any necessary rigidity. The dielectric constants of samples of expanded Marbon S of different densities are given in Sec. 13·13. These materials are tough at room temperature. However, the resistance of formed sheets to heat is poor, appreciable distortion taking place at a temperature far below the forming temperature. They are also weak and brittle at low temperatures and are attacked by aromatic motor fuels.

13·3. Molded Thermoplastic Materials.—The two thermoplastic radome materials that can be formed by low-pressure molding are "poly-

fiber" plastic (reduced-density microporous polystyrene) and molded polystyrene film (Polyflex). The former material has lower flexural strength and stiffness than polystyrene, but because of its lower dielectric constant it can be used in greater wall thicknesses. For a given wavelength and reflection coefficient, the specific strength and stiffness decrease as the density and dielectric constant of a reduced-density material is reduced, but the wall thickness increases. There is an optimum density that will result in the strongest (or stiffest) radome wall (*cf.* Secs. 13·8 and 13·15).

Polystyrene is marketed by different manufacturers under various trade names (e.g., *Lustron*, *Styron*, *Loalin*). It is usually supplied as a granular composition that is molded by conventional methods to form clear plastics. If polystyrene in the form of extremely fine fibers having a diameter of about one micron is used, however, it can be molded into clear polystyrene under moderate conditions of temperature (100°C) and pressure (15 lb/in.^{2}). Under these conditions the low-pressure molding technique can be used. More important still, if the molding process is interrupted at a suitable stage, a reduced-density plastic is produced that has certain marked advantages over full-density polystyrene for radome construction (see Secs. 13·13 and 13·15).

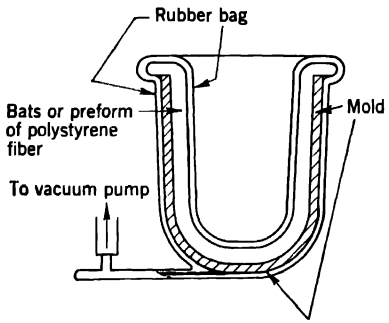

FIG. 13·1.—Bag-molding technique for polyfiber radome.

Three types of polystyrene fiber have been used for making radomes. They are the Dow Chemical Company's Q-107 and Q-274 Polyfibres and a third variety produced by the Bakelite Corporation. The Q-107 Polyfibre contains about 4 per cent of solvent, which markedly affects the molding conditions and reduces the heat resistance of the molded plastic. The other two varieties are free of solvent.

Radomes are molded from each of these types of polystyrene fiber by essentially the same process. The mold is fabricated most cheaply from laminated-paper phenolic plastic by a bag-molding operation such as is used in molding the radome itself. Bats of the fiber or a preform are laid in the mold and placed in a rubber bag (see Fig. 13·1). The bag is then evacuated, causing a pressure of approximately 15 lb/in.^{2} to be applied to the polystyrene fibers. The bag and its contents are placed in a hot-water bath for a closely controlled length of time. If a temperature higher than 95° is required, the bag is placed in a hot-air oven with efficient circulation of air or in an autoclave where heat and additional

pressure are provided by means of saturated steam. Further molding pressure can be provided by introducing compressed air into the autoclave. Careful control of the molding temperature and time is necessary in order to obtain the optimum density. If the density is too low, the fibers are not properly knitted together and the radome is weak. If the density is too high, the radome has too high a dielectric constant and is brittle. This is especially true in the case of the Bakelite fiber. For molded Dow Q-107, the optimum density is about 0.85 g/cc; for the other two types it is about 0.65 g/cc. In spite of the numerous voids in these molded plastics, they absorb but little water. Radomes molded from such materials are usually provided with a cemented-on outside skin made of a single layer of fine Fiberglas fabric (ECC-11-112). This skin, which is added to provide resistance to abrasion rather than additional mechanical strength, produces only a very slight increase of loss by reflection.

This type of radome is not especially useful in the 10-cm band, since there are other materials with higher dielectric constant that can be used, still keeping to a sufficiently small value of the electrical thickness. In the 3-cm band, however, this type of radome is of great value if the reflection is not to exceed about 10 per cent of the incident power. In order to achieve this, the thickness must be controlled by molding the radome to a thickness greater than the final value and then machining off the inside of the radome. This process has been used in quantity production. Radomes for the 1-cm band can also be made by this process. If the wall thickness is made slightly less than a half wavelength and thin skins of Fiberglas fabric impregnated in polystyrene lacquer are cemented on, the sandwich has a core dielectric constant of about $2.2\epsilon_0$ and thin skins with a dielectric constant of about $3.7\epsilon_0$. A sandwich of this construction can be used in the 1-cm band for a streamlined radome with perpendicular polarization. Electrically, it is nearly as good as a modified half-wavelength thickness wall of polyfiber plastic; mechanically, it is somewhat superior (*cf.* Sec. 13·10).

Polyfiber radomes do not absorb much water or water vapor but their heat resistance is marginal, particularly when they have been molded from fibers containing a considerable quantity of solvent. They are also susceptible to attack by aromatic liquids such as motor fuels.

The second type of material for making molded thermoplastic radomes is used in a similar way; it consists of sheets of stretched polystyrene 0.007 in. thick. It is marketed under the name of "Polyflex" by the Plax Corporation. Under suitable bag-molding conditions, the thin sheets, which can be easily tailored to fit the bag mold, fuse together to form a sheet of clear polystyrene. Radomes constructed of 10 layers of Polyflex sheet and outside and inside layers of ECC-11-112 Fiberglas cloth all

cemented together with polystyrene lacquer have moderate reflection and can be used for the 3-cm band satisfactorily. In this construction, the Fiberglas skins contribute greatly to flexural strength and stiffness yet introduce only a small additional reflection. It should be noted that this construction is not used in order to get zero reflection at normal incidence in the 3-cm band; the core spacing is much too small. Such a construction may be called a structural sandwich. If a sandwich having zero reflection at normal incidence and low weight is required, it is preferable to use a conventional sandwich with a core of low density as described in Sec. 13·6.

13·4. Molded Thermosetting Materials. *Thermosetting Resins.*—The materials considered in Secs. 13·2 and 13·3 undergo a physical change during the drawing or molding operation. The molded or drawn object is under internal stress and is accordingly somewhat deficient in resistance to heat. The resins to be considered in this section undergo an essentially irreversible chemical change consisting of the cross-linking of long molecular chains. The material usually changes from a viscous liquid or paste (at room temperature) to a hard resin in the molding process. It should be noted that the terms "thermoplastic" and "thermosetting" refer to the workability of fully cured material and not to heat resistance. For example, the thermoplastic materials polyvinyl carbazole and poly 2,5 dichlorostyrene are much more heat resistant in the conventional sense than the thermosetting glyceryl phthalate polyester.

So far, little information has been released on the chemical nature[1] of the liquid and paste types of thermosetting resins used for radome fabrication. It appears that in the uncured state, many of these resins consist of an unsaturated polyester with styrene monomer added ("polyester-styrene" resins).

Cured thermosetting resins by themselves are rather weak; their important field of application lies in the making of reinforced plastics with fibrous fillers such as paper; glass mats; and cotton, rayon, and glass cloth. Because closely controlled thicknesses and moldings with double curvature are required for radomes, fabrics are the best reinforcing fillers for low-pressure thermosetting resins. Dupont Fiber-A, woven Owens-Corning Fiberglas, and knitted glass fabric are almost completely nonhygroscopic and are therefore satisfactory for fabrication of radomes.

Laminated Panels Made with Thermosetting Resins.—The techniques of molding flat panels and radomes by using a suitable fabric and a thermosetting low-pressure resin in the form of liquid or paste are the following. The recommended amount of suitable peroxide catalyst is added to the resin and stirred in. (Paste resins must first be carefully

[1] *Cf. Modern Plastics Encyclopedia*, 1946, "Unsaturated Polyesters," p. 163; "Allyl Resins," p. 167.

heated to make them fluid.) A suitable mandrel is covered with a sheet of cellophane to act as a parting medium, as shown in Fig. 13·2. The requisite number of layers of fabric are then placed on the mandrel, and the liquid resin or heated paste resin is poured or brushed on and worked into the plies of fabric. Alternatively, the fabric may be dipped into a bath of resin; the excess resin squeezed out in a wringer; and the plies of fabric stacked on the mandrel. The fabric is covered with a second sheet of cellophane and placed in a rubber bag that is evacuated. The curing is effected by placing the bag in a heated glycerin bath or in an oven or an autoclave. Pressures up to 100 lb/in.^{2} may be obtained with a range of temperatures from 105° to 160°C (221° to 320°F). It is recommended that the bag be cooled before breaking the vacuum and removing the contents.

If the correct procedure has been followed, a rigid board is obtained and there is some clear hard brittle resin squeezed out around the edges

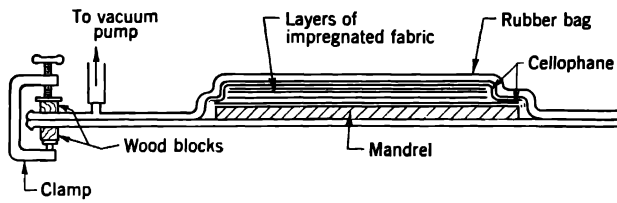

FIG. 13·2.—Bag molding of flat laminated panels.

of the laminate. With poor or incorrectly handled resin, unsatisfactory panels that are weak or nonuniform in a variety of ways will be obtained. Even the relatively simple process of making a flat laminated panel by this low-pressure molding procedure involves a complicated technique.

Fiberglas fabric, as ordinarily supplied, is white in appearance; the filaments are coated with sizing material and lubricating oil intended to facilitate weaving. Since the presence of these organic materials usually prevents a good bond to low-pressure resin, the fabric is heated under controlled time and temperature conditions. This volatilizes the oil and caramelizes the size and the resulting pale straw to dark brown fabric ("heat-treated Fiberglas") bonds much more satisfactorily to low-pressure resin (*cf.* Sec. 13·9). Extended heating of Fiberglas fabric removes all organic material ("heat-cleaned Fiberglas"); such fabric is nearly white. Heat-cleaned Fiberglas is not so good as heat-treated fabric for making laminates (*cf.* Sec. 13·9).

Although much work has been done on the technical problems of low-pressure laminating during the past few years, there are nevertheless considerable differences of opinion as to the best fabricating techniques to give the most uniform product with the best mechanical and weathering

qualities. There is also a difference of opinion as to which is the best of the numerous commercially available liquid or paste resins. Laminated panels made by the bag-molding process are subject to appreciable variations in thickness and in dielectric constant because of variation in the proportions of air, resin, and fabric in the final laminate (*cf.* Secs. 13·9 and 13·14.) The dielectric constant of the resin itself may vary as a result of styrene loss due to exposure to air of the uncured resin and the uncured impregnated fabric and possibly because of a variation in the nature of the cross-linking reaction as a result of variations in cure conditions and aging of the resin.

These low-pressure laminated plastics are more hygroscopic than the materials considered in Secs. 13·2 and 13·3. The thermosetting resins are somewhat polar, and the capillaries and voids make possible appreciable absorption of water, as can be demonstrated by the ASTM standard test for water absorption.[1] Thermosetting laminates differ from thermoplastic materials by being stable with respect to temperature up to the molding temperature at least and, in some instances, to much higher temperatures.

By a simple variation of the fabricating technique, laminated panels may be made by using thermoplastic resins instead of thermosetting resins. Fully polymerized resin is dissolved in the resin monomer; and when a satisfactory viscosity is reached, the catalyst is added. Impregnation and cure then follow as with the liquid thermosetting resins. The procedure is practicable only in the case of 2,5 dichlorostyrene, since this material is highly heat resistant when polymerized and the monomer is mobile and can dissolve a large amount of polymer before the viscosity becomes excessive; furthermore, the polymerization is sufficiently rapid to be feasible commercially. Thermoplastic laminates of poly 2,5 dichlorostyrene are less hygroscopic and have lower loss tangents than laminates of polyester-styrene resins (Table 13·13). Laminated plastics with high dielectric constants can be made by incorporating titanium dioxide. This material is added to the liquid resin containing a catalyst, and the fabric is then impregnated and cured in the usual way. The mechanical and electrical properties of such laminates are discussed in Secs. 13·9 and 13·14; the electrical properties of similar materials containing titanium dioxide are considered in Sec. 13·13.

Fabrication of Single-wall Laminated Radomes.—The technical problem of molding a single-wall laminated radome with uniform electrical properties and optimum mechanical properties is, of course, more complex than the molding of plane panels. Single-wall laminated radomes can be fabricated by essentially the same procedure as described for laminated

[1] American Society for Testing Materials, "Standard Method of Test for Water Absorption of Plastics," D 570-42.

panels with the exception that instead of a flat mandrel, a mold as was shown in Fig. 13·1 is used. The cellophane sheet next to the mold must be laid in place carefully, since any wrinkles will be reproduced on the outside surface of the radome. The cloth is "tailored" to fit the shape of the mold and have overlaps of about ½ to 1 in. These overlaps should be staggered to avoid excessive localized reflection and possible distortion of the pattern. While the fabric layers are being placed in position, or "laid-up," the resin tends to drain down toward the nose of the radome. This may be obviated by placing the evacuated bag in the oven or autoclave so that the nose of the radome is uppermost and the vacuum connection is near the rim.

An alternative procedure for making small laminated glass-fabric radomes is to draw knitted "socks" of glass fabric over a male mold.[1] Such radomes are largely handmade and require skillful and competent workmanship.

For any given wall thickness, it is preferable to laminate only a few layers of fabric (two to seven), because it is difficult to handle a large number of plies of impregnated fabric. When Fiberglas is used, the number of layers of material determines the grade of fabric to be used. It has been the practice to use square-woven Fiberglas fabric containing continuous filaments of "E" (electrical grade) glass. The fabrics most commonly used have been ECC-11-112, ECC-11-127 (or 128), and ECC-11-164 grades, corresponding roughly to thicknesses of laminate of 3, 7, and 14 mils per ply (*cf.* Sec. 13·9).

Reduced-density Thermosetting Laminates.—There is another radome material that is equivalent to polyfiber plastic in electrical and mechanical properties but has the superior heat resistance of thermosetting laminates. This material is made by using a leno (open-mesh) weave of Fiberglas fabric (grade X-1542) impregnated with resin. Several plies of the fabric are laid up in the usual way. The face plies are fine square-woven Fiberglas (say, ECC-11-112 grade). This laminate has a cellular structure and good mechanical and electrical properties. Its specific gravity is about 1.0, compared with 1.5 to 1.7 for a standard Fiberglas laminate.

An even better balance of mechanical and electrical properties is obtained with cotton or viscose rayon marquisette, ordinary household curtain material; the resulting laminates possess a specific gravity of 0.75, compared with about 1.5 for a regular cellulosic fabric laminate. Cotton and viscose rayon marquisette laminates, however, absorb water readily; they require the application of a suitable phenolic varnish to act

[1] For a detailed description of a technique of radome fabrication with knitted glass fabric, see Anon., "Radio Detection and Ranging," *Modern Plastics*, **23**, No. 1, 132A, September 1945.

as a barrier to moisture. Such materials might be of value for radomes to be used in temperate climates but not in the tropics. The mechanical and electrical properties of these materials are discussed further in Secs. 13·9 and 13·15.

Postforming.—When cross-linked thermosetting resins are heated, they acquire a certain amount of rubberlike elasticity and can be given a limited amount of single or double curvature, the extent depending largely upon the nature of the resin. This property is the basis of the technique of postforming.[1] When fully cured laminates that contain suitable thermosetting resins are heated to an appropriate temperature, they become quite flexible and can be formed over a wooden mold with very little effort. After cooling, they retain substantially the shape of the form. Thin laminates made with certain weaves of cotton fabric can be deep-drawn in this way. The process has recently been developed and extensively used for making quantities of aircraft components that are to be subjected to light stresses only.

This technique may be of value in radome engineering when a panel with a closely controlled thickness and dielectric constant has to be molded to a limited amount of double curvature, for example, streamlined radomes in the 1-cm band whose wall thickness (or sandwich skin thickness) is a modified half wavelength. Close control of the thickness and dielectric constant could be obtained by first making the radome wall (or each skin of the sandwich) in a platen press as a flat panel that could then be heated and bent over the form. An appreciable amount of double as well as single, curvature can be given to Fiberglas laminates of the appropriate thickness, with only a small variation in the thickness as a result of the heating and forming operations. Better formability can be obtained by some plasticization of the resin, but this results in a greater change of thickness in the laminate.

13·5. Materials for Construction of Sandwiches.—The choice of materials for fabrication of sandwich radomes is usually restricted to those which have low loss tangents and absorb but little moisture, especially if the skins are thick, if second-order spacing is used, or if perpendicularly polarized waves are to be incident at large angles. It is not possible to take full advantage of many recent structural improvements in sandwiches, because electrical requirements must first be satisfied. Design of the radome sandwich is based on the cancellation of the reflections of the two half sandwiches. It is not electrically necessary for the core to have a low dielectric constant; but in order that the sandwich may have good strength/weight and stiffness/weight ratios, the core must have as low a density as possible.

[1] See, for example, "Postforming Laminates," *Modern Plastics Encyclopedia*, 1946, p. 1093.

The low-density materials[1] for cores may be divided into three categories: cellular, fibrous, and granular. The first category includes several materials that may be considered as plastic foams, that is, expanded rigid plastics containing nonconnecting voids. Such foams can be made of hard rubber, synthetic hard rubber, polystyrene, cellulose acetate, phenolic resins, and polyester-styrene resins. Fibrous materials include balsa wood, Owens-Corning glass mat, and Forest Products Laboratory cellulosic fiber mat. Instead of a homogeneous material for the core, a laminated material can be used in the form of a corrugated sheet, a dimpled (waffle iron) sheet, or an egg-crate or honeycomb grid construction; of these, the last-mentioned type is in production.[2]

Of the plastic foam materials, cellulose acetate appears to be hygroscopic, while polystyrene foam does not hold up at high temperatures. The hard rubber foam with the best heat resistance is that based on the GR-N type of elastomer (butadiene-acrylonitrile copolymer); in general, this material has heat resistance superior to that of GR-S and natural hard rubber foams. Commercially available hard rubber foams differ appreciably in hygroscopic properties. Phenolic and polyester-styrene foams have excellent heat resistance but run somewhat higher in density for the same mechanical properties (*cf.* Sec. 13·11).

The low-density materials that have been used most successfully in cores are GR-N rigid foam, polyester-styrene resin foam, and the "honeycomb" (hexagonal Fiberglas grid) construction. The first-named material can be formed in flat sheets and then softened by heat to obtain a limited amount of double curvature. The same results do not seem to be possible with polyester-styrene resin foam. The Fiberglas honeycomb, as supplied, can also be bent to a certain amount of double curvature. The design of the radome determines both the choice of core material and the technique of fabrication.

Fabric laminates are used for the skins of sandwich radomes; these materials are strong and permit close control of skin thickness. Laminates of Fiberglas fabric and of Fiber-A that absorb but little moisture under conditions of high ambient temperatures and relative humidity are satisfactory for the skins of sandwich radomes (*cf.* Sec. 13·4).

13·6. Fabrication of Sandwich Radomes.—The four principal methods that have been used for the fabrication of sandwich radomes are the "foaming-in-place" technique, the single-stage and two-stage "wet layup" techniques, and the "cementing" technique.

Foaming in Place.—The inner and outer skins of the radome are made

[1] G. B. Rheinfrank, Jr., and W. A. Norman, "Core Materials for Sandwich Structures," *Modern Plastics*, **22**, No. 11, 127 (1945).

[2] L. S. Meyer and J. C. Case, "Honeycomb Core in Sandwich Structure," *Modern Plastics*, **22**, No. 11, 136 (1945).

separately with Fiberglas fabric and polyester-styrene resin, as described in Sec. 13·4 for single-wall laminated radomes. The fully cured outside skin is then placed in a female form, and the inside skin placed on a male form, as illustrated in Fig. 13·3. The polyester-styrene resin with foaming agent added is poured into the space between the skins. The assembly is heated, causing the core resin first to foam and then to cure to a rigid, brittle foam. Recipes have been developed for core resins that appear to give fine-pored cores with uniform density and good adhesion to the skins. After finishing the rim of the mounting area, the radome is complete. Because of the relatively high density of the core (about 20 lb/ft^3), this type of construction is suitable only for a small radome especially for one having a small radius of curvature at the nose. With this type of construction it is possible to arrange for gradation in thickness so as to get maximum transmission at each point of the radome.

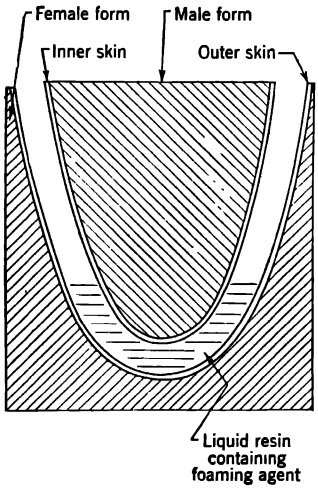

FIG. 13·3.—Foaming-in-place technique.

Single-stage Wet Lay-up.—The single-stage wet lay-up technique uses a fully cured and preformed core on which the skins are cured in the course of the molding operation. For core material, either rigid-foam board of the GR-N type or Plaskon "honeycomb" material is used. It is necessary to remove the original skin of the GR-N board to a depth of about $\frac{1}{16}$ in. because it is impossible to obtain a good bond with its original surface and because there appears to be a plane of weakness just beneath the surface.

When hard foam of the GR-N type is heated it manifests a high elasticity and is capable of some flow, so that it can be preformed to the shape of the radome. This process may be carried out in two ways. In one, each board is roughly cut to size and placed on a metal or laminated-paper phenolic mandrel or template. The board and template are then enclosed in a rubber bag and placed in a hot-air oven. When the bag and its contents reach the desired temperature, a vacuum is slowly drawn, causing the board to bend to the shape of the template. The bag is then removed from the oven and chilled in water; the vacuum broken; and the contents removed. The shaped boards are then carefully trimmed and fitted together, with a minimum of gaps, on the radome mold. A single mold as shown in Fig. 13·4 may be used. It may be of sheet metal, laminated-paper phenolic-resin plastic, or a laminated Fiberglas plastic. Molds of the last two varieties may themselves be made by the low-

pressure molding technique, so that the relatively large number of molds required for even a short production run can be prepared quickly and inexpensively. An alternative forming procedure for a core material of the GR-N type is to heat each board until it is limp and rapidly press it into the desired portion of the radome mold. The boards are then trimmed and fitted together on the mold, placed in a rubber bag, evacuated, and heated in an autoclave. This step results in a more perfect forming of the boards to the contour of the mold. Any lateral contraction of the boards caused by incomplete cure may be allowed for at this stage.

After the sections of the core have been formed, the single-stage wet lay-up can be made. In Fig. 13·4 a cross section is shown of the lay-up for a saucer-shaped streamlined radome for installation of the AN/

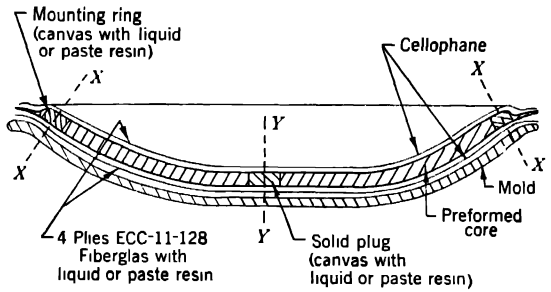

FIG. 13·4.—Single-stage wet lay-up technique.

APQ-13 system with 60-in. scanner on the Boeing B-29 (*cf.* Fig. 6·11). Upon the mold is first placed a layer of cellophane sheet to act as a parting material. A fourfold layer of heat-treated ECC-11-128 fabric impregnated with polyester-styrene resin containing a catalyst is next placed on the mold, care being taken to stagger the fabric overlaps. This becomes the outer skin. The sections of the core have in the meantime been coated with a solution of the catalyst used for the skin resin and dried in air. The core is laid in position on the layers of Fiberglas. A ring of impregnated cotton duck is laid around the edge of the core material, and a hole in the core at the center of the mold is similarly filled. Fiberglas fabric for the inner skin is then placed on the core and covered with cellophane. The completed lay-up is placed in a rubber bag which is then evacuated. Alternatively, a rubber "blanket" clamped to the rim of the mold can be used. Curing is effected in an autoclave as with the single-wall Fiberglas radome described previously (Sec. 13·4). A typical cure requires the following conditions: pressure, 20 lb/in.^{2}; temperature, 105°C; time, 1 hr. Upon removal of the fully cured radome from the mold, the mounting ring is trimmed along the line XX and drilled for the mounting attachments. The central plug is

drilled at *YY* to make a drain hole, and the radome is then ready for painting, if desired. The core is under heat and pressure for an appreciable time in this fabrication process, and there is a possibility of partial or complete collapse of the core. In Secs. 11·7 and 11·8 it was seen that the core spacing is critical for some streamlined radomes. For these, any plastic-foam core material used in this technique must have excellent uniform heat resistance. With a GR-N foam of good quality, a density of 12 lb/ft^3 should be sufficient to withstand these molding conditions without appreciable collapse. More severe molding conditions might produce stronger and more weather-resistant skins but with greater danger of local or complete collapse of the core. In some cases, such collapse appears to be attributable to chemical attack by the skin resin.

When the "catalyst wash" of the core is omitted or is insufficient, the core material will partially inhibit the cure of the skin resin, making the skin soft and poorly bonded to the core. If such a skin is stripped from its core, the resin on the inside of the skin will be found to be tacky and to smell strongly of styrene. When the core has been properly treated, the bond between a skin and its core is formed by the skin resin "keying" into the core (*cf.* Fig. 10·13), causing the bond between the skin and core to be stronger than the core. Generally speaking, the core should be as finely grained as possible, since the finer the pore size the less is the difference between the effective and actual skin thickness (Sec. 10·6). With the technique described above, an actual skin thickness of 0.030 $\pm$ 0.001 in. has been found to correspond to an effective skin thickness of 0.042 $\pm$ 0.002 in. The single-stage wet lay-up procedure can be used with Plaskon-type honeycomb core material; some details of the technique have been published.[1] Electrical tests on sandwich panels with both GR-N foam and honeycomb cores have already been discussed (Sec. 11·12), and the mechanical properties of such panels are considered in Sec. 13·10 and the properties of core materials in Sec. 13·11.

Two-stage Wet Lay-up.—For deep radomes, such as streamlined "bath-tub" or cylindrical-hemispherical radomes as shown in Fig. 9·3 a modification of the previous technique is used. The impregnated fabric for the outer skin is cured to completion on the mold, as for a single-wall laminated radome (Sec. 13·4). The inner surface of the cured outer skin is carefully sanded so as to remove only the surface film of resin and then coated with the same type of resin (containing catalyst) as was used to mold the skin. A preformed core previously washed with catalyst is next laid on the cured skin, followed by the impregnated fabric for the inner skin as before. In a second curing operation, there occurs both the bonding of the outer skin to the core and

[1] L. S. Meyer and J. C. Case, *loc. cit.*

the curing and bonding of the inner skin. This two-stage technique appears to be electrically and mechanically equivalent to the single-stage process, provided that the uncured resin is not adversely affected by prolonged exposure to air.

Cementing.—With this technique the precured skins are cemented to the core with cold- or warm-setting adhesive. Cold-setting resorcinol-formaldehyde cements such as Penacolite give an extremely good bond when heavily applied; but because these cements have high loss tangents, there is a reduction in transmission. Rubber cements are excellent electrically but do not give a good bond. With this type of construction, any errors or irregularities in forming the skin or core result in localized air gaps or adhesive-filled gaps that lead to serious distortion of the pattern. This technique is not recommended for the fabrication of radomes.

MECHANICAL PROPERTIES OF RADOME MATERIALS

13·7. Evaluation of Strength and Stiffness.—Because the design of a radome involves mechanical as well as electrical problems, methods must be devised by which radome materials can be evaluated both mechanically and electrically.

In this section are developed criteria for the strength and stiffness of the electrical portion of the radome wall. Although these are of some value in comparing radomes, they should be used with caution. They are of little use in determining the proper design of the nonelectrical parts of the radome. Furthermore, radome wall materials are isotropic in only a few cases; in a plane panel, for instance, the strength and stiffness criteria may vary in different directions. Also, a more ductile or flexible material may allow a plastic or elastic relaxation of stress that will strengthen a radome. If these limitations are borne in mind, the strength and stiffness criteria can be valuable guides in the selection, evaluation, and control of radome materials.

The forces that are exerted on the wall of a radome in use are likely to be complicated. In most cases, however, the important ones appear as bending and shearing couples. The latter are of relatively small consequence for fairly homogeneous materials but may be of some importance for sandwiches. The important properties of a wall construction are the flexural stiffness, the flexural strength, and sometimes the analogous quantities connected with shear stresses.

Since bending of a beam produces tension at the outer surface and compression at the inner surface, it is clear that the physical property of the material involved is its elasticity. In the elementary theory of the flexure of beams it is shown that

$$M\rho = EI = \frac{Ed^3}{12}, \tag{1}$$

where M = the bending moment per unit width of beam,
ρ = the radius of curvature of the originally straight beam (measured with respect to the neutral layer),
E = Young's modulus,
I = the moment of inertia about the neutral axis of a cross section of unit mass and unit width ($I = d^3/12$),
d = depth of the beam.

Within the elastic limit the bending moment is proportional to the reciprocal of the radius of curvature. The constant product $M\rho$ is thus the measure of the flexural stiffness of the beam and equals $Ed^3/12$. The proportionality to d^3 is verified experimentally.

Simple geometrical considerations show that the greatest value of the tensile and compressive stresses in the beam S_0 is proportional to the bending moment, the relation being

$$S_0 = \frac{6M}{d^2} \tag{2}$$

so long as the strains are within the elastic limit. When the strains become so great that the elastic limit is exceeded at either surface of the beam, Eq. (2) is no longer accurately valid. If, however, M_{max} is the value of the bending moment per unit width that causes failure of the beam, we can write

$$f_b = \frac{6M_{max}}{d^2}. \tag{3}$$

The quantity f_b has the dimensions of stress and is approximately equal to the maximum value of tensile or compressive stress that the material can withstand. It is found experimentally that M_{max} is not accurately proportional to d^2, so that f_b is not a property of the material, strictly speaking. The experimental values, however, are close enough to constancy to warrant looking upon f_b as a quantity that gives a measure of the strength of the material. It is called the flexural strength or the modulus of rupture.

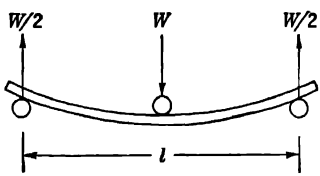

FIG. 13·5.– Simple bending test.

The most convenient type of test for this sort of panel is the simple bending test in which a beam of material resting upon two supports is loaded with a central load, as in Fig. 13·5. The bending moment varies linearly from zero at the supports to a maximum value at the center of the span. If the load carried by a test specimen of width b and span l is W, the corresponding maximum value of the bending moment per unit

width at the center of the beam is given by

$$M = \frac{Wl}{4b}. \tag{4}$$

When W_{max} is the load that just causes failure of the test sample, a corresponding value of M_{max} is given by Eq. (4). Put into Eq. (3) it gives

$$f_b = \frac{3W_{max}l}{2bd^2}. \tag{5}$$

If δ is the deflection of the center of the beam produced as the result of the load W at the center, it can be shown to equal $l^2/12\rho_{min}$, where ρ_{min} is the radius of curvature of the beam at the middle of the span. Putting this value of ρ_{min} and M from Eq. (4) into Eq. (1) yields the expression

$$\frac{\delta}{W} = \frac{l^3}{4Ebd^3}. \tag{6}$$

Young's modulus is thus given by

$$E = \frac{l^3}{4bd^3\left(\frac{\delta}{W}\right)}. \tag{7}$$

The load-deflection curve is often a straight line up to an appreciable fraction of the breaking load; δ/W is obtained from the slope of this line. If there is no straight portion of the load-deflection curve, δ/W is taken as the slope of the load-deflection curve at the origin.

There is also a constant shearing force of amount $W/2$ on each half of the beam. Thus, if the span l is great enough, the shear stress is negligible in comparison with the bending stress which, by Eq. (4), increases with increasing l for given W. For transverse test on plastics, a span/depth ratio of at least 16 has been standardized.[1] With a span/depth ratio equal to or greater than 16, the effect of shear on the measured values of f_b and E appears to be negligible in a beam of homogeneous material (see Sec. 13·10). In testing a sandwich construction having a core of low density, however, it may be necessary to use much greater values of the span/depth ratio in order to reduce the effect of shear in the core; in evaluating thin panels of a relatively weak material, such as Polyfibre, it may be necessary to use a span/depth ratio of 8 or less in order to obtain a reasonable value for W_{max}. The most heavily stressed central cross section is under the local concentration of stress from the loading foot and is, at the same time, adjacent to the more lightly loaded cross sections. It is not to be expected, therefore, that the value of M_{max} obtained from a

[1] American Society for Testing Materials, "Tentative Method of Flexural Test of Plastics," D790-45T.

simple bending test will agree too well with a value that would be obtained in pure bending.

Figure 13·6 shows a bending jig that has been designed to test panels having widths up to $\frac{5}{8}$ in. and spans from 0.64 to 5 in. The jig is provided

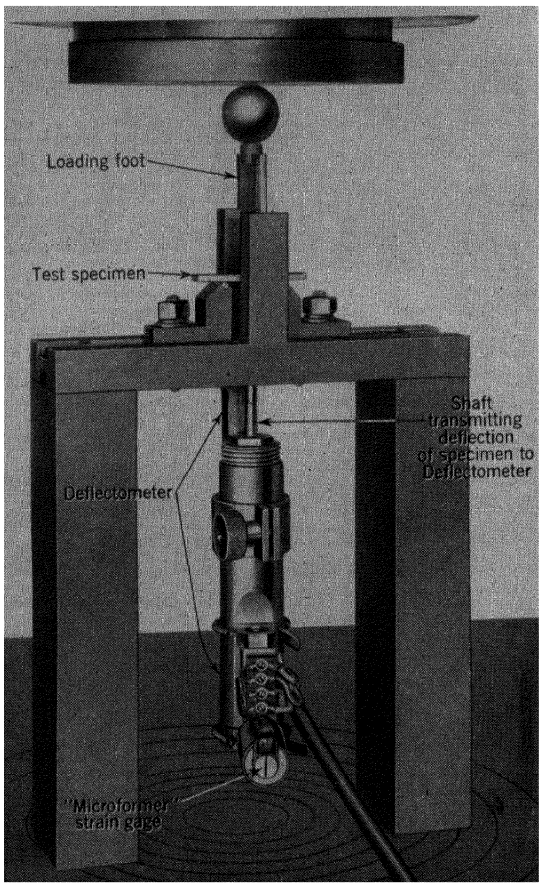

FIG. 13·6.—Testing of flexure on thin panels.

with an electronic deflection gauge of the "Microformer" type, whose range and sensitivity may be changed as required. The equipment has been used in a Baldwin-Southwark Universal Testing Machine having a scale with a range of 120 lb and with a recorder giving autographic load-deflection curves.

Actual panels made by the processes described in the preceding

sections are not likely to be truly uniform or homogeneous. If, however, test panels are made using the same materials and methods of fabrication as will be used for actual radomes, the results of the bending tests will be of some significance. With homogeneous materials such as cast acrylic plastic sheet and quasi-homogeneous materials like Polyfibre plastic and Fiberglas laminates, quantities are obtained (E and f_b) having the dimensions of stress that may be considered to be characteristic of the material to a first approximation. The values of these quantities usually depend upon the face of the panel that is in compression in the flexural test and on the original orientation of the length of the test beam in the panel from which it was taken. It is generally advisable to test some specimens with a given face in compression, others with the same face in tension, and still others with different orientations relative to the sheet. If the properties of a panel vary appreciably from point to point, a representative selection of test samples should be made. It is occasionally necessary to test specimens at high temperatures in order to find the temperature dependence of the mechanical properties.

13·8. Flexural Properties of Thermoplastics.—Table 13·1 gives the results of tests on polystyrene, molded Polyflex, and acrylic plastic.

TABLE 13·1.—FLEXURAL PROPERTIES OF THERMOPLASTICS

Material	d, in.	$\frac{l}{d}$	f_b, lb/in.²	E, lb/in.²
Polymethyl methacrylate ("Plexiglas")	0.057	18	15,900	0.40×10^6
Polymethyl methacrylate ("Plexiglas")	0.390	15	13,900	0.39×10^6
Polystyrene	0 112	16	9,390	0.49×10^6
Polyflex	0.075	13	13,300	0.38×10^6

Reduced-density Polystyrene Plastics.—Dow Q-107 polystyrene fiber is supplied in the form of bats of oriented fiber. It is usually inconvenient, in practice, to lay up these bats crossed, i.e., with the direction of the fibers in alternate layers of bat at right angles to each other. For this reason the strength and stiffness of a Polyfibre radome wall in the direction of the fibers may be two to three times the strength and stiffness transverse to the direction of the fibers. In order to evaluate the oriented molded plastic as a radome material and to compare it with other reduced density materials, the average should be taken between the values parallel and perpendicular to the fiber direction.

Figure 13·7 gives the results of flexural tests on four panels of Dow Q-107 molded Polyfibre plastic. The panels were all about 0.1 in. thick and were prepared by a standard procedure of fabrication for this material. The data given in Fig. 13·7 thus represent the specific flexural properties of radome walls for low-reflection thin-wall radomes to be used

for the 3-cm band. Material of two slightly different solvent contents was used for the preparation of the test panels, which presumably accounts for the mechanical properties of the panel of specific gravity 1.00 being slightly poorer than those of the panel of specific gravity 0.94. Figure 13·7 gives the values (obtained at 25°C) of the modulus of rupture f_b and of Young's modulus in bending E both when the span is parallel and when it is perpendicular to the direction of the fibers. The average values of f_b and E for each panel are also given. In Sec. 13·13 the dielectric constants of these materials are discussed; it is shown in Sec. 13·15 that material having a specific gravity of about 0.80 has the optimum combination of mechanical properties and dielectric constant for thin-walled radomes.

It has been pointed out (Sec. 13·3) that the heat resistance of molded polystyrene fiber plastics is marginal. If a radome is exposed to strong

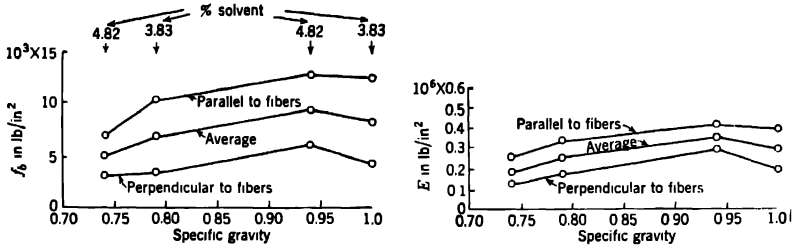

(*a*) Strength. (*b*) Stiffness.

FIG. 13·7.—Flexural strength and stiffness of molded Dow Q-107 Polyfibre.

sunlight, the direct radiation from the sun will make the surface temperature much higher than the ambient temperature; this effect is most severe when the radome is painted a dark color. If it can be assumed that the surface temperature of the radome under such conditions will not exceed 70°C, a polystyrene fiber plastic will be suitable for radome use at this temperature provided that the material remains stable (that is, if contraction in the direction of the fibers does not take place on exposure) and that the values of the mechanical moduli are appreciable fractions of the corresponding values at 25°C.

Figure 13·8 shows the average of the values of f_b and E measured parallel and perpendicular to the direction of the fibers in four panels of molded low-solvent Dow Q-107 Polyfibre (0.8 per cent solvent content). Data for both 25° and 70°C are given. Although the optimum specific gravity for this type of material appears to be about 0.75 (*cf.* Sec. 13·15), a higher density might have to be used in practice to facilitate the cementing of the reinforcement in the nonelectrical area. This low-solvent material thus seems to be adequately heat resistant for surface temperatures up to at least 70°C. If the reinforcing skins outside the elec-

trical area are cemented on by means of solvent-type cement, the presence of residual solvent reduces the heat resistance of that portion of the radome.

It has been mentioned (Sec. 13·3) that Dow Q-274 Polyfibre and the Bakelite polystyrene fiber are molded to an optimum density somewhat less than that for the Q-107 material. The results of flexural tests on early panels of these materials are given in Table 13·2. The first material

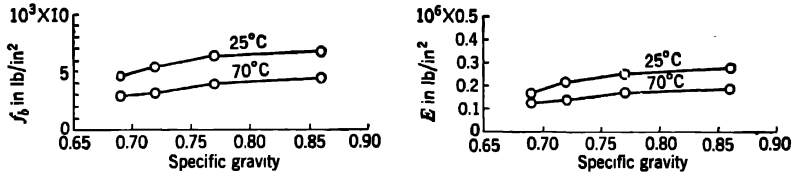

(*a*) Strength. (*b*) Stiffness.

FIG. 13·8.—Effect of temperature on flexural strength and stiffness of molded low-solvent Dow Q-107 Polyfibre.

in Table 13·2 compares well with Dow Q-107 molded Polyfibre, while the second one, because of its low strength and low density, is best used for the 3-cm band as the core of a sandwich with very thin Fiberglas-polystyrene skins.

TABLE 13·2.—FLEXURAL PROPERTIES OF REDUCED-DENSITY POLYSTYRENE PLASTICS

Material	d, in.	Specific gravity (approx.)	f_b, lb/in.^{2}	E, lb/in.^{2}
Dow Q-274 Polyfibre	0.147	0.62	3600	0 091 × 10^6
Bakelite polystyrene fiber	0.142	0 53	1200	0 044 × 10^6

13·9. Flexural Properties of Thermosetting Laminates. *Fiberglas Laminates.*—Laminates of Owens-Corning Fiberglas fabric and Dupont Fiber-A fabric with thermosetting resins have low loss tangents and low absorption of moisture and are suitable for use in radomes. Fiberglas fabric has been used extensively for radomes, whereas Fiber-A fabric has been used experimentally only. Laminates of knitted glass fabric have also been used successfully in the fabrication of small streamlined and other beacon housings where the lower specific strength and stiffness can be tolerated. It is well known that the tensile strength of a glass filament increases rapidly with decrease in diameter of the filament. This property has been taken into account in the development of Owens-Corning Fiberglas fabric, in which an extremely fine filament is used to obtain a fabric of high tensile strength.[1] Thus, laminates of Fiberglas

[1] F. O. Anderegg, *Ind. Eng. Chem.* **31**, 290 (1939).

fabric, when tested for tension in the direction of the fabric warp or filling, show high tensile strengths and moduli attributable largely to the reinforcing fabric. They are usually not so strong under compression. Under optimum conditions the compressive strength of a good Fiberglas laminate is about the same as its tensile strength, while the compressive strength of a poor laminate may be only one-tenth as great. When Fiberglas laminates are tested in simple bending, it is found that failure first occurs on the compression side at the cross section where the bending moment is maximum. If further deflection is applied to the specimen, failure occurs on the tension side. The first compression failure may not be observed if the load is applied by means of dead weights. A Fiberglas laminate tested parallel to the warp or filling behaves like wood tested parallel to the grain, showing greater strength in tension than in compression.[1] The properties of glass fabric laminates are thus in marked contrast to the properties of block glass, which is stronger in compression than in tension.

In view of the large number of factors, many of which are uncontrollable, that affect the modulus of rupture and modulus of elasticity in bending of Fiberglas laminates, significant data are difficult to obtain. The following paragraphs present some data obtained with carefully prepared laboratory samples in which undesired variables were eliminated as much as possible.

Effect of Treatment of Fabric and Thickness of Plies.—Flexural tests have been made on four Fiberglas laminates containing respectively 3 layers and 9 layers of ECC-11-162 Fiberglas fabric and 9 layers and 30 layers of ECC-11-112 Fiberglas fabric. For each arrangement, three samples were tested, one each with untreated fabric, heat-cleaned fabric, and heat-treated fabric. The resin contents ranged from 37 to 47 per cent.[2] The flexural tests summarized in Table 13·3 give the averaged results of tests made parallel and perpendicular to the warp direction. It is seen that the effect of heat-treatment of the fabric is always to improve the flexural strength greatly, whereas heat cleaning of the fabric results in a smaller improvement. The flexural stiffness follows a similar although less marked behavior. Comparing the first and third and also the second and fourth sections of Table 13·3, it appears that the modulus of rupture depends not upon the number of layers of fabric but upon the thickness of each ply.

The resin contents used in the above panels seem to be about optimum

[1] See, for example, "Form Factors of Beams Subjected to Transverse Loading Only," Forest Products Laboratory Report No. 1310 (reprinted from National Advisory Committee for Aeronautics Report No. 181), Forest Products Laboratory, Madison, Wis., October 1941.

[2] The specimens were supplied by the Owens-Corning Fiberglas Corporation and were cured with Bakelite BRS 16631 resin at contact pressure.

for mechanical properties. In practice lower resin contents are used, since in molding a radome with double curvature it is desirable to use appreciable pressure (15 to 50 lb/in^2) in order to obtain good contact between the plies. If the excess resin is squeezed out before gelation occurs, an equilibrium resin content of 25 to 30 per cent by weight is

TABLE 13·3.—EFFECT OF FABRIC TREATMENT AND NUMBER OF PLIES OF FABRIC ON THE FLEXURAL PROPERTIES OF FIBERGLAS LAMINATES

No. of layers of fabric	Grade of fabric	Treatment of fabric*	Thickness of laminate, in.	Modulus of rupture, lb/in.^{2} $f_b \times 10^{-3}$	Young's modulus, lb/in^2 $E \times 10^{-6}$	Specific dielectric constant $\frac{\epsilon'}{\epsilon_0}$
9	ECC-11-112	U	0.028	33 4	2.08	3.72
		HC	0 031	30.3	2.27	3.96
		HT	0.032	42.1	2.21	3.76
3	ECC-11-162	U	0.048	25.3	1.12	3.45
		HC	0.052	29.7	1.34	3.62
		HT	0.046	32.9	1.80	4 00
30	ECC-11-112	U	0.077	32.6	2 59	4 05
		HC	0.083	35.8	2 59	3.90
		HT	0.087	42.6	2.49	4.05
9	ECC-11-162	U	0.158	22.9	1 76	....
		HC	0.154	32.8	1.88	....
		HT	0.142	34.7	2.20	....

* U = untreated fabric,
HC = heat-cleaned fabric,
HT = heat-treated fabric.

obtained. With lower resin contents, poorer mechanical properties are obtained, and the improvement in mechanical properties resulting from heat-treatment of the fabric is more marked in practice than is indicated in Table 13·3. Table 13·4 gives the flexural properties of some laminates prepared by a commercial molder using his standard technique, following

TABLE 13·4.—EFFECT OF HEAT TREATMENT AND NUMBER OF PLIES; ECC-11-162 FIBERGLAS FABRIC, BAKELITE BRS 16631 RESIN

No. of plies	Treatment of fabric	Thickness of laminate, in. d	Modulus of rupture, lb/in.^{2} $f_b \times 10^{-3}$	Young's modulus, lb/in.^{2} $E \times 10^{-6}$	Specific dielectric constant $\frac{\epsilon'}{\epsilon_0}$
3	Untreated	0.054	16.6	1.15	3.36
3	Heat-treated	0.058	27.1	1.56	3.50
9	Untreated	0.146	16.0	1.66	3.77
9	Heat-treated	0.168	22 3	1.59	3.56

the procedure outlined in Sec. 13·4 (Fig. 13·2). It is seen that for samples prepared under industrial conditions, the effect of heat-treating is more pronounced than it is for samples prepared under laboratory conditions. Heat-treatment of fabric to be used in Fiberglas single-wall radomes is therefore to be recommended. It would also appear preferable to use very fine Fiberglas fabric, such as ECC-11-112 grade. The greatly increased difficulty of handling a large number of layers of fine fabric, however, makes it undesirable to use this material. For many purposes, including thin-wall radomes for the 10-cm band and sandwich radomes for the 3-cm band, a satisfactory compromise is to use the ECC-11-128 fabric. In the fabrication of radomes of half-wavelength thickness for the 1-cm band, ECC-11-162 fabric is preferable to avoid the necessity of using an excessive number of plies.

Effect of Resin Content on Properties of Fiberglas Laminates.—It was mentioned in Sec. 10·4 that where it is desired to de-ice a radome, the double-wall type of construction can be used because hot air can be passed through the space between the walls.[1] The Fiberglas laminates comprising the radome walls must possess good flexural properties at the maximum

TABLE 13·5.—EFFECT OF RESIN CONTENT ON FLEXURAL PROPERTIES OF FIBERGLAS LAMINATES AT 25° AND 120°C

Laminate: 7 Plies Heat-treated ECC-11-128 Fiberglas with Laminac X-4000 Resin.

Resin content, % by weight	Specific gravity	Specific dielectric constant $\frac{\epsilon'}{\epsilon_0}$	Thickness, in. d	Modulus of rupture, lb/in.^{2} $f_b \times 10^{-3}$		Modulus of elasticity, lb/in.^{2} $E \times 10^{-6}$	
				25°C	120°C	25°C	120°C
43.0	1.67	4.23	0.056	30 6	25.2	1.44	1.28
41.6	1.70	4.30	0.055	25.8	20.1	1.29	1.03
36.3	1.72	4.10	0.049	33.0	21.9	2.10	1.32
32.6	1 64	4.06	0 049	34 9	17.2	2.07	1.04
31.7	1 68	4.06	0 049	33.1	17.7	2.04	0.83
27 8	1.50	3.79	0.050	29.6	11.2	1.84	0.74
24.6	1.50	3.73	0.049	21.2	9.4	1.65	0.78

temperature of the hot air, perhaps 120°C. The flexural tests on the plastic material must then be carried out at an appropriate temperature. Table 13·5 gives data on flexural strength and stiffness of a series of Fiberglas laminates consisting of seven plies of heat-treated ECC-11-128 Fiberglas fabric and American Cyanamid Laminac X-4000 resin.[2] Five of these panels, with resin contents ranging from 24.6 to 36.3 per cent by

[1] As in the leading edge of the Eagle vane (see Sec. 14·5).

[2] These panels were kindly supplied by American Cyanamid Company.

weight, were cured under identical conditions, the content being varied by varying the impregnation of the fabric. Two of the panels, containing respectively 41.6 and 43 per cent resin by weight, were cured under different conditions in order to obtain the high resin content. With these two specimens, the load-deflection curves at 120°C were initially linear, making it easy to determine E in bending. With specimens containing only a small amount of resin there was no initial linear part, since they exhibited pronounced plastic flow at the higher temperature. The values of strength and stiffness at 120°C for these specimens are of slight significance.

It will be observed that for the last five panels in Table 13·5, the resin content increases with specific gravity and dielectric constant whereas the thickness remains unchanged. A reduction in resin content through under-impregnation of the fabric must therefore result in the creation of a large proportion of voids in the laminate. Although a low dielectric constant can be obtained in this way, the resulting mechanical properties are poor, especially at high temperatures. From Table 13·5, it appears that the best mechanical properties at 25°C correspond to a resin content of about 33 per cent; but in order to obtain the best properties at 120°C, the maximum possible resin content should be used.

Fiberglas Laminates with High Dielectric Constant.— It has been mentioned in Sec. 13·4 that Fiberglas laminates of high dielectric constant can be obtained by impregnating the fabric with a mixture of the laminating resin and titanium dioxide. In order to obtain a high dielectric constant, it is necessary to have an appreciable volume of titanium dioxide present in the laminate (see Sec. 13·13). Table 13·6 gives the properties of two laminates made in this manner. Eight plies of ECC-11-128 untreated Fiberglas fabric impregnated with BRS 16631 Bakelite were used for each. In practice, the proportions of resin, filler, and fabric have to be accurately controlled in order to obtain a closely controlled dielectric constant. It should be noticed that the thickness of the

TABLE 13·6.—PROPERTIES OF FIBERGLAS LAMINATES CONTAINING TITANIUM DIOXIDE

Thickness, in. d	Parts TiO_2 to 100 parts resin	Modulus of rupture, lb/in.^{2} $f_b \times 10^{-3}$	Modulus of elasticity, lb/in.^{2} $E \times 10^{-6}$	Specific dielectric constant $\frac{\epsilon'}{\epsilon_0}$
0.079	121	19.8	1.38	7.07
0.091	229	22.3	1.70	9.25

panels in Table 13·6 is greater than for such laminates without titanium dioxide. These laminates can therefore be considered as Fiberglas

laminates in which part of the glass fabric filler is replaced by titanium dioxide powder. In spite of the large amount of low-strength filler, the flexural properties of the panels compare well with those of regular Fiberglas laminates.

Reduced-density Laminates.—Regular Fiberglas laminates usually include a certain amount of air (or voids). To some extent the dielectric constant and mechanical properties are affected thereby. In a reduced-density laminate, the material contains an intentional and controlled proportion of voids (*cf.* Sec. 13·4), these voids being obtained by using an open-weave (leno) fabric such as marquisette. Table 13·7 gives data on the mechanical and electrical properties of a reduced-density thermosetting laminate having a core consisting of heat-treated leno-weave Fiberglas fabric and faces of one ply each of heat-treated ECC-11-112 Fiberglas fabric. The table also includes data on a laminate whose core is viscose rayon marquisette with faces of one ply of airplane cloth. These materials are evaluated more fully in Sec. 13·15.

TABLE 13·7.—REDUCED-DENSITY LAMINATES

Core	Faces	Thickness, in.	Modulus of rupture, lb/in.^{2}	Modulus of elasticity, lb/in.^{2}	Specific dielectric constant $\frac{\epsilon'}{\epsilon_0}$
11 Plies X-1542 leno-weave Fiberglas	1-ply ECC-11-112 Fiberglas	0 074	18,350	1,300,000	2.78
14 plies viscose rayon marquisette	1-ply airplane cloth	0.092	11,070	139,000	2.25

Laminates for Half-wavelength Radomes.—Laminated fabric plastics are of value for half-wavelength radomes. For the 1-cm band, laminates of Fiberglas fabric with polyester-styrene resins may be used. (If poly 2,5 dichlorostyrene, Monsanto Styramic HT, is used as the resin, a slightly lower loss tangent is obtained.) As Fiberglas laminates contain variable amounts of resin and voids, any given construction varies in thickness and dielectric constant, which might give trouble in streamlined radomes of modified half-length thickness. Fiber-A laminates have low loss tangents and appear to be more uniform in dielectric constant (see Sec. 13·14). Table 13·8 presents the flexural properties of several panels of approximately half-wavelength thickness for the 1-cm band.

TABLE 13·8.—LAMINATES FOR HALF-WAVELENGTH RADOMES
1-cm band

No. of plies	Fabric	Resin	Thickness, in. d	Modulus of rupture, lb/in.² $f_b \times 10^{-3}$		Young's modulus, lb/in.² $E \times 10^{-6}$	
				Parallel to warp and filling	45° to warp and filling	Parallel to warp and filling	45° to warp and filling
8	ECC-11-162 Fiberglas (heat-treated)	Bakelite BRS 16631	0 130	34.1	23.3	1.90	1 65
9	ECC-11-162 Fiberglas (heat-treated)	Monsanto dichloro-styrene	0.135	26.3	19.4	2.06	1.14
..	Knitted Fiber-A	Pittsburgh Plate Glass Co. Selectron	0.152	11.3	....	0.62	....
12	Woven Fiber-A	Bakelite BRS 16631	0.145	15.0	....	0.55	....

13·10. Mechanical Properties of Sandwiches.—The two types of loading to which an element of a sandwich radome may be subjected are illustrated in Fig. 13·9. At *a* the element is under pure bending stress, and at *b* it is under shear.

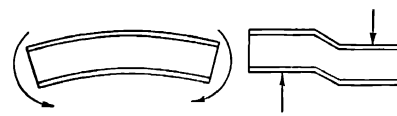

FIG. 13·9.—Types of loading.

Stiffness in Pure Bending.—For a symmetrical sandwich, the neutral layer is equidistant from the faces. The applied bending moment per unit width of beam is M, and ρ is the radius of curvature of the bent beam referred to the neutral layer. If the elastic limit is not exceeded, the appropriate generalization of Eq. (1) of Sec. 13.7 is

$$M\rho = EI = E_s I_s + E_c I_c = \frac{E_s(h^3 - d_c^3)}{12} + \frac{E_c d_c^3}{12}, \tag{8}$$

where E_s and E_c are Young's moduli for the skin (face) and core respectively, h is the over-all thickness of the sandwich, and d_s and d_c are the skin thickness and core thickness, respectively. (In this chapter the unprimed quantities d_s and d_c indicate the actual thicknesses rather than

effective thicknesses as in previous chapters.) For many practical sandwich arrangements, d_s is small compared with h, so the flexural stiffness can be approximated by

$$M\rho = EI \approx \frac{E_s h d_s d_c}{2} + \frac{E_c d_c^3}{12}. \tag{9}$$

With sandwiches having laminated Fiberglas skins and low-density cores, the second term on the right-hand side of Eq. (9), representing the contribution of the core to the flexural stiffness of the beam, is usually negligible. Take, for example, the following set of values:

$$\begin{aligned} E_s &= 2.5 \times 10^6 \text{ lb/in.}^2, \\ E_c &= 20{,}000 \text{ lb/in.}^2, \\ h &= 0.445 \text{ in.}, \\ d_s &= 0.030 \text{ in.} \end{aligned}$$

Then the first term of Eq. (9) equals 6430 lb-in.^{2} per inch of width, and the second term equals 95 lb-in.^{2} per inch of width. Thus, for sandwiches with low-density cores and thin skins, the flexural stiffness is given approximately by

$$M\rho = EI \approx \frac{E_s h d_s d_c}{2}. \tag{10}$$

This approximation does not apply to sandwiches where the core contributes appreciably to the stiffness of the sandwich, as, for instance, with a sandwich having a core of polyfiber plastic and faces of very thin Fiberglas laminates.

Strength in Pure Bending.—The strength of a sandwich construction in pure bending can be represented as with a homogeneous beam by the maximum terminal couples M_{max} that can be applied to a beam of unit width before it fails. Usually, with sandwiches having low-density cores, the flexural strength is primarily due to the skins of the sandwich. With laminated Fiberglas and Fiber-A faces, failure usually takes place in the face of the sandwich under compressive stress. It is assumed that the skins and core follow Hooke's law (stress is proportional to strain) up to failure. For a symmetrical sandwich, the distance from the neutral layer to the outside of the compression face is $h/2$; thus, the maximum bending moment carried by unit width of beam in pure bending is

$$M_{max} = \frac{f_s I_s}{\frac{h}{2}} = f_s d_s d_c, \tag{11}$$

where f_s is the compressive strength of the faces. The value of f_s, determined by means of a bending test on a panel of thin-skinned sandwich

with low-density core, is found to be somewhat higher than the value of f_s obtained directly by means of an edgewise compression test on the same panel. This discrepancy is the result of assuming that Hooke's law holds until failure.

Sandwich Beams under Transverse Load.—In actual practice, radomes are loaded by aerodynamic loads normal to the surface and by the reactions at the supports; thus, in addition to the longitudinal stresses in the skin and core, shear stresses are also present. The deflection of the radome under load is due partly to the action of longitudinal stresses and partly to the action of shear stresses; the deflection due to shear stresses may be an appreciable part of the total deflection. Breakdown may occur not only through compression (or tension) failure in the faces but also through failure in the core resulting from shear stress or combined longitudinal and shear stress; failure of the core-skin bond may also occur.

In order to evaluate the strength and stiffness of the sandwich construction under transverse load, it is necessary to study the behavior of beams cut from plane panels and tested in simple bending as illustrated in Fig. 13·5.

Assume that a beam of breadth b and of span l is loaded centrally with a load W. If the skin thickness d_s is small compared with the over-all thickness h, and if E_c is small compared with E_s, then the shear stresses in the core and at the core-skin interface at any section along the beam are given approximately by $W/2bd_c$ where d_c is the core thickness. The deflection of the beam at the center due to shear δ_s is then given by the approximation of

$$\delta_s \approx \frac{Wl}{4bd_cG_c} \approx \frac{Wl}{1.6bd_cE_c}, \tag{12}$$

where the shear modulus of the core G_c is assumed to be equal to $0.4E_c$. The deflection due to bending moment δ_b [*cf.* Eq. (6)] is

$$\delta_b = \frac{Wl^3}{48EIb}, \tag{13}$$

where EI is as in Eq. (10). Thus, the total deflection δ $(= \delta_s + \delta_b)$ is given by

$$\frac{\delta}{W} = \frac{l^3}{48EIb}\left[1 + e\left(\frac{h}{l}\right)^2\right], \tag{14}$$

where

$$e \approx 15\left(\frac{E_s}{E_c}\right)\left(\frac{d_s}{h}\right). \tag{15}$$

The term $e(h/l)^2$ therefore represents the ratio of the deflection due to

shear to the deflection due to bending moment.[1] If now the *apparent* flexural stiffness obtained from a simple bending test with span l be denoted by $(EI)_l$, then

$$\frac{\delta}{W} = \frac{l^3}{48(EI)_l b}, \tag{16}$$

and

$$\frac{1}{(EI)_l} = \frac{1 + e\left(\frac{h}{l}\right)^2}{EI}. \tag{17}$$

Thus $1/(EI)_l$ varies linearly with the square of the depth/span ratio.

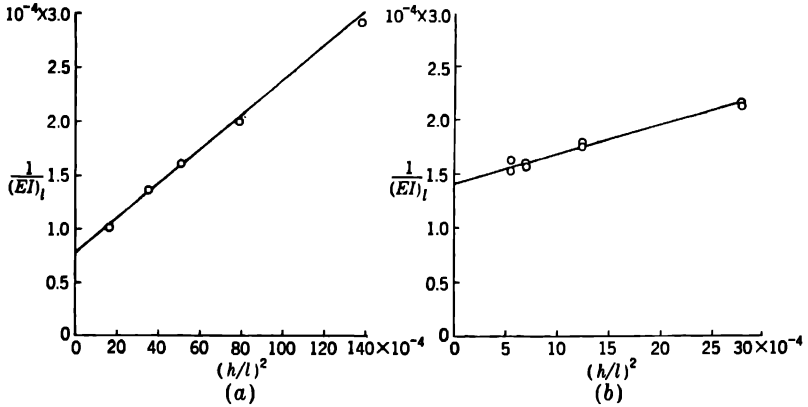

(*a*) Conditions for *a*:
EI = 12,500 lb-in.²/in.
d_s = 0.037 in.
h = 0.702 in.
E_s = 1.53 × 10⁶ lb/in.² (computed).
e = 199 (computed).

(*b*) Conditions for *b*:
EI = 7100 lb-in.²/in.
d_s = 0.030 in.
h = 0.423 in.
E_s = 3.09 × 10⁶ lb/in. (computed).
e = 202 (computed).

FIG. 13·10.—Effect of shear deformation in simple bending tests.

Figure 13·10 illustrates the effect of the shear deformation in such tests. A beam was tested[2] with successively shorter spans, being cut down each time to maintain an overhang of 1 in. The results plotted in Fig. 13·10*a* show that the reciprocal of the apparent flexural stiffness $1/(EI)_l$ varies linearly with $(h/l)^2$; the intercept gives a value of 1.53 × 10⁶ lb/in.² for Young's modulus of the skins, which were each two plies of ECC-11-162 Fiberglas fabric (not heat-treated). The apparent

[1] *Cf.* March and Smith, "Flexural Rigidity of a Rectangular Strip of Sandwich Construction," Forest Products Laboratory Report No. 1505, Forest Products Laboratory, Madison, Wis., February 1944.

[2] *Cf.* "Deflection of Beams with Special Reference to Shear Deformations," Forest Products Laboratory Report No. 1309 (reprinted from National Advisory Committee for Aeronautics Report 180), Forest Products Laboratory, Madison, Wis., October 1941.

value of flexural stiffness for a span/depth ratio of 16 is found from Fig. 13·10*a* to be 56 per cent of the true value, the coefficient e being found from the slope of the line to have a value of 199. For this sandwich $d_s = 0.037$ in., $h = 0.702$ in. If the theory is developed for a homogeneous beam, the coefficient e of Eq. (16) is found to have a value of 2.5. This would give a discrepancy between the true and apparent values of the stiffness of only 1 per cent for a span/depth ratio of 16.

Figure 13·10*b* gives the results of similar tests on a sandwich panel made by the single-stage wet lay-up technique (see Sec. 13·6). The faces consisted of four plies of heat-treated ECC-11-128 Fiberglas fabric. Two specimens were loaded to destruction at each span; in one of each pair of specimens the face of the sandwich molded in contact with the mandrel was in compression; in the other, this face was in tension. The skin was stripped off the beam after the test, and its thickness d_s measured. Because of the uncertainty in estimating d_s and large variations that may occur from point to point in the mechanical properties of commercial synthetic hard rubber foam, it is difficult to obtain a satisfactory result by this test procedure. For this sandwich the Young's modulus of the faces was found to be 3.09×10^6 lb/in.^{2} ($d_s = 0.030$ in., $h = 0.423$ in.; $e = 202$.)

The flexural stiffness is of interest in connection with radomes that have large nearly flat areas. A beam cut from a flat panel of the same construction should be tested in simple bending over a span comparable to the dimensions of the flat area of the radome. If it is found that the deflection due to shear is large, then it is known that the stiffness of the radome can be increased by increasing the shear modulus of the core. If the deflection due to shear in the simple bending test is small, the stiffness of the radome cannot be increased by increasing the shear modulus of the core.

Figure 13·11 shows a test jig for testing beams of sandwich construction in simple bending; autographic load-deflection curves are obtained by means of an electronic deflection gauge. For sandwiches with Fiberglas faces these curves are linear up to at least half the maximum load; hence δ/W can easily be found.

Flexural Strength in Simple Bending.—The flexural strength of a sandwich construction is also obtained most easily by means of the simple bending test. If W_{max} is the maximum load carried at the center of a beam of span l and breadth b, the flexural strength of the beam M_{max} in simple bending given by $M_{max} = W_{max}l/4b$ [*cf.* Eq. (4)], provided that the failure is attributable to longitudinal stresses, and not to shear. For the construction to be the most efficient, the flexural failure of the sandwich as a whole should result from such failure of the skin in compression (or tension) rather than from premature failure of the core. In other

words, the core must not be more brittle than the skin. Synthetic hard rubber foam like GR-N has been found to work well with laminates of Fiberglas fabric. With sandwiches having faces of laminated Fiberglas or laminated Fiber-A fabric, failure of the sandwich in simple bending usually takes place in the face under compression, as has been stated.

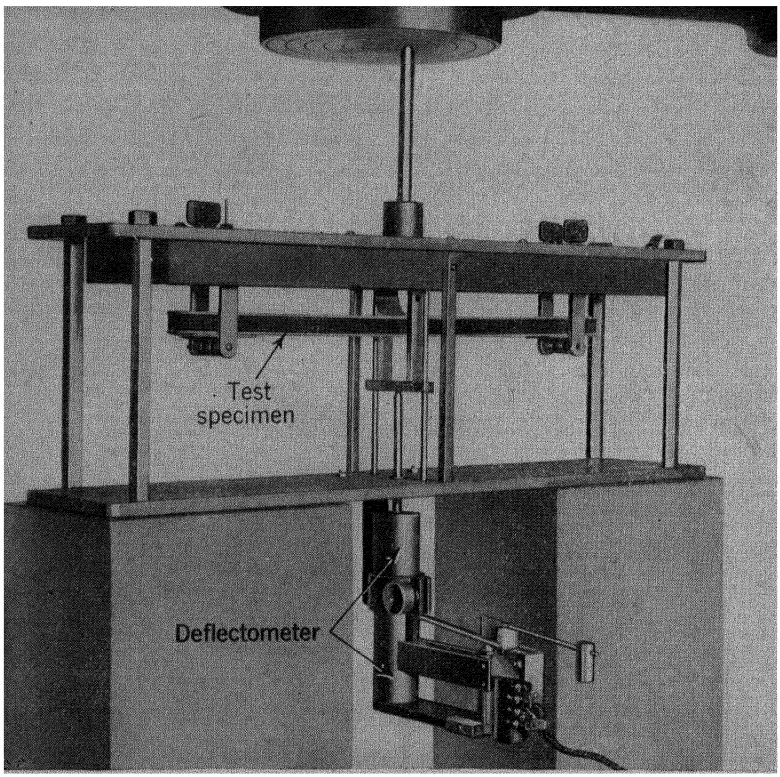

FIG. 13·11.—Test jig for beams of sandwich construction. Specimen arranged for test at 12-in. span.

This occurs if the span l exceeds a critical value that depends upon the sandwich construction. For spans greater than the critical value, M_{max} is found to be constant, and W_{max} varies inversely with l. Since M_{max} equals $f_s d_s d_c$, taking the contribution of the core to be negligible as before, $W_{max} = 4f_s b d_s d_c / l$, f_s being the critical compressive stress in the skin equivalent to f_b of Sec. 13·7. At the critical value of the span breakdown takes place either by failure of the skin under compression or by shearing of the core or core-skin bond. For smaller values, failure occurs by shearing only; the value of W_{max} per unit width of the beam is

found to be approximately independent of the span. This constant value of W_{max}/b is a measure of the shear strength of the beam of sandwich construction. It equals $2\tau_s d_s + \tau_{c(max)} d_c$ if $\tau_{c(max)}$ is the value of the shearing stress in the core at which it fails and τ_s is the average shear stress in the skin. An expression for the critical span can be obtained by equating the expressions for the two critical values of W_{max}/b at the critical length. It is

$$l_{crit} = \frac{4d_s d_c f_s}{2\tau_s d_s + \tau_{c(max)} d_c}. \tag{18}$$

So long as the skins contribute only a small amount to the shear strength, the first term of the denominator of Eq. (18) is small compared with the second, and larger values of l_{crit} are found with stronger and thicker skins or a weaker core, as in radomes with modified half-wavelength skins and low-density cores. If the critical length for a given construction is found to be large compared with the dimensions of a proposed radome, it is to be expected that any failure of the radome will result from shear failure in the core or core-skin bond rather than from failure of the skin under compression. The design must, of course, be one that does not produce other weakening local concentrations of stress.

The simple bending test thus gives information concerning the relative roles played by skins and core in determining both the strength and stiffness of sandwich construction. It generally indicates whether improvement in the strength of any particular radome is to be effected by improvement in the strength of the skin or of the core. It also tells whether stiffness can be improved by increase of the stiffness of the skin or of the core. Furthermore, it can be used to obtain information as to the relative value of different techniques of fabrication. When rubber-base cement or lightly spread resorcinol-formaldehyde cement is used, failure takes place in the core-skin bond when the span is less than the critical value. With a sandwich panel made by the single-stage wet lay-up technique or bonded with heavily spread resorcinol-formaldehyde cement, the failure takes place in the core. In the latter case the bond appears to be stronger than the core; this heavy glue line of resorcinol-formaldehyde cement is unacceptable, however, because it is found to absorb a large amount of energy (Sec. 10·7).

Simple bending tests on beams cut from panels of sandwich construction made by the single-stage wet lay-up technique indicate that both skins are of about equal strength in a properly made panel. If the core is properly sized, the strength of the skin is as good as in a sandwich in which the skins are cured separately from the core. Such tests have also indicated that mandrels of laminated paper $\frac{1}{2}$ in. thick and of laminated Fiberglas $\frac{1}{8}$ in. thick are as satisfactory as sheet steel; these two con-

structions can therefore be used to make relatively cheap and quickly fabricated molds (*cf.* Secs. 13·4, 13·6). This type of test has indicated, for a particular sandwich specification, that the flexural strength for any given combination of skin resin and core material can vary over a wide range for a fully cured sandwich. It is not very surprising then that the flexural strength of sandwiches fabricated by the wet lay-up technique depends largely upon the details of the technique. The most satisfactory laminating resin for this type of construction is, therefore, not the one from which the panel of highest strength can be made under laboratory

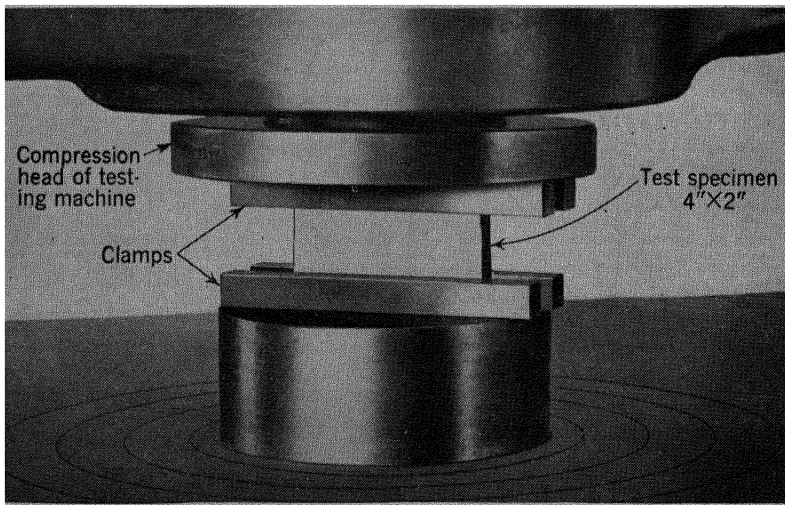

FIG. 13·12.—Edgewise compression test.

conditions but one that gives consistently good results under practical conditions.

Edgewise Compression Test.—In addition to the simple bending test, there are two further tests that are useful for the rapid evaluation of sandwich constructions having low-density cores.[1] These are the edgewise compression test (for the rapid evaluation of the skin and the bond between the skins and the core) and the normal tension test (for evaluation of the skin-core bond and the core). The edgewise compression test is carried out as shown in Fig. 13·12. The load is applied parallel to the faces of a plane rectangular section of a sandwich panel, the height of the specimen being chosen so that buckling will not occur. If W_{max} is the maximum compressive load and b is the dimension of the face at right angles to the direction of the load, the edgewise compressive

[1] Proposed by Aircraft Materials Laboratory, ATSC, Wright Field, Dayton, Ohio; see, for example, AAF Specification R-12046.

strength of the panel may be expressed as W_{max}/b. In most sandwiches practical for radomes the maximum load on a specimen in this test is reached when the faces fail in compression, the core still carrying only a small part of the total load. Hence, if d_s is the average skin thickness, the compressive strength f_s of the skins is given by the expression

$$f_s \approx \frac{W_{max}}{2bd_s}. \tag{19}$$

It should be noted that when the skin-core bond is poor, the sandwich fails through separation of the skins from the core and not through compression failure of the skins. Failure is likely to occur when brittle cements such as resorcinol-formaldehyde are used. With inferior bonds produced by rubber-base cements, such skin separation is likely to occur, causing extremely variable and unreliable values of W_{max}/b.

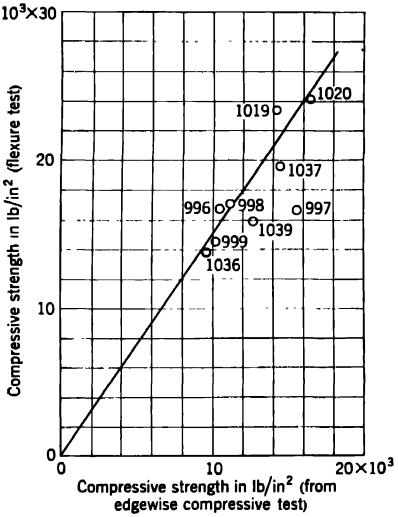

FIG. 13·13.—Compressive strength of sandwich faces made of laminated Fiberglas.

If the bond between the skin and the core is satisfactory, the edgewise compression test may be used for the rapid evaluation of techniques of fabrication; for example, f_s as determined by this test on sandwiches with faces of heat-treated Fiberglas fabric is usually found to be greater than for similar sandwiches made with fabric that has not been heat-treated. This test can be used to evaluate laminating resins and the efficiency of any sizing method in the wet lay-up technique. The edgewise compressive strength of properly cured heat-treated Fiberglas laminate faces of a sandwich made in this way ranges from about 10,000 to about 20,000 lb/in.^{2} for ECC-11-128 Fiberglas fabric.

For any given sandwich specification, the edgewise compressive strength of a sandwich panel having Fiberglas faces and a low-density core would be expected to be a measure of the flexural strength obtained in a simple bending test. Figure 13·13 shows the relationship obtained between f_s obtained from the edgewise compressive strength and f_s obtained from the corresponding flexural strength in tests on a series of sandwich panels made by the single-stage wet lay-up technique. For these panels, the skins were approximately 0.030 in. thick (four plies of

ECC-11-128 heat-treated Fiberglas fabric), and the over-all panel thickness was approximately 0.445 in. The core material was GR-N synthetic hard rubber foam of approximately 12 lb/ft^3 density. There is only a fair correlation, the value of f_s computed from the bending test being about one and a half times as great as the value computed from the edgewise compression test. Since the correlation is not good, the edgewise compression test gives only a rough indication of the flexural strength of a panel.

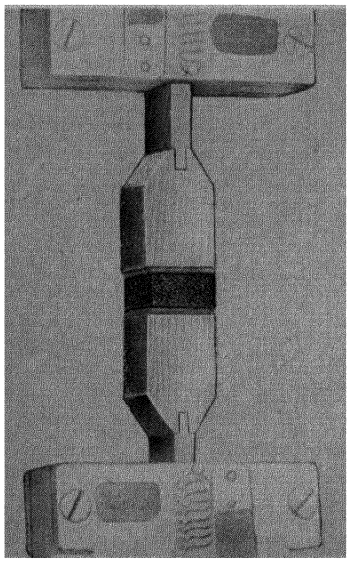

FIG. 13·14.—Normal tension test.

Normal Tension Test.—An arrangement for carrying out a normal tension test is shown in Fig. 13·14. If the strength of the bond is adequate and the core material is not defective, tension failure takes place in the core at a stress corresponding to the tensile strength of the core material. This test is a more critical test of the bond than the previous one.

Representative Sandwiches.—It is very difficult to make radomes of adequate strength if perpendicularly polarized 3-cm radiation is to be incident through a wide range of angles of incidence. In order to obtain the best transmission characteristics, it is necessary to use a first-order spacing and to make the skins as thin as possible. A construction that gives good transmission characteristics at perpendicular polarization for a wavelength of 3.2 cm over a range of angles of incidence from 0° to 70° has skins of four plies of heat-treated ECC-11-128 Fiberglas fabric and a core of GR-N synthetic hard rubber foam having a density of about 10 to 12 lb/ft^3, the dielectric constant of the core being about $1.4\epsilon_0$. When the sandwich is made by the wet lay-up technique, the actual skin thickness d_s is about 0.030 in.

If a resin of low dielectric constant ($3.7\ \epsilon_0$) is used in the skin the over-all thickness h should be about 0.445 in. For resins with higher dielectric constant ($4.0\ \epsilon_0$ to $4.2\ \epsilon_0$) the thickness h should be about 0.420 in. (*cf.* Sec. 11·12). For a properly cured sandwich built by the wet lay-up method to these specifications, the flexural strength M_{max} ranges from 200 to 350 lb-in./in., averaging about 250 lb-in./in. The flexural stiffness EI ranges from 6000 to 8500 lb-in.^{2}/in. The computed values of Young's modulus for the skin range from about 2.5×10^6 to about 3.2×10^6

lb/in.^{2} The correction coefficient for shear e [Eq. (14)] is about 150. The above data refer to a direction parallel either to the warp or to the filling of the Fiberglas fabric. The flexural strength and stiffness of such a sandwich at an angle of 45° to the direction of the warp and filling are approximately two-thirds of the values measured for the warp and the filling directions.

It has been pointed out that the compressive strength of a laminated Fiberglas face of a sandwich is less than its tensile strength. If the bending moments in a radome are such that one particular skin is always in compression, a radome of greater strength can be designed if the face under compression is made thicker than the one under tension. If the sandwich previously discussed were modified to have five layers of fabric in one face and three layers in the other, with a slight increase of the total thickness, it would then have a flexural strength much greater than that of the symmetrical sandwich. As we have seen (Sec. 11·12), this asymmetrical sandwich would have electrical transmission characteristics similar to those of the corresponding symmetrical sandwich.

In Sec. 13·6 it was mentioned that with the wet lay-up fabrication technique, gridded hexagonal Fiberglas material (Plaskon "honeycomb") may be used for the core instead of synthetic hard rubber foam. Panels fabricated with honeycomb core material and having specifications otherwise similar to those given for the sandwich with a core of hard rubber foam possess very similar electrical and mechanical properties (*cf.* Sec. 11·12). Sandwich radomes made with honeycomb cores may prove to absorb less water vapor than do similar radomes made with the more hygroscopic GR-N foams.

Preliminary data on sandwich panels incorporating Fiber-A fabric and GR-N foam indicated that these panels are mechanically comparable to Fiberglas panels with the same electrical properties. For example, panels having skins of Fiber-A 0.039 in. thick and an over-all thickness of about 0.50 in. were found to give values of the electrical transmission as a function of angle of incidence similar to those of the symmetrical Fiberglas sandwich panels discussed above (Sec. 11·12). The values for flexural strength and stiffness of such panels are about one-half of those for Fiberglas sandwich panels.

A comparison can now be made of the flexural strengths and stiffnesses and weights between a Fiberglas sandwich and a modified half-wavelength panel of acrylic plastic of equivalent electrical properties. If for the acrylic plastic a thickness of $0.36\lambda_0$ is chosen (see Fig. 11·5), the flexural strength and stiffness for a wavelength of 3.2 cm are equal to 480 lb-in./in. and 3020 lb-in.^{2}/in., respectively.[1] Thus, the strength of the acrylic plastic construction is somewhat greater than that of the good Fiberglas

[1] Taking f_b = 13,900 lb/in.^{2} and $E = 0.39 \times 10^6$ lb/in.^{2} (Table 13·1).

sandwich discussed previously. The stiffness is only about one-half that of the sandwich, while the electrical transmission characteristics are slightly better, provided that the tolerances are closely kept. The weight of the modified half-wavelength acrylic radome is, however, 2.8 lb/ft², compared with 1.1 lb/ft² for the sandwich radome. It should be noted that if the strength requirements will allow the thickness of the skins of the sandwich to be reduced below 0.030 in., the weight of the sandwich will be reduced and the electrical properties improved.

It has been pointed out that for the 1-cm band it is difficult to design a radome having adequate strength and stiffness if the radiation is incident over a wide range of angles at perpendicular polarization. One method of obtaining moderate strength and stiffness is to use a sandwich having a core of material such as Polyflex or polyfiber plastic and thin faces of Fiberglas fabric. In Table 13·9 some mechanical properties of such a panel are given; the core is of molded polystyrene fiber of specific gravity of about 1.0, and the faces are each a single ply of ECC-11-128 Fiberglas fabric. For this type of sandwich, failure in the simple bending

TABLE 13·9.—FLEXURAL PROPERTIES OF A SANDWICH PANEL WITH POLYFIBRE CORE

Core: Dow Q-107 Polyfibre, specific gravity 0.9–1.0, 0.160 in. thick.

Faces: Each face consists of a single layer of heat-treated ECC-11-128 Fiberglas fabric cemented with polystyrene lacquer.

Over-all panel thickness, 0.175 in.

Orientation of flexure test specimen relative to fiber direction	M_{max}, lb-in./in.		EI, lb-in.²/in.	
	With faces	Faces removed	With faces	Faces removed
Parallel to fiber direction	81.9	34.4	306	115
Perpendicular to fiber direction	65.8	24.3	282	117
Average	73.9	29.4	294	116

test occurs in the fabric face that is in tension. It is seen that the faces make an appreciable contribution to the flexural strength of the panel and that the effect of orientation of the fibers in the core is relatively slight.

If the radiation falling at a high angle of incidence on a radome is polarized parallel to the plane of polarization, a modified second-order spacing (Sec. 11·8) and a low-density core may be used. A typical sandwich specification for the 1-cm band has skins consisting of three plies of heat-treated ECC-11-112 Fiberglas fabric, 0.009 in. thick, and a core of GR-N foam of 20 lb/ft³ density. From tests on such a sandwich panel 0.355 in thick, a flexural strength M_{max} of 120 lb-in./in. and a flexural stiffness EI equal to 1900 lb-in.²/in. were obtained.

13·11. Mechanical Properties of Core Material.—In general, the low-density core in a sandwich arrangement suitable for radome construction usually contributes little to the flexural strength and stiffness of the radome. Failure of the radome, however, may take place through shear or tension failure in the core, and an appreciable part of the deflection of the radome may be due to shear strain in the core. For these reasons the mechanical properties of core materials deserve attention. Figure 13·15 gives the properties of a typical fine-cell GR-N hard synthetic

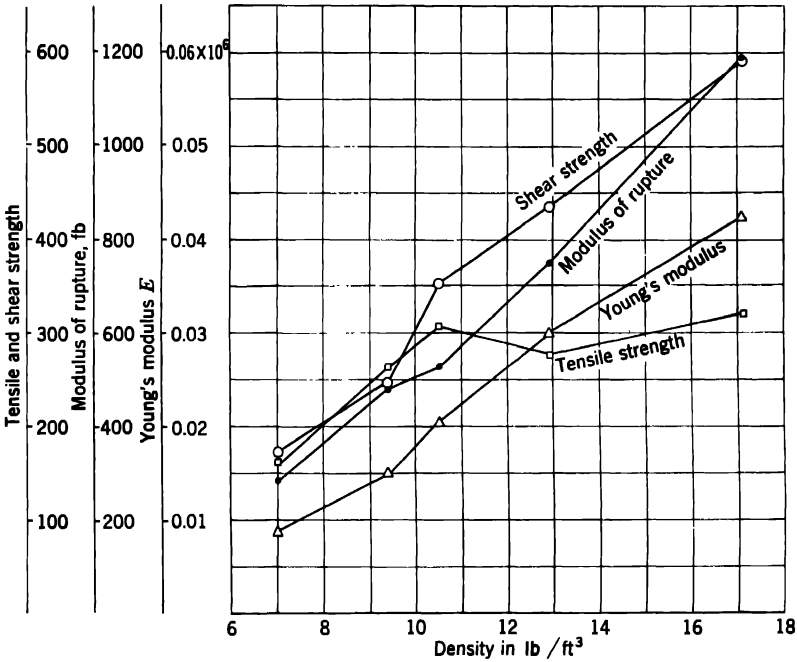

FIG. 13·15.—Mechanical properties of GR-N foam material for cores. (All ordinates in lb/in.²)

rubber foam[1] as a function of density. The shear strength, modulus of rupture, and Young's modulus of this particular material vary roughly linearly with density, and the tensile strength has a constant value at densities greater than about 10 lb/ft³. The mechanical properties of such materials depend largely upon the techniques of formulation, fabrication, and cure. Equivalent coarse-pored boards[2] have similar mechanical properties. Preliminary tests on polystyrene foam having a density of 6 lb/ft³ showed that this material is mechanically equivalent to GR-N

[1] Sponge Rubber Products Company; 5003R formulation.

[2] Sponge Rubber Products Company, 5003B formulation.

foam of the same density. Tests on polyester-styrene resin foam of about 20 lb/ft^3 density and on an early phenolic foam of 10 lb/ft^3 density showed that these materials were equivalent in strength and stiffness to GR-N foam of about 7 lb/ft^3 density.

ELECTRICAL PROPERTIES OF RADOME MATERIALS

13·12. General Remarks.—In order to make best use of the materials available for radome construction, it is necessary to know the electrical properties of these materials. For homogeneous materials (acrylic plastic) or ones in which the inhomogeneities are smaller than the wavelength (plastic foams), the electrical properties can be represented by a complex dielectric constant (Secs. 10·3 and 12·2). The complex dielectric constant ϵ equals $\epsilon'(1 - j \tan \delta)$, ϵ' being its real part and tan δ being the loss tangent. For radome materials, tan δ is very nearly equal to the power factor.

The electrical properties of a dielectric at microwave frequencies are generally obtained by observing the interaction between the dielectric and an electromagnetic field in free space, in a coaxial line or a rectangular waveguide, or in a resonant cavity. The electrical properties of high polymers at microwave frequencies depend, of course, on the atomic and molecular structure.[1]

In the subsequent discussion, consideration will be limited to the dielectric constants and loss tangents of materials of special interest for radomes. These are, in general, low-loss materials having dielectric constants that change only slowly in the wavelength region from 10 to 1 cm. Typical radome materials of fixed composition and physical structure are polystyrene, polymethyl methacrylate, and poly 2,5 dichlorostyrene. Their dielectric constants are nearly independent of frequency in the microwave region and are independent of the particular manufacturing methods. The loss tangents of extremely low-loss materials do depend upon the manufacturing process, but this is of no consequence in radome work. The dielectric constants of copolymer resins are variable, but this is to be expected, since they probably do not have compositions that are definite, either chemically or physically. One component is usually volatile, and the manner of the cross-linking is likely to depend upon cure and other conditions.

Most of the dielectrics used for radomes are actually mixtures. For example, polyfiber plastics consist of mixtures of polystyrene and air;

[1] See A. Von Hippel and R. G. Breckenridge, "The Interaction between Electromagnetic Fields and Dielectric Materials," NDRC 14-122, Laboratory for Insulation Research, M.I.T., January 1943; A von Hippel, L. G. Wesson, and S. L. Whitcher, "The Polystyrene Plastics as High-frequency Dielectrics," NDRC 14-276, Laboratory for Insulation Research, M.I.T., May 1944; Laboratory for Insulation Research, M.I.T., "Tables of Dielectric Materials, Vol. II," NDRC 14-425, June 1945.

low-density GR-N foam for sandwich radomes is a mixture of GR-N synthetic hard rubber and air; cyclized rubber is used in the expanded state. Mixtures of titanium dioxide and polystyrene form materials of high dielectric constant that may have some use in radome construction. The dielectric constants of such mixtures are discussed in Sec. 13·13. Fiberglas laminates can be regarded as mixtures of Owens-Corning "E" glass, a laminating resin, and air.

In Table 13·10 are presented average values (obtained from various sources) of the dielectric constant and loss tangent of single-phase dielectrics at microwave frequencies.[1]

TABLE 13·10.—DIELECTRIC CONSTANTS AND LOSS TANGENTS OF RADOME MATERIALS

Material	Specific dielectric constant, $\frac{\epsilon'}{\epsilon_0}$	tan δ (approx.)
Polystyrene	2.56	.....
Polymethyl methacrylate	2.66	0.01
Poly 2, 5 dichlorostyrene	2.57	0.0003
Bakelite BRS 16631, cast	2.69	0 019
Selectron 5003, cast	2 87	0.010
Plaskon 911, cast	3.06	0.020
Owens-Corning "E" glass	6.24	0.007
Penacolite G1131	3.86	0.10–0.15

13·13. Dielectric Constants of Polyfiber and Foam Plastics.—The ideal foam is an intimate mixture of air and a plastic of definite chemical and electrical properties. It is to be expected that variations would occur in the dielectric constant of foamed materials such as hard GR-N foam, even for a given density, because of possible variations in mixing the batches of stock and in curing the boards. Also, polyfiber plastic may contain an appreciable (and variable) amount of solvent, which has some effect on the dielectric constant.

If the dielectric constant of the unexpanded plastic is known, the dielectric constant of the expanded dielectric can be computed by assuming, for example, that the air spaces are in the form of regularly distributed cubes. Two empirical formulas, Eqs. (21) and (22), adequately represent the variation of dielectric constant with density.[2] If a dielec-

[1] For data on the electrical properties of radome materials at microwave frequencies, see E. M. Everhart and T. J. Suen, "Dielectric Constants and Loss Tangents of Radome Materials," RL Report No. 483-25, Jan. 11, 1946; also E. M. Everhart, RL Report No. 483-5, July 14, 1944; Laboratory for Insulation Research, M.I.T., "Tables of Dielectric Materials," NDRC 14-237, February 1944; also "Tables of Dielectric Materials, Vol. II," NDRC 14-425, June 1945.

[2] RL Reports Nos. 483-17 and 483-25.

tric consists of an intimate mixture of two components, the volume fractions of each component being a and b, respectively, and the real part of the dielectric constant of each component being ϵ_a' and ϵ_b', respectively,

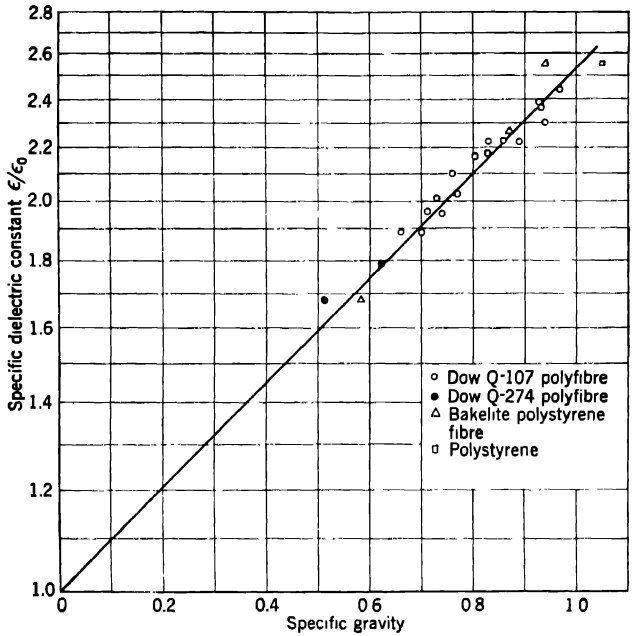

FIG. 13·16.—Dielectric constants of molded polystyrene fiber plastics.

the dielectric constant ϵ' of the mixture can be represented by the empirical expression[1]

$$\frac{\epsilon'}{\epsilon_0} = \left(\frac{\epsilon_a'}{\epsilon_0}\right)^a \cdot \left(\frac{\epsilon_b'}{\epsilon_0}\right)^b. \tag{20}$$

If the second component is air, a is equal to the ratio of the specific gravity ρ of the expanded plastic to the specific gravity ρ_0 of the unexpanded plastic, and Eq. (20) becomes

$$\log_{10}\left(\frac{\epsilon'}{\epsilon_0}\right) = \left(\frac{\rho}{\rho_0}\right) \log_{10}\left(\frac{\epsilon_a'}{\epsilon_0}\right). \tag{21}$$

[1] An equation of this form given by Lichtenecker and Rother, *Physik. Z.*, **32**, 255 (1931), is discussed by L. J. Berberich and M. E. Bell, *J. Applied Phys.*, **11**, 681 (1940). The latter authors give data on mixtures of polystyrene and titanium dioxide of Büchner (*Wiss. Veröff. a. d. Siemens Werken*, **18**, 204 (1939). These data are similar to ones reported below on such mixtures (see Fig. 13·18). The work discussed here was done without knowledge of the existence of these earlier papers.

Thus, the logarithm of the dielectric constant is proportional to the density.

Measurements on molded polystyrene fiber plastic, expanded Marbon S plastic, and a GR-N formulation of sandwich core material[1] are in

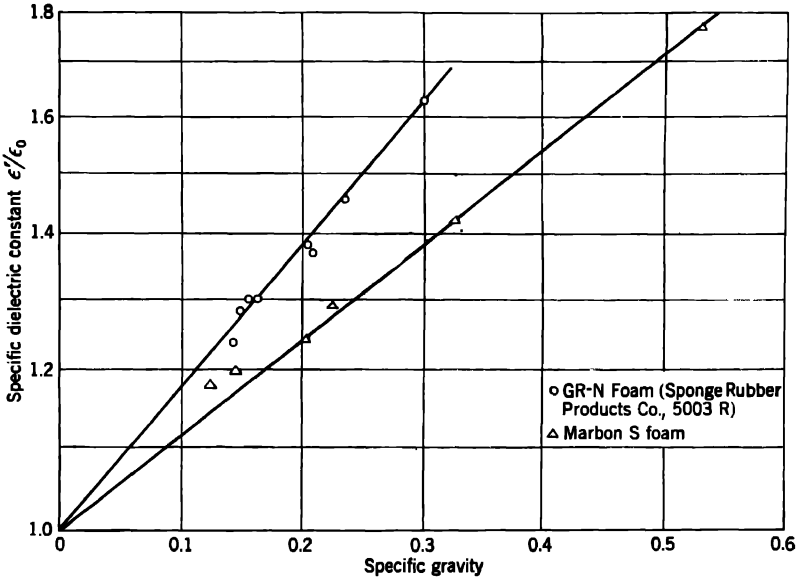

FIG. 13·17.—Dielectric constants of GR-N and Marbon S foams.

agreement with Eq. (21). In Fig. 13·16 the dielectric constants of three types of molded polystyrene fiber plastic of various densities are plotted to a logarithmic scale against specific gravity. The observations fall

TABLE 13·11.—DIELECTRIC CONSTANTS OF REDUCED-DENSITY AND LOW-DENSITY MATERIALS

Material	Specific gravity range of investigation	$\frac{1}{\rho}\log_{10}\left(\frac{\epsilon'}{\epsilon_0}\right)$
Molded polystyrene fiber (Polyfibre)	0.51–0.97	0.40
Expanded Marbon S	0.12–0.53	0.47
GR-N hard foam (Sponge Rubber Products Co., 5003R formulation)	0.14–0.30	0.71

near a straight line on this plot. Figure 13·17 shows similar results for the variation of dielectric constant with density for expanded hard

[1] Measurements made by the Laboratory for Insulation Research, M.I.T. For the same samples of GR-N core material the loss tangent was found to be nearly equal to the specific gravity multiplied by 0.03; see also Everhart and Suen, *op. cit.*

GR-N synthetic rubber foam and of expanded Marbon S. In Table 13·11 the values are given of the ratio of the logarithm of the specific dielectric constant (ϵ'/ϵ_0) to specific gravity ρ obtained from Figs. 13·16 and 13·17, as well as the ranges of specific gravity covered in the investigation. A second empirical expression[1] that seems to be in excellent agreement with available data is

$$\frac{\sqrt{\frac{\epsilon'}{\epsilon_0}} - 1}{\sqrt{\frac{\epsilon'_a}{\epsilon_0}} - 1} = \frac{\rho}{\rho_0}. \tag{22}$$

Thus, $\sqrt{(\epsilon'/\epsilon_0)} - 1$ is assumed to be proportional to density. It is seen that Eqs. (21) and (22) require the knowledge of the dielectric constant and density of only one sample for computation of the constant of proportionality.

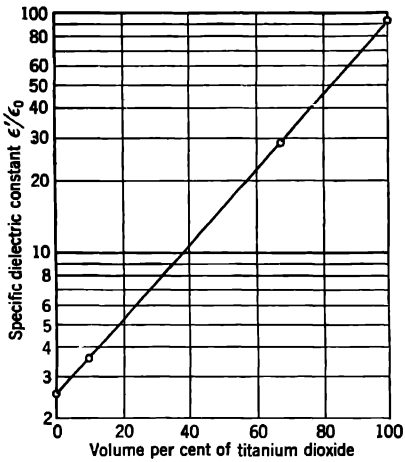

FIG. 13·18.—Dielectric constants of mixtures of polystyrene and titanium dioxide.

The effect of various ingredients in the rubber mix on the dielectric constant of GR-N foam materials has been investigated. A series of core materials containing respectively 0, 15, and 30 parts carbon black per 100 parts of elastomer were studied. These samples all had slightly different densities; the dielectric constant was accordingly adjusted to an arbitrarily chosen standard density of 7.3 lb/ft^3 by means of Eq. (21); thus, the effect of variation of carbon black on the particular formulation was determined. The results are given in Table 13·12. It is seen that increase in carbon black content results in a marked increase in dielectric constant. It is believed that an increase in the amount of carbon black in a formula results also in an increase in the strength and stiffness of a foam of any given density. It would seem that a material of higher carbon black content and lower density would be preferable for given strength and dielectric constant because of the resulting slight saving in weight.

Materials of high dielectric constant can be made by mixing titanium dioxide with polystyrene. Equation (20) can be used to represent the dielectric constants of such mixtures. In Fig. 13·18 the dielectric con-

[1] J. B. Birks, "Expanded Dielectrics," TRE Report No. T-1812, February 1945.

stants of various mixtures of polystyrene and titanium dioxide[1] are plotted to a logarithmic scale. As can be seen, there is a linear relationship between the logarithm of the specific dielectric constant and the volume percentage of either constituent.

TABLE 13·12.—EFFECT OF VARIATION OF AMOUNT OF CARBON BLACK ON THE DIELECTRIC CONSTANT OF GR-N SYNTHETIC HARD RUBBER FOAM (REDUCED TO 7.3 LB/FT³ DENSITY)

Parts carbon black per 100 parts elastomer	ϵ'/ϵ_0
0	1.168
15	1 275
30	1 311

13·14. Electrical Properties of Laminates. *Dielectric Constants of Fiberglas Laminates.*—The dielectric constant of a laminate made of woven Fiberglas fabric and a given low-pressure resin can vary between wide limits. Wide variations in density and resin content also occur; the variation in dielectric constant is therefore attributable, in part, to the variation of the volume percentages of glass, resin, and air in the laminate. For example, with one particular resin (Bakelite BRS 16631), the specific dielectric constants of a miscellaneous group of laminates obtained from various sources varied from 3.45 to 4.36, the specific gravities varied from 1.43 to 1.75, and the resin contents ranged from 24.2 to 47 per cent by weight. In Fig. 13·19, the specific dielectric constants of these laminates are plotted against specific gravity. There is seen to be a fairly good correlation between these properties. In Fig. 13·19 are also indicated the resin contents (in percentage by weight) for the various laminates. There does not appear to be much correlation between resin content and dielectric constant. From Fig. 13·19, it appears that the specific dielectric constant of a Fiberglas laminate with this resin can be held within the limits 3.7 ± 0.1 provided that the specific gravity lies within the limits 1.50 ± 0.05.

Dielectric Constants of Fiber-A Laminates.—The amount of air incorporated in a Fiberglas laminate appears to be variable, possibly because the glass fibers are not wetted by the resin. Furthermore, since the dielectric constant of the glass is very different from that of the resin, variation in the ratio of glass to resin, even in the absence of voids, must result in an appreciable variation in dielectric constant. Fiber-A, on the other hand, is evidently wetted by low-pressure laminating resins. Laminates of Fiber-A fabric have dielectric constants that are not much greater than those of the resins involved. Variation in resin content should therefore not result in any marked modification of the dielectric constant of the laminate.

[1] Everhart and Suen, *op. cit.*

Measurements in the 3- and the 1-cm band have been made on the dielectric constants of Fiber-A laminates. These incorporated knitted, fine-woven and coarse-woven fabrics. The resins included "Selectron" 5003, Bakelite BRS 16631, and poly 2,5 dichlorostyrene. The specific dielectric constant of all fell within the range 2.90 to 3.10.

Loss Tangents of Laminates.—The loss tangent of a laminate is important if it is to be used in a radome of approximately half-wavelength or

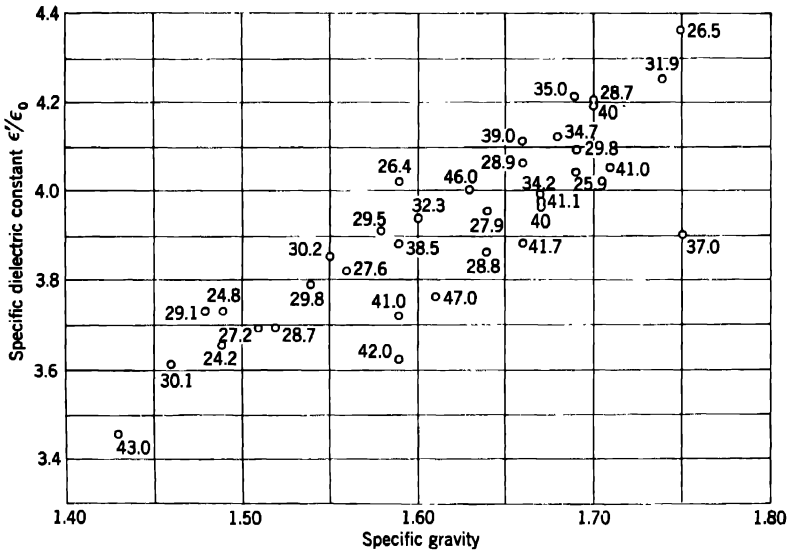

FIG. 13·19.—Dielectric constants of Fiberglas laminates made with Bakelite BRS 16631 resin. The number by each point is the per cent resin content by weight.

greater thickness. The absorption is given approximately by $\pi \tan \delta$ for half-wavelength thickness at normal incidence [Eq. (10·18)] but may rise to several times this value in a streamlined radome where the radiation is incident at a large angle of incidence and is polarized perpendicular to the plane of incidence (Secs. 11·5 and 11·11).

The following table represents the loss tangents to be expected with Fiberglas and Fiber-A laminates.

TABLE 13·13.—LOSS TANGENTS OF LAMINATES

Fabric	Resin	tan δ (approx.)
Fiberglas	Polyester-styrene	0.015
Fiber-A	Polyester-styrene	0.010
Fiber-A	Dichlorostyrene	0.007

13·15. Evaluation of Materials, Normal Incidence.—It will be recalled that there are three basic methods for the design of a normal-incidence radome with a homogeneous wall construction. One of these methods uses an expanded dielectric with a sufficiently low dielectric constant and loss tangent so that a thick wall can be used to satisfy mechanical requirements. Materials having a higher dielectric constant can be used only in walls that are thin compared with the wavelength or in walls that are of the order of half-wavelength thickness if the reflection is to be limited to a very small part of the incident power. In general, materials with higher dielectric constants are stronger and stiffer mechanically; the increase in the dielectric constant, however, is associated with a decrease in the allowable thickness for both walls that are thin and those which are half-wavelength. It is now possible to evaluate materials for the thin and half-wavelength normal-incidence radomes on the basis of their electrical and mechanical properties. If the reflection from the thin-walled radome is small, the expression for the amplitude-reflection coefficient at normal incidence reduces to

$$|R| \approx \frac{\left(\frac{\epsilon'}{\epsilon_0} - 1\right)\pi d}{\lambda_0}. \tag{23}$$

[See Eq. (10·10).] The amplitude-reflection coefficient for a thin low-reflection panel of a given material is proportional to the thickness,[1] and the permissible thickness is inversely proportional to $(\epsilon'/\epsilon_0) - 1$ for panels of given reflection coefficient. The flexural strength of a panel is proportional to $f_b d^2$ [Eq. (3)], while its flexural stiffness is proportional to Ed^3 [Eq. (1)]. It is thus possible to obtain ratings that measure the strength and stiffness of a thin panel having the thickness required for it to have a given reflection coefficient at normal incidence. They are

$$\text{Strength rating} = \frac{f_b}{\left(\frac{\epsilon'}{\epsilon_0} - 1\right)^2},$$

$$\text{Stiffness rating} = \frac{E}{\left(\frac{\epsilon'}{\epsilon_0} - 1\right)^3}.$$

These are only approximate in the region where Eq. (23) is not valid. In radomes of half-wavelength thickness [Eq. (10·4)] the thickness of the wall at a given free-space wavelength is inversely proportional to $\sqrt{\epsilon'/\epsilon_0}$. Accordingly, the following ratings are obtained for a half-wavelength thickness.

[1] This is true in general in the region in Fig. 10·8 where the curves are linear.

$$\text{Strength rating} = \frac{f_b}{\left(\frac{\epsilon'}{\epsilon_0}\right)},$$

$$\text{Stiffness rating} = \frac{E}{\left(\frac{\epsilon'}{\epsilon_0}\right)^{3/2}}.$$

These ratings may now be used to evaluate molded Dow Q-107 Polyfibre plastic as a function of density. The values of E and f_b from Fig. 13·7 have been used; the dielectric constants are obtained from Table 13·11. At *a* in Fig. 13·20 are plotted stiffness ratings for two types of Polyfibre for thin-walled radomes, while at *b* are plotted strength ratings. The corresponding ratings for half-wavelength radomes are plotted at *c* and *d*.

Making use of the information previously given on the mechanical and electrical properties of various other radome materials, it is also possible to derive the strength and stiffness ratings for each material in the two types of normal-incidence radome under discussion. These ratings are given in Table 13·14.

By examining Table 13·14 and Fig. 13·20 it can be seen that the strength ratings for the thin-wall radomes range from 3.0×10^3 to 7.1×10^3 while the stiffness ratings range from 0.07×10^6 to 0.265×10^6.

TABLE 13·14.—STRENGTH AND STIFFNESS RATINGS FOR HOMOGENEOUS-WALL NORMAL-INCIDENCE RADOMES

Material	Refer to	Thin-wall radome		Half-wavelength radome	
		Strength rating	Stiffness rating	Strength rating	Stiffness rating
Polymethyl methacrylate.	Table 13·1 Table 13·10	5.8×10^3	0.08×10^6	6.0×10^3	0.09×10^6
Polyflex.....	Table 13·1 Table 13·10	5.5	0.10	5.2	0.09
Dow Q-274 Polyfibre.	Table 13·2 Table 13·11	6.1	0.20	2.0	0.04
Bakelite polystyrene fiber.	Table 13·2 Table 13·11	3.0	0.18	0.7	0.02
Fiberglas laminate*	.....	3.4	0.09	6.8	0.24
Fiber-A laminate..	Table 13·8 Sec. 13·14	3.8	0.07	5.0	0.11
Fiberglas leno Viscose rayon marquisette	Table 13·7	5.8 7.1	0.23 0.23	.....	.....

* Assuming average values $f_b = 25{,}000$ lb/in.^{2}, $E = 1.7 \times 10^6$ lb/in.^{2}, $\frac{\epsilon'}{\epsilon_0} = 3.7$.

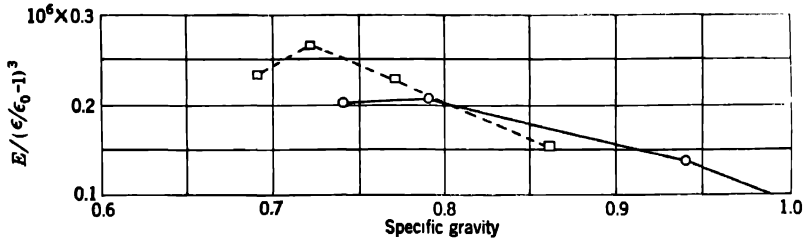

(*a*) Stiffness rating for thin-walled radomes.

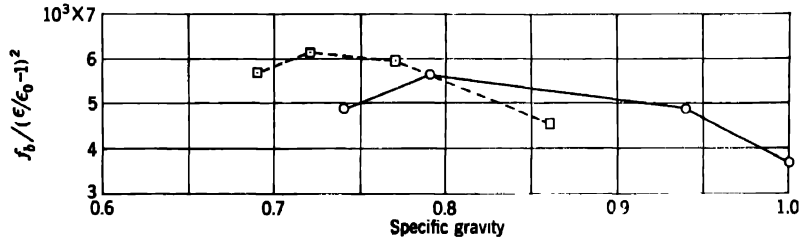

(*b*) Strength rating for thin-walled radomes

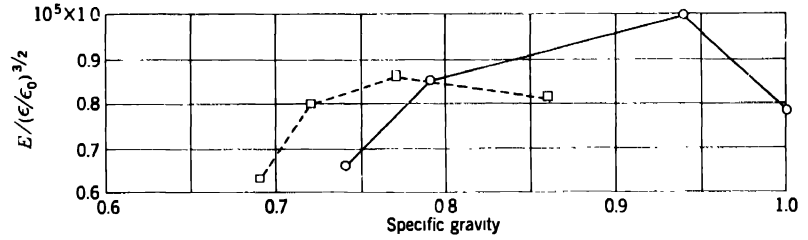

(*c*) Stiffness rating for half-wavelength radomes.

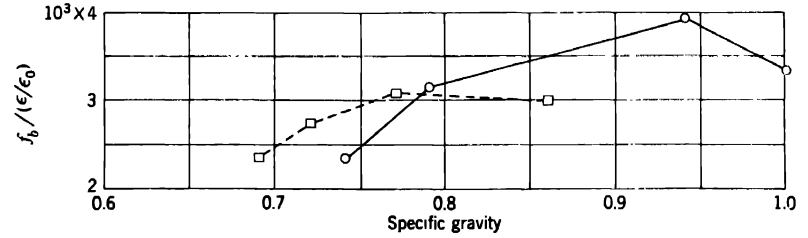

(*d*) Strength rating for half-wavelength radomes.

FIG. 13·20.—Strength and stiffness ratings for molded Dow Q-107 polystyrene fiber. Circled points refer to standard Q-107 Polyfibre; squared points refer to low-solvent Q-107 Polyfibre.

The reduced-density polystyrene plastics and reduced-density laminates are superior in stiffness to full-density thermoplastics and laminates. If the mechanical requirements are modest, as for a moderately large radome for the 10-cm band or in a small nonstreamlined housing for a linear array in the 3-cm band, a material having a low stiffness rating such as Fiberglas laminate or acrylic plastic can be used. Where the mechanical requirements become more severe, as for a moderately large radome for the 3-cm band, a material having a higher stiffness rating, such as Dow Q-107 Polyfibre, must be used. The latter material should be two to three times as stiff as a Fiberglas laminate for the same reflection behavior. The Fiberglas reduced-density laminate previously discussed (Sec. 13·9) is equivalent to Dow Q-107 Polyfibre plastic in strength and stiffness ratings. Laminated Polyflex is inferior to Polyfibre in stiffness; it has found its best use in thin sandwiches having inner and outer faces of a single layer of ECC-11-112 Fiberglas. The ratings for half-wavelength constructions suggest that the best material for such radomes is Fiberglas laminate. Laminated Fiber-A fabric is comparable to acrylic plastic and laminated Polyflex. Molded polystyrene fiber plastics are inferior to these materials for the half-wavelength construction; they are best used in sandwiches when the core is slightly less than the half-wavelength thickness and the faces are each a single layer of cemented-on Fiberglas fabric. These data for constructions of half-wavelength thickness for normal incidence radomes can be suitably modified for the modified half-wavelength walls of streamlined radomes.

CHAPTER 14

INSTALLATION AND TESTING OF RADOMES

By E. B. McMillan and F. J. Mehringer[1]

The previous chapters on radomes dealt with the theory of the electrical design and the mechanical and electrical properties of the materials. This chapter is an over-all consideration of problems that are encountered in actual installations.

The actual problem involves aerodynamic and structural aspects that are just as important as the electrical ones. The discussion of these aspects, however, is extremely brief, since numerous and excellent treatments[2] of the aerodynamic and structural problems are already available.

In order to prove the quality of a radome design and to have control of quantity production it was necessary to develop special tests, both structural and electrical. These testing procedures and examples of actual radome installations are discussed in detail.

14·1. Aerodynamic Considerations.—There is no simple or universal solution of the aerodynamic problems encountered in designing radomes. Each installation is individual and depends upon the airplane, its speed, the location of the radome, and the size and shape of the radome. Although a few simple generalities can be presented, only careful tests made in actual flight or on appropriate models in a wind tunnel can lead to a truly optimum aerodynamic design.

At velocities below 300 mph the effects of compressibility can be neglected and the problem can be considered as one of incompressible flow. For this type of flow, the expression for the drag of a body has the form

$$D_p = C_p \frac{\rho V^2}{2} A, \tag{1}$$

[1] E. B. McMillan is primarily responsible for the discussion of electrical problems. and F. J. Mehringer for the discussion of mechanical and aerodynamic problems. H. A. Perry supplied illustrative material on equipment for electrical testing.

[2] For information on aerodynamics see Prandtl and Tietjens, *Fundamentals of Hydro- and Aeromechanics* and *Applied Hydro- and Aeromechanics*, McGraw-Hill, New York, 1934; R. von Mises, *Theory of Flight*, McGraw-Hill, New York, 1945; E. P. Warner, *Airplane Design* (*Aerodynamics*, 1st ed., 1927; *Performance*, 2d ed., 1936), McGraw-Hill, New York; publications of National Advisory Committee for Aeronautics.

where D_p is the drag force in pounds; C_p, the drag coefficient;[1] ρ, the density of the fluid in slugs per cubic ft; V, the velocity of the air stream (velocity of airplane) in feet per second; and A, the reference area in square feet, usually frontal area. The drag coefficient is dependent upon the shape of the object and a dimensionless ratio called the Reynolds number.[2] The quantity $\rho V^2/2$ in Eq. (1) is known as the dynamic pressure and is represented by the symbol $q_0 = \rho V^2/2$. It is expressed either in pounds per square foot or pounds per square inch. Since the magnitude of the distribution of pressure on a given body varies in proportion with the dynamic pressure q_0, the pressure distribution is usually described by giving values of the dimensionless ratio q/q_0.

From Eq. (1) it can be seen that the drag force of a given shaped body will increase in proportion to the frontal area.[3] It is therefore desirable to reduce the projected area of a radome as much as possible and approach the ideal aerodynamic installation where the radome forms part of the skin of the plane.

The drag of a body can be reduced by fairing it or altering its shape in such a way that the turbulence of the air flowing over and around it is reduced to a minimum. For incompressible flow the best shape is moderately blunt in the front and tapers back gradually, the maximum section occurring at a distance of 0.2 to 0.3 of the length from the forward edge. Such a shaped radome is shown in Fig. 14·6. The drag of this radome mounted on a B-29 between the bomb bay doors is estimated at 3 mph, about two-thirds that for a cylindrical radome housing a reflector of the same size, like that of Fig. 9·3.

The drag of an appendage can be further reduced by taking advantage of the turbulent layer that is usually present in the air flow at the middle and aft sections of a plane. By putting a protuberance in this turbulent stream, further disturbance of unturbulent air is avoided, thus eliminating appreciable increase in the resultant drag that would come from putting the projecting member in otherwise quiet air. Figure 14·1 shows the AN/APQ-3 installation with a reflector 60 in. wide. By making the reflector quite shallow (12 in. in height) and partially retracting the antenna inside the fuselage, the extension of the radome below the keel line of the plane was kept down to only $10\frac{5}{8}$ in. Although this radome has a frontal area greater than that of the streamlined housing for the 29-in. reflector, its drag is only half as great.

There are further advantages in a low-drag radome, because lower

[1] At sea level the density of the air ρ is taken as 0.00238 slug/ft^3. This value is always used when the velocity V is indicated air speed, regardless of altitude of flight.

[2] See the texts cited in the introduction to this chapter.

[3] This is only approximately true, since there is no attempt in this equation to allow for the fact that the airplane as a whole does not increase in size proportionally.

drag and lower pressure on the radome go together. If the pressure is lower, the structural requirements are less severe and the electrical design can be better. Typical pressure distribution curves are shown in Fig. 14·2. These data were taken during actual flight with the radome mounted on a B-17E aircraft. The peak negative pressure is in the order of $0.9q_0$. For the shallow radome shown in Fig. 14·1, the peak pressure has been estimated to be only $0.5q_0$.

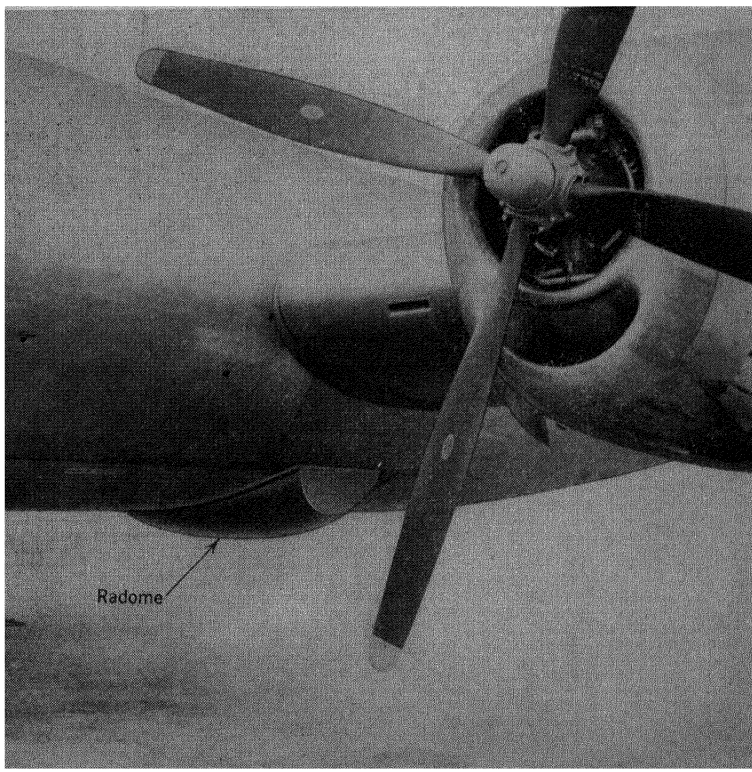

FIG. 14·1.—A belly installation of a 60-in. radar antenna on a B-29.

Determination of the optimum size and shape of a radome by a study of the radome alone is not sufficient to ensure that the shape will have a low drag when integrated with the airplane; the location on the plane and the manner of attachment can cause the resultant over-all drag to exceed the sum of the individual drag forces by a large amount. An example is given by the AN/APQ-7 radar system installed on a B-29; it is shown in Fig. 14·3*a*. The airfoil section shown at *a* has extremely low

drag, yet when this section was mounted on the B-29, the effect was more severe than that of the earlier cylindrical radome installation for the AN/APQ-13. This set had a radome, like that of Fig. 9·3, that was 35½ in. in diameter and extended about 32 in. beyond the skin of the plane.

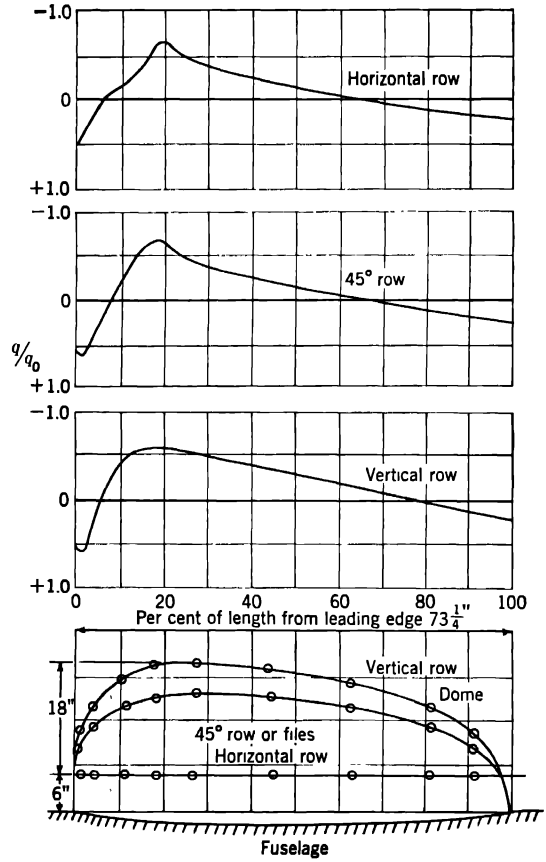

FIG. 14·2.—Pressure distribution on a streamlined radome mounted on the B-17E in place of the ball turret. The speed of the airplane during the test was 198 mph. (*Courtesy of U.S. Army.*)

It has been estimated that the cylindrical radome decreased the top speed of the plane by 4½ mph; the estimated effect of the airfoil for the AN/APQ-7 was 6 mph. This increase in the drag is attributable to new interference effects. Both installations shown in Fig. 14·3*a* and *b* resulted in extremely high drag. The constriction of the space between the airfoil and the fuselage restrains the flow in such a way that it is more advan-

tageous to fill in these spaces completely, as in Fig. 14·3*c*, even though the frontal area may be greatly increased.

With speeds in excess of 300 mph, compressibility effects become more and more critical. The drag of a body is no longer just a function of its size, shape, velocity, and Reynolds number but also involves a quantity known as the Mach number. The Mach number is the ratio of the velocity of the air stream to the velocity of sound in the air stream.

The available data on compressible flow are extremely meager at present. The theory involves the solution of nonlinear differential

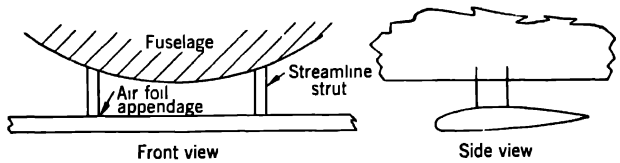

FIG. 14·3.—(*a*) Airfoil section connected by streamlined struts.

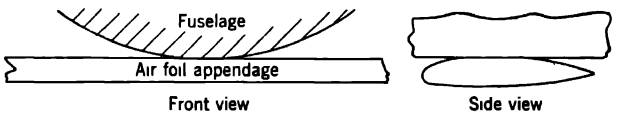

FIG. 14·3.—(*b*) Airfoil section mounted in contact with fuselage.

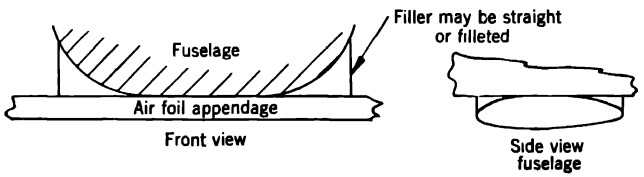

FIG. 14·3.—(*c*) Airfoil section mounted in contact with remaining intervening space filled.

equations, and only the simplest of these have been solved so far. The wind tunnel results have been few because the development of wind tunnels for compressible flow has been slow until very recently. The indications are, however, that the ideal aerodynamic shapes for noncompressible flow are not at all desirable for compressible flow.

Airfoils for noncompressible flow are characterized by rather blunt leading edges, the maximum thickness occurring at a distance of 0.2 to 0.3 of the length from the leading edge. This shape results in a very high peak pressure at the station of maximum thickness (see Fig. 14·2). A large negative pressure is indicative of large increase of the velocity in the air flow. When such a shape is used at high velocities the local velocity at this point of greatest velocity approaches the velocity of sound. The flow immediately becomes unstable; intense turbulence for

the remainder of the flow over the airfoil occurs and causes a rapid increase in the drag.

The tests on compressible flow made to date indicate that it is desirable to have a much longer and more gradual taper in the forward portion so that the maximum section occurs at about 0.6 to 0.7 of the length from the leading edge. This has two effects: One is to reduce the length over which turbulence might take place; the other is to decrease the peak pressure by making the taper more gradual. This lower peak pressure is associated with corresponding decrease in the velocity of flow at this point; the critical value of the Mach number, for which the drag for the body starts to increase very rapidly, is approached only at much higher speeds of the airplane. An additional decrease in drag has been produced by abruptly cutting off some of the rearward portion of the airfoil. This tends to decrease further the surface area over which turbulent flow occurs.

It should be emphasized that the above discussion on compressible flow applies only to airfoils. The design of an appendage to an airplane based on the suggested changes may not be at all satisfactory. The optimum aerodynamic design can be obtained, therefore, only by careful tests of models in a suitable wind tunnel or on an actual plane in flight.

14·2. Structural Design of Radomes.—A radome does not present any new demands on the theory of structural design. The unusual aspects are that the shape of the radome and the wall construction cannot be changed greatly because of structural requirements but are limited by aerodynamic and electrical requirements. The problem of structural design, therefore, is to determine the optimum construction and dimensions of the wall within a limited range of possibilities.

A detailed analysis of the structural design problem would be long; and as there are numerous sources of information on this subject,[1] this discussion will be extremely brief. It should be emphasized, however, that it is impossible to make an exact analysis for the structural design of a radome because of its irregular shape, the nonuniform distribution of pressure, the nonisotropicity of the radome material, and the variations in the physical properties of the materials even within one radome. Other factors, such as impact loads, cannot be predicted or estimated.

Structural analysis of a radome can yield two important results. The first is the deflection, or stiffness, that will determine the clearance necessary for the antenna. The other is the strength. It may be limited by either the ultimate strength of the material or the elastic stability of the

[1] S. Timoshenko, *Theory of Plates and Shells*, McGraw-Hill, New York, 1940, and *Theory of Elasticity*, McGraw-Hill, New York, 1934; J. E. Younger, *Mechanics of Aircraft Structures*, 2d ed., McGraw-Hill, New York, 1942; Niles and Newell, *Airplane Structures*, 3d ed., Vols. I and II, Wiley, New York, 1943.

radome. The latter may be the limiting factor when the air loading consists primarily of positive (compressive) pressure.

In proceeding with the structural design, several simplifying assumptions are often made. The first involves a simplification of the pressure distribution. When the radome is shallow and is mounted on the underside toward the rear of the fuselage, the pressure may be assumed to be uniformly distributed. A uniformly varying pressure is sometimes used in computations on radomes that are mounted well forward on the fuselage. Other simplifications may involve trigonometric or exponential functions. It is also helpful to assume a continuous function for the surface of an irregularly shaped radome so that the elastic equations may be reduced in complexity.

When the wall is very thin in comparison with its radius of curvature and the prevailing pressure is negative, the radome may be treated as a membrane which is not subject to the stresses of bending moments and thus experiences lower stresses. The occurrence of positive pressures prevents the use of the membrane approximation. It may then be desirable to simplify the solution by dividing the radome into longitudinal and transverse strips of unit width and treating the strips as individual arches. It is necessary to proportion the loads assigned to the various strips so that at any given point the deflection for the corresponding longitudinal and transverse strips will agree.

Whether the analysis is made on the basis of drastic simplifying assumptions or by more rigorous methods, it can at best be only approximate. The results of any analysis should be verified by structural tests.

14·3. Anti-icing and Deicing.—Anti-icing or deicing of radomes is applied for electrical or aerodynamical reasons when necessary. "Anti-icing" refers to the prevention of the formation of ice; "deicing," to the removal of ice already formed. Dry ice is a dielectric material. Its dielectric constant and loss tangent vary with frequency, but in the microwave region at $-12°C$ ϵ' is about 3.2 and $\tan \delta$ equals 0.00018. A uniform coating of ice on a dielectric wall has the same effect as a uniform increase of wall thickness, with a resulting increase in the reflection and a decrease of the transmission. A nonuniform coating will cause changes in the antenna pattern. As it forms, ice presents a highly reflective coating of water to the radiation, the dielectric constant at 0° varying from 80 to 3000 Mc/sec to 30 at 9500 Mc/sec. It is desirable, therefore, not only to anti-ice but to use measures to prevent the formation of the film of water, as it is easier to prevent the formation of ice than to remove it once it has formed.

Mechanical methods of checking ice formation are usually measures for deicing rather than for anti-icing. The use of expandable air ducts such as the rubber edge of airfoils is familiar. Pulsations of the ducts

force the constantly forming ice to break off. The expulsion of fluid under pressure through porous walls has also been used.

Chemical methods of anti-icing include the use of antifreeze pastes and liquids. These can be applied by external methods such as wiping or spraying, or they can be extruded through porous plastic walls. The dielectric properties of such a substance and the uniformity of covering are important. Surface treatment may include application of a non-wetting coating that does not need frequent renewal.

Thermal methods include conduction heating from an internal or external source and convection heating. The latter may involve the circulation of hot liquids or gases between double walls as for the radome of the AN/APQ-7 radar. This system requires auxiliary heaters, which are objectionable because of the weight added by the heaters and the additional fuel required.

Extensive use has not been made of methods for prevention or removal of ice. Ice was frequently encountered in the European Theater during World War II, but flights were usually able to avoid icing areas. The Pacific Theater was comparatively free of icing conditions.

Airborne radomes in the leading edge of the wing of the AN/APQ-7 type (Secs. 6·14 and 14·5) were required to meet the same anti-icing specifications as the rest of the airplane; the decrease of lift of the AN/-APQ-7 airfoil caused by ice would not be critical, but the increase in weight would be. This airfoil was flown in both theaters, but without heat in the Pacific.

Ship and ground radomes also have to be kept reasonably free of ice in order to avoid excessive structural load. On occasion, shipborne radomes have been deiced by hand chipping.

While anti-icing and deicing are highly desirable, the present available methods of anti-icing and deicing of radomes are not satisfactory. Much more development is needed.

14·4. Examples of Airborne Normal-incidence Radomes. *Cylindrical Radomes for the ASG (AN/APS-2).*—The original radome intended for installation in B-24's and PB4Y's was made of a single thin wall of a Fiberglas laminate using Plaskon 700 resin; the dielectric constant was over 5.0, and the wall thickness was 0.060 in. Initial tests of the ASG in such a radome resulted in complete disappearance of signals from certain sectors, as discussed in Sec. 9·2 and shown in Fig. 9·7 of that section.

A new design was made, consisting of a double-walled radome in which Laminac resin P4122 was used, thus reducing the dielectric constant to 4.0. Each wall was 0.060 in. thick and separated from the opposite wall by a distance of 0.825 in., the separation having been arrived at according to the methods of Sec. 10·5. The improvement resulting from use of this new design is shown in *c* of Fig. 9·7.

The AN/APS-6 Wing Nacelle Radome.—This is an example of the use of an electrically thin wall of a material having a moderately low dielectric constant ($\epsilon/\epsilon_0 = 2.2$) for a small normal-incidence radome for the 3-cm band. The material was Polyfibre. The AN/APS-6 wing nacelle is installed as shown in position *J* in Fig. 9·6. It deviates a little from the hemispherical shape to form a paraboloid that gives mild streamlining. It is classified as a normal-incidence radome, since a diagram of the incident and reflected rays shows that none departs more than 30° from the normal, as shown in Fig. 9·18.

The beam scans a continuous spiral from 0° to 60° and back to 0°. In the position of maximum nod of the antenna the radome presents its greatest area at nearly normal incidence and the antenna is subject to the maximum rate of change of impedance. A description of the scanning mechanism is given in Sec. 6·13.

Transmission tests of the radome provided by the airplane manufacturer showed a reduction in one-way transmission of power of at least 40 per cent. This radome had a wall section of phenolic laminated cotton duck nearly $\frac{3}{32}$ in. thick. A model submitted by a plastics manufacturer, made of laminated Fiberglas $\frac{1}{16}$ in. thick, resulted in a similar reduction. An accompanying reduction in range of 20 to 25 per cent resulted from this cause alone. The pulling of the transmitting magnetron beyond the capacity of the AFC also caused loss in power and efficiency. The reflected power was sufficient to result in most of the harmful effects of reflection discussed in Sec. 9·2. On the basis of comparison of the strength and stiffness ratings of the materials then available in usable form—polymethyl methacrylate, Fiberglas laminates, and Polyfibre plastic—the last-named, which had been developed for this sort of application, was selected for the new design. The minimum thickness that would withstand static load tests was found to be 0.090 in.

The tolerances specified were −0.00 in., +0.035 in. Since even greater thicknesses do not result in changes of impedance beyond the capacity of the AFC, the tolerances were chosen to get mechanical uniformity and to avoid excessive weight. Loss of power by absorption in the material is negligible because d/λ is small and the loss tangent does not exceed 0.001. The design proved satisfactory. The radome is lighter and more moisture resistant than earlier models. Some difficulty was experienced in service because of slow erosion of the plastic and changes of shape that resulted whenever the percentage of residual solvent in the Polyfibre was high.

The Design of the AN/APS-4 Radome.—This is an example of a small normal-incidence airborne radome, having an extremely thin wall of medium-high dielectric constant ($\epsilon/\epsilon_0 = 3.5$), that derives much of its rigidity from pressurization of the enclosed space. It is a cylinder

about 17 in. in diameter, terminated in a hemisphere. Its installation in a bomb rack is illustrated at M in Fig. 9·6. The antenna consists of a 14-in. dish for the 3-cm band. The "ray" diagram and other geometrical relationships are similar to those of Fig. 9·18.

The radome is required to hold two-thirds of its pressure for 10 hr without aid of the pressurizing pump after 10 severe weathering cycles that include temperature extremes, high humidity, and exposure to ultraviolet light. It is further required to withstand at least 150 per cent of the expected aerodynamic load with both low and high internal pressure.

A Polyfibre radome survived the pressurizing and cycling tests. A radome that was capable of passing the tests was made of nearly half the weight, however, by utilizing a carefully molded knit fiber glass fabric which is better able to withstand the internal pressure. With this material the radome wall is 0.050 in. thick in the cylindrical section and thins to 0.040 in. in the hemispherical end. The material consists of an Oneida knit fiber glass, including 25 per cent cotton, and laminated with Bakelite BRS 16631 polyesterstyrene resin. Its dielectric constant is 3.5.

While the loss tangent (0.015) exceeds that of Polyfibre (< 0.001), this is of little significance in so thin a radome. The power absorbed proved to be less than 1 per cent, and the power transmitted was 89 per cent, which agrees with theoretical calculations. A refocusing that strengthened the main lobe at the expense of the side lobes and gave an apparent power transmission of 100 per cent was observed in the zero azimuth position of the antenna. Although the performance did not quite equal that of the Polyfibre radome, it was well within design limits.

The mechanical advantage of this construction lies in its ability to hold the internal pressure, which gives it stiffness. Its rigidity without pressure is not equal to that of an equal weight of Polyfibre, so in recent models stiffening rings have been added to the nonelectrical area to take care of failure of the pressurizing. In addition, the stretch of the fabric makes for ease of fabrication which helps in meeting the very high production schedule. Every radome is tested mechanically, and representative radomes are given severe durability tests. Very few have failed to meet these standards.

After the radar and radome were far advanced in production and installation, it was found that radomes of AN/APS-4 sets carried in P-38 bomb racks were being destroyed by ejected shell cases. Similar destruction occurred with Marbon B and Marbon S (cyclized natural rubber and resin-modified GR-S rubber respectively) cylindrical radomes installed with AN/APQ-13 (29 in.) in B-29's. An example is shown in Fig. 14·4. Both cyclized and natural rubber caps cemented over the

exterior of the AN/APS-4 radome were tested by the ATSC, but they were not entirely satisfactory.

Design of Large Radomes.—For nearly normal incidence the optimum core thickness of a sandwich radome for the 10-cm band may prove to be impractically great. One very large normal-incidence radome was designed for an antenna that exceeded the airplane considerably in width. A sandwich of less than the optimum electrical thickness was used. It

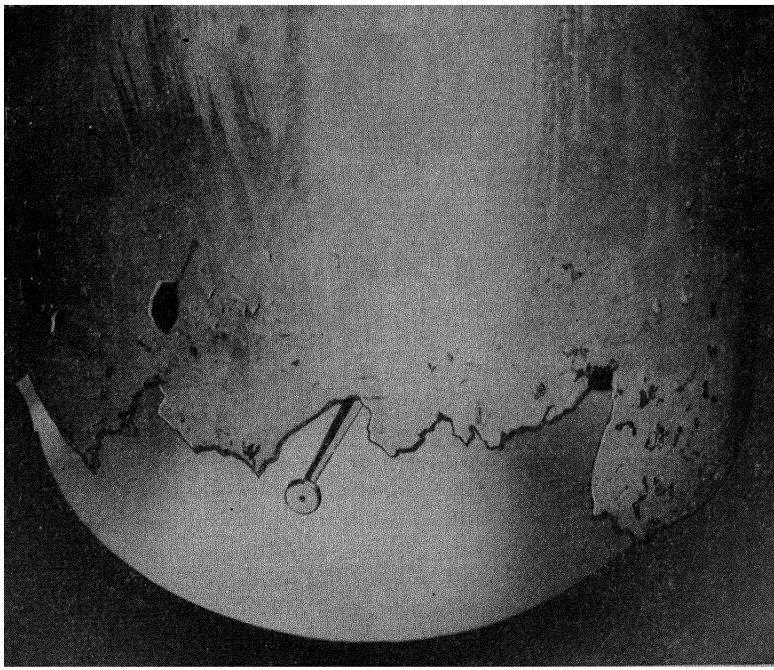

FIG. 14·4.—Rubber radome damaged by firing of lower guns. (*Courtesy of Air Transport Service Command.*)

was placed under the airplane streamlined to fair into the after part of the fuselage. Figure 14·5 shows this radome attached to a mount for testing the pattern of the antenna and radome.

The radome wall consisted of a structural sandwich using Fiberglas laminate skins 0.040 in. thick and a core of GR-A cellular hard rubber board 0.52 in. thick. Some reduction of reflection was obtained by this arrangement, although it was thinner than a first-order sandwich and served chiefly to give a very light, rigid, and strong structure. It was chosen primarily to save weight, because of the size of the radome.

The maximum deviation from normal incidence was not great, so transmission was good. In a later design, transmission to the rear was improved by increasing the thickness of the core. Tests of a radome of equal weight but having a wall consisting solely of a Fiberglas laminate confirmed the mechanical superiority of the sandwich construction.

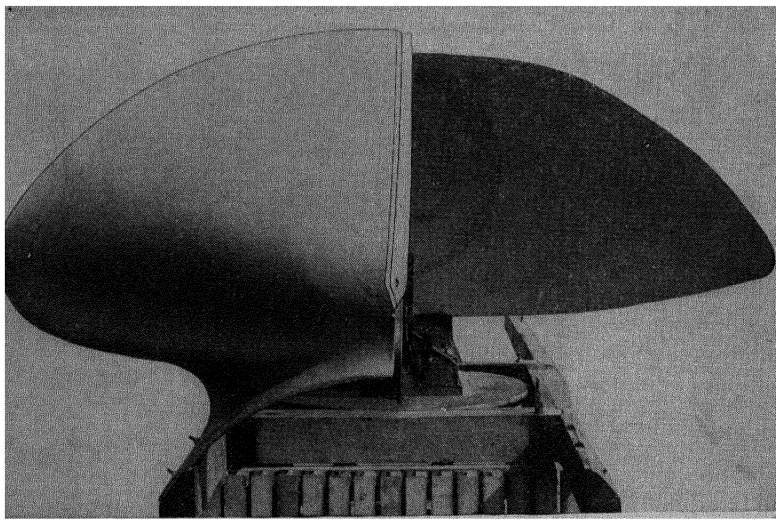

FIG. 14·5.—Front view of one side of radome inverted on test mount. The antenna shows at the right.

14·5. Examples of Streamlined Radomes. *Nose Radomes for the P-61.* Difficulties experienced with the SCR-720 radar installed in the P-61 airplane are discussed in Sec. 9·2. Figure 9·11 shows a plane with radome. The original radome was made of a laminate of Fiberglas with a polyester-styrene resin that had a dielectric constant of 4.0 and a loss tangent of 0.015. The radome was 0.125 in. thick in the electrical area and 0.185 in. elsewhere. It reflected 8 per cent of the incident power at normal incidence in the 10-cm band. Analysis showed that a thickness of 0.085 in. in the electrical area would lower the reflection to 2.8 per cent and give a mechanical safety factor of 1.5. A thinner radome was made and tested. It gave the satisfactory results shown in Fig. 9·13.

Radome for the ASG-3 Radar in the PBM-3C Airplane.— This radome was located on the PBM-3C airplane in position *C* of Fig. 9·5. It was approximately 8 ft long, 3 ft wide, and 4 ft high. The original design for this radome was made by structural designers at a time when it appeared to many that any material sufficiently strong and "fairly transparent" to radiation could be used. Many other radomes were built to satisfy only these basic requirements.

Serious limitation in range of the ASG-3 in operational flights was reported. Laboratory tests of the set disclosed a reduction in power of nearly 50 per cent. The power transmission coefficient of the radome was 94 per cent, but the loss of power by the system corresponded to a 30 per cent reduction in standard range. Frequency pulling of the magnetron was blacking out certain sectors in the scope in the forward direction, as shown in Fig. 9·7. Transmission through the streamlined tail was satisfactory.

The radome was constructed with a thin wall, 0.060 in. thick, of a Fiberglas laminate made with Plaskon 700 resin that had a dielectric constant over 5. The reflection was found to be 4.5 per cent, in accord with theory. To remove the cause of pulling, a reflectionless double wall was designed. An inner wall of the same thickness as the outer one was attached to the forward half of the radome and spaced 0.80 in. from the outer wall. The improvement that resulted from the double-walled design can be seen in Fig. 9·8*a*, *b*, *c*.

The AN/APQ-13 (60-*in.*) *Radome.*—Although satisfactory radomes had previously been designed, none of these had imposed so great a demand on the designer as the radome for the AN/APQ-13 (60-in.) 3-cm radar. Because of the high estimated loads on the radome and the high angles of incidence of the radiation, it was decided that a sandwich construction was needed for optimum all-round performance.

Theoretically the design appeared to be straightforward. The shape of the radome was based on a protrusion as small as the primary antenna pattern would permit and on a maximum angle of incidence of 70°. Test panels were molded to the theoretical values and found to give results in disagreement with predictions. Further investigation showed that the discrepancy was due to a film of resin between the skin and core of the sandwich, which behaved electrically as additional skin thickness (see Sec. 10·6).

In order to minimize the glue line and keep its thickness fairly uniform, it was necessary to refine the core of cellular hard rubber and also to develop a new molding technique, the "wet lay-up" method. With these developments it became practicable to hold the glue line to approximately 0.010 in.

No exact structural analysis of this radome was made. For an approximation, it was treated as a membrane because it was realized that the pressure distribution would be nearly uniform. The shape of a stressed membrane will be subject to minimum stresses and deflections under a uniform load because stresses involved in bending tend to disappear, especially when the wall thickness is small compared with the curvature of the structure. The radome was mounted to the plane by flexible straps so that the possibilities of bending moments would be further reduced.

On the basis of numerous electrical and mechanical tests it was decided to use the following sandwich construction: core of cellular hard rubber of 12 lb/ft³ density; faces, laminates of ECC-11-128 Fiberglas and BRS 16631 resin 0.030 in. ± 0.002 in.; over-all thickness, 0.440 in. ± 0.002 in.

The results of structural loading tests on this radome are discussed in Sec. 14·10. Crude measurements made on the initial flight test indicated that the radome deflection did not exceed ¼ in. An idea of the mechanical properties of the final radome can best be obtained by examining the specifications, some of which follow:

Bending moment per inch of width, lb-in./in	250
Stiffness coefficient (EI per inch of width), lb-in.²/in	5500
Edgewise compressive stress, lb/in.²	840
Tensile strength normal to the surface, lb/in.²	200

The sandwich construction was so balanced as to give as nearly uniform transmission as possible throughout the range of angles of incidence from 0° to 70°.

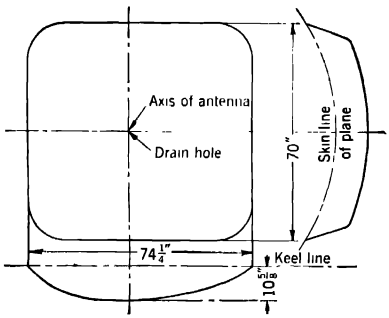

FIG. 14·6.—Outline of production radome for AN/APQ-13 60-in. antenna on the B-29.

Difficulties were encountered in the initial trials of this radar system, particularly in flights at low altitude when the beam was almost horizontal. It was learned later that interference resulted from diffraction at the edge of the airplane. The simple application of the primary antenna pattern for determining extension of the antenna is inadequate. This effect is discussed in detail in Vol. 12. The radome was arbitrarily extended an additional 2½ in. in order to lower the antenna. The outline of the final radome is shown in Fig. 14·6. No further difficulty from this effect was encountered.

The electrical testing of the radome is discussed in Sec. 14·9.

Nonprotruding Radome for the 60-*in. AN/APQ*-13.—The design of this radome is discussed because of interesting requirements that were not encountered in any other designs. It is thought to be representative of the problems that will be encountered in the high-speed airplanes of the future. The radome was never flight-tested.

A development model of the radome was molded for a location under the nose of a projected fast airplane as in installation *E* in Fig. 9·5. Its shape was that of the fuselage which it was to replace. The objective was to design the antenna, antenna installation, and airplane together to

get the desired aerodynamic and radar performance. Although the development of an entirely new radar was planned for use in the airplane, the AN/APQ-13 (60-in.) scanner or a modification of it was to be used in the first installations.

The length of the radome was 123 in.; its depth, 10 in. forward and $30\frac{1}{4}$ in. aft. Its forward end was located 30 in. aft of the tip of the nose. Its surface could very nearly be generated by revolution of a single element of its contour about a fore-and-aft axis, the radii being $18\frac{1}{2}$ in. forward and $38\frac{3}{4}$ in. aft.

The following factors were taken into consideration in planning the shape of the radome and the antenna system. Because vision through the nose of the airplane had to be unobstructed, the antenna had to be as close as possible to the undersurface of the fuselage. The need for placing other equipment above it also limited the location of the reflector to a position below the maximum width of the plane. Good resolution in azimuth was dependent upon having a reflector wide enough to separate individual targets.

The required shape of the radome necessitated cutting the ends and lower edge of the reflector in order to fit it in. The maximum width of the antenna feed also had to be adjusted to fit the radome. Upward radar vision was limited by the level of the floor. The amount of upward vision needed was determined from the expected roll and pitch of the airplane in rough air and in climbing, gliding, and banking. It also depended on the angle of depression of the beam from the horizontal, given by the AN/APQ-13 antenna. As the airplane could not be designed to allow unobstructed vision, nonreflecting screens were to cover all obstacles, both metallic and nonmetallic. By eliminating reflection, frequency pulling and the resulting azimuth errors and loss of power were to be prevented. Distortion of the wavefront by shift of phase in transmission through dielectric obstacles was also to be obviated by this masking. Diffraction at the edges of the screen, however, could not be prevented. The use of exponentially curved edges for such a purpose has been proposed but has not been adequately studied.

In order to get maximum range at low altitudes it was necessary to plan for a minimum depression of the nose of the beam. This required satisfactory transmission and low reflection by the radome over a wide range of angles of incidence from nearly normal to 85°, a difficult requirement to satisfy, especially for perpendicularly polarized radiation. In such an installation in the fuselage the radome comprises a large section of the skin of the airplane. It must support the corresponding aerodynamic loading; and where the floor above cannot be used to pressurize the cabin, the radome must do so, although this requirement is to be avoided if possible. An aerodynamic study disclosed a variable loading

over the radome. In normal flight a positive pressure would extend over its surface with a maximum of 85 lb/ft^2 near the forward end. Under other conditions the load would be entirely negative, reaching a peak of -210 lb/ft^2 a little aft of the forward edge.

Electrical design followed the techniques outlined in Secs. 11·6 to 11·8, and mechanical design was in accord with the principles discussed in Sec. 14·2. A family of curves similar to that of Fig. 11·18 was prepared in order to make it easier to compare various possible designs. It could be seen that the range of angles of incidence would be broadened by decreasing the skin thickness and that the corresponding core thickness would increase so rapidly that the stiffness would be improved. Consequently, the thinnest skins consistent with adequate surface resistance to puncture were sought. Four drawings (Figs. 11·19*a* and *b* and 11·20*a* and *b*) were prepared to determine manufacturing tolerances.

The design of the sandwich was begun by taking the skin thickness as the independent variable and then determining the core spacing, in accordance with Sec. 11·8. The wall was of uniform construction, unobstructed by reinforcements. The over-all thickness determined for the radome was 0.440 in. $\pm$ 0.020 in. The sandwich skins were 0.030 in. $\pm$ 0.002 in. in thickness, each consisting of four layers of ECC-11-128 Fiberglas cloth laminated with Bakelite resin BRS 16631. An average skin resin penetration into the core not exceeding 0.12 in. was permitted. The core consisted of cellular GR-A hard rubber board having a density of 12 lb/ft^3. The single-stage wet lay-up molding process, which had been developed for the AN/APQ-13 (60-in.) radome, was used because of the mechanical and electrical excellence of the adhesion to the core.

The design of a similar sandwich is discussed in Sec. 11·8, where it is shown that it is advantageous to use the minimum skin thickness. A value of d_s/λ_0 equal to 0.030 was used for this new radome rather than 0.040 as in the radome considered in Sec. 11·8.

A second design was to have an inner or compression skin, consisting of five layers of ECC-11-128 Fiberglas fabric, and an outer skin having three layers of the same, to increase its flexural strength by 25 per cent when the thicker face was in compression. The core was to consist of a honeycomb hexagonal grid possessing electrical and mechanical properties similar to those of Fiberglas—GR-A foam sandwiches. The over-all thickness was to be 0.482 in.

AN/APQ-7 Anti-iced Leading Edge.—A sketch of this installation is given in Fig. 14·3, and a photograph shown in Fig. 6·17; a description of the scanner may be found in Sec. 6·14.

The radome is an auxiliary wing, having a double-walled leading edge of Fiberglas molded with American Cyanamid Laminac X-4000 resin.

The entire forward section containing the antenna is pressurized. For anti-icing, heated air flows between the double walls. The walls are separated by vertical plastic spacers $\frac{1}{4}$ in. wide and 0.210 in. thick, arranged at random to prevent creation of extra side lobes.

In treating effects on the radiation of an obstacle as close to the source as is the wall of this radome, the wall itself should probably be considered as a source of scattering rather than as a reflecting surface. It was discovered in the design of streamlined beacon housings that a wall thickness intended for nonreflection distorted the E-plane pattern even though the E vector was in the plane of incidence. The radius of curvature was of the same order as the wavelength. The AN/APQ-7 antenna, also similarly polarized, was distorted in the H-plane by the radome. The flared weaker portion of the pattern seemed to be the most affected. In addition, it was found to be sensitive to the formation of a thin coating of ice along the most forward area of the leading edge. The distortion of the pattern was minimized by locating the housing in a more favorable position with respect to the antenna and by design of a new flap.

The leading edge has the following additional effects on the electrical characteristics of the antenna. The gain is reduced 0.5 db in one-way transmission. Pulling is observed at an azimuth of 0° but not at other azimuths.

Because of the difficulty of calculating the reflection from a combination of dielectric walls placed and shaped as these were, an approximation was made by assuming two parallel plane dielectric layers separated by air. Assuming the dielectric constant to vary from 3.8 to 4.6 in manufacture and selecting a wall thickness of 0.045 in. $\pm$ 0.005 in. for structural reasons, the proper spacing between the walls of 0.205 in. $\pm$ 0.010 was calculated, using Eq. (10·22).

The wear observed on the leading edges of these radomes in the Pacific was reproduced in the laboratory by causing samples of the plastic material to move at high speed through a water spray. A velocity of 250 mph was obtained by rotating small pieces at 3400 rpm on an arm 26 in. in diameter. All Fiberglas laminates tested showed wear regardless of the resin used, with little difference of practical importance among samples. The resins included a group of polyesterstyrenes and phenolics. It was interesting to note that a thermoplastic sheet (methyl methacrylate) containing no filler showed no wear. A $\frac{1}{32}$-in. rubber sheet was equally resistant, and various rubber cements gave more limited protection. The rapid deterioration of the plastic in flight appeared to result in part from the breaking of ribs during the pressurizing test made before acceptance. The broken ribs allowed flexing of the outer wall during flight.

Radome for the GEI Scanner.—The roll-stabilized GEI scanner antenna was designed for a 1-cm radar set. The radome was 73 in.

long, 52½ in. wide, and 24 in. deep. Its drag load coefficient (relative drag) was estimated by the Air Technical Service Command to be 2.5. Its outline was similar to that illustrated in Fig. 9·19, and its size and shape were based upon the dimensions of the space required for the swing of the antenna (see Fig. 14·7). A vertically polarized cosecant-squared roll-stabilized antenna, 42 by 10 in., was used. It is shown in side view in Fig. 14·7*a*, swinging from the pitch adjustment axis, which is within the skin of the airplane. The minimum inside diameter of the radome that provided for 1-in. clearance was 26 in. The depth below the normal horizontal, as determined by the motion of the antenna about the roll axis, was fixed at 21 in., as shown in Fig. 14·7*b*. The reader may refer

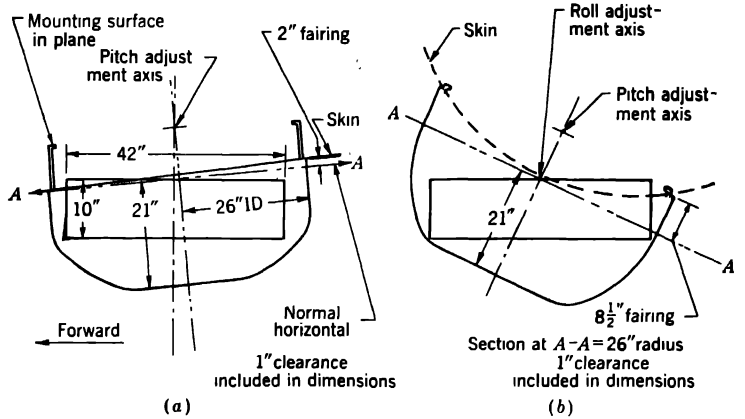

FIG. 14·7.—Minimum radome under B-17E airplane allowing ±25° roll stabilization.

to Sec. 7·2 for a description of roll-stabilized scanning mechanisms and to Sec. 7·5 for a comparison of the swept volumes for four types of stabilization.

A modified half-wavelength wall of Fiberglas was chosen for the radome because sandwiches for the 1-cm band were relatively unproved structurally. (A very thin-skinned Polyfibre sandwich later investigated proved to be superior electrically and adequate structurally.)

The radome was molded of nine layers of ECC-11-164 and one layer of ECC-11-127 Fiberglas cloth, with Bakelite resin BRS 16631. The specific dielectric constant of the laminate was about 4.0; tan δ was 0.015; and the thickness was 0.145 in. This design was in accordance with the theory given in Sec. 11·9.

The average power transmission as obtained from pattern measurements was 71 per cent. That of a flat control panel at normal incidence was 80 per cent. The reflection over a range of incident angles of a similar modified half-wavelength panel for which $d/\lambda_0 = 0.28$, where

d is thickness and λ_0 is free-space wavelength, is given in Fig. 11·9. The d/λ_0 of the 1-cm radome equaled 0.296.

Table 13·14 rates a laminate of Fiberglas-polyesterstyrene higher mechanically than Polyfibre plastic for the wall of a half-wavelength radome. In the 1-cm band the latter is more desirable because wider manufacturing tolerances are permitted and it has a much lower absorption of power.

Radome for Experimental 1-cm Radar.—The antenna of this radar set was similar to that of the GEI scanner. It was line-of-sight stabilized, and the tilt was manual. Its beam was cosecant-squared, the pattern extending from −12° to 68°. The polarization was vertical.

An antenna ray diagram similar to that shown in Fig. 9·19 was drawn up. This assumed, for convenience only, that the treatment of geometrical optics could be used. The surface of the radome was then shaped so as to avoid angles of incidences greater than 70°. In the final design the electrical area was largely confined to the bottom of the radome. A nearly flat-bottomed, streamlined radome was then manufactured. It was 73 in. long and 46 in. wide and extended 15 in. below the keel line.

As stated in Sec. 11·9, it is difficult to use the conventional Fiberglas sandwich in a 1-cm band streamlined radome. Consequently, a first-order sandwich having a core of molded polystyrene fiber (Dow Q-107 Polyfibre: dielectric constant, 2.2; density, 0.85 g/cc) and skins of one layer each of Owens-Corning ECC-11-128 Fiberglas impregnated with polystyrene lacquer ($\epsilon'/\epsilon_0 = 3.5$ to 3.7). The skins were first dried and then fused to the core. A nitrocellulose paint was used on the surfaces to protect them from spilt aircraft fuel.

The over-all thickness was 0.173 in. ± 0.010 in. This value was selected for the best average transmission for angles of incidence up to 70° at perpendicular polarization. When the antenna looked through the sides of the radome, the polarization was perpendicular and the angles of incidence were large. Transmission through the bottom of the dome was largely at parallel polarization and was uniformly excellent. At normal incidence the reflection loss was a little under 10 per cent and the absorption loss was a fraction of 1 per cent. At 60° the reflection loss was zero, increasing to 10 per cent again at 70°.

This radome design was also tested with horizontal polarization. In this case, the wave incident on the bottom of the radome was perpendicularly polarized. Transmission was not more than ½ db down, since the wall thickness had been chosen for that polarization.

In a flight test at 425 mph no change in stability or evidence of vibration or buffeting was detected. No deflection of the radome greater than ¼ in. could be measured. The radar performance was excellent.

Future 1-cm Band Designs.—In designing sandwiches for the 1-cm band it was concluded that a first-order thin-skinned Fiberglas-rubber foam sandwich for first-order spacing was not stiff enough and strong enough for medium and large radomes. Such a design, however, was used for an experimental 1-cm version of the AN/APS-6 radome and proved adequate for both the 1- and 3-cm bands.

The aerodynamic loadings for these radomes were smaller than are to be expected in high-speed planes of the future. Nothing thinner than a third- or fourth-order sandwich of this material is likely to be mechanically suitable for many future designs. Such a construction is not likely to be adequate electrically because the transmission for a third-order sandwich at angles of incidence above 45° is poor for perpendicular polarization. The constant reflection contours become steeper with increasing order of spacing, as shown in Sec. 11·8. For a sandwich, furthermore, the dimensions for zero reflection are not the same for perpendicular and parallel polarization except at normal incidence, and the difference becomes greater with increasing order of spacing. As a result, a design that is satisfactory for incidence at perpendicular polarization may be unsatisfactory for parallel polarization.

Design for the 1-cm band is further complicated by the high angles of incidence, which extend even to 85°. This results from the limitations on propagation in the 1-cm wavelength band, which will necessitate large reflectors when long range is required. Most of the large antenna will then have to be retracted within the airplane. Where ground coverage and a larger sector of scan than can be obtained from the nose is required, the antenna will have to be in the bottom of the fuselage and radiation will strike the surface of the radome at grazing incidence.

New solutions must be sought. It is shown in Chap. 11 that it is advantageous to plan for predominantly parallel polarization whenever possible. If this can be done, the radome wall can be a second-order sandwich with modified half-wavelength skins. Such a scheme is discussed in Sec. 11·9, where an example is given of a second-order sandwich with half-wavelength skins for the 1-cm band, in which $\alpha_s = 3.7$ and $\alpha_c = 1.4$. Theoretical considerations and experimental work have indicated that such a design would be practical with low-loss material. It could possess adequate strength and stiffness together with good transmission characteristics and might be used at perpendicular polarization if necessary.

14·6. Examples of Shipborne Radomes.—An example of a medium-sized normal-incidence sandwich radome is the one built for an antenna that is a cut paraboloid higher than it is wide and uses line-of-sight stabilization and AFC. The radome was 30 in. in diameter and 44 in. high. It was required to withstand the blast of 5-in. 38-caliber guns.

Figure 14·8 shows how two radomes were tested simultaneously. The radomes were mounted on portable platforms that were advanced toward the muzzle of a 5-in. 38-caliber gun along two radial lines progressively after each shot until damage occurred. Measurements of the blast pressure were made with a Williams blast gauge. The pressures at Positions 2, 5, and 6 were roughly 7, 15, and 20 lb/in.^{2}, respectively. The radomes were required to remain intact in Position 5.

Polystyrene solvent-fiber radomes proved adequate in the blast tests but distorted badly in service under the heat of the sun. Examination of samples showed that the solvent in the fibers had been insufficiently dried and that further solvent had been added in order to attach the outer Fiberglas skin. In view of the uncertain quality of these radomes a new

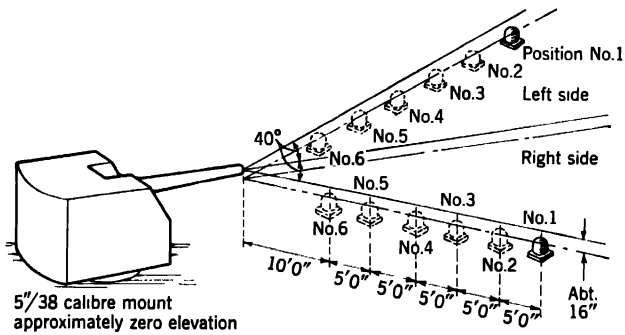

FIG. 14·8.—Test of radomes for resistance to gun blast. Successive positions of the radome are indicated.

design was substituted. This was a sandwich made of Fiberglas and cellular hard rubber. The dielectric constants of the skin and core were 3.5 and 1.2, respectively. The resin content of the skins was low. The design specification called for a total wall thickness of 0.316 in. ± 0.032 in. for areas in excess of 3 in. in diameter. Combinations of ECC-11-162 and ECC-11-128 Fiberglas cloth falling within a thickness of 0.042 in. ± 0.004 in. were permitted for the skins. Bakelite resin BRS 16631 was used to laminate the Fiberglas. Urea, resorcinol, melamine, phenolic, and other resins of higher dielectric constant were proposed for the skins. They were not used because larger variations are permissible in the spacing of the core in manufacturing if the reflection coefficient of the skins, or faces, of the sandwich is small. A cellular GR-A hard rubber board having a density of 8 lb/ft^3 was specified for the core.

It was necessary to show that the new sandwich of cellular hard rubber and Fiberglas was thermally stable. A radome of this construction was brought to 167°F at 90 per cent relative humidity in an oven. Over a

period of 55 min the temperature was slowly raised to 185°F. As expected, no dimensional change or obvious softening could be detected.

Early models were manufactured by the assembly and gluing of separate premolded skins and core. This technique introduced an additional skin thickness of lossy adhesive, resulting in transmission values as low as 80 per cent of the incident power (see Sec. 10·7). After an early version of the wet lay-up molding process was introduced, production radomes gave zero reflection and 90 to 94 per cent for the value of the power transmission. An ocean-gray naval paint (Bureau Ships Spec. 52P46) was used. The use of paints containing no free metal was found to result in negligibly small losses in transmission.

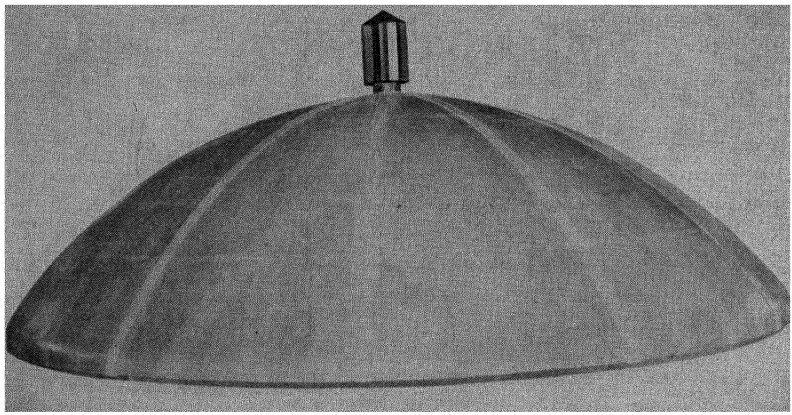

FIG. 14·9.—Top of radome for LST. (*Courtesy of U S Plywood Corporation.*)

Radome for LST Installations.—This is an example of a very large sandwich radome for shipboard use. A radome 26 ft in diameter was required for installation of a 10-cm radar on LST's. No gun-blast requirement was specified, but it had to withstand a 110-mph wind.

The shape of the design arrived at was a cylinder with a diameter of 26 ft and height of 15 ft, capped with a dome 7 ft high and a ventilator. The dome and cylinder were separate sections. The dome is shown in Fig. 14·9. It was divided into 12 pieces of 30° each. Sections were butt-jointed, and the joints secured with cover plates of Fiberglas $\frac{1}{8}$ in. thick. The wall section was a first-order normal-incidence sandwich for the 10-cm band, with sandwich skins of ECC-11-164 Fiberglas cloth 0.060 in. thick laminated with Bakelite resin BRS 16631 and a core of cellular Hycar GR-A hard rubber board having density of 12 lb/ft^3.

At the butt joint the core was strengthened with hardwood. Narrow vertical stiffeners of hardwood ($\epsilon/\epsilon_0 = 2.0$) 1 in. ($\lambda/4$) wide and 1.17 in.

(0.4λ) deep, arranged at random but not more than 20 in. apart, were also used to strengthen the core. They were put between the skins, replacing some of the core material. These compromised the electrical design for necessary structural reasons; but if the core material needed had been available, a second-order sandwich for the 10-cm wavelength could have been used without the stiffeners. Rubber cement was used for assembly of the sandwich. Reinforcement was augmented by the use of three horizontal laminated wooden rings, two located below the scanning area and one above at the juncture of the dome with the cylinder. A system of cables reinforced the dome and the upper end of the cylinder.

ELECTRICAL AND MECHANICAL TESTS

14·7. Equipment for Electrical Test.—Laboratory tests of radomes, as contrasted to actual or simulated flight tests, serve to locate particular sources of trouble. It has been found that such tests give results in good agreement with system tests whenever comparison is possible.

Laboratory tests must be designed to uncover defects in design or manufacture that would result in faults such as the following:

1. General reduction in range.
2. The complete disappearance of signals from certain sectors.
3. The shifting in apparent bearing of echoes.
4. Increased ground return to airborne radar systems intended for detecting other airplanes.
5. Creation of spurious signals.
6. Fluctuating signal strength.
7. Interference rings on the scope.

In a laboratory the cause of these harmful effects can be determined.

A general reduction in range may be attributed to fairly uniform loss from absorption and reflection over the area of the radome. In an early installation some reduction resulted because the magnetron was loosely coupled in an effort to isolate it from changes in the impedance that resulted from varying reflections from the radome.

The effects of pulling can be predicted from the measurement of the changes in the phase and magnitude of the standing waves in the transmission line as the antenna scans if the properties of the magnetron are well enough known to permit computation of the pulling. Complete disappearance of some signals may be caused.

The shift of the apparent bearing of certain echoes is discussed briefly in Sec. 9·2.

Reflection has resulted in both excessive ground return and spurious signals. The former is illustrated by the SCR-720 radar in the P-61 radar nose discussed in Sec. 9·2. Spurious signals resulting from power-

ful side lobes have been reported from targets not actually in the line of sight of the antenna. These are caused by obstacles in the path of the beam near the antenna and by high reflections from a radome wall redirected as a side lobe.

Fluctuating signal strength has been common in the pattern both of the antenna alone and of the antenna with the radome. Under operational conditions this results in complete or partial neglect of targets falling within the holes of lowered signal strength. This effect can readily be predicted in laboratory tests of the pattern of the antenna and of the antenna and radome combined.

Variations have been caused by ribs and by the interference of redirected power with the main beam. A strong side lobe inherent in the design of a particular antenna or created by a rib, joint, or similar obstacle in a radome or near-by structure can result in interference with the main lobe through diffraction and redirection of the diffracted power by reflection from near-by structures such as the skin of an airplane. Such a lobe not attributable to the radome, resulted in pronounced interference rings and was observed on the scope in an early design of the AN/APS-10. The photograph shown in Fig. 9·17 illustrates the interference caused by reflection of a portion of the main lobe of the AN/APQ-13 60-in. antenna installed under the B-29. It was produced by tilting the antenna upward while flying at 20,000 ft. Diffracted power may reinforce interfering side lobes, so that interference can be caused by both the antenna and the radome.

Testing of the radomes of aircraft installations has been conducted as part of flight tests of the entire system. Unfortunately, it has not been possible to conduct such tests without the radome in order to isolate effects attributable to it and thus obtain a significant standard of performance. When testing of airborne radar sets is done on the ground, the antenna is inverted to look upward. In this latter method, either the radar system or its antenna without the system, but with special test equipment to feed it, has been used. The latter combination has been favored, as it has proved not only more convenient and adaptable for making a series of varied tests but necessary for more exact diagnosis.

The effect of the radome on range can only be inferred, as a flight test cannot be made without a radome. Even if such tests could be made, a most elaborate target would be necessary if one were to try to draw conclusions as detailed as can be drawn from laboratory tests on the ground. Little could be learned about the causes of pulling by a flight test. Measurement of angular shift caused by the radome would demand very accurate navigation of an airplane flying over familiar and clearly detailed territory. This same sort of terrain would have to be flown over for investigation of variation in signal strength. The causes of excessive return

from the ground are hard to find; extended tests of the SCR-720 radar in the P-61 airplane failed to give enough information to disclose them. Differences among radomes are masked by the difference in the performance of the same system at two widely separate times, both in flight tests and in ground tests. Laboratory tests are valuable because the separate harmful effects can be isolated; they do not have to be examined simultaneously as in flight tests.

The laboratory test for reduction in range is simple and accurate. It is conducted in three steps: First a test is made with the antenna uncovered, then with the radome in position over the antenna, and finally with the antenna again uncovered, to make sure that nothing has changed

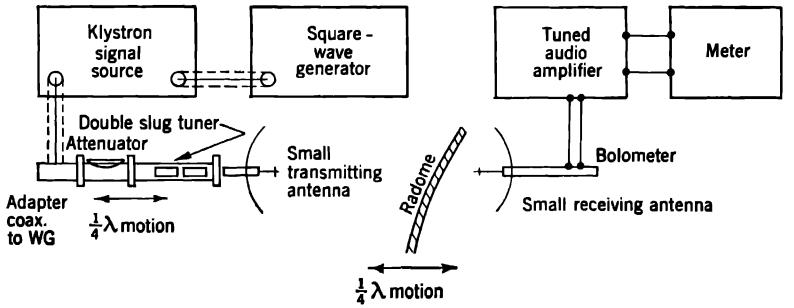

FIG. 14·10.—Apparatus for transmission tests.

during the test. Monitoring controls ensure comparison under identical conditions.

For examination of the radome wall in detail, an antenna that is small compared with the system antenna is placed within the radome in such a manner as to simulate various portions of the actual antenna in a series of its scanning positions. The system antenna is used when it is desired to determine the average transmission of the nose of the beam through a larger area. A pattern measurement also gives information about transmission. Usually, however, pattern tests have not been so accurate as transmission tests.

Either the antenna in the radome or a second external antenna may be the transmitting antenna in a test. It is preferable to use the antenna in the radome for receiving, in order to avoid indirect effects of the radome on the transmitting tube. Figure 14·10 gives a block diagram of the apparatus. The effects of interactions between dishes and between dishes and adjacent objects can be allowed for by making quarter-wavelength shifts as indicated.

Figure 14·11 shows how a small antenna can be used to simulate a larger antenna with a cosecant-squared pattern for examining small por-

tions of the radome. Due consideration must be given to the ray diagram of the antenna that is being simulated.

The obliteration of targets and the angular shift resulting from frequency pulling are investigated with standing-wave measurements made with the transmitting antenna located in the radome. With a small antenna the reflecting area can be gone over in detail. Pulling tests may also be made with the system at a ground test station. The setting of the

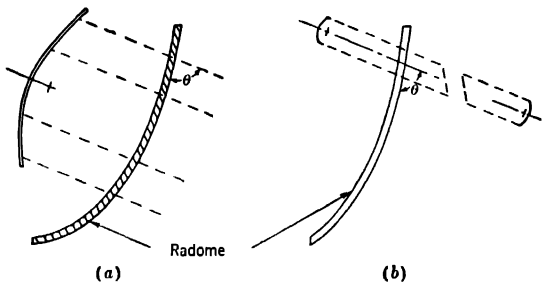

FIG. 14·11.—Use of a small antenna for the analysis of the interaction of antenna and radome.

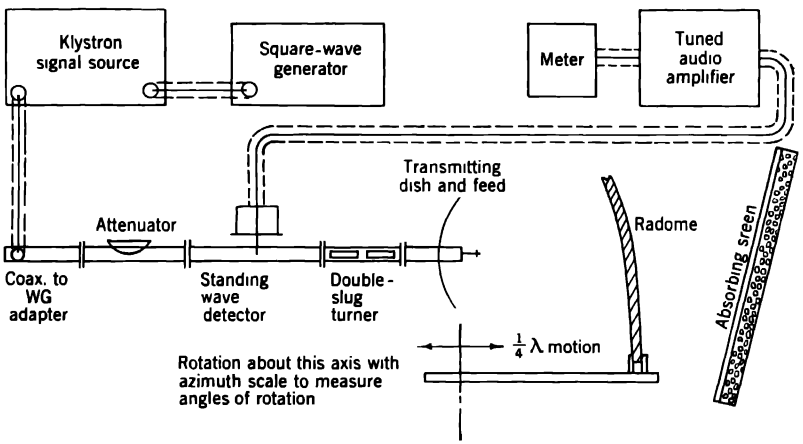

FIG. 14·12.—Apparatus for reflection tests.

local oscillator for maximum signal is read against azimuth with and without the radome. As the frequency shift per angular unit of dial setting has been previously determined by calibration, the shift of frequency in megacycles per second as a function of azimuth may be obtained.

An arrangement of laboratory apparatus for making measurements of reflection is shown in Fig. 14·12. The reflection coefficient of the radome in any position is derived as an arithmetic mean of reflection

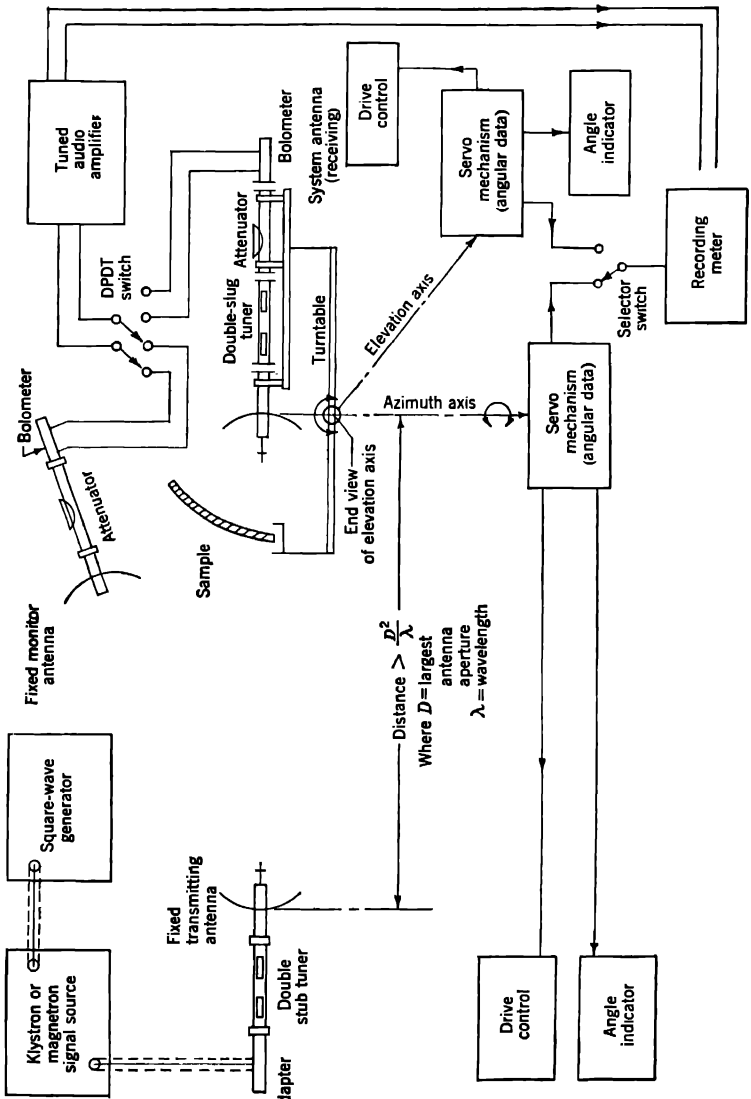

FIG. 14·13.—Apparatus for testing patterns with and without radomes.

coefficients computed from two standing-wave ratios measured at each angular position of the radome. The distance between the radome and antenna differs by $\frac{1}{2}\lambda$ in the two measurements.

Pattern measurements are best made with the aid of a mockup that simulates the actual installation and surrounding structure of the aircraft. Separate measurements are made with and without the radome. A study of the patterns obtained and correlation of them with the geometry of test conditions will disclose distortions caused by obstacles such as ribs, by focusing in the reflecting spherical sections of radomes, by fluctuations along the line of uniform illumination in cosecant-squared patterns, by interference, and by excessive ground return.

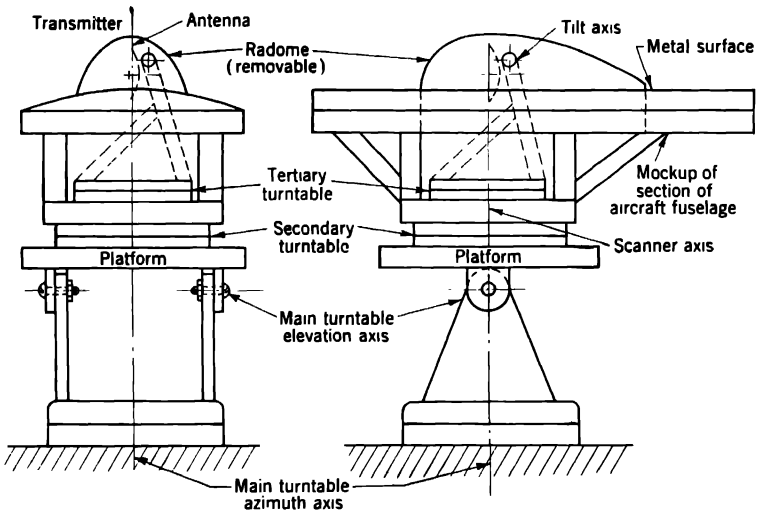

FIG. 14·14. - Mockup of aircraft installation for testing antenna pattern.

In Fig. 14·13 is shown a block diagram of an apparatus for making pattern measurements. The antenna of the radar system is placed in the radome and used only for receiving. The transmitting antenna is placed at a distance at least D^2/λ away, where D is the largest aperture of the antenna and λ is the free space wavelength, so that a substantially plane wavefront arrives at the receiving antenna. The procedure is first to record the antenna pattern and the monitor level. This is followed by installation of the radome and repetition of the test. A complete test covers both horizontal and vertical patterns for representative positions of the antenna.

Figure 14·14 shows schematically the test mockup of a typical aircraft installation. The structure was of wood covered with aluminum

sheet. This was mounted on a secondary turntable attached to the main turntable. The antenna was mounted on a third turntable attached to the mockup structure. United States Navy 30-in. machine-gun mounting rings fitted with handbrakes proved most useful for the second and third turntables. By means of the main and tertiary azimuth motions, patterns could be taken for successive positions of the antenna relative to the radome. The secondary turntable allowed the antenna and the drive from the main turntable to the automatic pattern recorder to be aligned without disturbing the position of the radome. To take a vertical pattern the main platform was tilted about the main elevation axis for various positions of the radome relative to the antenna. Azimuth and elevation patterns could also be taken with the entire assembly above the secondary turntable mounted on its side 90° from the previous position; both could be taken either horizontally or vertically, the choice depending upon the location of adjacent interfering structure.

The development of this test equipment was based partly upon the need for mechanization of the tests in order to simplify the work of conducting them. As the radar program progressed, the practical need for electrical quality in radomes compelled the testing of increasing percentages of production runs. By the end of the war, equipment had been developed at the request of the Air Technical Service Command for testing the transmission of every radome produced. Test data were taken by an Esterline-Angus recording milliammeter as the radome was moved automatically. The entire test required not more than 20 min. Interference in the motions of the turntable and trunnions by the antenna supports necessitated development of a design to keep the antenna aligned regardless of the motions of the radome. This is shown in Fig. 14·15. Transmission of mechanical control to the antenna has to pass along the same axis as the torque that adjusts the position of the radome in elevation. This is accomplished by mounting the standard horn antenna shown in Fig. 14·15 on an axis that coincides with that of the trunnions, from which the supporting radome swings in elevation. By means of a chain drive, the horn is held in a fixed position in space, pointed toward the transmitting antenna. The radome can be moved in azimuth or elevation without disturbing the antenna.

Ordinary mounts for antenna pattern tests proved too weak to handle radomes and mockups. In addition, their angular motions were in steps too large to disclose slight beam deviations. The top carriage[1] of a 40-mm Bofors antiaircraft gun was used and made a satisfactory mount. A servomechanism was used to drive the gun carriage in coordination with the drive of the recording mechanism. Photographs of the radome

[1] Further details of this carriage can be found in *War Department Technical Manuals* 9-252, 9-1252, and 9-1643.

and an aircraft mockup mounted on the modified Bofors carriage are shown in Fig. 14·5.

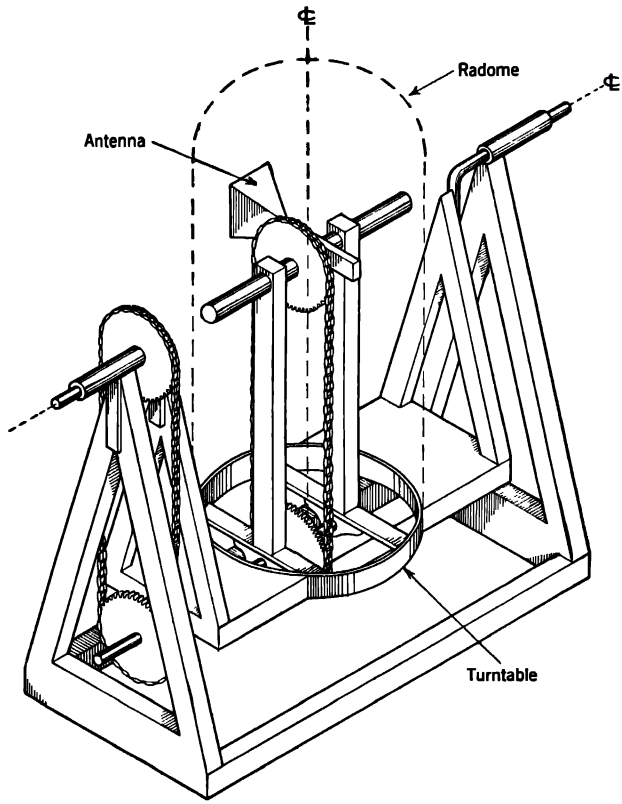

FIG. 14·15.—Design of test mount.

14·8. Procedure in Electrical Test.—The method of using the test equipment that was described in the preceding section will be illustrated by description of the tests that were made on an experimental radome, shown in Fig. 14·16. It was 20 in. deep, 35 in. wide, and 84 in. long and was streamlined back over the doors of the bomb bay to converge to the keel line at 20°. It had to meet difficult aerodynamic and mechanical requirements. The forward section completely enclosed the antenna; it included a transverse after bulkhead for that purpose. The tail section consisted of two fairings, one attached to each door of the bomb bay of the airplane. A pair of metal rods supported the leading edge of each of the fairings. A similar pair were located farther aft. The radome was attached with a mounting strip.

In the course of the tests it was discovered that the pattern was seriously distorted by interference with the main beam by energy diffracted by the following obstacles and discontinuities: (1) the intersection of the transverse bulkhead with the streamlined portion, (2) the thickened leading edge of each tail fairing, and (3) the thickened longitudinal edge of each fairing in the plane at which the fairing joined.

The equipment used to make the pattern tests was that shown in Fig. 14·13. The mockup of the radome and fuselage was arranged as in Fig. 14·14. Some of the elevation patterns taken with the mockup are shown in Fig. 14·17. The pattern of the antenna alone is given in *a*. The pat-

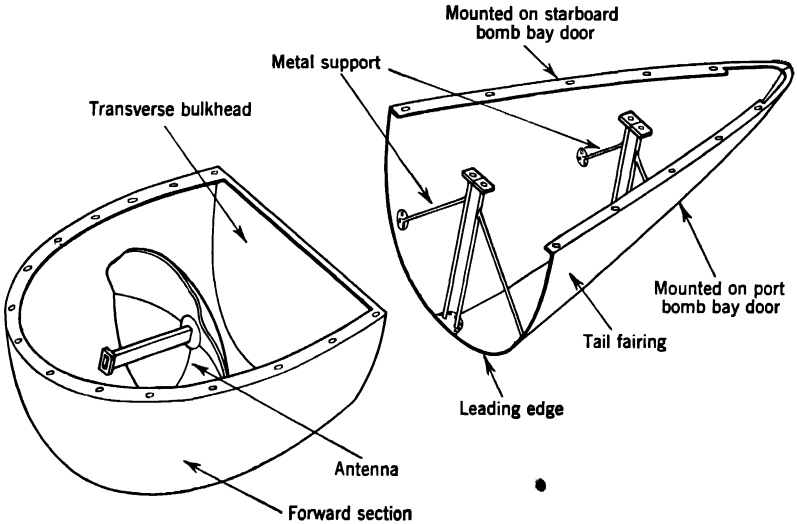

FIG. 14·16.—Experimental radome.

tern at −4° tilt and 180° az, with the antenna mounted in position on the mockup but with no radome, is given in Fig. 14·17*b*. Interference between the mockup and the top of the reflector disturbed the fan beam at angles below 16°. The effect of addition of the forward section of the radome is shown in Fig. 14·17*c*. The gain of the nose of the beam has been reduced 1.2 db. The half-power width and the position of the peak have not been changed. Fluctuations of 7 to 10 db in intensity and 3° in width have appeared near the 20°, 25°, and 30° depression angles, with others about 1.5° wide at greater angles. Using ray optics as an arbitrary guide it was found that much of the flared portion of the pattern converged near the thickened juncture of the transverse radome bulkhead with the streamlined portion of the forward section of the radome. The distortion of the wavefront was interpreted as the result of diffraction at

the edges of the thick part and a change of phase on transmission through it. The 1.5° holes were attributed to interference by diffracted and reflected power returning to the beam after reflection from the fuselage.

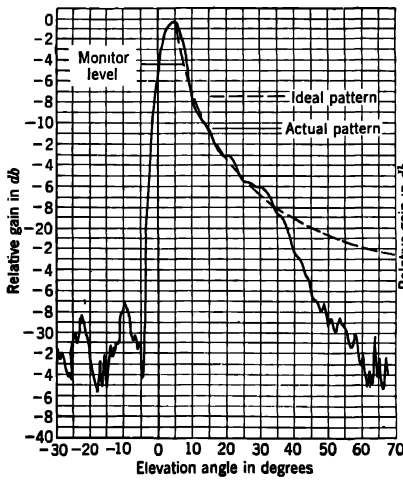

(*a*) Antenna in free space; radome absent.

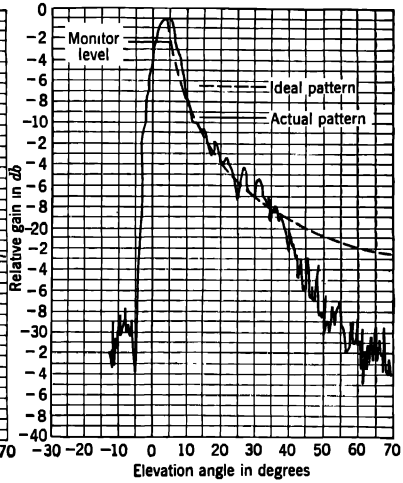

(*b*) Antenna with fuselage; radome absent.

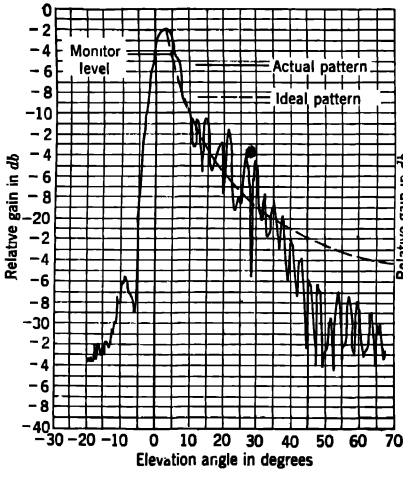

(*c*) Radome, front portion only.

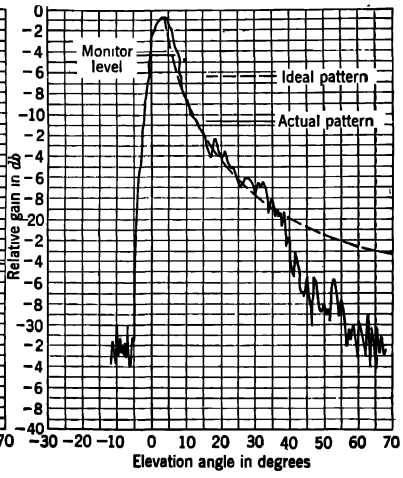

(*d*) Radome absent; braces present.

FIG. 14·17.—Elevation patterns of experimental antenna under various

As expected, the metal braces for the tail fairing had almost no effect (see Fig. 14·17*d*). To obtain this pattern, the forward section of the radome had been removed. When the metal braces were removed and

the tail fairings placed in position, distortions were observed. The peak was reduced by 3.8 db, and its position was directed upward 3°. The half-power beamwidth of the elevation pattern was increased from 6.5°

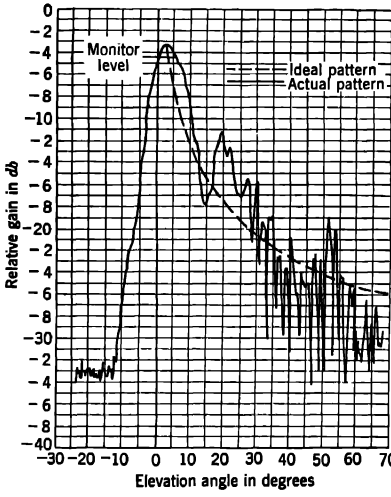

(*e*) Radome absent; fairing pieces in place.

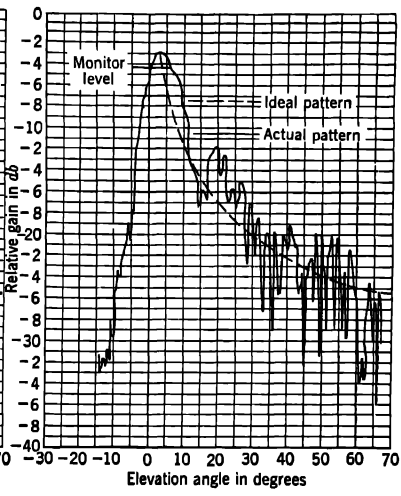

(*f*) Fairing pieces and braces in place.

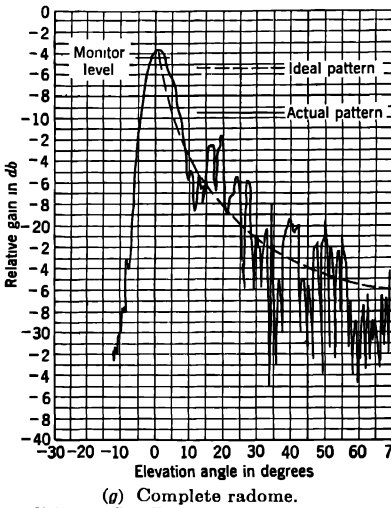

(*g*) Complete radome.

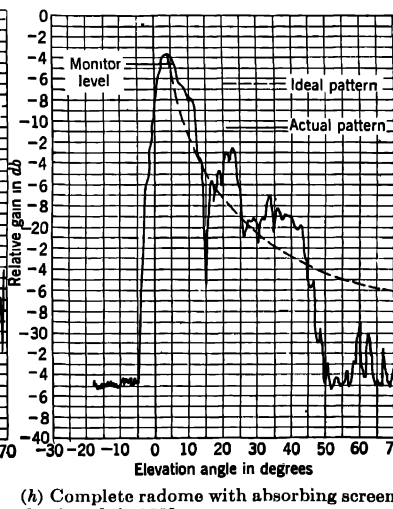

(*h*) Complete radome with absorbing screen.

conditions. In all cases tilt setting is −4° and azimuth is 180°.

to 10°. Fluctuations 5° wide and 7 and 3 db in depth appeared at 15° and 25°, respectively. These were followed at greater depression angles by jagged serrations 1½° wide. The latter were similar in appearance to

the one caused by the discontinuity in the rear of the forward section of the radome. They were thought to have been caused in the same manner, that is, by diffraction and reflection of power to the fuselage, from which it was then reflected into the flared portion of the beam. The diffracted power and some of the reflected power seemed to have come from the thickened leading edge of the fairing pieces. Some of the diffraction must have been caused by the thickening at the longitudinal split. The balance of the reflection to the fuselage was from the sandwich bottom of the fairings at perpendicular polarization. It is believed that the larger holes at 15° and 25° were the combined result of poor transmission through the thickened dielectric of the leading edge of the fairing and diffraction at the discontinuities it formed. The pattern with the completely assembled radome is shown in Fig. 14·17*g*. After an absorbing covering was placed over the fuselage under the tail fairings, the result was as shown in Fig. 14·17*h*. The loss in gain by the peak was not recovered, being accounted for by poor transmission through the longitudinal thickening and the sandwich and by power lost in the absorbing coating. As a result of the nearly complete removal of the fuselage as a cause of reflection, most of the serrations that were 1½° wide were removed, but enormous holes at 15° and 30° remained. Since the absorbing material reflects some power, which varies with angle of incidence, the resultant pattern did not represent the effect of the radome alone without the assistance of the fuselage.

The thickened parts at the corners and edges were about 0.68 thick and varied from 0.4λ to 1.0λ wide. If a loss tangent of 0.018 is assumed, a reflection of 50 per cent in amplitude or 25 per cent in power could be predicted for normal incidence. There would be a phase difference of nearly 0.34λ between the wavefront emerging from the sandwich walls and the portion passing through the thick parts. Considerable disturbance of the wavefront, diffraction, and interference by power reflected to the fuselage could therefore be predicted.

To meet the design requirements of this radome, a modified half-wavelength thickness of a homogeneous material might have adequate strength for use without ribs, stiffeners, or similar sources of diffraction. The weight of the radome would be increased, however.

AN/APQ-13 (60-*in.*) *Radome and Antenna.*—The following is an example of the testing of a radome and antenna that were designed with both electrical and mechanical requirements in mind, as described in Sec. 14·5. A description of the AN/APQ-13 (60-in.) scanning mechanism can be found in Sec. 6·11.

The antenna was installed in an inverted partial mockup of a B-29 airplane. The ordinarily lower edge of the antenna projected upward 4 in. above the surface of the inverted fuselage mockup when it was in the zero azimuth position.

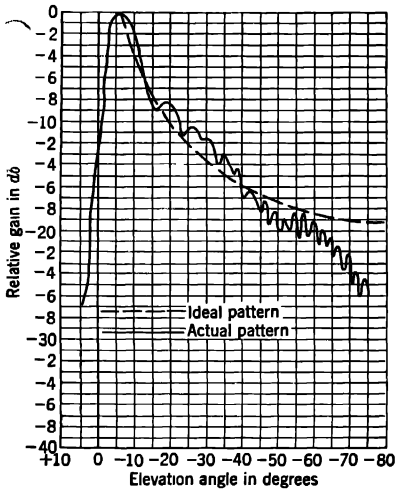

(*a*) Antenna extension 4 in. Radome absent. Tilt setting −6°, azimuth 0°.

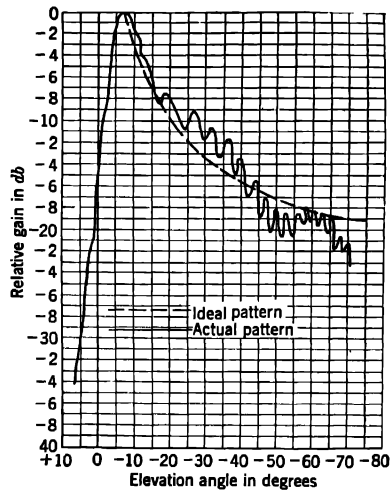

(*b*) Antenna extension 4 in. Radome extension 8 in. Tilt setting −6°, azimuth 0°.

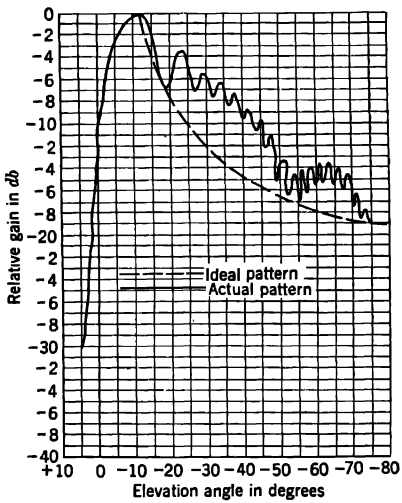

(*c*) Antenna extension 4 in. Radome absent. Tilt setting 0°, azimuth 0°.

FIG. 14·18.—Elevation patterns of 60-in. AN/APQ-13 antenna mockup under various conditions.

Figure 14·18*a*, *b*, and *c* shows three patterns of the AN/APQ-13 (60-in.) antenna. To record Curve *a* the antenna was placed in its −6° downward tilt position. The absolute gain proved to be 29.9 ± 0.2 db; the half-power width in elevation was 7.0°. The fuselage mockup had no effect on the tilt of the nose of the beam.

To record Curve *b*, the radome was added. It projected 8½ in. from the fuselage at its lowest point. The gain dropped 0.7 db, and the half-power width increased 1.0°. A broad bump at 60° was raised a little.

For *c*, the radome was removed and the antenna was tilted upward to the 0° tilt position. This placed a nearly 4-in. vertical section of the ray diagram of the beam within the hole in the aircraft. As a result, the nose of the beam was actually tilted to −12°, the half-power beamwidth increased to 12°, and the absolute gain reduced to 24 ± 1 db. The 1-db hole 7° below the nose of the beam was deepened to 3½ db. On a PPI this would be represented by a loss of maximum range on the zero azimuth heading and a dark area at a depression angle θ of 19°. A broad bump at 60° was raised (*cf.* Figs. 9·16 and 9·17).

14·9. Structural Test Methods and Equipment.—Because of the unusual shapes of radomes the structural design can ordinarily be based only on a rough approximation to the distribution of load and stress. Furthermore, the design is usually based on data taken from small samples that are molded under ideal conditions and may be much better than those actually present in the radome material. The strength of the material in the radome may be only 80 per cent or less of that of the laboratory control panel. In order to check the structural design and the quality of material in the actual radome it is desirable to make loading tests on a full-sized radome.

An attempt is made to approximate the loading that is anticipated under actual flight conditions. This loading may have to be estimated but is preferably the result of tests in a wind tunnel or in flight (see Fig. 14·2). The reliability of the results of the test naturally depends on the degree of the approximation of the test load.

The quantities that are of chief interest are the deflection of the radome at the rated load (when q takes on its maximum value for any condition of flight) and the maximum load that the structure can withstand before failure occurs. The deflection is important because it indicates the stability of the radome as a structure and because the allowed clearance for the motion of the antenna in operation is based on it. The maximum applied load gives the factor of safety (ratio of maximum load to rated load). For aircraft structures the factor of safety should be the smallest that does not jeopardize the safe performance of the airplane.

There are several means of approximating the pressure distribution, and they vary in their demands on special equipment and man power. The simplest is to load the structure or radome with dead weights, usually sand. This method, while involving a minimum of equipment and man power, assumes a uniform pressure distribution having only a vertical component, the side thrust of the sand being negligible. The

method is also limited in that only one type of pressure can be applied at a time, either positive or negative (inward or outward).

A second method is shown in Fig. 14·19. A closer degree of approximation is possible with this testing procedure than with the first. The negative pressure is obtained from an internal hydrostatic pressure, the water being restrained by an oversized rubber bag; the positive pressure is obtained from loading pads. By varying the number of loading pads

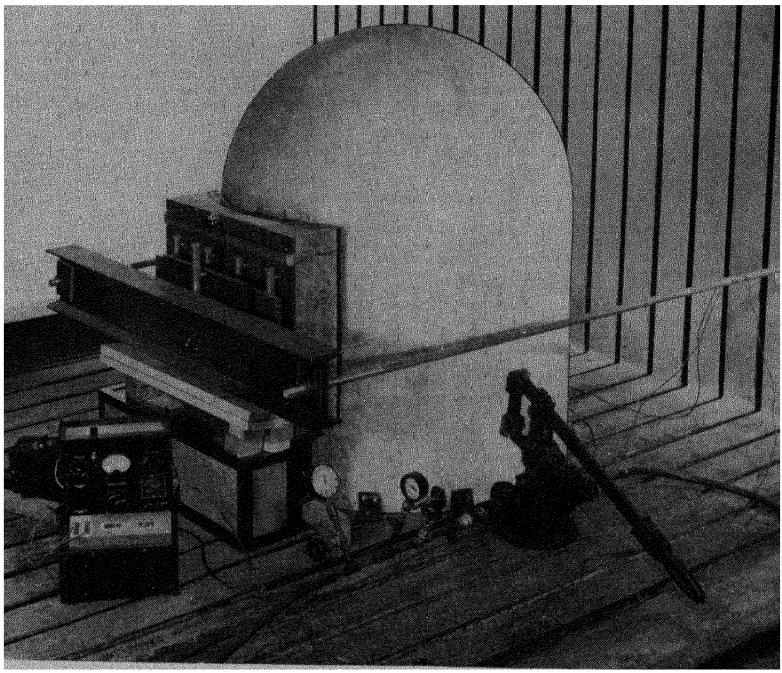

FIG. 14·19.—Structural test on a cylindrical radome.

and their loads, any degree of approximation can be obtained. The actual pressure distribution could be more nearly approached by the addition of a similar set of loading pads mounted directly opposite those shown in Fig. 14·19.

This method has the advantage of requiring very little special equipment and can be worked by one person. For these tests the positive load is measured by means of wire strain gauges mounted on the loading straps; the negative pressure is indicated directly on pressure gauges.

There are, however, two disadvantages to this system. One is that in order to test a radome to failure it is necessary for safety to use either water or oil to obtain the internal pressure; the pressure distribution,

therefore, will not be as indicated on the pressure gauge but will increase linearly with height. The variation in pressure per foot of height for water is 0.44 lb/in.^{2} For a radome that is 40 in. high (*cf.* Fig. 14·19), the pressure at the apex is 1.4 lb/in.^{2} less than that at the base. When the maximum pressure to be applied is small, this variation of pressure is a troublesome complication.

The major disadvantage, however, is that the negative loading is obtained by internal pressure and not by tension on the outer surface. For a homogeneous material this distinction is of little significance, but this method of testing will not disclose the tendency of a sandwich or laminate to come apart.

The third method overcomes these objections. In this procedure the radome is completely covered by loading pads similar to those shown in Fig. 14·19. The pads can be used to apply both negative and positive pressures, depending upon the prevailing load for the area in question. The more numerous and the smaller the loading pads the more nearly the actual distribution of pressure can be approximated. Limitation on man power or equipment limits the smallest practical size of the loading pad to about 6 to 8 in.^{2} In most cases the loading is done manually, the compressive forces being obtained by hydraulic jacks and the tensile forces, by dead weights and pulleys. Fifteen to twenty men are needed for making such a test on a radome of average size. A device has been developed by Lockheed Aircraft Company of Burbank, Calif., in which the pulley systems are replaced by special hydraulic jacks. All jacks, for both tension and compressive loads, are then controlled by a system of valves operated by cams; the load on each pad is thereby increased proportionally throughout the entire test. The apparatus requires only a single operator for the test run. The equipment, however, is expensive and complicated.

14·10. Examples of Structural Tests.—In this section a few typical tests on radomes are discussed.

AN/APG-13 Radome.—It was desired to approximate the loading conditions that this radome would have when mounted in the nose of a B-29 airplane. The pressure distribution was assumed to be that shown in Fig. 14·20. The maximum positive pressure was estimated to be $1.0q_0$ where $q_0 = \frac{1}{2}\rho V^2$, and the maximum negative pressure was equal to $\frac{1}{3}q_0$.

The negative pressure equal to $\frac{1}{3}q_0$ was applied by means of internal pressure; the positive pressure was obtained by means of a hydraulic testing machine. The load of the testing machine was applied through a heavy wooden block hollowed to the contour of the dome and lined with soft sponge rubber.

The failure of this radome occurred at a load equal to $5q_0$ where q_0

was based on a speed of 300 mph. The test setup and fractured radome are shown in Fig. 14·21.

AN/APQ-13 (60-in.) Radome.—For structural tests on this radome it was assumed that the stress was uniformly distributed. The actual distribution was more nearly as shown in Fig. 14·22, the peak pressure (negative) being about 0.5 lb/in.^{2} Deflection readings were taken at the center of the radome.

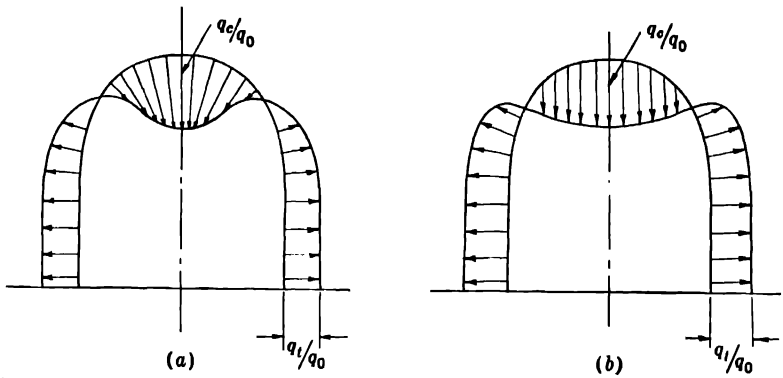

FIG. 14·20.—Load distribution on AN/APG-13 radome. (*a*) Probable distribution in flight; (*b*) probable distribution in structural test.

Test results on a radome whose mounting edge was reinforced with cotton duck were as follows:

Deflection:	
At $\frac{1}{2}$ lb/in.^{2} pressure	0.20 in.
At $5\frac{1}{2}$ lb/in.^{2} pressure	0.75 in.
Maximum applied internal pressure	9 lb/in.^{2}

Failure was due to the shearing of several of the mounting bolts at 9 lb/in.^{2}

A similar radome with a plywood reinforcement in place of the cotton duck showed similar loading characteristics except that failure in the mounting ring of the radome occurred at $7\frac{1}{2}$ lb/in.^{2} caused by shearing of the bolt holes. Both radomes, however, had ample stiffness and strength.

Structural Test of Beacon Housings.—Airborne beacon housings are generally small streamlined cylinders. Some of them are mounted on fighter planes, which often sideslip in the course of intricate maneuvers and cause high side thrusts on the radome. This side thrust considerably exceeds the thrust that is due to forward motion, since both the projected area and the drag coefficient are higher broadside. The bending strength is also weaker in that direction. The beacon housing is therefore tested for sidewise strength and stiffness.

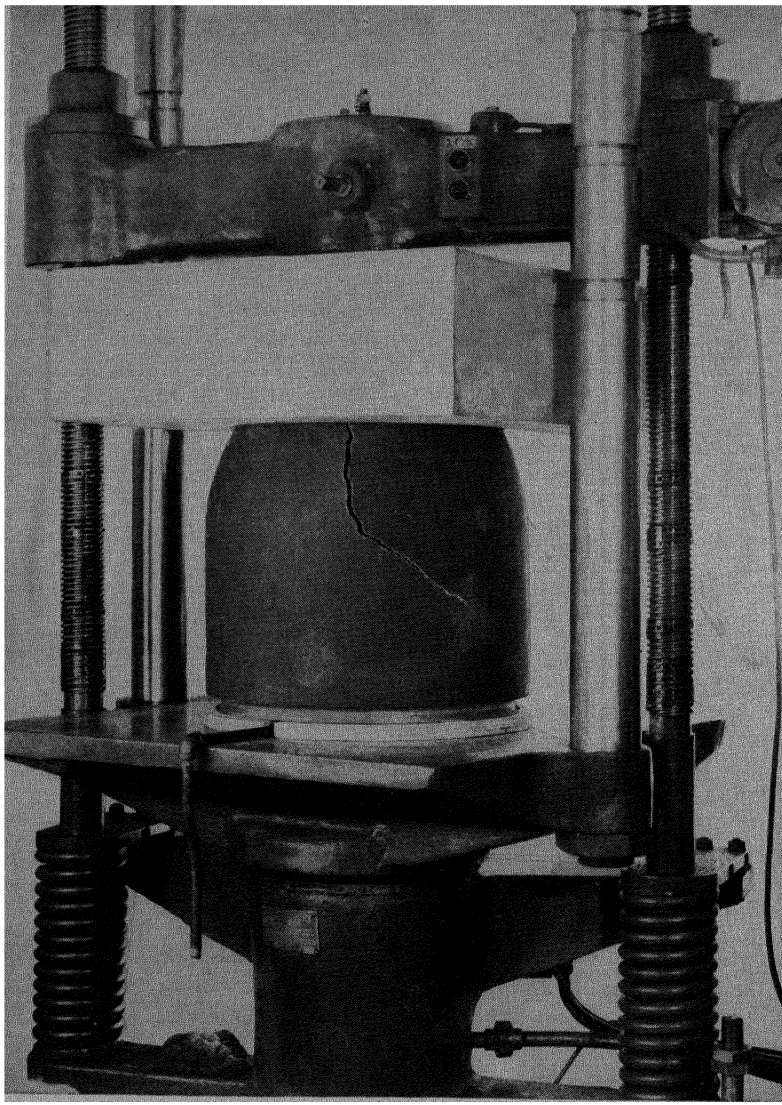

FIG. 14·21.—Structural test on AN/APG-13 radome.

Test on a 10-*cm Beacon Housing.*—This housing was molded of a Fiberglas laminate $\frac{1}{8}$ in. thick. It was 12 in. high, $7\frac{1}{2}$ in. long, and $2\frac{1}{2}$ in. wide, the slenderness ratio being 3. The housing was mounted on a cast-aluminum base so that the unsupported height was 11 in.

The distributed load was obtained by distributing a concentrated load through a system of yokes as shown in Fig. 14·23. The yoke bore on metal strips, 1 by $\frac{1}{4}$ by 12 in., which in turn rested on a cushion of soft

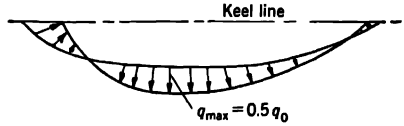

FIG. 14·22.—Distribution of air pressure on AN/APQ-13 60-in. radome.

rubber sponge. The deflection at the tip was measured by means of an Ames dial gauge.

The test results were as follows:

Deflection at 365 lb	0.387 in.
Maximum load	430 lb
Maximum bending moment	2040 in.-lb

The dome failed by buckling on the compression side.

A flat plate with its area equal to that of the lateral projected area of the radome would undergo a force of approximately $0.0015V^2$, where V

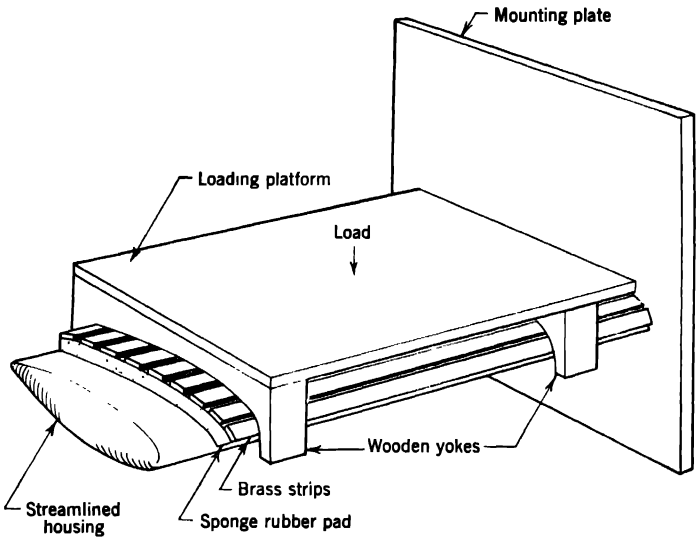

FIG. 14·23.—Structural loading test on 10-cm beacon housing.

is the velocity of the air stream in miles per hour. The velocity of sideslip seldom exceeds half the forward velocity. In order to cause failure due to sideslip, the velocity of sideslip would have to be about 500 mph. Since this velocity is in the order of magnitude of the forward velocity of the plane, the housing has a factor of safety of 2.

DESIGN AND TESTING OF HOUSING FOR BEACON ANTENNAS

14·11. Electrical Design and Testing of Beacon Antennas.—The electrical design of housings for beacon antennas has been a matter of empirical solution. Little difficulty was experienced in the beginning. At first, antennas for the 10-cm band were placed in cylindrical dielectric tubes. Later, streamlined shapes were used but did not distort the azimuth pattern noticeably.

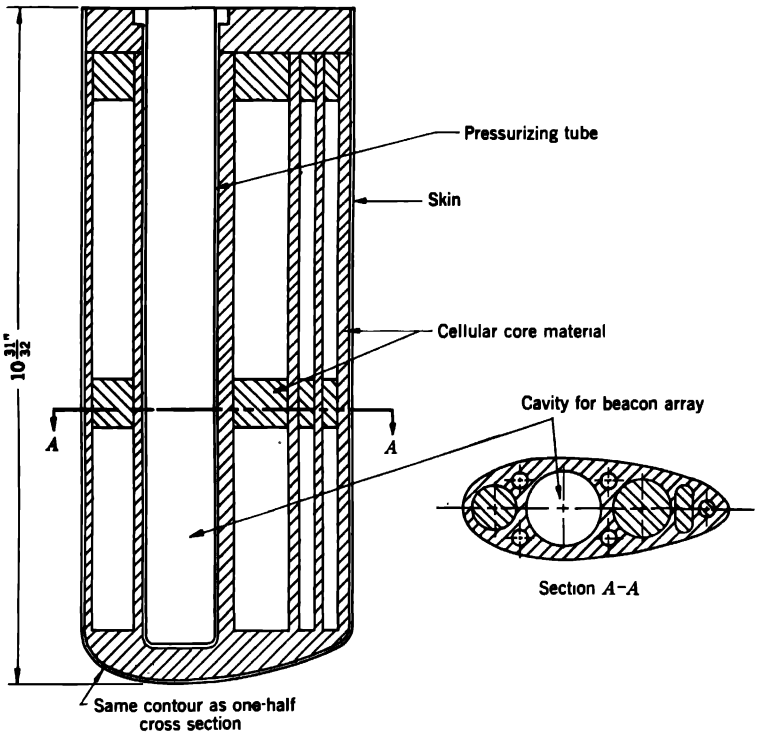

FIG. 14·24.—Radome for 3-cm-band beacon.

Serious difficulty first arose when an attempt was made to enclose the antenna of a beacon for the 3-cm wavelength band in a streamlined housing. The antenna was a horizontally polarized beacon for the 3-cm band, consisting of two slotted six-element linear arrays placed on the same axis. Several housings having a modified half-wave thickness for low reflection over a wide range of angles of incidence distorted the horizontal pattern seriously. So did one having a continually varying modified half-wave thickness intended to give no reflection at any point.

As an empirical solution it was decided to encase the antenna in a streamlined block of foam plastic, covering the exterior with a very thin surface and drilling as many holes in the block as the strength of the housing would permit. The aim was to reduce the amount of dielectric in the path of the circular wavefront, particularly in the streamline tail of the radome. This proved to be a successful solution.

Figure 14·24 is a drawing of this housing. Bakelite resin BRS 16631 was specified to laminate the skin; but since fireproofing was desirable,

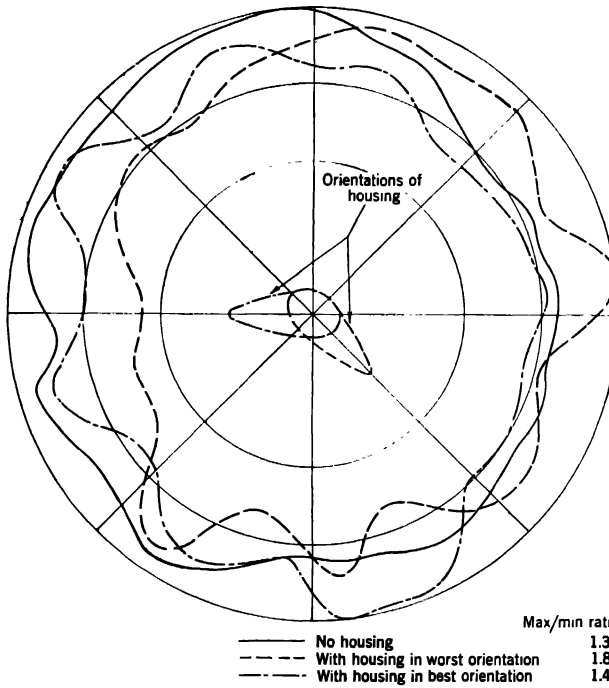

FIG. 14·25.—Pattern of radome for 3-cm beacon.

it was planned to substitute Monsanto Styramic HT, poly 2, 5 dichlorostyrene as soon as molders became accustomed to its use. A brief description of the method of manufacture follows. It proved difficult to use a cellular core material having a dielectric constant greater than 1.2. Sponge Rubber Products 5003P Celltite GR-A hard rubber board was selected as best meeting the electrical and mechanical requirements and being adaptable to the chemistry of plastic manufacture. Vertical holes as shown in Fig. 14·24 were drilled in the cellular block parallel to its faces and to the beacon antenna that was inserted in one hole.

For the molding process to follow, these holes were filled with wooden

dowels. Three layers of ECC-11-112 Fiberglas were then molded to the surfaces of the hard rubber by the single-cycle molding process. The central plastic tube immediately enclosing the antenna was molded around a cellophane-covered rod in two steps. One-half the final necessary thickness of impregnated fabric was molded at one time. The penetration of the resin of the second layer into the air leaks of the first layer served to seal it effectively for pressurizing.

The outer surface of the tube was ground to make it round, and it was then inserted in the streamlined cellular block and cemented. The bottom metal base was cemented to the cellular block and to the Fiberglas laminate skin overlapping it, as follows. The metal and laminate surfaces were first sized with a rigidly setting GR-A phenolic cement and then precured, after which the metal block and the plastic part were cemented together by a cold-setting resorcinol adhesive.

The azimuth patterns of the antenna and radome were measured indoors with the beacon array placed vertically and surrounded by absorbing screens. Elevation patterns were taken outdoors as for other types of antennas and radomes. A pickup was used to determine the field strength in the azimuth or E-plane. Ideally, a constant intensity would be found at all angles. The patterns actually obtained are shown in Fig. 14·25, in which the result without the housing is shown as a solid line; it varies in intensity with azimuth and has a ratio of maximum to minimum of 1.34. The housing was rotated in order to find its best and worst orientations with respect to the pattern of the antenna alone. These results are shown as a broken line having a ratio of maximum to minimum of 1.80 for the worst orientation and as a line with alternating dots and dashes having a ratio of maximum to minimum of 1.46 for the best orientation.

APPENDIX A

FORMULAS FOR STABILIZATION OF SHIP ANTENNAS

By F. E. Swain

The developments that follow are taken from work of H. M. James and represent a portion of his comprehensive study of antenna stabilization and associated problems.

A·1. Deck-tilt Correction; Elevation Order.—The relations for deck-tilt correction and antenna elevation order will be developed for the general problem of a target that is elevated above the horizon. From these relations can be obtained the expressions that are applicable to targets on the horizon. The notation used is as follows:

P = pitch angle of the plane of the deck. It is the angle between the fore-and-aft axis of the ship and the horizontal as measured in a vertical plane. P will here be taken as positive when the bow is down.

R = roll angle of the plane of the deck. It is the angle of rotation about the fore-and-aft axis in its pitched position. In general, it is not measured in a vertical plane. R will here be taken as positive when the deck is down on the port side.

α = relative bearing angle of the radar beam (measured clockwise in a horizontal plane).

α' = train order required for beam (measured clockwise in the plane of the deck).

β = true elevation angle of target (measured in a vertical plane).

β' = elevation order required for beam (measured in a plane normal to the deck and passing through the target).

The derivation of the desired expressions may be attacked by a consideration of the unit sphere shown in Fig. A·1. As shown on the diagram, GH represents a horizontal plane passing through the origin and center of the sphere O, while $JEKCF$ represents the deck plane of the ship, which also passes through the origin. The line CE is the fore-and-aft axis of the ship, and a vertical plane through this axis will intersect the unit sphere in a great circle of which the arc ABC is a part. The length of arc BC, which extends from the horizontal plane to the point of intersection of the fore-and-aft axis with the unit sphere, is equal to the pitch angle P. A plane normal to the deck, passing through the origin O

and perpendicular to the fore-and-aft axis, will intersect the unit sphere in a great circle of which the arc MWV is a part. The length of the arc WV, which extends from the plane of the deck to the horizontal plane, is equal to the roll angle R.

The arc ATD is a part of the great circle formed by the intersection of the unit sphere and a vertical plane passing through the origin O and the target T. The length of the arc DT, which extends from the horizontal plane to the target point T, is equal to the true elevation angle β of the

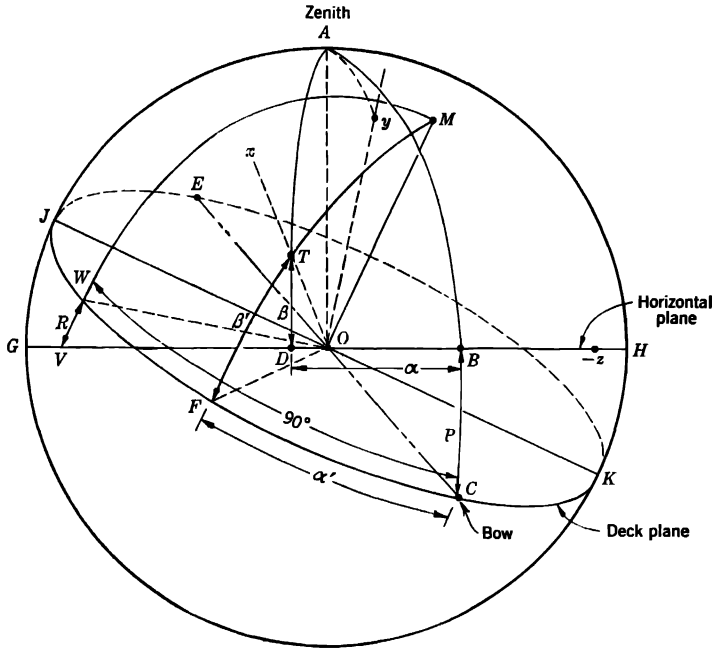

FIG. A·1.—Unit sphere showing various stabilization angles.

target above the horizon. The length of the arc BD, which is a portion of a great circle in the horizontal plane, is equal to the relative bearing angle α of the target. A plane that passes through points O and T and is normal to the deck plane will intersect the unit sphere in a great circle of which the arc MTF is a part. The length of the arc FT, which extends from the deck plane to the target point, is equal to the elevation order β' of the target. The length of the arc CF, which is a portion of a great circle in the deck plane, is equal to the train order α' of the target.

It is desired to determine the values of the angles α' and β' in terms of the given angles α, β, R, and P. The relations among these quantities can be determined by the use of a reference vector and a sequence of six

rotations of a given right-hand rectangular coordinate system. Let the x-axis of the original system lie along the line of sight to the target OT; the y-axis in the same vertical plane, intersecting the unit sphere in a point beyond the zenith; and the z-axis in the horizontal plane. The position of these initial axes is shown in Fig. A·1. For convenience, the intersection of the $-z$-axis with the unit sphere has been shown, rather than that of the z-axis, since the latter axis intersects the rear portion of the sphere. The fixed reference vector is taken to have a magnitude of unity and is assumed to lie along the initial x-axis and line of sight OT. The components of the reference vector in the initial coordinate system are thus

$$\left.\begin{aligned} x &= 1, \\ y &= 0, \\ z &= 0. \end{aligned}\right\} \tag{A·1}$$

Now let the original xyz-coordinate system be carried into a second $x'y'z'$-coordinate system by rotating the x- and y-axes about the z-axis through an angle $-\beta$ until the x'-axis lies along the horizontal line OD and the y'-axis lies along the vertical line OA. The components of the reference vector in this new coordinate system are

$$\left.\begin{aligned} x' &= \cos\beta, \\ y' &= \sin\beta, \\ z' &= 0. \end{aligned}\right\} \tag{A·2}$$

The $x'y'z'$-coordinate system is next carried into the $x''y''z''$-coordinate system by rotating the x'- and z'-axes about the vertical y'-axis through an angle α until the x''-axis lies along the line OB. The components of the reference vector in the second coordinate system are

$$\left.\begin{aligned} x'' &= \cos\beta\cos\alpha, \\ y'' &= \sin\beta, \\ z'' &= \cos\beta\sin\alpha. \end{aligned}\right\} \tag{A·3}$$

The third rotation of the coordinate system, carrying the x''-, y''-, and z''-axes into the x'''-, y'''-, and z'''-axes, involves a rotation[1] about the horizontal z''-axis through the angle $-P$ until the x'''-axis lies along the line OC which is a part of the fore-and-aft axis of the ship. The y'''-axis will then be perpendicular to the fore-and-aft axis and in a vertical plane. The components of the reference vector in this new coordinate system are

[1] In this treatment the signs of the angles of rotation of axes are taken as follows: A positive rotation about the z-axis is one that moves the x-axis most directly toward the former position of the y-axis; that is, it turns the x-axis into the y-axis. Positive rotation about x turns y into z; positive rotation about y turns z into x.

$$\left.\begin{aligned} x''' &= \cos\beta\cos\alpha\cos P - \sin\beta\sin P, \\ y''' &= \cos\beta\cos\alpha\sin P + \sin\beta\cos P, \\ z''' &= \cos\beta\sin\alpha. \end{aligned}\right\} \tag{A·4}$$

The fourth rotation of the coordinate system is a rotation about the fore-and-aft x'''-axis through the angle $-R$ from the z'''-axis toward the y'''-axis. The components of the reference vector in this new coordinate system are

$$\left.\begin{aligned} x^{iv} &= \cos\beta\cos\alpha\cos P - \sin\beta\sin P, \\ y^{iv} &= -\cos\beta\sin\alpha\sin R \\ &\quad + (\cos\beta\cos\alpha\sin P + \sin\beta\cos P)\cos R, \\ z^{iv} &= \cos\beta\sin\alpha\cos R \\ &\quad + (\cos\beta\cos\alpha\sin P + \sin\beta\cos P)\sin R. \end{aligned}\right\} \tag{A·5}$$

These relations give the components of the reference vector in a coordinate system fixed in the ship, the x^{iv}- and z^{iv}-axes lying in the deck plane with the x^{iv}-axis pointing forward along the fore-and-aft axis of the ship. The y^{iv}-axis is directed generally upward, normal to the plane of the deck, and lies along the line OM. Thus, all of the known angles α, β, P, and R have been utilized.

The first of the unknown angles α' is now introduced. The $x^{iv}y^{iv}z^{iv}$-coordinate system is carried into the $x^{v}y^{v}z^{v}$-system by rotating the former about its y^{iv}-axis through the angle $-\alpha'$ from the x^{iv}-axis toward the z^{iv}-axis[1] until the x^{v}-axis lies in the plane that is normal to the deck and includes the reference vector. The reference vector thus lies in the $x^{v}y^{v}$-plane and its z^{v}-component is zero. The components of the reference vector in the new coordinate system become

$$\left.\begin{aligned} x^{v} &= x^{iv}\cos\alpha' + z^{iv}\sin\alpha', \\ y^{v} &= y^{iv}, \\ z^{v} &= z^{iv}\cos\alpha' - x^{iv}\sin\alpha' = 0. \end{aligned}\right\} \tag{A·6}$$

Since $z^{v} = 0$, α' can be determined at once in terms of the known angles α, β, P, and R from the third of Eqs. (A·6),

$$\tan\alpha' = \frac{z^{iv}}{x^{iv}}, \tag{A·7}$$

or

$$\tan\alpha' = \frac{\cos\beta\sin\alpha\cos R + (\cos\beta\cos\alpha\sin P + \sin\beta\cos P)\sin R}{\cos\beta\cos\alpha\cos P - \sin\beta\sin P}. \tag{A·8}$$

As the final step, the $x^{v}y^{v}z^{v}$-coordinate system is rotated about the z^{v}-axis through the angle β' until the x^{vi}-axis of the new $x^{vi}y^{vi}z^{vi}$-system lies

[1] It should be noted that a positive bearing angle α', corresponding to a clockwise displacement from the fore-and-aft line as is customary on shipboard, is a negative angle in the right-hand coordinate system that is used here.

along the original reference vector and the y^{vi}-component of the vector is zero. The components of the reference vector in this coordinate system are

$$\left.\begin{aligned} x^{i} &= x^{v}\cos\beta' + y^{v}\sin\beta' = 1, \\ y^{vi} &= -x^{v}\sin\beta' + y^{v}\cos\beta' = 0, \\ z^{vi} &= z^{v} = 0. \end{aligned}\right\} \tag{A·9}$$

From the second of Eqs. (A·9) we have

$$\tan\beta' = \frac{y^{v}}{x^{v}} = \frac{y^{v}}{[1-(y^{v})^{2}]^{\frac{1}{2}}}, \tag{A·10}$$

since the sum of squares of the components of the reference vector in any system must be equal to 1. From Eq. (A·10) or from the geometry of the system (remembering that $z^{v} = 0$), it is seen that

$$\sin\beta' = y^{v}, \tag{A·11}$$

or

$$\sin\beta' = (\cos\beta\cos\alpha\sin P + \sin\beta\cos P)\cos R - \cos\beta\sin\alpha\sin R. \tag{A·12}$$

Equations (A·8) and (A·12), then, give the desired expressions for the train order angle α' and the elevation order angle β' for a target elevated above the horizon by an angle β and at a relative bearing angle of α in terms of the known angles α, β, R, and P.

Since the angle α' is measured in the deck plane and the angle β' is measured in a plane normal to the deck plane, the relations given in Eqs. (A·8) and (A·12) can be used to compute deck-tilt correction and elevation orders required for one-axis and two-axis pedestals. The one-axis pedestal, which has a train axis only, does not require the computation of any elevation orders and is intended for use with surface targets only. The deck-tilt correction for this type of mount can be obtained using Eq. (A·8) with the angle β equal to zero. For this condition we have

$$\tan\alpha' = \frac{\sin\alpha\cos R + \cos\alpha\sin P\sin R}{\cos\alpha\cos P}. \tag{A·13}$$

An expression for the deck-tilt correction angle $(\alpha' - \alpha)$ can be obtained by using Eq. (A·13) and the trigonometric relation for the tangent of the difference of two angles

$$\tan(\alpha' - \alpha) = \frac{\cos^{2}\alpha\sin R\sin P + \sin\alpha\cos\alpha(\cos R - \cos P)}{\sin^{2}\alpha\cos R + \sin\alpha\cos\alpha\sin R\sin P + \cos^{2}\alpha\cos P}. \tag{A·14}$$

Equation (A·14) represents an expression for the deck-tilt correction angle $(\alpha' - \alpha)$ for a one-axis mount used for surface targets only.

The train order angle α' for a two-axis mount dealing with a target at an elevation angle β above the horizon is given directly by Eq. (A·8). If the numerator and denominator of the right-hand member of the equation are divided by cos β, the following expression results:

$$\tan \alpha' = \frac{\sin \alpha \cos R + (\cos \alpha \sin P + \tan \beta \cos P) \sin R}{\cos \alpha \cos P - \tan \beta \sin P}. \quad \text{(A·15)}$$

The elevation order angle β' required for a two-axis mount dealing with surface targets only can be obtained from Eq. (A·12) by setting

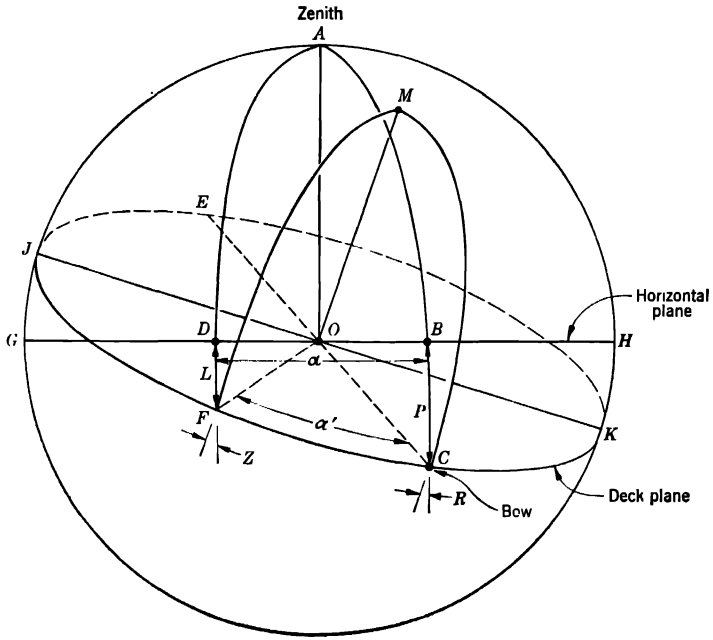

FIG. A·2.—Unit sphere showing relationship between α, α', P, R, L, and Z.

angle β equal to zero. When this is done, we obtain

$$\sin \beta' = \cos \alpha \sin P \cos R - \sin \alpha \sin R. \quad \text{(A·16)}$$

For a two-axis pedestal, where the center of the antenna beam is to be elevated to a target above the horizon by an angle β, the elevation order β' can be obtained from Eq. (A·12) directly.

A·2. Level and Cross-level Angles.—The expressions for the level and cross-level angles in terms of the known angles of roll R, pitch P, and relative bearing α or train order α', can be derived in a manner similar to that used previously for the deck-tilt correction and antenna

elevation order by a consideration of Fig. A·2, in which the following additional notation is used:

L = level angle (measured in a vertical plane),
Z = cross-level angle (measured in a plane normal to the plane of the deck).

Relations Where Train Order α' Is Available.—The right-hand xyz-coordinate system is first taken so that the x- and z-axes lie in the horizontal plane with the x-axis directed forward along a projection of the fore-and-aft axis of the ship. The y-axis is taken to be vertical. The unit reference vector is also taken to be vertical and the components of this vector in the initial coordinate system are

$$\left.\begin{aligned} x &= 0, \\ y &= 1, \\ z &= 0. \end{aligned}\right\} \tag{A·17}$$

If the original coordinate system is rotated about the z-axis through an angle $-P$ from the y-axis toward the x-axis, the reference vector will have the following components in the new system:

$$\left.\begin{aligned} x' &= -\sin P, \\ y' &= \cos P, \\ z' &= 0. \end{aligned}\right\} \tag{A·18}$$

The x'-axis is the fore-and-aft axis of the ship, and the y'-axis is directed upward, normal to the fore-and-aft axis, that is, in the vertical plane.

A second rotation about the x'-axis through an angle $-R$ from the z'-axis toward the y'-axis will bring the z'-axis to z'' in the deck plane. The y''-axis will be upward, normal to the deck. The components for the reference vector are

$$\left.\begin{aligned} x'' &= -\sin P, \\ y'' &= \cos P \cos R, \\ z'' &= \cos P \sin R. \end{aligned}\right\} \tag{A·19}$$

The x''- and z''-axes now lie in the plane of the deck. A third rotation about the y''-axis through an angle $-\alpha'$ from the x''-axis toward the z''-axis will produce the following components for the reference vector:

$$\left.\begin{aligned} x''' &= \cos P \sin R \sin \alpha' - \sin P \cos \alpha', \\ y''' &= \cos P \cos R, \\ z''' &= \cos P \sin R \cos \alpha' + \sin P \sin \alpha'. \end{aligned}\right\} \tag{A·20}$$

The desired cross-level angle Z is now the rotation about the x'''-axis, from the y'''-axis toward the z'''-axis, that will bring the $x'''y'''$-plane into coincidence with a vertical plane and make the z^{iv}-axis horizontal; thus the z^{iv}-component of the reference vector vanishes. This rotation about

the x'''-axis through the angle Z will produce the following components for the reference vector:

$$\left.\begin{aligned} x^{iv} &= \cos P \sin R \sin \alpha' - \sin P \cos \alpha', \\ y^{iv} &= y''' \cos Z + z''' \sin Z, \\ z^{iv} &= z''' \cos Z - y''' \sin Z = 0. \end{aligned}\right\} \tag{A·21}$$

It is seen that

$$\tan Z = \frac{z'''}{y'''}, \tag{A·22}$$

or

$$\tan Z = \frac{\cos P \sin R \cos \alpha' + \sin P \sin \alpha'}{\cos P \cos R}, \tag{A·23}$$

which may be reduced to

$$\tan Z = \tan R \cos \alpha' + \tan P \sec R \sin \alpha'. \tag{A·24}$$

Finally, a rotation of the coordinate system about the z^{iv}-axis, through the level angle L from the x^{iv}-axis toward the y^{iv}-axis, will make the x^{iv}-axis horizontal and the x^{iv}-component of the reference vector equal to zero. The reference vector will have the following components in the new coordinate system:

$$\left.\begin{aligned} x^{v} &= x^{iv} \cos L + y^{iv} \sin L = 0, \\ y^{v} &= y^{iv} \cos L - x^{iv} \sin L = 1, \\ z^{v} &= z^{iv} = 0. \end{aligned}\right\} \tag{A·25}$$

From the first of Eqs. (A·25) we find

$$\tan L = -\frac{x^{iv}}{y^{iv}} = -\frac{x^{iv}}{[1 - (x^{iv})^2]^{1/2}}, \tag{A·26}$$

or

$$\sin L = -x^{iv}. \tag{A·27}$$

Substituting in Eq. (A·27) we have

$$\sin L = \sin P \cos \alpha' - \cos P \sin R \sin \alpha'. \tag{A·28}$$

The converse of Eqs. (A·24) and (A·28), giving the values of the roll angle R and the pitch angle P in terms of the level angle L, the cross-level angle Z, and the train order α', can also be obtained by reference to Fig. A·2. The initial coordinate system is chosen so that the x- and z-axes lie in the horizontal plane with the x-axis being directed along the line OD from O to D. The y-axis and reference vector are taken to lie along the vertical line OA with the positive direction being from O toward A. Successive rotations of the coordinate system about the z-axis through the angle $-L$ from the y-axis toward the x-axis and about the x'-axis through the angle $-Z$ from the z'-axis toward the y'-axis will bring the

x''- and z''-axes into the plane of the deck. A third rotation about the y''-axis through the angle $+\alpha'$ from the z''-axis toward the x''-axis will make the x'''-axis lie along the line OC. Expressions for the angles R and P can now be obtained, through a method similar to that used to obtain the values for L and Z in the preceding derivation, by successive rotations of the coordinate system through the R and P angles. By comparing the successive transformations, it will be seen that the expressions for R and P can be obtained from Eqs. (A·24) and (A·28) by interchanging P and L, R and Z and substituting $-\alpha'$ for α'. Making these changes, we have

$$\tan R = \tan Z \cos \alpha' - \tan L \sec Z \sin \alpha', \tag{A·29}$$

and

$$\sin P = \sin L \cos \alpha' + \cos L \sin Z \sin \alpha'. \tag{A·30}$$

Relations Where Relative Bearing Angle α Is Available.—The xyz-coordinate system is now taken so that the x- and z-axes lie in the plane of the deck with the x-axis being directed forward along the fore-and-aft axis of the ship, which is the line OC in Fig. A·2. The y-axis is normal to the plane of the deck and lies along the line OM. The z-axis points to the starboard beam. The reference vector is also taken to lie along the line OM so that the components of this vector in the initial coordinate system are

$$\left.\begin{aligned} x &= 0, \\ y &= 1, \\ z &= 0. \end{aligned}\right\} \tag{A·31}$$

The coordinate system is now rotated about the x-axis through the angle R from the y-axis toward the z-axis. In this new system, the reference vector has the following components:

$$\left.\begin{aligned} x' &= 0, \\ y' &= \cos R, \\ z' &= -\sin R. \end{aligned}\right\} \tag{A·32}$$

A second rotation about the z'-axis through the angle P from the x'-axis toward the y'-axis will cause the reference vector to have the following components in the new system:

$$\left.\begin{aligned} x'' &= \cos R \sin P, \\ y'' &= \cos P \cos R, \\ z'' &= -\sin R. \end{aligned}\right\} \tag{A·33}$$

A third rotation about the vertical y''-axis through the angle $-\alpha$ from the x''-axis toward the z''-axis will produce the following components of

the reference vector:

$$\left.\begin{aligned} x''' &= \cos R \sin P \cos \alpha - \sin R \sin \alpha. \\ y''' &= \cos P \cos R, \\ z''' &= -\cos R \sin P \sin \alpha - \sin R \cos \alpha. \end{aligned}\right\} \tag{A·34}$$

The x'''-axis now lies along the line OD, and the y'''-axis along the line OA.

A fourth rotation of the coordinate system about the horizontal z'''-axis through the angle $-L$ from the y'''-axis toward the x'''-axis will produce the following components in the new system:

$$\left.\begin{aligned} x^{iv} &= x''' \cos L - y''' \sin L = 0, \\ y^{iv} &= y''' \cos L + x''' \sin L, \\ z^{iv} &= z'''. \end{aligned}\right\} \tag{A·35}$$

From the first of Eqs. (A·35) we obtain

$$\tan L = \frac{x'''}{y'''}, \tag{A·36}$$

or

$$\tan L = \frac{\cos R \sin P \cos \alpha - \sin R \sin \alpha}{\cos P \cos R}, \tag{A·37}$$

which reduces to

$$\tan L = \tan P \cos \alpha - \tan R \sec P \sin \alpha. \tag{A·38}$$

From the geometry of the figure, we see that

$$\sin Z = -\frac{z^{iv}}{1} = -z''', \tag{A·39}$$

or, by Eq. (A·34)

$$\sin Z = \sin R \cos \alpha + \cos R \sin P \sin \alpha. \tag{A·40}$$

The converse of Eqs. (A·40) and (A·38), giving the values of the roll angle R and the pitch angle P in terms of the level angle L, cross-level angle Z, and relative bearing angle α, can be determined by the method outlined in the previous transformation. The desired equations can be obtained by interchanging P and L, R and Z and substituting $-\alpha$ for α. When these substitutions are made, the following relations are obtained:

$$\sin R = \sin Z \cos \alpha - \cos Z \sin L \sin \alpha, \tag{A·41}$$

and

$$\tan P = \tan L \cos \alpha + \tan Z \sec L \sin \alpha. \tag{A·42}$$

GLOSSARY

Most of the following terms occur repeatedly in the text with recondite meanings or with meanings that they have only recently acquired. The definitions have no claim to completeness; rather, they explain only the usages peculiar to the present volume. Terms in small capital letters are defined elsewhere in the glossary.

AFC.—See AUTOMATIC FREQUENCY CONTROL.

amplitude reflection coefficient.—The ratio of the amplitudes of the electric vectors in PLANE WAVES reflected from a plane surface. It is usually a complex number that expresses relations of both amplitude and phase.

angle of incidence.—The angle between a ray and the normal to a surface that it intersects. See PLANE OF INCIDENCE.

antenna.—A unit that converts guided waves into free-space waves, or vice versa. It often includes both a FEED and a REFLECTOR.

antenna elevation.—(1) (Three-axis mount, Type 1, and four-axis mount, Fig. 4·1.) The angle between the deck and the LINE OF SIGHT, measured upward from the deck in the vertical plane through the line of sight. (2) (Two-axis mount, Type 1, and three-axis mount, Type 2.) The angle between the deck and the line of sight, measured upward from the deck in the plane perpendicular to the deck through the line of sight.

antenna mount.—The assembly that produces a scanning BEAM of radiant energy. It includes the ANTENNA, the PEDESTAL, and any other radar or electronic equipment located on the antenna or pedestal. The term "antenna mount" is commonly used in connection with SURFACE-BASED radar, and the term SCANNER with airborne radar.

antenna train.—(1) (Three-axis mount Types 1 and 4, and four-axis mount, Fig. 4·1.) The angle between the fore-and-aft axis of own ship and the vertical plane through the LINE OF SIGHT, measured in the deck plane clockwise from the bow. (2) (One-axis mount, two-axis mount Type 1, and three-axis mount Type 2). The angle between the fore-and-aft axis of own ship and the plane through the line of sight perpendicular to the deck, measured in the deck plane clockwise from the bow.

asymmetrical sandwich radome.—A SANDWICH RADOME whose two skins differ in thickness or material.

attack, angle of.—The angle between the horizontal and the fore-and-aft axis of the fuselage or fuselage reference line, in an airplane flying at a constant altitude. It is positive if the airplane is high at the nose.

automatic frequency control.—AFC. A device providing continuous automatic adjustment to the tuning of the local oscillator of a radar receiver so as to maintain a constant beat frequency between the local oscillator and the transmitting tube.

axis.—(1) A line about which rotation takes place. (2) One of the torque tubes of an ANTENNA MOUNT.

azimuth.—See RELATIVE AZIMUTH ANGLE, TRUE AZIMUTH ANGLE.

azimuth plane.—The horizontal plane.

bank.—An airplane maneuver in which one wing is higher than the other and the direction of flight is changing.

base.—The part of the PEDESTAL that is rigidly fixed to the ground or to the structure carrying the radar system.

beacon.—A device that transmits a characteristic pulsed reply signal immediately upon receiving an interrogating pulse from a radar set.

beam.—The concentration of radiation transmitted by a directional ANTENNA.

beamwidth.—The angular separation between the two directions to the right and left of the NOSE of the BEAM, at which the GAIN is one-half that at the nose. This is the beamwidth in AZIMUTH or in the horizontal plane; beamwidth is also measured in ELEVATION or in the vertical plane, or in an inclined plane.

bearing.—(1) The support for a rotating member. (2) See RELATIVE TARGET BEARING and TRUE TARGET BEARING.

beavertail beam.—A FAN BEAM that is rather wide in AZIMUTH but narrow in elevation.

bolometer.—A device for measuring power. It consists of an electrical resistor that becomes heated by the absorption of the power and accordingly increases in resistance. The increment in resistance is nearly proportional to the power absorbed. In MICROWAVE work the bolometer is usually attached to a TRANSMISSION LINE and absorbs R-F power.

Brewster's angle.—The ANGLE OF INCIDENCE at which the reflection of PARALLEL-POLARIZED radiation at the interface between two dielectric media equals zero.

cellular hard rubber.—A foam (expanded) hard rubber used for RADOME construction. Each cell is watertight.

choke.—In MICROWAVE technique, commonly a groove approximately one-quarter wavelength deep in a metal surface, which prevents the escape of microwave energy. See FLANGE.

circular scan.—A SCAN in which the BEAM revolves continually around a vertical axis.

coaxial transmission line.—A TRANSMISSION LINE consisting of a metal rod or tube supported concentrically inside a metal tube.

conical scan.—A SCAN widely used in TRACKING, in which the axis of a PENCIL BEAM rapidly and continuously generates a circular cone about an axis directed toward the target.

cosecant-squared beam.—A BEAM that is narow in AZIMUTH and wide in ELEVATION. The NOSE of the beam is usually nearly horizontal, and the GAIN at other elevations varies approximately as the square of the cosecant of the angle from the horizon.

course.—(1) The angle between the north and south vertical plane and the vertical plane through an airplane's path, measured in a horizontal plane clockwise from north. (2) See OWN SHIP'S COURSE.

cross-level angle.—The angle, measured about the axis given by the intersection of the deck plane with the vertical plane through the LINE OF SIGHT, between this vertical plane and a plane perpendicular to the deck through this axis. It is positive if the right-hand side of the deck is above the horizontal plane as one faces the target.

cross-linking.—Interconnection of molecular chains in a high POLYMER.

cross-traverse angle.—The angle, measured about the LINE OF SIGHT, between the vertical plane through the line of sight and the plane perpendicular to the deck through the line of sight. It is positive if the right-hand side of the deck is above the horizontal plane as one faces the target.

data stabilization.—The intentional rotation or distortion of the DISPLAY in such a way as to compensate automatically for changes in the location or angular position of the ship or airplane carrying the radar.

data transmission.—The technique of signaling to the radar operator the angular position of the BEAM.

depression angle.—The negative of the ELEVATION angle.

dielectric.—A material having negligible electrical conductivity.

dielectric constant.—The quantity ϵ in the expression $F = qq'/\epsilon d^2$, where F is the force between point charges q and q' at a distance d apart. The numerical value of ϵ depends on the system of units and on the medium. It is also called the permittivity. See SPECIFIC DIELECTRIC CONSTANT, LOW DIELECTRIC CONSTANT MATERIAL, and HIGH DIELECTRIC CONSTANT MATERIAL.

dipole.—A simple form of ANTENNA approximately one-half wavelength in width.

dish.—A paraboloidal REFLECTOR.

display.—The information visually presented to the radar operator by means of a cathode-ray tube or by dials.

ditching load.—The impact load on the airplane or radome during a forced landing on water.

double-wall radome.—A radome composed of two dielectric sheets separated by an air space.

drag.—The component of the total air force on a body, that is parallel to the direction of flight.

electrical area of a radome.—The portion of the RADOME wall through which energy is to be transmitted.

electrical scanner.—A SCANNER in which the scanning is accomplished without motion of the ANTENNA as a whole. Scanners in which the scanning is the result of the relative motion of a point FEED and a REFLECTOR are, however, not commonly included.

electrical thickness.—The actual thickness of a homogeneous DIELECTRIC slab, multiplied by the ratio of the wavelength in free space to the wavelength of the same radiation in the slab. It is often expressed in terms of the wavelength in the dielectric.

elevation.—See TARGET ELEVATION and ANTENNA ELEVATION.

error signal.—(1) The signal, usually a voltage, applied to the controller of a SERVOMECHANISM, that indicates the misalignment between the controlling and the controlled members. (2) In a TRACKING radar, a voltage depending upon the SIGNAL received from the TARGET, which in sign and magnitude depends on the angle between the target and the center of the scan. In CONICAL SCANNING there are separate error signals for ELEVATION and AZIMUTH.

E-vector.—The vector representing the electric field of an electromagnetic WAVE. In free space it is perpendicular to the direction of propagation. See H-VECTOR.

fairing.—A streamlined surface on an airplane introduced to reduce aerodynamic resistance, commonly employed beside or behind a RADOME.

fan beam.—A BEAM whose PATTERN is broad in one dimension and narrow in the other.

feed.—The termination and immediately adjacent portion of the TRANSMISSION LINE. The R-F energy radiated from the ANTENNA FEED falls directly on the REFLECTOR. The feed may be a point source or a line source of waves.

Fiber A.—A synthetic organic fiber or yarn made by the Dupont Company.

Fiberglas.—Glass fibers or cloth woven from glass yarn, manufactured by the Owens-Corning Fiberglas Corporation.

flange.—A coupling flange at the end of a section of WAVEGUIDE. It may be a CHOKE

flange, in the flat surface of which is a circular choke groove, or it may be a plain or blank flange, intended to mate with a corresponding choke flange.

flexural stiffness.—An index of the resistance of a member to deflection due to bending. It is proportional to the product of Young's modulus and the cube of the thickness, for a homogeneous member.

flexural strength.—The maximum apparent outside fiber stress in a member at rupture due to an applied moment.

friction, coulomb.—A force that is substantially independent of velocity and always acts in opposition to the motion.

friction, viscous.—Frictional force proportional to velocity.

gain.—The ratio of the power radiated by an ANTENNA per unit solid angle in any direction to the power radiated per unit solid angle by an isotropically radiating antenna of the same total power output. Gain is a variable, being different in different directions. The maximum gain, or gain at the most intense part of the beam, is sometimes loosely termed the gain.

GR-N rubber.—A Buna-N synthetic rubber made to government specification. A copolymer of butadiene and acrylonitrile similar to rubber in mechanical properties but almost unaffected by oils.

ground return.—Also referred to as ground clutter. Reflections from objects on the ground observed with a radar set; more particularly such reflections observed by an airborne radar used for locating other airborne targets.

GR-S rubber.—A Buna-S synthetic rubber made in government plants. It is a copolymer of butadiene and styrene similar to natural rubber but more nearly saturated. It is often used where low-temperature flexibility is required.

gyro, gyroscope.—An assembly consisting of a rapidly rotating wheel, gimbals, a take-off at one or at each gimbal axis, a dustproof case and other items. See STABLE ELEMENT and STABLE VERTICAL.

half-sandwich.—A mathematical abstraction used in RADOME calculations that consists of one skin and an infinitely thick core.

half-wavelength panel or **radome.**—(1) One whose thickness is a half wavelength in the material. (2) MODIFIED HALF WAVELENGTH PANEL OR RADOME. One that behaves for waves incident obliquely at a particular angle as a half-wavelength panel or radome does for normally incident waves.

heading.—The angle between the north and south vertical plane and the vertical plane through the fore-and-aft axis of an airplane, measured clockwise from the north.

heat distortion temperature.—For almost any polymer, a characteristic narrow temperature range in which the mechanical properties undergo changes. Below this temperature range the high polymer is dimensionally stable; above it, creep appears.

high dielectric constant material.—One having a SPECIFIC DIELECTRIC CONSTANT of 4.0 or higher.

hinge joint.—A coupling between two WAVEGUIDES that allows a few degrees of angular misalignment in one plane only. Commonly it employs a choke FLANGE, slightly separated from a plain flange which may be beveled to allow motion.

hole.—A deficiency, in a certain direction, in the GAIN of an imperfect FAN-BEAM ANTENNA PATTERN.

honeycomb core.—A RADOME core material consisting of a hexagonal grid of laminated fabric.

horn feed.—The flared termination of a WAVEGUIDE, used to illuminate a paraboloid REFLECTOR.

H-vector.—The vector representing the magnetic field of an electromagnetic wave. In free space it is perpendicular to the E-VECTOR and to the direction of propagation.

hybrid plane wave.—A wave corresponding to complex values of the quantities that are the direction cosines of an ordinary plane wave.

IFF.—Identification, friend or foe. The equipment elicits a replying pulse SIGNAL from a transpondor on friendly airplanes or vessels. See BEACON. It often uses a special ANTENNA, sometimes mounted on or in front of the radar antenna.

incidence.—See PLANE OF INCIDENCE and ANGLE OF INCIDENCE.

indicator.—The cathode-ray tube and associated apparatus on which the radar SIGNALS are made visible.

instability.—Elastic instability of the RADOME wall; the inability of a radome to sustain more than a certain critical load, owing to elastic buckling.

interference fringes.—Bands in the radar DISPLAY, representing a fluctuation in the pattern due to the alternating addition and subtraction of waves propagated by different paths.

jamming.—Intentional interference with the normal operation of a remote radio or radar receiver.

level angle.—The angle between the horizontal plane and the deck plane, measured in the vertical plane through the LINE OF SIGHT. It is positive if the deck toward the line of sight is below the horizontal plane.

line of sight.—The line from the ANTENNA in the direction of the NOSE of the BEAM or in the direction of a TARGET.

line-of-sight stabilization.—ANTENNA STABILIZATION by means of the ELEVATION axis in a two-axis SCANNER.

line-stretcher.—A device for making slight adjustments in the effective length of a TRANSMISSION LINE.

linear array.—A straight row of DIPOLES or other radiating elements, energized in such phase relationships as to produce a PATTERN which is broadside, end-fire, or intermediate in direction.

load, matched.—A termination of a TRANSMISSION LINE that absorbs all R-F energy reaching it from the line.

loss.—The absorption of radiation within a dielectric. See also LOSS ANGLE, LOSS TANGENT, LOSSY DIELECTRIC, LOW-LOSS DIELECTRIC, and TRANSMISSION LOSS.

loss angle δ.—The complement of the phase angle θ; the angle by which the polarization lags behind the charging current.

loss tangent $\tan \delta$.—The ratio of loss factor of a material to its PERMITTIVITY. For small LOSS ANGLES, the loss tangent is approximately equal to the power factor $\cos \theta$.

lossy dielectric.—One whose LOSS TANGENT is different from zero, especially one whose loss tangent exceeds 0.015.

low-loss dielectric.—One whose LOSS TANGENT does not exceed 0.015.

low dielectric constant material.—One having a specific dielectric constant of 2.2 or less.

low-pressure molding.—A method of molding plastic sheets, in which atmospheric or other moderate pressure is applied, usually through a rubber bag, at an elevated temperature, and forces the sheet against a mold. Also known as bag molding and impression molding.

magnetron.—The type of transmitting tube used in nearly all MICROWAVE radars. It must be used in a magnetic field of proper strength.

Marbon B.—A brand of cyclorubber prepared by the Marbon Corporation by the cyclization of natural rubber, changing it from an elastomeric material to one that is tough and hard.

Marbon S.—A brand of cyclorubber prepared by the Marbon Corporation by the cyclization of GR-S rubber, changing it from an elastomeric material to one that is tough and hard.

match.—The extent to which a reflectionless condition is realized, as waves are propagated from one region into another (e.g., through an elbow in WAVEGUIDE or from a TRANSMISSION LINE into space).

mechanical scanner.—A SCANNER that moves the BEAM by a motion of the ANTENNA as a whole or by relative motion of the external portion of a point FEED and the REFLECTOR.

microwaves.—Radio waves whose wavelength is less than approximately 25 cm or whose frequency exceeds about 1200 megacycles per second.

mockup.—A nonfunctioning full-scale model intended to facilitate design studies.

mode.—See *TE*-mode, *TEM*-mode, $TM_{0,1}$-mode.

modulator.—The component of a radar set that energizes the transmitting tube during each pulse. It is sometimes carried on the PEDESTAL.

monomer.—An organic compound of molecules of relatively simple structure that may be combined in groups to form molecules of the corresponding POLYMER.

mount.—See ANTENNA MOUNT.

nacelle.—An excrescence on the leading part of a fuselage or wing, housing an engine, scanner or the like.

normal-incidence radome.—A RADOME for which the ANGLE OF INCIDENCE is less than 30°. See STREAMLINED RADOME.

nose.—(1) The part of a BEAM in the direction of maximum intensity or GAIN. (2) The leading portion of an airplane fuselage.

nutating feed.—A VERTEX FEED which describes an orbit at the focus of a paraboloid without spinning, i.e., by a wobbling motion. It maintains a steady PLANE OF POLARIZATION of the radiation.

order.—(1) The voltage sent through a SERVO SYSTEM to control the TRAIN or ELEVATION of an ANTENNA. (2) The angles defining the position of an antenna, e.g., train order and elevation order. See also ORDER OF A SANDWICH RADOME.

order of sandwich radome.—As in "second-order SANDWICH," etc., the number identifying a member of the series of optimum low-reflection RADOMES, which differ by a half-wavelength in the ELECTRICAL THICKNESS of the core. The order is $n + 1$ where n is the number of half-wavelengths added to the electrical core thickness of the thinnest member of the series.

own ship's course.—The angle between the north and south vertical plane and the vertical plane through the fore-and-aft axis of own ship, measured in a horizontal plane clockwise from north.

pattern.—The angular distribution in space of the energy from the ANTENNA; a graph of this distribution. It is sometimes termed the "secondary pattern." The primary pattern is the angular distribution of energy from an antenna FEED.

pedestal.—The structure supporting the ANTENNA, including the BASE, the mechanical drives, the TRANSMISSION LINE as far as the antenna FEED, the data TAKE-OFFS, and such other electronic equipment as may be mounted thereon.

pencil beam.—A BEAM having nearly circular symmetry about an axis. It is equally sharp in all planes passing through its axis.

pillbox.—A type of antenna FEED, commonly energized through a WAVEGUIDE, that provides a source of radiation distributed along a line.

perpendicular (parallel) polarization.—Polarization in a plane perpendicular (parallel) to the plane of incidence.

pip.—(1) A single TARGET as seen on the DISPLAY. (2) An artificial signal added to the

DISPLAY for reference purposes. It is sometimes produced by a "pipper" switch on the SCANNER.

pitch angle.—The angle, measured about the axis given by the intersection of the horizontal plane with the athwartship plane perpendicular to the deck, between this plane and the zenith direction. It is positive when the bow is up. A similar definition applies to the pitch of an airplane. The ROLL and pitch angles would be indicated directly by protractors attached to the outer and inner gimbal bearings respectively of a STABLE VERTICAL if the outer gimbal axis is installed in a fore-and-aft direction.

plane of incidence.—The plane including a ray and the normal to a surface that it intersects. See ANGLE OF INCIDENCE.

plane wave.—A wave whose wavefronts are planes.

plane polarized wave.—In free space, a wave in which the E-VECTOR is always parallel to one plane, which includes the direction of propagation.

plane of polarization.—The plane through the direction of propagation which is parallel to the E-VECTOR in plane polarized radiation. If the beam axis is horizontal, the plane of polarization is usually either horizontal or vertical, as determined by the antenna.

polarization.—See PLANE POLARIZED WAVE, PLANE OF POLARIZATION, and PERPENDICULAR (PARALLEL) POLARIZATION.

polyesterstyrene resin.—A polycondensation product resulting from vinyl polymerization of styrene so as to cross-link polyester chains.

Polyfibre.—A brand of polystyrene fibers made by the Dow Chemical Company.

polymer.—A chemical compound whose molecule consists of a closely bound group of like molecules of a compound of simpler structure known as the MONOMER.

polystyrene.—A clear colorless thermoplastic molding material made by polymerizing styrene, a colorless organic liquid. A pure nonpolar hydrocarbon of excellent DIELECTRIC properties.

postforming.—Permanent deformation of plastic sheets to change their curvature.

power contour.—A curve connecting points of a given value of the power reflection coefficient.

power reflection coefficient.—The ratio of the intensity of plane waves reflected from a plane surface to that incident upon it; the square of the AMPLITUDE REFLECTION COEFFICIENT.

PPI, plan position indicator.—A very common type of DISPLAY, in which surface objects surrounding the radar are shown as on a circular map, usually with the radar at the center.

pressurization.—Maintaining a pressure in excess of the ambient pressure in a TRANSMISSION LINE, R-F HEAD, etc.

pulling.—A change in the frequency of a TRANSMITTER output, resulting from STANDING WAVES in the TRANSMISSION LINE. It is generally undesirable.

radome.—Radar dome. The housing for an ANTENNA, transparent to R-F radiation. It may include certain nontransparent areas.

range.—(1) The distance to a TARGET. In airborne usage this is termed slant range. (2) The ground range, or horizontal component of the slant range. (3) The maximum range at which a given type of target can be detected with a given radar.

reflection.—See POWER REFLECTION COEFFICIENT, AMPLITUDE REFLECTION COEFFICIENT.

reflector.—The portion of an ANTENNA that reflects the radiation from the FEED into space, collimating the BEAM or otherwise shaping the secondary PATTERN. Some antennas have no reflector.

relative azimuth angle.—RELATIVE TARGET BEARING.

relative target bearing.—The angle between the fore-and-aft axis of own ship and the vertical plane through the LINE OF SIGHT, measured in the deck plane clockwise from the bow.

resolution.—The ability of a radar set to distinguish two reflecting objects that lie close together.

resolver.—A transformer having two primary windings in space quadrature and two secondary windings in space quadrature. The secondary may be rotated in relation to the primary. Sometimes one winding is absent.

r-f.—Radio frequency. In the 1-, 3-, and 10-cm bands the frequencies are about 30,000; 10,000; and 3000 megacycles per second, respectively.

r-f head, r-f unit.—The unit containing the TRANSMITTER and the parts of the receiver in which R-F currents are present. It is sometimes mounted on the PEDESTAL.

roll angle.—The angle, measured in the athwartship plane perpendicular to the deck, between its intersections with the horizontal plane and with the deck plane. It is positive when the starboard side of the ship is raised or when the right wing of an airplane is depressed. See PITCH ANGLE.

rotary joint.—A connection between two portions of a TRANSMISSION LINE that allows rotation of one with respect to the other.

sandwich radome.—A RADOME composed of three layers: a core of one DIELECTRIC, bonded between skins of a different dielectric. See also ASYMMETRICAL SANDWICH RADOME.

scan.—The path periodically described by a BEAM in space; does not include the motion of TRACKING.

scanner.—The entire mechanism employed to produce a scanning BEAM of radiation and to actuate its motion. See ANTENNA MOUNT.

Selsyn.—A trade name for a SYNCHRO.

servomechanism, servo system.—A device whereby a remote member is caused to assume a position dependent upon the position of a control member. The controlling force on the remote member is a function of the difference between the actual and desired positions of the remote member. The design of a servomechanism may be such as to provide great amplification of torque.

side lobe.—A portion of the radiation from an ANTENNA outside the main BEAM and usually of much smaller intensity. A side lobe is a region between two minima in the PATTERN.

signal.—A radar echo; pip. See also ERROR SIGNAL.

specific dielectric constant.—The ratio of the DIELECTRIC CONSTANT of the material to the dielectric constant of vacuum.

square-law detector.—A detector whose output is proportional to the square of the amplitude of the received SIGNAL, i.e., to the intensity.

stabilization.—The use of a SERVOMECHANISM to control the angular position of an ANTENNA, in such a way as to compensate automatically for changes in the angular position of a ship or airplane on which the antenna is mounted.

stable element.—A gyroscope whose wheel maintains a vertical axis and whose gimbal axes may be oriented in TRAIN.

stable vertical.—A gyroscope whose wheel maintains a vertical axis and whose gimbal axes are fore and aft and athwartship.

standing waves.—The spatial alternation of regions of high and low R-F electric field, caused by the reflection of waves, as in a faulty TRANSMISSION LINE or ANTENNA FEED. The voltage standing wave ratio (VSWR or SWR) is the ratio of maximum to minimum field intensity.

stowing pin.—A means of inhibiting the motion of an ANTENNA during periods when the radar is not in use.

streamlined radome.—A radome whose electrical area is steeply inclined to the WAVEFRONTS. The rays of high intensity are incident on the wall at ANGLES OF INCIDENCE in excess of 30°. See NORMAL-INCIDENCE RADOME.

strength and stiffness ratings.—Figures of merit of a RADOME panel, in terms of the strength (or stiffness), DIELECTRIC CONSTANT(S), and thickness of the panel.

structural radome sandwich.—A sandwich designed with primary regard for structural considerations at the expense of electrical characteristics.

surface-based.—Located on the ground or on a tower, vehicle, or vessel. Not airborne.

synchro.—A transformer of which the coupling is varied by the relative orientation of the primary and the secondary. Continuous rotation is possible. Usually one or both windings are three-phase.

SWR.—Standing wave ratio. See STANDING WAVES.

take-off.—A SYNCHRO, potentiometer, or other device for DATA TRANSMISSION. Take-offs are mounted on SCANNERS to indicate the direction of the BEAM and on gyros to indicate the angular position of a ship or aircraft.

target elevation.—The angle between the horizontal plane and the LINE OF SIGHT, measured upward from the horizontal in the vertical plane through the line of sight.

target.—Any object reflecting a radar pulse back to the ANTENNA.

TE-mode.—Any mode of propagation in WAVEGUIDE or between parallel plates, in which the electric field is wholly transverse to the direction of propagation. The $TE_{1,0}$-mode is commonly used in rectangular WAVEGUIDE TRANSMISSION LINES.

TEM-mode.—A mode of propagation of electromagnetic energy between parallel plates (or in a COAXIAL TRANSMISSION LINE), in which the electric field is everywhere perpendicular to the conductors and the wavelength is independent of the spacing between them.

thermoplastic material.—An organic material that becomes deformable and workable upon heating.

thermosetting material.—One that is cured, i.e., undergoes an irreversiblee hemical change consisting of a CROSS-LINKING of molecular chains upon heating. After curing it resists change in physical form. See THERMOPLASTIC MATERIAL.

thick-skinned sandwich radome.—A sandwich radome in which the skins have a low dielectric constant and an ELECTRICAL THICKNESS of one-half wavelength.

thickness, electrically effective.—Especially of a RADOME skin, the thickness as determined by electrical (i.e., R-F) rather than by mechanical measurements. It is influenced by the penetration of the skin resin into the core.

thin-walled radome.—One whose ELECTRICAL THICKNESS is small in comparison with a quarter-wavelength.

tilt angle.—The DEPRESSION ANGLE.

$TM_{0,1}$-mode.—A mode of propagation of electromagnetic energy which has axial symmetry if excited in a circular WAVEGUIDE. It is widely employed in ROTARY JOINTS.

tracking.—Directing an ANTENNA continuously toward a moving TARGET. This may be effected manually while watching the INDICATOR or automatically.

train.—Angle measured in the deck plane, clockwise from the bow. See also ANTENNA TRAIN.

train axis.—An axis of an ANTENNA MOUNT, perpendicular to the deck.

transmission coefficient, power transmission coefficient.—The ratio of the intensity of

the PLANE WAVE transmitted through a plane surface or panel to the intensity that would exist if the surface or panel were removed. *Amplitude transmission coefficient* is the corresponding ratio of amplitudes, usually a complex number.

transmission line.—The conductor or system of conductors carrying R-F energy from the TRANSMITTER to the ANTENNA. See COAXIAL TRANSMISSION LINE and WAVEGUIDE.

transmission loss.—Unity minus the power TRANSMISSION COEFFICIENT.

transmitter.—(1) the R-F transmitting tube, in MICROWAVE practice usually a MAGNETRON. (2) A data TAKE-OFF.

true azimuth angle.—TRUE TARGET BEARING.

true target bearing.—The angle between the north and south vertical plane and the vertical plane through the LINE OF SIGHT, measured in a horizontal plane clockwise from the north.

tuner.—In MICROWAVE R-F practice, any device for altering the STANDING WAVES in a TRANSMISSION LINE; an adjustable impedance transformer.

vertex feed.—A FEED at the focus of a paraboloid REFLECTOR; it is mounted at the end of the TRANSMISSION LINE, which penetrates through the paraboloid at its vertex.

wavefront.—An imaginary surface in a field of radiation, at all points of which the r-f variation of the E-VECTOR is in the same phase. In free space the wavefronts are one wavelength apart and are perpendicular to the direction of propagation.

waveguide.—A metal tube, usually of rectangular cross section, within which electromagnetic energy may be propagated.

wet lay-up molding.—The low-pressure curing of the skin of a sandwich RADOME in contact with the core material. In the single-stage process both skins are cured simultaneously.

wobble joint.—See HINGE JOINT.

Index

S